

013.57.11
Program and
Extended
Abstracts

International
Conference on
the Physics of
X-ray Spectra
August 30 -
Sept. 2, 1976
National Bureau of
Standards
Gaithersburg, Md.



Sponsored by:
International Union of
Pure & Applied Physics
U.S. Dept. of Commerce
National Bureau of
Standards
U.S. Naval Research
Laboratory
U.S. Army Research Office
U.S. Energy Research &
Development Admin.
U.S. Office of Naval
Research

PREFACE

This International Conference on the Physics of X-ray Spectra at the U.S. National Bureau of Standards follows a sequence begun in Ithaca, New York, USA (1965) and followed biennially in Kiev, USSR (1968), Paris, France, (1970), Munich, Federal Republic of Germany (1972), and Helsinki, Finland (1974). The Conference is sponsored by the International Union of Pure and Applied Physics, the U.S. Energy Research and Development Administration, the U.S. National Bureau of Standards, the U.S. Naval Research Laboratory, the U.S. Army Research Office and the U.S. Official Naval Research.

The 1976 Conference provides a forum for the discussion of current work in the physics of X-ray spectra as obtained under a wide variety of conditions and from a diversity of points of view. Sessions have been arranged under the topics: Many-Body Effects in Metals, Hole State Dynamics, Continuum Oscillator Strength Distributions, Ion-Atom Collisions, X-rays from Astrophysical and Laboratory Plasmas, and X-ray Lasers. Other discussions are included in the areas of spectra from Molecules and Compound Solids, Metals and Alloys, and Synchrotron Studies of Extended Absorption Fine Structure. In addition to a considerable number of reports on related spectroscopies (APS, AES, XPS and Isochromats), there will be papers concerning recent work on Compton and Raman Scattering. Finally, a session has been planned to permit exchanges of experience regarding Instruments and Methods.

The organization of the Conference and its program has relied upon the functioning of its two principal committees:

International Advisory Committee

T. Åberg (Finland)
M.A. Blokhin (USSR)
J. Drahokoupil (Czechoslovakia)
D.J. Fabian (United Kingdom)
B.S. Fraenkel (Israel)
S. Hagstrom (Sweden)
R. Manne (Norway)
W. Mehlhorn (Federal Republic of Germany)
T. Sagawa (Japan)
F.J. Wuilleumier (France)

Program Committee

R.D. Deslattes
R.C. Elton
M.O. Krause
R.E. LaVilla
S.T. Manson
D.J. Nagel
P. Richard
S.E. Schnatterly
H.W. Schnopper

As is usually the case in any gathering such as this, the transition from an initial state of a conference that will take place to a final state that is a smoothly operating conference has been the result of much labor by a small number of people. R.E. LaVilla has borne the major part of the burden of arranging the sessions, communicating with authors about the mechanics of their contributions, and assembling this Proceedings volume. I am greatly indebted to him for dedicated efforts. I also extend my grateful thanks to Miss Robyn Hoy who did all the typing and record-keeping for the Conference. Finally, I appreciate the contributions of Dr. W.G. Schweitzer, Jr. and Mrs. Sara Torrence in handling administrative details.

R.D. Deslattes
August 1976
Gaithersburg, Maryland

INTERNATIONAL CONFERENCE ON THE PHYSICS OF X-RAY SPECTRA PROGRAM

MONDAY, AUGUST 30, 1976

	<u>PAGE</u>
SESSION 1 - PREAMBLE AND MANY-BODY EFFECTS IN METALS	
Chairman - W.T. Oosterhuis	
0900 Keynote Address - X-ray Physics After Eighty Years Bernd Crasemann	1
0930 Many-Body Effects at X-ray Edges in Metals G.D. Mahan	7
1000 Prediction of Many-Body Lineshapes Using Sum Rules J.D. Dow	10
1020 Coffee	
1040 Exchange Effects in the Li K Edge S.M. Girvin and J.J. Hopfield	13
1100 Band Theory of Edge Shapes in Metals R.P. Gupta and A.J. Freeman	16
1120 Photoabsorption and Photoyield Measurements of Li K-Edge C. Kunz, H. Petersen and B. Sonntag	19
1140 Inelastic Electron Scattering Determination of Edge Shapes in Simple Metals P.C. Gibbons, S.G. Slusky and S.E. Schnatterly	23
1200 Impurity Spectra and the Optical Threshold Profile in Metals C.P. Flynn	26
1220 Understanding of X-ray Absorption Edges in Simple Metals Using X-ray Photoemission P.H. Citrin, G.K. Wertheim, M. Schlüter and Y. Baer	29
1240 Lunch	
SESSION 2a - HOLE STATE DYNAMICS	
Chairman - J.P. Briand	
1340 Categorization of Two-Electron Processes According to the Major Many-Electron Interaction M.O. Krause	32
1410 Effects of Relaxation and Continuum Interaction on the Ne KLL Auger Spectrum G. Howat, T. Åberg and O. Goscinski	35

MONDAY, AUGUST 30, 1976 - continued

		<u>PAGE</u>
1430	Double L-vacancy States in the Electron Capture Decay of ^{181}W P.V. Rao	38
1450	Multipolarity of Some Transitions in ^{231}Th By Application of Gamma-X-rays Coincidence Technique E. Vano and L. Gonzalez	40
1510	Simplified Calculation of Autoionization Rates in Two and Three-Electron Atoms D.R. Franschetti and D.L. Miller	43
1530	Theoretical X-ray and Autoionization Rates for Four-Electron Ions with $2s^n 2p^m$ Configurations M. Ahmed, S.C. Soong and C.P. Bhalla	46
1550	Tea	

SESSION 2b - MOLECULES AND COMPOUND SOLIDS-I

Chairman - T. Sagawa

1340	Interpretation Schemes for Core Electron Excitation Spectra of Small Molecules W.H.E. Schwarz	49
1410	An Ab Initio Calculation of a Vibrational Structure in X-ray Spectra of Molecules L.N. Mazalov, F.K. Gel'mukhanov, A.V. Kondratenko and V.I. Avdeev	53
1430	Soft X-ray Absorption of Molecular Alkali Halides K. Radler, B. Sonntag and H.W. Wolff	54
1445	Interpretation of the X-ray Emission and Photoelectron Spectra of Simple Solid Compounds G. Leonhardt, A. Kosakow, H. Sommer and M. Petke	57
1500	The Oxygen X-ray Emission Spectrum of Some Oxyanions N. Kosuch, E. Tegeler, G. Wiech and A. Faessler	60
1520	X-ray Investigation of the Energy Level Structure of Tetrahedrally Coordinated Transition Metal Atoms R. Szargan and A. Meisel	63
1535	On the 1s-Absorption Line Spectra of Li in Lithium Halides and of B in BCl_3 and BF_3 T. Hayasi and Y. Hayasi	64
1550	Tea	

	<u>PAGE</u>
SESSION 3 - COMPTON AND RAMAN SCATTERING Chairman - Cully Sparks	
1610 Resonant X-ray Scattering from Solids Philip M. Platzmann	67
1640 Compton Spectroscopy William Reed	70
1710 X-ray Inelastic Scattering - Relation Between Compton - Raman- and Plasmon Scattering T. Suzuki	72

TUESDAY, AUGUST 31, 1976

PAGE

SESSION 4 - RESONANCE AND CONTINUUM OSCILLATOR STRENGTH DISTRIBUTION-I
Chairman - R. Haensel

0900	Shape Resonance Effects in X-ray Absorption Spectra of Molecules J.L. Dehmer and D. Dill	75
0920	Partial Photoionization Cross-Sections in the Soft X-ray Region I. Lindau, P. Pianetta and W.E. Spicer	78
0940	X-ray Resonance Scattering by Atoms with A Partially Empty Localized Shell C. Bonnelle and R. Barchewitz	81
1000	Coffee	

SESSION 5 - EXTENDED ABSORPTION FINE STRUCTURE
Chairman - A. Bienenstock

1020	White Lines and EXAFS: Complementary Effects D E. Sayers, E.A. Stern and F.W. Lytle	84
1050	Extended Structure in X-ray Photoabsorption: Principles and Applications P. Eisenberger, W.E. Blumberg, G.S. Brown, P.H. Citrin, B.M. Kincaid, J. Reed and R.G. Shulman	86
1120	X-ray Photoabsorption Studies of Superconducting Al5 Compounds G.S. Brown and L. Testardi	88
1140	EXAFS in Photoelectron Yield Spectra: Comparison with Photoabsorption and Determination of Electron Escape Depths R. Haensel, G. Martens, P. Rabe, N. Schwentner, M. Skibowski and A. Werner	89
1200	EXAFS of a Single Crystal of Galium W.M. Weber	90
1220	Lunch	

SESSION 6a - APS, XPS AND ISOCHROMATS
Chairman - M.A. Blokhin

1320	On Newer Developments in Isochromat Spectroscopy K. Ulmer	92
------	--	----

	<u>PAGE</u>
1350 X-ray Continua Near the High Frequency Limit R.J. Liefeld and A.F. Burr	95
1420 Bremsstrahlung Isochromat from Aluminum P.E. Best and C.C. Chu	98
1435 Bremsstrahlung Isochromat of Tungsten at 16 eV H. Humberg and H. Merz	101
1450 Studies of the 4f States in Ba and La by Electron and Photon Excited APS J. Kanski, P.O. Nilsson and I. Curelaru	102
1505 Diffraction Effects in Appearance Potential Spectroscopy M.L. den Boer, Y. Fukuda and R.L. Park	105
1520 X-ray Photoelectron Studies of the Heavy Rare-Earth Metals and Their Oxides D.J. Fabian, W.C. Lang, P.R. Norris, B.D. Padalia and L.M. Watson	108
1540 Tea	
1600 Determination of Empirical Atomic Continuum Charge Densities, Phase Shifts, and Local Pseudo-Potentials from Angular- Dependent Photoemission Data for Rare Gases D.L. Miller and J.D. Dow	111
1615 Satellites in the 1s and 2s XPS Spectra of Nickel Oxide E.-K. Viinikka and P.S. Bagus	114
1630 Multiplet Splitting of Core 2p and 3p Photoelectron Lines of Transition Metal Halides M. Okusawa, T. Ishii and T. Sagawa	116
1645 Importance of Relaxation Effect During Ionization of Molecules J.J. Pireaux, S. Svensson, E. Basilier, P.-Å. Malmqvist, U. Gelius, R. Caudano and K. Siegbahn	119
1700 ESCA Studies of the Alkali-Halides, LiF, LiCl and LiBr, and of Li Metal L.I. Johansson, S.B.M. Hagström and S.-E. Karlsson	122
1715 X-ray Spectra of Transition Metal Alloys and Their Interpretations E.Z. Kurmaev	125

	<u>PAGE</u>
SESSION 6b - MOLECULES AND COMPOUND SOLIDS-II	
Chairman - A. Meisel	
1320 Formation of Band Structures in Quasi One Dimensional Molecules J.J. Pireaux, S. Svensson, E. Basilier, P.-Å. Malmqvist, U. Gelius, R. Caudano and K. Siegbahn	126
1340 Beryllium K Spectra of Beryllium Compounds Yasuo Iguchi	130
1355 Characterization of Silicon Monoxide by X-ray Spectroscopy M.T. Costa Lima and C. Senemaud	133
1410 The Effect of Temperature on X-ray Emission Spectra J.B. Jones, M. Kasrai and D.S. Urch	136
1425 The Chemical Bonding in Spinel ($MgAl_2O_4$) Studied by X-ray Emissions and X-ray Photoelectron Spectroscopies D. Haycock, C.J. Nicholls and D.S. Urch	139
1440 An XES Study of the Structure of As-S Glasses M. Lähdeniemi and E. Suoninen	142
1455 Investigation of the X-ray Emission and Photoelectric Yield Spectra of Beryllium in Its Compounds M.A. Blokhin, E.G. Orlova and I.G. Schweizer	145
1510 Chemical Shifts of the K-Absorption Discontinuity of Cobalt in Intermetallic Systems C. Mande and V. Kondawar	148
1525 K-Absorption Spectra of Some Polynuclear Copper Complexes J. Prasad, V. Krishna and H.L. Nigam	151
1540 Tea	
1600 The K-Emission and Absorption of Gallium in GaP, GaAs and GaSb J. Drahokoupil, H. Klokocníková and A. Šimůnek	154
1615 Effect on Chemical Environment on Sulfur $K\alpha$ X-ray Spectra G. Graeffe, H. Juslén and E.-K. Viinikka	157
1630 X-ray Emission Spectra of Rare Earth and Transition Elements and Their Oxides S.I. Salem	160

		<u>PAGE</u>
1645	X-ray Spectroscopic Studies of Some CaCu_5 Type Intermetallic Compounds A.R. Chetal and P.R. Sarode	163
1700	Positron Annihilation and X-ray Spectroscopic Studies of Heavy Rare Earth Elements S.N. Gupta and V.P. Vijayavargiya	166
1715	X-ray Spectra of Transition Metal Disulfides: FeS_2 , CoS_2 , and NiS_2 C. Sugiura, S. Nakai, T. Matsukawa, M. Obashi, J. Kashiwakura and Y. Gohshi	168

	<u>PAGE</u>
SESSION 7 - ION ATOM COLLISIONS	
Chairman - E. Merzbacher	
0900 Multielectron Transitions in K X-ray Spectra of Ion-Atom Collisions T. Åberg	171
0940 Measurement of Cross Sections for the Two-Electron One-Photon Transitions in Heavy-Ion Collisions R. Schuch, G. Nolte, H. Schmidt-Böcking, R. Schulé, W. Lichtenberg, K.E. Stiebing and I. Tserruya	174
1000 Evidence for $2e-1\gamma$ Transitions in Cl^{n+} Bombardment of KCl W.W. Jacobs, B.L. Doyle, S.M. Shafroth, J.A. Tanis and A.W. Waltner	177
1020 Coffee	
1040 Excitation of 2 Electron - 1 Photon K X-ray in Ni-Ni Collisions J.S. Greenberg, P. Vincent and W. Lichten	180
1105 Effects of Collisional Quenching on the X-ray Yield from Ion-Atom Collisions D. Matthews and R. Fortner	183
1130 K X-rays and REC from Cl^{N+} Bombardment of Targets in the Region $19 < Z < 35$ J.A. Tanis, B.L. Doyle, W.W. Jacobs and S.M. Shafroth	186
1155 $K\alpha$ Satellite Structure in Ion-Atom Collisions R.L. Watson, B.I. Sonobe, A.K. Leeper, T. Chiao and F.E. Jenson	189
1220 Lunch	
SESSION 8a - VALENCE BAND STUDIES OF METALS AND ALLOYS	
Chairman - Derek Fabian	
1320 Calculations of X-ray Band Spectra D.A. Papaconstantopoulos	192
1350 Valence Band Structure of Diamond, Graphite and Amorphous Carbon Obtained by X-ray and Photoelectron Spectroscopy G. Wiech	195
1405 Polarization and Anisotropy of the C K-Spectrum J. Kieser	198

		<u>PAGE</u>
1420	Calculation of the K-Absorption Spectrum of Aluminum F. Szmulowicz and B. Segall	202
1435	Valence Band Spectra of Aluminum Noble-Metal Alloys L.M. Watson, D.J. Fabian, J.C. Fuggle, E. Källne and P.R. Norris	205
1450	SXS and XPS in the Investigation of Order in Alloys and Liquid Metals C. Hague, J.M. Mariot, G. Dufour, and R.C. Karnatak	208
1505	A New Comparison Between Experiment and Theory for the X-ray K-Absorption Edge of Nickel D.M. Pease and T.K. Gregory	211
1520	Application of Pt L Emission and Absorption Spectra for the Investigation of Cluster Structures J. Finster, P. Muller, F. Thiel and A. Meisel	214
1540	Tea	
1600	Configuration Interaction Interference Effects in the Core- Electron Excitation Edges of Transition Metals R.E. Dietz and E.G. McRae	217
1615	Valence Band and Conduction Band Spectra of Transition-Metal Compounds K. Tsutsumi, K. Ichikawa and O. Aita	220
1630	Interpretation of the Rhenium L ₃ Absorption Discontinuity in Rhenium Metal and in Some of Its Compounds A.V. Pendharkar and C. Mande	223
1645	Coherent- Pseudopotential- Pair Calculation for X-ray Photoemission Studies of Ag-Pd Alloys V. Srivastava and S.K. Joshi	226
1700	On the Electronic Structure of Palladium in the Pd-H System E. Gilberg	229
1715	Characteristic and Continuous X-ray Emission Measurements on TiNi H. Föll	232

	<u>PAGE</u>
SESSION 8b - INSTRUMENTS AND METHODS	
Chairman - R. Liefeld	
1320 Resolution-Enhanced Cu and Co $K\alpha_{1,2}$ X-ray Emission Spectra Obtained by the Deconvolution Method J. Kashiwakura, Y. Gohshi and I. Suzuki	235
1335 A New Computer Controlled Soft X-ray Spectrometer H.-E. Goldstein, R. Pfliegl and H. Kirchmayr	238
1350 Ultra High Resolution Capabilities of a 5M Grating Spectrometer in the 10 to 250 Å Region G. Andermann, L. Bergknut, M. Karras and G. Griesehaber	240
1405 K-Absorption Spectra of Fluorine in Alkali-halide Crystals S. Kiyono, Y. Hayashi and T. Muranaka	241
1420 A High-Resolution X-ray Spectrometer: Description and Preliminary Experimental Results W.C. Sauder and R.E. LaVilla	243
1435 Holographic Transmission Gratings - A New Analyzer in the X-ray Region E. Källne, H.W. Schnopper, L.P. Van Speybroeck, J.P. Delvaille, A. Epstein, R.Z. Bachrach, J.H. Dijkstra and L.J. Lantwaard	245
1450 Vapor X-ray Spectra of Rare-Earth Metals I.A. Brytov, L.E. Mstibovskaya, N.I. Komyak and L.G. Rabinovitch	248
1505 Determination of the Depth of Impurity Atoms in Bulk Material by Proton Induced X-rays O. Benka, M. Geretschlager, A. Kropf, H. Paul and J. Kepler	249
1520 High Resolution L X-ray Emission Spectrum of Argon J. Nordgren, H. Ågren, C. Nordling and K. Siegbahn	250
1540 Tea	
1600 The Use of Long Wavelengths for Low-Angle Scattering Y. Siota and M. Yokota	253
1615 X-ray Detection for Measurement of Inner Shell Ionization by Relativistic Electron Impact H. Genz, D.H.H. Hoffmann, W. Low and A. Richter	256
1630 A New Type of Kossel-Borrmann Radiation from Germanium Crystal K. Das Gupta	260

		<u>PAGE</u>
1645	Theory and Measurement of X-ray Diffraction Several Acid Phthalates D.M. Barrus, R.L. Blake and A.J. Burek	263
1700	A Spectrograph for Studies of High Speed Discharge B. Sundbom and S.K. Händel	266
1715	X-ray Spectroscopic Investigation of Energy Bands Fine Structure and the Interpretation of Conductivity Character of Phosphorous Compounds of Various Chemical Bond Types A.N. Gusatinski, M.A. Blokhin, G.I. Alperovich, M.A. Bunin and I.A. Topol	269

SESSION 8c - MORE ION ATOM COLLISIONS

Chairman - P. Richard

1320	Target K X-ray Production for Heavy Ions Moving in Thin Solid Films T.J. Gray, P. Richard, R.K. Gardner, K.A. Jamison and J.M. Hall	272
1340	Ar $K\alpha$, $K\beta$ and K-REC X-ray Energies and Intensities vs. Ar^{+12} \rightarrow C-Foil Thickness F. Folkmann, K.-O. Groeneveld, P. Mokler, J. Schader and K.D. Sevier	275
1400	Absolute Measurements of L-Shell Excited Ar Projectiles Emerging from Carbon Foils Between 100 and 800 keV P. Ziem, R. Baragiola and N. Stolterfoht	278
1420	Continuous Thermal X-ray Spectrom from Hot Plasmas, Bremsstrahlung and Radiative Electron Capture Process C.M. Lee and R.H. Pratt	281
1435	Relative Intensities of Ion-Induced $K\alpha$ X-ray Satellite Spectra of Si and Mg as a Function of the Chemical Environmental R.L. Kauffman, L.C. Feldman and P.J. Silverman	284
1450	Impact Parameter Dependence of Non Characteristic Radiation Emitted in Cl-Cl Collisions I. Tserruya, H. Schmidt-Böcking, R. Schulé, R. Schuch, K. Bethge and H.J. Specht	287
1505	Angular Distribution and Projectile-Energy Dependence of the Radiative Electron Capture X-rays R. Schulé, H. Schmidt-Böcking and I. Tserruya	289

WEDNESDAY, SEPTEMBER 1, 1976 - continued

	<u>PAGE</u>
1520 Continuous X-ray Spectra Below 2 MeV in Relation with Nuclear Resonance Y. Cauchois	292
1540 Tea	

SESSION 9 - X-RAYS FROM ASTROPHYSICAL AND LABORATORY PLASMAS

Chairman - H.W. Schnopper

0900	Solar X-ray Astronomy A.S. Krieger	293
0930	K-Shell Excitation and X-ray Spectra in Hot Laboratory and Astrophysical Plasmas L.P. Presnyakov	296
1000	X-rays from Tokomaks W. Stodiek	298
1030	Coffee	
1050	300 - 500 Å Lasers and Possible Lasers of Shorter λ I. Sobelman	299
1120	Electron Temperature and Density Measurements from Laser Produced Plasmas T.C. Bristow	300
1135	K X-ray Emission Spectra from a High Power-Density Plasma	301
1150	Spatially Resolved Spectra from Exploded Wire Plasma C.M. Dozier, P.G. Burkhalter and D.J. Nagel	304
1205	Picosecond Proximity-Focused X-ray Streak Camera A.J. Lieber, H.D. Sutphin and C.B. Webb	307
1220	Lunch	

SESSION 10a - RESONANCE AND CONTINUUM OSCILLATOR STRENGTH

DISTRIBUTION II

Chairman - H.P. Kelly

1320	Theoretical Investigations Concerning the Evolution of the Atomic Effects Contribution in the Spectra (40 to 400 eV) F. Combet Farnoux and F. Keller	310
1340	Analytic Calculation of Screened Photoeffect Cross Sections J. McEnnan, S.-D. Oh and R.H. Pratt	311
1355	Low Energy Photoionization Cross Sections from Proton Induced X-ray Spectroscopy A. Lurio, W. Reuter and J. Keller	316

	<u>PAGE</u>
1410 Study of 4d Shell Excitations by Electron Scattering C. Franck, P.C. Gibbons and S.E. Schnatterly	319
1425 Experimental Study of Photoabsorption in Gd and Dy in the Vicinity of the 4d Ionization Threshold M. Cukier, P. Dhez and P. Jaegle	321
1440 Exact Numerical Calculation of Rayleigh Scattering L. Kissel and R.H. Pratt	324
1455 Angular Correlation Between K and L X-rays in Platinum A.L. Catz	327
1510 Soft X-ray Photoionization of Xenon by Photoelectron Spectroscopy with Synchrotron Radiation F. Wuilleumier, M.Y. Adam, V. Schmidt, N. Sandner and W. Mehlhorn	329
1540 Tea	
 SESSION 10b - EMISSION SATELLITES Chairman - K. Tsutsumi	
1320 About the $L\alpha$ Satellite Spectrum - Can $L\alpha$ Diagram Lines Be Observed J.P. Briand, M. Frilley, P. Chevallier, A. Chetoui, A. Touati, M. Tavernier and J.P. Rozet	332
A Direct Proof of the Shake Model: The $K\alpha$ Satellite Spectrum Following Electron Capture J.P. Briand, P. Chevallier, A. Chetoui, J.P. Rozet, M. Tavernier and A. Touati	335
1340 Rigorous Screening and Effective Principal Quantum Numbers Z.J. Horak, M.N. Lewis and H. Rihova	338
1355 Contribution of Radiative and Auger Transition on K_{β}' Satellite of Transition Elements T. Watanabe and C. Horie	341
1410 Theoretical X-ray Spectra for Double Vacancy in 2p Shell of Argon C.P. Bhalla	344
1425 Systematics of X-ray Satellites S. Rai	347

		<u>PAGE</u>
1440	On the Satellites of the $K\alpha$ -Doublet of Fluorine in Lithium-Fluoride Y. Hayasi	351
1455	Electron Excited K Series Spectra of Neon Gas T. Tooman and R. Liefeld	352
1510	Plasmon Satellites in Auger Spectra of Metals D. Chastenot and P. Longe	354
1525	Multiple Plasmon Excitation in Characteristic Energy Loss Spectrum of Polycrystalline Al K.S. Srivastava, S.P. Singh and R.L. Shrivastava	355
1540	Tea	
SESSION 11 - X-RAY LASERS		
Chairman - James M. Forsyth		
1600	Review and Status of X-ray Laser Research R.W. Waynant	358
1630	Time Resolved Negative Absorption of a Laser-Produced Plasma G. Jamelot, A. Carillon, P. Jaeglé and A. Sureau	361
1700	Population Inversion and the Measurement of Gain in Laser Produced Plasmas W.T. Silfvast, O.R. Wood and J.M. Green	364
1715	Gain Calculation for Electron Collision Pumped X-ray Lasers L.J. Palumbo	365

X-RAY PHYSICS AFTER EIGHTY YEARS*

Bernd Crasemann

Department of Physics, University of Oregon, Eugene, Oregon 97403

Two days before Christmas, 1895, Wilhelm Conrad Röntgen in his chambers in the Physical Institute of the University, Würzburg, recorded a radiograph of the hand of his wife, Bertha. The event marks the birth of our field of study, which is named after Röntgen's rays. Yet radiative transitions play only a relatively minor role in the deexcitation of deep atomic vacancies, the preponderant majority of inner-shell transitions being radiationless. The world had to wait another quarter of a century until Pierre Auger, ca. 1923, performed the ingenious cloud-chamber experiments that led to the unambiguous characterization of what the Germans called "strahlenlose Quantensprünge." The close interplay between experiment and theory during the advent of wave mechanics, in the second half of the twenties, led to a basic understanding of atomic transitions [1]. In 1927, Wentzel formulated the ansatz through which Auger rates are being computed to this day, and in 1935, Coster and Kronig deduced from x-ray satellites the existence of an Auger process in which a vacancy bubbles up among subshells with the same principal quantum number--a kind of transition that is being studied intensely now.

The physics of x rays came to be pursued vigorously in the United States as well. At Harvard, W. Duane and his students used a 43,000-v storage battery made from test tubes to measure Planck's constant. We recall the pioneering contributions of F. K. Richtmyer, L. G. Parratt, J. A. Bearden, and J. W. M. Du Mond, to name a few.

At the present time, we are experiencing a resurgence of interest in the field of inner-shell atomic physics, of which x-ray physics is an integral and historically the oldest part. Modern experimental and theoretical techniques have made important problems accessible that were once intractable. Applications to astrophysics, solid-state and plasma physics, surface studies, and other areas of practical concern have stimulated work in this field. The high level of current activity in x-ray physics is well illustrated by the comprehensive scope of the present conference, and by that of the Second Inner-Shell-Ionization Conference held in Freiburg only five months ago.

It is my task here to attempt to relate one person's assessment of the present status of the subject, to single out some problems and accomplishments, and to try some crystal-ball gazing. This effort is bound to be very subjective, reflecting my own interests and limitations, for which I ask your forbearance. Of the many possible topics, I shall limit myself to commenting briefly on many-body effects, advances in the understanding of transitions among multiple-vacancy configurations, new work on energies, and some developments in technology and instrumentation.

Many-electron interactions.

If one were asked to identify a single feature of this field that is moving into the focus of activity and is likely to characterize much of our research in the near future, then, I believe, he would have to point toward the role of many-electron effects. Not only in connection

with solid-state physics (as exemplified by the following papers in this session), but also in "pure" atomic physics some of the most significant recent work has been done in this direction: as the apex of refinement in relativistic HF independent single-particle calculations has been reached, increasing attention is being given to electron correlations and their effect on photoelectron spectra, partial photoionization cross sections, and multi-electron excitation.

The simultaneous excitation of two atomic electrons, in particular, is a manifestation par excellence of a departure from independent-particle behavior; progress is being made in understanding shakeup and shakeoff in terms of contributions from core rearrangement, ground-state correlations, virtual Auger transitions, and final-state configuration interaction [2].

The converse process--the simultaneous deexcitation of two electrons--has only been discovered within the last year, through Wölfl's identification of two-electron transitions to an empty K shell, accompanied by the emission of a single photon [3], and through the work of Afrosimov et al. on the complementary three-electron Auger transition, in outer shells [4]. There has been intense activity in the search for the production of Wölfl lines in various ion-atom collision systems, and in the measurement and calculation of cross sections for their production.

Perhaps some of the most astonishing manifestations of atomic many-body effects are found in connection with certain short-lived hole states, such as the 4p levels of Xe. Here the independent-particle model predicts super-Coster-Kronig transitions of extraordinary intensity: the hole lifetime is shortened so that ionization and decay processes can no longer be separated clearly, and the transition rate is such that perturbation theory may well be pushed beyond its limits. Indeed, the levels are wide--so wide, that the 4p_{1/2} "line" virtually disappears from the Xe photoelectron spectrum [5]. A combination of energy degeneracy and strong overlap between configurations, and of a wide exit channel, produces a situation in which the independent-particle model indeed appears to break down [2]: virtual super-Coster-Kronig transitions cause the hole to fluctuate with great strength. The level is broadened and redistributed as a result of many-electron interactions, so that the simple picture of a well-defined hole loses much of its meaning [6]. The arduous task is now being undertaken of formulating a description of atoms that sometimes seem to behave more like a breathing plasma than the traditional model, and of reformulating traditional transition theory that cannot be generalized to the many-electron case involving non-orthogonal orbitals [7].

Multiple inner-shell ionization, x-ray yields, and satellites.

Already at the time of the Atlanta Inner-Shell Ionization Conference in 1972, increased interest in the properties of atoms with several deep-lying holes had become apparent [8]. Rapid progress has taken place since then in the understanding of the deexcitation of multiply ionized atoms. Efforts in this area were primarily motivated by work on ion-atom collisions, where inner-shell excitation under quasi-adiabatic molecular conditions can result in gutting of a collision partner. But the significance of the insights gained here reaches much farther. In

the complex cascade of radiative and (mostly) radiationless transitions through which an atom with a single initial inner vacancy rids itself of its excitation energy, only the very first one or two steps constitute single-hole decay and have heretofore been treated theoretically with reasonable accuracy. Recent advances will make it possible to extend calculations to further steps in the cascade. The clue has been the improved understanding of the decay properties of multiplet states, and the development of computational techniques to treat transitions among multiplets [9]. Unfortunately, the overwhelming complexity of these calculations has forced their limitation, so far, to a few cases of particular practical interest.

The drastic differences in decay properties of different multiplet states pertaining to one and the same vacancy configuration have interesting consequences. The fluorescence yield of the products of ion-atom collisions is profoundly affected by the distribution among final states, a fact that entails promising possibilities for diagnosing details of collision mechanisms. Moreover, x-ray yields from ion-atom collisions in gases differ strikingly from those in solids. A noticeable decrease in x-ray yields from solids has been found to arise from collisional quenching--not only the quenching of vacancies through such processes as electron capture and vacancy transfer, but also quenching through redistribution among multiplet states. This phenomenon lends itself to a new approach to the study of the dynamics of ions traversing solid targets [10].

In x-ray spectra, the presence of multiple vacancies manifests itself through satellite lines. Many satellites are as yet not well identified. The improved understanding of the properties of multi-vacancy states and better methods for calculating their energies now promise to resolve many of the difficulties in this area. On the experimental side, the use of coincidence counting techniques, long since employed in the disentanglement of nuclear decay schemes, has been applied successfully to the characterization of definite multiple inner-shell vacancy states and to the study of their decay. This technique has permitted the identification of some $L\alpha$ satellites. The finding that the radiative deexcitation of an L_3 hole in the presence of an N vacancy leads to a satellite that is shifted by less than the natural width of the $L\alpha_1$ line raises the spectre that indeed other diagram lines may be contaminated with satellites of nearly the same energy, distorting if not invalidating intensity determinations [11].

Energies.

Progress in understanding the energetics of both radiative and radiationless transitions holds promise for very interesting application.

Free-atom transition energies have been computed by several groups; semiempirical approaches to the calculation of transition energies have been refined [12] and even superseded by ab initio calculations of the energies of the pertinent hole states [13]. Relativistic effects are being included through the full Breit operator, not as corrections made a posteriori. Vacuum polarization and self energy are taken into account. The importance of these QED corrections for heavy atoms can be considerable: in the case of hahnium (element 105), for example, vacuum

polarization lowers the 1s level by ~ 190 eV (out of 161 keV), and self energy raises it by ~ 570 eV. Delicate tests of the QED calculations become possible, but first, a substantial effort toward extension and completion of these calculations is called for. Thus, the effect of screening on the self energy, for example, has not yet been calculated, and no one has as yet worked out the self-energy shifts of levels above $2p_{1/2}$.

One striking illustration of the importance of accurate high-Z energy calculations arose a few months ago in connection with the discovery of fluorescent x rays attributed to the L series of naturally occurring superheavy elements. A search for the corresponding K peaks, unsuccessful at the time of this writing, was seriously hampered by the lack of a reliable prediction of the expected energy.

Aside from the familiar problems of finding a tractable yet fairly realistic atomic model and taking care of relativity and QED, the big uncertainty in the area of energetics appears to lie with the topic of relaxation. The adjustment of the electron cloud of one isolated atom (or even a molecule) to the removal of an inner electron can be accounted for by performing separate SCF calculations for the initial and final states. Such relaxed-orbital (" Δ SCF") calculations, while time-consuming, do adequately reproduce the redistribution of charge that represents the static monopole screening of the hole, including its self energy.

It is more complicated to evaluate the result of interatomic relaxation, the "solid-state effect." Mostly semi-empirical considerations have been brought to bear on this subject so far, although absolute measurements of changes in reorganization energy between related compounds have been performed and successfully interpreted [14]. It appears that a closer evaluation of the absolute values of interatomic relaxation energies is now becoming possible, due to two factors: (i) the increasing availability of theoretical free-atom transition energies, and (ii) the possibility, with new techniques, of comparing transition energies in solids and vapors [15].

The solid-state effect shows itself in the widths of XPS lines, reflecting the hole-state lifetimes, and in the intensities of x-ray satellites and the related Coster-Kronig electron peaks. The extreme sensitivity of Coster-Kronig and super-Coster-Kronig rates to the transition energy, especially near threshold, appears to have great potential for investigating extraatomic relaxation. One may speculate that the exploration of detailed features of the interatomic relaxation energy, once better understood, could grow to become a very useful technique in materials science.

Technological developments.

Many papers at this conference deal with advances in instrumentation and techniques that are reaching ever increasing sophistication. The development of facilities for obtaining Auger and x-ray spectra from liquids [16] and vapors [15] will be of great help in checking free-atom calculations. Channel-cut crystals [17] and holographic gratings [18] imply a significant advance in diffraction techniques. Elaborate new spectrometers are being constructed in several laboratories [17, 19].

Auger-electron appearance potential spectra have been shown to

exhibit diffraction properties, not unlike those found in EXAFS, that may prove very valuable in surface studies [20].

Last but not least, the vast possibilities of synchrotron radiation are beginning to be exploited, though clearly only the surface is being scratched. Measurements of extended x-ray absorption fine structure are probably the most widely utilized application of synchrotron radiation to date, and EXAFS is now seen not only in absorption, but also in fluorescence and even in photoelectron yield spectra [21], and is observed as a function of polarization [22]. The energy dependence of partial photoionization cross sections is being measured [23], yielding information that is badly needed. The potential of synchrotron radiation, with its intensity, tunability, polarization, and time structure, is likely to lead to many important innovations yet.

All considered, then, we may well be justified in concluding that the field of x-ray physics, after its first eighty years, is as stimulating and challenging as ever, and that we can look forward to continued exciting work in the time ahead.

*Work supported in part by the National Aeronautics and Space Administration, and by the U.S. Army Research Office.

1. E. Merzbacher, in Proceedings of the Second International Conference on Inner-Shell Ionization Phenomena, Freiburg, 1976 (hereinafter referred to as 1976 Freiburg Proceedings), Invited Papers, ed. by R. Brenn and W. Mehlhorn (Fakultät für Physik, Universität Freiburg, 1976).
2. M. O. Krause, in Photoionization and Other Probes of Many-Electron Interactions, ed. by F. Wuilleumier (Plenum, New York, 1976), and this Conference.
3. W. Wölfl et al., Phys. Rev. Lett. 35, 656 (1975).
4. V. Afrosimov et al., JETP Lett. 21, 249 (1975).
5. U. Gelius, J. Electr. Spectr. 5, 985 (1974).
6. G. Wendin and M. Ohno, in 1976 Freiburg Proceedings.
7. G. Howat, T. Aberg, and O. Goscinski, in 1976 Freiburg Proceedings, and this Conference.
8. Proceedings of the International Conference on Inner-Shell Ionization Phenomena and Future Applications, ed. by R. W. Fink et al. (U.S. Atomic Energy Commission Report No. CONF-720404, 1973).
9. E. J. McGuire, Phys. Rev. A 10, 13 (1974) and 11, 1889 (1975); M. H. Chen and B. Crasemann, Phys. Rev. A 10, 2232 (1974) and 12, 959 (1975); C. P. Bhalla, Phys. Rev. A 12, 122 (1975) and this Conference.
10. D. Matthews and R. Fortner, this Conference.
11. J. P. Briand et al., this Conference.
12. F. P. Larkins, J. Phys. B: Atom. Molec. Phys. 9, 37 (1976).
13. Ch. Briançon and J. P. Desclaux, Phys. Rev. A (in press); K.-N. Huang et al., At. Data Nucl. Data Tables (in press).
14. J. J. Pireaux et al., this Conference.
15. I. A. Brytov et al., this Conference.
16. C. Hague et al., this Conference.
17. W. C. Sauder and R. E. LaVilla, this Conference.
18. H. W. Schnopper et al., this Conference.

19. G. Andermann, et al., this Conference. H.-E. Goldstein et al., this Conference.
20. M. I. den Boer et al., this Conference.
21. R. Haensel et al., this Conference.
22. W. M. Weber, this Conference.
23. I. Lindau et al., this Conference.

G. D. Mahan
Physics Department
Indiana University
Bloomington, IN 47401

Current practice ascribes the shape of the x-ray absorption edge in metals to four or five contributions.[1-4] The first of these are the normal one electron processes, which are determined by calculating wave functions in the suitable metallic environment.[5] Second is the Auger decay of the core hole, which gives a lorentzian broadening to the edge shape.[3] Third are the atomic vibrations--phonon contributions. They contribute a Poisson broadening to the distribution, which can usually be approximated by a gaussian.[6] Fourth is the exciton and many-electron effects, which are described by MND theory.[6] Fifth are possible spin flip processes.[7] The early theories considered each of these processes as independent. Thus the final edge shape was constructed by a successive convolution of the shape of each contribution. This also seems to be the current experimental practice. In XPS analysis, lorentzian contributions are labeled "Auger," and gaussian contributions are labeled "phonon." This successive convolution is equivalent to having each term a separate factor in the time response of the system

$$A(\omega) = \int_{-\infty}^{\infty} dt e^{i\omega t} A_0(t) \exp[-\Gamma|t| - \phi_P(t) - \phi_{e1}(t)]$$

where $A_0(t)$ is the fourier transform of the one electron spectra, while other factors are for Auger, phonon, and many electron contributions. This simple separation may not be valid. Recently Sunjic and Lucas[8] noted that the Auger decay may also effectively reduce the phonon matrix elements. It is possible that a similar modification takes place, as we shall discuss, for the electron-electron contribution.

A. One Electron Theory

Although this contribution is the one which everyone thinks they understand, it is by no means easy to calculate. This may be appreciated by reviewing the different theoretical methods of calculating atomic photoionization spectra of, for example, neon.[9] These different methods mostly vary the procedure for including exchange, correlation, and relaxation into the continuum wavefunctions. The same problems are encountered in the solid, with the additional necessity of including band structure. The theoretical formula for the absorption

$$A_0(\omega) = [C_{\ell-1} M_{\ell-1}(\omega)^2 + C_{\ell+1} M_{\ell+1}(\omega)^2] \theta(\omega - \omega_T) \quad (1)$$

$$M_{\ell} = \int \psi^{(f)} \hat{\epsilon} \cdot \vec{p} \psi^{(i)} \quad (2)$$

The initial and final state wave functions which enter the matrix element are really Slater determinants of 10^{23} orbitals of the solid. Generally these are replaced by one electron wave functions for the primary orbital in the transition. Atomic shake-up processes are very small, and the integrals over the other atomic orbitals provide typi-

cally a 5% reduction in the intensity. The conduction electrons provide a shake-up process which is discussed separately in D.

The initial orbital is taken for a ground state potential $V_i(Z,R)$ where Z is the ion charge as viewed from outside of the atom. The final state orbital is evaluated for the potential $V_f(Z+1,R)$. Both potentials should be calculated with the inclusion of the screening charge of conduction electrons. These two potentials, if evaluated self consistently, are quite different, so that the two wave functions are not solutions of the same Hamiltonian. This is quite well known in atomic physics, and accounts for the different results obtained using the length, velocity, or acceleration forms of the transition matrix element.[9] In the solid, band structure effects must also be included, and are regarded as being important in even changing the edge shapes.

B. Auger Decay

In atoms of low atomic number, the core hole mostly decays by an Auger process. In metals, one possible event is where a conduction band electron falls into the core hole, while exciting another conduction electron to a state of high kinetic energy. The rate of this process is calculated by assuming the particles interact via the coulomb potential. It provides a lorentzian broadening to the spectra. The widths Γ are typically 0.1 eV or larger.[1-4]

C. Phonon

Nearly all electronic transitions in solids are accompanied by the emission or absorption of phonons. For coupling to a core hole, the form of $\phi_p(t)$ is well known to be

$$\phi_p(t) = \sum_q M(q)^2 [(N(q) + 1) (1 - e^{-i\omega_q t}) + N(q) (1 - e^{i\omega_q t})]$$

At zero temperature this gives a Poisson distribution. Since it is usually true that $\Gamma \gg \omega_q$, then $\omega_q t \ll 1$ and the small time limit may be used, which is $\phi_p(t) \rightarrow t^2 \sum_q M(q)^2 (N(q) + 1/2)$. Thus this contribution usually provides gaussian broadening. Whether this process is important depends upon the size of the matrix element $M(q)$. There has been much debate over the size of this quantity.

Sunjic and Lucas recently questioned the use of this simple formula. They argue that the energy denominator ω_q^2 should be replaced by $\omega_q^2 + \Gamma^2$. Since $\Gamma \gg \omega_q$, this significantly reduces the effective coupling to phonons. We have derived a formula similar to the one they propose. We find that the reduction in phonon broadenings is only about a factor of two. This is, however, still a significant factor.

D. Exciton and Electron-Electron

The MND theory predicts in simple metals an edge shape of the form [6]

$$A(\omega) = \theta(\omega - \omega_T) \left[C_{\ell-1} M_{\ell-1}(\omega)^2 \left(\frac{\xi_0}{\omega - \omega_T} \right)^{\alpha_{\ell-1}} + C_{\ell+1} M_{\ell+1}(\omega)^2 \left(\frac{\xi_0}{\omega - \omega_T} \right)^{\alpha_{\ell+1}} \right] \quad (3)$$

where $C_\ell M_\ell^2$ are the normal one-electron amplitudes described above, and the exponents $\alpha_\ell = 2\delta_\ell/\pi - \Sigma (2\ell'+1)(\delta_{\ell'}/\pi)^2$ are obtained by calculating $\delta_\ell(k_F)$ for conduction electron scattering from the core hole. This formula applies just at threshold, and there have been several methods suggested to convolute the theory with a full spectrum.[10-11] There have been numerous calculations of the phase shifts, using either a screened point charge, or else a pseudopotential.[10-12] It would seem that Auger decay would affect this potential. One should use, as is commonly done in nuclear physics, a complex potential, wherein the imaginary part relates to the absorptive part of the potential: the electron can get absorbed by the core hole. The two terms in α_ℓ arise from two processes: $2\delta_\ell/\pi$ is from an exciton-type enhancement of the absorption edge, while the other is from shake-up processes involving the conduction band electrons.

Our eqn. 3 for the MND theory is slightly different than the one we have used in the past. The difference is in the ordinary matrix elements. Previously we used matrix elements evaluated with $\psi(f)$ and $\psi(i)$ both calculated from $V(Z,R)$, and the core hole potential $V_c(R) = V(Z+1,R) - V(Z,R)$ is treated as a perturbation which gives rise to the edge anomalies. As first suggested by Friedel,[13] and argued persuasively by Flynn,[14] the form in eqn. 2 is more correct. It can be derived by starting with a Kubo formula in which the current operator is expanded in final state basis set (eigenstates of $V_f(Z+1,R)$) instead of those of the initial state. One can derive the edge singularity in the standard fashion, except that it is obvious that the matrix elements should be those in eqn. 2.

References

1. P. H. Citrin, G. K. Wertheim, Y. Baer, Phys. Rev. Letters 35, 885 (1975).
2. J. J. Ritsko, S. E. Schnatterly, P. C. Gibbons, Phys. Rev. B 10, 5017 (1974).
3. L. Ley, F. R. McFeely, S. P. Kowalczyk, J. G. Jenkin, D. A. Shirley, Phys. Rev. B 11, 600 (1975).
4. H. Neddermeyer, Phys. Rev. B 13, 2411 (1976).
5. R. J. Gupta and A. J. Freeman, Phys. Rev. Letters 36, 1194 (1976).
6. G. D. Mahan, Solid State Physics, Vol 29 (Academic Press, 1974) pg. 75.
7. Y. Onodera, J. Phys. Soc. Japan 39, 1482 (1975).
8. M. Sunjic and A. A. Lucas, preprint.
9. J. W. Cooper, Phys. Rev. 128, 681 (1962).
10. P. Longe, Phys. Rev. B 8, 2572 (1973).
11. G. D. Mahan, Phys. Rev. B 11, 4814 (1975).
12. P. Minnhagen, Phys. Letters 56A, 327 (1976).
13. J. Friedel, Comments Solid State Physics 2, 21 (1969).
14. C. P. Flynn, private communication.

PREDICTION OF MANY-BODY LINESHAPES USING SUM RULES*

John D. Dow

Department of Physics and Materials Research Laboratory
University of Illinois at Urbana-Champaign
Urbana, Illinois, U.S.A. 61801

Sum rules, conservation laws, and other general theoretical relations can be used (i) to predict many-body lineshapes with higher confidence and accuracy than straightforward computations, and (ii) to test existing theories of x-ray edges. Here we consider three general theories: (A) The MND theory, which is the version of the Nozieres-de Dominicis (ND) theory [1], widely accepted three years ago, and discussed in Mahan's review article [2] (this theory includes the prediction that $L_{2,3}$ edges should be peaked, $\alpha_0 \gtrsim 0.4$, whereas K edges should be rounded, $\alpha_1 \ll 0$); (B) The ND theory, with any reasonable exponents α_ℓ ; and (C) Extensions of the ND theory.

(A) MND THEORY AND THE PARITY SELECTION RULE

Three years ago the first x-ray edge controversy arose when Robinson, Carver, Franceschetti and I proposed that the K edge of Li was rounded primarily because of phonon and Auger broadening, not by the MND effect [3,4]. Our phonon model was an extension of work by Overhauser and McAlister [5] to approximately include phonon effects on both ground and excited states; it obtained an order of magnitude estimate of the K-edge breadth from Knight shift and radioactive decay constant data.

The MND theory attributes lithium's rounded K absorption edge to a parity selection rule ($A_0 = 0$) [6] and a negative exponent ($\alpha_1 < 0$): $\epsilon_2(\omega) \propto [A_0^2(\hbar\omega - E_T)^{-\alpha_0} + A_1^2(\hbar\omega - E_T)^{-\alpha_1} + \dots] \theta(\hbar\omega - E_T)$. Here E_T is the threshold energy, θ is a step function Fermi factor, and the exponents α_0 and α_1 are positive and negative, respectively. The A_ℓ are proportional to one-electron dipole matrix elements between the core (1s for Li) and conduction band states of angular momentum $\ell\hbar$; therefore A_0 vanishes by virtue of the inversion symmetry of the core hole's environment, making α_1 (which is negative) the dominant exponent, and producing a rounded edge.

Sonntag destroyed inversion symmetry in Li by adding Cu impurities, thereby making A_0 non zero; he did not observe the strongly peaked edge ($\alpha_0 \gtrsim 0.4$) expected for an MND threshold [7]. Subsequently Kunz, Petersen, and Lynch showed that lithium's K edge breadth is temperature dependent, at least for temperatures near the melting temperature [8]. Several other experiments [9] have lent further support to the broadening model as the dominant mechanism of K-edge rounding.

(B) ND THEORY: CHARGE CONSERVATION

With experiments casting doubt on the MND interpretation of the K edge of lithium, attention shifted to the $L_{2,3}$ edges of Na, Mg, and Al, and a second controversy arose over the interpretation of these edges: "Does the ND theory, with any reasonable exponents α_ℓ , account quanti-

tatively for the observed x-ray edge anomalies?" (In particular, values $\alpha_0 \lesssim 0.2$, $\alpha_1 \gtrsim 0$ are required by the data.)

The first experiment designed to test the ND theory was by Slowik and Brown on $\text{Mg}_{1-x}\text{Sb}_x$ alloys [10]. This test, and most subsequent ones, concentrated on the exponents

$$\alpha_\ell \equiv 2 \frac{\delta_\ell}{\pi} - \Delta$$

$$\Delta \equiv \sum_{j=0}^{\infty} 2(2j+1)(\delta_j/\pi)^2$$

[Other authors refer to Δ as α or $-\alpha_\infty$.] Here δ_ℓ are the phase shifts of a Fermi energy electron in the presence of a hole, and must satisfy several constraints. Chief among these is the constraint of charge conservation, which is embodied in Friedel's sum rule for a fully screened hole:

$$1 = \sum_{j=0}^{\infty} 2(2j+1)(\delta_j/\pi).$$

Moreover, reasonable phase shifts for alkali (noble) metals assign most of the screening to s- and p-electrons;

$$\sum_{j=2}^{\infty} 2(2j+1)(\delta_j/\pi) < z_0,$$

where $z_0 < 0.3$ (0.5) for alkalis (noble metals). Finally, to a very good approximation, the phase shifts δ_j should be the same for $L_{2,3}$ thresholds (α_0), K thresholds (α_1), x-ray photoemission (XPS) asymmetries (Δ), and impurity resistivity data. These constraints provide many useful relations among experimental data, which should be satisfied if the ND interpretation is valid. The data violate these restrictions [11]. Given one datum (e.g., α_0) and various constraints, it is possible to predict other data (e.g., Δ , α_1) with higher precision than they can presently be measured or calculated a priori; however the predicted exponents generally disagree with the measured values, indicating that interpretation of the data in terms of a pure ND effect is not generally tenable.

Nevertheless the $L_{2,3}$ edge controversy lingers on. One reason for this is that the ND lineshape formula has several parameters, is very flexible, and can be well-fitted to data unrelated to the ND effect. Another reason is that recently virtually every conceivable exponent α_0 has been computed by one theorist or another; and different experiments have likewise produced virtually every possible value of α_0 . Hence every experiment agrees with at least one theory and every theory describes at least one experiment -- even though the experimental results are not mutually compatible. This is an important point which should be kept in mind when analyzing data.

Other important tests of the theory are experiments which produce inconceivable exponents: XPS lines which are unacceptably symmetric ($\Delta \lesssim 0.03$) [11], and allowed absorption thresholds which are nearly linear ($\alpha_0 = -0.9 \pm 0.1$) [12].

(C) OTHER THEORIES

Sum rules and general constraints not only are capable of predicting ND lineshapes with high precision, they are also useful for indicating the form an improved theory must take; that is the principal purpose of this work. The relative importances of band-structure effects, exchange, and electronic recoil will be discussed, with attention paid to the general theoretical requirements. Particularly useful in this regard are the experiments of Flynn and coworkers [12], which suggest that general features of initial and final state charge distributions, not just the Fermi energy phase shifts δ_j , strongly influence the edge shapes.

* Research supported by the National Science Foundation under grants DMR-73-07661 and DMR-72-03026.

- [1] P. Nozieres and C. T. de Dominicis, Phys. Rev. 178, 1097 (1969).
- [2] G. D. Mahan, Solid State Phys. 29, 75 (1974).
- [3] J. D. Dow, J. E. Robinson and T. R. Carver, Phys. Rev. Lett. 31, 759 (1973).
- [4] D. R. Franceschetti and J. D. Dow, J. Phys. F. 4, L151 (1974).
- [5] A. J. McAlister, Phys. Rev. 186, 595 (1969).
- [6] J. D. Dow and D. L. Smith, J. Phys. F 3, L170 (1973).
- [7] B. F. Sonntag, J. Phys. F 3, L255 (1974).
- [8] C. Kunz, H. Petersen, and D. W. Lynch, Phys. Rev. Lett. 33, 26 (1974).
- [9] J. J. Ritsko, S. E. Schnatterly, and P. C. Gibbons, Phys. Rev. B10, 5017 (1974); P. Citrin, G. K. Wertheim et.al., Bull. Amer. Phys. Soc. [II] 21, 425 (1976); H. Neddermeyer, Phys. Rev. B13, 2411 (1976).
- [10] J. H. Slowik and F. C. Brown, Phys. Rev. B10, 416 (1974).
- [11] J. D. Dow (to be published).
- [12] C. P. Flynn (these proceedings, and to be published); see also R. A. Tilton, D. J. Phelps, and C. P. Flynn, Phys. Rev. Lett. 32, 1006 (1974).

EXCHANGE EFFECTS IN THE Li K EDGE

S.M. Girvin and J.J. Hopfield

Department of Physics
Princeton University
Princeton, New Jersey
08540

The Mahan, Nozières, and De Dominicis [1,2] (MND) theory of x-ray edges in metals predicts a power law absorption shape whose exponent is determined by the phase shifts for the core hole potential. One feature of this potential which has been previously neglected is the exchange interaction. This is of particular importance in lithium where exchange produces a 0.5 ev splitting in the free ion.

The edge exponent is given by the modified formula [3]:

$$\alpha_{\ell', \sigma'} = 2\delta_{\ell'\sigma'}/\pi - \Delta \quad (1) \quad \Delta = \sum_{\ell=0}^{\infty} \sum_{\sigma=\pm 1} (2\ell+1) (\delta_{\ell\sigma}/\pi)^2, \quad (2)$$

where ℓ' and σ' are the orbital and spin quantum numbers in the channel into which the core electron is injected. Since spin is unaffected by the optical transition, σ' refers to the singlet orientation relative to the core.

In the Born approximation, the diagonal part of exchange leads to a symmetric modification of the phase shifts by some amount μ_{ℓ} :

$$\delta_{\ell\pm} = \delta_{\ell}^0 \pm \mu_{\ell} \quad (3)$$

where δ_{ℓ}^0 is the phase shift without exchange and (\pm) refers to the spin orientation. Equations (1) and (2) become

$$\alpha_{\ell} = (2\delta_{\ell}^0/\pi - \Delta^0) + (2\mu_{\ell}/\pi - \mu) \quad (4)$$

$$\Delta^0 = 2 \sum_{\ell=0}^{\infty} (2\ell+1) (\delta_{\ell}^0/\pi)^2 \quad (5) \quad \mu = 2\lambda \sum_{\ell=0}^{\infty} (2\ell+1) (\mu_{\ell}/\pi)^2 \quad (6)$$

where $\lambda = 1$. The effect of the off-diagonal part of exchange (spin flip scattering) may be included to lowest order by invoking rotational invariance which gives $\lambda = 3$. Note that μ_{ℓ} must be negative since the phase shift for the singlet orientation is reduced by exchange. Exchange decreases threshold exponents because the excitonic enhancement factor, $2\delta_{\ell\sigma}/\pi$ is reduced and because the orthogonality index, Δ is increased.

The phase shifts obtained for lithium from a self-consistent model potential calculation are displayed in Table I along with results for sodium for comparison purposes. The lithium phase shifts differ substantially from those for a simple screened point charge [4], emphasizing the importance of details of the core. The absence of orthogonality effects accounts for the anomalously large p phase shift in

lithium which is unique among the alkali metals for its lack of p core levels. The sodium results more closely resemble the point charge values.

The phase shift correction, μ_l may be calculated by treating exchange as a local perturbation and adjusting the coupling constants to fit the atomic level splittings. The coupling constants in the metal are scaled by the metal to ion ratio of electron density inside the core radius. In addition, the electron-electron exchange interaction in the bulk contributes a factor of the ratio of the measured electronic susceptibility to the ordinary Pauli susceptibility.

Calculation of the exchange corrections from the numerical lithium wave functions yields $\mu_0 = .24$, $\mu_1 = .07$, and $\mu_2 \approx 0$. The threshold exponents corrected for exchange are displayed in Table II. Note that Δ is increased by some 50% and that the edge exponents are substantially reduced. The predicted value of Δ is smaller than that obtained by XPS [5,6] measurements by about 0.08 for both sodium and lithium. Exchange does increase the orthogonality index but is insufficient to prevent this important discrepancy.

The best absorption edge test of the lithium results is a measurement of the difference between α_0 and α_1 . The point charge model predicts $\alpha_0 - \alpha_1 = +.58$, while the present calculation yields $\alpha_0 - \alpha_1 = -.21$. Inelastic electron scattering measurements [7] find that α_0 and α_1 are both close to zero with their difference probably not exceeding 0.1 in magnitude. Calculations on lithium by Freeman and Gupta [8] show that band structure effects increase the value of α_0 and reduce the value of α_1 which would be deduced from experiment. These effects appear to bring the present calculation into good agreement with the data. However, quantitative results for the band structure corrections to the exponents are not available at present.

Exchange plays a fundamental role in the lithium K edge by reducing all the threshold exponents while at the same time increasing the orthogonality index--a possibility not otherwise allowed by the Friedel sum rule. This mechanism partially resolves the troubling paradox that the MND many-body effects appear only weakly in x-ray edge data but are strikingly large in x-ray photoemission.

- [1] G.D. Mahan, Phys. Rev. 163, 612 (1967).
- [2] P. Nozières and C.T. DeDominicis, Phys. Rev. 178, 1097 (1969).
- [3] S.M. Girvin and J.J. Hopfield, to be published.
- [4] George A. Ausman, Jr. and Arnold J. Glick, Phys. Rev. 183 (1969).
- [5] P.H. Citrin, G.K. Wertheim, and Y. Baer, Phys. Rev. Letters 35, 885 (1975)
- [6] Y. Baer, P.H. Citrin, and G.K. Wertheim, submitted for publication in Phys. Rev. Letters.
- [7] J.J. Ritsko, S.E. Schnatterly, and P.C. Gibbons, Phys. Rev. B10, 5017 (1974).
- [8] Raju P. Gupta and A.J. Freeman, Bull. Am. Phys. Soc. 21, 310 (1976).

Table I. Phase shifts δ_ℓ^I , δ_ℓ^{II} with and without the core hole, the change in the phase shifts $\Delta\delta_\ell$, and the exponents α_ℓ for lithium and sodium without exchange corrections.

ℓ	δ_ℓ^I	δ_ℓ^{II}	$\Delta\delta_\ell$	α_ℓ	
0	-.375	-.115	+.260	+.059	Li $\Delta = .106$
1	+.126	+.516	+.390	+.141	
2	-.001	+.026	+.027	-.089	
0	-.011	+.607	+.618	+.276	Na $\Delta = .117$
1	-.001	+.249	+.250	+.042	
2	+.003	+.043	+.040	-.091	

Table II. Phase shifts δ_ℓ^I , δ_ℓ^{II} with and without the core hole, the change in the phase shifts $\Delta\delta_\ell$, and the exponents α_ℓ for lithium with exchange corrections

ℓ	δ_ℓ^I	δ_ℓ^{II}	$\Delta\delta_\ell$	α_ℓ	
0	-.375	-.357	+.018	-.164	Li $\Delta = .159$
1	+.126	+.451	+.325	+.044	
2	-.001	+.026	+.027	-.142	

RAJU P. GUPTA, Physics Department and Materials Research Center, Northwestern University, Evanston, Illinois 60201, and
A.J. FREEMAN, Physics Department, Northwestern University, Evanston, Illinois 60201, and Argonne National Laboratory, Argonne, Illinois 60439

The shapes of the observed threshold edges in simple metals are either sharp and peaked (e.g. $L_{2,3}$ edges of Mg and Al) or broad and rounded (e.g. K edges of Li, Be, Mg, and Al) over energies ≈ 1 eV. Since these features cannot be explained using one-electron theory based on the free-electron model, efforts have been made by Mahan, Nozières and de Dominicis (MND) [1] to explain them as many body effects in which conduction electron-core hole final state interaction effects play a dominant role.

We have attempted to assess the importance of the generally ignored one-electron effects on both emission and absorption spectra of Mg, Na, and Li using the energy eigenvalues and wave functions obtained from augmented plane wave (APW) calculations. We have found that there are important and significant departures from the behavior expected of free-electron metals, especially near the threshold and above it. To assure numerical accuracy of both the density of states (DOS) $N(E)$ and the x-ray intensity $I(E)$ (the energy E is measured from the bottom of the valence band), the ab initio Bloch eigenvalues and wavefunctions were calculated on a dense mesh (495 inequivalent points in the irreducible $1/24$ th zone for Mg, and 285 inequivalent points in the irreducible $1/48$ th zone each for Na and Li).

The x-ray emission or absorption intensity $I(E)$ in the one electron approximation is given by Fermi's Golden Rule

$$I(E) \propto \sum_n \int d^3k |\langle \psi_c | \nabla | \psi_{n\vec{k}} \rangle|^2 \delta(E - E_{n\vec{k}} + E_c), \quad (1)$$

with transition matrix elements between core (ψ_c) and Bloch states ($\psi_{n,\vec{k}}$). Note from Eq.(1) that in the constant transition matrix elements approximation, the intensity depends on the projected or partial DOS (associated with different angular momentum quantum numbers) because of the dipole selection rule and not on the total DOS. Fig. 1 presents our DOS results for Mg. We first note that the DOS is remarkably parabolic over the bottom three-fourths of the occupied part of the band but at higher energies (which is also the region of interest for the edge problem) some large peaks appear, including an important peak at the Fermi energy itself. Since we are concerned with transitions involving a 2p core state for the $L_{2,3}$ spectrum we also show in Fig. 1 the projected DOS of s, p and d character (only s and d will contribute to the $L_{2,3}$ spectrum because of dipole selection rules and only p to the K spectrum). Fig. 2 shows the results for the $L_{2,3}$ emission/absorption spectra obtained entirely on the basis of the band model including the transition matrix elements calculated from APW Bloch functions. The results of Fig. 2 show that essentially all features of the partial DOS (not the total DOS) are also present in the calculated x-ray spectrum. As discussed in ref [2], the $L_{2,3}$ emission results are in very good agreement with experiment, band structure effects are significant in Mg at the x-ray edge and the $L_{2,3}$ edge of Mg is a poor testing ground for many body threshold effects.

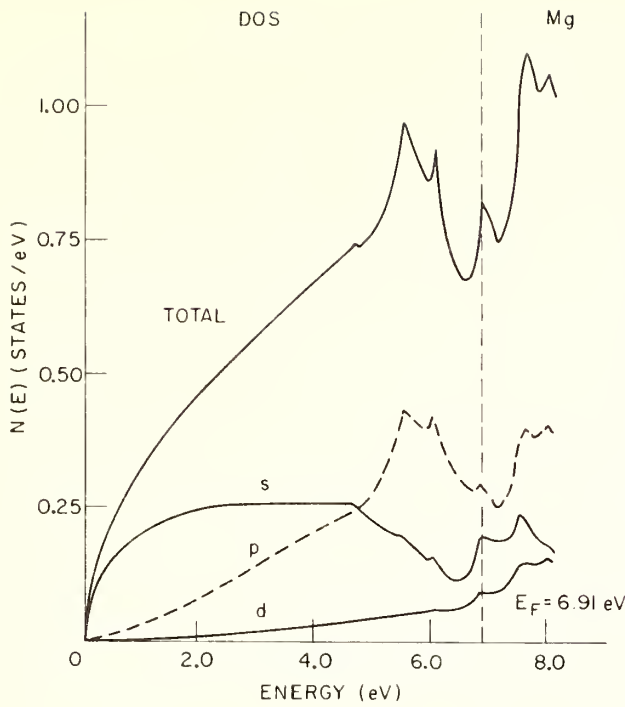


Fig. 1

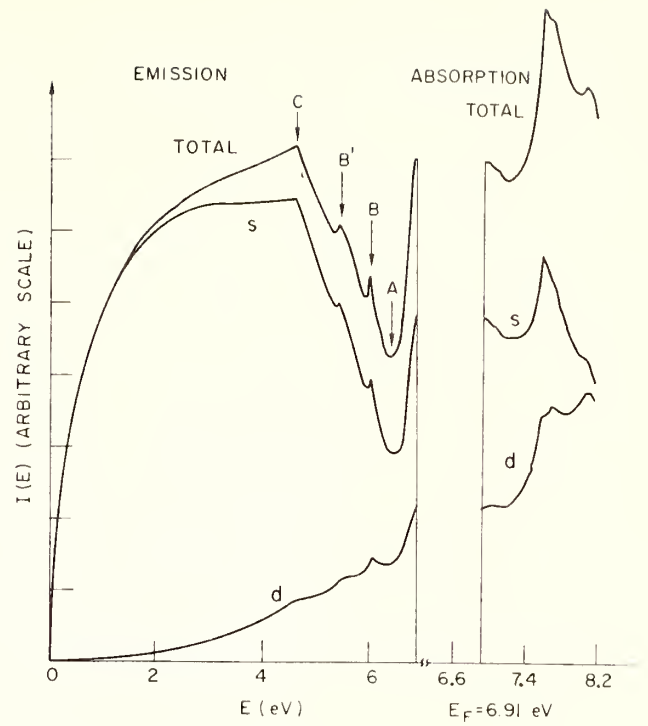


Fig. 2

Fig. 3 shows the calculated $L_{2,3}$ x-ray spectrum for Na; for comparison we give the free electron total and partial DOS in Fig. 4. We see that features in the APW x-ray spectrum (especially in absorption) are totally absent in the free-electron case. The positions of the calculated absorption peaks are in agreement with the experimental data of Crisp and Williams [3]. Note that if one includes the TME in the free-electron case using a single plane wave ($\psi_k \approx \exp(ik \cdot r)$) then even the intensity ratio s/d will be wrong ($=0.5$ at all energies).

We have also calculated the K spectrum of Li and the results are shown in Fig. 5. There is no peak below threshold in the calculated emission spectrum, indicating that an observed rounded peak would have to be associated either with a) broadening and emission-absorption overlap or b) with an electron-hole scattering resonance (in which

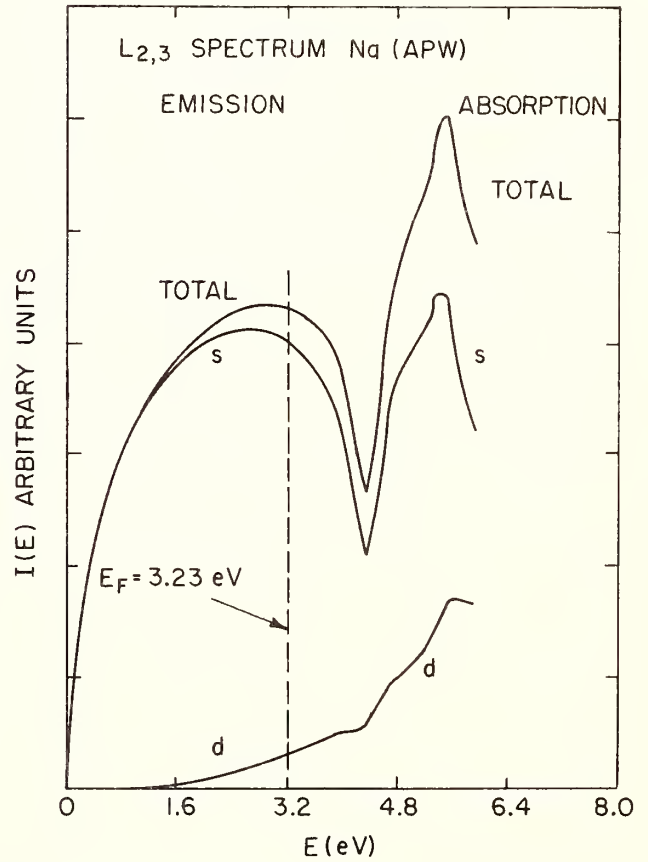


Fig. 3

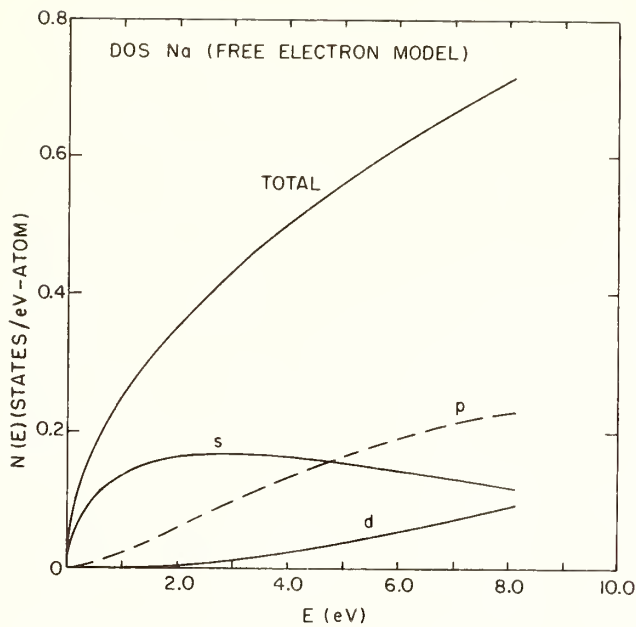


Fig. 4

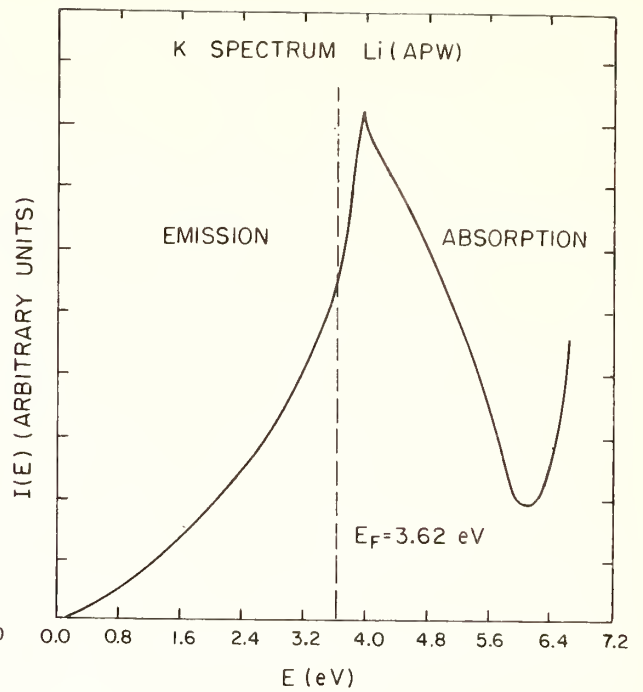


Fig. 5

case the emission-absorption overlap should be small). There is a peak in the calculated absorption spectrum about $\frac{1}{2}$ eV above threshold, in agreement with most data. The calculations suggest that absorption and emission edges near threshold should not be mirror images of each other.

In conclusion, our calculations do not necessarily show that Nozières - de Dominicis type many body threshold divergences are absent, but they may effectively remove the necessity of invoking such effects to explain the observations. Hence the $L_{2,3}$ edge of Na, like the $L_{2,3}$ edge of Mg and the K edge of Li, is a poor testing ground for the many body theory. Therefore, experimental attention should focus on the $M_{2,3}$ edge of potassium and the possibility of many-body effects there.

* Supported by the NSF, AFOSR and ERDA.

1. G. D. Mahan, Phys. Rev. 153, 882 (1967); P. Nozières and C. T. de Dominicis, Phys. Rev. 178, 1097 (1969).
2. R. P. Gupta and A. J. Freeman, Phys. Rev. Letters 36, 1194 (1976).
3. R. S. Crisp and S. E. Williams, Phil. Mag. [8] 6, 365 (1965).

PHOTOABSORPTION AND PHOTOYIELD MEASUREMENTS OF THE Li K-EDGE

C. Kunz, H. Petersen and B. Sonntag⁺

Deutsches Elektronen-Synchrotron DESY, Hamburg, Germany

⁺Universität Hamburg, Hamburg, Germany

The rounded threshold of the Li K-edge, which has been a puzzle since its first observation, for a long time was considered as one of the clear cut examples for the break-down of the one-electron approximation. From the different explanations proposed, the many electron theory of the threshold anomaly put forward by Mahan (1), Nozieres and de Dominicis (2) was the most attractive one because of its capability to account for both, the rounding of the Li K-edge and the spike at the Na L_{II,III} edge. Quantitative tests of the theory based on detailed analyses of the existing absorption and emission data (3) and new experimental results on the q-dependence of the edge shape (4) indicate that the influence of the Mahan-Nozieres-de Dominicis (MND) many body effect on the x-ray edges is much weaker than thought previously. To assess the importance of the MND effect it has to be disentangled from one-electron bandstructure effects and broadening effects, a task which has not been fulfilled in an unambiguous way.

For Li, recent measurements of the partial photoyield of massive specimens kept at 77 K showed that the Li K-edge breaks up into two parts (5). The photoyield spectrum given in Fig. 1 shows a well detectable

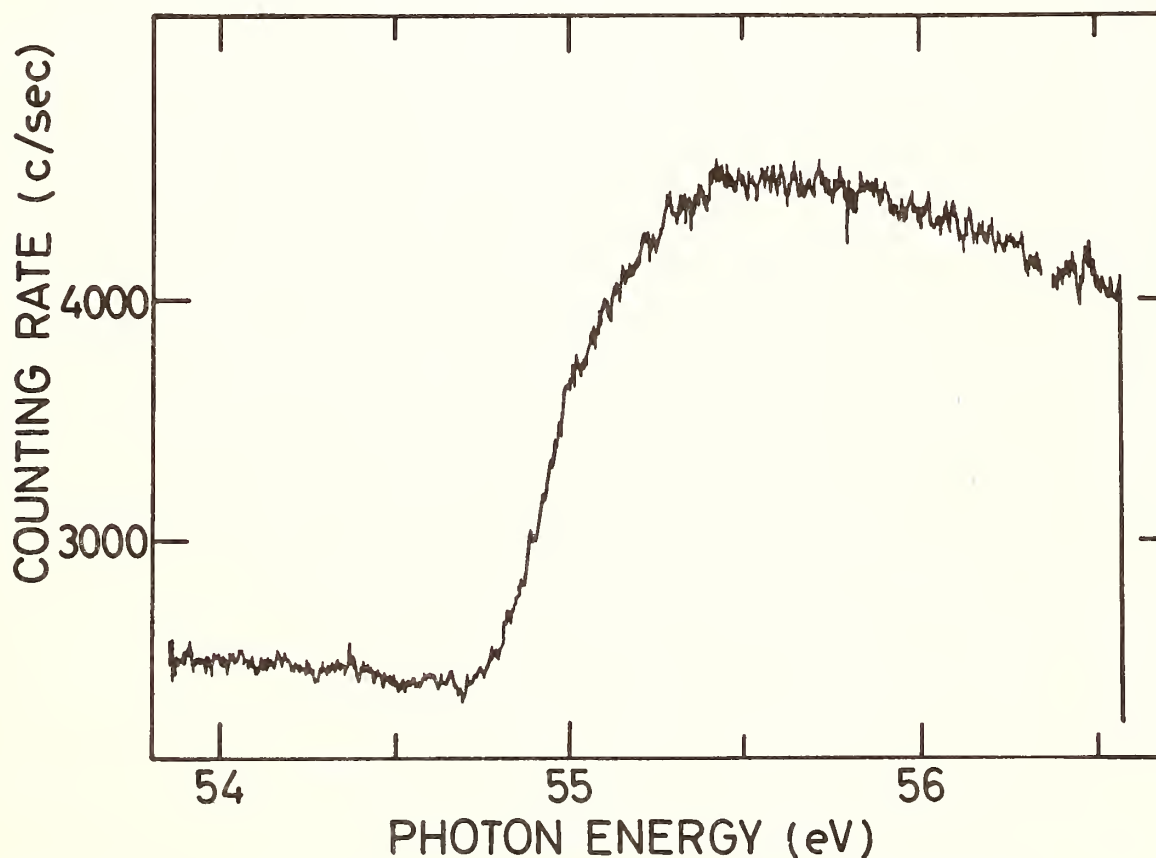


Fig. 1 Li K-absorption edge at LNT measured with photoyield spectroscopy

kink between the steep rise at the onset and the significantly slower increase at higher energies. The correspondence of photoyield and absorption spectra is demonstrated for a considerable number of substances (6) and therefore it is very improbable that the kink is an artifact of the photoyield technique. Contamination of the samples and lack of long range crystalline order are some of the explanations brought forth to account for the fact, that so far the kink has not been detected in thin film absorption measurements. In order to dispel any doubt the results, however, should be confirmed by high-resolution ultra-high vacuum absorption measurements.

Fig. 2 shows the photoyield together with the model potential density of states calculated by Shaw and Smith (7) (comprising all symmetries) and the transition density to p-symmetric final states given by McAlister (8). The Li K-edge extends from the onset of the absorption to the kink. The increase towards higher energies peaking at 55.3 eV is well described by the density of states. Taking into account the width of the core hole, the Fermi function broadening and the phonon broadening the Li K-edge can be reconciled with the predictions of the one-electron band theory without invoking a prominent MND effect.

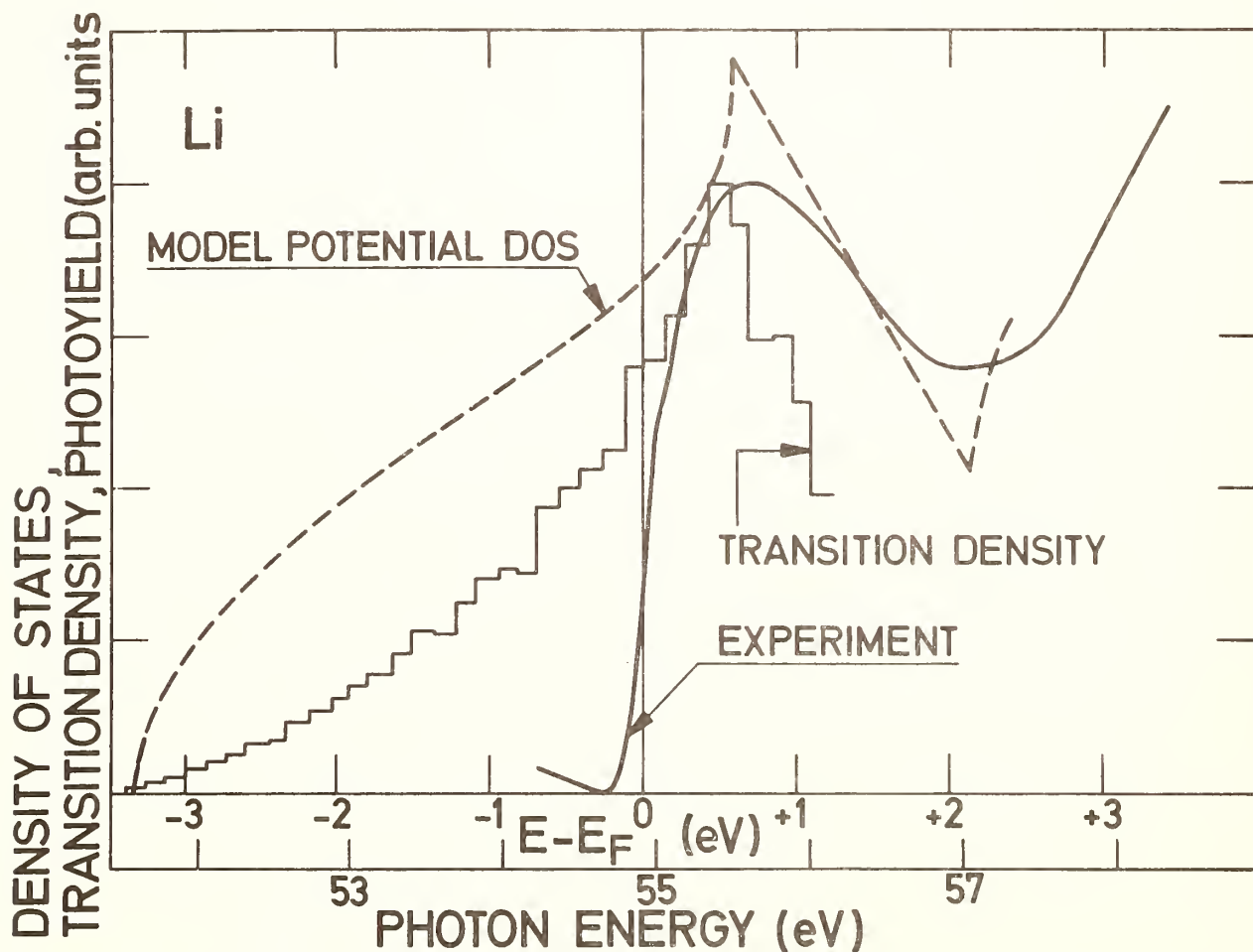


Fig. 2 Li K-absorption edge at 77 K, model potential density of states (Ref. 7), and transition density to p-symmetric final states (Ref. 8)

The importance of the phonon broadening in shaping the edge clearly manifests itself in the strong temperature dependence of the edge shown in Fig. 3. Increasing the temperature from 77 K to temperatures above the melting point the edge broadens considerably and at the same time the maximum above the edge shifts towards higher energies. A pronounced kink is only detectable at 77 K and therefore an exact determination of the temperature dependence of the edge width is very difficult. The 10 % to 90 % widths of the edge listed in Table 1 have been estimated by positioning the 10 % and 90 % values as indicated in Fig. 3. In order not to add to the already existing confusion, which to our opinion is partially due to an overinterpretation of the data we refrain from presenting numbers for the different broadening mechanisms contributing to the width of the edge. The resolution function of the monochromator (~ 0.11 eV full width at half maximum at 55 eV) is also contained in the widths given below. The theoretical 10 % to 90 % widths calculated by Hedin (10) for $\Gamma_{\text{Auger}} = 20$ meV are included for comparisons.

Table 1 Temperature dependence of the Li 1s edge width (10 % - 90 %)

Temperature (K)	79	300	370	440	480
Edge-width (10%-90%) (meV)	230	330	400	460	510
(after Hedin (10)) (meV)	180	250	280	310	330

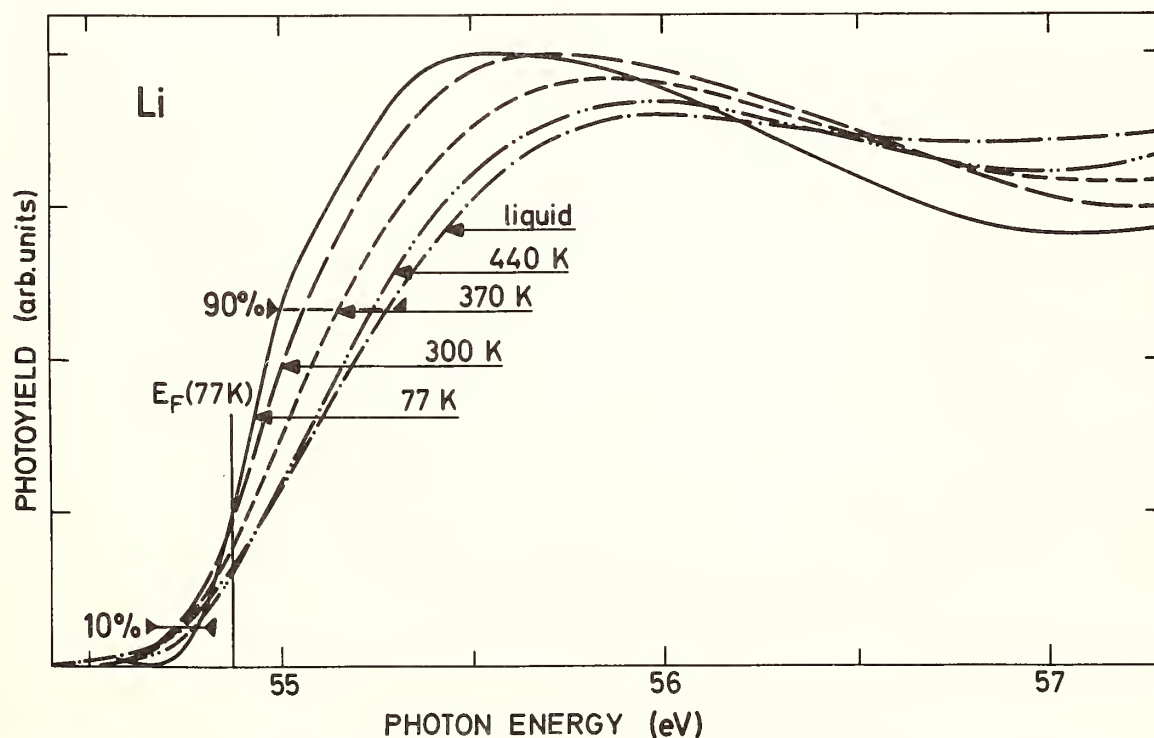


Fig. 3 Photoyield spectra (normalized with respect to each other) of the Li K-edge for different temperatures (Ref. 9)

1. G.D. Mahan, Phys.Rev. 153, 882 (1967) and 163, 612 (1967)
and Solid State Physics 29, 75 (1974)
2. P. Nozieres and C.T. de Dominicis, Phys.Rev. 176, 1097 (1969)
3. see e.g. J.D. Dow, J.E. Robinson, J.H. Slowik and B.F. Sonntag,
Phys.Rev. B10, 432 (1974)
J.D. Dow, D.L. Smith and B.F. Sonntag, Phys.Rev. B10, 3092 (1974)
4. J.J. Ritsko, S.E. Schnatterly and P.C. Gibbons, Phys.Rev. B10, 5017
(1974)
S.G. Slusky, P.C. Gibbons, S.E. Schnatterly and J.R. Fields, Phys.
Rev.Lett. 36, 326 (1976)
5. H. Petersen, Phys.Rev.Lett. 35, 1363 (1975)
6. see e.g. W. Gudat, C. Kunz and H. Petersen, Phys.Rev.Lett. 32,
1370 (1974)
7. R.W. Shaw and N.V. Smith, Phys.Rev. 178, 985 (1969)
8. A.J. McAlister, Phys.Rev. 186, 595 (1969)
9. H. Petersen, thesis Universität Hamburg (1976)
10. L. Hedin, private communication

INELASTIC ELECTRON SCATTERING DETERMINATION OF EDGE SHAPES IN SIMPLE METALS

P. C. Gibbons*, S. G. Slusky, S. E. Schnatterly

Joseph Henry Laboratories
Princeton University
Princeton, New Jersey 08540

The Princeton Inelastic Electron Scattering Spectrometer was designed to study electronic excitations in solids.[1] Electrons from an oxide-coated cathode pass through a series of electrostatic lenses and deflectors which define the energy and momentum of the beam. The beam is accelerated to 300 keV, passed through a thin solid sample, and decelerated. A second set of lenses and deflectors then selects electrons of one specific energy and momentum and transmits them to an electron multiplier. By lowering the potential of the emitting system with respect to the detecting system, we increase the energy loss of the electrons which reach the electron multiplier. Transverse momentum transfer is determined by deflecting the beam before and after it is scattered, so that the only electrons which reach the electron multiplier are those which receive a compensating deflection in the sample.

Both energy and momentum resolutions are variable by adjusting the electrostatic lenses. The experiments described below were performed with energy FWHM of 70 to 90 meV and momentum FWHM of $\sim 0.3 \text{ \AA}^{-1}$, with the exception of the lithium experiment. That data was acquired with momentum FWHM of $\sim 0.1 \text{ \AA}^{-1}$.

Using the Born approximation one derives [2]:

$$\frac{d^3\Sigma}{dEd\Omega} \propto \frac{1}{q} \text{Im} \frac{-1}{\epsilon(q, \omega)} \quad (1)$$

and

$$\text{Im} \left(-\frac{1}{\epsilon} \right) \propto \frac{1}{2} \left| \langle \psi_f | e^{iq \cdot r} | \psi_i \rangle \right|^2 \delta(E_f - E_i - \hbar\omega) \quad (2)$$

where $\frac{d^3\Sigma}{dEd\Omega}$ is the macroscopic differential cross section for electron scattering, $\hbar q$ is the total momentum transfer, $\hbar\omega$ is the energy loss and ϵ is the dielectric constant. ψ_f and ψ_i are the initial and final states of the system.

The major advantage of electron scattering over optical absorption or emission for the study of x-ray edges is the ability to vary momentum transfer independently of energy loss. We can then

*Present address: Department of Physics, Washington University,
St. Louis, MO. 63130

compare the energy loss spectrum at large momentum transfer to that at small momentum transfer.

For core excitations, it is useful to expand the operator:

$$e^{iq \cdot r} = 1 + iq \cdot r - \frac{1}{2} (q \cdot r)^2 + \dots \quad (3)$$

The first term does not contribute to the matrix element since ψ_f and ψ_i are orthogonal. When q is very small compared to the inverse of the relevant core radius, the second term dominates the series. Thus, for small q our count rates show a general $1/q^2$ dependence, and dipole transitions are being observed. As q is increased, the third term in the series becomes important and monopole and quadrupole transitions are observed.

Applied to x-ray edges, this means that different partial waves in the conduction band become available as the final state. For example, transitions from an s core state can only go to conduction band p-waves when q is small, but can also go to s-waves when q is large.

The Mahan-Nozieres-De Dominicis (MND) theory of x-ray edges [3,4] predicts that transitions to different partial waves will have different threshold shapes. High angular momentum partial wave final states are expected to contribute more rounded threshold shapes than low ones. Thus electron scattering is well suited to the investigation of this problem and provides information not obtainable by optical measurements.

In our analysis of our electron scattering data we include the effects of spectrometer resolution, lifetime and phonon broadening, Fermi surface thermal width, spin-orbit and exchange [5] interactions in the excited state and one-electron transition density in a simple approximation. Multiple scattering and background from low energy excitations are removed from the data before analysis.

To date the threshold shapes of the K edge in Li [6] and the $L_{II,III}$ edge in Mg [7] have been studied in detail and the $L_{II,III}$ edge of Na has been subjected to some investigation. The Li, Mg, and Na samples studied were polycrystalline films evaporated within the vacuum chamber of the spectrometer onto thin carbon substrates.

The lithium edge remained the same at momentum transfer up to 1.2 \AA^{-1} , implying either that the MND theory doesn't apply at all to the Li K edge or that the threshold shapes characteristic of s and p wave final states are the same. The data showed that the edge shape was consistent with a simple step function convoluted with a Gaussian.

The magnesium $L_{II,III}$ threshold is peaked at low momentum transfers. When momentum transfer is increased, the edge becomes

rounded as expected but by more than MND theory would predict. The general conclusion is that in Mg, some effect other than the MND theory influences the edge shape in a significant way.

In preliminary results, the sodium $L_{II,III}$ threshold appears peaked at low momentum transfers and rounded at high momentum transfers.

Most recently we have studied the potassium $L_{II,III}$ and $M_{II,III}$ edges using a potassium film on a carbon substrate. Our efforts at improving sample preparation techniques were rewarded by a potassium sample which provided high count rates in the edge and very low carbon background rates. This eliminates the need for elaborate background subtraction schemes. The data thus obtained is, at this writing, in analysis. The spin-orbit splitting of the edge is large enough that we should be able to ascertain whether the two portions have different shapes. In addition, we have obtained spectra of the $M_{II,III}$ edge at a range of momentum transfers rather than only a high and low value.

We have observed that the $M_{II,III}$ threshold shape changes with momentum transfer. It becomes less peaked as momentum transfer increases. We shall discuss these data in relation to the various mechanisms proposed to explain x-ray threshold shapes.

References

1. P. C. Gibbons, J. J. Ritsko, and S. E. Schnatterly, Rev. Sci. Instr. 45, 1546 (1975).
2. J. R. Fields, Thesis (unpublished), Princeton University (1975).
3. G. D. Mahan, Phys. Rev. 163, 612 (1967).
4. P. Nozieres and C. T. De Dominicis, Phys. Rev. 178, 1097 (1969).
5. Y. Onodera, J. Phys. Soc. Japan 39, 1482 (1975) and Y. Onodera and Y. Toyozawa, J. Phys. Soc. Japan 22, 833 (1967).
6. J. J. Ritsko, S. E. Schnatterly, and P. C. Gibbons, Phys. Rev. B10, 5017 (1974).
7. S. G. Slusky, P. C. Gibbons, S. E. Schnatterly, and J. R. Fields, Phys. Rev. Lett., 36 326 (1976).

C. P. FLYNN, Physics Department and Materials Research Laboratory,
U. of Illinois, Urbana, Ill. 61801

It would stretch the truth too far to call 10 eV photons x-rays. At first sight our work with $5 \leq \hbar\omega \leq 12$ eV therefore appears misplaced among contributions dealing with keV x-rays. In fact, the "persistence" spectra [1] discussed here closely resemble those at high energy, and provide unusually rich information about the physics of photon-induced core processes in metals. Some of the specific results discussed here are: (1) the MND formula [2] makes qualitatively incorrect predictions in some cases; (2) the shapes of the observed optical edges are determined by chemical properties of the active center; (3) in some cases the optical process in metals is decoupled from the electron gas and gives sharp lines.

Persistence spectra characterize a single site in the lattice. They occur in metals whenever the hole localizes for times much longer than ω_p^{-1} (the reciprocal plasma frequency). Conduction electrons can then screen the perturbation within a distance $\sim k_F^{-1}$, and the entire excitation is localized inside the cell it characterizes. This happens whenever the hole energy lies outside a band; it is invariably the case for deep levels but, for impurity atoms, may often occur even at $\hbar\omega \sim E_F$. The many-particle electronic readjustments commonly pursued in high energy spectroscopies are then accessible at low energy and high resolution. A variety of results from this emerging valence spectroscopy are described in what follows. Electronic recoil, phonon broadening, Fano interferences, spin-orbit splittings and other "x-ray" threshold effects are all observed at $\hbar\omega < 12$ eV.

The absolute absorption per atom is given in Figs. 1 and 2 for rare gas and halogen impurities in K films ~ 4000 Å thick. Samples of this type are made [3] by coevaporation of the constituents onto a LiF crystal held at He temperatures. The "persistence" of the spectra is established by threshold energies and profiles that are mainly host-independent, as for Xe in K, Rb and Cs hosts (see Fig. 1) [3]. An unusually broad scale of persistence is shown in Fig. 2 by data [4] for 1% Br in metallic K and for the "interband" absorption in the salt KBr (broken line). Halogens do enter alkali metals as ions, and the structure of their excitations in metals does resemble that of excitons in salts (see below); the persistence of spectral features from salt to metal therefore is not accidental.

A chemical understanding of metallic screening allows the excitation energies to be calculated accurately. The conduction band responds mainly to the core charge. Sketches showing the electron density near Cl^- , Ar^0 , K^+ and Ca^{++} $2p^6$ cores in K are given in Fig. 3 (the $2p$ orbitals bind below the band bottom [5]). But a core excitation that promotes one core electron into the conduction band also changes the core charge by $+|e|$. A halogen excitation therefore causes a transition $2(a) \rightarrow 2(b)$ in the electron gas distribution; $2(b) \rightarrow 2(c)$ and $2(c) \rightarrow 2(d)$ describe rare gas and alkali metal core excitations. Calculations based on this insight, and atomic levels,

estimate the threshold to ~ 0.1 eV for suitable rare gases (arrow for Cs in Fig. 1). For halogens the predictions (some years before the experiments! [6]) agree with the data and a Stokes shift of 1.5 ± 0.1 eV for each halogen [4]. A similar accuracy appears feasible for deep levels predictions.

The halogen spectra in Fig. 2 show much structural detail. Fano interferences [7] with conduction band continua, visible below threshold, are most pronounced for F. Spin-orbit splittings similar to those in the salts break phonon broadened threshold edges. From the known Stokes shift E_s one predicts [4] a rms phonon broadening of $\sim \sqrt{(2 E_s E_0)} \approx 110$ MeV, with E_0 the potassium zero-point energy. A gaussian step of this width (dotted line) agrees well with the observed Br edge profile. The intrinsic Br profile, due to the electron gas, is therefore a sharp step. Analogous results and conclusions hold for other halogens in potassium.

We thus reach the central topic of x-ray threshold effects in metals. Lacking a quantitatively predictive theory of optical threshold profiles, our past efforts have aimed to uncover the physical parameters relevant to the threshold shape. Three results will be mentioned:

1. The profile is determined by chemical properties of the optical center. We find that different halogens have almost identical threshold characteristics in K: sharp steps of similar height, when corrected for phonon effects. The rare gas profiles for Xe (Fig. 1) and Kr (Fig. 2c) resemble each other and are quite distinct from the halogen edges. They rise smoothly to a maximum ~ 1 eV above threshold. The Na L_{23} edge [10] resembles the K M_{23} edge [11]; both are sharp, with small cusps at threshold. The different characteristic shapes are sketched next to the ground state of the relevant element in Fig. 2. These different shapes characterize elements from successive columns of the periodic table. We deduce that the profile is determined by the chemical structure of the active center.

2. Some optical excitations are decoupled from quasiparticle-pair creation processes. Sharp lines that emerge [8] with increasing Xe content in Fig. 1 have widths comparable with exciton lines observed in pure Xe, with no sign of broadening by the conduction electron response. The spectra are due to near neighbor Xe_2 pairs, and have been observed also for Kr_2 and XeA pairs in potassium [8]. In a determinantal theory this occurs when the excited (molecular) orbital is a virtual bound state [9].

3. The MND formula gives qualitatively incorrect predictions in some cases. The rare gas profiles can be parameterized for ~ 0.5 eV above threshold by an exponent $\alpha_0 \approx -0.9 \pm 0.1$. Realistic estimates of this parameter from the impurity structure gives the contrary prediction of a cusped threshold with $\alpha = 0.35 \pm 0.1$ [3]. The prediction thus has the wrong magnitude and sign. It is provocative that halogens, also repulsive, have sharp edges (α positive?).

Acknowledgement. This research was completed through the efforts of R. Avci, D. J. Phelps and R. A. Tilton, using funds provided by the National Science Foundation under Grant DMR-72-03026.

References.

1. Y. Onodera and Y. Toyozawa, J. Phys. Soc. Jap. 24, 341 (1968).

2. P. Nozières and C. T. deDominicis, Phys. Rev. 178, 1097 (1969).
3. R. A. Tilton, D. J. Phelps and C. P. Flynn, Phys. Rev. Lett. 32, 1206 (1974).
4. R. Avci and C. P. Flynn (to be published).
5. C. P. Flynn and N. O. Lipari, Phys. Rev. Lett. 27, 1356 (1971).
6. C. P. Flynn, Phys. Rev. B 9, 1984 (1974).
7. U. Fano and J. W. Cooper, Rev. Mod. Phys. 40, 441 (1968).
8. R. A. Tilton and C. P. Flynn, Phys. Rev. Lett. 34, 20 (1975).
9. C. P. Flynn (to be published).
10. See J. Dow and B. F. Sonntag, Phys. Rev. Lett. 31, 1461 (1973).
11. P. R. Norris, Phys. Lett. 45A, 387 (1973).

Fig. 1

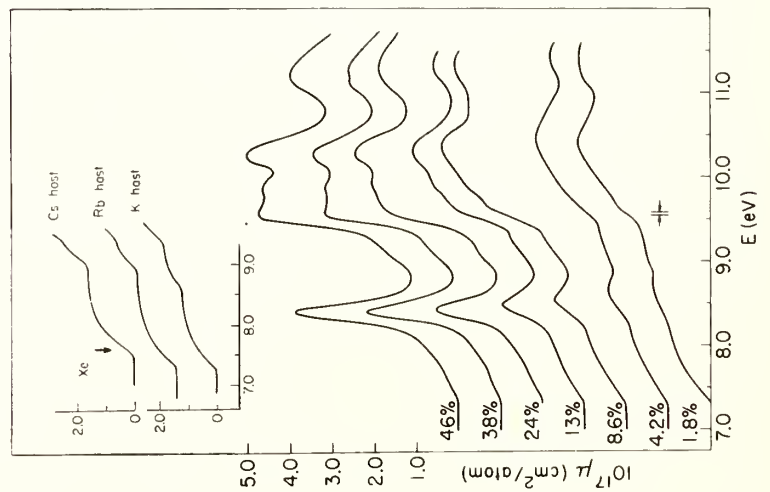


Fig. 2

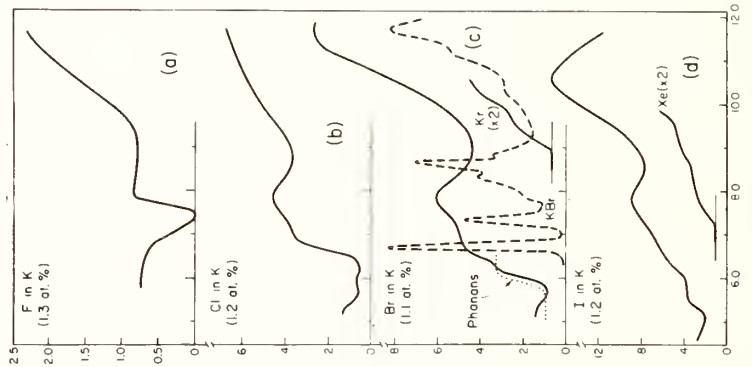
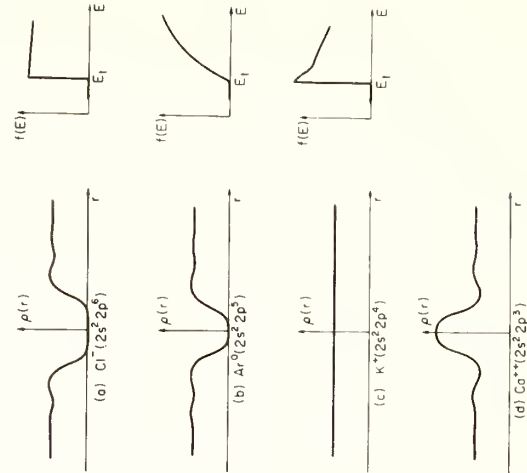


Fig. 3



- Fig. 1. Rare gas spectra in K, and Rb and Cs (inset).
- Fig. 2. Halogen spectra in K, and KBr, Kr and Xe spectra.
- Fig. 3. Electron density near various ions in K. Also the characteristic profiles are shown (right).

UNDERSTANDING X-RAY ABSORPTION EDGES IN SIMPLE METALS
USING X-RAY PHOTOEMISSION

P. H. Citrin, G. K. Wertheim, and M. Schlüter
Bell Laboratories, Murray Hill, New Jersey 07974

and

Y. Baer
Laboratorium für Festkörperphysik, ETH
CH-8049 Zürich, Switzerland

The many-body theory of Mahan and Nozières and DeDominicis (MND) [1,2] has historically predicted [3] peaked $L_{2,3}$ and rounded K edges in the simple metals Li, Na, Mg, and Al. In spite of its qualitative agreement with the observed x-ray edges in these systems [4] more quantitative analyses [5] have raised serious doubts about the theory's validity. X-ray photoemission (XPS) lineshapes contain three pieces of information which are essential for resolving this issue: the hole-state lifetime, the phonon broadening contribution, and the Anderson singularity index [6]. The latter quantity describes the many-body response of the conduction electrons to the sudden creation of a core hole in terms of the partial phase shifts which are contained in the MND threshold exponents. Since these phase shifts are constrained by Friedel's sum rule, it is possible to predict x-ray edge threshold exponents from measured XPS singularity indices by assuming that in the simple s,p metals phase shifts δ_ℓ are negligible for $\ell \geq 3$.

There are two additional effects that must be considered in x-ray edge measurements. One is the exchange mixing between spin-orbit components [7] and the other is the optical transition density of states (TDOS) [8,9,10]. These effects have been known to exist for some time, but their possible importance in x-ray edge measurements of simple metals is only now being considered seriously [11,12,13]. A similar statement applies to the hole-phonon broadening mechanism, but its magnitude can be empirically determined rather unambiguously from XPS measurements (exchange mixing and TDOS are absent in XPS experiments).

High resolution AlK α x-ray photoemission has been measured from all the accessible core levels in Na, Mg, and Al [14], and from Li as a function of temperature [15]. The data were analyzed using procedures previously described [14]. Briefly, a lineshape function after Doniach and Šunjić [16], containing the singularity index α and the hole-state lifetime width Γ , is convoluted with the spectrometer response function of known width. Subsequent convolution with an additional gaussian lineshape of width Γ_{ph} is then performed to take into account the effects of phonon broadening. Detailed analysis of the high binding energy side of the XPS peak determines α while that of the low binding energy side determines Γ and Γ_{ph} .

Transition density of states for the $L_{2,3}$ absorption edges in Na, Mg, and Al and for the K absorption edge in Al have been calculated using a combined pseudopotential-OPW formalism. The pseudopotential input parameters were extracted from accurate Fermi surface studies. The pseudo-valence wavefunctions are orthogonalized to atomic-like core states and the transition matrix elements are calculated directly. TDOS's are obtained by sampling k-space using the Gilat-Raubenheimer scheme.

In order to assess the relative importance of the five independent mechanisms which may affect x-ray absorption edges (MND, lifetime, phonons, TDOS, and exchange), we have analyzed the $L_{2,3}$ edge data from Na, Mg, and Al [17], and the K edge data from Li [12,18,19] and Al [20]. Wherever applicable, structure and/or broadening from these mechanisms, along with broadening from the appropriate Fermi function and spectrometer response, were taken into account and compared with the edge data. Lifetimes measured from the XPS data were used in the analyses while phonon contributions were determined from the absorption edge data directly. In all cases phonon broadening from the edge data was consistent with that from the XPS measurements. In all cases MND threshold exponents empirically determined from our edge analyses were consistent with values predicted from the measured XPS singularity indices and Friedel's sum rule [21].

Results and conclusions of our work are as follows: (1) The K edges in Li, Na, Mg, and Al are essentially unaffected by the consequences of the MND theory [1,2], in agreement with proposed arguments [5] and with electron energy loss measurements in Li [17]. However, this result does not imply [5] the MND theory is invalid; quite the contrary, that theory predicts [3,22,23,24] small threshold exponents for Na, Mg, and Al, that are in excellent agreement with our analyses [21]. (2) In Na, Mg, and Al the K edge rounding is primarily due to lifetime broadening. Structure in the TDOS and broadening from phonons are only weakly important in these metals. (3) In Li, the reverse is true for explaining the K edge rounding. Contrary to previous proposals [25,26], lifetime broadening is negligible. In agreement with the suggestion by Petersen [12], structure in the TDOS [9] is important, but is only partly responsible for the rounding. The primary mechanism is the hole-phonon coupling, suggested [9,27] and rebutted [26,28] by a number of workers. The new XPS temperature dependence studies [15], which are consistent with those reported earlier on edge measurements [19], provide magnitudes of the broadening which are not in good agreement with any published theory [27,29,30]. (4) The peakings of the $L_{2,3}$ edges in Na, Mg, and Al are in quantitative agreement with predictions [3,22,23,24] of the MND theory [1,2]. While this result strongly confirms the validity of the MND theory in these metals, it is obtained only after including the effects of phonon broadening (small in absolute magnitude but large relative to kT) and exchange coupling [11]. This latter mechanism appears to be important only for Na. (5) Structure from the TDOS has virtually negligible effect on the peaked edges in Na and Mg. For the case of Al, inclusion of such effects are moderately important for achieving quantitative agreement comparable to

that for Na and Mg. (6) The quality of agreement between the edge data and our fitted lineshapes including all the effects mentioned above deteriorates > 1.5 eV above the edge. It is not clear, however, up to what energy above threshold the MND theory remains valid. (7) Previous neglect or incorrect consideration of phonons, lifetimes, or exchange appears to be responsible for the apparent discrepancies between predictions of the MND theory near threshold and previous analyses of experimental data.

1. G. D. Mahan, Phys. Rev. 163, 612 (1967).
2. P. Nozières and C. T. DeDominicis, Phys. Rev. 178, 1097 (1969).
3. G. A. Ausman, Jr. and A. J. Glick, Phys. Rev. 183, 687 (1969).
4. G. D. Mahan, in Solid State Physics, edited by H. Ehrenreich, F. Seitz, and D. Turnbull (Academic, New York, 1974), Vol. 29, p.75.
5. J. D. Dow, J. E. Robinson, J. H. Slowik, and B. F. Sonntag, Phys. Rev. B10, 432 (1974); J. D. Dow, Phys. Rev. B9, 4165 (1974).
6. P. W. Anderson, Phys. Rev. Lett. 18, 1049 (1967).
7. Y. Onodera and Y. Toyozawa, J. Phys. Soc. Japan 22, 833 (1967).
8. G. A. Rooke, J. Phys. C: Solid State Phys. 1, 767 (1968).
9. A. J. McAlister, Phys. Rev. 186, 595 (1969).
10. L. Smrčka, Czech. J. Phys. B21, 683 (1971).
11. Y. Onodera, J. Phys. Soc. Japan (to be published).
12. H. Petersen, Phys. Rev. Lett. 35, 1363 (1975).
13. R. Gupta and A. J. Freeman, Phys. Rev. Lett. 36, 1194 (1976).
14. P. H. Citrin, G. K. Wertheim, and Y. Baer, Phys. Rev. Lett. 35, 885 (1975).
15. Y. Baer, P. H. Citrin, and G. K. Wertheim, Phys. Rev. Lett. (to be published).
16. S. Doniach and M. Šunjić, J. Phys. C: Solid State Phys. 3, 285 (1970).
17. C. Kunz, R. Haensel, G. Keitel, P. Schreiber, and B. Sonntag, "Electronic Density of States", edited by L. H. Bennet, NBS Spec. Publ. 323 (U.S. G.P.O. Washington, D.C., 1971), p.275.
18. J. J. Ritsko, S. E. Schnatterly, and P. C. Gibbons, Phys. Rev. B10, 5017 (1974).
19. C. Kunz, H. Petersen, and D. W. Lynch, Phys. Rev. Lett. 33, 1556 (1974).
20. H. Neddermeyer, Phys. Rev. B13, 2411 (1976).
21. For the case of Li, S. Girvin and J. J. Hopfield, Bull. Am. Phys. Soc. 21, 309 (1976), argue that spin exchange modifies the conventional sum rule, thus destroying simple phase shift analyses of XPS singularity indices. Our analyses of the LiK data, however, indicate a very small exponent in agreement with Ref. 18.
22. P. Longe, Phys. Rev. B8, 2572 (1973).
23. C. O. Almbladh and U. von Barth, Phys. Rev. B13, 3307 (1976).
24. P. Minnhagen, Phys. Lett. 56A, 327 (1976).
25. D. R. Franceschetti and J. D. Dow, J. Phys. F4, L151 (1974).
26. G. D. Mahan, Phys. Rev. B11, 4814 (1975).
27. J. D. Dow, J. E. Robinson, and T. R. Carver, Phys. Rev. Lett. 31, 759 (1973).
28. B. Bergersen, P. Jena, and T. McMullen, J. Phys. F4 L219 (1974).
29. A. W. Overhauser, footnote 23 in Ref. 9.
30. B. Bergerson, T. McMullen, and J.P. Carbotte, Can. J. Phys. 49, 3155 (1971).

CATEGORIZATION OF TWO-ELECTRON PROCESSES ACCORDING TO THE
MAJOR MANY-ELECTRON INTERACTIONS*

M. O. Krause

Transuranium Research Laboratory
Oak Ridge National Laboratory
Oak Ridge, Tennessee 37830

One important class of x-ray satellites derives from a single-electron jump in a multi-hole configuration that is created in the initial excitation process of the atom. Hence the study of multiple, especially two-electron, processes is basic to the understanding of x-ray satellites.

Two-electron processes are a manifestation of electron correlation (EC), which is probed readily by photoionization. If all EC effects are included in the description of the atom, the transition matrix elements contain the exact wavefunctions of the initial and final states of the atom and give finite values for all allowed transitions, whether single or multiple. Similarly, the sharp distinction between single and multiple transitions fades away, when we visualize the following sequence of events: (i) before the perturbation by the incident photon, the atom is in its ground state; (ii) during the interaction none of the electrons is in a stationary state; and (iii) following the interaction, the remaining orbital electrons will be in the various stationary states of the resulting ion.

However, since exact wavefunctions are available only for the simplest systems and since single-electron processes usually dominate, it is a realistic approach to start a calculation with the single, independent particle model and then apply successive EC corrections.

The multi-body perturbation theory (MBPT) has proven successful and lucid in its application to two-electron transitions. Chang and Poe's MBPT calculation [1] of the double photoionization probability in the 2p shell of neon is in excellent accord with experiment [2,3]. The following effects, represented in Fig. 1 in the diagrams of MBPT, were shown to be major contributors at photon energies sufficiently far above threshold: (a) Core rearrangement (CR), or core relaxation, or shakeoff (in the restricted sense of the term); (b) Ground-state correlation, or initial-state configuration interaction (ISCI); and (c) Virtual Auger process, or final-state configuration interaction (FSCI).

In this paper, Chang and Poe's results [1] are used as a framework for the categorization of two-electron ($\epsilon\ell$, $\epsilon'\ell'$ or $n\ell$, $\epsilon\ell'$) processes,

*Research sponsored by the U. S. Energy Research and Development Administration under contract with the Union Carbide Corporation.

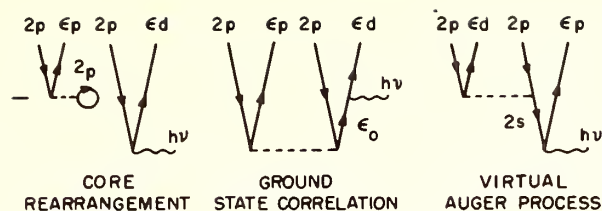


Fig. 1. The major contributing effects for the $\epsilon l, \epsilon' l'$ process in the 2p subshell of neon [1].

the process to be classified as either CR, ISCI or FSCI.

The CR mechanism is the major contributor when the two-electron process involves electrons from different principal shells. Examples are given in Fig. 2. for an $\epsilon l, \epsilon' l'$ and an $n l, \epsilon l'$ event. In Ne (1s,2p), about 90% of the intensity comes from CR and the remainder from ISCI. If the same many-electron interactions are considered to improve the K-level energy of Ne, an analogous result is obtained: the CR correction of 20 eV [5] is about 20 times the ISCI correction. [6]. To use the rare gases as examples, CR should be predominant for Ar(1s,n); Ar(L,n); Kr(1s,n); Kr(L,n); Kr(3s,n); Kr(3p,n); Xe(1s,n); Xe(L,n); and Xe(M,n), where n denotes the less tightly bound shell of a pair.

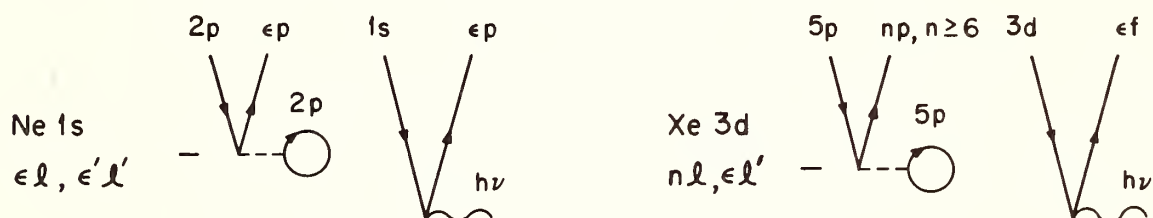


Fig. 2. The CR term, major contributor in two electron processes involving an inner and an outer electron.

The ISCI term is of significance when $(\epsilon l, \epsilon' l')$ and $(n l, \epsilon l')$ involve electrons of the same subshell. A specific case is depicted in Fig. 3., where the term shakeup is used in a generalized sense. In He, ISCI is dominant at all photon energies; in Ne(2p,2p), and the outer p levels of the other rare gases [1], ISCI is large; and it is important

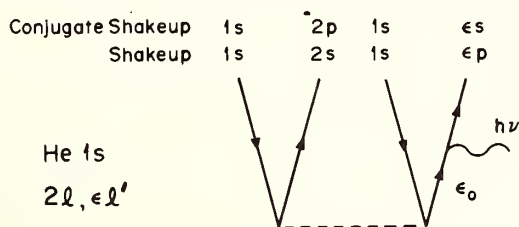


Fig. 3. The ISCI term; for $\Delta L = 1, l = 0$ or 1.

for processes involving inner K and L shells, for example, in double-internal conversion and $2e \rightarrow h\nu$ events [8]. In elements with an ns^2 nominal configuration, ISCI plays a significant role [9].

The FSCI mechanism assumes importance when configurations of the same symmetry are closely

spaced, as in the presence of partially filled or empty subshells. In Fig. 4., evidence is shown for FSCI involving $2S$ states in Ar by way of photoelectron [10] and x-ray emission spectra [11]. FSCI also appears

in Auger spectra [2] and in the form of interchannel coupling in partial photoionization cross sections [13]. A particularly interesting manifestation of FSCI occurs in the $4p$ shell of elements near $Z = 50$ because of the strong coupling of $4p$ with $4f^2$ states [14].

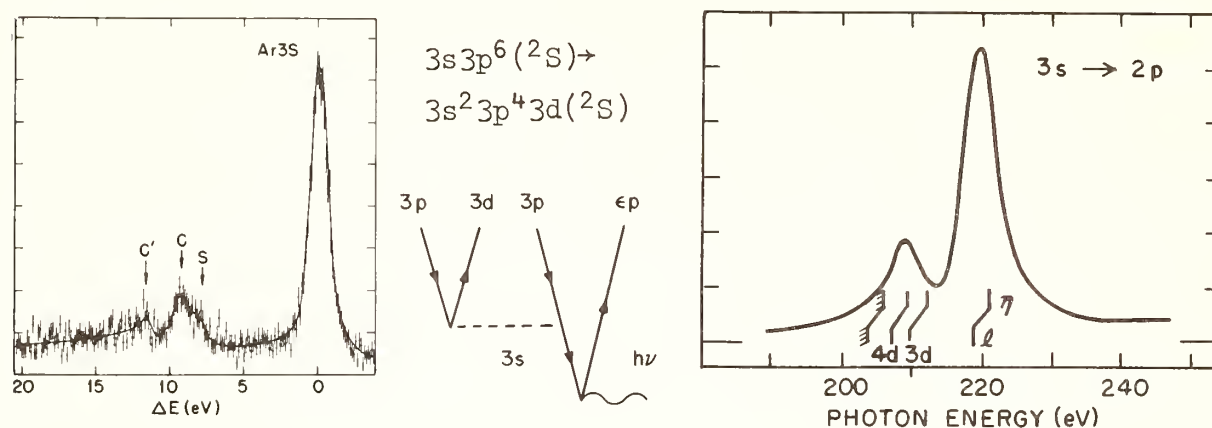


Fig. 4. The FSCI term, depicted for Ar3s as a diagram (center), and as evidenced in a photoelectron spectrum (left, C', C) and an x-ray spectrum (right); [10 and 11]. CR contribution is designated as S in photoelectron (left) and unresolved in x-ray spectrum (right).

At this stage of theoretical development and with the still limited number of experiments, the proposed categorization and treatment of two-electron processes is mainly of heuristic value, affording a systematization of data and hopefully an impetus for more extensive and detailed experimental and theoretical studies.

- (1) T. N. Chang and R. T. Poe, Phys. Rev. A 12, 1432 (1975).
- (2) V. Schmidt, N. Sandner, H. Kuntzemüller, P. Dhez, F. Wuilleumier, and E. Källne, Phys. Rev. A 13, 1748 (1976).
- (3) G. R. Wight and M. J. Van der Wiel, J. Phys. B (1976). (To be publ.)
- (4) M. O. Krause in "Photoionization and Other Probes of Many-Electron Interactions" NATO Advanced Institute Series. F. Wuilleumier editor, Plenum Press (1976), pp. 133 - 163.
- (5) U. Gelius, Physica Scr. 9, 133 (1974).
- (6) H. P. Kelly, Phys. Rev. A, 11, 556 (1975).
- (7) V. L. Jacobs and P. G. Burke, J. Phys. B 5, L67 (1972).
- (8) W. Wolfi, Ch. Stoller, G. Bonani, M. Suter, and M. Stockli, Phys. Rev. Lett. 35, 656 (1975).
- (9) See e.g. S. Süzer and D. A. Shirley, J. Chem. Phys. 61, 2481 (1974).
- (10) D. P. Spears, H. J. Fischbeck and T. A. Carlson, Phys. Rev. A 9, 1603 (1974).
- (11) J. W. Cooper and R. E. LaVilla, Phys. Rev. Lett. 25, 1745 (1972).
- (12) W. Mehlhorn, W. Schmitz, and D. Stalherm, Z. Phys. 252, 399 (1972).
- (13) For example Ar3s: P. G. Burke and K. T. Taylor, J. Phys. B 16, 2620 (1975) and References therein.
- (14) G. Wendin in Proc. of 2nd Conference on Innershell Ionization Phenomena, W. Mehlhorn et al., eds., Univ. Freiburg (1976).

EFFECTS OF RELAXATION AND CONTINUUM INTERACTION ON THE NEON KLL AUGER SPECTRUM

G. Howat*

Department of Chemistry
Edinburgh University
Edinburgh EH9 3JJ, Scotland

T. Åberg[†]

Department of Physics
Kansas State University
Manhattan, Kansas 66506

and

O. Goscinski

Department of Quantum Chemistry
Uppsala University
S-75120 Uppsala 1, Sweden

In this report we discuss generalizations of the conventional Auger theory which is based on Wentzel's Ansatz [1]. Previously we have demonstrated that it is not possible to generalize Wentzel's approach to the many-electron case involving non-orthogonal spin orbitals by replacing the perturbing two-electron Coulomb interaction by its many-electron counterpart [2]. Hence a systematic investigation of the effect of relaxation on Auger rates requires a consideration of the full Hamiltonian unless the relaxation can be adequately described by using transition orbitals (TO's) [3]. We indicate, however, that the use of the TO's does not significantly improve the frozen-core restricted Hartree-Fock (RHF) KLL Auger rates of Ne. The Hartree-Slater (HS) approach [4] gives better agreement with experiment than the HF method especially when the $2s^{-2} 1S_0 - 2p^{-2} 1S_0$ configuration interaction is included. However, the HS rates are expected to approach the frozen core HF rates if the interaction within each outgoing channel of the Auger electron is included [5]. Hence a consistent theory of the Auger effect requires the consideration of other interactions like the interaction between the final $2S$ continuum states which we shall include in the lowest order by generalizing Fano's variational configuration interaction approach [6]. As indicated by the many-body-perturbation calculation of Kelly [7] this interchannel mixing is very important.

Since the inner-shell hole states of the same symmetry are usually well separated, it is sufficient to consider an isolated discrete stationary state ϕ interacting with N continuous stationary states ψ_{iE} . The corresponding energy submatrix to be diagonalized is

$$\begin{aligned} \langle \phi | H - E | \phi \rangle &= E_\phi - E, & \langle \psi_{iE'} | H - E | \phi \rangle &= M_i(E', E), & \langle \psi_{iE'} | H - E | \psi_{jE''} \rangle &= V_{iE', jE''} \\ & & i, j &= 1 \dots N, \end{aligned} \quad (1)$$

where the bound state wave function ϕ is not necessarily orthogonal to the continuum wave functions ψ_{iE} [8]. In Fano's work [6] it is assumed that $V_{iE', jE''} = \delta_{ij} \delta(E'' - E') (E' - E)$. This assumption is usually not valid for basis sets which are used in Auger calculations so that a pre-diagonalization [9] of the continuum submatrix must be carried out.

If we choose a HF basis, then there is no intrachannel interaction so that $V_{iE',iE''} = \delta(E''-E')(E'-E)$. With this assumption it can be shown [10] that the diagonalization of the matrix (1) leads to the following lowest order result. The total resonance width $\Gamma(E)$ of the Lorentzian decay curves is a sum of the partial widths $\Gamma_i(E) = 2\pi|V_i(E,E)|^2$, where

$$V_i(E,E) = M_i(E,E) + \sum_{j \neq i}^N P \int d\epsilon \frac{V_{j\epsilon,iE} M_j(\epsilon,E)}{E - \epsilon} \quad (2)$$

In the sum which represents the continuum interaction, P denotes the "principal part" of the integral and E coincides with the resonance energy which is given by E_ϕ to a high accuracy. The matrix elements $M_j(\epsilon,E)$ and $V_{j\epsilon,iE}$ are given by Eq. (1).

As a first step to explore the orbital dependence and relaxation we consider the calculation of the Ne KLL HF rates. Two sets of one-electron bound state spin orbitals were employed in these calculations. The first set consisted of TO's obtained from the variation of $(1/2) \times [E(1s^{-1}) + E(L^{-2})_{av}]$, where $E(L^{-2})_{av}$ refers to the LS average energy of a particular L^{-2} configuration. Hence there are actually three sets of TO's corresponding to the final $2s^{-2}$, $2s^{-1}2p^{-1}$, and $2p^{-2}$ configurations. The second set consisted of RHF spin orbitals of the initial $1s^{-1}$ state. In both cases the continuum orbital ϵl was solved in the field of the residual ion with two L vacancies. The wave functions of each term of the ion were constructed from the TO's or the initial state HF orbitals and coupled to the continuum orbital ϵl to yield the $2S$ wave function. The corresponding Fock operator was constructed and the orthogonality of the continuum orbital to the bound state orbitals was imposed by the introduction of the appropriate non-diagonal Lagrangian multipliers. The calculation of the continuum orbitals and the rates was performed using a computer program (ALKO) constructed by one of us (GH). The bound state orbitals were those provided by the Froese-Fischer program [11]. The energies of the Auger electrons were the experimental energies which practically coincide with the corresponding TO energies [12]. In Table 1 we compare our results with the HS results of Bhalla [4] and with the HF results of Kelly [7]. Bhalla [4] employs initial bound state orbitals and solves the continuum orbital in the initial state HS potential which approaches $2r^{-1}$ for large r . Kelly's HF rates [7] are based on final state orbitals except that the $2s$ orbitals are spin polarized HF orbitals associated with the initial state configuration. None of the calculations reproduces the experimental results very well. However, the inclusion of relaxation via the TO's improves the $KL_1L_{2,3}^{-1,3}P$ and $KL_{2,3}L_{2,3}^{-1}D$ Auger HF rates somewhat.

We compare also our improved Auger rates which are based on initial $1s^{-1} 2S$ bound orbitals with Bhalla's HS rates involving the $2s^{-2} 1S_0 - 2p^{-2} 1S_0$ mixing [4] and with Kelly's many-body-perturbation results [7]. Our HF results modified by the $2s^{-2} 1S_0 - 2p^{-2} 1S_0$ mixing and our results based on Eq. (2) are shown. It is seen that the inclusion of the final state interchannel interaction in the lowest order results in a significant improvement of the HF results. Note that the mixing of the final

$2s^{-2} 1S_0$ vs $2S$ and $2p^{-2} 1S_0$ vs $2S$ configurations is equivalent to the mixing of the corresponding configurations of the residual ion. Our result suggests that the success of the HS approach involving the $2s^{-2} 1S_0 - 2p^{-2} 1S_0$ mixing is partially due to a cancellation of the intra- and interchannel mixing in the final state. An analysis [13] of intra- and interchannel effects on HS rates is in progress.

References:

*Supported by Imperial Chemical Industries (U.K.)

†Permanent Address: Laboratory of Physics, Helsinki University of Technology, 02150 Espoo 15, Finland, partial support by USERDA Contract.

- 1 G. Wentzel, Z. Phys. 43, 524 (1927).
- 2 G. Howat, T. Åberg, and O. Goscinski, in Abstracts of the 2nd International Conference on Inner Shell Ionization Phenomena (Freiburg, 1976) p. 126, and to be published.
- 3 O. Goscinski, G. Howat, and T. Åberg, J. Phys. B 8, 11 (1975).
- 4 C. P. Bhalla, Phys. Lett. 44A, 103 (1973) and private communication.
- 5 See e.g. U. Fano and J. W. Cooper, Rev. Mod. Phys. 40, 441 (1968) for a discussion of the intrachannel interaction in the context of photoabsorption.
- 6 U. Fano, Phys. Rev. 124, 1866 (1961).
- 7 H. P. Kelly, Phys. Rev. A 11, 556 (1975).
- 8 F. H. Mies, Phys. Rev. 175, 164 (1968).
- 9 A. Starace, Phys. Rev. B 5, 1773 (1972).
- 10 G. Howat, T. Åberg, and O. Goscinski, to be published.
- 11 C. Froese Fischer, Comp. Phys. Comm. 1, 151 (1969).
- 12 G. Howat, O. Goscinski, and T. Åberg, Physica Fennica 9, Suppl. S1, 241 (1974).
- 13 C. P. Bhalla, M. Ahmed, and C. S. Soong, private communication.

Table 1. Ne KLL Auger rates. Units are 10^{-3} a.u.

Transition	T0 ^a	RHF ^a	HF ^b	HS ^b	CI(I) ^c	CI(II) ^c	HSCI ^d	CI(I) ^d	Expt ^e
KL ₁ L ₁	¹ S	1.09	1.14	0.95	0.83	0.85	0.60	0.62	0.51
KL ₁ L _{2,3}	¹ P	1.82	2.31	2.03	1.83	2.31	1.95	1.83	1.48
	³ P	0.75	1.07	0.79	0.61	1.07	1.01	0.61	0.54
KL _{2,3} L _{2,3}	¹ S	0.41	0.44	0.46	0.39	0.71	0.95	0.61	0.76
	¹ D	5.18	5.44	5.68	5.14	5.44	6.06	5.14	5.15

^a Our calculation using bound T0 orbitals and $1s^{-1}$ RHF orbitals.

^b The HF rates are from Ref. 7 and the HS rates from Ref. 4.

^c Our CI(I) calculation includes the $2s^{-2} 1S_0 - 2p^{-2} 1S_0$ configuration mixing and CI(II) the mixing between the final continuum states in the lowest order according to Eq. (2).

^d The HSCI results are from Ref. 4 and CORR(I) includes the diagrams described in Fig. 1 of Ref. 7.

^e The absolute total rate measured by U. Gelius et al. (Chem. Phys. Lett. 28, 1, 1974) has been scaled by the experimental relative rates of M. O. Krause et al. (Phys. Lett. A31, 81, 1970).

P. Venugopala Rao
 Department of Physics
 Emory University, Atlanta, Ga., U.S.A. 30322

The double L-vacancy atomic states are produced in the decay of W-181 by the following mechanisms: a) KLL Auger electron emission following K capture decay to the ground and 6.25-keV levels in Ta-181, b) KLL Auger electron emission following K electron conversion of 136- and 153-keV transitions in Ta-181 (K electron capture decay is energetically forbidden to the levels at 136- and 159-keV), and c) Internal ionization in K or L shells following electron capture or internal conversion. The mechanism (a) contributes predominantly resulting in the formation of 0.02 double L-vacancy states per decay approximately. The remaining two mechanisms contribute very little of the order of 10^{-4} or 10^{-5} per decay according to the present theories.

Konstantinov et al. [1] measured the rate of production of these double vacancy states by measuring L X-ray - L X-ray coincidences with two proportional counters and found three times larger than the expected number. In their opinion these additional states arise because "the change in the total binding energy of all electrons of an atom in electron capture is spent on production of additional vacancies in the electron shells, starting with the L-shell, and is not carried off by the neutrino as has been assumed previously."

In the present work two Si(Li) detectors, placed at 180° to each other in a fast coincidence arrangement with a resolving time of 200 nsec, are employed to measure the Ta L x rays, $C_{L(L)}$ and Ta $K\alpha$ x rays, $C_{K\alpha(L)}$ in coincidence with Ta L x rays. The ratio of these two coincidence rates is related to the number, $a(LL)$, of double L-vacancy states created per decay and the number, $b(L)$, of single L-vacancy states created in $K\alpha$ x ray emission per decay through the following relation,

$$\frac{C_{L(L)}}{C_{K\alpha(L)}} = \frac{2a(LL)}{b(L)} \cdot \frac{\bar{\omega}(LL)}{\omega_{K\alpha L}}$$

where $\bar{\omega}(LL)$ is the average L x ray fluorescence yield of double L vacancy states and $\omega_{K\alpha L}$ is the average L x ray fluorescence yield of single L vacancies created in $K\alpha$ x ray emission. A value of 0.096 ± 0.002 is obtained for this ratio which is corrected for the directional correlation between L x rays and K x rays and the presence of the true L x ray - L x ray coincidences from cascade nuclear transitions.

Assuming that all the double L-vacancy states are created in K Auger electron emission, the ratio $a(LL)/b(L)$ is calculated from the knowledge of KLL Auger electron branching ratios, K x ray branching ratios and K fluorescence yield (reviewed by Bambynek et al. [2]) for $Z = 73$. Using this value of 0.036 in the above relation, $\bar{\omega}(LL)/\omega_{K\alpha L}$

ratio is found to be 1.33. The estimated value for this ratio, based upon the knowledge of the relative population of L subshell vacancies and their average L x-ray yields from Bambynek et al. [2], is 0.97, thus showing a substantial discrepancy.

One possible explanation is an increase in the fluorescence yield of double L-vacancy states. But in a recent measurement by Campbell et al. [3] in which they measured L x rays in coincidence with KLL Auger electrons no such increase is reported. The angular correlation between the two cascade L x rays emitted during the decay of double L-vacancy states can also be a source of discrepancy. No theoretical studies of such effects are available but a measured value of 18% for the anisotropy in the angular correlation of cascade L x rays in the decay of W-181 is reported [1]. Thus the present result obtained with 180° between the two coincident L x rays needs to be reduced by about 10 or 12% approximately. Such a correction still leaves the experimental value 20% higher than the estimated value, but not three times larger as reported by Kanstantinov et al. [1].

Before searching for other mechanisms for the production of double L-vacancy states, it is important to recognize that the estimated value of $a(LL)$ depends heavily upon the K x ray fluorescence yield through the factor $(1-\omega_K)/\omega_K$. A one percent decrease in the presently accepted value of ω_K (0.956) can increase the estimate of $a(LL)$ by about 20%. At $Z = 73$ neither reliable experimental values nor theoretical estimates are available for K x ray fluorescence yield. A direct measurement of KLL Auger electrons per decay of W-181 would be of considerable value.

References:

1. Kanstantinov et al., in Proc. Int. Conf. Inner-Shell Ionization Phenomena and Future Appl., Atlanta, U.S. Atomic Energy Comm. Report No. CONF-720404, edited by R.W. Fink, S.T. Manson, J.M. Palms and P. Venugopala Rao, p. 2035 (1973).
2. Bambynek et al., Rev. Mod. Phys. 44, 716 (1972).
3. Campbell et al., Proc. Second Int. Conf. Inner-Shell Ionization Phenomena, Freiburg (1976).

MULTIPOLARITY OF SOME TRANSITIONS IN Th-231, BY APPLICATION OF GAMMA-X-RAY COINCIDENCE TECHNIQUE

E. VAÑO AND L. GONZALEZ

JUNTA DE ENERGIA NUCLEAR. SECCION DE FISICA NUCLEAR DE BAJA ENERGIA. MADRID -3-. SPAIN.

Research on the nuclear level schemes needs in many cases the multipolarity measurement of some transitions, to establish the level angular momenta. In this field conversion electron spectrometry is the most common method, but its convenience for nuclides having a very low specific activity is questionable, because spectra with sufficient statistics require long measurement times, compromising the spectrometer stability.

A gamma-X-ray coincidence experiment can provide, at times, sufficient information for the determination of multipolarity mixing in the gamma transitions involved, having the advantage that it can be performed simultaneously with the routine gamma-gamma coincidences, if an adequate low energy detector choice is made.

The U-235 decays to Th-231 by alpha emission, with a 7.13×10^8 y half-life. Due to its low specific activity, about $2 \mu\text{Ci/U-235 gram}$, the use of electron spectrometry for multipolarity determination becomes practically impossible. The more recent works on the level scheme of Th-231 (1,2,3) have been made without direct measurement of multipolarities. For this reason we have applied to this nuclide the method described here.

This method has been applied for a 42 keV transition deexciting a level of that energy to the ground state. This level is populated via alpha decay, with an intensity of 4,5%. It is also filled by some gamma transitions. One of them, with an energy of 163 keV, arises from a 205 keV level, which is also deexcited to the ground state by means of a 205 keV transition, both 163 and 205 keV gammas having practically equal intensities, about 5 photons per 100 α -decays.

Bidimensional coincidences have been made using a 47 cm^3 CANBERRA Ge (Li) coaxial detector, covering an energy range between 75 and 220 keV and $0,37 \text{ cm}^3$ ORTEC Ge (Li) plane detector, operating from 10 to 45 keV. The electronics was conventional, ORTEC and CANBERRA, for this type of experiment. The data acquisition system was an INTERTECHNIQUE TRIDAC-C, which allowed simultaneous recording on magnetic tape of the coincident events and their convenient display in a reduced matrix. The employed dynamics were,

in this experiment 512 channels for the coaxial detector and 1024 channels for the low energy detector. Stability of the linear electronic chains was assured by means of two digital gain stabilizers, placed in the analogic-to-digital converters, surveying the position of an electronic pulse supplied by an ORTEC 448 pulse generator and driven into the detector preamplifiers for obtaining a coincidence peak, which was placed at the most energetic end of the biparametric coincidence map. Computer programs COIN, DENSIS, STEREO and ANYS (4) permit the general treatment of the results on a 1106 UNIVAC Computer. The first one classifies the coincident events in a matrix, the second and the third are used for the matrix digital plot, either as a contrast map or as an isometric projection display. ANYS program permits row-or-column superimposition in the matrix.

The process that follows the matrix classification consists in selecting one transition arising from a determined level, coincident with that whose multipolarity is to be investigated, as well as another placed between the same issuing level and the ground state. In the present work, the involved transitions are the 163 keV gamma, in coincidence with the 42 keV line and the 205 keV one.

The difference between the 163 keV and 205 keV coincidence spectra (obtained by superimposition of some lines on the coincidence matrix) after adequate detector efficiency corrections and corresponding normalization to the intensity unit, becomes a neat coincidence spectrum, due exclusively to the 42 keV transition, this spectrum containing information about the 42 keV photons and also about the XL-Rays following the internal conversion of the 42 keV transition.

From this spectrum, the peak areas can be calculated and by using the low energy detector efficiency values and the XL-ray emission ratios (5) one can obtain the intensities of the XL-rays proceeding from every subshell L1, L2 and L3. Calculation of the L3 subshell X-ray intensity presents no difficulties and it can be estimated from the referred ratios, using $L\epsilon$ or $L\alpha$ peak areas. To separate the L2 and L3 subshell X-ray contributions one can make use of the $L\gamma$ group, fundamentally constituted by the L2-N4 and (L2-04+L1-N3) lines. So, if the theoretical $L2-N4/L2-04$ ratio is supposed sufficiently precise, it is possible to find the ratio $L1-N3/L2-04$ (placed in the second doublet peak) calculating the peak gravity-center and establishing a proportionality between its energy position and the L2-04 and L1-N3 respective contributions. In this way, the XL-rays from every subshell are obtained, these values corresponding to the Coster-

Kronig modified vacancy distribution.^f Coster-Kronig factors and the w L-subshell fluorescence yields (6) permit one to obtain the primary vacancy distribution, produced by the 42 keV transition internal conversion. The values are, in this case 17, 47 and 36%, for L1, L2 and L3 respectively. Internal conversion coefficients for M1 and E2 42 keV transitions (which are the possible multipolarities assumed for the 42 keV transition, taking into account the level angular momenta and parities), lead to the results, 75% for M1 and 25% for E2.

The same neat coincidence spectrum due to the 42 keV transition permits the measurement of the total internal conversion coefficient for this transition, using the X-rays and 42 keV peak areas, so determining the transition intensity (this calculation is normally very difficult by others procedures).

The validity of this method must be judged with regard to the high sensibility of the multipolarity mixing obtained from the L1, L2 and L3 vacancy percentages. If the L2 and L3 vacancies calculated shift by 10%, this can produce variations of up to 50% in the E2 calculated mixing. Consequently, this point must be taken closely into account when calculating multipolarity mixing.

References

- (1) E. VAÑO, R. GAETA, L. GONZALEZ and C.F. LIANG, Nucl. Phys. A251 (1975) 225
- (2) W.TEOH and R.D. CONNOR, Nucl. Phys. A 228 (1974) 432
- (3) L.A. KROGER, C.W. REICH and J.E. CLINE, ANCR-1016 (1971)
- (4) J.M. LOS ARCOS. No published
- (5) J.H. SCOFIELD, Phys. Rev. 179 (1969) 9
- (6) E.J. MCGUIRE, Phys. Rev. A 3 (1971) 587

SIMPLIFIED CALCULATION OF AUTOIONIZATION RATES
IN TWO AND THREE-ELECTRON ATOMS*

Donald R. Franceschetti[†]
Department of Physics and Astronomy
University of North Carolina
Chapel Hill, North Carolina 27514

and

Donald L. Miller[‡]
Department of Physics and Materials Research
Laboratory
University of Illinois at Urbana - Champaign
Urbana, Illinois 61801

The Auger decay, or autoionization, of atomic inner shell vacancy states has been the subject of numerous theoretical calculations [1,2]. Most of this work falls into one of two categories; high accuracy studies of autoionization of two-electron systems - He and H^- [1], and broad surveys of autoionization in many-electron systems [2]. The calculation of energies, widths, and lineshape asymmetries for two-electron atoms has served as a testing ground for many-electron and scattering-theoretic methods. The existence of such high-accuracy results also permits the testing of simpler, physically motivated, methods more readily applicable to complex systems, and the development of a qualitative understanding of the role of electron-electron correlation in the autoionization process.

We present here some simple calculations of energy widths for KLL Auger transitions in He, Li and Be^+ . Comparison of our results for He with those of high accuracy calculations and with available experimental data permits a rough estimate of the reliability of our approach. The results for He, Li and Be^+ together provide an indication of qualitative trends in going from one system to another.

Our method is motivated by the realization that the best single- (or few-) determinant approximations to the wavefunctions of two different atomic states would employ two different sets of atomic orbitals. By determining atomic orbitals for the initial and final states of each autoionization process in independent calculations, we are able to take into account, in an approximate way, the difference in electron-electron repulsion of the two states. This difference should be particularly significant for atoms of only a few electrons. Autoionizing states were taken to be Slater determinants or linear combinations thereof as required in LS coupling. The atomic orbitals employed were of simple form and were determined by a variational procedure described in detail elsewhere [3]. Continuum wavefunctions were determined by self-consistent solution of a one electron Schrodinger equation including Coulomb and exchange interactions with the atomic core.

Table I. Autoionization widths (eV.) for He

$2s^2\ ^1S$	$2s2p\ ^3P$	$2s2p\ ^1P$	$2p^2\ ^1S$	$2p^2\ ^1D$	Source
0.091	0.018	0.032	0.049	0.105	1 configuration calc.
0.149	-	-	0.00095	-	2 term C.I.
0.138	0.0094	0.038	0.0067	0.072	Expt. (see Ref.[3]) or Calc. [1]

The lifetime half-widths obtained for He autoionizing states are shown in Table I, together with accurate values. In addition to single configuration calculations, a two-term configuration-interaction calculation was performed for the $2s^2$ and $2p^2\ ^1S$ states. Our results agree with the accurate values to within a factor of 2, except for the $2p^2\ ^1S$ state, for which the Auger matrix element involves small differences between large terms. We feel that the agreement is quite good considering the approximate nature of the method. It has been realized for some time that the major contribution to the Auger matrix element in He comes from the region of configuration space with both electrons near the atomic core [4]. A qualitative examination of energy terms suggests that our variational determination of atomic orbitals for the autoionizing state provides a fair description of the outer shell orbitals in the core region, and that the effects of instantaneous electron-electron correlation in this region are, in most cases, smaller than in the atom as a whole [3].

Within the atomic orbital approximation employed, the Auger transition matrix element for He involves only conventional Coulomb terms of the form

$$\langle 1s_f\ k\ell_f | r_{12}^{-1} | 2\ell_i'\ 2\ell_i'' \rangle, \quad (1)$$

where the subscripts i and f designate initial and final state orbitals, respectively. For the three-electron atoms Li and Be^+ , the use of different sets of atomic orbitals leads to a transition matrix element which is the sum of (i) conventional matrix elements (Eq. 1), multiplied by near unity overlap factors, (ii) other Coulomb matrix elements between initial and final state orbitals, multiplied by small overlap factors, and (iii) matrix elements of the electron kinetic energy and electron-nuclear attraction operators between initial and final states orbitals, multiplied by products of orbital overlaps. Lifetime widths obtained from the full Auger matrix element and from the conventional Coulomb terms alone are given in Table II.

The conventional Auger matrix elements (Eq. 1) for He, Li and Be⁺ were found to correlate well with the amplitudes of the wavefunctions in the core region. For given ℓ , ℓ' , ℓ'' the matrix elements were found to be proportional to

$$a^4 \psi_{1s}(a) \psi_{k\ell}(a) \psi_{2\ell'}(a) \psi_{2\ell''}(a) \quad (2)$$

(a is the final state 1s radius), to within about 25%.

In Table II, the conventional Coulomb matrix elements are seen to account for most of the energy width of the $1s2s^2$ and $1s2p^2$ states but not for the $1s2s2p$ states. In the latter case the dominant contribution to the Auger matrix element is

$$\langle 1s_f | 2s_i \rangle \langle kp_f | -\frac{1}{2} \nabla^2 - \frac{Z}{r} | 2p_i \rangle. \quad (3)$$

Although results obtained using more accurate wavefunctions will differ somewhat from those presented here, this result does indicate the possible importance of one-electron operator contributions to autoionization in few electron atoms.

Table II. Autoionization widths (eV.) for Li and Be⁺. Values in parentheses are widths computed from conventional Coulomb terms (eq. 1) alone.

	$1s2s^2 \ ^2S$	$1s2s2p \ ^2P$	$1s2s2p \ ^2P$	$1s2p^2 \ ^2D$	$1s2p^2 \ ^2S$
Li	0.026 (0.017)	0.037 (10 ⁻⁶)	0.098 (0.003)	0.013 (0.013)	0.011 (0.009)
Be ⁺	0.038 (0.028)	0.073 (0.002)	0.258 (0.011)	0.030 (0.030)	0.009 (0.007)

*Research supported by the National Science Foundation under Grants DMR-72-03026 and GH-39132

†National Science Foundation Energy-Related Postdoctoral Fellow 1975-76.

*National Science Foundation Predoctoral Fellow.

1. A. K. Bhatia and A. Temkin, Phys. Rev. A 11, 2018 (1975) and references cited therein.
2. W. Bambynek, B. Craseman, R. W. Fink, H.-V. Freund, H. Mark, C. D. Swift, R. E. Price, and P. V. Rao, Rev. Mod. Phys. 44, 716 (1972).
3. D. L. Miller and D. R. Franceschetti, J. Phys. B (to be published).
4. J. W. Cooper, in M.R.C. McDowell, Atomic Collision Processes (North Holland, Amsterdam, 1964), p. 595.

THEORETICAL X-RAY AND AUTOIONIZATION RATES FOR FOUR-ELECTRON IONS
WITH $2s^n 2p^m$ CONFIGURATIONS*

M. Ahmed, S. C. Soong and C. P. Bhalla

Kansas State University, Department of Physics
Manhattan, Kansas 66506 USA

The theoretical investigations of few-electron ions are important for the diagnostic applications to plasmas and for the analysis of x-ray relative intensities as observed in solar flares. These calculations are also relevant to the recent high-resolution spectral measurements in heavy ion-atom collisions.

Bhalla, Gabriel and Presynakov [1], and Bhalla and Gabriel [2] have recently published theoretical results for the $1s\ 2p^2$, $1s\ 2s^2$ and $1s\ 2s\ 2p$ configurations. A detailed discussion and the analyses of the experimental data from laser-produced plasmas and from solar flares were presented [1].

Using the formalism developed by Fano [3], the autoionization rates were calculated for all the spectroscopic terms [4,5]. Similarly, the theoretical expressions relevant to the radiative decay for the four-electron configurations were derived. Configuration mixing between all the various terms of the following electron configurations

$$2p^4, 2s^1 2p^3, 2s^2 2p^2, 1s^1 2p^3, 1s\ 2s\ 2p^2, 1s\ 2s^2\ 2p$$

were calculated. The spin-orbit parameter for the 2p shell was computed with the Hartree-Fock [6] program. The Hamiltonian was then diagonalized for each value of J_i to obtain the eigenvectors. The autoionization and x-ray rates were then calculated using the generalized Slater integrals and the transition matrix elements.

Table 1 contains the numerical results for Fe^{+22} . The dominant electronic configuration and the spectroscopic term are identified in the first two columns for each value of the total angular momentum. The individual transition rates to the various final states are not listed, since the total number of x-ray transitions are very large. The sum of the autoionization rates and x-ray rates gives the total transition probability in a.u. (1 a.u. = 2.419×10^{-17} sec.).

TABLE 1

Total autoionization (R_A) and x-ray (R_X) rates in a.u. for Fe^{+22} , calculated with the inclusion of configuration mixings and in the intermediate coupling scheme.

Initial State	J_i	$R_A \times 10^4$	$R_X \times 10^4$
$2s^2 2p^2$	3P	0	105.8
	1S	0	163.0
$2p^4$	3P	0	130.7
	1S	0	137.0
$2s^2 2p^2$	3P	1	107.1
$2p^4$	3P	1	130.9
$2s^2 2p^2$	1D	2	185.7
	3P	2	106.9
$2p^4$	1D	2	207.6
	3P	2	130.5
$2s2p^3$	3P	0	115.4
	3D	1	92.41
	3P	1	68.73
	1P	1	92.58
	3S	1	47.50
	3D	2	97.66
	1D	2	115.2
	3P	2	39.41
	5S	2	7.284
	3D	3	146.1
			183.6
			186.2
			188.4
			185.3
			203.1
			184.3
			174.7
			187.8
			183.4

REFERENCES

*Supported by the U. S. Energy Research and Development Administration under Contract No. E(11-1)-2753

- [1] C. P. Bhalla, A. H. Gabriel, and L. P. Presynakov, Mon. Not. R. Astr. Soc. 172, 359 (1975).
- [2] C. P. Bhalla and A. H. Gabriel, in Beam-Foil Spectroscopy, ed. Sellin and Pegg (Plenum Press 1976) p. 121.
- [3] U. Fano, Phys. Rev. 140, A67 (1965).
- [4] C. P. Bhalla, Phys. Rev. A 12, 122 (1975).
- [5] C. P. Bhalla, J. Phys. B 8, 2787 (1975).
- [6] C. Froese Fischer, Comp. Phys. Commun. 4, 107 (1972).

INTERPRETATION SCHEMES FOR CORE ELECTRON EXCITATION SPECTRA OF SMALL MOLECULES

W.H. Eugen Schwarz, Institute of Theoretical Chemistry,
University of Bonn and Gesamthochschule Siegen,
Wegeler Str. 12, D 5300 Bonn, Germany

1. Introduction

In order to obtain chemical information on a molecule from an experimental X-ray absorption spectrum, one has usually at first to assign it within the one-electron-orbital representation. This can be achieved on the basis of more or less sophisticated ab initio calculations. However, often it is sufficient to have recourse to simple rules of thumb and to other experimental data. Several model concepts of this kind will be discussed below. Examples are presented, for which these models work, and also other ones, which exhibit specific deviations from the simple schemes. Explaining such "irregularities" will help to get a deeper understanding of the physics of core electron excitation phenomena in molecules.

2. The Equivalent Core or Z+1 Core Analogy Model

The basic premise of this model (1-4) is that the energy levels and valence shell properties of a system with an excited core electron (Z^*) should be very similar to those of a species with one more proton in the nucleus and a fully occupied core shell (Z+1). This model is applied in two directions: 1) If the valence electron spectrum of the Z+1 molecule is known, this helps to assign the Z^* spectrum. 2) If the Z+1 species is a radical difficult to investigate, its properties may be deduced from the Z^* spectrum (3-10).

2.1 Geometric Corrections

2.1.1 caused by different valence configurations of the initial states of the Z and the Z+1 molecules

2.1.1.1 Bond length effects: Since in their ground states the Z+1 molecule has one more valence electron (of antibonding character in most cases), the equilibrium bond lengths

of the ground state of Z , of its core excited Rydberg and ionized states, and of the Rydberg states of $Z+1$ are very similar, but are different from that of the ground state of $Z+1$. Therefore the vibrational structure of the excitations 1) core to valence of Z ; 2) core to Rydberg or free electron of Z ; 3) valence to Rydberg of $Z+1$; exhibit specific differences. They explain some of the discrepancies already showing up in diatomics (11). Neglecting them means to identify vertical and adiabatic ionization potentials and electron affinities.

2.1.1.2 Bond angle effects: Since bond angles are more sensitive than bond lengths, bond angle effects may be quite drastic in polyatomic molecules (12,13). Not only valence but also Rydberg orbitals may undergo significant changes.

2.1.2 Geometric corrections caused by different core sizes. The closed shell core of $Z+1$ is slightly more compact than the core shell of core excited Z^* . This effect will be of significance for very light atoms only. It then results in Franck-Condon shifts not only of valence but also of Rydberg transitions (9). Whereas core to Rydberg excitations usually show very short vibrational progressions, the contrary holds for compounds of light atoms like Li.

2.2 Exchange and Coulomb Corrections

2.2.1 Exchange effects

The exchange interactions of the valence electrons with the closed shell core of $Z+1$ and with the open shell core of Z^* is not negligible in many cases (4,6,9,13). A rough rule states that the doublet to doublet term values of $Z+1$ correspond to the singlet to triplet term values of core excited Z^* , whereas the singlet to singlet term values of Z^* are smaller by twice the exchange integral.

2.2.2 Corrections due to different Coulomb interactions.

So far we have accepted the frozen orbital approximation which, however, will result in significant errors for pene-

trating orbitals of light atoms, since they perceive different effective nuclear charges in the $Z+1$ and Z^* systems (9,14).

3. The 'Constancy of Rydberg Term Values' Model

Whereas in section 2 we have compared the core spectrum of Z^* with the UV spectrum of $Z+1$, we will now compare with the UV spectrum of Z . At least the Rydberg term values are transferable from valence to core excitations in many cases (15-17), but sometimes this model fully breaks down.

3.1 The 's-Type Rydberg' Difficulty

The lowest Rydberg MO's, especially those of s-type, are very sensitive to perturbations by virtual valence orbitals. The most dramatic example is represented by the core spectra of second row hydrides (8,18).

3.2 Exchange and Coulomb Corrections

Even within the frozen orbital approximation two corrections have to be applied to the model (11): The difference in exchange energies of the core and valence excited states will usually increase the term values of the core excitations. The difference in Coulomb energies is difficult to predict generally. It is symmetry-dependent, but will often decrease the term values.

3.3 Comment on Selection Rules

The atomic symmetry symbols of core excitations do not represent the molecular symmetry. E.g. $C1s$ to $3s$ is electronically forbidden in CH_4 but not in other hydrocarbons. The short and long range behavior of MO's may be very different.

4. SCF Models

4.1 Equivalent Ionic Core Virtual Orbital Model

The term values of core excitations are approximately given by the virtual orbital energies of the $Z+1$ species. Although this model neglects the exchange and coulomb corrections, it is usually of much help (8-10,13).

4.2 Correlation Corrections

Usually the model underestimates the term values, because orbital reorganization has been neglected and because the correlation energy will often increase with the number of electrons. The contrary happens, if the excited electron strongly disturbs the correlation of the other valence electrons as in the case of CO₂ (13). Specific correlation effects occur in molecules with two equivalent nuclei (14).

4.3 Koopmans' Theorem

Koopmans' Theorem is useful to estimate the magnitude of extra structure due to core orbital splittings. Failure of Koopmans' theorem (14,19) may sometimes be explained by a rule based on Green's Function method (11,20).

4.4 Intensities

Although intensities predicted within the framework of the independent particle model are often qualitatively correct (8,9,21), initial and final state correlations have an enormous effect in other cases (11).

- 1 M.Nakamura et al. Phys.Rev. 178(1969)80
- 2 W.L.Jolly,D.N.Hendrickson JACS 92(1970)1863
- 3 G.R.Wight,C.E.Brion,M.J.Van der Wiel J.El.Spect. 1(1973)
457
- 4 W.H.E.Schwarz Ang.Chem.Intern.Ed. 13(1974)454
- 5 W.H.E.Schwarz Ber.Bunsenges. 78(1974)1206
- 6 G.R.Wight,C.E.Brion J.El.Spect. 4(1974)313
- 7 G.R.Wight,C.E.Brion Chem.Phys.Let. 26(1974)607
- 8 W.H.E.Schwarz Chem.Phys. 11(1975)217
- 9 K.Radler et al. Chem.Phys. 13(1976)363
- 10 M.E.Schwartz Chem.Phys.Let. 40(1976)1
- 11 W.H.E.Schwarz et al. to be published
- 12 G.R.Wight,C.E.Brion J.El.Spect. 3(1974)191
- 13 W.H.E.Schwarz,R.J.Buenker Chem.Phys. 13(1976)153
- 14 W.H.E.Schwarz,T.C.Chang Int.J.Quant.Chem. 10S(1976)ooo
- 15 F.J.Comes,U.Nielsen,W.H.E.Schwarz J.Chem.Phys. 58(1973)
2230
- 16 M.B.Rubin Chem.Phys.Let. 31(1975)140
- 17 U.Nielsen,W.H.E.Schwarz Chem.Phys. 13(1976)195
- 18 W.H.E.Schwarz Chem.Phys. 9(1975)157
- 19 F.J.Comes et al. J.Chem.Phys. 58(1973)516
- 20 L.S.Cederbaum Chem.Phys.Let. 25(1974)562
- 21 U.Nielsen,R.Haensel,W.H.E.Schwarz J.Chem.Phys. 61(1974)
3581

AN AB INITIO CALCULATION OF A VIBRATIONAL STRUCTURE IN X-RAY SPECTRA OF MOLECULES

L.N. Mazalov, F.K. Gel'mukhanov, A.V. Kondratenko, and V.I. Avdeev
Institute of Inorganic Chemistry
Novosibirsk, USSR

We suggested a theory of a vibrational structure in X-ray spectra of molecules in a one-particle approximation in [1]. An X-ray fluorescence arises as a result of an inelastic scattering of an X-ray photon with a frequency ω by a molecule ($\hbar = m = e = 1$)

$$\begin{aligned} \frac{d\sigma}{d\Omega'} &\sim \sum_{\nu k} |W_{\nu i} W'_{ki}|^2 \sum_{\hat{n}_{\nu k}} \delta(\omega' - \omega + \epsilon_{\nu} - \epsilon_k + \hat{\omega}^{\nu k} \hat{n}_{\nu k} + \Delta\epsilon^{\nu k}) \\ &\times \left| \sum_{\hat{n}_{\nu i}} \frac{\langle \hat{n}_{\nu k} | \mu^{\nu k+} \mu^{\nu i} | \hat{n}_{\nu i} \rangle \langle \hat{n}_{\nu i} | \mu^{\nu i+} | \hat{0} \rangle}{[\omega' - (\epsilon_k - \epsilon_i + \hat{\omega}^{\nu i} \hat{n}_{\nu i} + \Delta\epsilon^{\nu i} - \hat{\omega}^{\nu k} \hat{n}_{\nu k} - \Delta\epsilon^{\nu k})] + i\frac{\Gamma}{2}} \right|^2 \\ &= G(\omega') + IG(\omega'). \end{aligned} \quad (1) \quad (1)$$

Here $G(\omega')$ - the main member, $IG(\omega')$ describes an interference between vibrational sublevels of intermediate states. An absorption cross section of a photon with a frequency ω has a form

$$\sigma_a \sim \sum_{\nu i} \sum_{\hat{n}_{\nu i}} |W_{\nu i}|^2 \frac{\frac{\Gamma}{2\pi} |\langle \hat{n}_{\nu i} | \mu^{\nu i+} | \hat{0} \rangle|^2}{[\omega - (\epsilon_{\nu} - \epsilon_i + \hat{n}_{\nu i} \cdot \hat{\omega}^{\nu i} + \Delta\epsilon^{\nu i})]^2 + \frac{\Gamma^2}{4}} \quad (2)$$

In Eqs. (1) and (2) $|\langle \hat{n}_{\nu i} | \mu^{\nu i+} | \hat{0} \rangle|^2$ and $|\langle \hat{n}_{\nu k} | \mu^{\nu k+} \mu^{\nu i} | \hat{n}_{\nu i} \rangle|^2$

-Franck-Condon factors, $U^{\nu i}$ - the unitary shift operator. A vibrational structure in X-ray and ESCA- spectra of molecules N_2 , CO, BF, HF, HCl are calculated from Eqs. (1), (2). A good agreement with experiment is obtained, when experimental data are available [2].

References

1. F.K. Gel'mukhanov, L.N. Mazalov, A.V. Nikolaev, A.V. Kondratenko, P.I. Wadash, V.G. Smyrny, A.P. Sadovskii, Dokl. Acad. Nauk SSSR 225, N3 (1975).
2. L.O. Werme, J. Nordgren, H. Ågren, C. Nordling and K. Siegbahn, UUIP-876 (1974).

SOFT X-RAY ABSORPTION OF MOLECULAR ALKALI-HALIDES

K. Radler, B. Sonntag, and H.W. Wolff

II. Institut für Experimentalphysik, Universität Hamburg,
D-2000 Hamburg, Germany

The absorption spectra of molecular LiF, LiCl, NaCl, CsF, CsCl, and CsBr have been determined in the energy region of the Li^+1s , $\text{Na}^+2p,2s$ and Cs^+4d transitions. The alkali-halide vapours were contained in a tubular furnace mounted in front of a 2 m grazing incidence spectrograph. The synchrotron radiation of the 7.5 GeV electron synchrotron DESY, transmitted through the vapour column, was registered on photographic plates bent along the Rowland circle.

The absorption bands dominating the spectrum of molecular LiF at the onset of the Li^+1s transition are presented in Fig. 1. Due to the high concentration of dimers present in the vapour there is a considerable overlap of the spectra of LiF and Li_2F_2 . By analyzing the vibrational structure superimposed on the broad bands the contributions of monomers and dimers can be separated. The assignment of the bands (1), based on SCF calculations, is indicated in Fig. 1.

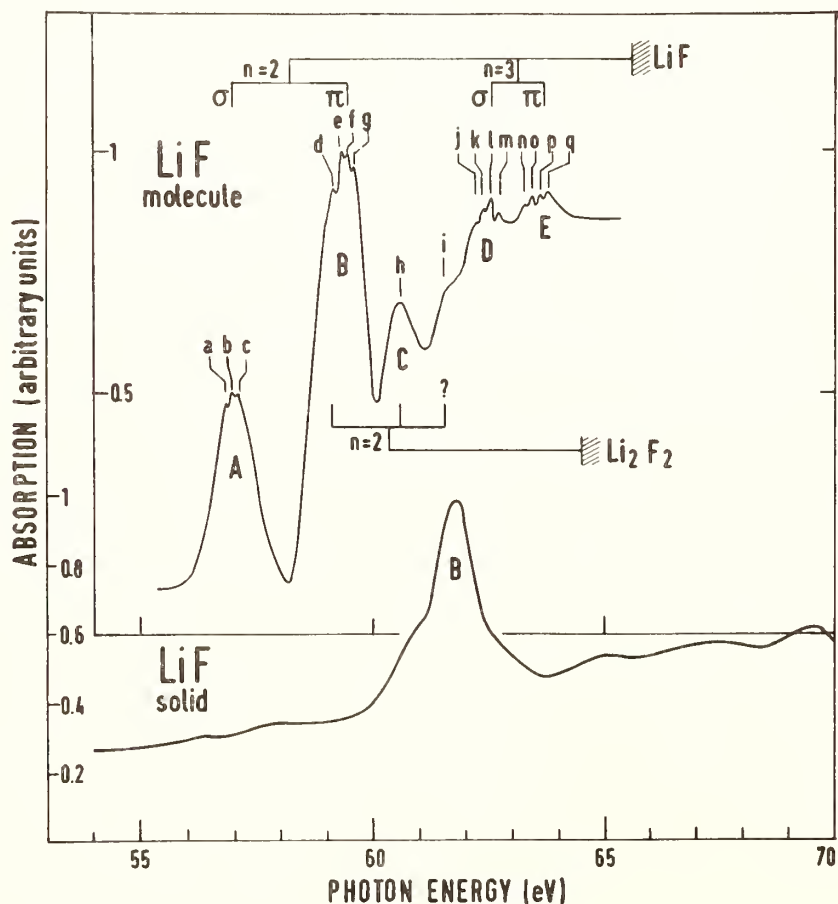


Fig. 1 Li^+1s absorption of molecular and crystalline LiF

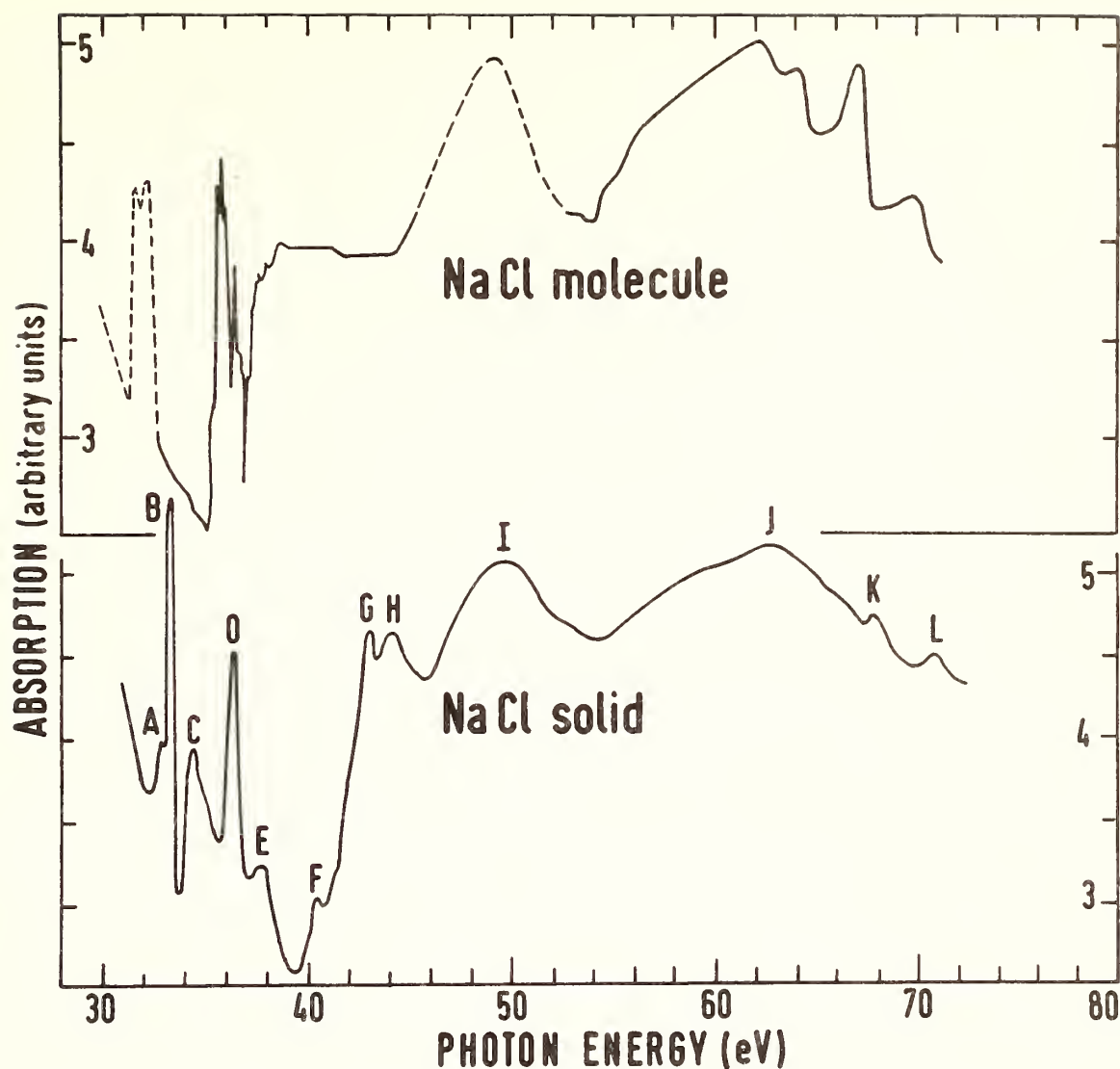


Fig. 2 $\text{Na}^+2p,2s$ absorption of molecular and crystalline NaCl

A doublet shows up at the threshold of the Na^+2p excitations in molecular NaCl (Fig. 2). Towards higher energies this doublet is followed by absorption bands, which show a rich vibrational fine structure. The low energy doublet and the maximum at 50 eV are only given by a dashed line because of the uncertainties involved in the determination of the relative heights. Transitions from the Na^+2s level give rise to the maxima at 64.5 eV, 67.5 eV and 70.2 eV. In the framework of a simple ionic model the absorption bands at the onset of the $\text{Na}^+2p,2s$ transitions can be ascribed to transitions to final states mainly originating from the 3s, 3p and 3d states of the free Na^+ ion. The same final states have been invoked by Åberg and Dehmer for the interpretation of the exciton lines A to E detected in the spectra of crystalline NaCl (2). Above 45 eV there is a striking similarity of the spectra of molecular and crystalline NaCl.

Close correspondence has also been found between the Cs^+4d spectra in molecular and crystalline CsCl (3). The absorption spectra of molecular

and crystalline CsF, CsCl and CsBr at the Cs^+4d threshold are presented in Fig. 3. In all molecular spectra there is a weak peak A at the onset followed by four prominent bands B, B', C, C'D. The separation of B, B' and C, C' is determined by the spin orbit splitting of the 4d hole. These bands are due to transitions of the Cs^+4d electrons to final states with dominant $\text{Cs}^+6s, 6p$ parentage. Going from the molecular Cs halides to the crystalline Cs-halides the small peak A persists whereas the maxima B, C and B', C' coalesce. The strong band E shows up at almost the same energy in all spectra. In contrast to this the other maxima shift considerably. The insensitivity of the peak position to the environment supports the assignment of E to transitions to highly localized f-symmetric final states. This is in agreement with Hartree-Fock calculations for the $\text{Cs}^+4d^9 4f$ states.

1. K. Radler, B. Sonntag, T.C. Chang, and W.H.E. Schwarz, Chem.Phys. 13, 363 (1976)
2. T. Åberg and J.L. Dehmer, J.Phys. C6, 1450 (1973)
3. K. Radler and B. Sonntag, Chem.Phys.Lett. 39, 371 (1976)

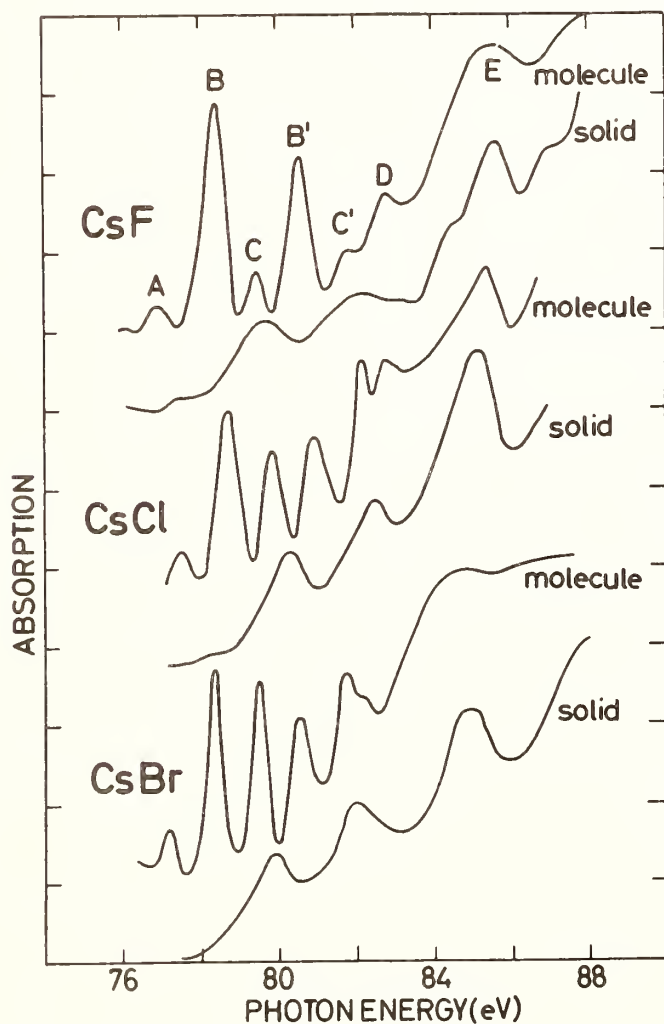


Fig. 3

Cs^+4d absorption of molecular and crystalline CsF, CsCl and CsBr.

INTERPRETATION OF THE X-RAY EMISSION AND PHOTO-ELECTRON SPECTRA OF SIMPLE SOLID COMPOUNDS

G. Leonhardt, A. Kosakow, H. Sommer, M. Petke
Sektion Chemie der Karl-Marx-Universität,
DDR-701 Leipzig, Linnéstr. 2

We have investigated the electronic structure of the valence bands of some $A^{IV}B^{VI}$ - and A_2B_3 -compounds using X-ray emission and photoelectron spectroscopy. The Ge $K\beta$ emission and K absorption spectra of GeS and the As $K\beta$ band of As_2O_3 were measured with a double crystal spectrometer (secondary excitation, experimental resolution about 1.5 eV) [1,2]. The photoelectron spectra excited by UV- and Al $K\alpha$ -radiation (VG instrument, resolution 0.2 and 1.2 eV, resp.) were got from evaporated samples of GeS, GeSe, GeTe, As_2O_3 , As_2S_3 , Sb_2O_3 , and Bi_2O_3 (base pressure 10^{-9} torr, substrate temperature $20^\circ C$). The results are shown in fig. 1-3 and tab.1.

Having in mind the interpretation of the valence bands of the A^NB^{8-N} and A^NB^{10-N} crystals [3,4,5] one can conclude:

1.) The valence band is built up from two lower bands with mainly s-character and several p-bands on the top. The symmetry character of the states can be derived from the X-ray emission (see fig.1 and 2). For an exact calculation of the shape of the X-ray spectra, a computation of the transition probability involved is needed [6]. In the calculation of the photoelectron spectra, there are important cross products [7] and final hole state effects [8].

2.) The energy distance between the s-bands and the width of the antisymmetric gap can be described by a chemical bond parameter with an accuracy of several 0.1 eV. A model including covalent and ionic parts gives better agreement with the experiment than a pure ionic model including Madelung and polarisation corrections. The ionic part can be described via a Madelung energy. Conclusions concerning the absolute energy scale of the spectra can also be made.

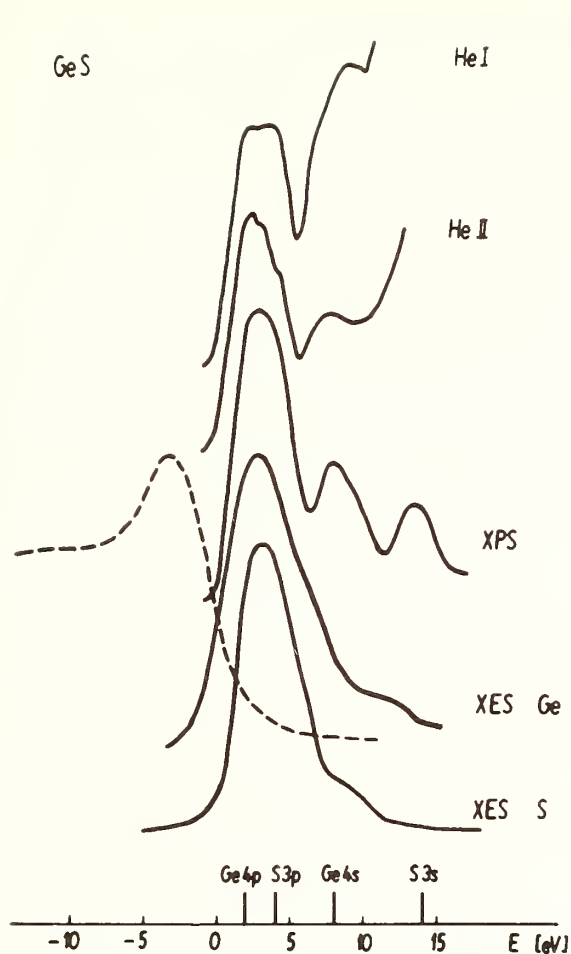


Fig.1 Photoelectron spectra excited by X- and UV-radiation and Ge K β - and S K β -emission bands of GeS (in the lower part are given the atomic ionization energies)

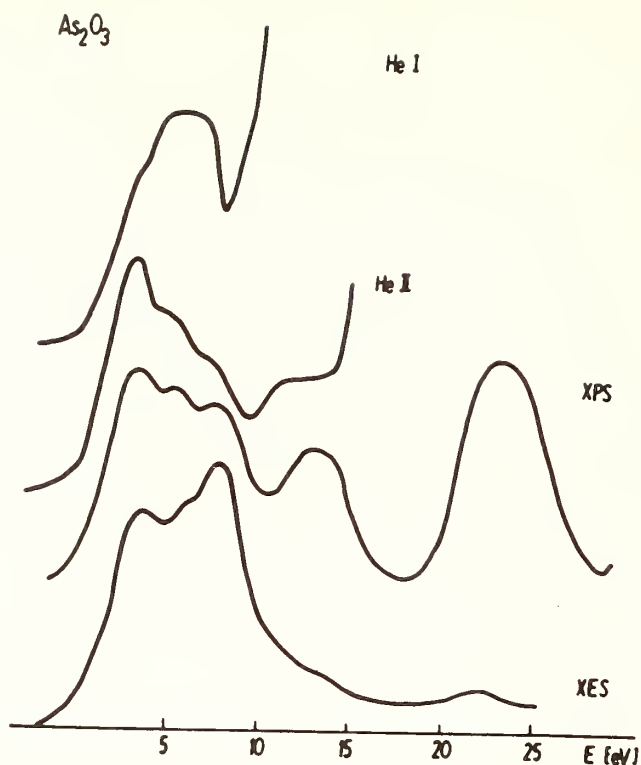


Fig.2 Photoelectron spectra and the As K β emission band of As_2O_3

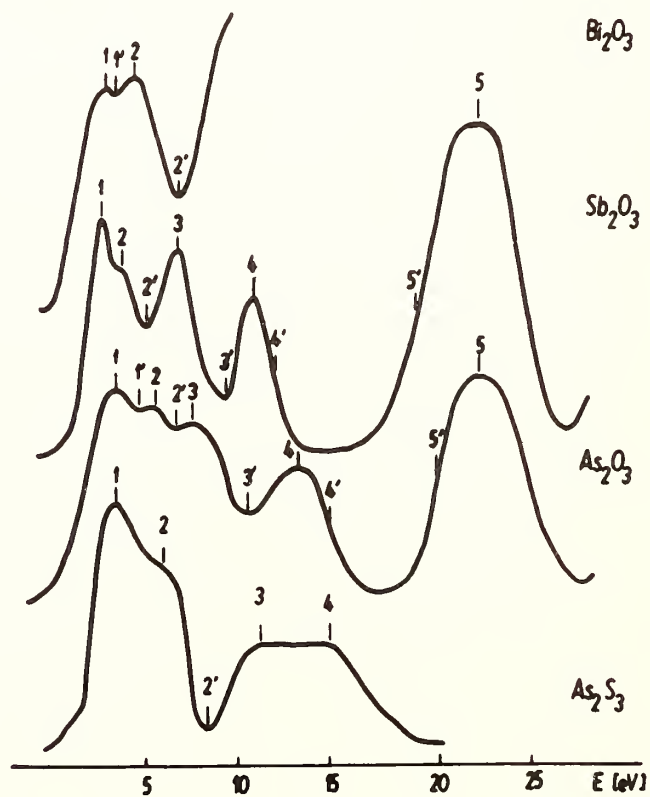


Fig.3 X-ray photoelectron spectra of As_2O_3 , Sb_2O_3 , Bi_2O_3 , and As_2S_3

3.) The p-bands on the top of the valence band can be described by an LCAO-model. For the IV-VI compounds we have got a good agreement between experiment and such a calculation[9].

Table 1. Energies of characteristic structures of the spectra (all values in eV relative to the top of the valence band)

Label of the structure	Bi ₂ O ₃	Sb ₂ O ₃	As ₂ O ₃	As ₂ S ₃	GeS	GeSe	GeTe
1	2.9	1.8	3.6	2.0	2.2	1.9	1.5
1'	3.3		4.5				
2	4.5	3.7	5.55	4.2	3.5	3.0	3.0
2'	6.8	4.4	6.45	6.9			4.0
3		5.5	7.65	11.2	4.9	4.15	4.5
3'		8.6	10.5		6.6	6.5	6.4
4		9.9	13.35	15.0	8.1	8.2	8.2
4'		11.0	15.3		11.5	11.5	9.8
5		22.0	23.2		13.6	13.9	12.5
5'		19.0	20.6				
Width of p-states	6.8	8.6	10.5	6.9	6.6	6.5	6.4
Width of the valence band		24.7	25.5	18	15.8	15.8	14.7

References

- 1 A.Kosakow, G.Graeffe a.o., to be published
- 2 I.Topol, J.Tilgner, G.Leonhardt, A.Meisel, J.Phys.Chem.Sol. 35(1974), 1657
- 3 S.P.Kowalczyk, L.Ley a.o., J.chem.Phys. 61(1974), 2850
- 4 G.Leonhardt, J.Electr.Spectr. 5(1974), 603
- 5 G.Leonhardt, A.Kosakow, H.Sommer, Proc.Int.Symp.ESCA, Kiev 1975, in press
- 6 I.Topol, K.Unger a.o., phys.stat.sol.(b) 61(1974), 485
- 7 A.Kosakow, K.Unger, G.Leonhardt, phys.stat.sol., in press
- 8 A.Kosakow, E.Kurmajew, G.Leonhardt, to be published
- 9 A.Kosakow, H.Neumann, G.Leonhardt, to be published

THE OXYGEN X-RAY EMISSION SPECTRUM OF SOME OXYANIONS

N. Kosuch, E. Tegeler, G. Wiech and A. Faessler

Sektion Physik der Universität München, 8 Munich 40, Germany

The O K-emission spectrum of ions of the type XO_2^- , XO_3^{n-} , and XO_4^{n-} were excited in fluorescence using the synchrotron radiation of the storage ring DORIS in Hamburg and recorded in a 2m concave grating spectrometer with an open multiplier. The main intensity of the spectra with pronounced structures appears between 520 and 530 eV, a structure of very low intensity is observed at 500-510 eV. Positions and relative intensities of the structural features differ considerably depending upon the nature of the central atom and the symmetry of the anion. The nature of the cation is without noticeable influence.

For many of the anions studied, as for CO_3^{2-} and PO_4^{3-} , photoelectron spectra (XPS) of the valence states are available. In some cases where the binding energy of the O 1s level with respect to the vacuum level was determined, an unambiguous correlation of photoelectron and X-ray spectra is possible. In the examples mentioned above the X-ray spectra of the central atoms are also known. They provide additional information on the sequence and position of the orbitals and the symmetry character of the valence electrons.

Fig. 1 shows the O K-spectrum of CO_3^{2-} . The C K-spectrum of CO_3^{2-} was also measured and is shown below. The photoelectron spectrum and results of a MO-calculation (1) fitted to the main maximum of the O K-spectrum are shown above. There is good correspondence between the experimental observations. The calculated orbitals can be satisfactorily

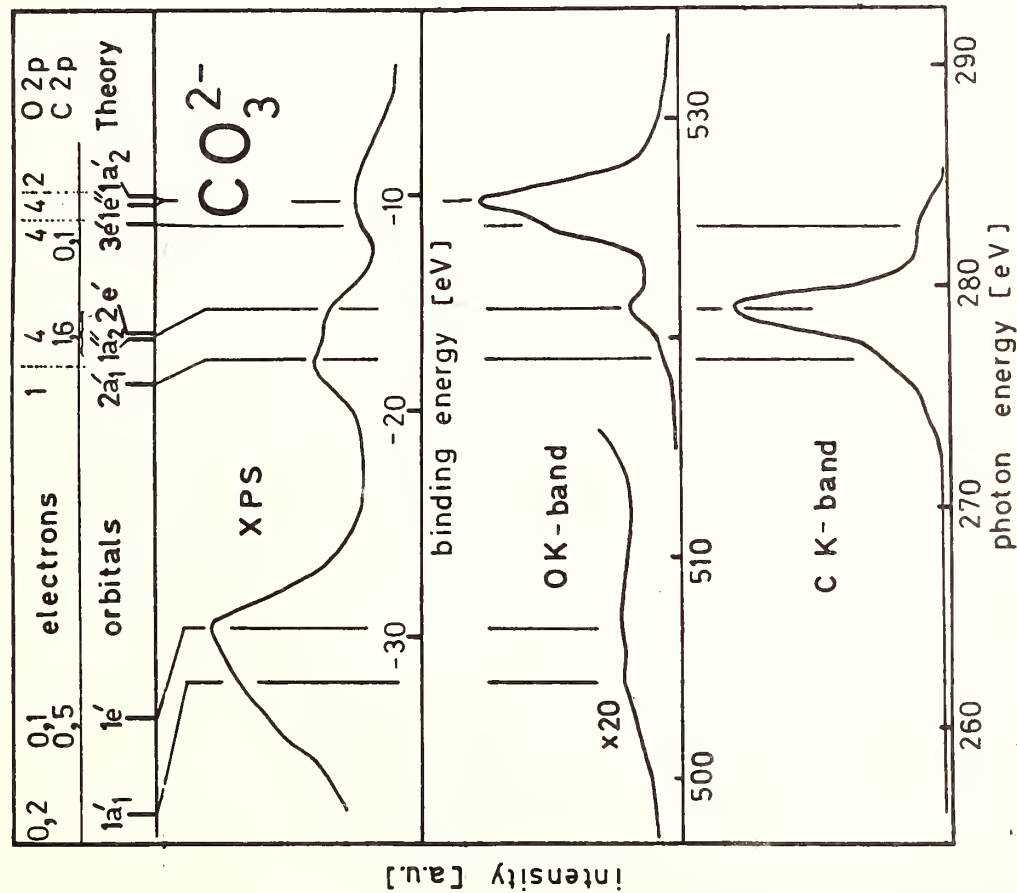


Fig. 1. O K- and C K-spectrum of CO_3^{2-} together with photoelectron spectrum and MO-calculations

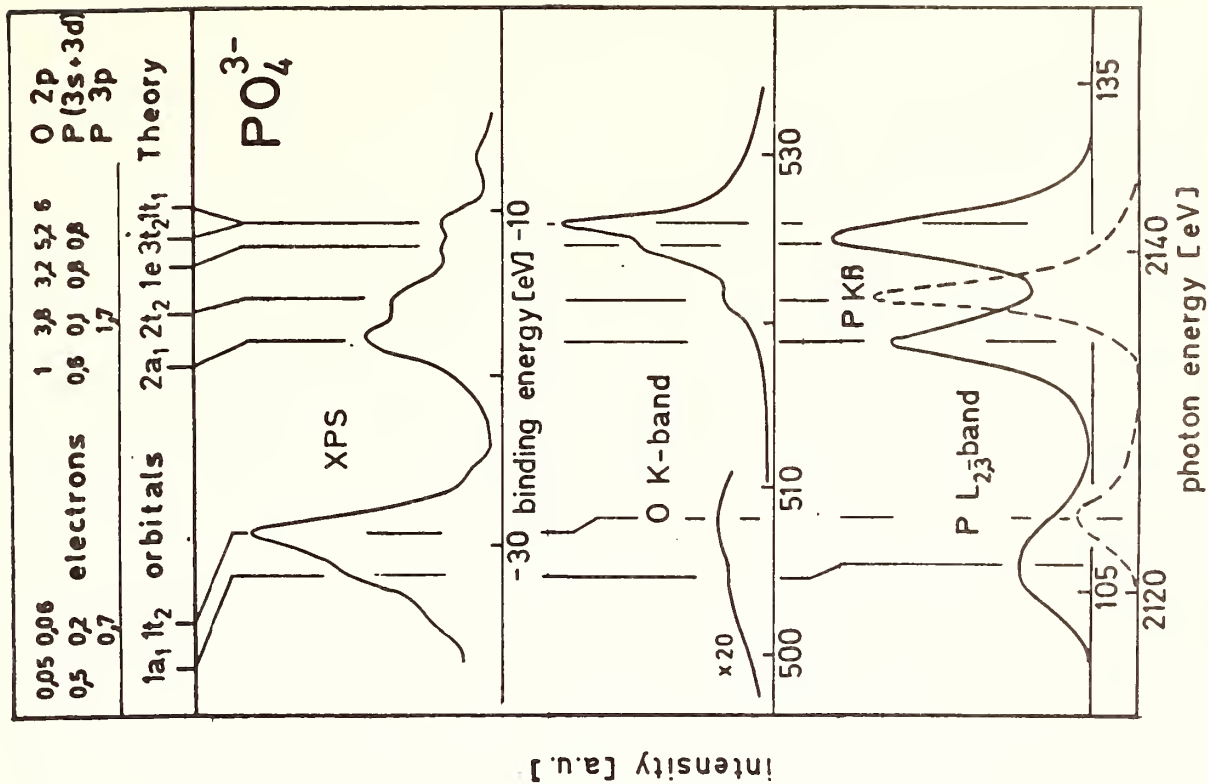


Fig. 2. O K-spectrum of PO_4^{3-} together with $\text{P K}\beta^-$, $\text{P L}_{2,3}^-$, photoelectron spectrum, and MO-calculations

coordinated to the structural features of the spectra, but the energy position of the orbitals is not quite in agreement with the experimental data. The regions of high intensity of the oxygen and carbon spectra correspond to the orbitals with high population of O 2p- and C 2p-electrons, respectively.

In Fig. 2 the O K-spectrum of PO_4^{3-} is shown together with the $\text{K}\beta$ - and $\text{L}_{2,3}$ -spectrum (2,3) of the central phosphorus atom. In this case we obtain information on the valence electrons not only with p symmetry but also with s and d symmetry. The photoelectron spectrum (4) and results of MO-calculations of PO_4^{3-} (1) are also shown. The correspondence of the orbitals to the features of the spectra is again satisfactory, with the exception of discrepancies at lower energies. It will be seen that in the case of PO_4^{3-} the X-ray spectra provide more detailed informations concerning the energy of the orbitals and the symmetry character of the electrons than do the photoelectron spectra. Here too the orbitals with high electron population correspond to high intensity of the corresponding X-ray transitions.

References:

- (1) J.A. Connor, I.H. Hillier, V.R. Saunders, and M. Barber,
Molec. Phys. 23, 81 (1972)
- (2) M. Fichter, Spectrochim. Acta B 30, 417 (1975)
- (3) G. Wiech, Z. Physik 216, 472 (1968)
- (4) V.I. Nefedov, Yu.A. Buslaev, N.P. Sergushin, Yu.V. Kokunov,
V.V. Kovalev, L. Bayer, J. Electron Spectrosc. 6, 221 (1975)

X-RAY INVESTIGATION OF THE ENERGY LEVEL STRUCTURE OF TETRAEDRICALLY COORDINATED TRANSITION METAL ATOMS

R. Szargan and A. Meisel, Karl-Marx-Universität Leipzig
701 Leipzig DDR Linnéstr. 2

The X-ray emission bands and the photoelectron spectra of the core and valence regions of the tetraedrical oxyanions and thioanions of some 3d and 4d elements have been measured /1,2/. To determine the order of energy levels the presented experimental results were analyzed with the aid of published ab initio /3,4/ and semiempirical calculations. Discrepancies in the results of recently published XPS /4,5/, UPS /7,8/, X-ray emission /9,10/ and optical absorption work /11,12/ on this subject are discussed and details open to question are pointed out. The value of the above mentioned techniques in confirming the assignment of the electronic structure is illustrated in the light of limited resolution and accuracy in photon and electron binding energy measurements.

References

- 1 R. Szargan, E. Suoninen et al., Spectrochim. Acta B, :
2 R. Szargan, unpublished result in press
- 3 I. H. Hillier and V.R. Saunders, Chem. Phys. Letters and
2 (1971) 219, and references therein
- 4 J. A. Connor, I. H. Hillier et al., Mol. Phys. 24 (1972) 497
- 5 R. Prins and T. Novakov, Chem. Phys. Letters 16 (1972) 86
- 7 E. Diemann and A. Müller, Chem. Phys. Letters 19 (1973) 538
- 8 S. Foster, S. Felps et al., J. Amer. Chem. Soc. 95 (1973) 5521
- 9 D. W. Fischer, J. Phys. Chem. Solids 32 (1971) 2455
- 10 A. P. Sadowski, Izv. Sib. Otd. Akad. Nauk SSSR, Ser. Chim.
2 (1975), 62
- 11 S. Foster, S. Felps et al., J. Amer. Chem. Soc. 95 (1973) 6578
- 12 A. Müller and E. Diemann, Chem. Phys. Letters 2 (1971) 369

ON THE 1S-ABSORPTION LINE SPECTRA OF LI IN LITHIUM HALIDES AND OF B IN BCL₃ AND BF₃

T. Hayasi Iijima-cho Nagano-ken Japan 399-37.
and Y. Hayasi Department of Applied Physics, Faculty of Engineering, Tôhoku University, Sendai Japan 980.

1. An attempt was made for interpretation of the chemical shift of absorption threshold and the line absorption spectra appearing near the threshold. For this purpose we calculated the x-ray terms of free atom and ions. We considered also the bond dissociation energies, which are necessary to define the initial states of the atoms and ions. The results are compared with the measured absorption peaks of Li 1s-absorption spectra in Li-halides and of B 1s-absorption spectra in BCl₃ and BF₃. In the following the method is illustrated by application to Li 1s-absorption spectra.

2. The 1s-excited states of Li atom as a whole are approximately calculated by the following procedure. The Li 1s² ion has two terms 1s2s ^{1,3}S as the lowest 1s-excited states of the ion. Adding a 2s electron to these states results in two Li 1s2s² ²S, which are the low energy 1s-excited states of a neutral Li atom. For simplicity we assume that these two ²S terms have the same energy separation as that of the parent terms, this assumption is approximately valid in the optical energy levels (1). The error is estimated about 10 per cent or less of the parent term separation.

The method to obtain the term values of the two ²S terms is as follows. Adding a 2s electron to Be 1s²2s and Li 1s²2s leads to Be 1s²2s², Li 1s²2s² respectively, where the spin of core 1s² is 0. If the spin of the 1s electron in Li 1s2s is ignored, which we denote by 1s', then Li 1s'2s becomes iso-electronic with Be 1s²2s, Li 1s²2s. Upon them we apply the procedure of iso-electronic sequence.

The effective core charges Z_e are defined by term values T of Li 1s²2s ²S, Be 1s²2s² ²S and Li 1s'2s² ²S respectively, expressed as $T = RhcZ_e^2/n^2$ for $n=2$, taking the core states Li 1s², Be 1s², Li 1s' as $T=0$. Optically known term values of Li 1s²2s² ²S, Be 1s²2s² ²S determine Z_e of Li 1s² and Be 1s² respectively. For the term value of Li 1s'2s, we assume Li 1s' - Li 1s'2s is equal to the mean value of Li 1s - Li 1s2s ^{1,3}S, then we obtain the Z_e for Li 1s'.

The term Be 1s²2s² is optically known, referred to $T=0$ mentioned above, and the term Li 1s²2s² is the sum of electron affinity 0.82 eV and 1s² - 1s²2s. If we assume, as a modified Moseley's law, that the x-ray term value T is proportional to the effective core charge square Z_e^2 , then the term Li 1s'2s² is obtained by linear interpolation.

Subsequently the term Li 1s2s² ²S is obtained from Li 1s'2s² ¹S; since the separation ¹S - ²S in the parent terms approximately remains, the former lies lower than the latter by half the separation of Li 1s2s ^{1,3}S terms. Another term Li 1s2s(³S)2s ²S lies lower than this by the separation of the parent terms. So we find Li 1s2s(³S)2s ²S - Li 1s²2s² ²S = 54.97 eV. This corresponds to the 1s-excitation threshold of a free Li atom, to which the transition from 1s²2s² ²S is allowed by the selection

$\Delta J = 0, \pm 1$ for jj-coupling.

This method is applied also to obtain the term of the ls-excited state $1s2p(^1P)2s\ ^2P$ or other states by repeating the procedure from the beginning. The energies of ls-excited states of Li atom of small quantum number, referring to the ground state, are shown in Table 1.

Table 1. The ls-excitation energies from the ground state for Li atom in eV.

$1s2s(^3S)2s\ ^2S$	54.97	$1s2s(^3S)3s\ ^2S$	62.37
$1s2s(^1S)2s\ ^2S$	56.71	$1s2s(^1S)3s\ ^2S$	63.78
$1s2p(^3P)2s\ ^2P$	57.32	$1s2s\ ^3S, e$	64.41
$1s2p(^1P)2s\ ^2P$	58.86	$1s2s\ ^1S, e$	66.15

3. The bond energy determines the energy of the atom as a whole. Generally any ls-excitation breaks or changes the bond. As a result the energy required for ls-excitation is larger than that for the free atom by the amount of bond energy change, which means the shift of free atom spectra.

The bond energy D^0 for lithium halides are, in eV (2)

Li-F 6.00, Li-Cl 4.91, Li-Br 4.37, Li-I 3.66

The calculated ls-excitation energies of Li atom in lithium halides are compared with the absorption peaks measured by Haensel, Kunz and Sonntag (3) as shown in Table 2, where fairly well agreements are found.

Table 2. The ls-excitation energies of Li atom in lithium halides and the photon energies of absorption peaks measured, in eV.

D^0	LiF		LiCl		LiBr		LiI	
	6.00		4.91		4.37		3.66	
	Meas.	Calc.	Meas.	Calc.	Meas.	Calc.	Meas.	Calc.
A	61.13	60.97	60.75	59.88	60.44	59.34	59.42	58.65
B	61.91	62.71	62.87	61.62	61.68	61.08	59.82	60.37
		63.32		62.25		61.69		60.98
C	64.9	64.86	63.54	63.77	62.96	63.23	61.5	62.52
D	67.4	68.37	65.4		64.8		65.6	66.05
				67.28		66.74		67.44
E	69.6	69.78	68.8	68.69	67.7	68.15		68.07
						68.78		69.81
F					70.2	70.52	71.4	

4. The ls-excitation energies of B atom are calculated in a similar procedure as in the case of Li atom. Table 3 shows the ls-excitation energies from the ground state in eV for free B atom.

Table 3. The ls-excitation energies for B atom in eV from the ground state $1s^2 2s^2 2p\ ^2P$ to $1s2s^2 2p^2$

4P	185.703, 2D	186.807, 2S	188.240, 2P	188.323, 2D	189.427, 2S	190.860
-------	----------------	----------------	----------------	----------------	----------------	---------

Bond energies for BCl_3 and BF_3 are taken in eV (2). The ls-excited B atom behaves almost like C atom for valence bonds. We can obtain the energies needed for bond changes $BCl_3 - CCl_2$ 6.28, $BCl_3 - CCl$ 10.22, $BCl_3 - B$ 13.65 and $BF_3 - CF_2$ 8.31, $BF_3 - CF$ 13.61, $BF_3 - B$ 19.15 in eV.

In Table 4 the photon energies of ls-absorption peaks of BCl_3 measured by Fomichev and Barinski(4) are compared with the calculated ls-excitation energies. In Table 5 the photon energies of ls-absorption peaks measured by Fomichev(5) of BF_3 are compared with the calculated ls-excitation energies. In both Tables we find almost agreements.

Table 4. The photon energies of measured absorption peaks of B for BCl_3 (4) and the calculated ls-excitation energies of B, in eV.

Measured peaks	Calculated ls-excitation energies with bond change			
	$\text{BCl}_3 - \text{B}$ 13.65	$\text{BCl}_3 - \text{CCl}$ 10.22	$\text{BCl}_3 - \text{CCl}_2$ 6.28	
a 192.4			191.98	
b 195.4			193.08	
c 194.4			194.52	194.60
d 195.8		195.92	195.90	
e 197.3		197.02	197.14	
f 198.7		198.46 198.54		
	199.35 200.45	199.64		
	201.89 201.97	201.08		
	203.07 204.51			

Table 5. The photon energies of measured absorption peaks of B for BF_3 (5) and the calculated ls-excitation energies of B, in eV.

Measured peaks	Calculated ls-excitation energies with bond change			
	$\text{BF}_3 - \text{B}$ 19.15	$\text{BF}_3 - \text{CF}$ 13.61	$\text{BF}_3 - \text{CF}_2$ 8.31	
a 195.4			194.01 195.11	
			196.55 196.63	
b 198.3		199.31	197.74 199.17	
c 200.7		200.41		
d 202.3(202-203)		201.85 201.93		
		203.03		
e 205.8	204.85 205.95	204.47		
(205.5-209)	207.39 207.47			
	208.57			
f 212(210-212)	210.01			

5. In conclusion the ls-absorption line spectra near the threshold of the bonded atom are interpreted as the ls-excitation spectra of free atom shifted by the energy of bond changes, or the superposition of those spectra.

- (1) C.E. Moore, Atomic Energy Levels I, NBS-Circular 467 1949, Cf. e.g. O II $3s^4P$, $3s^3 2D$, $3s^2 2S$.
- (2) B.deB. Darwent, Bond Dissociation Energies in Simple Molecules, NSRD S-NBS 31 1970. V.I. Vedeneyev et al, Bond Energies, Ionization Potentials and Electron Affinities, Acad. Sci. USSR Moscow 1962.
- (3) R. Haensel, C. Kunz and B. Sonntag, Phys. Rev. Letters 20 262, 1968.
- (4) B.A. Fomichev and R.P. Barinski, J. Str. Chimi, 11 875, 1970.
- (5) B.A. Fomichev, Ph.T.T., 2 3167, 1967.

RESONANT X-RAY RAMAN SCATTERING FROM SOLIDS

P. M. Platzman

Bell Laboratories

Murray Hill, New Jersey 07974

Historically x-ray scattering has been one of the oldest and most useful tools for the investigation of the microscopic properties of solid state systems. [1] Until about ten years ago most of the applications utilizing x-rays were confined almost exclusively to elastic or Bragg scattering. Recently there has been a renewal of interest in the phenomenon of inelastic x-ray scattering. [2] This rebirth owes its origins to the availability of new and more powerful sources of x-ray radiation including synchrotron radiation

In a typical inelastic scattering process for a photon of frequency ω_1 most of the information is contained in the angle of scattering (momentum transfer $k = 2k_1 \sin \theta / 2$) and frequency shift $\omega = \omega_2 - \omega_1$. In some cases the relevant cross sections can depend on the frequency of the incoming or outgoing photon if this frequency is near a resonant absorption frequency for the system. In this talk we will focus on several aspects of the frequency dependent inelastic scattering of x-rays from simple metals.

Qualitatively the general properties of such scattering arises from the nature of the one electron excitation spectrum of such materials. (See Fig. 1) Electrons occupy levels starting with K shell which are bound for materials like Cu by thousands of electron volts. The electrons in the L shell are typically bound by hundred's of electron volts while those electrons in the

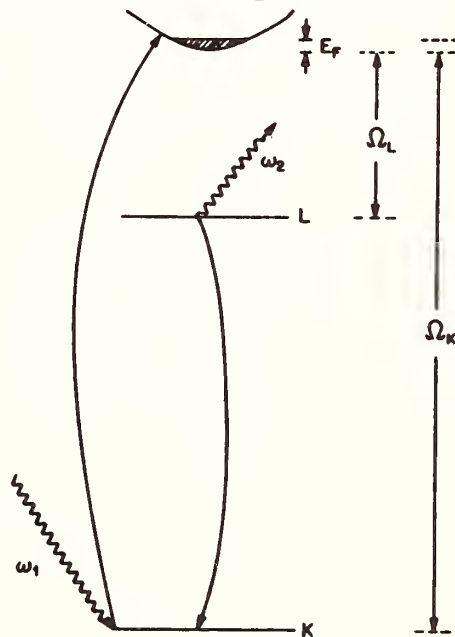


Fig. 1

conduction band have energies in the several electron volt range. X-rays which scatter from such a system leave it in varying states of excitation which are well separated in energy. The excitation of conduction electrons leads to so called plasmon and Compton scattering. The excitation of the L and K shell electrons has been called x-ray Raman scattering. Since x-rays which have

the appropriate wavelength to probe the microscopic spatial behavior of the outer electrons are in the 10 KeV range, the resonant process which is involved in all such scattering experiments involves the virtual excitation of a K electron. No scattering experiments to date have investigated the real excitation of such a K shell electron.

In this talk we will consider two kinds of resonant processes. In the first a real hole is left in the L shell leading to Raman scattering while in the second, a hole is left in the conduction band leading to Compton scattering. Schematically the basic coupling of nonrelativistic x-rays is given by,

$$H_c = \int dx^3 \left[\frac{e}{mc} \vec{p} \cdot \vec{A} + \frac{e^2}{2mc^2} \rho A^2 \right] . \quad (1)$$

Here \vec{A} is the vector potential, ρ the density and \vec{p} the momentum density of the electronic system. In general the $\vec{p} \cdot \vec{A}$ term taken to second order is small unless a resonance exists. To lowest approximation the second order matrix element for L shell Raman scattering is

$$M_{ti} = \frac{\langle P | \vec{p} \cdot \vec{\epsilon}_2 | S \rangle \langle K | \vec{p} \cdot \vec{\epsilon}_1 | S \rangle}{m(\omega_1 - \epsilon_K - \Omega_K + i\Gamma_K)} \quad (2)$$

Here $|S\rangle$, $|P\rangle$ are the one electron K and L shell wave functions and Γ_K is the K hole lifetime. The resonance is immediately put into evidence.

The matrix element given in Eq. 2 is strictly one electron in character and is obtained by evaluating dipole matrix elements of the momentum operator \vec{p} between various filled and empty levels. In reality the excited electrons and holes may interact with one another and with the sea of electrons which remain by means of coulomb interaction. Since the Raman scattering experiments of Sparks,[3] Eisenberger, Platzman and Winick[4] are extremely new and in many ways rather crude we will discuss these experiments within the framework of the one electron approach. This approach gives an accurate description of all such experiments to date. The inclusion of both the K and L shell lifetime in a detailed analysis of line shapes and positions predicts a variety of interesting resonance phenomenon which have been observed. These phenomenon are analogous to, but not precisely equivalent to, similar phenomenon in the visible. One of these effects, the narrowing of the inelastic spectrum as one approaches resonance is shown in Fig. 2. We will discuss this effect in some detail.

For Compton or conduction electron scattering the nonresonant situation has developed rapidly over the last few years and much information regarding electronic wave functions and collective modes in simple metals has been obtained.[5] However, at this writing no experiments on resonant Compton scattering exist. A theoretical investigation of this phenomenon indicates that a variety of interesting physical phenomenon are contained in such experiments. One such new phenomenon i.e. the interference effect arising from the $\vec{p} \cdot \vec{A}$ and A^2 has been analyzed and we conclude that this interference effect can be directly related, in the Compton regime to the overall phase of the wave function as referred to its nuclear center. This means that we can in principle solve the "phase" problem for Compton scattering and determine the position of the wave functions of the other electrons. The theory of this effect will be presented.

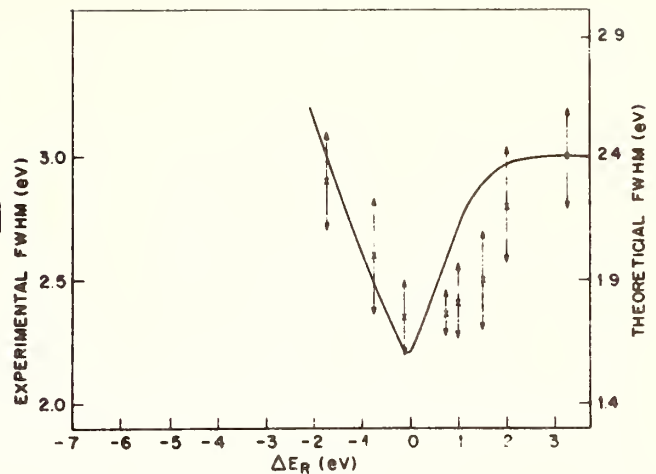


Fig. 2

References

1. R. W. Jones, The Optical Principles of the Diffraction of X-Rays. (Cornel U.D. New York 1965).
2. P. M. Platzman and N. Tzoar, Phys. Rev. 139, 410 (1965).
W. Phillips and R. J. Weiss, Phys. Rev. 171, 790 (1968).
M. Cooper and J. A. Leake, Phil. Mag. 15, 1201 (1967).
R. J. Weiss and W. Phillips, Phys. Rev. 176, 900 (1968).
P. Eisenberger and P. M. Platzman, Phys. Rev. A 4 15 (1970).
3. C. J. Sparks, Jr., Phys. Rev. Lett. 33, 262 (1974);
Y. B. Bannett and I. Freund, Phys. Rev. Lett. 34 372 (1975).
4. P. Eisenberger, P. M. Platzman and H. Winick, Phys. Rev. Lett. 36, 623 (1976).
5. Compton Scattering, Editor, B. Williams, McGraw-Hill, (To be published in 1976).

COMPTON SCATTERING: WHAT HAS IT DONE FOR US LATELY?
W. A. Reed, Bell Laboratories, Murray Hill, N. J. 07974

The observation that scattered x-rays are shifted in energy, and the explanation of this effect, earned A. H. Compton the Nobel prize in 1927. The subsequent realization that Compton scattering could be used to study the momentum of electrons excited considerable interest in the late 1930's and early 1940's. From the work of people like Dumond, Kirkpatrick, Ross, Coulson and Duncanson there developed an understanding that the "modified line" (the Compton profile) contained information about electron momentum distributions and these distributions could be calculated from electron wave functions obtained from theoretical models[1]. Despite this initial activity, the field hibernated until the 1960's when interest was revived by Weiss, Leake, Cooper, Platzman, Tzoar and others. From this renewed activity has come improved methods for the measurement and calculation of Compton profiles, and a better understanding of how to apply this technique to obtain a better knowledge of electron momentum states.

Initial steps in the revival were aimed at showing that carefully measured profiles of simple systems such as He gas[2] did in fact agree with profiles calculated from the best theoretical wave functions. Agreement of 1% or better was generally obtained. From there more complicated systems, such as Li[3] and Si[4], were measured which demonstrated the sensitivity of the technique to the details of the electron wave function. A study of some aliphatic hydrocarbon molecules showed that chemical bonds have characteristic momentum distributions[5] which in some cases carry over to bonds in solids[6]. Numerous other measurements demonstrated the ability of Compton scattering to provide information which was difficult to obtain by other techniques[1].

What are the areas of current interest and what are the prospects for the future? A detailed study of urea[7] which is yielding information on how the wave functions in a molecule are modified as the isolated molecule forms a crystal, and measurements of niobium hydride[8,9] which indicate that the hydrogen donates its electron to the niobium conduction band, are typical of problems now under study, and are indicative of the direction the field will probably take in the near future. The wide variety of problems to which Compton scattering can be applied, the promise of improved detector resolution and the expanded use of synchrotron radiation as a source insure that Compton scattering will continue to provide definitive information about problems in both chemistry and physics.

References

1. The Compton Effect, edited by B. G. Williams, to be published by McGraw-Hill (London) 1976. This is an up-to-date review of the experimental and theoretical technique in this field.
2. P. Eisenberger, Phys. Rev. A2, 1678 (1970).
3. P. Eisenberger, L. Lam, P. M. Platzman and K. C. Pandey, Phys. Rev. B6, 3671 (1972).
4. W. A. Reed and P. Eisenberger, Phys. Rev. B6, 4596 (1972).
5. P. Eisenberger and W. C. Marra, Phys. Rev. Letters 27, 1413 (1971).
6. W. A. Reed, P. Eisenberger, K. C. Pandey and L. C. Snyder, Phys. Rev. B10, 1507 (1974).
7. W. A. Reed and L. C. Snyder, to be published.
8. P. Pattison, M. Cooper and J. R. Schneider, to be published.
9. N. G. Alexandropoulos and W. A. Reed, to be published.

X-RAY INELASTIC SCATTERING

Relation between Compton, Raman and Plasmon Scattering

T. Suzuki, Department of Physics, Sophia University
Chiyodaku Kioicho, Tokyo, Japan 102

As is well known, X-ray Compton scattering and X-ray Raman scattering were both discovered in the early stages of the study of X-ray physics. The former served as one of the bases of quantum mechanics, but the latter has been confirmed only recently because of its very small scattering cross section. By contrast, the beginning of the study on X-ray plasmon scattering is comparatively new. These forms of X-ray inelastic scattering have been studied recently by many workers interested in the electronic states of solids. They are interrelated and transform from one to another according to the scattering conditions, principally the degree of momentum transfer.

In general, in X-ray inelastic scattering including phonon scattering, the incident X-ray photon suffers momentum and energy changes:

$$\hbar(k_0 - k) \equiv \hbar q \quad \text{and} \quad \hbar c(k_0 - k) \equiv \hbar \omega.$$

The electronic states of the scatterer are excited from the ground state Ψ_0 to the excited states $\{\Psi_F\}$, and the differential cross section can be denoted by

$$\frac{d^2\sigma}{d\omega d\varepsilon} = \left(\frac{e^2}{mc^2}\right)^2 \left(\frac{k}{k_0}\right)^2 \frac{1 + \cos^2\theta}{2} S(q, \omega),$$

$$S(q, \omega) = 2 \sum_F |\langle \Psi_F | \hat{p}(q) | \Psi_0 \rangle|^2 \delta[\hbar\omega - (E_F - E_0)].$$

Assuming a rigid lattice and in the one-electron approximation, the dynamical structure factor $S(q, \omega)$ can be expressed using one-electron wave functions:

$$S(q, \omega) = 2 \sum_{i,f} |\langle \varphi_f | e^{i q \cdot r} | \varphi_i \rangle|^2 \delta[\hbar\omega - (\varepsilon_f - \varepsilon_i)].$$

(a) Compton scattering:

$$S_{Comp}(q, \omega) = \frac{2}{(2\pi)^3} \int \delta[\hbar\omega - \frac{k^2}{2m} \{(\mathbf{k} + \mathbf{q})^2 - k_0^2\}] d\mathbf{k}.$$

(b) Raman scattering: In the dipole approximation $S(q, \omega)$ can be rewritten as:

$$S_{Ram}(q, \omega) = N_K q^2 \mathbf{e} \cdot T(\omega) \cdot \mathbf{e},$$

where $T(\omega) = \sum \langle \varphi_k | \mathbf{r} | \varphi_f \rangle \delta[\hbar\omega - (\varepsilon_f - \varepsilon_k)] \langle \varphi_f | \mathbf{r} | \varphi_k \rangle$.

$T(\omega)$ is known as the K-absorption tensor. The dipole approximation is satisfied when $qa_K \lesssim 1$, where a_K is the mean radius of the K-electron orbital.

(c) Plasmon scattering is a collective excitation, in contrast with the above two cases. However, since q is small, it is a modulation of the ground state. Therefore, it can also be expressed by an individual excitation formula similar to that for Compton scattering. Using the random

phase approximation, $S(q, \omega)$ for plasmon scattering is

$$S_{plas}(q, \omega) \approx \frac{Nq^2}{2m\omega_q} (\hbar\omega - \hbar\omega_q),$$

where ω_q depends upon the plasmon frequency and the Fermi velocity.

From the above described dynamical structure factors, the profile of each spectrum and dispersion relation can be seen. The Compton profile is parabolic, corresponding to the area of a section of the Fermi sphere for the ideal electron-gas model. However, a small modification due to the anisotropy in the electron momentum distribution or the many-body effect can be seen. The Raman profile corresponds to that of K-absorption depending upon the unoccupied state density above the Fermi level. The plasmon profile is of the δ -function type due to the definite energy of the plasmon oscillation.

The dispersion relations for Compton and plasmon scattering are well-known and are given by

$$\omega = \frac{\hbar}{2m} q^2 \quad \text{and} \quad \omega = \omega_p \left(1 + \frac{3}{10} \frac{q^2 V_F}{\omega_p} \right),$$

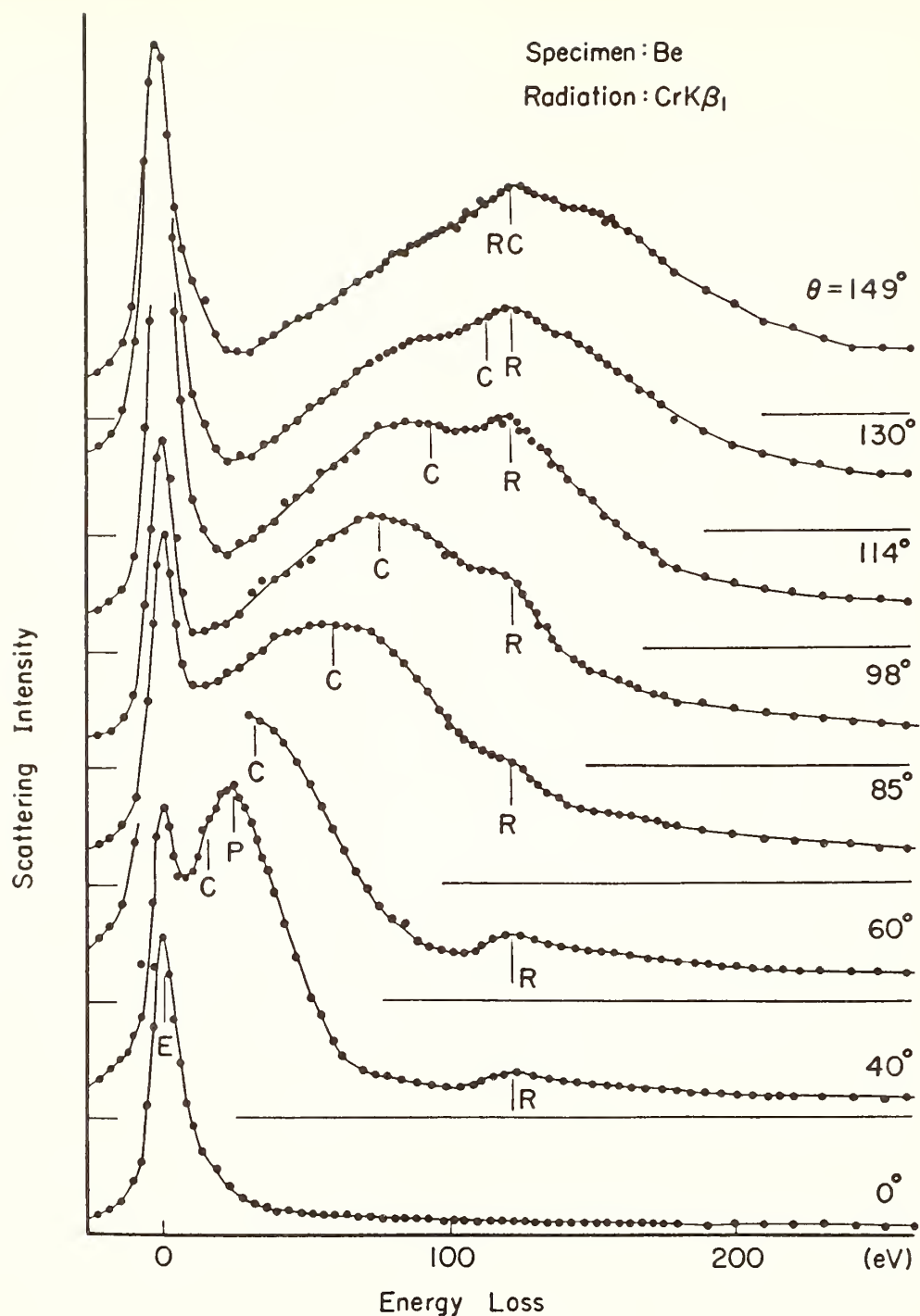
respectively, where ω_p is the plasmon frequency and V_F is the Fermi velocity. ω_p Raman is scarcely dispersive.

Usually it is thought that Compton scattering is associated with nearly free valence electrons and Raman scattering is associated with bound electrons, and that Raman scattering should appear as spectral lines. However, generally speaking, this is not valid. The difference between the conditions for the two types of scattering is decided only by the value of qa , where a is the mean radius of the orbit of the target electron, in general. For Raman scattering, $qa \leq 1$ and for Compton scattering, $qa > 1$.

Details of the features of each type of scattering will also be discussed.

Literatures can be seen in the references of the following articles:

- B.I.Lundquist and C.Lyden, Phys.Rev.B. 4(1971)3360
 G.G.Cohen, N.G.Alexandropoulos and M.Kuriyama,
 Phys.Rev.B. 8(1973)5427
 P.Eisenberger, P.M.Platzman and K.C.Pandey,
 Phys.Rev.Lett. 31(1973)311
 T.Suzuki and H.Nagasawa, J.Phys.Soc.Japan 39(1975)1579



Spectra observed at different scattering angles. Symbols E, R, C and P indicate respectively the TDS, Raman, Compton and plasmon scattering peak. Although not presented in this figure, the plasmon peak can be observed at the scattering angles, $\theta = 10^\circ \sim 50^\circ$. The peak of the Raman band does not shift appreciably with scattering angle.

T. Suzuki and A. Tanokura, J. Phys. Soc. Japan 29(1970)972

T. Suzuki and H. Nagasawa, J. Phys. Soc. Japan 39(1975)1579

SHAPE RESONANCE EFFECTS IN X-RAY ABSORPTION SPECTRA OF MOLECULES*

J. L. Dehmer

Argonne National Laboratory, Argonne, Illinois 60439

and

Dan Dill⁺

Department of Chemistry, Boston University
Boston, Massachusetts 02215

Following the key measurements of x-ray absorption spectra of SF_6 [1,2] ten years ago, a burgeoning body of data (see, e.g., [3-7]) demonstrate that spectra of deep molecular core levels depart markedly from the corresponding atomic spectra, especially within a few tens of volts of the inner-shell threshold. Although inner-shell photoabsorption takes place in essentially an "atomic" local environment, the subsequent escape of the photoelectron through the molecular field causes a major redistribution of oscillator strength over tens of volts. In particular, molecular inner-shell spectra commonly exhibit strong concentrations of oscillator strength in narrow bands both below and above threshold, in contrast to the monotonic decrease characteristic of the corresponding spectra in the free atom. Based on this very suggestive empirical evidence, early interpretations [8-12] postulated an effective potential barrier on the perimeter of the molecule which blocked the classical escape of the photoelectron and led to shape resonances and related quantum mechanical effects in the molecular spectrum. A more concrete understanding of these new phenomena required a realistic and practical means for computing molecular photoionization cross sections which was not then available.

Fortunately, the multiple-scattering method, adapted to molecular photoionization two years ago [13], has succeeded in several cases [14-17] to reproduce and reveal the cause of resonance features in molecular inner-shell spectra. In our work on the K-spectra of N_2 [14,17], we have reproduced nearly all prominent features in the discrete and continuum parts of the experimental spectrum and have predicted the corresponding photoelectron angular distributions [14,17,18]. This detailed prototype system demonstrated conclusively that the resonance features in the N_2 K-shell spectrum are caused by centrifugal barriers acting on high- ℓ components of the final state wavefunction. Specifically, $\ell = 2$ and $\ell = 3$ shape resonances are observed below and above the K-shell edge, respectively.

At the conference we will present new results which emphasize developments in two areas: (1) Energy dependence of photoelectron angular distributions from oriented molecules. [18,19] These calculations bear on future experiments on molecules adsorbed on surfaces and oriented by molecular beam techniques. Moreover, they have great pedagogic value as they express the complete spectral and spatial aspects of the photoionization process. A highlight of this study is the distribution for the case of K-shell photoionization of N_2 and CO. If the electric vector is parallel to the molecular axis, the $\ell = 3$ shape resonance described earlier is reflected as a narrow band (in energy) of enhanced photocurrent with f-type symmetry. (2) Examination of inner-shell photoionization in other simple molecules, e.g., acid halides and halogens [20].

FOOTNOTES AND REFERENCES

* Work performed in part under the auspices of the U.S. Energy Research and Development Administration.

+ Alfred P. Sloan Foundation Fellow.

1. R. E. LaVilla and R. D. Deslattes, J. Chem. Phys. 44, 4399 (1966).
2. T. M. Zimkina and V. A. Fomichev, Dokl. Akad. Nauk USSR 169, 1304 (1966) [Sov. Phys. Dokl. 11, 726 (1966)].
3. T. M. Zimkina and A. C. Vinogradov, J. Phys. Paris 32, Colloque C4, 3 (1971).
4. V. A. Fomichev, Fiz. Tverd. Tela. 9, 3167 (1971) [Sov. Phys. Solid State 9, 2496 (1968)].
5. G. R. Wight, C. E. Brion, and M. J. van der Wiel, J. Electron Spectrosc. 1, 457 (1973).
6. See also reference 12 for a discussion of numerous other data.
7. G. R. Wight and C. E. Brion, J. Electron Spectrosc. 4, 313 (1974).
8. R. L. Barinskii, Proceedings of the International Symposium on X-Ray Spectra and the Structure of Matter, Kiev, USSR, September 1968, p. 222.
9. V. I. Nefedov, Zh. Strukt. Khim 11, 299 (1970) [J. Struct. Chem. 11, 277 (1970)].
10. V. A. Fomichev and R. L. Barinskii, Zh. Strukt. Khim. 11, 875 (1970) [J. Struct. Chem. 11, 810 (1970)].
11. R. L. Barinskii and I. M. Kulikova, Zh. Strukt. Khim. 14, 372 (1973) [J. Struct. Chem. 14, 335 (1973)].
12. J. L. Dehmer, J. Chem. Phys. 56, 4496 (1972).
13. D. Dill and J. L. Dehmer, J. Chem. Phys. 61, 692 (1974).
14. J. L. Dehmer and Dan Dill, Phys. Rev. Letters 35, 213 (1975); also J. Chem. Phys., to be published.

15. V. P. Sachenko, E. V. Polozhentsev, A. P. Kovtun, Yu. F. Migal, R. V. Vedrinski, and V. V. Kolesnikov, *Phys. Letters* 48A, 169 (1974).
16. L. N. Mazalov, F. Kh. Gel'muskhonov, and V. M. Chermoshentsev, *Zh. Strukt. Khim.* 15, 1099 (1974) [*J. Struct. Chem.* 15, 975 (1974)].
17. J. L. Dehmer and D. Dill, Proceedings of the 2nd International Conference on Inner-Shell Ionization Phenomena, March 29–April 2, 1976, Freiburg, West Germany, to be published.
18. D. Dill, J. Siegel, and J. L. Dehmer, *J. Chem. Phys.*, to be published.
19. D. Dill, *J. Chem. Phys.*, to be published.
20. J. Siegel, D. Dill, and J. L. Dehmer, to be published.

PARTIAL PHOTOIONIZATION CROSS-SECTIONS
IN THE SOFT X-RAY REGION*

by

I. Lindau, P. Pianetta, and W. E. Spicer
Stanford Synchrotron Radiation Project
and
Stanford Electronics Laboratories
Stanford University
Stanford, California 94305

In this paper, we report on the experimental determination of the partial photoionization cross-section [1] for a few subshells (3d, 4d, 4f) from the ionization threshold and a few hundred eV up by using the photoemission technique. The measurements were done at the Stanford Synchrotron Radiation Project utilizing the synchrotron radiation from the SPEAR storage ring [2]. Synchrotron radiation from this source provides an intense, continuous spectral distribution from the infrared into the hard X-ray region [2]. A grazing incidence monochromator [3] was used to monochromatize the radiation in photon energy region 32-400 eV. The average distributions of the photoemitted electrons from the different subshells were determined by a double-pass cylindrical mirror analyzer. The experiments were performed on solid surfaces under ultra high vacuum conditions, 10^{-11} Torr [4].

In Fig. 1, we present experimental data for the energy dependence of the cross-section of the 3d levels for Ga and As. The Ga and As 3d levels are located 19 and 41 eV, respectively, below the Fermi level [5] and the energy dependence can thus be followed continuously from threshold to about 350 eV above threshold. The experimental points in Fig. 1 are obtained from the photoemission experiment where the energy distribution of the photoemitted electron is measured and can be plotted as a function of the electron binding energy. The energy dependence of the photoionization cross section is then quite simply obtained by measuring the area under the photoelectron peak as a function of the excitation energy making proper normalizations for the incoming photon flux and the transmission of the energy analyzer. Thus, the energy dependence of the partial cross-section can be mapped out in detail from the threshold and up. As seen from Fig. 1, the 3d photoionization cross-section for Ga (and As) has a weak energy dependence with a broad maximum 70 - 80 eV above threshold and a monotonic decrease towards higher energies. The experimental results are in good agreement with Kennedy and Manson's calculation [5] for the 3d levels of gaseous krypton.

The 4d partial cross section for In and Sb is plotted in Fig. 2 as a function of electron energy above threshold. The experimental data are shown as crosses. The cross-section goes through a maximum at 45 eV above threshold and then decreases rapidly before passing through a broad minimum around 130 eV. A flat and extended minimum is observed about 220 eV above threshold before the cross section starts to decrease

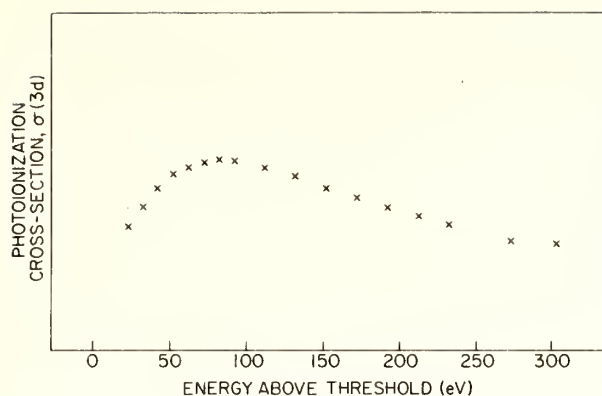


Fig. 1. Partial photoionization cross section (relative units) for 3d levels as a function of electron energy above threshold (x = experimental points).

functions and in the length approximation. The relative amplitudes of the theoretical curve and the experimental data have been fitted at the peak 45 eV above threshold. In overall, there is thus a remarkable agreement between theory and experiment with the energy positions of two maxima and the Cooper minimum reproduced. The cross-sections for the 3d and 4d levels for elements (solids) in the 3rd and 4th rows of the periodic table are thus in good agreement with Kennedy and Manson's atomic one-electron Hartree-Fock calculations for the corresponding noble gases [6]. However, care should be taken to generalize these results indiscriminatorily to other subshells where shake-up [9], shake-off [9], collective resonances [10,11], and other effects may considerably complicate the picture.

The photoionization cross-sections of the 4f levels (e.g., in Au, Pt, W) show a very slow onset at the threshold and a photon energy about twice the threshold value is required before they gain considerably in strength [12]. Again, this energy dependence can be understood from a one-electron picture, where electrons from any energy level with high angular momentum have a large repulse barrier to overcome. The effective potential contains a centrifugal term, which becomes important for $f \rightarrow g$ transitions.

In conclusion, we want to emphasize that the availability of synchrotron radiation makes it possible to map out in detail experimentally the energy dependence of the partial photoionization cross-section from threshold and up in the soft X-ray region. In the case of the 3d and 4d subshells for elements in the 3rd and 4th rows of the periodic table, good agreement is obtained for the general energy dependence with one electron Hartree-Fock calculations by Kennedy and Manson [6] for the corresponding subshells of the noble gases.

monotonically towards higher energies. Overall, the 4d partial cross section has a very dramatic energy dependence for the first 200 eV above threshold. The minima observed at 130 eV is termed the Cooper minima [7,8] and arises from the fact that the 4d wave functions have nodes. In comparison, the 3d wave functions do not have any nodes, and the cross-section shows a weak energy dependence as pointed out in connection to Fig. 1.

The solid line in Fig. 2 is the theoretical calculation of the atomic 4d levels in Xe by Kennedy and Manson [6], again using Hartree-Fock wave-

REFERENCES

* Work supported by ARPA, NSF, and ONR.

1. I. Lindau, P. Pianetta, and W. E. Spicer, *Phys. Letters A* (in press).
2. S. Doniach, I. Lindau, W. E. Spicer, and H. Winick, *J. Vac. Sci. Technol.* 12, 1123 (1975).
3. F. C. Brown, R. Z. Bachrach, S. B. M. Hagstrom, N. Lien, and C. H. Pruett, in "Vacuum Ultraviolet Physics," ed. by E. E. Koch, R. Haensel, and C. Kunz (Pergamon, New York, 1975), pp. 795-798.
4. I. Lindau, P. Pianetta, K. Y. Yu, and W. E. Spicer, *J. Vac. Sci. Technol.* 13, 269 (1976).
5. P. Pianetta, I. Lindau, C. M. Garner, and W. E. Spicer, *Phys. Rev. Letters* 35, 1356 (1975).
6. D. J. Kennedy and S. T. Manson, *Phys. Rev. A* 5, 227 (1972).
7. J. W. Cooper, *Phys. Rev.* 128, 681 (1962).
8. U. Fano and J. W. Cooper, *Rev. Mod. Physics* 40, 441 (1968).
9. M. Mehta, C. S. Fadley, and P. S. Bagus, *Chem. Phys. Letters* 37, 454 (1976).
10. M. Y. Amusia and N. A. Cherephov, *Case Studies in Atomic Physics* 5, 47 (1975).
11. G. Wendin, in "Vacuum Ultraviolet Physics," ed. by E. E. Koch, R. Haensel, and C. Kunz (Pergamon, New York, 1974), pp. 225-240.
12. I. Lindau, P. Pianetta, K. Y. Yu, and W. E. Spicer, *Phys. Rev. B* 13, 492 (1976).

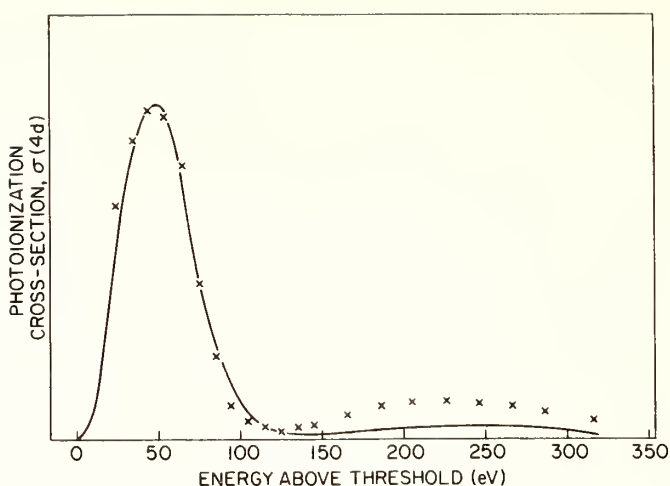


Fig. 2. Partial photoionization cross section (relative units) for 4d levels as a function of electron energy above threshold (x = experimental points, solid line = theoretical curve from Kennedy and Manson [6]).

X-RAY RESONANCE SCATTERING BY ATOMS WITH A PARTIALLY EMPTY LOCALIZED SUB-SHELL.

C. BONNELLE and R. BARCHEWITZ

Laboratoire de Chimie Physique, 11, rue Pierre et Marie Curie - 75231 Paris Cedex 05 - France.

The theoretical treatment of the scattering of light by atomic electrons had shown that the scattering cross section is very large if the incident radiation frequency, ν , becomes equal to one of the characteristic atom frequencies, ν_c . Then, the variation of the cross section must present a very sharp maximum in the neighbourhood of $\nu = \nu_c$ (1). This process is called resonance scattering of light or resonance fluorescence.

It is possible to suppose that the resonant amplitude is much larger than the sum of the non-resonant amplitudes. In this approximation, the expression of the amplitude scattered by a sample in the vicinity of $\nu = \nu_c$ is proportionnal to the probability of finding a strongly resonant state R which may be formed by the absorption of a photon. Indeed, such a resonant state is surely present if a resonant line is observed in the X-ray emission spectrum of the sample at the frequency ν_c (2) (3). Thus, we thought it would be interesting to study the amplitude scattered by various solid samples whether they contained atoms with a partially filled localized sub-shell or not.

We have attempted to analyze the intensity scattered elastically in the forward direction under specular reflection conditions. The distribution of X-rays reflected by films deposited on mirrors has been recorded under glancing angles between 10 and 80 mradians in the neighbourhood of a characteristic absorption. A large number of different substances have been used (4). From our results we class these in two groups : in the first, the distribution of X-ray radiation after reflection by the mirror is analogous to an absorption spectrum whatever the glancing angle ; in the second, a large variation in the spectrum is observed with a changing glancing angle and, for a value of the angle which is function of the wavelength, we observed an intense asymmetrical line situated towards the higher energies of the absorption line (figures 1 and 2). Its intensity is about 15 % at 70 mradians after reflection by La_2O_3 in the neighbourhood of the M_γ absorption.

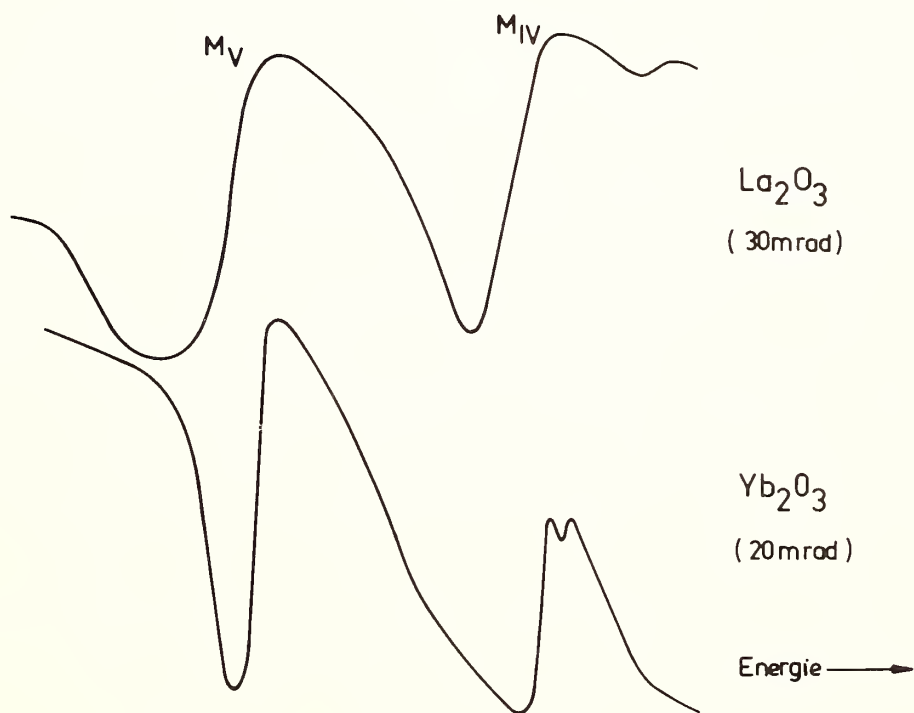
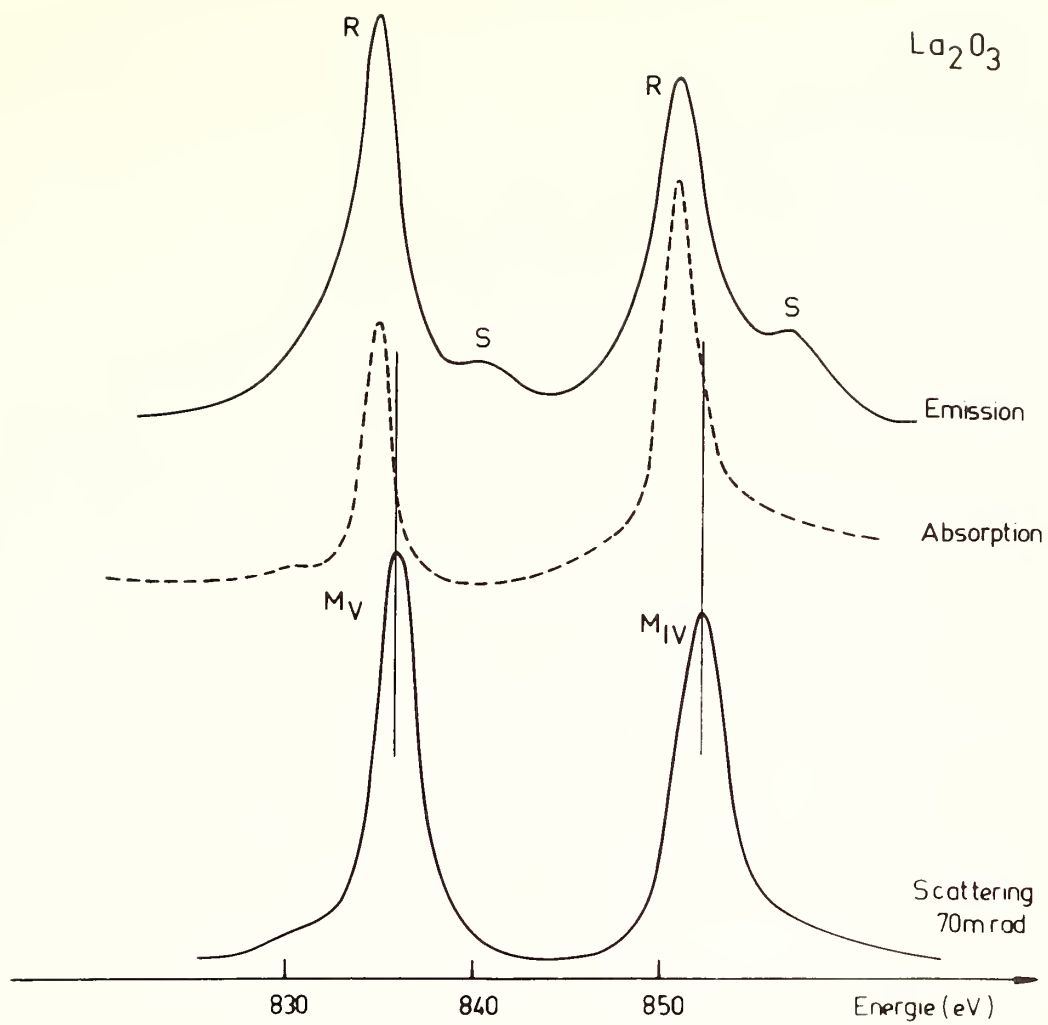
The observed phenomena are complex because it is necessary to take into account the variation of the refrac-

tive index in the anomalous region. However, it seems at present that intense lines can be observed only in the M_V and M_{IV} spectrum of the reflected intensity by samples containing a rare earth element. Thus during the interaction with the photon, the rare earth atom can be excited to a strongly localized virtual state and the process of de-excitation to the fundamental state is the most probable one because the speed of this transition is very large with respect to that of other interactions of the excited state in the solid.

Before a complete interpretation can be given many other experiments must be made in particular for samples containing transition elements. These results are of interest both from a fundamental and an experimental point of view. In fact this is a method for selecting a narrow energy band-pass (2 to 3 eV at 1 200 eV) with an intensity of up to 50 % of the incident radiation.

REFERENCES

- (1) W. HEITLER- The quantum theory of radiation, Oxford University Press, 3rd edition 1970.
- (2) C. BONNELLE, R.C. KARNATAK, J. de Phys. 32, C4-230 1971.
- (3) C. BONNELLE, Structure and Bonding Vol. 31 to be published.
- (4) R. BARCHEWITZ - Thèse de Doctorat d'Etat, Paris, 1976.



D. E. Sayers* and E. A. Stern, Department of Physics, University of Washington, Seattle, Washington 98195 and F. W. Lytle, The Boeing Company, Seattle, Washington 98124

In this paper we discuss the extension of our studies of K edge absorption spectra to the L edges. Using the EXAFS on the L₃ edge for structural studies would greatly expand the number of elements which can be studied by the EXAFS technique including Sm through the rest of the periodic table. A natural extension of these measurements has been a systematic study of the "white lines" (the large peak in the absorption coefficient within $\sim 10\text{eV}$) of some L₂ and L₃ edges. We have found variation in these white lines with changes in the chemical environment of the element being studied thus providing information about the local electronic environment which complements the structural information from the EXAFS.

To understand the origins of the "white lines" more completely we have studied the L₂ and L₃ edges of the elements W, Ta, Ir, Pt and Au as well as compounds of Ta, Pt and Au and catalysts containing Pt and Au. Qualitatively it has long been known that "white lines" arise from the high density of unfilled d states near the Fermi energy (1). Recently, Brown, et al. (2) have made a quantitative study of Pt including band effects and have shown that the calculated strength of the white line at the L₃ edge using band-calculation values for the number of d-holes of 0.3 is in agreement with the measured value. This quantitative agreement does not extend to Ta and W which have a large number of holes. Our studies find that the measured strength of the white line is less than one would expect theoretically if all of the d holes contribute. We interpret this to mean that only a fraction of the d-holes closest to the Fermi energy contribute to the white line. The reason for this result is not fully understood. We have also found a considerable variation in the Ta L₃ white line intensity for Ta, TaH, Ta₂O₅ and TaB₂ whose changes, although in qualitative agreement with the number of holes expected on valence considerations, again do not agree quantitatively. Despite the lack of quantitative understanding for transition metals with large numbers of d-holes, it appears that for atoms with a small number of d-holes, such as Pt, there is a quantitative correlation between the strength of the white line and the number of d-holes. Lytle (3) has carried out such a study with Pt catalysts and Pt compounds in order to understand the d character of these catalysts, demonstrating the usefulness of the white lines in understanding the electronic arrangement about a particular kind of atom in a complex system.

To determine structure information from the L edge EXAFS we have applied the fourier transform techniques which have been successful in analyzing the K edge data. The additional complications of the L edge are that the initial p state can couple to both s and d symmetric final states so that the expression for EXAFS can be written as

$$\chi_L = \sum_j A_j(k) \{ \mu_s(k) \sin(2kr_j + 2\delta_s(k)) + \mu_d(k) \sin(2kr_j + 2\delta_d(k)) \}$$

where $A_j(k)$ is the amplitude of the EXAFS as described elsewhere (4), μ_s and μ_d are the relative probabilities of making transitions to final s and d states, respectively, and δ_s and δ_d are the total s and d phase shifts, respectively. As we have shown (5), the s and d phase shifts are significantly different so that for each shell there are two peaks in the Fourier transform, one for the $p \rightarrow s$ transitions and one for the $p \rightarrow d$ transitions. The relative height of these two peaks are related to the appropriately weighted average of μ_s and μ_d over the range of data which is transformed. By taking transforms of $k^N \chi_L$ ($N=0,1,2,3$) we have been able to determine μ_d/μ_s as a function of k which shows that $p \rightarrow s$ contributions dominate or are equal to $p \rightarrow d$ up to $k \sim 8 \text{\AA}^{-1}$ after which $p \rightarrow d$ transitions then dominate. These measurements represent the first experimental measurements of these relative transition probabilities and are contrary to the usual arguments of complete domination by $p \rightarrow d$ transitions. These studies do show, moreover, that once the doublet structure for each shell is understood then useful structural information (particularly for the first neighbor) can be obtained as directly from L edge EXAFS as from K edge. To illustrate the usefulness of L edge EXAFS we will show results from a study of a heterogeneous catalysts (i.e. 1% Pt on SiO_2) which was examined in situ in a specially designed cell both after reduction by H_2 at 400°C and after chemisorption by O. The data show a clear rearrangement of the Pt atoms on the lattice after exposure to oxygen.

In conclusion, studies of L edge absorption spectra from elements in complex environments can give information on both the electronic structure about the absorbing atoms by studying the white lines and the atomic structure by studying the EXAFS.

† Supported by National Science Foundation Grant No. DMR73-02521, in cooperation with the Stanford Linear Accelerator and the U.S. Energy Research and Development Administration.

* Present address - Department of Physics, North Carolina State University, Raleigh, N.C. 27607.

- (1) N. F. Mott, Proc. Roy. Soc. 62, 416(1949).
- (2) M. Brown, R. E. Peierls, E. A. Stern, to be published.
- (3) F. Lytle, J. Catalysis (accepted for publication).
- (4) E. A. Stern, D. E. Sayers, F. W. Lytle, Phys. Rev. B11, 4835(1975).
- (5) E. A. Stern, D. E. Sayers, F. W. Lytle, to be published.

EXTENDED STRUCTURE IN X-RAY PHOTOABSORPTION PRINCIPALS AND APPLICATIONS

by

P. Eisenberger, W. E. Blumberg, G. S. Brown, P. H. Citrin,
B. M. Kincaid, J. Reed, and R. G. Shulman
Bell Laboratories
Murray Hill, New Jersey 07974

The first portion of this paper will describe the underlying phenomena responsible for the extensive structure observed above the x-ray absorption edge extending in some cases to 1-2 Kev above threshold. Schematic and simplistic mathematical formulations of the electron backscattering model will be presented. The presentation will stress the techniques ability to provide important interatomic distance determinations between atoms of ones choice if one can determine the energy dependence of the phase shift which the recoiling electron experiences.

Experiments on simple gaseous molecular systems will be described [1] and comparison with ab-initio calculations [1] will be made. Initial Hartree-Fock calculation of the energy dependent phase shift provided only 5-10% accuracy in interatomic distance determination [1]. More recent Kohn-Shan type calculations yield phase shifts which allow 1 to 2% accurate interatomic distance determinations [2].

To attempt to improve the accuracy of interatomic distance determinations an attempt has been made to empherically determine the energy dependence of the phase shifts [3]. The cornerstone of this empherical approach is the concept of the chemical transferability of the electron phase shifts; the phase for a pair of atoms (absorber and scatterer) is the same for all chemical environments for energies greater approximately 50 eV above the edge. The successful validation of this concept will be presented.

Examples will then be given of the ability to determine interatomic distances of importance to a wide range of scientific problems. Examples that will be discussed in detail will include the following:

Biology

1. Rubredoxin
2. Hemoglobin
3. Ions in Membranes

Chemistry

1. Ions in Solutions
2. Catalysis - Solid, Liquid, and polymer bound

Solid State

1. Single crystal anisotropy studies of zinc

Following this presentation a summary of the current theoretical and experimental status will be given as well as a discussion of possible future studies.

-
- [1] Kincaid, B. M. and Eisenberger, P., Phys. Rev. Lett. 34, 1361 (1975).
 - [2] Lee, P. A. - Private Communication
 - [3] Citrin, P. H., Eisenberger, P., and Kincaid, B. M., Phys. Rev. Lett. 36, 1346 (1976).

X-RAY PHOTOABSORPTION STUDIES OF SUPERCONDUCTING A15 COMPOUNDS^{††}

G.S. Brown and L. Testardi
Bell Laboratories
Murray Hill, New Jersey 07974

High superconducting transition temperatures have been obtained for thin films of Nb₃Ge prepared by sputtering at deposition temperatures in the neighborhood of 900°K. X-ray diffraction studies show that the material condenses principally in the A15 beta-tungsten phase. For lower deposition temperatures the transition temperature is much lower, despite the fact that the crystal symmetry remains body-centered cubic.

We have performed EXAFS measurements on the germanium and niobium K-edges of 4000 Å sputtered Nb₃Ge films. The samples were prepared at a variety of deposition temperatures, on both sapphire and silica substrates. The measurements were performed with the fluorescence technique, using a Ge semiconductor detector as well as a NaI scintillation counter. The EXAFS spectra were dramatically different among the samples, reflecting a large change in the interatomic distances. A preliminary analysis of the data indicates that the Ge-Nb distance contracts by about 0.2 Å for the low T_c material, despite a slight expansion (0.02 Å) of the lattice parameter. The data cannot be accounted for by reasonable vacancy concentrations or by anti-site disorder. Several models will be presented which are consistent with the X-ray diffraction data but which involve distortion of the atomic distribution within the unit cell.

^{††}The experimental work was performed at the Stanford Synchrotron Radiation Project (SSRP) which is supported by the National Science Foundation Grant No. DMR73-07692, with the cooperation of the Stanford Linear Accelerator Center and the U.S. Energy Research and Development Administration.

EXAFS IN PHOTOELECTRON YIELD SPECTRA: COMPARISON WITH
PHOTOABSORPTION AND DETERMINATION OF ELECTRON ESCAPE DEPTHS

R. Haensel, G. Martens, P. Rabe, N. Schwentner, M. Skibowski, A. Werner
Institut Für Experimentalphysik Der Universität Kiel
Kiel, Germany

K-shell photoelectron yield spectra of metal and insulator films prepared in situ under UHV conditions have been investigated above 3 keV photon energy. The spectra show a structure comparable to EXAFS in photoabsorption spectra. From the increase of the electron yield with the angle of incidence of the X-ray beam electron escape depths are deduced. Due to the short escape depth the electron yield at grazing incidence of the light is sensitive to the surface properties of the sample. The possibility to determine surface and overlayer structures will be discussed.

EXAFS OF A SINGLE CRYSTAL OF GALLIUM

W.M. Weber

Laboratorium voor Algemene Natuurkunde der Rijksuniversiteit Groningen,
Westersingel 34, The Netherlands.

In the last several years in Groningen the extended X-ray K absorption fine structure (EXAFS) of single crystals of gallium and cadmium was investigated for different orientations of the wave vector k and the polarization vector P of the X rays with respect to the crystallographic axes of the absorber; the degree of polarization could also be varied. The results obtained for an effectively unpolarized beam, for nearly 100 % linearly polarized X rays and for 37 % polarization of the beam can be summarized as follows: the more dominant the K photoejection perpendicular to the c axis of the gallium and the cadmium absorber, the more *pronounced* are the gallium and cadmium K fine structures. *No* significant change in the positions of absorption maxima and minima was found [1,2].

Interpretation of single-crystal K -absorption data for polarized and unpolarized X rays were given by Kostarev [3] and Izraileva [4]. In these interpretations the maxima and minima of the extended X-ray absorption fine structure (EXAFS) are conceived as variations of transition probability of the photoelectron due to elastic scattering of that electron from separate atoms in the nearest neighbourhood of the absorbing atom. In Kostarev's theory, the relative absorption coefficient can be calculated for all orientations of the wave vector k and the electric vector E , encountered in the experiments, by giving the vectors k and E fixed but arbitrary orientations with respect to the crystal axes of the absorber. Kostarev's theory gives good agreement with the experimental data for cadmium and especially for gallium in the energy region up to 300 eV from the main absorption edge. For gallium, the positions of EXAFS maxima and minima, the orientation effects, the general shape of the curves and some features of the hyperfine structure could be verified [5-8].

If the electric vector E of a linearly polarized X-ray beam is parallel to the c axis of a gallium single-crystal absorber, Kostarev's theory predicts a very weak fine structure, and the appearance of two extra pairs of absorption maxima and minima in the energy region between 100 and 300 eV (see Fig. 1). To investigate this, measurements at liquid helium temperature were carried out on the gallium single crystal. An EXAFS pattern in satisfactory agreement with the calculated one was found.

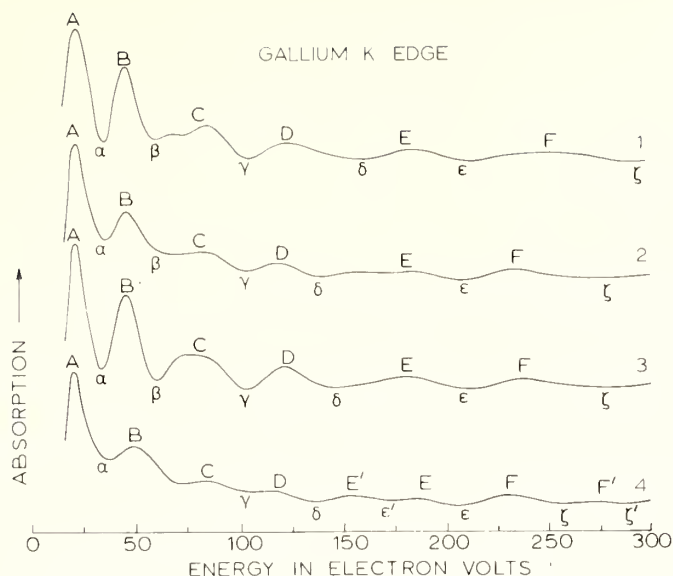


Fig. 1. Four theoretical curves of the gallium K fine structure, calculated from Kostarev's theory for 28 scattering atoms.

Curve 1: Electric vector E of the X rays almost parallel to the a axis of the absorber.

Curve 2: Angle between electric vector E and c axis 38° ; the vector E , the wave vector k of the X rays and the c axis lie in one plane perpendicular to the plane of the absorber.

Curve 3: Electric vector E almost parallel to the b axis of the absorber.

Curve 4: Electric vector E parallel to the c axis of the absorber.

REFERENCES

1. W.M. Weber, *Physica* **28** (1962) 689; **30** (1964) 2219.
2. W.M. Weber, *Phys. Letters* **25A** (1967) 590.
3. A.I. Kostarev, *Fiz. Metal. i Metalloved.* **19** (1965) 801.
4. L.K. Izraileva, *Doklady Akad. Nauk (USSR)* **168** (1966) 777; translation: *Soviet Phys. Doklady* **11** (1966) 506; *Doklady Akad. Nauk (USSR)* **169** (1966) 1048; translation: *Soviet Phys. Doklady* **11** (1967) 709.
5. A.I. Kostarev, *Fiz. Metal. i Metalloved.* **20** (1965) 26.
6. A.I. Kostarev and W.M. Weber, *Phys. Rev.* **B3** (1971) 4124.
7. W.M. Weber, Thesis, Groningen, 1972.
8. W.M. Weber, in *X-ray Spectra and Electronic Structure of Matter, Proceedings of the International Symposium, München, 1972*, edited by A. Faessler, G. Wiech (Sektion Physik der Universität München, 1973).

K. Ulmer

Physikalisches Institut, Universität, 7500 Karlsruhe (FRG)

Isochromat spectroscopy is fitted in the classical spectroscopies and its peculiarities are given. It is emphasized that isochromat spectroscopy makes disposable a new free parameter: The quantum energy $\hbar\omega$ of the radiative transition (Fig. 1). Contrary to the essentially fixed quantum energies of absorption edges for example, spectroscopy at optimal quantum energies can be performed with continuum isochromats.

An example utilizing this new degree of freedom is given. It concerns a simple absolute determination of the 2d-value of a spectrometer crystal. Result: $2d = (6.3390 \pm 0.0005)$ nm for OHM (Octadecyl Hydrogen Maleate) [1].

As a second example illustrating successful cooperation of different spectroscopies a comparison is given of the lanthanum M-series emission-spectrum for nearly threshold excitation [2] to the structure of isochromats (superposition of continuum and characteristic isochromats) [3]. The rich energy dependent structures of the spectra and of the isochromats can consistently be interpreted applying a theoretical electron-density-of-states (EDOS) of Glötzel (Fig. 2 and [4]) and a special two-electron-transition model. As a result of this consideration the essential features of the La-EDOS of Glötzel can be verified. The binding energy of the 3d 5/2-electrons in lanthanum for example turns out to be (831.0 ± 0.2) eV bringing this value nearer to expectations from XPS-energies [5] than from SXS-values given in the literature [6]. Likely due to angular momentum conservation in connection with the 4f-electron states in lanthanum, both spectra and isochromats cannot be interpreted in a simple one electron picture (Fig. 3).

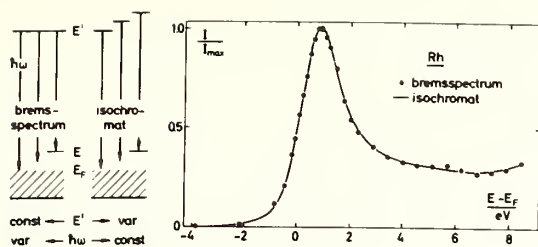


Fig. 1
Skeleton sketch of
continuum-isochromat and
bremspectrum with
Rh-example.

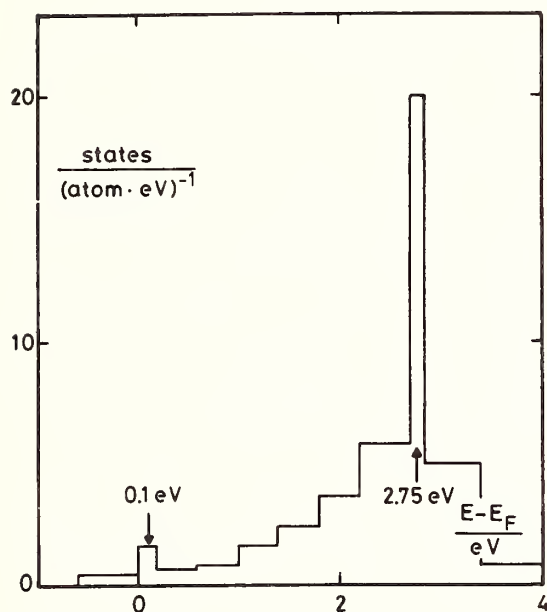


Fig. 2
f-electron-density-of-states
of lanthanum after Glötzel
(1976). Simplified version.

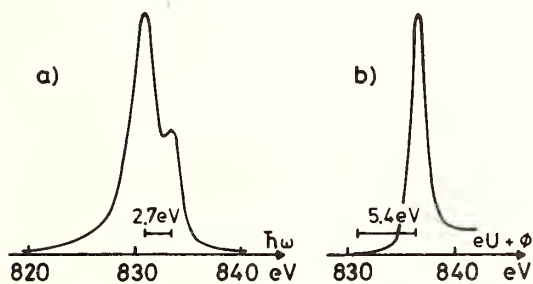


Fig. 3
a) La-spectrum ($eV+\phi=836,5eV$)
measured by LBC 1974
b) La-isochromat ($\hbar\omega=831,0eV$)
measured by Riehle 1976

References:

- [1] Föll H. and Ulmer K.: Verhandl. DPG (VI) 11, 612 (1976).
- [2] Liefeld R.J., Burr A.F., and Chamberlain M.B.:
Phys. Rev. A9, 316 (1974).
- [3] Noll H., Riehle F., and Ulmer K.: Verhandl. DPG (VI)
11, 614 (1976).
Riehle F.: to be published.
- [4] Fritsche L., and Glötzel D.: Verhandl. DPG (VI)
10, 541 (1975).
Glötzel D.: Diss. Clausthal FRG 1976 unpublished.
- [5] Bearden J.A. and Burr A.F.: Rev. Mod. Phys.
39, 125 (1967).
- [6] Bearden J.A.: Rev. Mod. Phys. 39, 78 (1967).

R.J. Liefeld and A.F. Burr - New Mexico State University
Las Cruces, New Mexico, 88003

The x-ray continuum near the high frequency limit may be regarded simply as the result of inelastic scattering of incident energetic electrons into available states above the Fermi level of the sample with emission of a photon as diagrammed in Fig. 1. A more complete view must acknowledge the role of the matrix element of the transition and its energy dependence. It will

be shown that this can be very important. The continuum intensity is then proportional to the density of available final states above the Fermi level times the matrix element for the transition from the particular initial state to the particular final state. Hence elucidation of densities of states in solids from studies of continuum limit spectra is frustrated by the need to know part of the "answer", (final state wave functions), to analyze the data to get another part of the "answer", (densities of states). Other complications are the presence of secondary processes such as the excitation of surface or

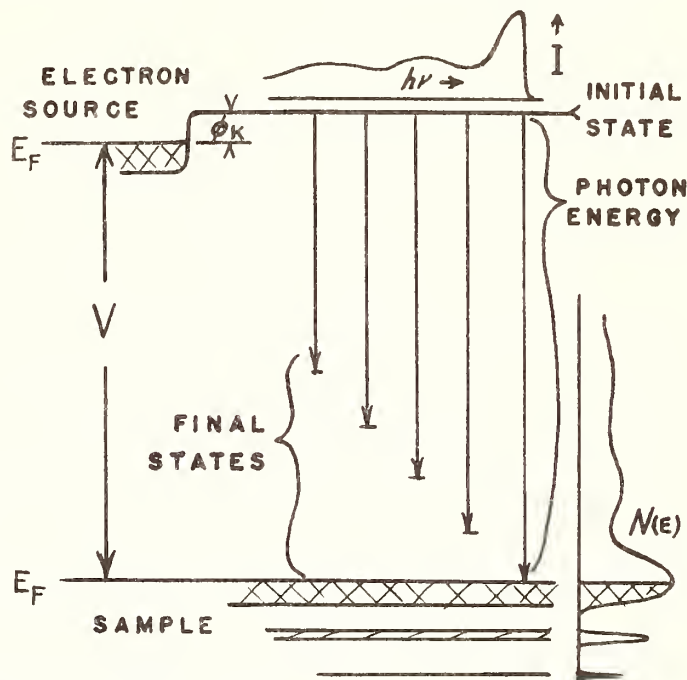


FIG.1. Simplified energy diagram of the continuum limit process

bulk plasmons, (characteristic losses), of phonons, and of valence electrons, resulting in an "incident" electron spectrum in the sample which is not single valued. Also, the presence of the scattered electron may distort the electronic structure in the solid. Thus a complete view of the continuum near the high frequency limit regards the intensity as the convolution of the "incident" electron spectrum in the sample with the (possibly modified) density of final states above the Fermi level times the matrix element for the transition.

At the N.M.S.U. x-ray physics laboratory continuous spectrum isochromats are recorded at a photon energy of 530 eV with a two crystal monochromator because a reflectivity peak of KAP crystals there yields high signal to background data, because the "incident" electron spectrum in the sample is more nearly single valued for the lower electron energies, and because isochromats do not require corrections for spectral sensitivity. Their equivalence to continuous spectra for single energy incident electrons depends on the shape of the continuum near the high frequency limit being independent of incident electron energy over the range of interest. Such isochromat spectra have been corrected for spectral smearing by unfolding the spectral window of the monochromator and have been corrected for the non-single valued nature of the "inci-

dent" electron spectrum by unfolding x-ray photo electron spectra of nearly the same energy as an approximation to the actual incident electron spectra in the samples. The results of studies of some of the first transition group and neighboring elements [1] and of Mg, Al, and Si [2], and comparisons with recent one electron densities of states calculations are convincing evidence that continuum limit spectra can yield useful information about the electronic band structures of solids.

However, for some elements, if the incident electron energy is close to the ionization energy of an inner shell which couples strongly with available orbitals lying close to the Fermi level, the intensity and shape of the continuum limit spectrum depends markedly on the energy of the incident electrons. An example of this effect is x-ray emission spectra from lanthanum for a succession of incident electron energies in the neighborhood of the M_5 and M_4 shell ionization energies. A time sequenced film of 35 spectra for incident electron energies in increments of 1 volt in this region shows the dramatic intensity resonance of a portion of the continuous spectrum as the incident electron energy is varied. Figure 2 shows a continuum limit spectrum from the lanthanum sample for an energy far from the M_5 , M_4 shell ionization energies. In it we recognize the abrupt onset at the Fermi level and a broad peak representing transitions to empty 4f levels on a continuum background. The broad peak is the feature which resonates so dramatically as the incident electron energy is varied through the M_5 , M_4 region. Data from cerium [3] show a similar behavior. In this case the area corresponding to the cross hatched area of Fig. 2 has been obtained from each graph of a series of more than 60.

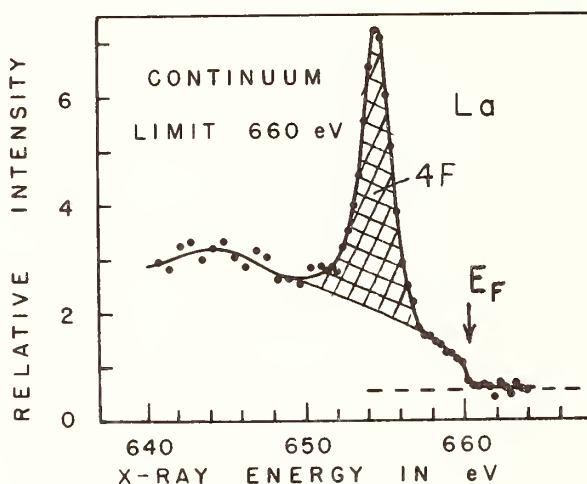


FIG. 2. A continuous spectrum from lanthanum for incident electrons of 660 eV.

These areas are plotted in Fig. 3 as the relative cross section for scattering to 4f levels as a function of incident electron energy. Note that the cross section for production of this part of the continuum varies significantly before the M_5 and M_4 energies are reached. A slow decrease is observed as the M_5 energy is approached. As the M_5 energy is closely approached the cross section increases by over two orders of magnitude. Between the M_5 and M_4 energies it is reduced to a very small value before increasing greatly again as the M_4 energy is closely approached. For incident electron energies greater than the M_4 energy the cross section decreases again, but slowly, with increasing electron energy. This distinct energy dependent resonance behavior of the matrix element of the continuum transition shows how important it can be for certain elements in particular energy regions. Other lanthanides also

exhibit this phenomena as do elements of the first transition group and the actinides. It can be seen that some "satellite lines" in x-ray emission spectra are actually due to this resonant continuum effect, that it dominates some appearance potential spectra, and thoroughly frustrates determinations of relative densities of states from continuum limit spectra. It has been speculated [3] that negative ion bound states with single channel decay modes are responsible for the continuum resonance, however, such speculations merely emphasize the need for an adequate theoretical exposition of the phenomenon.

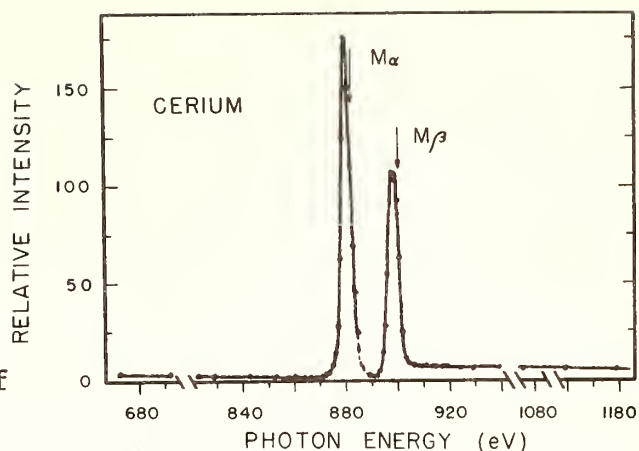


FIG. 3. Crosshatched area illustrated in Fig.2. plotted vs the energy of the continuum peak. The graph shows the variation with energy of the cross section for production of continuum photons.

- [1] R.R. Turtle and R.J. Liefeld, Phys. Rev. B, 3411 (1973).
- [2] D. Bruce, Ph.D. Dissertation, New Mexico State University, 1975.
- [3] M.B. Chamberlain, A.F. Burr, and R.J. Liefeld, Phys. Rev. A. 663 (1974).

BREMSSTRAHLUNG ISOCHROMAT FROM ALUMINUM.†

P. E. Best and C. C. Chu

Department of Physics and Institute of Materials Science
University of Connecticut, Storrs, Conn. 06268

We report a measurement of the bremsstrahlung isochromat (BI) from aluminum, and describe how the characteristic electron energy loss spectrum is unfolded from the raw data to simulate the BI from a thin target. This corrected data is discussed.

The raw BI data for an aluminum film evaporated within the experimental chamber in a pressure of $<10^{-10}$ Torr is shown as dots in Fig. 1. The data was recorded with the apparatus described elsewhere (1), using a monochromator set to pass 2.290 Å photons. The angular divergence of the incident electron beam and of the monochromator entrance aperture are less than 30 mR and 15 mR, respectively, the x-ray take-off direction being $87 \pm 1^\circ$ from the incident electron-beam direction.

From the step of the Duane-Hunt limit at 0 eV the BI intensity decreases slightly out to a second step which occurs at about 15 eV. The intensity then decreases slightly out to a third step centered at about 30 eV. The fine-structure peaks evident in the raw data curve, having widths of about 2 eV and intensities of about 10% of the step height, are believed to be due to density-of-states variations and will not be considered in this talk.

The three steps in the raw data of Fig. 1 can be understood as follows: The threshold and subsequent slow fall of intensity is the thin target BI appropriate to the incident monochromatic electron

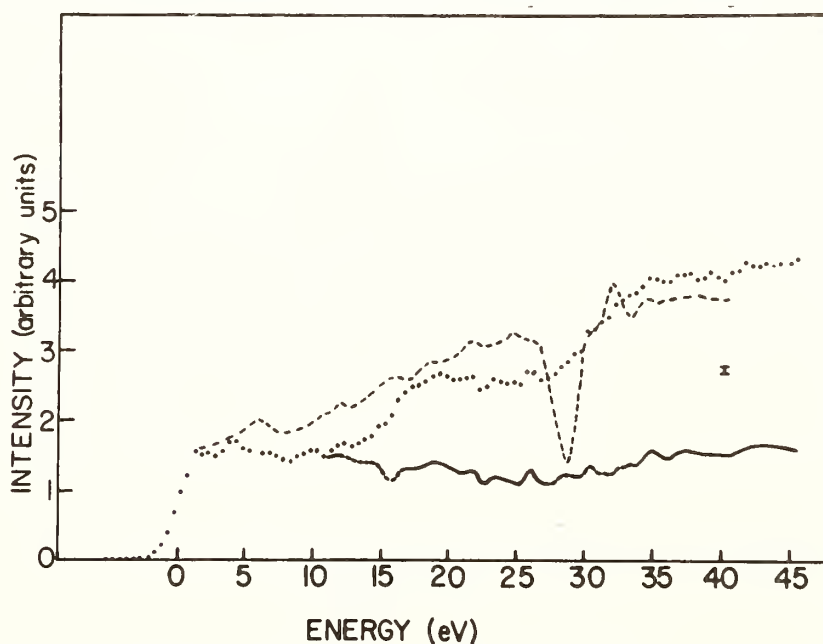


Fig. 1 Bremsstrahlung isochromat from aluminum: raw data, ——— corrected, - - - - - calculated density-of-states (9).

beam. At about 15 eV this thin target spectrum is augmented by a replica or echo of the threshold (2), which replica is the thin target BI from electrons which have excited a plasmon ($\hbar\omega=15.3\text{eV}$) (3). From 15 to about 30 eV above threshold the spectrum is the sum of the BI from the above two classes of electrons. Above about 30 eV a new thin target BI component, due to electrons that have excited two plasmons in separate events, is added to the spectral intensity.

To deduce the approximate thin target BI we must remove the plasmon echoes from the raw data. Before an unfolding technique can be considered we should know the relative number of electrons that have energies E_0 , E_1 and E_2 in the target, where E_0 is the energy of the incident beam, $E_1=E_0-\hbar\omega$, and $E_2=E_0-2\hbar\omega$. Also, we should ask whether electrons of energy E_0 , E_1 and E_2 , respectively, have similar cross-sections for bremsstrahlung production, and similar mean free paths (MFP's).

An electron entering the solid has a MFP of about 90A for inelastic scattering (4), and a similar MFP between elastic scattering events (5). The angular distribution of elastically scattered electrons is peaked in the forward direction, as the Bragg angles for these 0.16A electrons are very small for the intensely scattering low index planes.

About 0.9 of the total cross section for inelastic scattering is due to plasmon excitation (4). A rough description of the path of "typical" electron, therefore, can be given as follows: After entering the solid it travels 1 MFP with energy E_0 , another MFP with E_1 , a third MFP with E_2 , etc., all with little deflection. The relatively few electrons that contribute to the thin target BI of interest do so relatively close to the surface.

Electrons that excite K or L-shell electrons, or bremsstrahlung, are removed from the flux that can contribute bremsstrahlung intensity to the energy region of interest. These losses account for 0.1 of the total cross section (4), so the fluxes available for bremsstrahlung production are in the approximate ratios of $1:0.9:(0.9)^2$ for the E_0 , E_1 and E_2 components, respectively. For electrons whose energies are well removed from atomic excitation thresholds (6), bremsstrahlung cross-sections vary slowly with energy and angle. For our purposes it can be concluded that the bremsstrahlung production rates are in the ratios of $1:0.9:(0.9)^2$ for the E_0 , E_1 and E_2 components of the electron flux. It can be shown that there is virtually no loss of intensity due to x-ray absorption in the aluminum for the conditions of this experiment.

We describe a simple procedure to "unfold" the electron energy spectrum to reveal the gross behavior of the thin target BI. From the discussion above it can be concluded that the fully developed heights of the three steps in the data of Fig. 1 are in the ratios of $1:0.9:0.8$. From threshold to about 12 eV the spectrum represents the thin target BI from the E_0 part of the electron flux. When the bremsstrahlung component due to the E_1 part of the electron flux has reached its full height, at about 17 eV, the experimental curve is made up of

a thin target BI due to E_1 , which is 0.9 of the intensity due to E_0 at 15.3 eV lower energy, plus the unknown component due to E_0 . By displacing 0.9 of the thin target BI due to E_0 by 15.3 eV to the right, and subtracting it from the data, we are left with the thin target BI from the E_0 flux out to about 25 eV. This is shown in Fig. 1 by the solid line. The process was extended to the third step, revealing the E_0 thin target data out to 40 eV.

This "unfolding" procedure gives no direct information about the regions of the spectrum in the immediate vicinities of the steps in intensity. These regions are shown dashed in Fig. 1. While unresolved structure due to density-of-states effects can occur in these regions, there seems little doubt that the solid curve of Fig. 1 represents the gross nature of the aluminum BI out to 40 eV. In particular, there are no abrupt changes of levels or slopes in the corrected curve, features which would indicate an error in the model used.

The BI corrected in the above manner decreases from threshold out to a broad minimum at about 25 eV. The rise of intensity after 25 eV, and therefore the minimum itself, are probably artifacts caused by the neglect of structure in the energy loss spectrum due to both single particle excitations (7) and two-plasmon excitations (8). The calculated density-of-states curve for aluminum is shown by the dashed line in Fig. 1 (9). Over small energy regions it has been shown that the structure in the BI reflects structure in the density-of-states (1,10). It is clear from Fig. 1 that over an extended energy range the BI is not directly proportional to the density-of-states.

The BI from a free electron metal and a free atom, respectively, will have the same form. Inasmuch as aluminum is free-electron like, the corrected curve of Fig. 1 is a representation of the BI from free aluminum atoms.

Helpful discussions with Drs. L. V. Azaroff, D. Pease, and F. Szmulowicz are gratefully acknowledged.

Footnotes

†Supported in part by a grant from the National Science Foundation.

1. C. C. Chu and P. E. Best, Phys. Rev. B12, 4575 (1975).
2. G. Bohm and K. Ulmer, Z. Physik 228, 473 (1969).
3. C. J. Powell and J. B. Swan, Phys. Rev. 115, 869 (1959).
4. C. J. Powell, Surf. Sci. 44, 29 (1974).
5. V. W. Cosslett and R. N. Thomas, Brit. Journ. App. Phys. 15, 883 (1964).
6. M. B. Chamberlain, A. F. Burr and R. J. Liefeld, Phys. Rev. A9 663 (1974).
7. A. J. Glick and R. A. Ferrell, Ann. of Phys. 11, 359 (1960).
8. J. C. Ashley and R. H. Ritchie, Phys. Stat. Sol. 38, 425 (1970).
9. J. W. D. Connolly, Int. J. Quantum Chem. 3, 807 (1970) and F. Szmulowicz, private communication.
10. K. Ulmer, in "X-ray Spectra and Electronic Structure of Matter," Proc. Int. Symp. Kiev, 2, 79 (1968).

BREMSSTRAHLUNG ISOCHROMAT OF TUNGSTEN AT 16 eV

H. Humberg and H. Merz
Universitaet Muenster
Physikalisches Institut
D 4400 Muenster, Schlossplatz 7
Germany

In the case of transition metals photoelectron spectra of the valence bands and bremsstrahlung isochromats are complementary (e.g., Ulmer, Strathclyde, 1971); they give information about the distribution of filled resp. unfilled states in the valence and conduction bands.

Photoelectron spectra have been measured over an extended region of photon energies: there are significant differences in the spectra between the UV-region (UPS) and the X-ray region (SPS).

When transferring this classification to the analogous isochromat spectroscopy all known isochromats ($h\omega_0 > 150$ eV) are due to the X-ray region. With a grating (normal incidence) it was possible to get a tungsten isochromat at $h\omega_0 = 16$ eV (electron energy: 10-30 eV).

The tungsten curve shows the known "d-peak", but the ratio $I_{\max}/I_{\min} = 1,5$ is significantly smaller than near $h\omega_0 \approx 1000$ eV.

A comparison with tungsten isochromats of other authors, taken at some higher photon energies, shows a strong dependence of the ratio I_{\max}/I_{\min} from the photon energy. This dependence will be discussed.

STUDIES OF THE 4f STATES IN Ba AND La
BY ELECTRON AND PHOTON EXCITED APS*

J.Kanski, P.O.Nilsson and I.Curelaru, Physics Dept., Chalmers University of Technology, Fack, S-402 20 Göteborg, Sweden

In the present paper the $M_{5,4}$ and $N_{5,4}$ excitations in Ba and La are studied by means of electron and photon excited APS (EXAPS and XEAPS resp.) /1/. Both methods are probes of electron states above the excitation threshold. The final state in EXAPS contains two excited electrons and a core hole. In an independent particle picture an EXAPS spectrum is therefore to be interpreted as a self-convolution of the density of unoccupied electron states. This model has been applied successfully to various kinds of materials /2,3,4/, in which the final electron states are delocalized.

XEAPS is in principle a photoelectron yield experiment and the results are expected to be similar to photoabsorption data for the same core level excitation /5/.

Ba and La are the elements immediately preceding the rare-earth series in the periodic table. They contain therefore empty 4f states, which are localized in the region near the ion cores. This leads to a breakdown on the one-electron excitation description of the spectra.

Our experimental arrangement has been described earlier /1/. The measurements were performed on films evaporated from W-coils. During evaporations the pressure in the experimental chamber was around 5×10^{-8} torr. Within a few minutes of evaporation the base pressure of 5×10^{-10} torr was restored and was maintained during the measurements. In the EXAPS experiment the primary electrons were produced from a hot W-filament. For XEAPS we used the bremsstrahlung from a Ni-anode. This radiation was "monochromatized" by potential modulation /6/. All relevant experimental parameters are specified in the figure captions. The energy values quoted here include a 5.0 eV correction for the filament work function and for the thermal energy of the primary electrons.

Core level binding energies were determined by separate XPS experiments, using a HP-5950A ESCA instrument. These data were also obtained on evaporated films and were recorded within $\frac{1}{2}$ min of evaporation as the base pressure in the ESCA chamber was in the high 10^{-9} torr region. Only faint oxygen signals could be observed in these spectra. A few minutes after evaporation these peaks became more pronounced, and simultaneously "chemically" shifted metal structures appeared. Since the Ba data have been published earlier /1/, we restrict ourselves to show only the La spectra here, fig.1. The EXAPS $N_{5,4}$ spectrum is quite complex, and we cannot at present give any detailed interpretation of all the structures. It does however have some features in common with the photoexcited spectra (XEAPS, SXA), which are better understood. We see for example that all $N_{5,4}$ spectra extend over

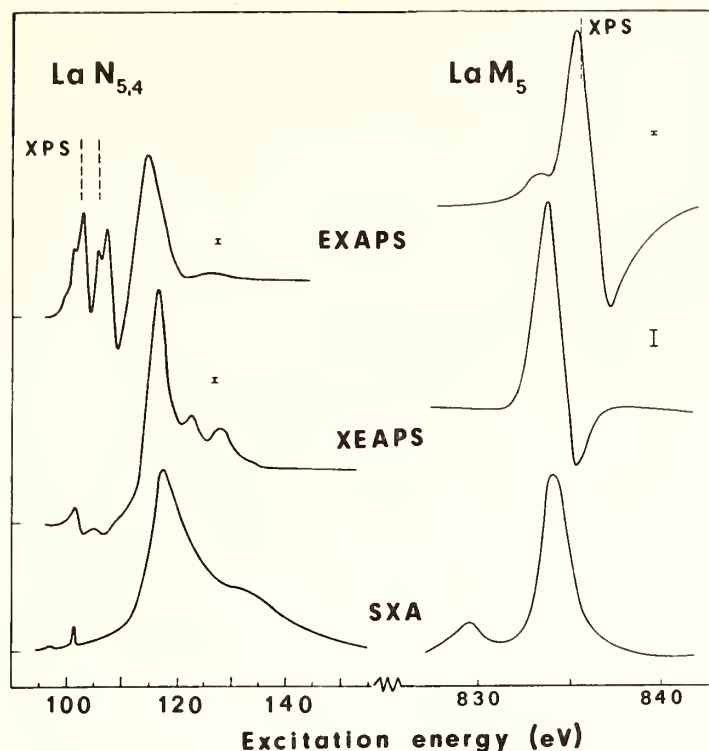


Figure 1. $N_{5,4}$ and M_5 spectra for La. The data were obtained using the following parameters for primary current, modulation amplitude (peak-to-peak) and time constant:

$N_{5,4}$ EXAPS:
1.0 mA, 0.5 V, 3 s

$N_{5,4}$ XEAPS:
4.0 mA, 1.4 V, 3 s

M_5 EXAPS:
1.0 mA, 0.5 V, 1 s

M_5 XEAPS:
6.0 mA, 1.1 V, 3 s

The resulting noise levels are indicated with bars.

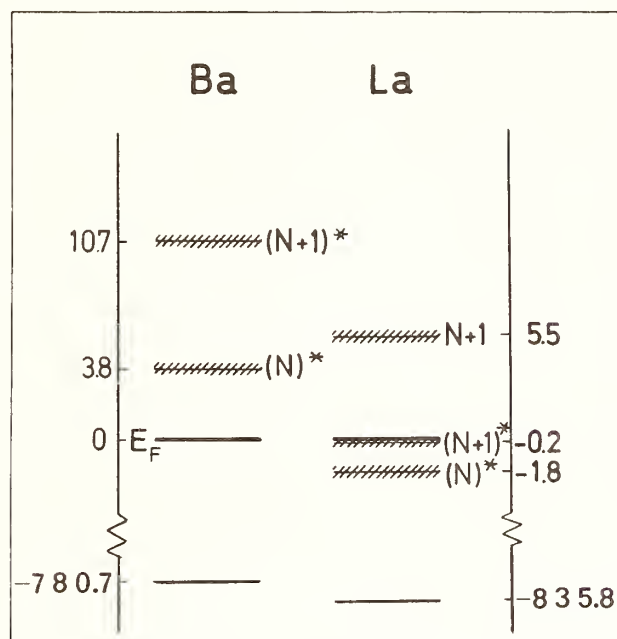
The SXA data are taken from refs. 9 and 10.

a wide energy range due to strong multiplet splitting. Further, the general structure of the spectra is similar, they are all dominated by one strong peak at about 115 eV, which is assigned as a collective dipole resonance of the $(4d^9 4f)^1 P$ state /7/.

As the processes in EXAPS and XEAPS are not subject to the same selection rules, one may however expect different results. In particular, the EXAPS spectrum should be richer in structure when multiplet splitting is a dominant effect. The M_5 spectra in fig. 1 are clearly less complicated. The EXAPS curve is qualitatively similar to the corresponding Ba curve /1/. In both cases the spectra are dominated by one peak, which on its low-energy side has a shoulder-like structure. The analysis of these data is greatly facilitated by comparison with the XEAPS spectra. Thus both for Ba and La the position of the shoulder corresponds to the position of the dominant peak in the XEAPS spectrum. Considering dipole selection rules and the narrow width of this peak, one can interpret it as the $3d \rightarrow 4f$ excitation. This is also our assignment of the shoulder-like feature in EXAPS. In this excitation the second electron in the EXAPS process is thought to enter an itinerant state, not affecting the local configuration at the excited atom. The main EXAPS peak is then interpreted as approximately the process $3d^9 4f^1 + e^- \rightarrow 3d^9 4f^2$.

It is now interesting to note that both EXAPS peaks appear

at excitation energies lower than our XPS binding energy, 835.8 eV (dashed line in fig. 1). Furthermore, the position of the 4f level is determined by continuum isochromat (CI) spectroscopy to be 5.5 eV above the Fermi level [8]. Combining the XPS and the CI results, one would expect the $3d \rightarrow 4f$ excitation to occur at 841.3 eV in an independent particle model. The present results thus demonstrate the



breakdown of this model when electron transitions are considered between localized states.

The M_5 results for Ba and La are summarized in fig. 2. It is evident that the position of the 4f states is very sensitive to the final state configuration, and therefore to the particular experiment by which it is examined.

Figure 2. One-electron 4f levels eV of Ba and La in different configurations as deduced from various experiments. N and N+1 denote the number of electrons and * the presence of a M_5 core hole.

* Work supported by the Swedish Natural Science Research Council.

1. J.Kanski and P.O.Nilsson, Physica Scripta 12,103 (1975)
2. R.L.Park and J.E.Houston, Phys. Rev. B6,1073 (1972)
3. P.O.Nilsson and J.Kanski, Surface Science 37, 700 (1973)
4. J.E.Houston, Solid State Comm. 17,1165 (1975)
5. W.Gudat and C.Kunz, Phys. Rev. Letters 29, 169 (1972)
6. R.Voparil, J. Phys. E3,793 (1970)
7. P.O.Nilsson, J.Kanski and G.Wendin, Solid State Comm. 15,287 (1974)
8. R.J.Liefeld, A.F.Burr and M.B.Chamberlain, Phys. Rev. A9 316 (1974)
9. P.Rabe, thesis, Universität Hamburg (1974)
10. D.W.Fischer and W.L.Baun, J. Appl. Phys. 38,4830 (1972)

DIFFRACTION EFFECTS IN APPEARANCE POTENTIAL SPECTROSCOPY

M. L. den Boer, Y. Fukuda and Robert L. Park

Center of Materials Research

and

Department of Physics

University of Maryland

College Park, Maryland 20742

Appearance potential spectroscopy (APS) falls into a class of experiments which measure threshold potentials for creation of excited states in matter. No analysis of decay products is required, since the relevant quantity is the energy of the exciting particle, which makes such experiments conceptually simple. In APS, electrons are used to excite core levels of atoms. The energy of the exciting electron is determined by the potential between a hot filament cathode and the sample. In the widely used soft x-ray appearance potential experiment, the excitation of the core level is signaled by its radiative recombination via emission of an x-ray. In the simplest method [1], a photocathode measures the total x-ray yield of the sample, and abrupt changes in the yield are detected as the incident electron energy is increased through a particular core level binding energy. There is, of course, in addition to the desired x-ray signal, a smoothly rising bremsstrahlung background. Differentiation, usually by the potential modulation technique, enhances the threshold structure relative to this smooth background.

At threshold, only electrons which have not lost energy participate. The appearance potential technique is therefore sensitive only to the first several angstroms of the sample, since for low energy electrons the mean free path for inelastic scattering is very short [2]. It is therefore used to investigate the composition and electronic structure of the surface region of solids. Measurement of the threshold energy gives the binding energy of a particular core level. Above threshold, the incident electron and the excited core electron must both occupy empty states just above the Fermi energy, and the probability for their doing so depends, in the absence of matrix element variations, on the density of states available for two electrons. The lineshape above threshold will therefore reflect the self-convolution of the local density of unfilled states for each species in the surface region of the

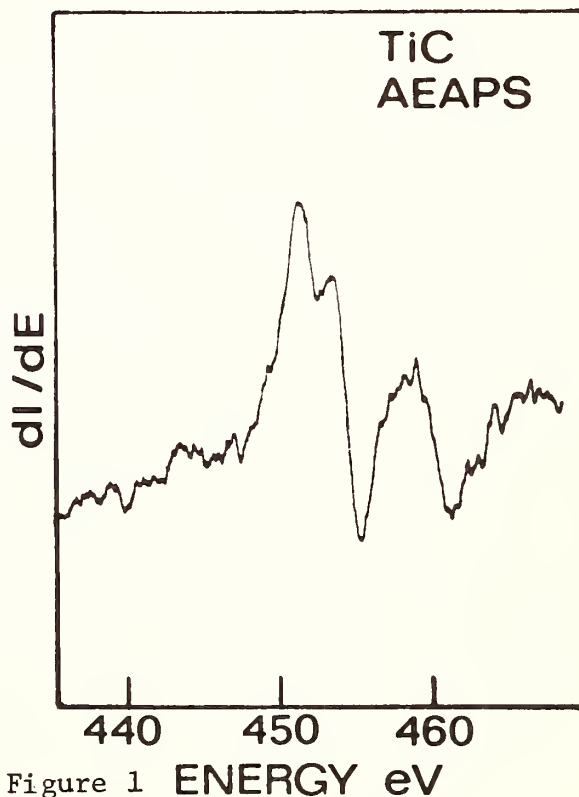


Figure 1

ENERGY eV

sample. For example, Figure 1 shows the APS spectrum of the 2p level of Ti in the compound TiC. The first feature, which in this case measures the unfilled d-band density of states, is wider than in pure Ti, indicating some charge transfer to the C. This information is of course broadened by the core level width. Apart from this intrinsic width, the experimental resolution is determined by the spread in incident electron energy and the smoothing necessarily introduced by differentiation. These can be kept below 0.5 eV, independent of incident energy. This makes appearance potential one of the highest-resolution core-level spectroscopies available.

The large sample currents in SXAPS, however, creates a serious problem for some systems. Using a conventional photocathode, with a quantum efficiency no better than 10^{-2} for x-ray detection, one needs sample currents of 1 to 10 mA, resulting insignificant sample heating and desorption of adsorbed species. By using a surface-barrier detector and an aluminum window, Andersson and coworkers [3] can reduce the current required to 10 to 100 μ A, enabling them to study certain strongly adsorbed species.

There is another approach which has been less widely explored. In the energy region of interest for surface studies, 10 to 1000 eV, radia-

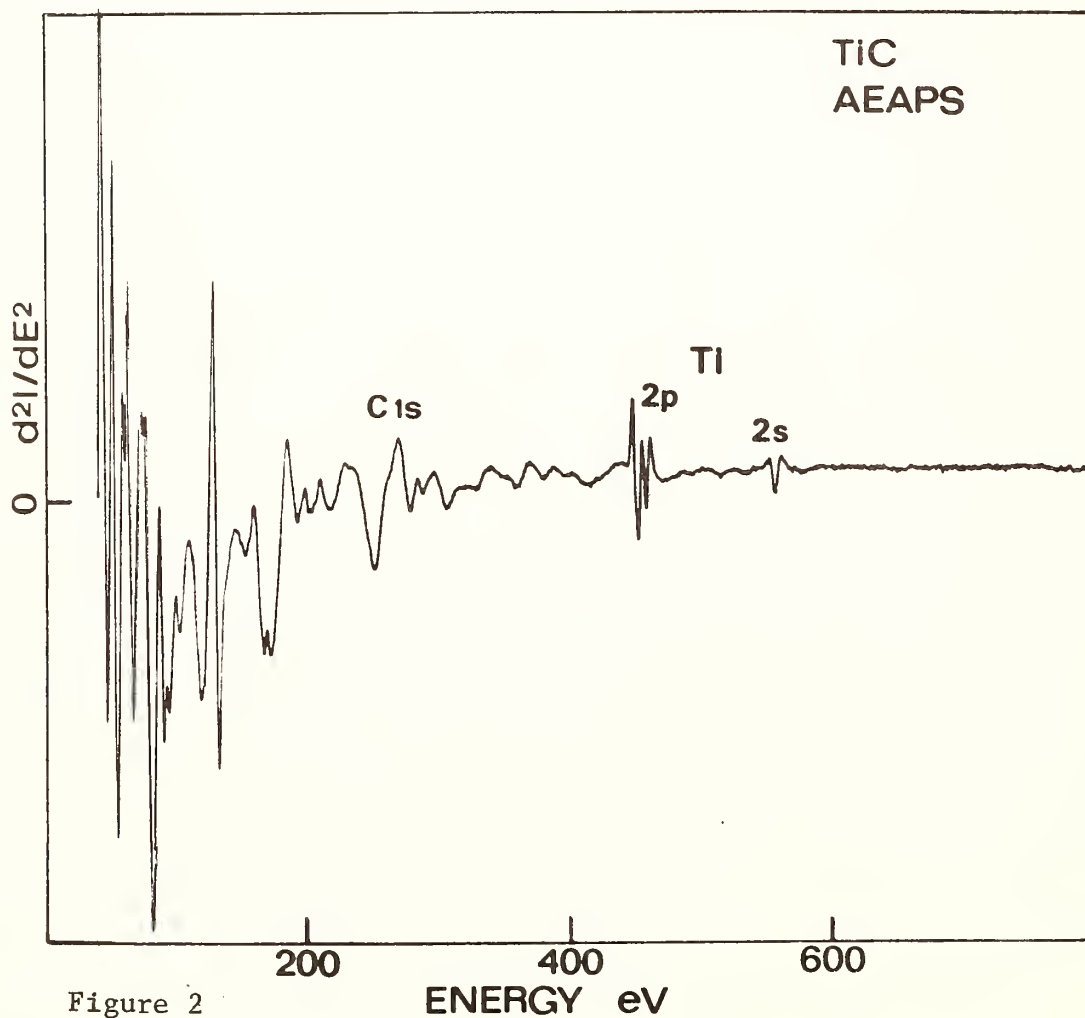


Figure 2

ENERGY eV

tive recombination of the core hole is rare, occurring at least 100 times less often than recombination by an Auger process. Excitation of the core hole is thus signalled as well by an increase in the secondary electron emission. Moreover, electrons are easily detected with 100% efficiency. This is exploited in Auger electron appearance potential spectroscopy [4], which simply measures the sample current as a function of incident electron energy, in an experimental arrangement with a constant primary current. Both because of the ease of detecting electrons, and the greater probability of non-radiative decay, the primary current can be reduced to a few microamperes, greatly reducing problems of sample heating and desorption. The experimental apparatus consists merely of a hot filament and an accelerating electrode with a small hole. Electrons passing through the hole are decelerated to the sample just beyond. Since the hole is small, the incident current does not depend on the sample potential. The sample current, or its derivative, is then measured as a function of sample voltage. Because only small incident currents are needed, one can also use a cold field-emission source, which draws electrons directly from the cathode Fermi level. Not only does this reduce the thermal energy spread of the incident electrons, improving the resolution, it also allows binding energies to be measured absolutely rather than relative to the emitter work function.

The method has a major disadvantage, in that the background, at energies below a few hundred eV, is very poorly behaved, as illustrated in Figure 2. In this second derivative spectrum of a TiC surface, appearance potential features below about 250 eV are obscured by a rapidly varying background, believed to be due to diffraction effects. This is in contrast to the soft x-ray experiment, where there is only a smoothly-rising bremsstrahlung background. Measurements taken as a function of sample temperature support the diffraction interpretation, although matters are complicated by the physical situation. In a customary diffraction experiment, one looks at a particular coherent beam as the sample is heated, which has the effect of reducing coherent scattering to the benefit of incoherent scattering. In this experiment, one is looking at the angular-integrated sum of all coherent and incoherent scattering.

REFERENCES

1. R.L. Park and J.L. Houston, J. Vac. Sci. Technol. 11, 1 (1974).
2. J.J. Quinn, Phys. Rev. 126, 1453 (1962).
3. S. Andersson, H. Hammarquist and C. Nyberg, Rev. Sci. Instrum. 45, 877 (1972).
4. J.E. Houston and R.L. Park, Phys. Rev. B 5, 3808 (1972).

X-RAY PHOTOELECTRON STUDIES OF THE HEAVY RARE-EARTH METALS AND THEIR OXIDES

D.J. Fabian, W.C. Lang, P.R. Norris, B.D. Padalia, and L.M. Watson

Department of Metallurgy, Materials Physics Group,
University of Strathclyde, Glasgow G1 1XN.

EXPERIMENTAL

Systematic measurements of the core-electron binding energies of the rare-earth metals terbium to lutetium, and their surface and bulk oxides, were made with a VG-ESCA3 instrument, using AlK_{α} and MgK_{α} radiations as excitation sources. Clean samples were prepared by evaporating spectroscopically pure rare-earth metals under vacuum of $\sim 10^{-9}$ torr onto the tip of the sample probe. The deposited films were transferred, without disturbing vacuum, from the sample preparation chamber to the analyser held at a base pressure of 6×10^{-10} torr. Controlled oxidation of the samples was achieved by exposing the clean evaporated films to measured amounts of clean dry oxygen before transfer to the analyser chamber.

Monitoring of the oxygen 1s spectra during surface oxidation revealed no measureable shift of the peaks, and we conclude that no charging of the oxidised films occurs. The absence of a charging effect was confirmed by evaporating gold onto the oxide surface and observing the characteristic gold 4f peaks which showed no broadening nor shift such as is generally attributed to charging of the sample.

Pure bulk oxide samples of the rare earths were examined by mounting the oxide powders onto the sample probe using double-sided 'Scotch' tape. In this case the magnitude of charging was estimated by imbedding a piece of pure gold in the powder and monitoring the Au 4f peaks. Bulk oxides were also prepared *in situ* by evaporating the pure metal in an oxygen atmosphere (at pressures $\sim 10^{-4}$). Monitoring for contamination was achieved by observing the C 1s region of the spectrum; however, no attempt was made to determine the extent of charging for these evaporated oxides. Further details of the experimental method have been described by Fuggle *et al* [1], and Lang *et al* [2].

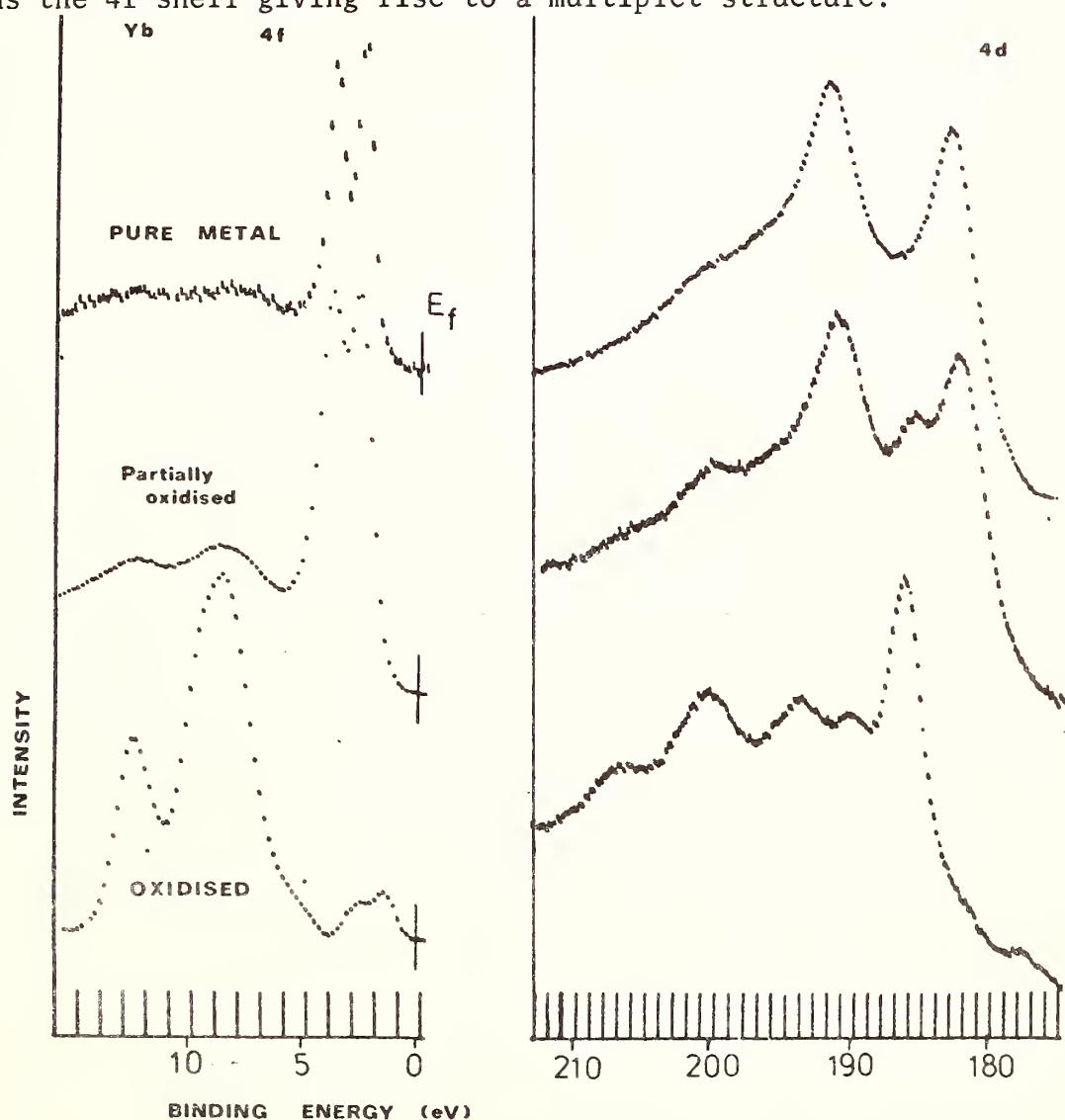
RESULTS

Multiplet splitting of the 4f, 4d, 4p, 4s and 5s levels for the metals terbium to thulium, which have open 4f-shells, is observed. The 4f and 4d spectra of pure ytterbium and lutetium metals, with closed 4f-shells, exhibit spin orbit doublets. Multiplet splitting was also detected for the oxidised ytterbium, while for oxidised lutetium the simple 4f and 4d doublets are retained. The degree of 4s and 5s multiplet splitting, for the metals terbium to thulium with open 4f shells, increases with number of unpaired spins.

Existing data for core-level binding energies for the series are

included in the compilation by Bearden and Burr [3]. Comparison with the present results reveals many discrepancies, some of which are certainly associated with chosen reference levels. Binding energies for the core levels of surface-oxidised samples do not correlate well with those measured for the bulk oxides, which stresses the importance of surface effects.

The 4f and 4d spectra for Yb, where oxidation produces notable modification to both these levels, are shown in figure 1 (4f to the left, 4d to the right). The clean metal spectra (uppermost) are dominated by simple doublets. On partial oxidation two features begin to appear, at 8.5eV and 12.3eV below the Fermi level in the 4f spectrum (the valence band), and at binding energies of 186eV and 201eV in the 4d spectra. On full oxidation these features become peaks that dominate the 4f spectrum and are prominent in the 4d multiplet. These observations reflect the divalent character of Yb. The effect of oxidation is quite different for example in the case of lutetium, which also has a closed 4f shell in the pure metal. With Yb the promotion of a 4f electron to a bonding orbital opens the 4f shell giving rise to a multiplet structure.



Oxidation also modifies the widths and intensity ratios in the multiplet structure for the trivalent metals terbium to thulium, though the effect is not large and indicates that the 5d63 valence electrons only are involved in the bonding with oxygen atoms.

In the 4d spectra for terbium to thulium (metals with incomplete 4f shells) additional structure is observed at ~ 26 eV to the high energy side of the most intense peak. This is attributed to correlation peaks in the multiplet structure predicted by the multiplet-hole theory proposed by Bagus *et al* [4] and confirmed for Mn^{3+} by Kowalczyk *et al* [5].

References

- [1] Fuggle J.C., Burr A.F., Watson L.M., Fabian D.J. and Lang W.C., 1974 J. Phys. F. 4, 335-42.
- [2] Lang W.C., Padalia B.D., Fabian D.J. and Watson L.M., 1975b Faraday Discussion no. 60 (1975), p37-43.
- [3] Bearden J.A. and Burr A.F., 1967, Rev. Mod. Phys. 39, 125-142.
- [4] Bagus P.S., Freeman A.J. and Sasaki F, 1973, Phys. Rev. Lett. 30, 850-853.
- [5] Kowalczyk S.P., Ley L., Pollak R.A., McFeely F.R. and Shirley D.A., 1973, Phys. Rev. B, 7, 4009.

Acknowledgements

This work is supported by funds from the UK Science Research Council; in addition B.D.P. wishes to thank the SRC for a Senior Visiting Fellowship, P.R.N. for a Research Fellowship, and W.C.L. for a Research Studentship.

DETERMINATION OF EMPIRICAL ATOMIC CONTINUUM CHARGE DENSITIES,
PHASE SHIFTS, AND LOCAL PSEUDO-POTENTIALS FROM ANGULAR-DEPENDENT
PHOTOEMISSION DATA FOR RARE GASES.*

Donald L. Miller[‡] and John D. Dow
Department of Physics and Materials Research Laboratory
University of Illinois at Urbana-Champaign
Urbana, Illinois 61801

The differential cross section $d\sigma/d\Omega$ for atomic photoemission of electrons with energy E into a direction at an angle θ with respect to the propagation direction of the absorbed light is

$$\frac{d\sigma}{d\Omega}(E) = \frac{\sigma(E)}{4\pi} \left[1 - \frac{1}{2} \beta(E) P_2(\cos \theta) \right], \quad (1)$$

where $P_2(\cos \theta)$ is a Legendre polynomial, $\sigma(E)$ is the total cross section, and we have assumed the dipole approximation, L-S coupling, and unpolarized light. For electrons photoemitted from the 3p level of Ar, the function $\beta(E)$ is a measure of the interference between outgoing s- and d-waves, and should be a sensitive function of the atomic charge distribution. Here we show how this sensitivity of $\beta(E)$ can be exploited to produce an empirical pseudopotential which reproduces the Ar 3p data for $\beta(E)$ and $\sigma(E)$, at all energies $E \lesssim 70$ eV, even though the pseudopotential is constructed from data in a limited spectral region ($E < 25$ eV). For Ar, we find better agreement with the experiments than either Hartree Fock or correlation calculations [1].

The method assumes a potential of the form $V(r) = -Z(r)e^2/r$ with $Z(r)$ depending on adjustable parameters, e.g.

$$Z(r) = \begin{cases} 1 + (Z_0 - 1) \frac{(1-r/R)^2}{(1+Cr+Dr^2)} & \text{for } r < R \\ 1 & \text{for } r > R. \end{cases} \quad (2)$$

Here Z_0 is the nuclear charge (18 for Ar) and C , D , and R are the adjustable parameters. Note that $Z(R) = 1$ and $Z'(R) = 0$. The potential is employed to compute phase shifts $\delta_\ell(E)$ and the matrix-element ratios

$$A \equiv \int_0^\infty P_{3p} r_{op} P_{Es} dr / \int_0^\infty P_{3p} r_{op} P_{Ed} dr, \quad (3)$$

which come into the Cooper-Zare model [2]:

$$\beta(E) = \frac{2 - 4 A \cos(\delta_0 - \delta_2)}{2 + A^2} \quad (4)$$

Here P_{3p} is the radial 3p wavefunction of Ar [3], P_{Es} and P_{Ed} are continuum s- and d-waves, and r_{op} is an average of the length and velocity forms of the dipole operator.[†] The parameters of the potential (C , D , and R) are adjusted to achieve optimal agreement between the computed $\beta(E)$ and experimental data at selected energies E_i . Here we have

employed the data of Dehmer *et al.* [4], at only three energies $E_i = 5.37$, 11.01, and 24.96 eV. Using this pseudopotential we have computed the cross section $\sigma(E)$ in Fig. 1, and $\beta(E)$ at energies as large as 70 eV. Our results agree well with the data, including Houlgate's *et al.*'s [5] measurements which show considerable structure of $\beta(E)$ for $25 < E < 70$ eV (well outside the range of input data). For example, in Fig. 1, our results (solid line) are in better agreement with the data [6] (dotted), than Hartree-Fock length [1] (dot-dashed), Hartree-Fock velocity [1] (dot-dot-dashed), or RPAE [1] (dashed) calculations. The resulting empirical charge distribution $Z(r)$ is reassuringly similar to the Hartree distribution calculated using wavefunctions of Bagus *et al.* [3]. Moreover, preliminary analyses of Ne 2p data indicate that the success for Ar is not accidental.

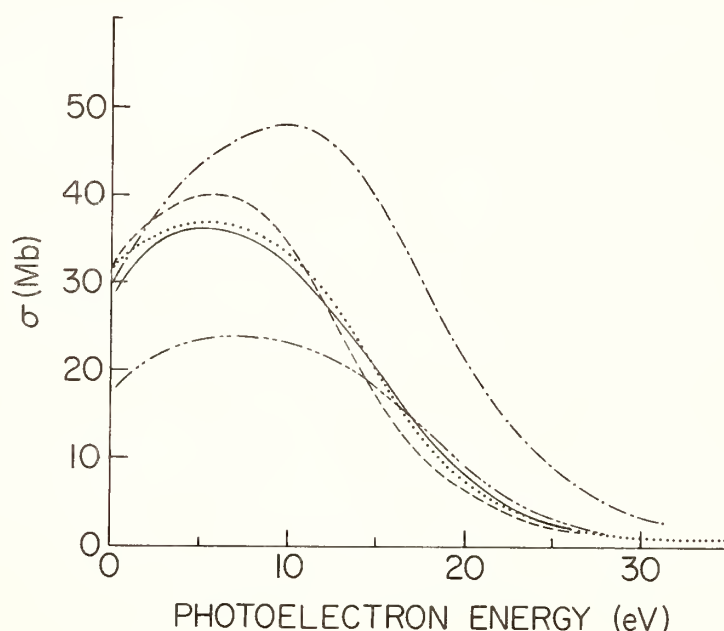


FIG. 1. Photoionization cross-section for the 3p subshell of Ar. (dotted) - experimental data [6], (solid) - present work, (dashed) - RPAE [1], (dot-dashed) - Hartree-Fock Length [1], (dot-dot-dashed) - Hartree-Fock Velocity [1].

It should be emphasized that semi-empirical phase-shifts, continuum wavefunctions, and bound charge distributions are all byproducts of the pseudopotential determination. We are optimistic that the method can be extended to a wide class of atoms, and expect that it will prove useful, not only for the description of soft x-ray excitations of atoms, but also for theories of photoemission and of low energy electron diffraction from surfaces and adsorbates.

[†]We use
$$r_{op} = \frac{1}{2} r + \frac{\hbar}{2m\omega} \left[\frac{d}{dr} - (1 - 2\delta_{l,2}) \frac{1 + \delta_{l,2}}{r} \right]$$

where $\hbar\omega$ is the energy of the photon, m is the electron mass, and the Kronecker delta, $\delta_{\ell,2}$, applies only to the d-wave. This form reduces the deviations from the oscillator-strength sum rule [1] which occur for Hartree-Fock wavefunctions (P_{3p}); the deviations are a direct consequence of the non-local nature of the Hartree-Fock potential.

References

- [1] M. Ya. Amusia, N. A. Cherepkov, and L. V. Chernysheva, *Sov. Phys. JETP* 33, 90 (1971).
- [2] J. Cooper and R. N. Zare, in Lect. in Theoretical Physics, Vol. XI-C edited by S. Geltman, K. Mahanthappa, and W. Brittin (Gordon and Breach, New York, 1969) p. 317.
- [3] P. S. Bagus, T. L. Gilbert, and C. C. J. Roothaan, *J. Chem. Phys.* 56, 5195 (1972).
- [4] J. L. Dehmer, W. A. Chupka, J. Berkowicz, and W. T. Jivery, *Phys. Rev. A* 12, 1966 (1975).
- [5] R. G. Houlgate, J. B. West, K. Codling, and G. V. Marr, *J. Phys. B* 7, L470 (1974); and *J. Elec. Spec.*, to be published.
- [6] J. A. R. Samson, in Advances in Atomic and Molecular Physics, edited by D. R. Bates and I. Estermann (Academic Press Inc., New York, 1966), Vol. 2, p. 177.

*Research supported by National Science Foundation grants DMR 73-07661 and 72-03026.

†National Science Foundation Predoctoral Fellow.

SATELLITES IN THE 1s- AND 2s-XPS SPECTRA OF NICKEL OXIDE

Eeva-Kaarina Viinikka^{*)} and Paul S. Bagus
IBM Research Laboratories
5600 Cottle Road, San José
California 95193, U.S.A.

The satellite structure in the inner-shell XPS spectra of first row transition metal compounds has been a subject of some experimental studies (1-2). However, there has been no detailed theoretical study on the origin of the satellites.

With correlated many-electron wave functions for a molecular cluster it has been possible to provide a correct description for the valence- and 3s-shell XPS spectra (3-4) of transition metal compounds. Here we make a report of similar calculations for the 1s- and 2s-hole states of nickel oxide. Our model for a wave function of bulk NiO is characterized by:

1. NiO_6^{10-} cluster, with distances between atoms taken from the NiO crystal. All electrons of the cluster are treated explicitly.
2. A point charge field around the cluster fitted to represent the crystal Madelung field.
3. Extended LCAO basis set. ALCHEMY/MOLECULE program system.
4. Calculations for both the ground and ionic state wave functions have been performed both at the Hartree-Fock (HF) and the configuration interaction (CI) level. The latter allows for electron correlation.

From our results we can conclude the following:

1. The intensive satellite at 6-8 eV from the main peak is due to a $\text{O}(2p)e_g \rightarrow \text{Ni}(3d)e_g$ charge transfer and to the different relaxation of the Ni3d orbitals in the two ionic states involved.
2. A weak satellite at about 12-15 eV comes from a $(\text{O}(2p)e_g)^2 \rightarrow (\text{Ni}(3d)e_g)^2$ charge transfer.
3. The satellite structure in the 1s- and 2s-spectrum are essentially similar. The larger multiplet splitting in the 2s together with the broad lines makes the analysis difficult.
4. It is essential for the model not only to allow for the $\text{O}(2p) \rightarrow \text{Ni}(3d)$ charge transfer, but also to allow for the different relaxation of the Ni(3d) orbitals in the ionic ground state and in the "shake-up" states.

*) Present address: Laboratory of Physics
Helsinki University of Technology
SF-02150 Espoo 15, Finland

An example of our results is given in table I.

Table I. Computed ${}^5A_{2g}$ 1s-hole states of NiO_6^{10-} .

Both $O(2p) \rightarrow Ni(3d)$ charge transfer and $Ni(3d)$ relaxation included.

Configuration \ E	State 1 0.0	State 2 6.6 eV	State 3 12.9 eV
1. $(Ni(3d)e_g)^2(O(2p)e_g)^4$	0.94	0.32	0.06
2. $(Ni(3d)e_g)^3(O(2p)e_g)^3$	0.28	0.92	0.05
3. $(Ni(3d)e_g)^4(O(2p)e_g)^2$	-0.10	-0.08	-0.91
Relative Intensity	0.51	0.26	0.01
I_s/I_l		0.51	0.02

1. R.A. Pollack, Ph.D. Thesis (University of California at Berkeley) unpublished.
2. K.S. Kim, Phys.Rev. 11, 2177 (1975)
3. P.S. Bagus, A.J. Freeman, F. Sasaki, Phys.Rev. Letters 30, 850 (1973).
4. P.S. Bagus, U.I. Wahlgren, Physica Fennica 95, 275 (1974).

MULTIPLY SPLITTING OF CORE 2p AND 3p PHOTOELECTRON LINES OF TRANSITION METAL HALIDES

M. Okusawa, T. Ishii, and T. Sagawa

Department of Physics, Tohoku University, Sendai 980, Japan

In X-ray photoemission spectra of core levels of some compounds, fine structures other than spin-orbit splitting are observed, and this phenomenon is one of the remarkable aspects of photoemission. A lot of arguments have been made concerning the origin of the fine structure, and its qualitative explanation appears to have been established. Recent studies in this problem aim at more quantitative analysis of the spectra. Energies of correlation between an outer-shell electron and an inner-shell electron as well as the energy of charge transfer from a ligand ion to a metal ion may be obtained through the analysis of the fine structure. Spectral resolution attainable with presently available experimental instruments is not high enough, but the observable line-profile may be given as an overlap of essentially-unresolved component-lines. We have carried out an experimental investigation of the 2p, 3s, and 3p lines of transition-metal ions in transition-metal halides. In this report, the results on the chlorides and the bromides are presented.

Measurements were performed with an electron-energy-analyzer of the hemispherical type with a mean radius of the electron trajectory of 132mm. Samples were prepared by evaporation and subsequent annealing at 150°C. Pressure during measurements and sample evaporation was in the range of 10^{-8} Torr. Measurements and data accumulation were controlled by a Yokogawa-Hewlett-Packard 2100A computer.

All spectra observed here have profiles which are dependent on ligand anions. This feature is quite clearly observed when comparison is made with the spectra of compounds other than halides, for example, the oxides and the sulfides.[1] As the metal ion in the sample changes from chromium to nickel, the profiles of the core level lines change markedly. This dependence of the spectrum on the number of 3d-electrons in a metal ion, along with the ligand-dependence, is favorable to the interpretation that the fine structures are due to the charge-transfer transition from the ligand p-orbital to the 3d-orbital of the metal ion.[2, 3] The multiplet-coupling between 3d-electrons and a core-hole is appreciable. In the analysis of the spectra the line distributions theoretically predicted are usually convoluted with a window function giving a broadening about 1eV and then compared with the experimental data. Recently, Satoko[4] proposed a method of the analysis where the moment of a spectrum around its center of gravity, defined as $\mu^N = \int (\omega - \omega_0)^N I(\omega) d\omega / \int I(\omega) d\omega$, is used.

Figure 1 shows the second and third moments of the 2p and 3p lines of transition metal ions calculated from the observed spectra.

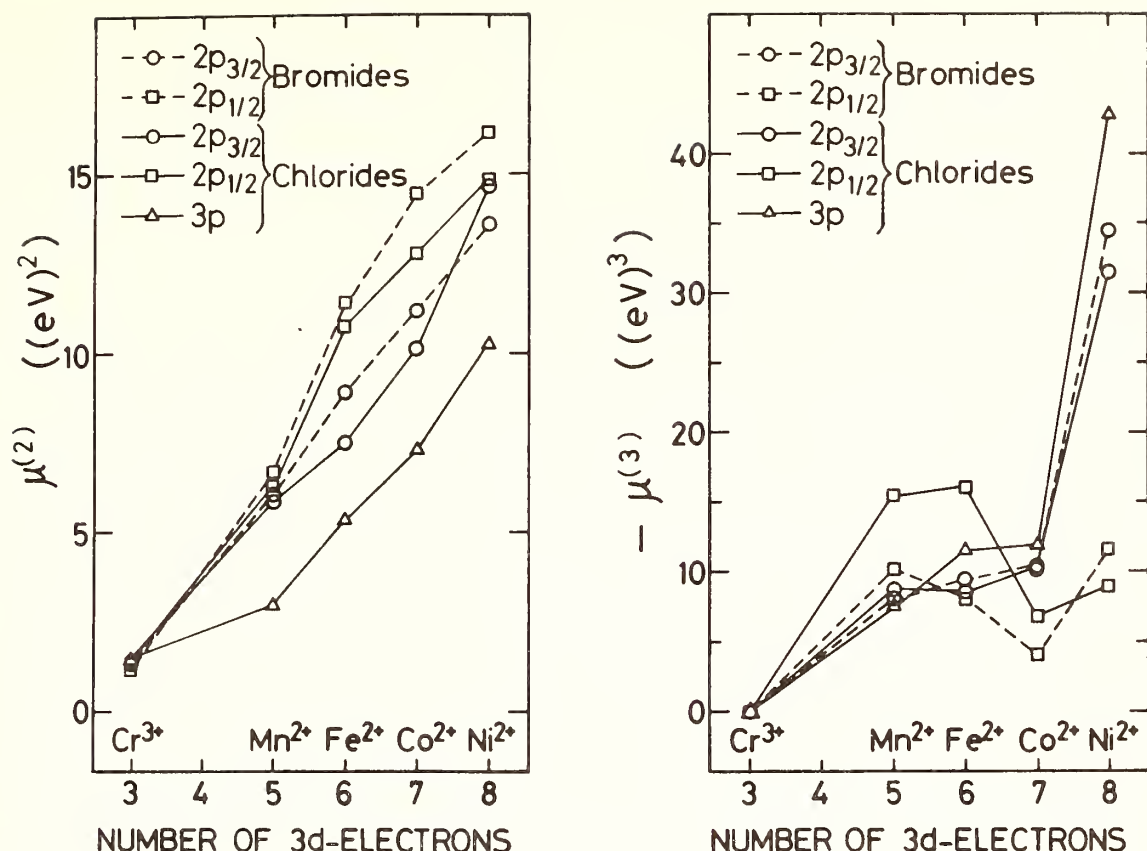


Fig. 1. The second and third moments of the 2p and 3p lines of transition metal ions in the chlorides and the bromides.

The moments are calculated from the overall profiles of the lines including satellites. In the 2p spectra, the spin-orbit energies are sufficiently large as compared with multiplet splitting and charge-transfer energies to make the 2p_{1/2} and 2p_{3/2} components be separated completely. The moments were obtained for both component-lines. In the 3p spectra, the spin-orbit energies are not large and the moments were calculated for the whole spectra. Before the moments were calculated, the backgrounds of the spectra caused by inelastically scattered electrons were subtracted under the assumption that the intensity of the overlapping background is proportional to the integrated intensity of the true line.

The second moments of both 2p and 3p lines decrease as the atomic number of transition metal decreases. If the line distribution is determined by the multiplet splitting only, the width of the spectrum is expected to become broader as the number of energy levels arising from the 3d-electrons of a metal ion increases. Satoko's calculation[4] suggests that the second moment is largest in Mn-compounds. Monotonic decrease towards Cr-compounds in Fig.1 is brought about by the contribution of the charge-transfer satellite. The contribution of the satellite is largest in Ni-compounds. The main line of a 2p_j spectrum is broadened by the multiplet splitting. It might be possible to separate the main line and calculate the

moments for this line. We actually tried this. However, the overlap between the main line and the satellite was not negligible and the results of calculation included appreciable errors. With the inevitable errors thus introduced, the difference in the second moments among different materials was not large and the systematic change due to the difference of the number of 3d-electrons was not found.

In the case of the 3p lines, the situation is slightly complicated. According to Satoko's theory [4], that the spin-orbit components are unable to be separated is not serious at all, and the analysis can be made with the inclusion of the spin-orbit interaction. As is obvious in Fig.1, the dependence of the second moments on the number of 3d-electrons in a metal ion is quite similar to the 2p lines. However, the interpretation may not be unique. According to the calculation by Asada et al. [5], the 3p spectrum of NiCl_2 is explained in terms of multiplet splitting with appropriately-scaled Slater-Condon parameters. Incorporation of the separate contribution of satellites appeared unnecessary. Thus, the result shown in Fig.1 may be ascribed to the following two possibilities: (1) In the case of the 3p lines, the charge-transfer excitation of p-electrons has appreciable effects, and the multiplet splitting and the satellite effect mix each other completely. (2) As the number of 3d-electrons decreases, the energies of high-energy components of the multiplet increase but their intensities decrease at the same time. Low signal-to-noise ratio makes it too difficult to find them. As regards to this point, it is worth noting that high-energy multiplet components are found in both XES and XPS spectra of MnF_2 . [6, 7] More detailed analyses concerning these points are now under progress.

References

- 1 M. Okusawa, T. Ishii, and T. Sagawa: *Physica Fennica* 9 suppl. S1, 298 (1974)
- 2 K. S. Kim: *Phys. Rev.* B11 (1975)
- 3 S. Asada and S. Sugano: *Tech. Repts. ISSP A.750* (1976), to be published in *J. Phys. Soc. Japan*
- 4 C. Satoko: Private Communication
- 5 S. Asada, C. Satoko, and S. Sugano: *J. Phys. Soc. Japan* 38 855 (1975)
- 6 V. M. Pessa: *J. Phys.* C8 1769 (1975)
- 7 C. S. Fadley and D. A. Shirley: *Phys. Rev. Lett.* 30 850 (1970)

J.J. PIREAUX⁺§, S. SVENSSON, E. BASILIER, P-Å MALMQVIST, U. GELIUS, R. CAUDANO§ and K. SIEGBAHN.

University of Uppsala, Institute of Physics, P.O.Box 530, S-751 21 UPPSALA 1 Sweden

§ Facultés Universitaires, Laboratoire de Spectroscopie Electronique, Rue de Bruxelles 61, B-5000 NAMUR, Belgium

INTRODUCTION

One observes generally that core electron binding energies are larger for isolated atoms or molecules than for the corresponding liquids or solids. This is also the case when comparing free atoms and their corresponding diatomic molecules. The effect is due to the fact that the larger systems have available more degrees of freedom for electronic reorganization of a core orbital, increasing the relaxation energy.

The alkanes (C_nH_{2n+2}) constitute a suitable series to study the influence of the molecular size on the electronic relaxation energy, since the molecule size can be progressively increased by choosing molecules with different n .

ALKANES C1s CHEMICAL SHIFTS

High resolution ESCA measurements have been performed on the C1s core levels for the alkanes with $1 \leq n \leq 13$. Table I reports the experimental C1s chemical shifts, referred to the methane C1s binding energy [1,2]. The alkane chemical shifts, determined to within ± 0.02 eV, are small, ranging over an energy scale of about 0.6 eV only. A very smooth variation of binding energies is observed. We report here a negative chemical shift for the alkanes, the C1s binding energies decreasing with an increasing length of the molecules.

KOOPMANS' THEORETICAL CORRELATIONS

ESCA chemical shifts arise generally [3,4] because of different electronic distribution around the atom to be ionized. In the simple electrostatic approximation, a positive chemical shift corresponding to an increasing binding energy is correlated to an increase of the positive charge on the atom. Table I (third column) shows that this trend is not encountered for the alkanes series, since the chemical shifts are predicted to be positive from *ab initio* charges on the carbon atoms. The electrostatic interaction from the other atoms in the molecules have been accounted for in the *ground state potential model* [4]. This model, using CNDO/2 charges, does not improve the previous correlation since signs and trends of the calculated shifts still are incorrect (Table I, fourth column).

These two models rest on the Koopmans' approximation. This does not account for the final state influence, generally included in a relaxation

+ Aspirant du Fonds National Belge de la Recherche Scientifique.

energy term [5]. The fact that the Koopmans' approach is not successful in describing the alkanes chemical shifts is evidence that in this case the variation in the relaxation energy is a dominant term compared to the classical electrostatic effect.

Table I. Alkanes Cls chemical shifts. Comparison between experimental ESCA data with various theoretical models

Molecule	Experimental shift(eV) ^a	Ab initio charge ^b	Potential Model shift ^c (eV)	Transition Potential Model shift ^d (eV)	ΔSCF shift (eV) b
CH ₄	0.0	-0.2511	0.0	0.0	0.0
C ₂ H ₆	-0.12	-0.1627	0.37	-0.40	-0.32
C ₃ H ₈	-0.26	-0.1468	0.50	-0.62	-0.60
n-C ₄ H ₁₀	-0.35	-0.1293	0.57	-0.82	-0.68
n-C ₅ H ₁₂	-0.41	-0.1122	0.66	-0.93	---
n-C ₆ H ₁₄	-0.47	-0.1068	0.68	-1.00	---
n-C ₈ H ₁₈	-0.52	-0.1014	--	---	---
n-C ₁₀ H ₂₂	-0.56	---	0.70	-1.09	---
n-C ₁₃ H ₂₈	-0.57	---	--	---	---

a : shift relative to the Cls line; its centroid was measured at 290.83 eV [1,2]

b : ab initio minimal basis calculations

c : $\Delta E = k_A Q_A + V_A + L$ with $k_A = 22.11$ eV/unit charge

d : $\Delta E = k_A^T Q_A^T + V_A^T + L^T$ with $k_A^T = 24.3$ eV/unit charge

RELAXATION EFFECT

The relaxation effects are implicitly included in the *transition potential model* [6,7], where charges are calculated for a fictitious transition state, intermediate between the ground and final states of the molecules. The correlation obtained between the experimental chemical shifts and data calculated with this model is good as can be seen by comparing columns 2 and 5 of Table I. The correct experimental trend is finally reproduced.

This reorganisation process can be discussed in terms of a charge redistribution within the whole molecule, with the effect that the created positive charge is screened. Fig. 1 illustrates this charge flow for a n-hexane molecule. As can be seen, all the atoms effectively participate in the screening of the core hole. With increasing molecu-

lar size, the electron flow can be taken from more and more distant atoms, resulting in an increasing total relaxation contribution to the chemical shift.

In order to estimate the accuracy of this model, explicit Δ SCF calculations were performed on both the initial and excited states of the molecules using the equivalent core approximation. It was found that the ab initio Δ SCF binding energies reproduce the decreasing behaviour of the experimental shifts (Table I, column 6). These results show that a satisfactory description of the alkane core orbitals energies has to include the relaxation effect.

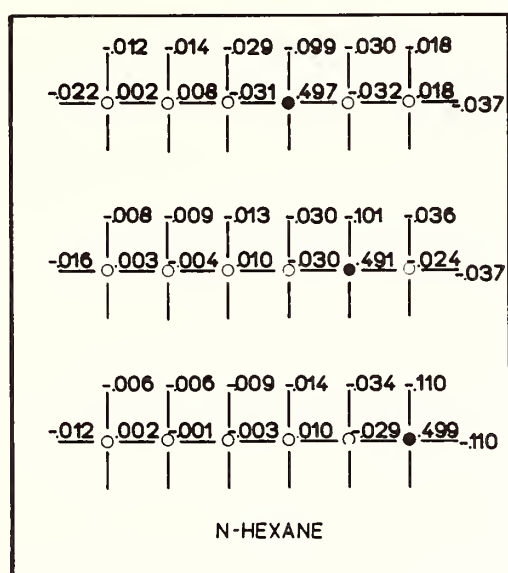


Fig. 1. : charge flow ΔQ in n-hexane (difference in charge before and after ionization of the atoms marked by a black dot).

ACKNOWLEDGEMENT

One of the authors (J.J.P.) is grateful to the belgian F.N.R.S. for financial support.

REFERENCES

- [1] J.J. Pireaux, Ph.D Thesis, Facultés Universitaires, Namur, 1976.
- [2] J.J. Pireaux, S. Svensson, E. Basilier, P-Å Malmqvist, U. Gelius, R. Caudano and K. Siegbahn. Uppsala Report UUIP 920 (March 1976); subm. for publ.
- [3] K. Siegbahn et al. ESCA. Atomic, molecular and solid state structure studied by means of electron spectroscopy. (Almqvist and Wiksells, Uppsala 1967).
- [4] K. Siegbahn et al. ESCA applied to free molecules (North Holland, Amsterdam 1969).
- [5] U. Gelius and K. Siegbahn. Trans. Far. Soc. 54 (1972) 2571.
- [6] G. Howat and O. Goscinski. Chem. Phys. Lett. 30 (1975) 87.
- [7] H. Siegbahn, R. Medeiros and O. Goscinski. J. Electr. Spectr. 8 (1976) 149.

ESCA STUDIES OF THE ALKALI HALIDES,
LiF, LiCl AND LiBr, AND OF Li METAL.

L.I. Johansson, S.B.M. Hagström* and S.-E. Karlsson

Department of physics and measurement technology,
Linköping University, S-581 83 Linköping, Sweden.

Controversies in the interpretation of soft x-ray absorption spectra of alkali halides have arisen because excitonic enhanced absorption peaks may appear below the band edges. These peaks are difficult to distinguish accurately from the thresholds for interband transitions. An approach has recently been proposed [1,2,3] in which x-ray photoemission (ESCA) is used in conjunction with optical band gap data to determine these thresholds. For insulators the threshold for transitions from a core level to the conduction band $\Delta\epsilon_{\ell\lambda}$ can be represented as the sum of two energy differences [1] ; $\Delta\epsilon_{\ell\lambda} = \Delta\epsilon_{\ell\ell}' + \Delta\epsilon_{\ell\lambda}'$. The first $\Delta\epsilon_{\ell\ell}'$ is the difference between the top of the valence band and the core level of interest. The second $\Delta\epsilon_{\ell\lambda}'$ is the difference between the bottom of the conduction band and the top of the valence band, i.e. the optical band gap. The first energy difference can be obtained by subtracting ESCA measurements for the ionization energies of electrons in the core level from those at the top of the valence band. We have performed such measurements on the alkali halides LiF, LiCl and LiBr.

The photoelectrons, expelled by $MgK\alpha_{1,2}$ or $AlK\alpha_{1,2}$ radiation, were energy analysed in an electrostatic instrument which operates under high vacuum conditions, 10^{-7} torr. The overall resolution of the instrument was set at 1.3 eV FWHM for the $Au4f_{7/2}$ peak excited by $MgK\alpha_{1,2}$ radiation. The measurements were performed on single crystals of LiF, on films evaporated in situ and on pressed powder samples of LiCl and LiBr. It was possible to ignore charging effects because the samples were irradiated for at least one hour before any actual measurement and valence band and core levels were then recorded in the same spectrum. The top of the valence band was experimentally determined from the intersection of a line extrapolated from the segment of maximum negative slope with the line defining the background level in the recorded spectrum. Our estimated uncertainty in this determination is ± 0.2 eV. Our valence band spectra will be presented and compared with available UPS results.

The energy separations, obtained between the top of the valence band and the $Li1s$ level, in these three halides are summarized in Table 1. Literature values of the optical band gap are also given in Table 1 as are

* Present address: Xerox Corporation, Palo Alto Research Center,
3333 Coyote Hill Rd, Palo Alto, California 94304, USA

Table 1 Summary of energy differences concerning the Li1s level. The figure in the parentheses represents the estimated uncertainty in the last digit of our measured values. The symbols introduced are defined in the text and their values are given in eV.

Compound	$\Delta\epsilon_{\ell\ell}'$	$\Delta\epsilon_{\ell\lambda}'$	$\Delta\epsilon_{\ell\lambda}$
LiF	49.8(3)	13.6 ^a	63.4
LiCl	53.2(3)	9.4 ^a	62.6
LiBr	54.1(4)	7.6 ^a	61.7

^ataken from ref. 4.

the interband transition thresholds represented by the sum of those two terms. The agreement between the present results and previously published results on LiF and LiCl is quite satisfactory. Our result of 51.4 eV for LiBr confirms the estimated value of 54.2 eV [1,3] which previously has been used for the interpretation of the soft x-ray absorption spectrum. The observed dominant peaks [5], in the soft x-ray absorption spectrum, lie at 61.9, 60.8 and 60.4 eV respectively for LiF, LiCl and LiBr. Thus, these can be identified as purely excitonic since their energies are 1.5, 1.8 and 1.3 eV smaller than the thresholds listed in Table 1 for LiF, LiCl and LiBr respectively. Our results on the energy separation between the Li1s level and the valence band also agree well with the predictions of the point charge model including corrections for polarization effects. Further experimental results as well as references are to be found in ref. 6.

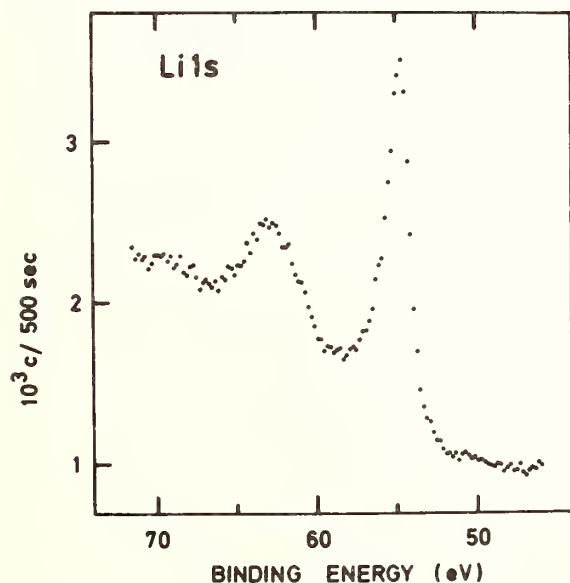


Fig 1. ESCA spectrum from Li metal showing the Li1s line and structure due to plasmon losses.

For comparison metallic Li was also studied. In this case the measurements were performed under ultrahigh vacuum conditions ($\leq 2 \times 10^{-10}$ torr). The resolution was set at 1.6 eV FWHM and films of Li were prepared by electron gun evaporation onto a polished copper backing. During deposition the pressure was kept below 1×10^{-7} torr. A weak O1s line was observed in the photoelectron spectrum a few hours after deposition so repeated evaporations were made. A recording of the Li1s spectrum is shown in Fig. 1. The binding energy is given with respect to the Fermi level and the Au4f_{7/2} line was used as re-

ference level (83.8 eV). The larger peak in Fig. 1 corresponds to the Li1s level. Its binding energy was found to be 54.7 (1) eV in good agreement with an earlier investigation [7]. Extra atomic relaxation contributes a shift of several eV as estimated from values for free atoms [7].

The broad structure in the spectrum is due to plasmon losses. The maximum of the structure lies at 8.0(3) eV below the Li1s level which corresponds rather well to the bulk plasmon loss. The shoulder on the low binding energy side corresponds to the surface plasmon loss.

The Li1s level could not be related to the valence band because the valence band spectrum was too weak probably because of the low photoionization cross section.

REFERENCES

1. S.T. Pantelides, Phys. Rev. B 11, (1975) 2391
2. F.C. Brown, Solid State Phys. 29, (1974) 1
3. S.T. Pantelides and F.C. Brown, Phys. Rev. Lett. 33, (1974) 298
4. W.H. Strehlow and E.L. Cook, J. Phys. Chem. Ref. Data 2, (1973) 163
5. R. Haensel, C. Kunz and B. Sonntag, Phys. Rev. Lett. 20, (1968) 262
6. L.I. Johansson and S.B.M. Hagström, to appear in Physica Scripta
7. S.P. Kowalczyk, L. Ley, F.R. McFeely, R.A. Pollak and D.A. Shirley, Phys. Rev. B 8, (1973) 3583

X-RAY SPECTRA OF TRANSITION METAL ALLOYS AND THEIR INTERPRETATION

E.Z. Kurmaev
Institute of Metal Physics
The Ural Scientific Centre
Academy of Sciences of the USSR
Sverdlovsk GSP-170, USSR

The experimental results of $\text{MeK}\beta_5$ -emission bands ($\text{Me}=\text{V}, \text{Cr}, \text{Fe}$) investigation in alloys with transition metals of II and III periods are represented. The influence of relative arrangement of alloyed components, atomic and electron concentration, type of crystal structure on the electron energy spectra of alloys is analysed. The question about short-order manifestation in X-ray emission spectra is considered and a new interpretation of $\text{MeK}\beta_5$ -bands is proposed. These investigations show that the CPA theory gives a good description of the electron structures formed in the alloys of transition metals. The state of order and the crystal structure of the studied alloys hardly affects the global features of electron structures in these alloys. The values of δ -parameter for CPA theory are determined from X-ray emission spectra of alloys under investigation.

FORMATION OF BAND STRUCTURES IN QUASI ONE DIMENSIONAL MOLECULES

J.J. PIREAUX⁺§, S. SVENSSON, E. BASILIER, P-Å MALMQVIST, U. GELIUS, R. CAUDANO§ and K. SIEGBAHN.

University of Uppsala, Institute of Physics, P.O.Box 530, S-751 21 UPPSALA 1 Sweden

§ Facultés Universitaires, Laboratoire de Spectroscopie Electronique Rue de Bruxelles, 61, B-5000 NAMUR, Belgium

INTRODUCTION

X-Ray and UV photoelectron spectroscopies have emerged over the last ten years as powerful methods for studying experimentally the electronic band structures of solids. In this work [1-3] we propose to follow and study by electron spectroscopy the construction mechanism of an electronic energy band during the progressive formation of a solid. The basic idea rests on the following simple model. When two identical atoms approach each other to form a molecule, their electronic clouds start to overlap and this results in a splitting of the electronic levels in the molecule. The splitting will be more pronounced for the outermost shells of the molecule where the overlap between the atomic orbitals is larger. The Pauli principle then prevents the electrons from all going into the orbitals with lowest energy, i.e. we have the *aufbau principle*. As the number of identical atoms in the molecule increases, the level density will increase correspondingly, and gradually this will become a band structure.

Another illustration of a band structure formation was recently reported through the ESCA analysis of the 4d band of silver particles with varying radii [4]. As for us we found that the carbon compounds in the series of the alkanes (formula C_nH_{2n+2}) are suitable to study step by step the formation of a band structure. The successive molecules with increasing number n are in fact considered as progressive steps in constructing a quasi one dimensional solid.

EXPERIMENT

The valence electronic levels of the alkanes have been recorded by high resolution photoelectron spectroscopy using monochromatized Al K α radiation source. Spectra from methane to n-tridecane ($n = 1$ to 13) were recorded in the gas phase with an ESCA spectrometer previously described [5]. Measurements in the condensed phase were performed for n-pentane to polyethylene ($n = 5$ to ∞) on an HP 5950A ESCA spectrometer.

FORMATION OF A BAND STRUCTURE

The linear saturated hydrocarbons contain $6n + 2$ electrons distributed between $3n + 1$ energy levels in their valence electronic region. These levels are divided into two groups : a C2p-H1s band containing carbon-hydrogen bonding orbitals, and a C2s band of essentially carbon-

+ Aspirant du Fonds National Belge de la Recherche Scientifique.

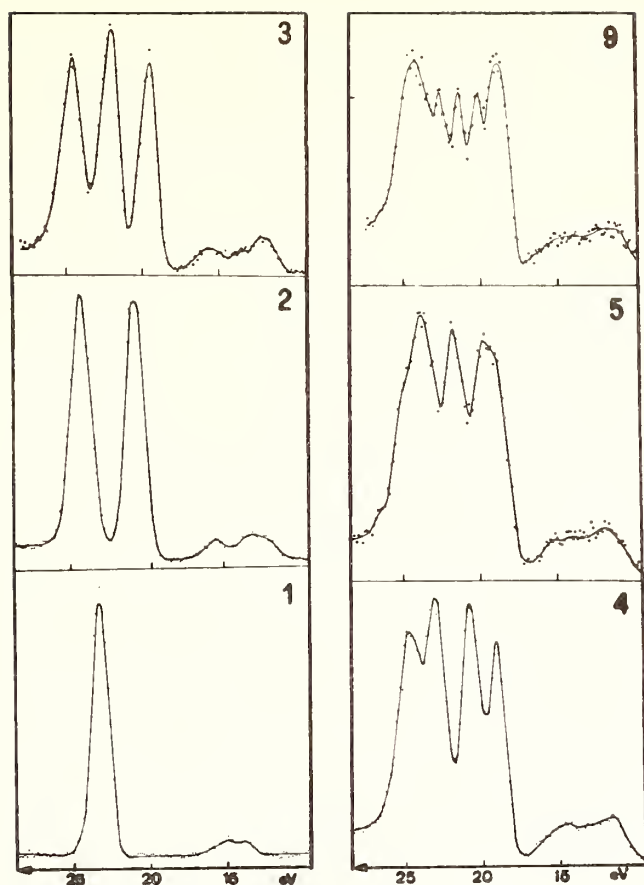


Fig. 1. : Valence electron spectra of the alkanes ($1 \leq n \leq 9$) recorded in the gas phase.

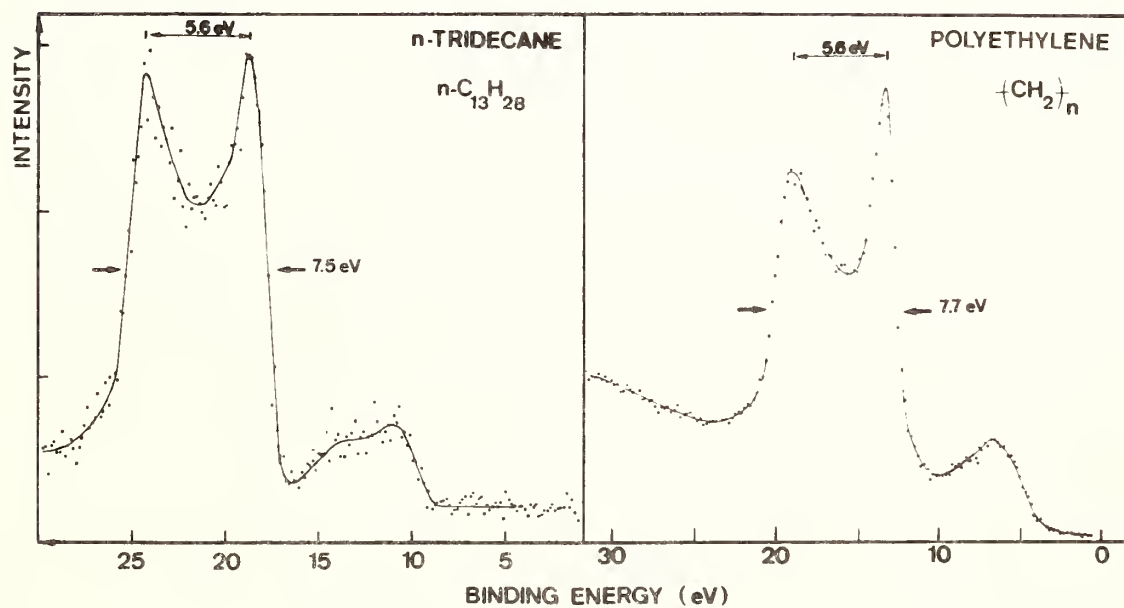


Fig. 2. : Valence electron spectra of n-tridecane and polyethylene recorded respectively in the gas and solid phases.

carbon bonding character. The number of electronic levels in this last region equals the number of carbon atoms in the linear alkane chain [6].

As discussed above, the C2s molecular orbital splits with the increasing number of carbon atoms in the molecule. The single $2a_1$ (C2s) level in methane is divided into two components in ethane, three components in propane, etc. (Fig. 1).

Since the C2s band is spread out over a limited energy range of about 7.5 eV, the spacing between each level decreases with an increasing number of carbon atoms. Progressively, the distinction between the levels vanishes and, for larger n , the peaks overlap and form a band structure.

It is interesting to find out for which number n , the ESCA spectrum of an alkane becomes essentially similar to the one of polyethylene [7]. This would in fact give the minimal system length necessary to successfully simulate the real band structure of an infinite one dimensional solid. Fig. 2 shows that no sub-structure can be resolved already for the n -tridecane ($n = 13$) spectrum. Moreover, this valence band is evidently quite similar to the spectrum of polyethylene recorded in the solid phase [7]. We conclude that thirteen atoms in the alkane chain are sufficient to simulate the electronic properties of polyethylene.

The magnitude of the C2s level splitting depends on the overlap between the corresponding electronic wave functions on the neighbouring atoms. Consequently, it is a function of the distance between the atoms in the molecule. The ethane (C_2H_6), ethylene (C_2H_4) and acetylene (C_2H_2) molecules constitute a suitable series to study this effect, their carbon-carbon distances being 1.54, 1.33 and 1.21 Å, respectively. Indeed, the splitting ΔE between the two components of the C2s band increases with the shortening of the C-C distance, being 3.49, 4.41 [8] and 4.74 [9] eV.

Finally spectra recorded in the gas and solid phases have been compared in search of a phase transition effect, i.e. influence of inter-molecular interactions on the band structure spectra. For n -pentane taken as an example, Fig. 3 shows that the two spectra are essentially similar, presenting the same number of structures in the C2s band. The most significant difference between the two spectra is a slight increase in the peak widths recorded in the solid phase. As the alkane molecules do not contain any polar group or dipole moment, it is in fact understandable that the inter-molecular interactions will not affect the solid state spectra significantly.

ACKNOWLEDGEMENTS

One of the authors (J.J.P.) wishes to thank the "Fonds National de la Recherche Scientifique, Belgique" for financial support.

REFERENCES

- [1] J.J. Pireaux. Ph.D. Thesis, Facultés Universitaires Namur 1976.
- [2] J.J. Pireaux, S. Svensson, E. Basilier, P-Å Malmqvist, U. Gelius, R. Caudano and K. Siegbahn. Uppsala UUIP 920; subm. for publ.
- [3] J.J. Pireaux, R. Caudano, J. Riga and J.J. Verbist, to be publ.
- [4] S.T. Manson and R.C. Baetzold. J. Chem. Phys. 64 (1976) 271.

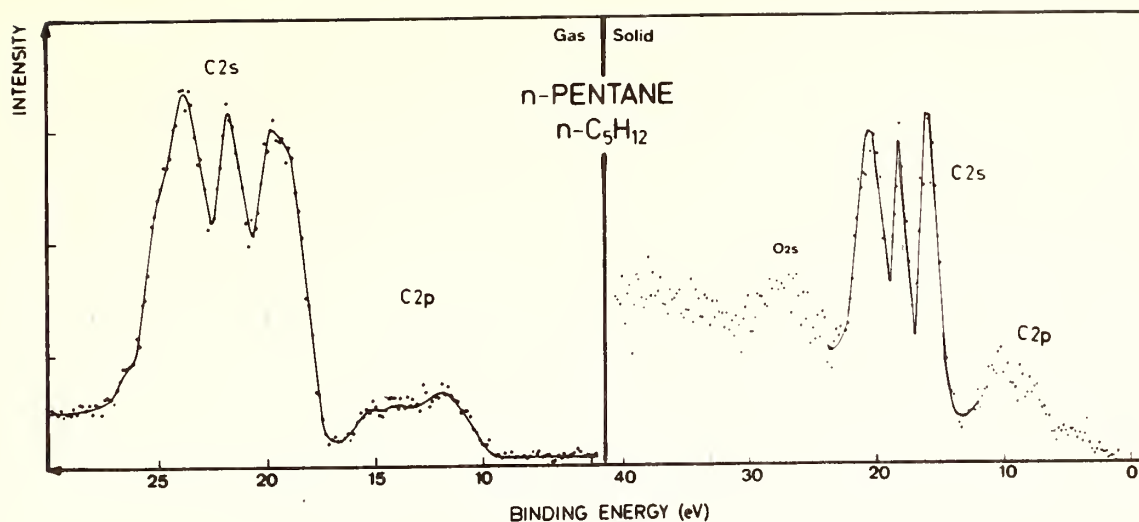


Fig. 3. : Valence electron spectra of n-pentane recorded in the gas and solid phases.

- [5] U. Gelius, E. Basilier, S. Svensson, T. Bergmark and K. Siegbahn. *J. Electr. Spectr.* 2 (1973) 405.
- [6] See e.g. R. Hoffman. *J. Chem. Phys.* 40 (1963) 2047.
- [7] J. Delhalle, J.M. André, S. Delhalle, J.J. Pireaux, R. Caudano and J.J. Verbist. *J. Chem. Phys.* 60 (1974) 595.
- [8] A. Berndtsson, E. Basilier, U. Gelius, J. Hedman, M. Klasson, R. Nilsson, C. Nordling and S. Svensson. *Phys. Scripta* 12 (1975) 235.
- [9] P-Å Malmqvist, E. Basilier, U. Gelius, J.J. Pireaux, S. Svensson and K. Siegbahn. To be published.

BERYLLIUM K SPECTRA OF BERYLLIUM COMPOUNDS

Yasuo IGUCHI

Institute for Optical Research, Kyoiku University
Shinjuku-ku, Tokyo 160, Japan

Beryllium K emission spectrum of beryllium metal has been one of the important subjects of the soft x-ray spectroscopy for a long time. The spectra of beryllium compounds, however, have been studied in a few cases. Among them, BeO, which is known as a very important substance for material research and for practical purpose, has been studied exceptionally from many aspects. There are excellent papers, for example, on the soft x-ray spectra of it (1), the fundamental absorption spectrum (2), the XPS spectrum (3), and theoretical study of the electronic structure of the valence band (4). These previous studies give us many informations on the electronic structure of BeO, though they are still not enough.

In the present study, beryllium K emission spectra and relative photoelectric yield spectra near the beryllium K absorption edge of BeO, BeF₂, BeSO₄, and activated BeCu have been measured by means of a three meter grazing incidence monochromator and a soft x-ray tube as a light source to add some more informations on the electronic structure of these substances.

A glass grating with 1080 lines per mm was mounted at an angle of incidence of 84.73°. The resolution of the monochromator was better than 300 for the present experiments. The soft x-ray tube was operated at 3.5 kilovolts and at 10 mA for the emission spectrum and 200 mA for the yield spectrum. A photomultiplier with twenty dynodes was used as a detector. LiF photocathode was used to take the emission spectrum, and a sample plate or Ni plate, on which sample powder was spread over, was used as a photocathode to take the yield spectrum. Pressure of the apparatus was maintained at 2×10^{-6} Torr.

BeO has the wurtzite structure, and on the other hand, BeF₂ has α -quartz structure. Therefore, long range ordering of the crystals has nothing in common. However, if we see the short range ordering, we can find tetrahedrons. A beryllium atom is situated in the center of each tetrahedron, and the other atoms on the vertexes of it. As for BeSO₄, it is well known that Be(H₂O)₄ tetrahedron is important for the crystal growth.

These facts as well as the circumstance that the core state strongly localizes, suggest that the molecular orbital picture is useful for interpretation of soft x-ray spectra of the substances. As K shell electrons of beryllium atom have a₁ symmetry in the tetrahedron (T_d symmetry), the allowed state for electronic transitions giving rise to beryllium K spectra must have t₂ symmetry. Height of the structure of the spectra may reflect

amount of p-component in the t_2 state.

Some of the experimental results are shown in Fig.1 and Fig. 2. As for BeO, dominant structures have been observed in the emission spectrum at 89.4 eV, 105.0 eV, and 106.1 eV, and in the yield spectrum at 119.6 eV, 124.6 eV, and 138.6 eV. Corresponding structures of BeF₂ have been observed in the emission spectrum at 89.8 eV, 104.5 eV, and 106.4 eV, and in the yield spectrum at 120.5 eV, 124.8 eV, and 138.4 eV. An extra structure has been observed in the emission spectrum of BeF₂ at about 110 eV. The widths of main bands of the emission spectra are 10 eV and 12 eV for BeO and BeF₂ respectively. These values of the band widths agree with the ones determined by XPS (3) and UPS (7). The structures at 118 eV observed in both of the emission spectra of BeO and BeF₂ are considered due to double ionization (5). The yield spectrum of BeSO₄ agrees with the one reported by Brohin et al. (6), and it shows corresponding structures to the ones of the yield spectra of BeO and BeF₂. The yield spectrum of activated BeCu has closely similar structures to the ones of the yield spectrum of BeO. This fact and surface composition of activated BeCu observed by Ruttenberg and Haas (8) may support the molecular orbital picture for the interpretation of BeO spectra.

Tentative molecular orbital levels with t_2 symmetry of the tetrahedron are shown in Fig.3 together with experimentally determined energy scale. Atomic energy levels of Be, O, and F atoms are also shown in the figure. Anyhow, K spectra of the atom centered in the tetrahedron are useful for observing t_2 molecular orbitals selectively.

References

- (1) A.P.Lukirskii and I.A.Brytov: Soviet Phys.Solid State 6 33 (1964)
- (2) D.M.Roessler and W.C.Walker: J.Phys.Chem.Solids 30 157 (1969)
- (3) K.Hamrin et al.: Phys.Scripta 1 277 (1970)
- (4) W.O'Sullivan: J.Chem.Phys. 30 379 (1959)
- (5) Y.Hayashi: Sci.Rep.Tohoku Univ. (1) 51 1 (1968)
- (6) T.A.Brohin et al.: Izv.Akad.Nauk SSSR 38 652 (1974)
- (7) R.T.Poole et al.: Phys.Rev. B 12 5872 (1975)
- (8) F.E.Ruttenberg and T.W.Haas: J.Vac.Sci.Technol. 12 1043 (1975)

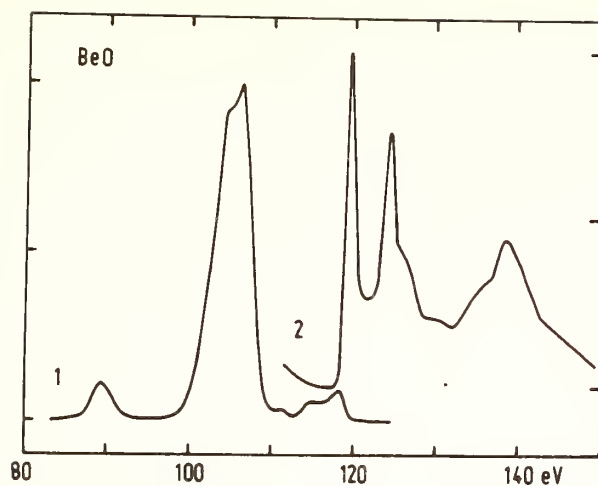


Fig.1 Beryllium K spectra of BeO.

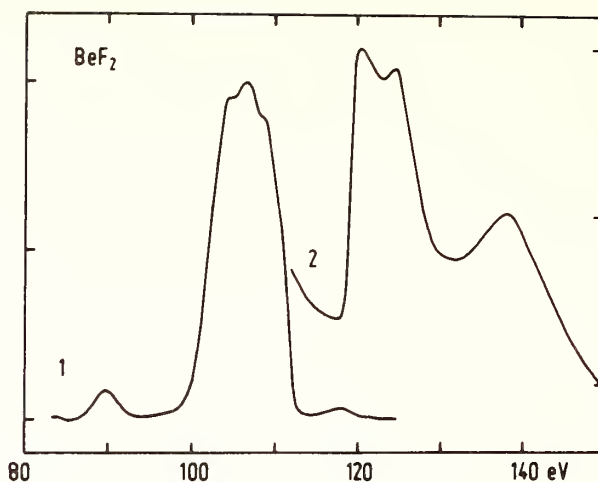


Fig.2 Beryllium K spectra of BeF₂.

1: Emission, 2: Photoelectric yield.

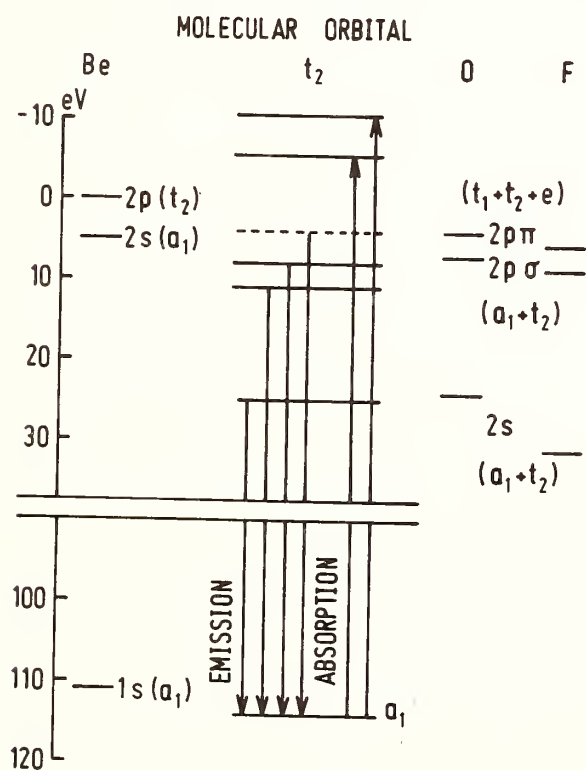


Fig.3 Energy level diagram for t_2 molecular orbitals of the tetrahedron.

M.T. COSTA LIMA - C. SENEMAUD

Laboratoire de Chimie Physique 11, rue Pierre et Marie
Curie 75231 Paris Cedex 05 - France.

Silicon monoxide, which has interesting properties for microelectronic applications, has often been considered as a mixture of pure silicon and quartz SiO_2 . However, some recent measurements from optical properties⁽¹⁾, nuclear analysis and infrared spectroscopy (2) are not accounted for by the same hypothesis. We have studied comparatively the K X-ray emission and absorption spectra of silicon in amorphous samples of pure silicon, SiO and SiO_2 . The influence of the crystalline state of Si and SiO_2 on their spectra is discussed elsewhere (3,4).

Without any adjustment in the energy scale, the absorption spectrum of SiO shows that this oxide is not a mixture Si + SiO_2 (5): no structure appears on the recordings, neither at the Si K edge position, nor at the wavelength of the strong SiO_2 absorption line. On the other hand, the SiO $\text{K}\beta$ emission has two structures, separated by about 4 eV, which appear at the position of Si $\text{K}\beta$ and SiO_2 $\text{K}\beta$ maxima, in agreement with previous results (6) (7).

The two electronic distributions involved in the X-ray transitions are affected by the chemical state of the element. In fact, the relative energetic position of the silicon valence and conduction bands in the element and in the oxide can be deduced from their K spectra, only if we know the shift of the K level. The Si 2p energy has been measured by ESCA in Si, SiO and SiO_2 (8). From our measurements of the energy of the $\text{K}\alpha$ emission ($2p \rightarrow 1s$) (3), we have deduced the energy of the 1s level in Si, SiO and SiO_2 , and, consequently the shift of this level in SiO and SiO_2 compared to the pure element. This shift is relatively high and is different for the two oxides = + 2,9 and 5,0 eV respectively.

Taking into account these values, we have adjusted the spectra of Si, SiO and SiO_2 , relatively to the position of the Fermi level obtained from the photoelectron spectra. (Fig. 1). This adjustment gives the relative position of the valence band and the limit of the conduction band of Si, SiO and SiO_2 . It appears that the SiO $\text{K}\beta$ emission is not a superposition of Si and SiO_2 spectra (9). This result is the same than deduced from the X-ray absorption spectra. A comparison with photoelectron spectra is shown on the figure. It will be discussed in details.

A tetrahedral model $\text{Si-Si}_y\text{O}_{4-y}$ has been proposed by Philipp (1) for the silicon monoxide. Following a statistical distribution, the arrangements Si-SiO_3 , $\text{Si-Si}_2\text{O}_2$ and $\text{Si-Si}_3\text{O}$ are the most likely. Then three types of binding are possible for the silicon atoms. They can be related to the three structures observed on the X-ray absorption curve of SiO , and to the maximums of the $\text{K}\beta$ emission, assuming that the broadest one corresponds to non-resolved transitions involving two different kinds of Si binding. So our X-ray spectra are consistent with Philipp's model.

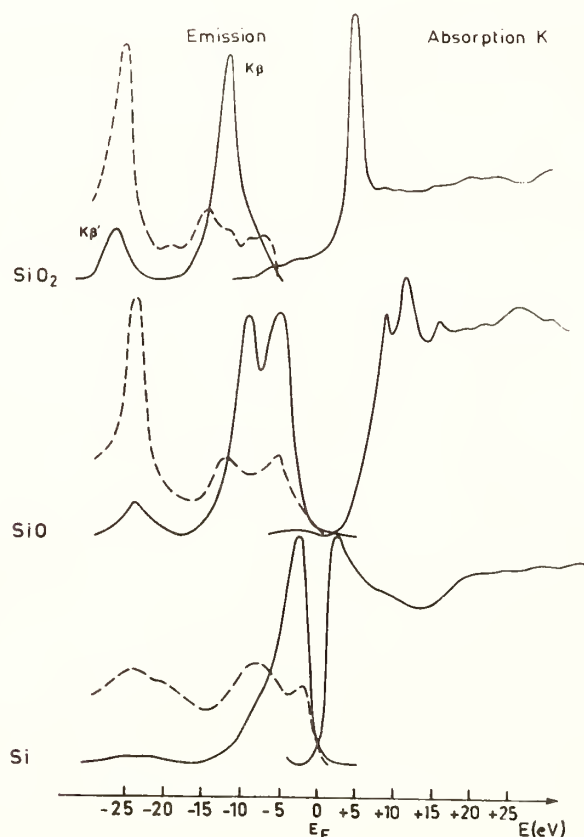


Fig. 1. ————— X-ray spectra
 ----- photoelectron spectra :
 Si (10)
 SiO (8)
 SiO₂ (11)

REFERENCES

- (1) H.R. PHILIPP - J. Phys. Chem. Solids 32, 1935, 1971
- (2) A. CACHARD, J.A. ROGER, Phys. Stat. Sol. 5a, 637, 1971.
- (3) M.T. COSTA LIMA, Thèse de Doctorat d'Etat, Paris 1976.
- (4) M.T. COSTA LIMA, C. SENEMAUD, to be published.
- (5) C. SENEMAUD, M.T. COSTA LIMA, J.A. ROGER, A. CACHARD, Chem. Phys. Lett. 26, 431, 1974.
- (6) E.W. WHITE, R. ROY, Solid St. Comm. 2, 151, 1964.
- (7) W.L. BAUN, J.C. SALOMON, Vacuum, 21, 165, 1971.
- (8) G. HOLLINGER, J. TOUSSET, TRAN MINH DUC, Intern. Conf. on Tetrahedrally bounded amorphous Semi Conductors, York town Heights 1974, p. 102.
- (9) M.T. COSTA LIMA, C. SENEMAUD, Chem. Phys. Lett. 40, 157, 1976.
- (10) L. LEY, S. KOWALCZYK, R. POLLAK, D.A. SHIRLEY, Phys. Rev. Lett. 29, 1088, 1972.
- (11) T.H. DI STEPHANO, D.E. EASTMAN, Phys. Rev. Lett. 27, 1560, 1971.

THE EFFECT OF TEMPERATURE ON X-RAY EMISSION SPECTRA

J.B. Jones, M. Kasrai and D.S. Urch

Department of Chemistry, Queen Mary College,

Mile End Road, London E1 4NS, U.K.

[M. Kasrai, on leave from, Tehran University, Institute of Nuclear Science & Technology, Tehran, Iran]

A Philips PW1410 X-ray fluorescence spectrometer has been modified so that the temperature of the sample can be controlled during irradiation (1). The sample is placed at the end of the probe of an Oxford Instrument CF100 cryostat which permits the temperature to be varied in the range 80° - 400°K when liquid nitrogen is used. Preliminary results using vanadium pentoxide and neodymium titanate, (see Table) showed that cooling causes a large reduction in peak intensity and that small changes in peak position can also be observed.

Table				
Sample	Peak	Intensity 350°K	(counts sec ⁻¹) 97°K	% Decrease
V ₂ O ₅	{ V Kβ _{1,3}	165	128	22
	{ V Kβ _{2,5}	12	10	15
Position (electron volts)				
		350°K	97°K	Shift
V ₂ O ₅	{ V Kβ _{1,3}	5418.4	5419.0	+0.6
	{ V Kβ _{2,5}	5455.1	5454.9	-0.2
Nd ₂ Ti ₂ O ₇	{ Ti Kβ _{1,3}	4932.4 (8.2) ^a	4933.0 (7.6) ^a	+0.6
	{ Ti Kβ _{2,5}	4963.8	4963.9	

(a) full width at half-height

It is also interesting to note that peak widths are somewhat reduced at lower temperatures.

The reduction in intensity upon cooling was the most dramatic observation, however, and so this phenomenon was investigated further by measuring the intensity of the vanadium Kβ_{1,3} peak from vanadium pentoxide at a variety of temperatures in the range 90-400°K. The results are shown in fig.1. A linear increase in peak intensity with temperature is observed. This increase in intensity may be due to vibronic coupling effects which would make a greater number of states available at higher temperatures. Such effects might also be expected to cause an increase in peak width as is observed.

It has been proposed by many authors (2,3,4) that the structure of the Kβ', Kβ_{1,3} peak in first row transition metal X-ray emission spectra is closely related to the magnetic moment of the metal ion in the sample. Some complexes are known in which the magnetic moment is temperature dependent. A study of the structure of the Kβ' Kβ_{1,3} peak as a function of temperature of one such compound was therefore made;- iron-bis(diethyl dithio carbamate)nitrosyl, the magnetic susceptibility of

which diminishes with temperature (5). The results at 328, 160 and 93 °K are shown in fig. 2. Whilst the reduction in main peak intensity with temperature is apparent it is most interesting to notice that the relative intensity of $K\beta'$ also diminishes. This is of course exactly the behaviour that would be expected if the $K\beta':K\beta_{1,3}$ intensity ratio is related to the magnetic moment of the iron.

These preliminary experiments show that temperature can profoundly affect the intensity of Xray emission spectra and also that when certain physical properties (e.g. magnetic moment) are temperature dependent, corresponding effects can also be observed in the Xray spectra.

References

1. J.B. Jones and D.S. Urch, J.Physics E, Sci.Inst., 8, 541 (1975).
2. K.J. Tsutsumi, J.Phys.Soc.Japan, 14, 1696 (1959).
3. R.A. Slater and D.S. Urch, J.Chem.Soc.D. Chem.Comm., 1972, 564.
4. V.F. Demekhin, G.F. Lemeshku and A.T. Shavaev, Izv.Akad.Nauk.SSR. Ser.Fiz. 38, 587 (1974) - Eng.trans.p.136.
5. A.H. Ewald, R.L. Martin, G.I. Ross and A.H. White, Proc.Roy.Soc., A280, 235 (1964).

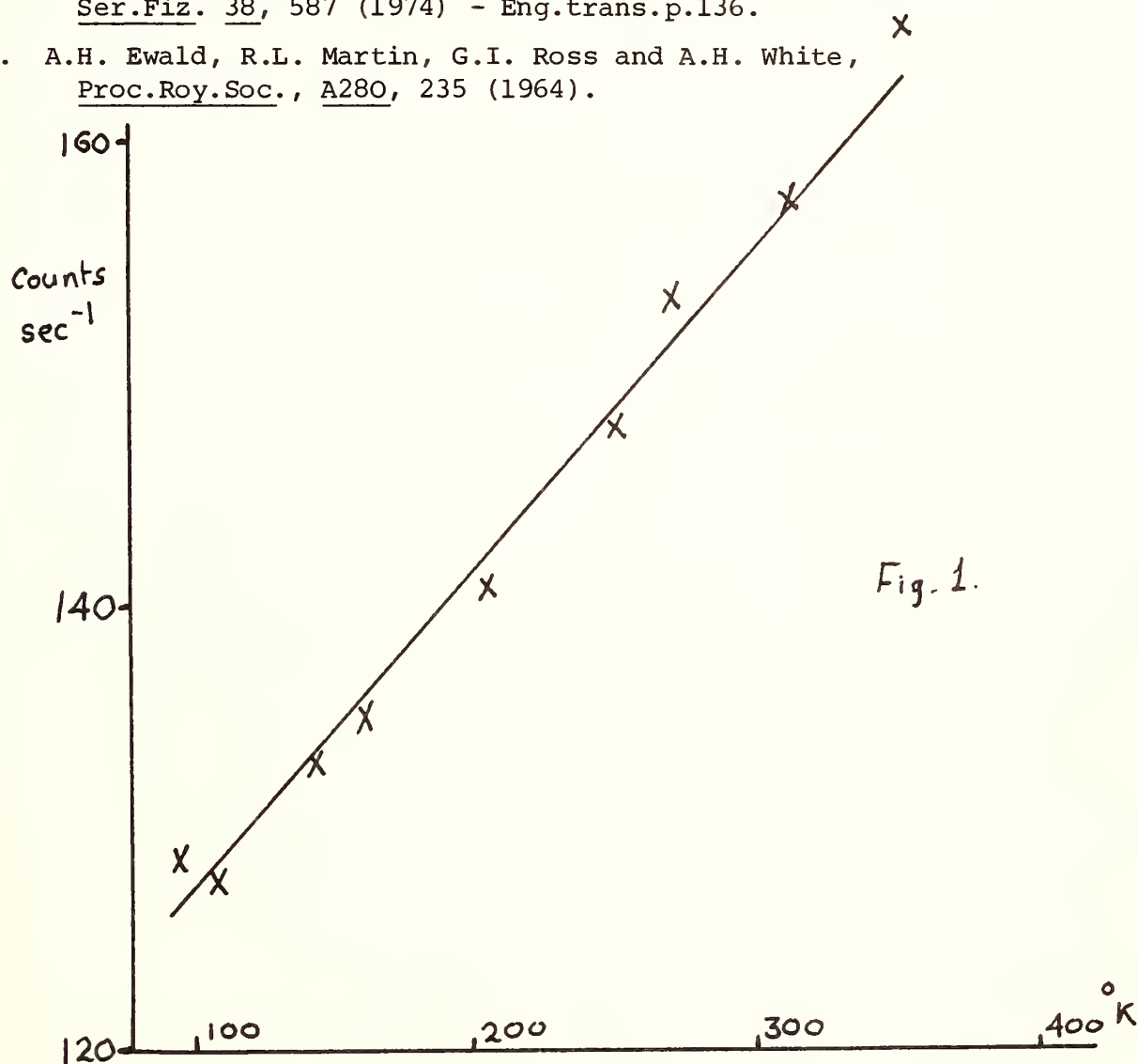
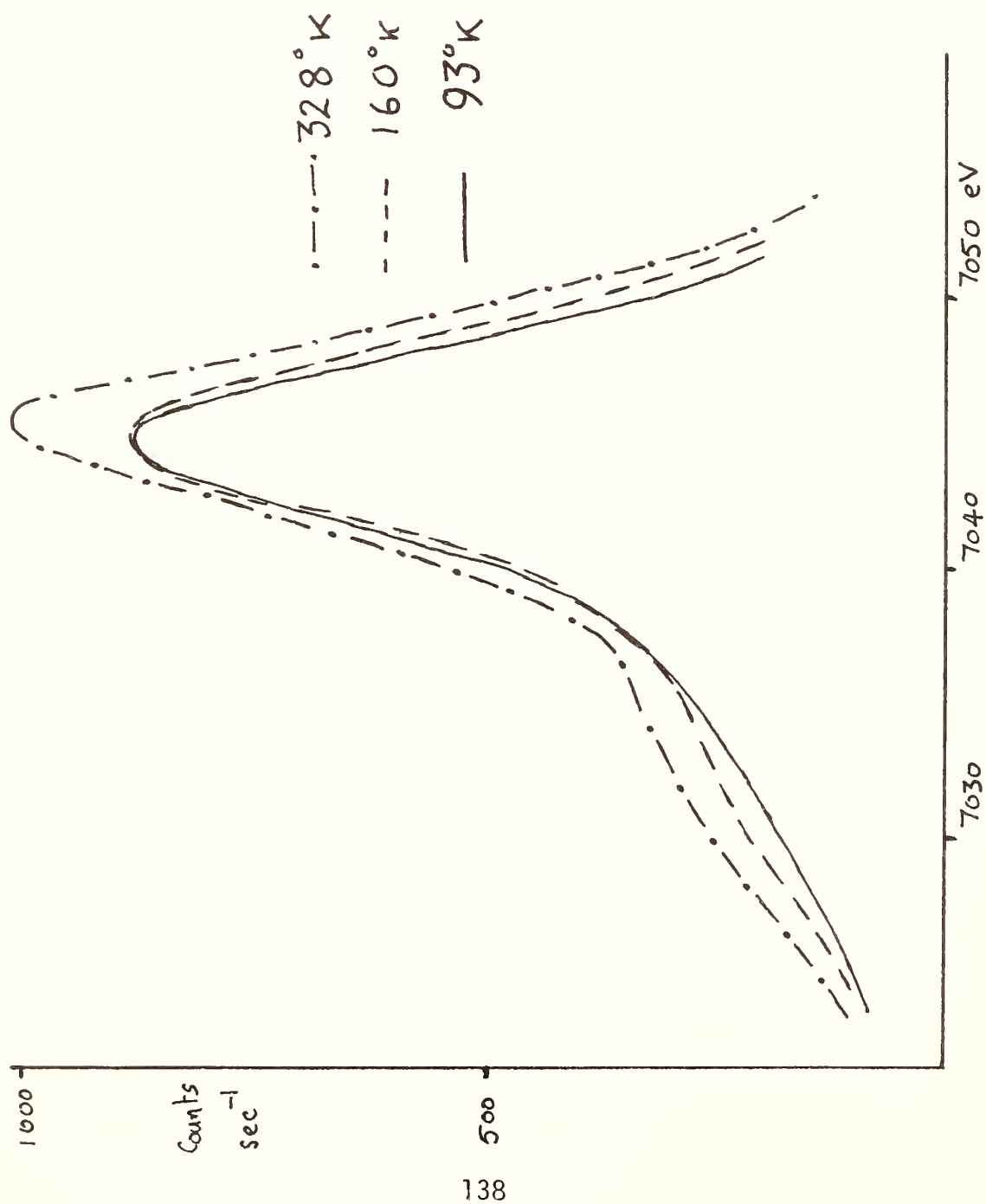


Fig. 1.

Fig. 2.

Fe $K\beta'$ - $K\beta_{1,3}$
in
iron nitrosyl
bis(diethyldithio-
carbamate).



THE CHEMICAL BONDING IN SPINEL (Mg Al₂O₄) STUDIED BY
XRAY EMISSION AND XRAY PHOTOELECTRON SPECTROSCOPIES

D. Haycock, C.J. Nicholls and D.S. Urch,
 Chemistry Department, Queen Mary College,
 Mile End Road, LONDON E1 4NS, U.K.

The structure of Xray emission peaks that arise from electronic, valence-band-inner orbital, transitions reflects the participation of specific valence shell atomic orbital(s) in the molecular orbitals which comprise the chemical bond. A study of all possible Xray emission peaks from a particular chemical compound thus enables the structure of the bonding to be investigated in great detail. In order that such a study can be carried out it is also necessary to know the ionisation energies of the inner orbitals so that all spectra may be placed on a common energy scale. This can be done using Xray photoelectron spectroscopy.

In this paper Xray emission and Xray photoelectron spectra for spinel, Mg Al₂O₄ are discussed. The former were obtained using a Philips PW 1410 Xray fluorescence spectrometer; the latter with a Vacuum Generators ESCA III instrument.

The results which are shown in fig. 1 display considerable unresolved structure. By the use of a simple computer procedure, it was, however, possible to resolve the spectra into three or in one case, four Gaussian components, details of which are given in the table.

	Oxygen K α			Magnesium K $\beta_{1,3}$			
position	521.2	522.7	524.9	1290.1	1293.2	1294.7	1296.9
intensity -arbitrary units	312	156	1092	182	1325	383	2268
full-width half-height	2.13	1.15	1.46	1.75	1.95	1.36	1.82
	aluminium K $\beta_{1,3}$						
				1545.7	1549.4	1552.3	
				306	2916	2370	
				2.58	2.46	2.25	

The positions and relative heights of these resolved peaks are indicated in the figure. It can be seen that two distinct bands of orbitals are present separated by about 2 eV.

The positions and relative intensities of these peaks can be rationalised using a simple molecular orbital model for the bonding in spinel. The structure of spinel (1,2) is such that each magnesium is tetrahedrally coordinated by oxygen and each aluminium is octahedrally coordinated by oxygen and that each oxygen is bound to one magnesium and three aluminium atoms in a trigonally distorted tetrahedron.

The bonding between oxygen and aluminium can be discussed in terms of an Al_4O_4 cube in which the sp hybrids from Al and p orbitals from oxygen are orientated towards the centre. This model predicts that two sets of m.o.'s should be formed, the least tightly bound (A) having an excess of oxygen 2p character compared with the more tightly bound set (B) and also that set A should be skewed, with an excess of more tightly bound orbitals. Al 3p character should be greater in set B than A but not exceeding 3:1. When the bonding between the m.o.'s of sets A and B and the magnesium atoms is considered it is found that Mg 3p character is concentrated in orbitals A rather than B (limiting ionic case for Mg 3p A:B = $\sqrt{3}$:1). A simple qualitative m.o. discussion thus provides an explanation for the main features and relative intensities of the X-ray emission peaks from spinel.

References

1. W.H. Bragg, Phil.Mag. 30, 305 (1915).
2. G.E. Bacon, Acta Cryst. 5, 684 (1952).

Fig. 1.

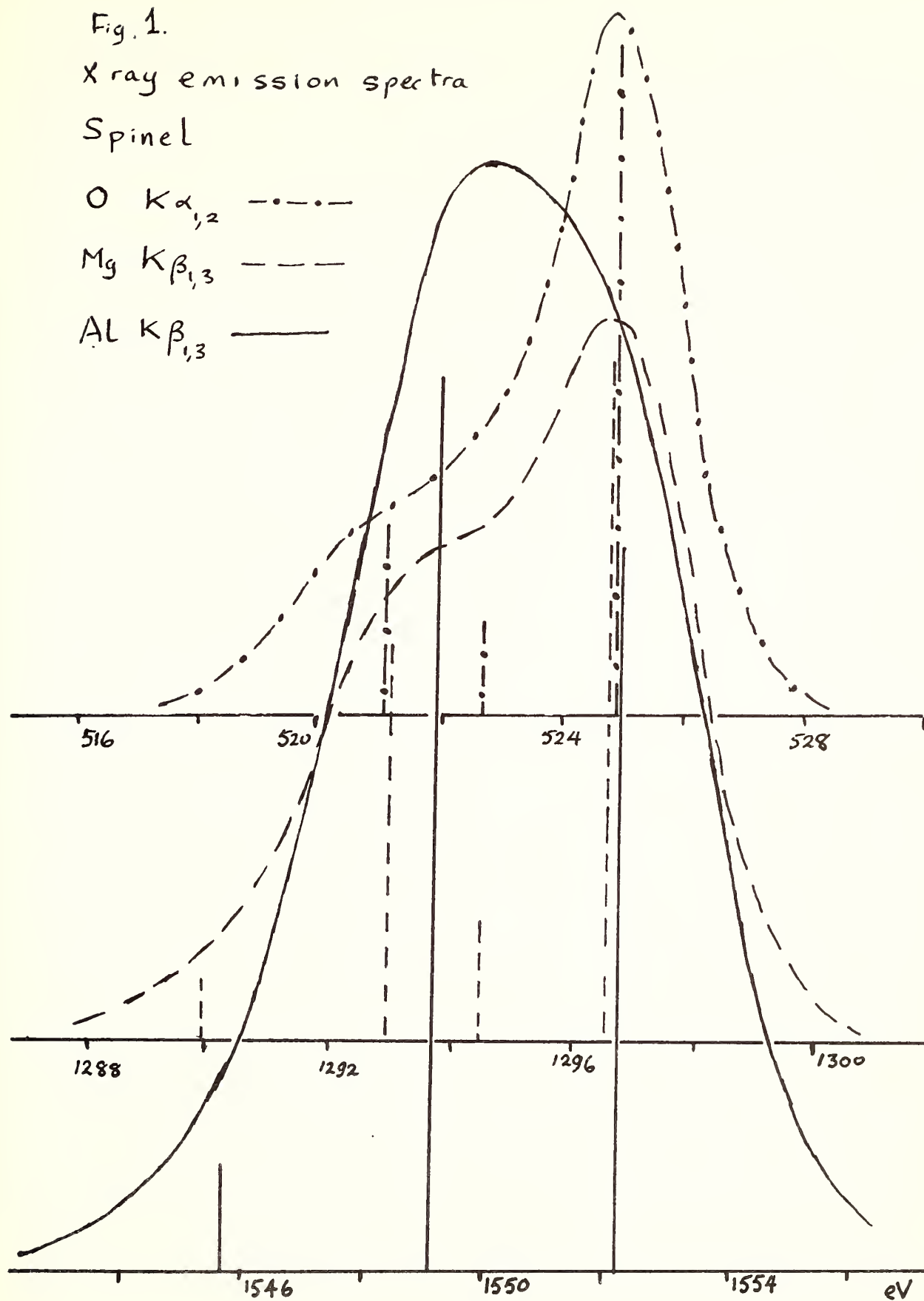
X ray emission spectra

Spinel

O $K\alpha_{1,2}$ - · - · - ·

Mg $K\beta_{1,3}$ - - - - -

Al $K\beta_{1,3}$ ———



AN XES STUDY OF THE STRUCTURE OF As-S GLASSES

M. Lähdeniemi and E. Suoninen
Department of Physical Sciences/Materials Sc.
University of Turku
SF-20500 Turku 50, Finland

The mechanism of dissolving As atoms in arsenic glasses was studied in this work by measuring the S K emission spectra of As-S alloys in the region 0 - 40 at% As. The main question to be decided was whether the dissolving takes place through the formation of clusters of As_2S_3 . Previous similar studies by Salaneck et al [1] were judged inconclusive. Our measurements were made with a double crystal spectrometer [2] using Si(111) crystals in the (1,1) position and fluorescence excitation.

The samples were given a homogenization anneal of several days at a temperature depending on the composition. X-ray diffraction runs of each sample indicated an amorphous structure.

The S K β band was measured for each alloy. The result for samples with 0 at%(S) and 40 at%(As_2S_3) arsenic are shown in Fig. 1. The energy scale refers to the position of the β_x peak of pure S. The Fermi energy is defined as the half-maximum intensity at the high-energy shoulder (c.f.

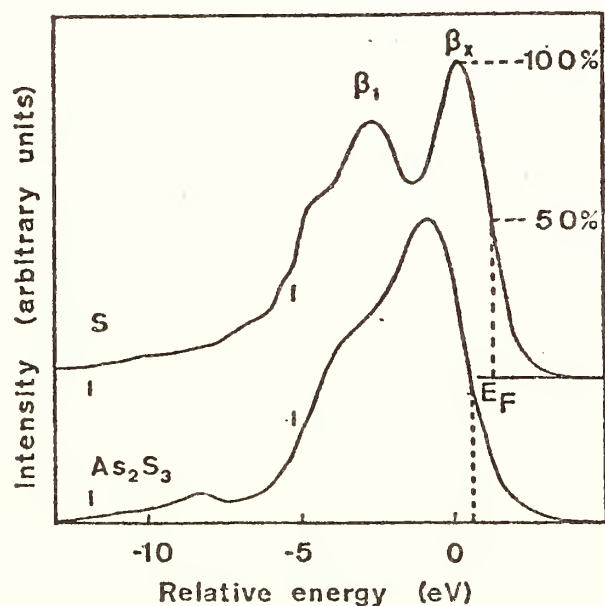


(Fig. 2). The measured energy shifts and half width of the S K β bands are shown in Table 1 (indicated by A).

The band shape is seen to change gradually with increasing As content. The low-energy part of the band getting relatively weaker. There is also a negative energy shift of the high-energy part of the band.

Fig. 1. S K β band of S and As_2S_3 .

Table 1

At% As	Energy shift (eV)		Half width (eV)	
	A	B	A	B
0	-	-	6.14	6.14
10	-0.15	-0.16	5.79	6.00
20	-0.27	-0.28	5.59	5.75
30	-0.53	-0.60	5.35	5.37
40	-0.84	-0.84	4.60	4.60

The measured S $K\beta$ band can be quite well interpreted as a weighted superposition of the band shapes of S and As_2S_3 . Parameters for the band obtained through superposition are given in Table 1 (indicated by B). A gradual small negative

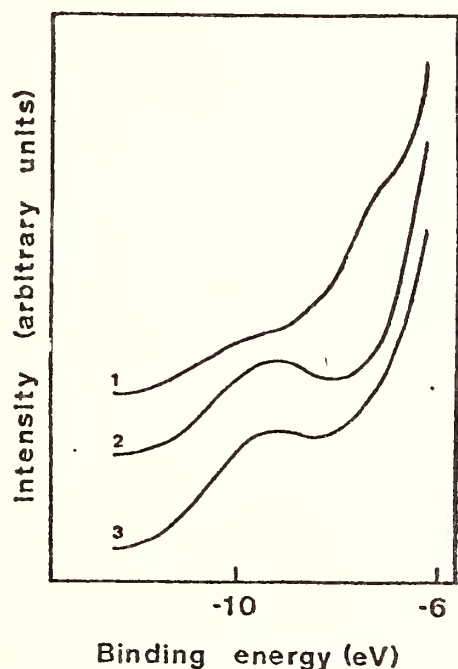


Fig. 2. Low energy structure of the band:
1. S, 2. As_2S_3 , 3. 30 at% As. The binding energies were obtained by using Fermi energies obtained as shown in Fig. 1.

energy shift with alloying is also found for the S $K\alpha_1$ line. This supports the above superposition interpretation. The results are compatible with the assumption that arsenic atoms enter the alloy as As_2S_3 molecules. The above tentative interpretation agrees with the previous work of Salaneck et al [1], but the measured data upon which they based their conclusions are found to be very different from ours.

According to calculations by Chen [3] , the s-p hybrid molecular orbitals 3_v with a substantial amount of p character of As_2S_3 have binding energies in the region 9.3-11.65 eV. They can be expected to give rise to satellite lines at the low energy side of the main band. No estimates for the line intensities to be expected are, however, available. It is seen from Fig. 2 that a broad satellite is indeed present in the samples containing arsenic, which again supports the above interpretation.

Acknowledgements

The authors are grateful to Ms. E.-K. Viinikka for interesting discussions. This research was financially supported by the Academy of Finland.

References

1. W.R. Salaneck, N.O. Lipari, W. McCain and R. LaForce, Solid State Commun. 15, 1453(1974).
2. E. Suoninen and M. Pessa, Phys. Scripta 7, 89(1973).
3. I. Chen, Phys. Rev. B 8, 1440(1973).

INVESTIGATION OF THE X-RAY EMISSION AND PHOTOELECTRIC YIELD SPECTRA OF BERYLLIUM IN ITS COMPOUNDS

M.A. Blokhin, E.G. Orlova, and I.G. Schweizer
Department of Solid State Physics, Rostov State University
344006 Rostov-on-the-Don, USSR

The Be K-photoelectric yield spectra of BeO , Be(OH)_2 , BeCO_3 , BeSiO_3 , $\text{BeSO}_4 \cdot 4\text{H}_2\text{O}$, $\text{Be}_3(\text{PO}_4)_2$, BeF_2 , Na_2BeF_4 and K_2BeF_4 are measured with a resolution of 0.3 eV by means of the RSM-500 soft X-ray spectrometer. For the last two compounds BeK-emission spectra were also measured. As is generally known [1,2] the photoelectric yield spectra, as well as the X-ray absorption spectra, give information about the free electron states. In this work compounds were investigated in which the Be atom is surrounded with oxygen or fluorine atoms or with hydroxyl groups $(\text{OH})^-$ or water molecules.

From the comparison of ESCA data [3,4] and photoelectric yield spectra one can see that the whole fine structure of the last one is situated above the ionization potential in the continuous absorption region. The discrete absorption lines correspond to the electron transitions from the Be 1s-level into quasi-stationary states. In Fig. 1 the photoelectric yield spectra are given for some of the compounds investigated. In the next table energies corresponding to the position of the first peak A are listed. We have revealed a systematic displacement of the peak A in the low energy side by changing ligands in the first coordination sphere of Be accordingly to the known spectrochemical series: $\text{O} - \text{H}_2\text{O} - \text{OH} - \text{F}$.

The influence of the second coordination sphere on the position of the first absorption peak can be observed by examining the photoelectric spectra of Na- and K-fluoberyllates, where the alkali metal atoms are located [5] between the BeF_4^{2-} tetrahedra cations. When the Na^+ cation is substituted by K^+ the negative charge on F atoms rises and the Be 1s-level energy decreases. As the photoelectron data [4,6] shows, the energy difference between Be 1s-levels of Na_2BeF_4 and K_2BeF_4 is 0.6 eV (the results in [6] were recalculated relative to the traditional calibration C 1s-line of the hydrocarbon contamination layer). Such a substitution shifts the photoelectric yield spectra to the low energy side: the peak A energy for K_2BeF_4 is 1.1 eV lower than for Na_2BeF_4 . It follows therefore that a change of a Na^+ ion in fluoberyllates causes a rise of the first free level of p-symmetry by 0.5 eV roughly. The smeared structure of the Be photoelectric yield spectra of Be(OH)_2 can be explained by low symmetry surrounding of the Be atom in the crystal lattice of the hydroxide (the space group is D_2^4 the possible point group of symmetry for the Be atom is very low $2'_1\text{C}_1$).

There is no information about the metasilicate BeSiO_3 crystal structure. A comparison of BeK-photoelectric spectra for BeO and for BeSiO_3 and also of $\text{SiL}_{2,3}$ -spectra for BeSiO_3 and for silicates with differing coordination of the SiO_4 -tetrahedras allows us to suggest the following structure for BeSiO_3 : slightly distorted BeO_4 -tetrahedra bonded through oxygen atoms with the SiO_4 -tetrahedra, which form an infinite chain $(\text{SiO}_3)_\infty$. The distortion of SiO_4 -tetrahedra is low.

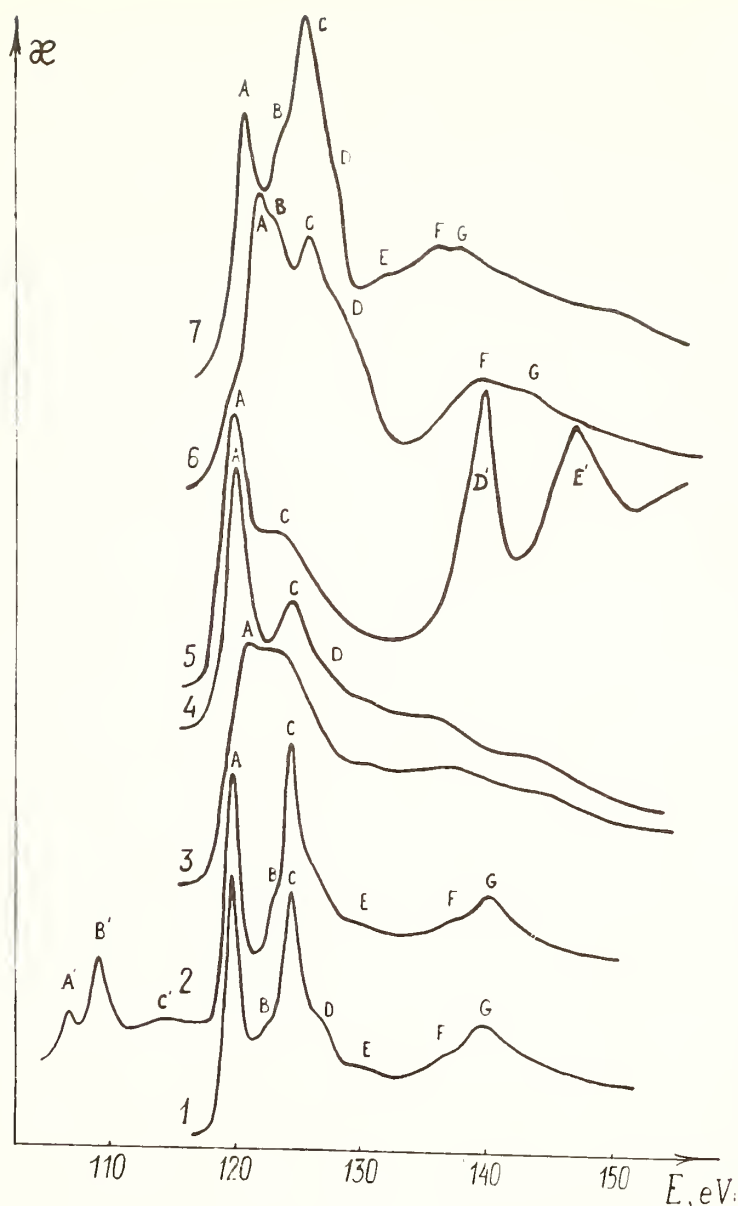


Fig. 1. Photoelectric yield spectra from the Be 1s-level for compounds: 1 - BeO, 2 - BeSiO₃, 3 - Be(OH)₂, 4 - BeSO₄·4H₂O, 5 - Be₃(PO₄)₂, 6 - Na₂BeF₄, 7 - K₂BeF₄. The scale on the ordinate axis is arbitrary. The peaks A', B', C'(2) belong to the SiL_{2,3}-spectrum and the peaks D', E'(5) - to the PL_{2,3}-spectrum.

The crystal structure of Be₃(PO₄)₂ is unknown. Generally one assumes that by normal conditions the Be ortho-phosphate is a hydrate. A comparison was made between BeK-photoelectric spectra in Be₃(PO₄)₂ and in BeSO₄·4H₂O in which the Be atoms are tetrahedrally surrounded with water molecules. The shape and

Table

Compound	Energy of Peak A, eV
BeO	119.5
BeSiO ₃	119.5
Be ₃ (PO ₄) ₂	119.8
BeSO ₄ ·4H ₂ O	120.0
Be(OH) ₂	120.8
Na ₂ BeF ₄	121.7
K ₂ BeF ₄	120.6

energy position of the phosphate spectra peaks confirm the last assumption.

A superposition of beryllium and oxygen K-spectra of BeO [7] had shown an ~ 8 eV shift of the Be and O absorption K-spectra and it allows us to conclude that the states near the bottom of BeO conductivity band can be described with Be p-functions in the main. By using ESCA data we have superimposed BeK-photoelectric spectra and FK-absorption spectra. In this case the K-edges of both spectra are practically coinciding and the spectra fine structures of both components are in good agreement with each other. So the more complicated character of the absorption spectra, initial part for fluoberyllates, compared to the same part of BeO-spectra can be a consequence of a strong wave function hybridization of the excited Be- and F-states.

The BeK-emission spectra are shown in Fig. 2. According to the molecular orbital scheme for the BeF₄²⁻ tetrahedra [8] the transition from Be 1s-state to the 1t₂-state (in which the part of Be 2p-states is low) displayed in the emission spectrum as a

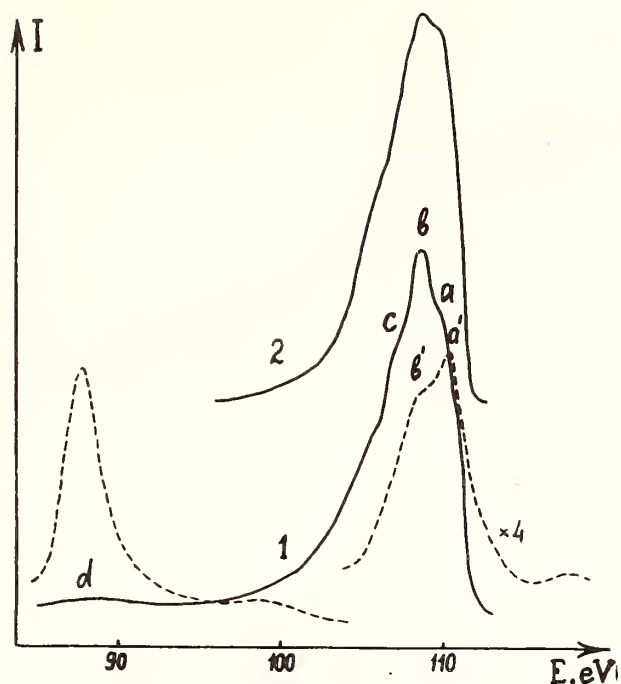


Fig. 2. BeK-emission spectra for fluoberyllates: 1 - Na_2BeF_4 , 2 - K_2BeF_4 . The dashed line shows the X-ray photoelectron spectrum for the valence band of the BeF_4^{2-} ion in the Li_2BeF_4 salt [9].

very faint band d with a relative intensity $\sim 2\%$, located ~ 20 eV to the low energy side from the main peak b (the transition $\text{Be } 1s \rightarrow 2t_2$). The main emission band has a complicated shape. The low energy shoulder c is apparently a consequence of lower symmetry of the BeF_4^{2-} tetrahedron in the fluoberyllates and of the resulting Be 2s- and 2p-levels mixing. The peaks a' and b' of the X-ray photoelectron spectrum (Fig. 2) with a distance 1.0 eV between them corresponds to $3t_2$ - and $2t_2$ -levels, the main contribution to which give the F 2p- and Be 2p-levels correspondingly. The same distance 1.0 eV is also seen on the X-ray spectrum between the peak b and the shoulder a. The last one corresponds apparently to the $\text{Be } 1s \rightarrow 3t_2$ transition and from its great intensity one can conclude that a considerable hybridization of F and Be 2p-states exists.

References

1. A.P. Lukirski, T.M. Zimkina, *Izv. AN SSSR, Ser. Phys.* **28**, 765 (1964) (in Russ.).
2. W. Gudat, C. Kunz, *Phys. Rev. Lett.* **29**, 169 (1972).
3. K. Hamrin, G. Johansson et al, *Physica Scripta* **1**, 277 (1970).
4. V.I. Nefedov, J.V. Kokunov et al, *Journ. Neorganich. Khimii* **18**, 931 (1973) (in Russ.).
5. Landolt-Börnstein, B.1 Atom und Molekularphysik, Tl.4 Kristalle, Springer-Verlag, 1955, S.62, 74.
6. Ch.K. Jørgensen, H. Berthon, *Mat.-Fys. Medd. Kgl. Dan. Vid. Selsk.* **38**, 1 (1972).
7. V.A. Fomichev, *Phys. Tverd. Tela* **13**, 907 (1971) (in Russ.).
8. B.F. Shchegolev, E.L. Rosenberg et al, *Journ. Strukt. Khimii* **14**, 581 (1973) (in Russ.).
9. V.I. Nefedov, J.V. Kokunov et al, *Journ. Neorganich. Khimii* **18**, 1208 (1973) (in Russ.).

CHEMICAL SHIFTS OF THE K ABSORPTION DISCONTINUITY OF COBALT IN INTERMETALLIC SYSTEMS

Chintamani Mande and Vivek Kondawar

Department of Physics
Nagpur University
Nagpur (India)

It is well known that X-ray absorption spectra are affected by chemical combination. Several types of effects due to chemical combination on X-ray absorption discontinuities are reported in literature. They include the effects on the position, shape and fine structure - near edge as well as extended - of the discontinuities. Amongst all these effects, the chemical shifts have attracted the greatest attention and in a very large number of papers the chemical shifts of X-ray absorption discontinuities have been reported. Kunzl(1) was the first worker to show that the chemical shifts depend upon valency. Later work has shown that the chemical shifts are influenced not only by valency, but also by other factors, such as coordination number, chemical bonding and structure of the compounds. However, it is not yet clear in what way exactly the different factors contribute to the chemical shifts.

It should be borne in mind that the chemical shifts should ideally refer to the completely free absorbing atom, such as that in the case of monoatomic gases. However, in practice the chemical shifts are always measured with respect to the discontinuity in the pure element in the solid state, mostly in metals. Probably because of this, one observes altogether different orders of magnitudes in the case of chemical shifts of different elements. Also, one finds that most often the chemical shifts are positive, i.e. the discontinuities in the compounds shift to the higher energy side with respect to the discontinuity in the pure metal. However, occasionally negative shifts have also been reported. In our laboratory, we have been making systematic efforts to unfold the various causes which determine the positive and negative chemical shifts in X-ray absorption spectra.

Our earlier work(2) on gallium, germanium, arsenic and selenium has shown that the chemical shifts are positive whenever the absorbing atom is a cation and are negative when the absorbing atom is an anion. It has also been shown that the magnitudes of the chemical shifts for a given

absorbing element mainly depend upon the effective charge on the absorbing atom. In the present paper, our study on the chemical shifts of the K absorption discontinuity of cobalt in some intermetallic compounds, viz. CoO, CoS, CoAs, CoSe, CoTe, CoAsS, CoS₂, CoAs₂, CoSe₂, CoTe₂, CoGe₂ and Co₂As is reported. The spectra were recorded using a 40 cm Cauchois type bent crystal spectrograph. The other experimental details are described elsewhere(2,3).

We have observed that the main cobalt K absorption discontinuity in the above compounds shifts to the high energy side with respect to that in the pure metal. The observed chemical shifts (ΔE) have been found to depend upon the effective charge (q) on the cobalt ions in different compounds, which have been calculated on the basis of Suchet's model. The ΔE vs q curves obtained by us in the present case are somewhat different than those obtained in our earlier work on gallium, germanium, arsenic and selenium. Whereas the ΔE vs q curves for the latter elements pass through the origin, the ΔE vs q curves for the cobalt K discontinuity do not show this behaviour. Also, instead of a single ΔE vs q curve for all the compounds, we have obtained two separate curves for the compounds of MX and MX₂ types, both of which do not pass through the origin. We have tried to explain our observations by considering the possible differences in the nature of the final levels available for absorption. Our work shows that the final level responsible for absorption in the MX type of compounds is situated at least 1.5 eV higher than the Fermi level in the metal and that it goes on shifting towards the high energy side as the effective charge on the cobalt atom increases in the compounds. Similarly, the final level responsible for absorption in the ternary compounds is situated at least 2.2 eV away from the Fermi level of the metal. The final level for the MX₂ family of compounds also shifts gradually towards the high energy side as the effective charge on the cobalt atoms increases in the series.

The positive chemical shifts obtained confirm that the cobalt atom behaves as a cation in all the compounds studied in the present work. It is interesting to mention here that recently it has been shown(4,5) in our laboratory that the cobalt discontinuity shifts to the low energy side in RCo₂ and RCo₅ types of compounds, where R stands for a rare earth atom, indicating that the cobalt ion behaves as an anion in these compounds.

Our work shows that the chemical shifts in X-ray absorption spectra can be used to obtain fruitful

information regarding chemical bonding prevailing in a compound.

References

- 1) Kunzl, V. Coll. Trav. Chim. Tchecoslovaquie, 4(S) (1932) 213.
- 2) Mande, C. and Sapre, V.B. Proc. Int. Symp. X-ray Spectra and Electronic Structure of Matter, München, 1 (1972) 237-248.
- 3) Kondawar, V.K. and Mande, C. J. Phys. C, 9 (1976) 1351-1359.
- 4) Chetal, A.R. and Sarode, P.R. J. Phys. F, 5 (1975) L217.
- 5) Sarode, P.R. and Chetal, A.R. Physica Stat. Solidi (in Press).

K-ABSORPTION SPECTRA OF SOME POLYNUCLEAR COPPER COMPLEXES

Jagdish Prasad, Vijai Kriahna and Hira Lal Nigam

Chemistry Department, Allahabad University, Allahabad-2, India.

The shifts in the K-absorption edges and the principal absorption maxima have been shown to depend primarily on the valence state of the metal in question[1,2]. An observation has been recorded to show that the edge shift notwithstanding its valence dependence is boosted in case of compounds which involve metal-metal interaction[3]. Very little X-ray spectroscopic work has been done on such compounds. In fact, the nature of metal-metal bonds remains an open question[4]. The present communication therefore, is an attempt to apply this technique in case of some especially chosen set of polynuclear copper complexes known to involve metal-metal interaction. The spectra were recorded using a 40-cm curved crystal (mica) spectrograph on Kodak X-ray films.

The data on edge shifts and the relative energies of the principal absorption maxima of these complexes are given in Table 1, a perusal of which would readily show that the edge shift as also the energy of the main peak, E_A are significantly larger for compounds involving Cu(II) than those involving Cu(I). Surprisingly, however, the magnitudes of edge shifts for the compounds (Nos. XIX-XXII) are seen to fall in the range of Cu(I) and are too small to be expected for Cu(II). The possibility of copper ion, being in the +1 state in these complexes has been ruled out earlier[5]. The relative energies of the main peak of these compounds however, fall close to the value observed for Cu^{2+} ion[6]. Hence, the criterion based on E_A rather than edge shift seems to be more reliable in regard to correct assignment of the oxidation state of the absorbing atom. The suppression in edge shifts may probably be due to enhanced covalency or band formation in these complexes[7,8]. Further, these observations do not support the hypothesis of boosting in edge shift as a consequence of metal-metal interaction.

The extended fine structure spectra of the square planar complexes show a general broadening in case of mixed oxygen and halogen ligands as against sharp peaks for only oxygen ligands. This leads to the conclusion that the fine structure is determined not only by the number of surrounding donor atoms, as hitherto believed[9], but also by their nature. The difference in energy, ΔE from the second absorption maximum, B to the next minimum, β in the fine structure spectra may be used to compute[10], the radius of the first coordination sphere around the central metal ion through the Bragg relation

$$r_1 = \left(151 / \Delta E \right)^{1/2} \text{ \AA}$$

As evident from Table 2, the estimated bond lengths are close to those obtained from crystallographic data.

Table 1. Shifts in the K-absorption edge and the main peak of copper in some complexes (in eV)

No.	Oxd. State	C o m p l e x	Edge shift ± 0.6	Main peak (E_A) ± 0.6
I	+1	$\text{Cu}(\text{C}_2\text{HN}_2\text{S}_3)$	1.1	8.0
II		$\text{Cu}(\text{NO}_3)(\text{PPh}_3)_3$	1.4	12.8
III		$\text{Cu}(\text{NO}_3)(\text{PPh}_3)_2$	2.2	12.2
IV		$\text{Cu}_4(\text{tu})_9(\text{NO}_3)_4$	3.0	13.7
V	+2	$\text{Cu}(\text{Cl}_3\text{C}\cdot\text{COO})_2$	5.8	17.0
VI		$\text{Cu}(\text{ClCH}_2\cdot\text{COO})_2$	7.7	19.1
VII		$\text{Cu}(\text{HO}\cdot\text{C}_6\text{H}_4\cdot\text{COO})_2$	8.6	19.3
VIII		$\text{Cu}(\text{C}_6\text{H}_5\cdot\text{COO})_2$	10.1	21.3
IX		$\text{Cu}(\text{CH}_3\cdot\text{COO})_2$	10.2	21.7
X		$\text{Cu}(\text{C}_{11}\text{H}_{23}\cdot\text{COO})_2$	11.7	22.8
XI		$\text{Cu}(\text{C}_{17}\text{H}_{35}\cdot\text{COO})_2$	11.0	22.5
XII		$\text{Cu}_2(\text{OCH}_3)_2(\text{C}_5\text{H}_7\text{O}_2)_2$	10.9	22.7
XIII		KCuCl_3	4.7	16.3
XIV		KCuBr_3	6.0	18.7
XV		$\text{Cu}(\text{C}_5\text{H}_5\text{NO})\text{Cl}_2$	5.4	17.5
XVI		$\text{Cu}(\text{C}_5\text{H}_5\text{NO})\text{Br}_2$	4.3	17.9
XVII		$\text{Cu}_5(\text{T})_2(\text{TH})_2\cdot 10\text{H}_2\text{O}$	6.5	20.6
XVIII		$\text{Cu}(\text{C}_4\text{H}_2\text{N}_2\text{OS})\cdot 2\text{H}_2\text{O}$	5.8	17.5
XIX		$\text{Cu}(\text{C}_2\text{HN}_2\text{S}_3)_2$	1.6	16.3
XX		$\text{Cu}_2(\text{C}_8\text{H}_4\text{N}_2\text{S}_2)\text{Q}_2$	1.4	15.8
XXI		$\text{Cu}(\text{C}_7\text{H}_5\text{N}_4\text{S})_2$	1.2	16.3
XXII		$\text{Cu}(\text{C}_7\text{H}_4\text{N}_4\text{SBr})_2$	1.5	16.0

* tu = thiourea, T = $\text{C}_4\text{HN}_2\text{S}_3$, Q = $\text{C}_8\text{H}_5\text{N}_2\text{S}_2$

Table 2. Average metal-ligand bond lengths

Compound	$\Delta E(\beta - B)$ (eV)	Computed value $r \pm 0.1$ (Å)	X-ray diffraction r (Å)	Ref.
$\text{Cu}(\text{CH}_3 \cdot \text{COO})_2$	42.2	1.88	$\text{Cu} - \text{O} = 1.97$ $\text{Cu} - \text{O}(\text{H}_2\text{O}) = 2.20$	a
$\text{Cu}(\text{C}_6\text{H}_5 \cdot \text{COO})_2$	39.4	1.95	$\text{Cu} - \text{O} = 1.91$ $\text{Cu} - \text{O}(\text{H}_2\text{O}) = 1.97$	b
$\text{Cu}(\text{HO} \cdot \text{C}_6\text{H}_4 \cdot \text{COO})_2$	40.5	1.92	$\text{Cu} - \text{O} = 1.84$ $\text{Cu} - \text{O}(\text{H}_2\text{O}) = 1.92$	c
KCuCl_3	28.5	2.30	$\text{Cu} - \text{Cl} = 2.25$ $\text{Cu} - \text{Cl} = 2.32$	d
$\text{Cu}(\text{C}_5\text{H}_5\text{NO})\text{Cl}_2$	34.2	2.10	$\text{Cu} - \text{O} = 2.03$ $\text{Cu} - \text{Cl} = 2.20$	e

a. J.N. Van Niekerk and F.R.L. Schoening, *Acta Cryst.* 6, 227 (1953).
 b. H. Koizumi, K. Osaki and T. Watanabe, *J. Phys. Soc. Japan*, 18, 117 (1963).
 c. F. Hanic and J. Michalov, *Acta Cryst.* 13, 299 (1960).
 d. R.D. Willet, C. Dwiggin (Jr.), R.F. Kruh and R.E. Rundle, *J. Chem. Phys.* 38, 2429 (1963).
 e. R.S. Sager, R.J. Williams, and W.H. Watson, *Inorg. Chem.* 6, 951 (1967).

REFERENCES :

1. G. Boehm, A. Faessler and G. Bittmayer, *Z. Naturforsch.* B9, 509 (1954).
2. G.L. Glen and C.G. Dodd, *J. Appl. Phys.* 39, 5372 (1968).
3. B.K. Agarwal and L.P. Verma, *J. Phys. C.* 3, 535 (1970).
4. R.S. Nyholm, *Advancement of Science*, January, 436 (1967).
5. U. Agarwala and S.K. Dikshit, *D.Phil. Thesis (Dikshit)*, I.I.T., Kanpur (1968).
6. W.W. Beeman, J. Forss, and J.N. Humphrey, *Phys. Rev.* 67, 212 (1945).
7. U.C. Srivastava and H.L. Nigam, *Coord. Chem. Rev.* 9, 275 (1973).
8. V.G. Bhide and N.V. Bhat, *J. Chem. Phys.* 48, 3103 (1968).
9. D. Coster and S. Kiestra, *Physica* 14, 75 (1949).
10. R.M. Levy, *J. Chem. Phys.* 43, 1846 (1965).

THE K-EMISSION AND ABSORPTION OF GALLIUM IN

GaP, GaAs AND GaSb

J.Drahokoupil, H.Klokočnicková and A.Šimůnek
Institute of Solid State Physics, Czech.Acad.Sci.,
Cukrovarnická 10, 162 53 Praha 6, Czechoslovakia

The $K\beta_2$ - emission band and the K-absorption edge of gallium were measured and computed in the isostructural compounds GaP, GaAs and GaSb.

In emission the shape and the integral intensity of the bands (normalized to $K\beta_{1,3}$) were studied. The shape of the bands is very similar for all the studied compounds while the intensity increases from GaP to GaSb. This is an evidence of the increasing valence electron localization on gallium (notice that $A^{III}B^V$ compounds are of the same structure), in agreement with the ionicity and gap width of these materials.

In absorption the shape, position of the K-edge and K-absorption "jump" were studied. For GaP and GaAs the shapes are very similar, only the magnitude of the "jump" for GaAs is greater; to compare with the theory it was necessary to measure the absorption coefficient in the region of several hundred eV from the edge for normalization (see [1]). The shape for GaSb was found distinctly different. The K-edges of these materials were formerly measured ([1],[2]) but the results concerning the position of the edge significantly

differ. Our analysis of the measured and computed curves shows that the edge position is not a good parameter: its experimental value is very sensitive to the form of the apparatus smearing; moreover it does not describe adequately changes of the conduction band bottom. As an example the results for GaP are given in Fig.1. Experiment-

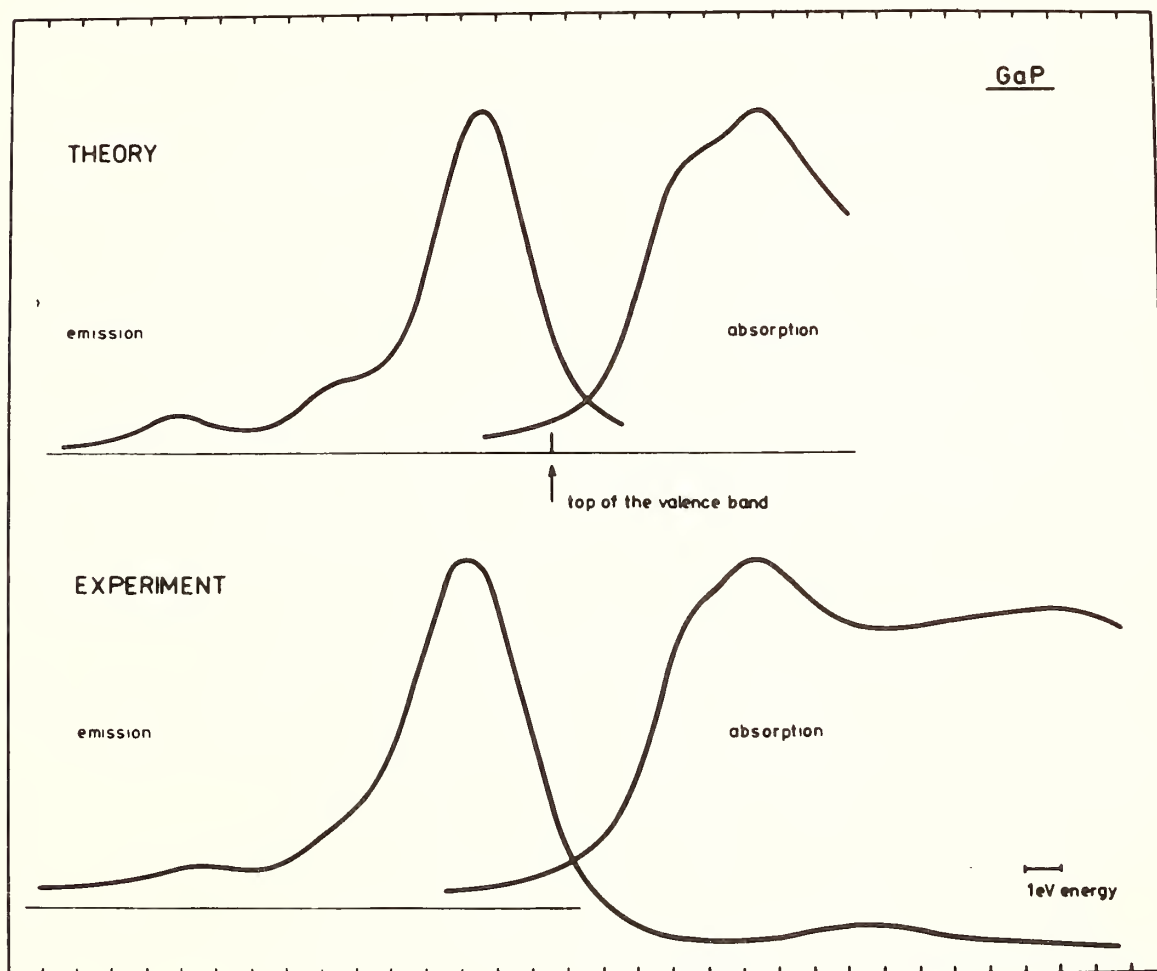


Fig.1. Profiles of K-emission intensity-curves on the left; absorption coefficient-curves on the right.

tal curves are not corrected and so the mirror-like correspondence of the K-absorption structure on the high energy side of emission is visible.

The measurements were performed on the double crystal spectrometer; the OPW band structure, transition probability and partial densities of states were computed. The details of the methods can be found in our paper [3], in which the system Ge, GaAs and ZnSe was studied in a similar way.

- [1] Kantelhardt D. and Waidelich W., Z.Angew.Phys.
26, 239 (1969)
- [2] Mande C., Chetal A.R. and Sapre V.B., Curr.Sci.
39, 391 (1970)
- [3] Drahokoupil J., Klokočnicková H. and Šimůnek A.,
J.Phys.C: Solid St.Phys. 9, 2667 (1976)

EFFECT ON CHEMICAL ENVIRONMENT ON SULFUR
 K_{α} X-RAY SPECTRA

G.Graeffe and H.Juslén
Tampere University of Technology,
33101 Tampere 10, Finland

and E.K. Viinikka
Helsinki Technical University,
02150 Espoo, Finland

Chemical effects in x-ray emission spectra was observed as early as for fifty years ago. The chemical shifts for $K_{\alpha_{1,2}}$ lines have been measured for many different chemical compounds for different elements by various authors [1]. The chemical shift for x-ray satellites (from double ionized states) is even larger but the satellite intensities are weak and only quite few measurements have been performed [2]. There are also other chemical effects, which occur but which have not been so much measured or are not so well understood. One of them is the satellite intensities. The integrated intensities relative to $K_{\alpha_{1,2}}$ line vary from one compound to another but not too remarkably. The fine structure of the satellite lines, however, depend strongly on the chemical environment [2]. In heavy ion bombardments where the multiple L-shell ionization has a large probability, the x-ray satellite spectra are also sensitive to the chemical environment [3].

The XPS (x-ray photoemission spectroscopy) method seems to have some limitations in studying the lifetimes for core hole states. It has been found that in some cases a large portion for the XPS linewidths is due to phonon effects [4, 5]. The observation of x-ray emission spectra may provide a useful tool for studying some core hole states even though in x-ray spectra one has both the effects of the initial and final states.

In the present work we have measured sulfur K_{α} x-ray spectra from rhombic sulfur and some sulfur compounds by a double crystal spectrometer. The K_{α} x-ray spectrum from sulfur was measured already by Parrat [6] using a double crystal spectrometer and by using the electron excitation. We used a chromium x-ray fluorescence tube for excite the sample. Two sets of analyzer crystals were used, quartz $[(10\bar{1}0), 2d = 0.849 \text{ nm}]$ and calcite $[(211), 2d = 0.606 \text{ nm}]$. The rocking curve half width for the former was 0.4 eV and for the latter 0.5 eV. Fig. 1. shows the K_{α} spectra from S_8 , Na_2SO_4 and ZnS . There are several chemical effects which can be observed as chemical shifts, line widths and intensities for K_{α_1} and K_{α_2} lines, line widths for satellite lines and the fine structure of the satellites.

Chemical shifts are quite well understood [1, 7, 8].

The effects on $K_{\alpha_{1,2}}$ lines are not large but a careful examination indicates some. The satellite spectra are quite complex. In LS coupling there are five components (α' , α^3 , α^4 , $\alpha^{2'}$, α_3') [9]. In spectra, in fig. 1, at least five lines can be seen. One striking feature is the change of the intensity of these lines especially that of the α_4 line.

These phenomena are probably due to interatomic Auger or Coster-Kronig type of transitions [3, 10].

References

- [1] W. Nefedow, Phys.Stat.Sol. 2, 904(1962).
- [2] e.g. W.L. Baun and D.W. Fischer, Spectrochimica Acta 21 1471 (1965), V.J. Demekhin and V.P. Sachenko in Röntgenspektren und chemische Bindung, VEB, Leipzig 1966, p. 68. K. Läufer, J. Phys. Chem.Solids, 33, 1343 (1972).
- [3] R.L. Watson, T. Chiao and F.E. Jenson, Phys.Rev.Lett., 35, 254 (1975)
- [4] P.H. Citrin, Phys.Rev.Lett, 31, 1164 (1973)
- [5] P.H. Citrin, P.M. Eisenberger, W.C. Marra, T. Åberg, J. Utriainen and E. Källne, Phys.Rev. 10 B, 1762 (1974).
- [6] L.G. Parrat, Phys.Rev. 50, 1 (1936).
- [7] R. Manne, J. Chem.Phys. 46, 4645 (1967).
- [8] H.-U. Chun in the proceedings, X-ray Spectra and Electronic Structure of Matter, vol. 1, München 1973, p.4.
- [9] T. Åberg in the proceedings, X-ray Spectra and Electronic Structure of Matter, vol.1, München 1973, p. 1.
- [10] P.H. Citrin, J. Electron Spectroscopy and Rel. Phenomena 5, 273 (1974).

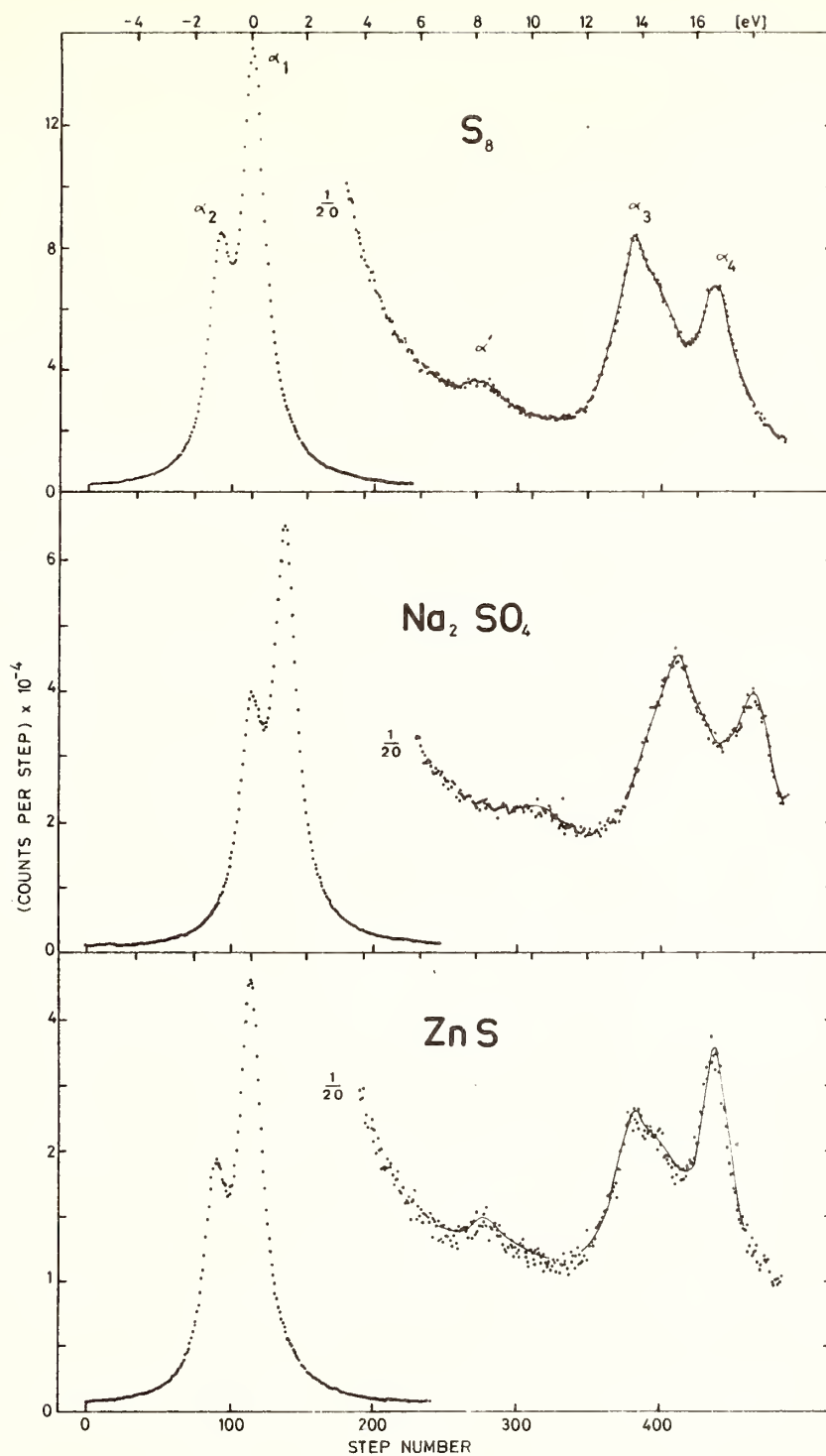


Fig. 1. Sulfur K α x-ray emission spectra from S₈, Na₂SO₄ and ZnS measured in the first order reflection by a double crystal spectrometer using calcite crystals (211).

X-RAY EMISSION SPECTRA OF RARE EARTH AND TRANSITION ELEMENTS AND THEIR OXIDES

S. I. SALEM

Dept. of Physics-Astronomy; California State University
at Long Beach, Long Beach, California, U.S.A. 90840

The elements in the two groups referred to as transition ($21 \leq Z \leq 29$) and rare earth elements ($59 \leq Z \leq 70$) have emission x-ray spectra quite different from those of other elements. They exhibit sets of nondiagram emission lines, or bands, not found in other spectra. In the transition elements, these nondiagram bands are found at the low energy side of the $K\beta_{1,3}$ lines (Fig. 1); and at the low energy side of the $L\gamma_1$ and $L\beta_2$ lines in the rare earth elements (Fig. 2). These nondiagram structures are the results of the splitting of the 3p levels in the transition elements^{1,2} and the splitting of the $4d_{3/2}$ and $4d_{5/2}$ levels in the rare earth elements.^{3,4} In the transition elements, the splitting is the result of the exchange interaction between the 3d and 3p electrons; and the same exchange interaction between the 4f and the 4d electrons in the rare earth elements further splits these levels.⁵

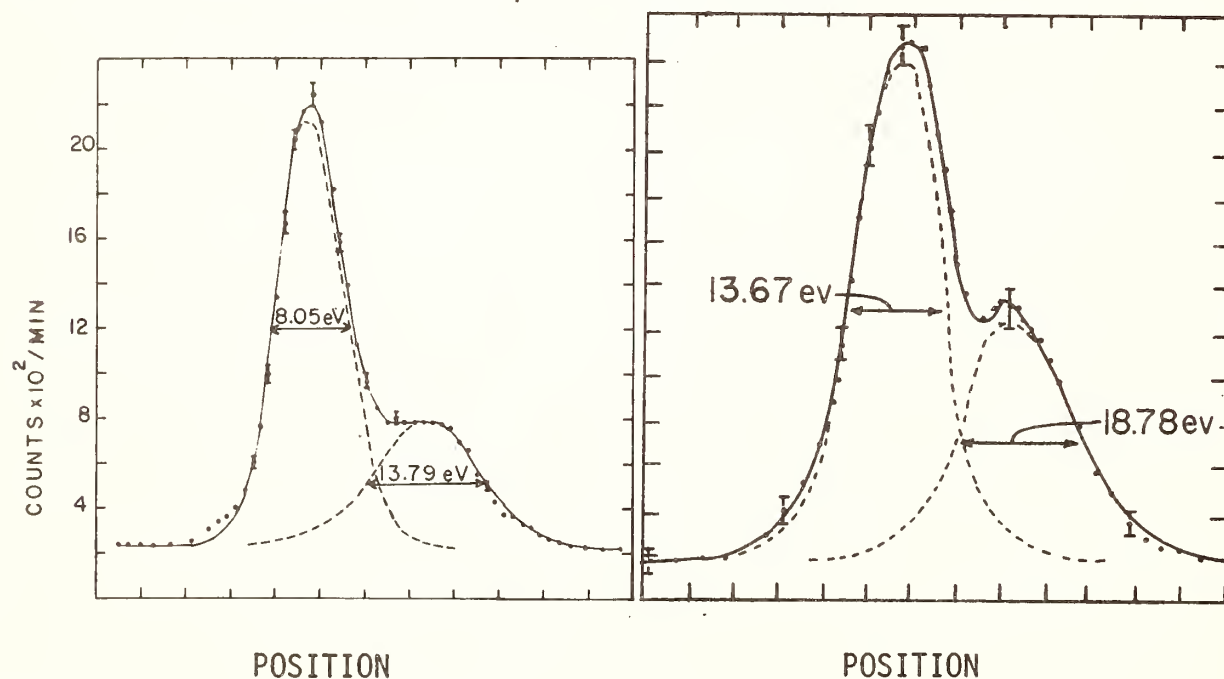


Fig. 1. Computer fit to the $K\beta_{1,3}$ emission lines of iron from an Fe_2O_3 sample, separating the experimental data into a $K\beta_{1,3}$ line and a single nondiagram line. The instrumental width at this energy is 3.90 eV.

Fig. 2. Computer fit to the $L\gamma_1$ emission line of terbium from metal sample, separating the experimental data into an $L\gamma_1$ line and a single nondiagram line. The instrumental width at this energy is 4.93 eV.

The splitting of the 4f level in the rare earth elements has been satisfactorily explained on the basis of exchange interaction.⁶ Theoretical calculations based on a simple exchange interaction^{7,8} between electrons from different levels give values of a mean energy separation between the diagram lines and the nondiagram bands, resulting from the splitting of the 4d levels in the rare earth elements⁸ as:

$$\Delta E = (2S+1) \left[\frac{3}{35} G^1(4d4f) + \frac{4}{105} G^3(4d4f) + \frac{10}{231} G^5(4d4f) \right]$$

and those resulting from the splitting of the 3p levels in the transition elements as:

$$\Delta E = (2S+1) \left[\frac{2}{15} G^1(3p3d) + \frac{3}{15} G^3(3p3d) \right]$$

where S is the total spin of the electrons in the partially filled levels [3d in the transition elements and 4f in the rare earth elements], and G^1 , G^3 , and G^5 are the Slater integrals.

Calculated energy separations are in reasonably good agreement with experimental values. On the other hand, the calculated values of the relative intensities of these bands are about twice as large as the experimentally observed intensities. The fact that calculations are made on free atoms and experiments are performed on solids should account for some of the discrepancy. Within experimental uncertainty, the pure metal and its oxide give the same energy separation ΔE for all the transition and the rare earth elements; while in general, the relative intensity of the nondiagram band is enhanced by oxidation.^{2,4}

Another aspect of the x-ray spectra of the transition elements is the observed asymmetry^{9,10} of the $K\alpha_1$ and $K\alpha_2$ "lines" which is the result of the exchange interaction between the 3d and $2p_{1/2}$ and $2p_{3/2}$ electrons.^{1,11} Thus, each of the $2p_{1/2}$ and $2p_{3/2}$ levels splits into several adjacent levels, and the $K\alpha_1$ and $K\alpha_2$ lines are in actuality bands with energy separation between components, understandably, considerably smaller than that observed in the $K\beta$ complex of the same element. As a result, the Z-dependence of the observed widths of the $K\alpha_1$ and $K\alpha_2$ "lines" of the transition elements exhibit considerable deviation from the trend established with elements having full 3d shells;¹⁰ and these widths are considerably larger than the predictions of the most recent theory;¹² of special interest is the ratio of the $K\alpha_1$ to $K\alpha_2$ line widths¹⁰ which, when plotted as a function of atomic number, exhibits a well pronounced dip at $Z=29$.

The effect of the partially full 3d shell on the radiative transition rates has been observed as a "flat" region¹³ when the ratio $K\beta/K\alpha$ is plotted as a function of atomic numbers. When the intensity of the nondiagram band is added to that of the $K\beta$ lines in evaluating the $K\beta/K\alpha$

ratio, experimental results and values calculated on the basis of a relativistic Hartree-Slater potential are in excellent agreement.^{14,15}

Both the $L\gamma_1/L\beta_1$ and the $L\beta_2/L\alpha_1$ radiative transition ratios, for atoms with partially filled 4f shell, exhibit similar "flat" regions when plotted vs. atomic numbers. Theory and experiments agree as to the existence of these irregularities, but the discrepancies between the experimental and the theoretical values of the $L\beta_2/L\alpha_1$ ratio are significant.

Recent calculations of level width¹⁶ predict a large drop in the value of the $L\beta_2$ and $L\gamma_1$ line width between $Z = 70$ and $Z = 60$, where the value of line width falls by a factor of about three. Experimental measurements show some possible irregularities in that region, but their magnitude is nowhere near what theory predicts.

REFERENCES

1. S. P. Kowalezyk, L. Ley, F. R. McFeeby, and D. A. Shirley, Phys. Rev. B 11, 1721 (1975).
2. S. I. Salem, G. M. Hockney, and P. L. Lee, Phys. Rev. A 13, 330 (1976).
3. S. I. Salem, C. W. Schultz, B. A. Rabbani, and R. T. Tsutsui, Phys. Rev. Lett. 27, 477 (1971).
4. S. I. Salem and Bruce L. Scott, Phys. Rev. A 9, 690 (1974).
5. G. K. Wertheim, A. Rosencwaig, R. L. Cohen, and H. J. Guggenheim, Phys. Rev. Lett. 27, 505 (1971).
6. J. L. Dehmer, A. F. Starace, U. Fano, J. Sugar, and J. W. Cooper, Phys. Rev. Lett., 26, 1521 (1971); and Jack Sugar, Phys. Rev. B 5, 1785 (1972).
7. B. Ekstig, E. Källne, E. Noreland, and R. Manne, Physica Scripta, 2, 38 (1970).
8. K. Tsutsumi, J. Phys. Soc. Jpn. 14, 1696 (1959); J. Phys. Soc. Jpn. 25, 1418 (1968).
9. L. G. Parratt, Phys. Rev. 50, 1 (1963).
10. P. L. Lee and S. I. Salem, Phys. Rev. A 10, 2027 (1974).
11. V. I. Nefdov, J. Struct. Chem. 5, 603 (1964); 7, 672 (1966).
12. S. I. Salem and P. L. Lee (to be published).
13. S. I. Salem, T. H. Falconer, and R. E. Winchell, Phys. Rev. A 6, 2147 (1972).
14. J. H. Scofield, Phys. Rev. A 9, 1041 (1974); and At. Data Nucl. Data Tables, 14, 121 (1974).
15. S. I. Salem, S. L. Panossian, and R. A. Krause, At. Data Nucl. Data Tables, 14, 91 (1974).
16. O. Keski-Rahkonen and M. O. Krause, At. Data Nucl. Data Tables 14, 139 (1974).
17. S. I. Salem and P. L. Lee, Phys. Rev. A 10, 2033 (1974).

X-RAY SPECTROSCOPIC STUDIES OF SOME CaCu_5 TYPE INTERMETALLIC COMPOUNDS

A.R. Chetal and P.R. Sarode

Department of Physics, Nagpur University, Nagpur (India)

Intermetallic compounds of the composition RCo_5 (where R stands for a rare earth element or yttrium), crystallizing in the hexagonal CaCu_5 type of structure, have received considerable attention because of their industrial applications. Magnetic and electrical properties of these compounds have been investigated in detail but these studies have thrown little light on the behaviour of the rare earth and cobalt atoms in these compounds and the nature of the chemical bonding between them. In our laboratory, we have carried out X-ray spectroscopic work on these compounds in order to understand the chemical behaviour of the constituent atoms.

From the positions of the cobalt K and rare earth L_{III} absorption discontinuities in these compounds, it is concluded that (1) the rare earth and cobalt atoms behave as cations (donors of electrons) and anions (acceptors of electrons) respectively, (2) the covalent character of the chemical bond between the rare earth and cobalt atoms increases progressively from LaCo_5 to TmCo_5 , and (3) the magnitude of the chemical shift depends upon the number of electrons participating in covalent bonding. The degree of hybridization of bonding orbitals has been estimated from the shapes of the discontinuities.

A bent crystal X-ray spectrograph of diameter 40 cm with a mica crystal oriented to reflect from its (100) planes was used for recording the spectra. Uniform absorbing screens of the compounds were prepared by spreading their fine powders on cellophane tape. Microphotometer records of the spectra were obtained with magnification X100 on the spectroline scanner made by Applied Research Laboratories, U.S.A. The experimental technique has been described elsewhere in greater detail(1).

In the case of the compounds studied (LaCo_5 , CeCo_5 , PrCo_5 , NdCo_5 , SmCo_5 , GdCo_5 , TbCo_5 , DyCo_5 , HoCo_5 , ErCo_5 , TmCo_5 and YCo_5) the K absorption spectrum of cobalt and the L_{III} absorption spectrum of the rare earth atom have been recorded and measured. The corresponding spectra for these elements in the pure form have also been recorded. It is observed that the K absorption discontinuity of cobalt shifts towards the low energy side whereas the L_{III} discontinuity of rare earth shifts towards the high energy side. Although the chemical shifts are of the same order our measurements consistently show that the magnitude of

the cobalt K absorption shift, which is maximum in LaCo_5 , decreases in the sequence CeCo_5 , PrCo_5 , NdCo_5 , SmCo_5 , GdCo_5 , TbCo_5 , DyCo_5 , YCo_5 , HoCo_5 , ErCo_5 , TmCo_5 . The magnitude of the rare earth L_{III} shift decreases in the sequence SmCo_5 , GdCo_5 , TbCo_5 , DyCo_5 , HoCo_5 , ErCo_5 , TmCo_5 .

In respect of X-ray absorption shifts, it has been shown (2) that the absorption edge of an atom shifts towards the high or low energy side relative to its position in the pure element, depending upon whether the absorbing ion is a cation or an anion. In the case of the compounds under study the K edge shifts of cobalt are towards the low energy side whereas the L_{III} edge shifts of rare earths are towards the high energy side, suggesting that the cobalt ions play the role of anions and rare earth ions act as cations. The directions of the shifts are consistent with what one would expect on the basis of Pauling's electronegativity criterion.

The decrease in the magnitude of the K absorption shift of cobalt as one goes from LaCo_5 through TmCo_5 may be explained by considering the number of electrons taking part in covalent bonding which can be calculated from a semiempirical relation given by Pauling (3). The magnitude of the shift decreases with increase in the number of ~~covalent~~ covalent electrons. The shift decreases with the decrease in the difference between the number of covalent electrons for cobalt metal and for the compound (1 to 2).

The magnitude of K and L_{III} chemical shifts depend upon the electronegativity difference between cobalt and rare earth, which is essentially a measure of the covalent character of the bond between them. Decrease of this electronegativity difference from LaCo_5 through TmCo_5 would mean that the covalent character of the bond between R and Co increases. This, in turn, means that the magnitude of the shift should decrease with decrease of this difference as observed by us (1).

It is found that the K absorption discontinuity of cobalt splits into two components K_1 and K_2 in all the systems studied, while no such splitting is observed in the L_{III} discontinuities of the rare earth, in the metals or in the compounds. Pronounced absorption maxima (white lines) are observed on the high energy side of these discontinuities. The overall shape of the K absorption discontinuity of cobalt in compounds is found to be more or less similar to that of cobalt in the metal. We have employed the density of states picture derived from the bidirectional orbital theory (3) proposed by Carter for the RCO_5 compounds to interpret the salient features of the discontinuities. Electronic transitions are given to the bands of appropriate symmetry (4). Comparison of the

lengths of the K_1 and K_2 components of the K absorption discontinuity of cobalt² in these compounds shows that the length of K_1 component varies slightly from compound to compound while the length of K_2 component remains almost constant. This variation indicates a change in the p and d characters in the hybridized band. According to Carter, however, the d character of bonding orbitals in cobalt remains nearly constant in the bidirectional orbital approach and hence only p character varies in the hybrid state. The K_2 component corresponds to the 1s electron transition to the band of pure 4p character which remains almost constant. The electronic transitions to the rare earth L_{III} discontinuities and the white lines associated with these discontinuities have been suggested. Thus, this study helps in estimating approximately the extent of hybridization of p and d characters of the bonding orbitals in RCo_5 compounds.

We wish to thank Professor C. Mande for his interest in the present work.

1. P.R. Sarode and A.R. Chetal, J. Phys. Soc. Japan, Vol. 40, (1976) In Press.
2. A.R. Chetal and P.R. Sarode, J. Phys. F 5, L217 (1975) and references therein.
3. F.L. Carter, Proc. 9th Rare Earth Research Conf. Blacksburg, Virginia P 617 (1971).
4. P.R. Sarode and A.R. Chetal, Communicated to J. Phys. C (1976).

POSITRON ANNIHILATION & X-RAY SPECTROSCOPIC

STUDIES OF HEAVY RARE EARTH ELEMENTS

S.N. GUPTA & V.P. VIJAYAVARGIYA

Madhav Science College, Ujjain, India.

Holkar Science College, Indore, India.

In recent years attempts have been made to correlate the X-ray spectroscopic studies in the other fields. Important work in this direction is of Bhide et al (1) who have correlated the results with Mossbauer spectroscopy and Magnetic Susceptibilities in case of second transition series elements. In the present work an attempt has been made to correlate the X-ray spectroscopic results of the heavy rare earth metals (2) with the positron Annihilation rates (3) and other structural properties (4) of these metals. The results are collected in the following table :

Element.	Annihilation rate (10^9Sec^{-1}). (3)	Width of the white line (ev). (2)	Metallic radius (\AA). (4)
Gd	4.029 ± 0.044	8.0	1.802
Tb	4.043 ± 0.043	8.2	1.782
Dy	4.158 ± 0.042	9.0	1.773
Ho	4.113 ± 0.057	9.3	1.766
Er	4.128 ± 0.043	9.8	1.757
Tm	4.071 ± 0.042	10.5	1.746
Yb	3.746 ± 0.035	12.3	1.940
Lu	4.056 ± 0.041	7.6	1.734

From the conclusions drawn by Rodda and Stewart from their experimental studies on the positron life times and Annihilation rates in rare earth metals it is noticed that, the 4f electrons are well shielded

and do not participate in the Annihilation process and the core Annihilation takes place only with the 5s and 5p electrons, the annihilation rate depending on the density of conduction electrons.

The study of white line associated with L-absorption edges provide information about the vacant part of the conduction band (2). Hence, it is natural to look for a correlation between the X-ray spectroscopic and positron annihilation studies in these metals. For this purpose a plot of the annihilation rates in the heavy rare earth metals and the width of the white line associated with the L_3 edges of these metals is made.

It is seen that a dip is obtained in the plot of annihilation rates at Yb, while a peak is obtained at the same metal in the plot of the width of the white line. It is also observed that for all other metals, both of these quantities remain nearly the same. Thus, it follows that when the number of conduction electrons remains the same both of these quantities remain nearly the same, but whenever the number decreases, the annihilation rate decreases and the width of the white line increases. The former depending on the filled part of the conduction band, while the later on the unfilled part. Thus a combined study of both can give information about the whole of the conduction band.

Further, the table shows a close relationship of the width of the white line with the well known Lanthanide contraction (Metallic radius) and consequently with the structural and other properties of these metals. This variation in the width of the white line can also be connected with the melting points and elastic constants (4) of these metals as they also show similar but reasonably smooth variations with increasing atomic numbers. However, deviation are observed in the case of Lu and Yb, which may be ascribed to the absence of 4f vacancies in these metals.

References :

1. V.G. Bhide & M.K. Bhal, J. Chem. Phys. 52 (1970).
2. B.D. Padalia, S.N. Gupta, V.P. Vijayavargiya and B.C. Tripathi, J. Phys. F (Metal Phys.), 4 (1974).
3. Rodda J.L. & Steward M.G. Phys. Rev. 131 (1963).
4. Taylor K.N.R. & Darby M.I. Phys. of rare earth solids (Chapman & Hall) 1972.

X-RAY SPECTRA OF TRANSITION METAL DISULFIDES :
FeS₂, CoS₂ AND NiS₂

C. Sugiura and S. Nakai
Department of Applied Physics, Faculty of Engineering,
Utsunomiya University, Utsunomiya, Japan

T. Matsukawa and M. Obashi
Department of Physics, College of General Education,
Osaka University, Toyonaka, Osaka, Japan

J. Kashiwakura and Y. Gohshi
Toshiba Research and Development Center, Kawasaki, Japan

The electronic properties of FeS₂, CoS₂ and NiS₂ with pyrite structure have been the subject of recent experimental as well as theoretical interest because of a wide variety of electric and magnetic properties. The experimental studies of the valence- and conduction-band structure have been made by several different research groups [1-4] investigating the X-ray and ultraviolet photoelectron spectra, the X-ray valence-band spectra and the optical spectra. The molecular levels and energy bands have been calculated by Li et al.[2] using the self-consistent-field X α cluster method and by Khan [5] using the LCAO method, respectively.

The characteristic points obtained from the experimental and theoretical studies are as follows: (1) The narrow 3d-like band of the metals lies at the top of the valence band. (2) Going from FeS₂ to NiS₂, the narrow 3d-like band is broadened and overlaps by degrees with the broad sulfur 3p-like band. (3) The lowest unoccupied band e_g is very strongly mixed with the sulfur 3p band. There is still some uncertainty about the valence and conduction bands.

The metal (Fe, Co and Ni) and sulfur K-absorption spectra of these compounds were measured on a two-crystal spectrometer and a 50-cm bent-quartz-crystal vacuum spectrograph, respectively. The sulfur K β emission spectra were obtained by fluorescent excitation and measured on a vacuum two-crystal spectrometer.

In the metal disulfides used here, FeS₂ was natural pyrite and CoS₂ and NiS₂ were synthetic compounds [6]. The absorbing layers were prepared by uniformly rubbing the fine powder on a sheet of thin paper. Their thicknesses were about 7 and 5 mg/cm² for the metal and sulfur K-absorption spectra, respectively.

The Fe, Co and Ni K-absorption spectra of FeS₂, CoS₂ and NiS₂ are shown in Fig.1. The sulfur K absorption spectra and sulfur K β emission spectra of these disulfides are shown

in Figs.2 and 3, respectively. The metal K absorption spectra are alike and the sulfur K absorption spectra are also alike. However the metal K absorption spectra are quite different from the sulfur K absorption spectra : the former spectra consist of a steplike structure, while the latter spectra are characterized by a prominent absorption maximum at the threshold. Going from FeS_2 to NiS_2 , the presence of the first shoulder in the metal K absorption spectra becomes ambiguous and the first and second bands A and B in the sulfur K absorption spectra move to lower energies and the width of the band A is narrowed. Considering that the lowest empty band e_g is strongly mixed with the sulfur 3p band, the first absorption band A or the shoulder is probably due to the transition to the e_g band.

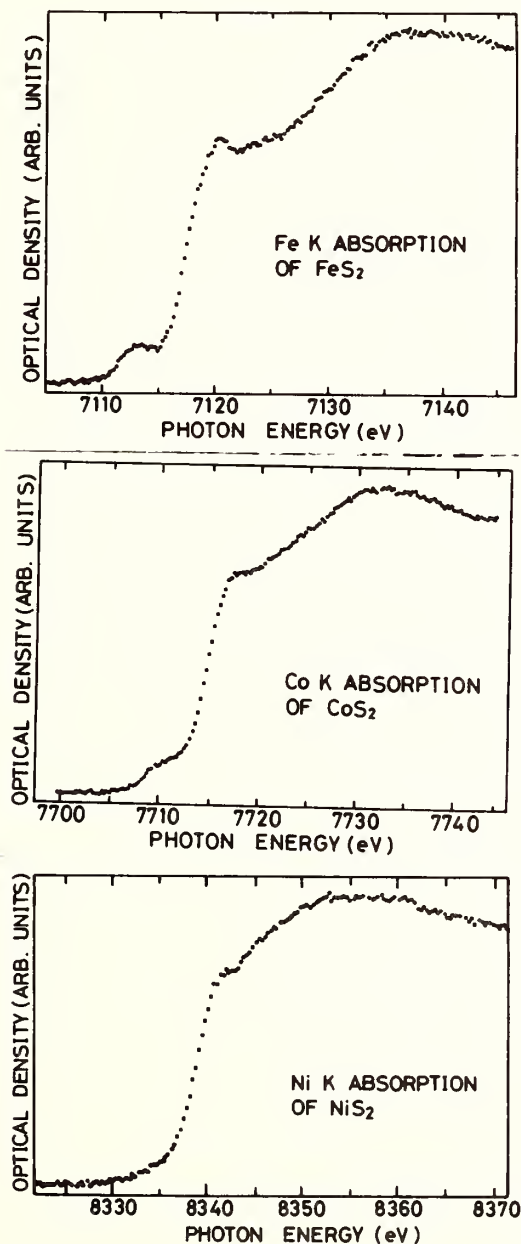


Fig.1. Fe, Co and Ni K-absorption spectra.

In the sulfur $\text{K}\beta$ emission spectra, the main peak $\text{K}\beta_1$ occurs at nearly the same energy. The shoulder $\text{K}\beta_x$ in FeS_2 is clearly separated from the main peak $\text{K}\beta_1$, while in CoS_2 and NiS_2 the presence of the corresponding shoulder is somewhat ambiguous. The structure $\text{K}\beta_1$ of NiS_2 is separated from the main peak $\text{K}\beta_1$, whereas those of FeS_2 and CoS_2 are ambiguous. The low-energy hump $\text{K}\beta'$ appears clearly in CoS_2 .

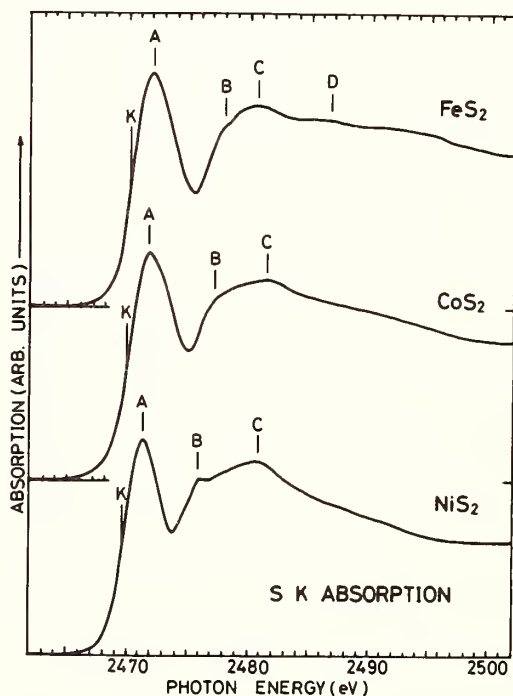


Fig.2. Sulfur K absorption spectra.

Comparisons of the Fe and S K-absorption spectra and S K β emission spectrum of FeS₂ and the molecular levels [2] of an octahedral FeS₆¹⁰⁻ cluster are shown in Fig.4, where the lowest empty e_g level is tentatively associated with the first absorption bands labelled A and a. As can clearly be seen, the first band A in the S K absorption spectrum is much stronger in the intensity than the first shoulder a in the Fe K absorption spectrum. This indicates that the empty band e_g is strongly mixed with the sulfur 3p band. In the Fe K absorption spectrum, the second shoulder b is attributed to the transition to the empty 4s band of the Fe²⁺ ion, having p-character and the third intense and broad band is attributed to the transitions to the higher lying p-like bands (arising from the 4p states of iron). The intensity difference between the two absorption curves is probably due to the different transition probabilities.

In the S K β emission spectrum, the main band K β_1 and its high-energy shoulder K β_x correspond well to a group of levels t_{1g}, t_{1u}, e_g, t_{2u}, t_{1u}, t_{2g} and a_{1g} and the highest occupied t_{2g} level, respectively. A good correspondence of the shoulder K β_x and the t_{2g} level suggests that the t_{2g} band has some sulfur 3p character. According to Khan's calculations [5] the mixing of the p state to the t_{2g} band is about 7 %.

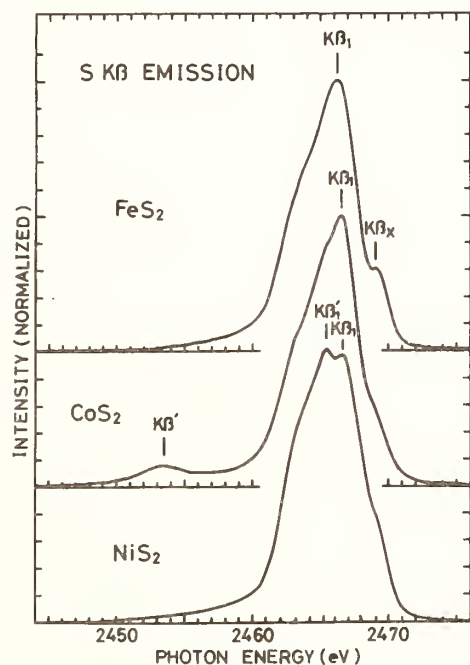


Fig.3. Sulfur K β emission spectra.

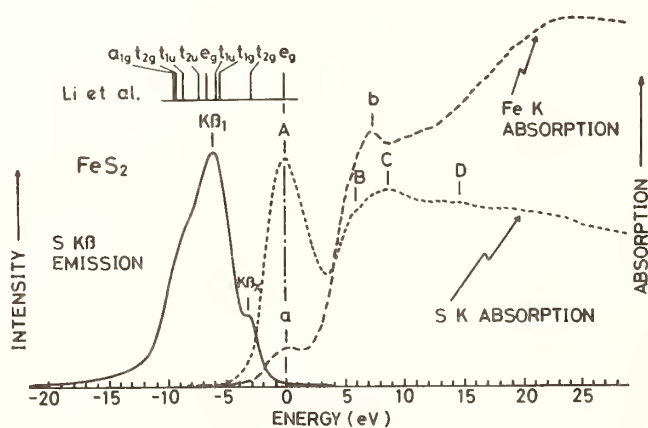


Fig.4. Comparisons of the Fe and S K-absorption spectra and S K β emission spectrum of FeS₂ and the molecular levels [2].

References

1. A. Ohsawa et al. : J. Phys. Soc. Japan 37, 568 (1974).
2. E. K. Li et al. : Phys. Rev. Letters 32, 470 (1974).
3. G. Wiech and E. Zopf : J. Phys. (Paris) 32, C4-200 (1971).
4. T. A. Bither et al. : Inorg. Chem. 1, 2208 (1968).
5. M. A. Khan : J. Phys. C 9, 81 (1976).
6. S. Ogawa et al. : Int. J. Magnetism 5, 349 (1974).

T. Åberg†

Department of Physics
 Kansas State University
 Manhattan, Kansas 66506

Recent experiments by Richard *et al.* [1] and Wölfl *et al.* [2] have revealed novel features in characteristic K spectra which are associated with the strong inner-shell multiple ionization in ion-atom collisions. Related to the former experiment [1] Fig. 1a shows a typical K spectrum [3], where the new features are the four almost equidistant peaks, denoted by KL^nRER (radiative electron rearrangement; n is the number of 2p holes.), below the $K\alpha L^n$ structure. The Si K x-ray spectrum was obtained by a curved crystal spectrometer. These peaks have been found to increase with increasing KL^n ionization in Mg, Al, and Si targets [3]. The two low-energy peaks corresponding to $n=1$ and 2 have also been observed in photon and electron impact [4] but there they are much weaker than the KLL radiative Auger [5] structure which is barely visible below the KL^nRER lines in Fig. 1a.

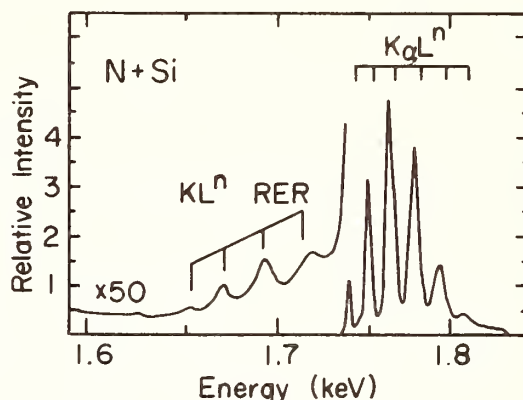


Fig. 1a

The Ne K spectrum [6] shown in Fig. 1b reveals a new peak, $K_{\alpha\alpha}$ ($K_{\alpha\alpha}^h$), far above the K_{α} structure. The energy of this peak is more than twice the K_{α} energy which suggests that it is associated with double K ionization. Observations of $K_{\alpha\alpha}^h$ have been made in the range $7 \leq Z \leq 28$ with solid state detectors [2,6,7]. Neither the K_{α} nor the $K_{\alpha\alpha}^h$ structure is resolved in these measurements.

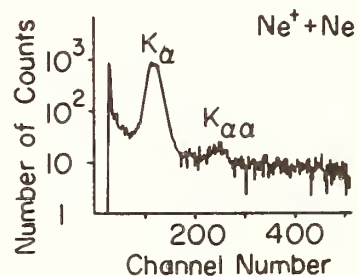


Fig. 1b

Term averaged Hartree-Fock (HF) calculations indicate that the KL^nRER peaks are due to one-photon $1s2s^22p^m - 1s^22s02p^{m+1} (m \leq 5)$ electric dipole (E1) transitions [8]. In the case of $K_{\alpha\alpha}^h$ various energy calculations [6,9,10] indicate that the principal initial and final configurations of this E1 transition are $1s^02s^22p^m$ and $1s^22s2p^{m-1}$, respectively. Hence there is a simultaneous transfer of a 2s and 2p electron in both cases which demonstrates the breakdown [11] of the single-configuration frozen core model of the atom. A schematic energy diagram of the KL^nRER and $K_{\alpha\alpha}^h L^n$ transitions ($n=6-m$) is shown in Fig. 2. The influence of the M electrons and of the multiplet splitting is neglected.

In analogy to theory of the radiative Auger effect [5] the origin of these transitions can be described in terms of configuration

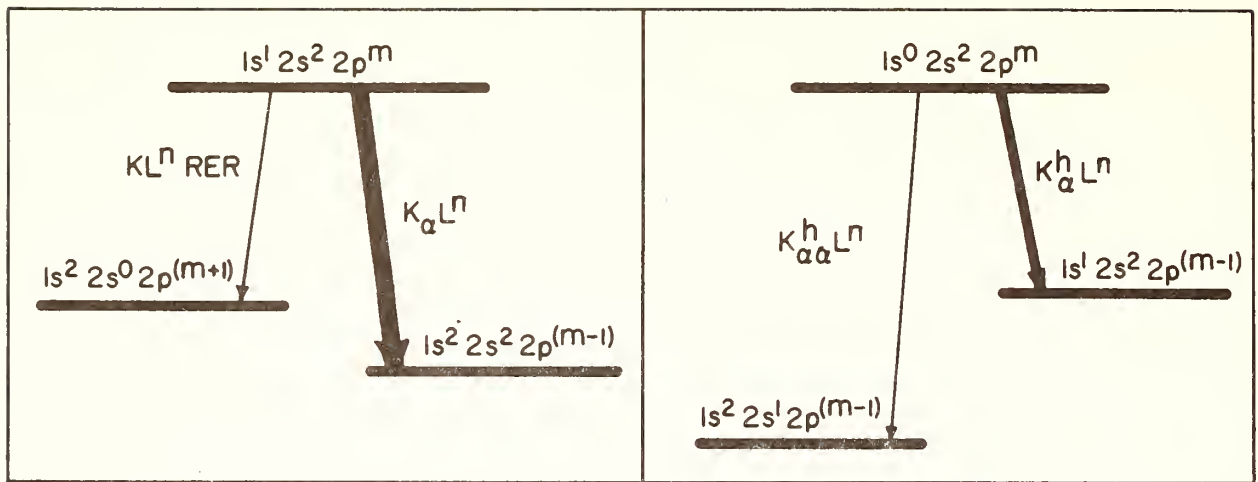


Fig. 2

interaction (CI) and the relaxation of the electronic cloud. It has been suggested [3] that the final state $2s^2 2p^x - 2s^0 2p^{x+2}$ ($x \leq 4$) CI, known to affect the KLL Auger transition rates, is responsible for $KL^n RER$. A detailed analysis [12] indicates that this CI together with the same CI in the initial state for $m \leq 3$, is the major mechanism. The influence of the relaxation with the leading contribution coming from the monopole-dipole amplitude term $D_0(1s2s)D_1(2p2s)$, where $D_0(1s2s)$ is the $1s2s$ monopole radial overlap and $D_1(2p2s)$ the $2p2s$ radial dipole integral, is small. The branching ratio defined as the intensity ratio $I(KL^n RER)/I(KL^n)$, is approximately proportional to $f(2s2p) = G^1(2s2p)^2 \Delta^{-2}$, where $G^1(2s2p)$ is the $2s2p$ Slater exchange integral and Δ twice the $2s$ - $2p$ electron energy difference. As a consequence of the $2s2p$ near degeneracy $f(2s2p) \approx 0.3$ is large and almost independent of Z and m . Hence the relative branching ratios are determined almost solely by the proportionality constants which reflect the electron coupling. Predictions of this model will be compared with experimental evidence regarding intensities and linewidths. It is also suggested that $1s^2 2s^0 2p^m - 1s^2 2s^2 2p^{m-3}$ ($m \geq 3$) $E1$ transitions, involving three jumping $2p$ electrons, may be observable on the high-energy side of $K_{\alpha} L^n$.

It has been proposed [10] that the principal mechanism of the $1s^0 2s^2 2p^m - 1s^2 2s^2 2p^{m-1}$ $E1$ transitions is the $2p$ - $1s$ dipole transition accompanied by the "shake down" of a $2s$ electron into the second $1s$ hole. This model predicts a branching ratio (with respect to the K_{α}^h hypersatellite transitions) which is proportional to the square of the $1s2s$ monopole radial overlap integral $D_0(1s2s)$ multiplied by an energy factor $\omega(K_{\alpha\alpha}^h)^3 / \omega(K_{\alpha}^h)^3$. According to HF calculations $D_0(1s2s)^2 \approx 0.035Z^{-2}$ for $12 \leq Z \leq 30$. These calculations pertain to atoms with two $2p$ holes. However, $D_0(1s2s)$ is fairly independent of the number of the $2p$ holes [10]. The large $1s2s$ overlap is due to the drastic change of the K shell screening of the $2s$ electron which does not occur in the case of $KL^n RER$, where the role of the $1s$ and $2s$ electrons is reversed. The calculated branching ratios [10] agree within a factor of two with the measured ones [13]. It is suggested that the inclusion of K shell correlation in the final state improves the "shake down" model. The mixing between the final $1s^2 2s^2 2p^{m-1}$ and $1s^2 2s^2 2p^{m-1}$ configurations is not

important within the framework of the HF approximation [10]. Note also that $D_0(1s2s)$ may be affected by relativistic effects for $Z \gtrsim 20$.

In conclusion, a unified model of KL^nRER and $K_{\alpha\alpha}^h L^n$ transitions [12] is presented in terms of configuration interaction and relaxation of the electronic cloud. This model indicates that whereas the KL^nRER transitions are governed by the $2s2p$ exchange interaction, the major mechanism of the $K_{\alpha\alpha}^h L^n$ transitions is the "shake down" of a $2s$ electron.

The author would like to thank K. Jamison and P. Richard for fruitful cooperation and P. Bagus and U. Fano for helpful discussions.

References:

*Supported in part by U.S. ERDA Contract No. E(11-1)-2753.

†Permanent Address: Laboratory of Physics, Helsinki University of Technology, 02150 Espoo 15, Finland.

- [1] P. Richard, C. F. Moore and D. G. Olsen, Phys. Lett. A43, 519 (1973).
- [2] W. Wölfli, Ch. Stoller, G. Bonani, M. Suter, and M. Stöckli, Phys. Rev. Lett. 35, 656 (1975).
- [3] K. A. Jamison, J. M. Hall, J. Oltjen, C. W. Woods, R. L. Kauffman, T. J. Gray, and P. Richard, Phys. Rev. A, to be published.
- [4] See e.g. T. Åberg and J. Utriainen, J. de Physique 32, C4, 295 (1971).
- [5] See e.g. T. Åberg, Atomic Inner Shell Processes, edited by B. Crasemann (N.Y.: Academic Press, p. 353, 1975).
- [6] Th. P. Hoogkamer, P. Woerlee, F. W. Saris, and M. Gavrilu, J. Phys. B 9, L145 (1976).
- [7] Ch. Stoller, W. Wölfli, G. Bonani, M. Stöckli, and M. Suter, to be published.
- [8] K. A. Jamison, J. M. Hall, and P. Richard, J. Phys. B 8, L458 (1975).
- [9] H.-D. Betz, Abstracts of Contributed Papers of Second International Conference on Inner Shell Ionization Phenomena (Freiburg, 1976) p. 155; private communications by J.-P. Briand and B. Hodge.
- [10] T. Åberg, K. Jamison, and P. Richard, to be published.
- [11] S. Goudsmit and L. Gropper, Phys. Rev. 38, 225 (1931).
- [12] T. Åberg, K. Jamison, and P. Richard, to be published.
- [13] See Ref. 7; According to Ref. 7 a many-body perturbation calculation of the $K_{\alpha\alpha}^h$ rate by H. P. Kelly (to be published) for $Z=26$ underestimates the rate somewhat whereas our calculation overestimates the rate by almost the same amount. H. Nussbaumer's (to be published in J. Phys. B) CI results are smaller than ours by a factor of 10^{-2} . The agreement between estimates based on J. P. Vinti's calculations (Phys. Rev. 42, 632, 1932) of oscillator strengths of $1s^2 1S - qs2p^1P$ ($q=1,2$) transitions in He and measurements seems to be fortuitous since the $1s^2 1S - 1s2p^1P$ transition corresponds to K_{α} rather than K_{α}^h . Furthermore the transition energy correction should be applied to Vinti's results.

MEASUREMENT OF CROSS SECTIONS FOR THE TWO-ELECTRON ONE-PHOTON TRANSITION IN HEAVY-ION COLLISIONS

R. Schuch and G. Nolte

Physikalisches Institut der Universität Heidelberg, 69 Heidelberg, Germany

H.Schmidt-Böcking, R.Schulé, W.Lichtenberg, and K.E.Stiebing

Institut für Kernphysik der J.W. Goethe Universität

6 Frankfurt/Main, Germany

I. Tserruya

Max-Planck-Institut für Kernphysik, 69 Heidelberg, Germany

Measurements of the two-electron one-photon transitions ¹ are interesting for two reasons: they yield information on the production of inner double-hole states, similar to the measurement of hypersatellite lines and they open the field of correlation effects in inner shells which is also investigated by measurements of the radiative Auger effect ² and the three electron Auger effect ³ .

In this paper we are mostly concerned with the production of double-hole states deduced from the absolute and relative intensity of the two-electron one-photon ($K_{\alpha\alpha}$) transition. However, first some comments on the identification of the $K_{\alpha\alpha}$ transition are in order. The relative intensity of the $K_{\alpha\alpha}$ transition is independent on the rate of K_{α} - and K_{β} x-ray events and thus cannot be due to pile-up. Also the energy of $K_{\alpha\alpha}$ x-rays is slightly different from the double

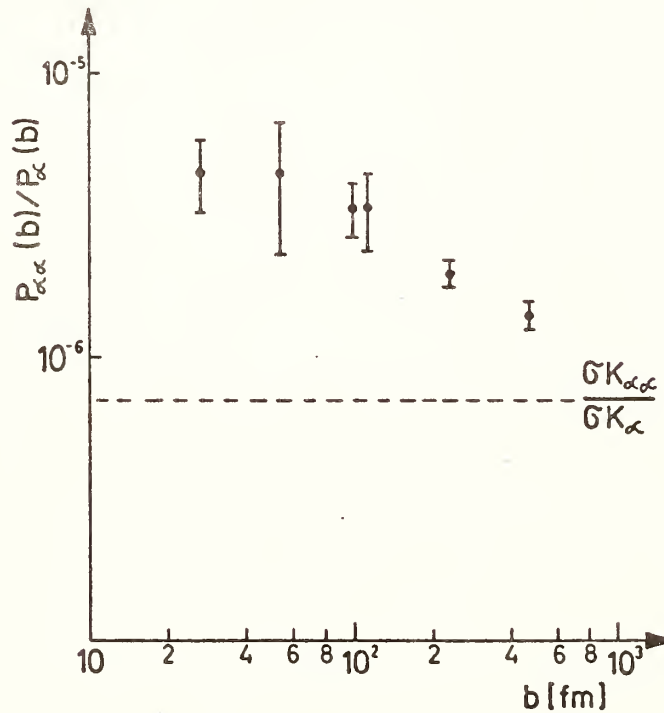
K_{α} energy and is in excellent agreement with Hartree Fock calculations for the $K_{\alpha\alpha}$ transition. This, however, would not exclude the existence of two correlated photons. The use of different absorbers in front of the x-ray detector proved the existence of a single photon with energy $E_{K_{\alpha\alpha}}$. We measured the intensity of the $K_{\alpha\alpha}$ transition for near-symmetric collision systems in the region of S and Cl for different impact energies and solid as well as dilute gas targets.

The results are in accordance with the assumption of a M0 excitation for the double-hole states similar to the production of single vacancy states under the same condition. The occurrence of the $K_{\alpha\alpha}$ transition under single-collision conditions proves the one-step production of both K-vacancies.

The reinvestigation of the impact parameter dependent x-ray spectra for 35 MeV Cl incident on Cl-targets ⁴ yielded the differential cross section for the $K_{\alpha\alpha}$ production. In contrast to the (single vacancy) K_{α} emission probability, which was found to be flat within the region of the K-shell radius (3100 fm) ⁵, the $K_{\alpha\alpha}$ emission probability is strongly dependent on the impact parameter even for very close collisions. The ratio of the emission probabilities $P_{K_{\alpha\alpha}}/P_{K_{\alpha}}$ is increased by almost a factor of 5 relative to the ratio of the single spectra yields $8 \cdot 10^{-7}$, for this case. The results indicate the existence of a new ionization mechanism,

occurring only in close collisions.

- 1 W. Wölfli et al., Phys.Rev.Lett. 35 (1975) 656;
Th.P. Hoogkamer et al., J.Phys. B 9 (1976) L 145.
- 2 T.Aberg and J.Utriainen, Phys.Rev.Lett. 22 (1969) 1346.
- 3 V.V. Afrosimov et al., JETP Lett. 21 (1975) 249.
- 4 I. Tserruya et al., Phys.Rev.Lett. 36 (1976) 1451.
- 5 I. Tserruya, H. Schmidt-Böcking, R. Schuch, R. Schulé,
to be published.



The ratio of the two-electron to one-electron-one-photon transition probability as function of the impact parameter measured with 35 MeV Cl on NaCl. The dashed line indicates the ratio of the total cross sections.

EVIDENCE FOR $2e-1\gamma$ TRANSITIONS IN Cl^{n+} BOMBARDMENT OF KCl^{\dagger}
W. W. JACOBS, B. L. DOYLE, S. M. SHAFROTH and J. A. TANIS[†]
University of North Carolina, Chapel Hill, N. C. 27514 and
Triangle Universities Nuclear Laboratory, Durham, N. C. 27706,
and A. W. WALTNER

North Carolina State University, Raleigh, N. C. 27607 and TUNL

The possibility of two-electron one-photon ($2e-1\gamma$) transitions, in which two electrons simultaneously fill an empty K-shell resulting in the emission of a single photon at approximately twice the K x-ray energy, was predicted nearly 50 years ago by Heisenberg [1]. Recently, evidence for such transitions was presented by Wölfl *et al.* [2] following collisions of Fe and Ni ions with Fe and Ni targets.

In the present work, we report similar evidence resulting from 30 to 80 MeV Cl^{n+} beams incident on thin ($\sim 100 \mu g/cm^2$) targets of KCl evaporated onto carbon backing foils ($20 \mu g/cm^2$). The x-rays were detected with an $80 mm^2 \times 5mm$ intrinsic Ge detector (170 eV FWHM at 5.9 KeV) located in air at 90° to the beam. In order to eliminate pulse-pileup, pure Al absorber, typically $20 mg/cm^2$, was used to reduce the characteristic x-ray counting rate. Scattered projectile ions were counted at 60° to the incident beam in a solid-state detector for normalization purposes.

Typical raw x-ray spectra for 30, 50, and 70 MeV Cl^{n+} incident on KCl are shown in Fig. 1. The Cl characteristic x-rays are completely attenuated by the Al absorber; the largest peaks near 4 KeV are the potassium K_{α}^* and K_{β}^* (the asterisks denote the shifted x-ray lines due to multiple ionization) whose

relative intensities have been reversed due to the large Al absorption. At higher energies, one sees small peaks riding on a background composed of the non-characteristic x-ray continuum. The peak near 5.6 keV is slightly greater than twice the measured K_{α}^* energy (2.7 keV) of Cl and the peak near 7.0 keV is slightly greater than twice the potassium K_{α}^* energy (3.4 keV). These peaks do not correspond to any known contaminant radiation. We attribute these peaks to $2e-1\gamma$ transitions, denoted by $K_{\alpha\alpha}^{h*}$, in Cl (due to both projectile and target x-rays) and potassium, respectively. At the higher bombarding energies, one sees, perhaps, evidence for the $K_{\alpha\beta}^{h*}$ transition for both Cl and K at slightly higher energies than the $K_{\alpha\alpha}^{h*}$ peaks. One also notes that as the bombarding energy is reduced, the

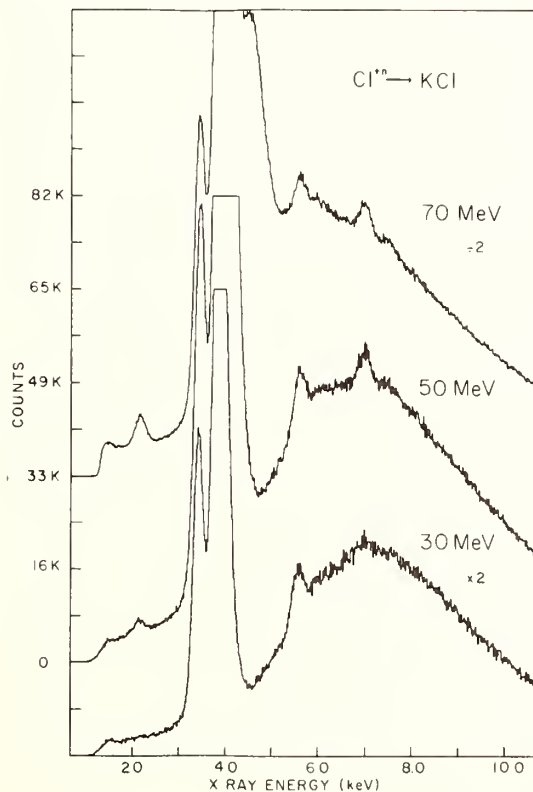


Fig. 1. $Cl \rightarrow KCl$ X-Ray Spectra.

intensity of the K 2e-1 γ peak goes down relative to the Cl 2e-1 γ peak. This may reflect a difference in the double K-shell vacancy-production mechanism for the two cases.

A summary of the observed energies for potassium x-rays is shown in Fig. 2 plotted as a function of Clⁿ⁺ bombarding energy. The straight lines are least-squares fits to the data. One notes that the K_{α}^{h*} and K_{α}^* energies (actually, $2E_{K_{\alpha}^*}$ is plotted) slowly increase with incident Cl energy indicating an increasing degree of L-shell ionization.

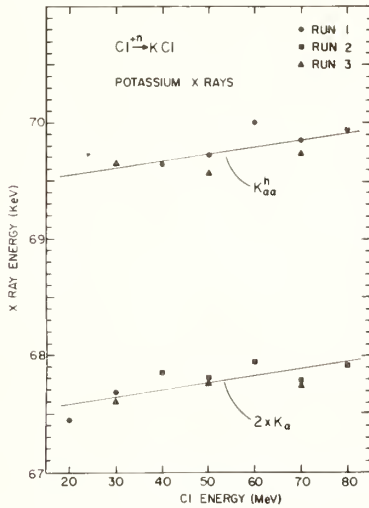


Fig. 2. K_{α}^* and K_{α}^{h*} energies

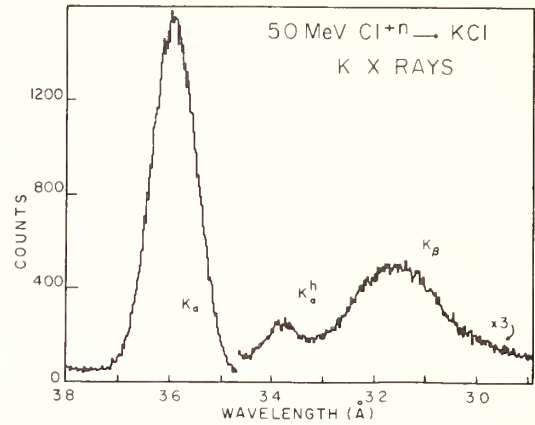


Fig. 3. High resolution spectrum showing K_{α}^* , K_{β}^* , and the hypersatellite K_{α}^{h*} .

In order to compare the observed K_{α}^* and K_{α}^{h*} energies with theoretical predictions and to determine the number of L vacancies present we compare the x-ray energies with appropriate unshifted x-ray energies. For the K_{α}^* line the energy shift is taken to be $\Delta E_{K_{\alpha}^*} = E_{K_{\alpha}^*} - E_{K_{\alpha}^0}$ where $E_{K_{\alpha}^0}$ is the unshifted K_{α} energy. For K_{α}^{h*} we define the energy difference $\Delta E_{K_{\alpha}^{h*}} = E_{K_{\alpha}^{h*}} - E_{K_{\alpha}^{h0}}$ where $E_{K_{\alpha}^{h0}}$ is the unshifted K_{α} hypersatellite energy [3]. This choice for $\Delta E_{K_{\alpha}^{h*}}$ is based on the fact that each of the transition energies involved result from initial states with two K-shell vacancies.

We have used the HFS computer code of Herman and Skillman [4] to calculate $\Delta E_{K_{\alpha}^*}$ and $\Delta E_{K_{\alpha}^{h*}}$ for increasing numbers of L vacancies. The justification for using the HFS code is based on a comparison of the energy shifts so obtained with the same energy shifts obtained from the code of Desclaux [5] for the cases of Fe and Ni in which it is found that the predicted shifts are nearly the same.

The results of our calculations are shown in Table 1. A comparison of the potassium experimental energy shifts for both K_{α}^* and K_{α}^{h*} with their theoretical values shows that both transitions take place in the presence of nearly the same number (~ 4) of L vacancies, as one might expect. Similar results are obtained for the Cl K_{α}^* and K_{α}^{h*} transitions.

Finally, we have determined the branching ratio, $K_{\alpha}^{h*}/K_{\alpha}^*$, for the 2e-1 γ transition to the hypersatellite transition. To do this, we measured the K_{α}^* and K_{α}^{h*} x-ray spectrum with a high resolution ARL

Table 1. Observed K_{α} and $2e-1\gamma$ ($K_{\alpha\alpha}^h$) x rays compared to calculated values of ΔE as defined in the text.

X Rays/ Target	$E_{C\ell}$ (MeV)	Experimental				Theoretical		
		$E(K_{\alpha}^*)$ (eV)	$E(K_{\alpha\alpha}^{h*})$ (eV)	ΔE (K_{α})	ΔE ($K_{\alpha\alpha}^h$)	Vacancy ^a Config.	ΔE (K_{α})	ΔE ($K_{\alpha\alpha}^h$)
K/KC ℓ	30	3387 \pm 10	6964 \pm 20	74	3452	-	-	3260
K/KC ℓ	50	3389 \pm 10	6957 \pm 20	76	3445	(2p) ⁻¹	19	3306
K/KC ℓ	70	3395 \pm 10	6977 \pm 20	82	3465	(2p) ⁻²	40	3355
						(2p) ⁻³	63	3409
						(2p) ⁻⁴	88	3466
						(2p) ⁻⁵	114	3528
C ℓ /KC ℓ	30	2683 \pm 10	5545 \pm 20	61	2746	-	-	2580
C ℓ /KC ℓ	50	2704 \pm 10	5562 \pm 20	82	2763	(2p) ⁻¹	16	2619
C ℓ /KC ℓ	70	2718 \pm 10	5575 \pm 20	96	2776	(2p) ⁻²	34	2662
						(2p) ⁻³	54	2709
						(2p) ⁻⁴	76	2759
						(2p) ⁻⁵	99	2814

a. Other than K-shell vacancies. In addition to the (2p) vacancies shown, outer-shell configurations of (3p)⁻³ and (3p)⁻³ (4s)⁻¹ were used for C ℓ and K respectively.

curved-crystal spectrometer, as shown in Fig. 3, to determine the ratio $K_{\alpha}^*/K_{\alpha\alpha}^{h*}$. Combining this measurement with the $K_{\alpha\alpha}^{h*}/K_{\alpha}^*$ ratio obtained from the low resolution intrinsic Ge spectra gives the desired branching ratio. Our preliminary results indicate values for $K_{\alpha\alpha}^{h*}/K_{\alpha}^*$ of about $2-4 \times 10^{-5}$ for both C ℓ and K. This value is nearly an order of magnitude lower than that measured by Wölfl *et al.* [2] for Fe and Ni and is nearly the same factor smaller than that predicted by Åberg *et al.* [6].

†Supported in part by the U. S. Energy Research and Development Administration

‡Supported by the North Carolina Board of Science and Technology

References

1. W. Heisenberg, Z. Physik 32, 841 (1925).
2. W. Wölfl *et al.*, Phys. Rev. Lett. 35, 656 (1975), and W. Wölfl *et al.*, (to be published).
3. D. J. Nagel *et al.*, Phys. Rev. Lett. 36, 164 (1975).
4. F. Herman and S. Skillman, Atomic Structure Calculations, (Prentice-Hall, N. J., 1963).
5. H.-D. Betz, Contributed Papers, 2nd Int. Conf. on Inner Shell Ionization Phenomena, (Freiburg, 1976); W. Hodge, (to be published).
6. T. Åberg, K. A. Jamison, and P. Richard, (to be published).

EXCITATION OF 2 ELECTRON - 1 PHOTON K X-RAYS IN Ni-Ni COLLISIONS†

by J. S. Greenberg and P. Vincent,
Wright Nuclear Structure Laboratory,

and W. Lichten,
Becton Center
Yale University, New Haven, Conn. 06520

According to the electron promotion model [1], the number of K-shell vacancies produced in a collision is proportional to the vacancy factor R , the number of prior vacancies in the L shell orbitals of the colliding atoms [2]. Thus, the theoretical calculation of Briggs and Macek [3] gives the cross-section for single K-shell vacancy production as a product of the vacancy factor R and the cross section for a single L-shell vacancy prior to the excitation process.

We report measurements of the energy dependence of the cross-sections for both the $K\alpha$ (1 electron, 1 photon) and $K\alpha\alpha$ (2 electron, 1 photon) x-ray emissions for Ni-Ni collisions in the energy range 17.9 - 91.5 MeV. The measurement of both cross-sections yields valuable information on the excitation mechanism of both single and double K-shell vacancies. In particular, two experimental cross-sections make it possible for the first time to make independent tests of both the vacancy factor and the theoretical cross-section per L-shell vacancy.

Figure 1 shows data points* for $\sigma(K\alpha)$, and $\sigma(K\alpha\alpha)$ (multiplied by 10^5)

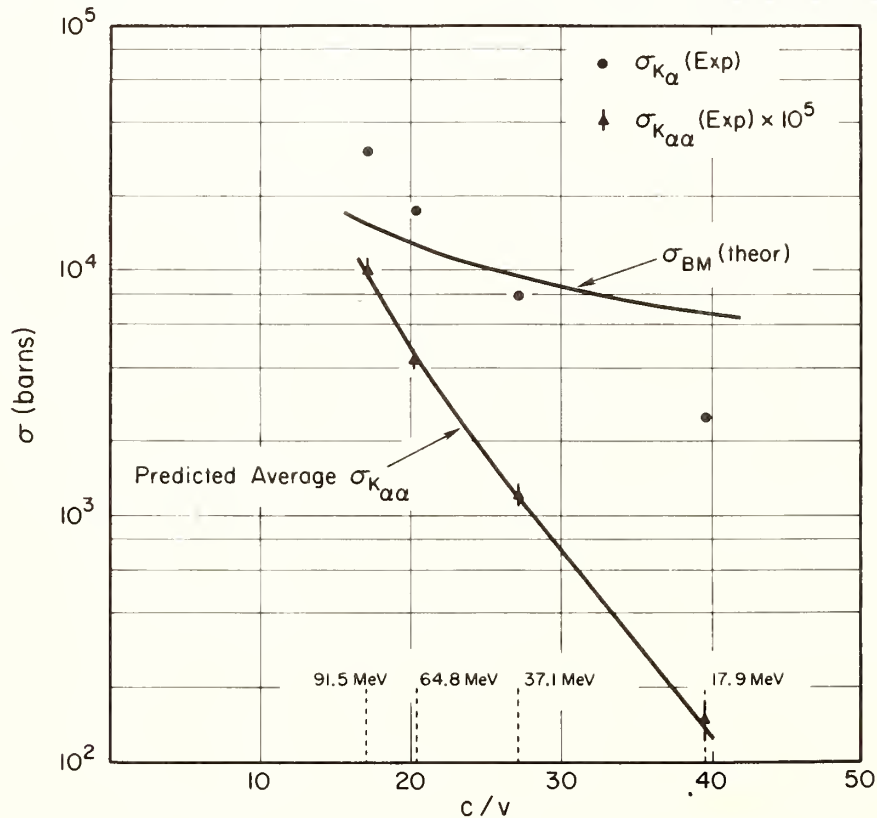


Fig. 1 Comparison of experimental data points with theory.

† Support: USERDA Control E(11-1)-3074 and NSF grant PHY 74-09408 A02.

as a function of reciprocal velocity. The curve marked σ (BM) in Fig. 1 is a scaled Briggs-Macek [3] calculation [4] of the $K\alpha$ cross-section, for a single prior L-shell vacancy and a fluorescence yield of 0.41. In the Briggs-Macek theory, the ratio of these two quantities gives the vacancy factor $R = \sigma(K\alpha)/\sigma(BM)$. This ratio is plotted as a function of reciprocal velocity in Fig. 2. Briggs and Macek predict that the number of double K-shell vacancies is proportional to the square of R , the number of prior L-shell vacancies [3]. Thus, the ratio of cross-sections for double and single K-shell vacancy production should be proportional to R . As a test of this idea, the ratio $\sigma(K\alpha\alpha)/\sigma(K\alpha)$ also is plotted in Fig. 2.* The agreement between the slopes of both curves in Fig. 2 is an excellent confirmation of the theory.

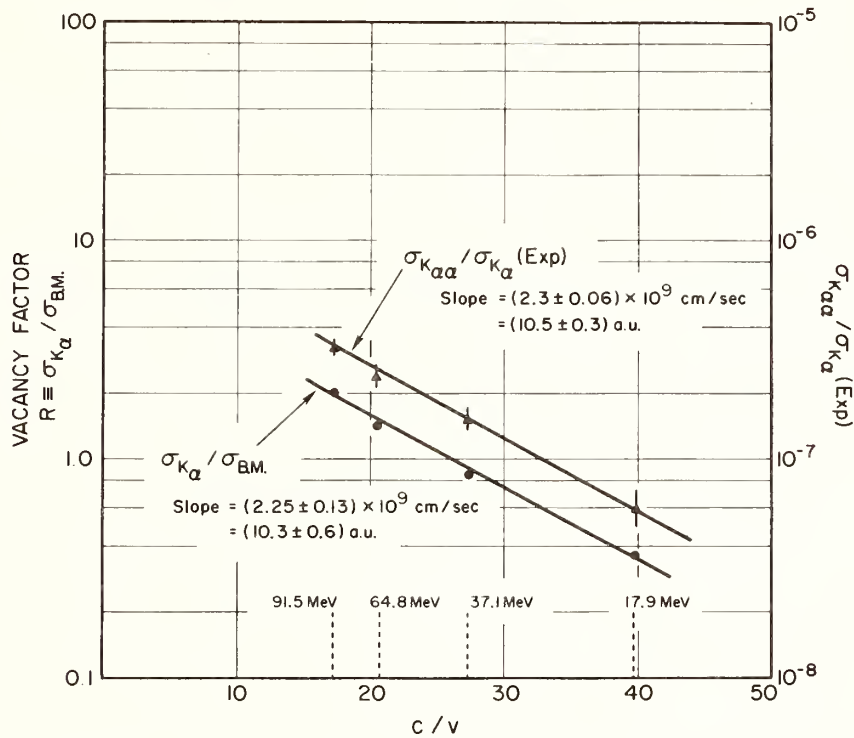


Fig. 2 A critical test of the dynamically induced exit channels mechanism, which predicts that both curves should have the same slope.

The absolute cross section for the 2 electron - 1 photon $K\alpha$ is given by the Briggs-Macek theory, extended to cover two electron excitations:

$$c_{K\alpha\alpha} = \sigma_{K\alpha} \frac{B.R. \times S \times R}{24} \left[\frac{\int_0^\infty b P^2(b) db}{\int_0^\infty b P(b) db} \right]$$

where $P(b)$ is the probability of a rotationally coupled $2P\sigma \rightarrow 2P\pi$ transition, b is the collision impact parameter, and $B.R. = 1/(5000 \pm 600)$ is the branching ratio for $K\alpha\alpha$ x-rays for double K-shell excitation [5]. We have used the Demkov-Olson-Meyerhof formula [6] to calculate $S = 1/(1 + \exp [2/v])$, a vacancy sharing factor, which gives the probability that both K-shell vacancies will end on the same atom. In the present experiment, S ranges from 0.36 to 0.44. We estimate the ratio of integrals in the bracket to be 0.5. The predicted and experimental $K\alpha\alpha$ x-ray crosssections are compared in Fig. 1. The agreement is excellent.

As pointed out by Fastrup et al. [7], the velocity dependence of the factor R (Fig. 2) is a measure of dynamically induced vacancies in the L-shell, prior to rotational excitation of K-shell vacancies. The slope of the curves in Fig. 2, when scaled to $Ne(+)-Ne$ collisions becomes $a(Ne) = a(Ni) \times Z(Ne)/Z(Ni) = (10.3 \pm 0.6)/2.8 = 3.7 \pm 0.2$, in fair agreement with the results of Stolterfoht et al. [8] for neon [3.0 for $Ne(+)$, 3.4 for $Ne(++)$] projectiles.

These results confirm the general correctness of the Briggs-Macek picture of K-shell excitation [3] within the framework of the electron promotion model [1,2]. The dynamically induced exit channel factors of Fastrup et al. [7] have been checked independently for the first time, and also have been found to be correct.

References

- [1] U. Fano and W. Lichten, Phys. Rev. Letters 14, 627 (1965).
- [2] W. Lichten, Phys. Rev. 164, 131 (1967).
- [3] J. Briggs and J. Macek, J. Phys. B: Atom. Molec. Phys. 5, 579 (1972); 6, 841 (1973); 6, 982 (1973).
- [4] R. Laubert et al., Phys. Rev. A11, 135 (1975) and R. Laubert, private communication.
- [5] W. Wolfli et al., Phys. Rev. Letters 35, 656 (1975); Paper presented at the Second International Conference on Inner Shell Ionization Phenomena, Freiburg, 1976.
- [6] Yu. N. Demkov, J. Soviet Physics, JETP 18, 138 (1964); R. E. Olson, Phys. Rev. A6, 1822 (1972); W. E. Meyerhof, Phys. Rev. Letters 31, 1341 (1973).
- [7] B. Fastrup et al., J. Phys.: Atom. Molec. Phys. B1, L206 (1974).
- [8] N. Stolterfoht et al., Phys. Rev. A12, 1313 (1975).

* All uncertainties shown are statistical only. Systematic errors are $\pm 20\%$.

EFFECTS OF COLLISIONAL QUENCHING ON THE X-RAY YIELD FROM ION-ATOM COLLISIONS*

Dennis Matthews and Richard Fortner
Lawrence Livermore Laboratory, Livermore, California 94550

A topic of current interest is the x-ray yield from ions which are excited while traversing target media of varying density and thickness. Betz et al.[1] and other researchers[2] have used a simple two-state model which describes the vacancy production and destruction in terms of inner-shell rearrangement processes. The basic categories of rearrangement are 1) inner-shell vacancy production, 2) natural decay by x-ray or Auger electron emission (which fills the vacancy), and 3) collisional quenching (which eliminates the inner-shell vacancy through processes such as electronic capture and vacancy transfer). Note that for most collision systems the probability of collisional quenching of the inner-shell vacancy is small[1-3] in comparison to the other types of rearrangement. To the extent that x-ray yields depend on the presence of inner-shell vacancies, one could conclude that these yields are not significantly affected by collisional quenching. However, recall that the probability of x-ray emission (the fluorescence yield ω) for high degrees of ionization depends sensitively on the multiplet states formed in the collision. Consider that outer-shell rearrangement collisions can easily change the ion from one multiplet state into another state having a different and perhaps smaller ω . In addition, only large impact parameter collisions are necessary for this type of rearrangement to occur. Thus, under certain conditions collisional quenching of x-ray emitting states (not quenching of vacancies) can seriously effect the yields of x rays from ions traversing gas, foil or solid targets. In fact, if the mean-free-path for quenching is comparable to that of natural decay then non-linearities in the yields of x rays vs target thickness or density will be observed (see ref. 4). The subject of this talk is to discuss the quenching mechanism in some detail as well as discuss how it effects the yields of x rays from ions moving in gas, foil and solid targets. We determine that the technique of determining inner-shell vacancy lifetimes via the non-linear yield of x rays with foil target thickness (see ref. 1,2) must include quenching of x-ray emitting states to get accurate lifetimes. On the other hand, this type of quenching does not effect the number of inner-shell vacancies in the beam. Thus the measurements[3] of target x-ray yields which require the presence of inner-shell vacancies are insensitive to these effects.

First, a definition of what we call collisional quenching. Collisional quenching of a state refers to any type of collision process which changes a given excited state into another. An obvious example of the process is Coulomb excitation of outer shell electrons from one n state to the next higher. This mechanism occurs with a high probability in ion-atom collisions whenever there are nearby energy states requiring no change of spin in going from the initial to final electronic state (i.e., dipole excitations dominate). Other collisional quenching mechanisms such as collisional deexcitation as well as excitation transfer can also contribute to the quenching of excited states.

Within the two-state approximation[1-4] a theoretical formulation of the beam population in terms of the various rearrangement modes is given by the following differential equation (neglecting energy loss and beam absorption):

$$\frac{df_j}{dx} = \frac{-f_j}{v\tau_j} - f_j N\sigma_{Qj} + (1 - f_j)N\sigma_{vj} \quad (1)$$

where f_j is the fraction of beam ions in state j as a function of distance x since centering a homogeneous target, v is the beam velocity, τ_j is the spontaneous lifetime of state j , N is the target density (cm^{-3}), σ_{Qj} is the total cross section for quenching the state and σ_{vj} is the $f_j(x=0) = 0$ then eq. 1 has solution

$$f_j(x) = \frac{N\sigma_{vj}}{\beta} [1 - e^{-\beta x}], \quad \beta \equiv \frac{1}{v\tau_j} + N(\sigma_{Qj} + \sigma_{vj}) \quad (2)$$

However for most collision systems of interest $\beta x \gg 1$, i.e., the state has achieved a steady state population. This implies $f_j(x) = f_{Qj} = N\sigma_{vj}/\beta$. The yield of x rays from a target of thickness L is given by

$$Y(L) = \int_0^L f_{Qj} \frac{dx}{v\tau_R} = N\sigma_{vj} \tilde{\omega}_j L, \quad \text{where } \tilde{\omega}_j = \omega[1 + N(\sigma_{Qj} + \sigma_{vj})v\tau_j]^{-1} \quad (3)$$

is the effective fluorescence yield inside medium. The numerator from the expression for $Y(L)$ is the standard thin target yield but note that it is reduced by the quenching term $[1 + N(\sigma_{Qj} + \sigma_{vj})v\tau_j]$. Similarly for a foil target, where we have contributions from both inside and outside the foil (see ref. 1) we obtain the solution $Y_{\text{foil}}(L) = N\sigma_{vj}\tilde{\omega}_j L + \omega f_{Qj}$. Following Betz and coworkers[1] we can determine the spontaneous lifetime τ_j from this expression by fitting $Y(L)$ vs L and extrapolating to $L \rightarrow 0$, thus $\tau_j = Y(0)/\tilde{\omega}_j N\sigma_{vj} v$. Note that any measurements of lifetimes using this technique depend sensitively on the magnitude of quenching. Fortner and Matthews[5] have determined that $\sigma_{Qj} \gg \sigma_{vj}$ for He-like fluorine states following F on C collisions. So presume that $\tilde{\omega}_j$ is strictly dependent on N , σ_{Qj} and τ_j . To illustrate the effects of quenching in more detail it is convenient to consider two types of collision conditions. Consider collisions where the mean-free-path for quenching, $\lambda_Q \equiv 1/[N\sigma_Q]$, is either 1) much greater than or 2) much less than the mean-free-path for natural decay, $\lambda_d \equiv v\tau$. Condition 1) is the single collision case where quenching has no effect since $N\sigma v\tau \ll 1$ thus $\tilde{\omega} \approx \omega$ and $Y(L) = N\sigma\omega L$. For prompt states ($\tau \leq 10^{-14}$ s) and ions with 1 MeV/amu velocities ($\sim 10^9$ cm/s), this condition is satisfied even with targets having solid densities ($N \sim 10^{23}$) provided that $\sigma_Q < 10^{-18}$ cm^2 . However, for metastable states (e.g., if $v\tau \sim 1$) this condition is not satisfied unless $N\sigma_Q \ll 1$. Assuming σ_Q is geometric (see ref. 4) would require that $N \ll 10^{-16}$ for the case of low z ions such as oxygen or fluorine impinging on argon targets. Obviously the satisfaction of this condition is sensitive to the size of σ_Q for the collision system of interest. Figure 1 illustrates what can happen to metastable states in a Li-like and He-like fluorine beam as the target density is increased from the gas to solid realm. Complete extinction of the metastable x-ray lines is observed when using a solid target. This situation is more closely described as condition 2)i.e., near complete

quenching of the state. This implies that $N\sigma_Q v\tau \ll 1$ hence $\tilde{\omega} \rightarrow \omega \ell_Q/\ell_d \ll 1$, consequently a very low probability of photon emission. Complete quenching can even occur for prompt states ($\tau \sim 10^{-14}$) provided $\sigma_Q \sim 10^{-16}$ since the condition $N \gg 10^{20}$ is easily accomplished with a solid target. Figure 2 illustrates this situation. The prompt He-like and H-like $np \rightarrow 1S$ ($n \geq 3$) transitions are greatly reduced in a solid over that of a thin foil target.

Outside the two extremes outlined above we observe that, in general, quenching is responsible for a noticeable decrease in x-ray yield whenever $N\sigma_Q v\tau \sim 1$. This condition covers a good number of the collision systems studied in ion-solid and ion-gas interactions.

More detailed descriptions of the quenching mechanism and its relationship to the final charge states observed for ions emerging from foil targets will be discussed. Suggested further measurements on quenching in ion-atom collisions include 1) a determination of why we observe non-equal quenching cross sections for states having widely differing lifetimes, 2) does σ_Q depend on different configurations or multiplets, 3) is σ_Q/σ_V ratio constant with ion atomic number, and 4) is σ_Q collision energy dependent?

References: /1/ H. D. Betz, F. Bell, H. Panke, G. Kalkoffen, M. Welz and D. Evers, Phys. Rev. Lett. 33, 807 (1974); /2/ S. L. Varghese, C. L. Cocke, B. Curnotte and G. Seaman, private communication; /3/ F. Hopkins, Phys. Rev. Lett. 35, 270 (1975); /4/ D. L. Matthews, R. J. Fortner and G. Bissinger, Phys. Rev. Lett. 36, 664 (1976). R. J. Fortner and D. L. Matthews (submitted to Phys. Rev. A.).

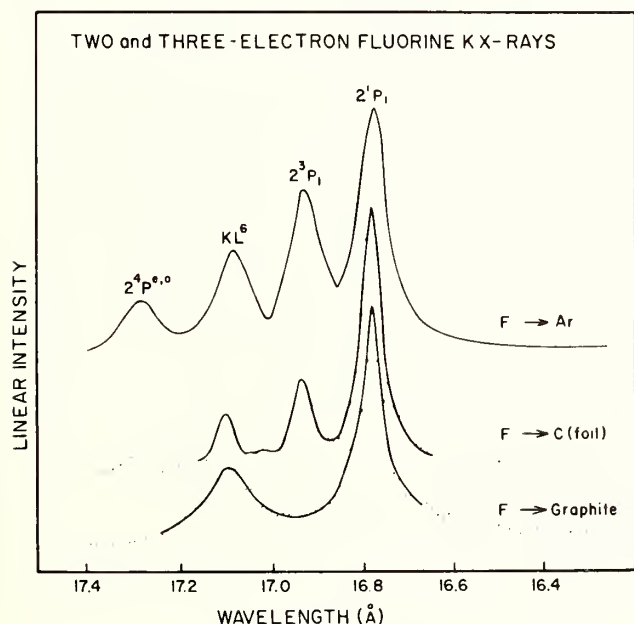


Fig. 1

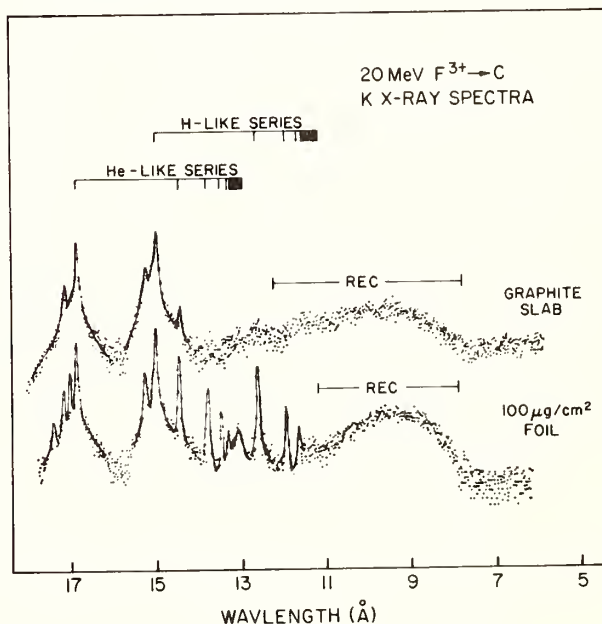


Fig. 2

*Work performed under the auspices of the U.S. Energy Research and Development Administration, W7405-Eng-48.

K X RAYS AND REC FROM Cl^{n+} BOMBARDMENT OF TARGETS IN THE REGION $19 \leq Z \leq 35^*$

J. A. TANIS[†], B. L. DOYLE, W. W. JACOBS, AND S. M. SHAFROTH
University of North Carolina, Chapel Hill, N. C. 27514 and
Triangle Universities Nuclear Laboratory, Durham, N. C. 27706

We have examined the characteristic K x-rays resulting from 20-80 MeV Cl^{n+} bombardment of C, KBr, Ti, Mn and Cu and the radiative electron capture (REC) resulting from Cl^{n+} incident on C. The purpose of this study is to determine the effects of multiple ionization on the observed x-ray spectra and to compare the measured x-ray cross sections with the predictions of Coulomb excitation¹ and K vacancy² sharing theories. Further, we examine the REC resulting from bombardment of a thin solid target and determine the REC energies, widths and cross sections as a function of projectile energy.

Figs. 1 and 2 show the observed target K_α and K_β energy shifts and K_β/K_α intensity ratios, respectively. The increase in the x-ray energy shifts with projectile energy implies an increasing degree of L-shell ionization while the increase in the K_β/K_α ratio implies an increasing degree of L-shell ionization with respect to M-shell ionization. At the highest incident energies, the energy shifts and intensity ratios are seen to level off, probably reflecting the projectile velocity matching with the target L-shell which occurs over the range of energies studied here.

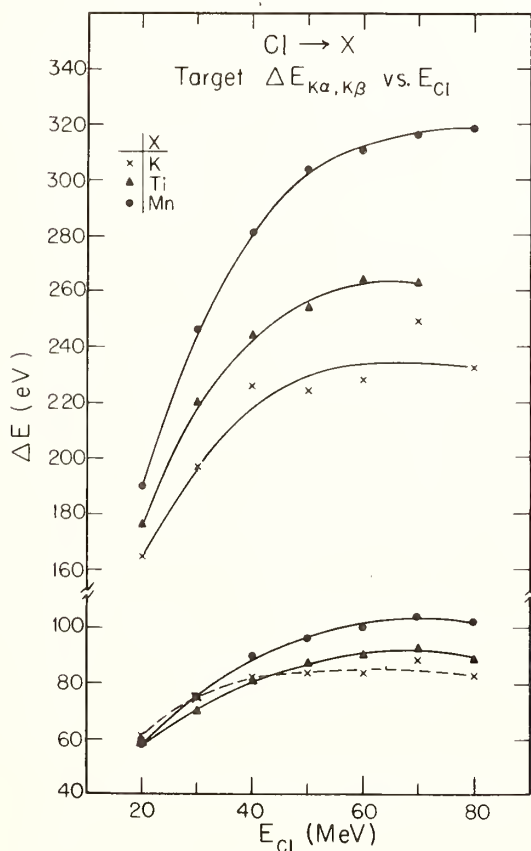


Fig. 1 Energy Shifts

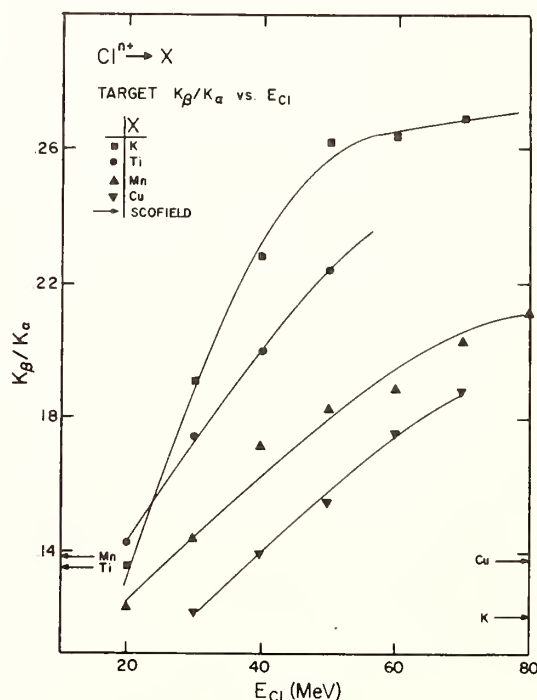


Fig. 2 K_α/K_β Ratios

The observed x-ray cross sections are compared with those predicted by the various Coulomb-excitation theories as shown in Fig. 3. Single vacancy fluorescence yields have been used to calculate the theoretical cross sections and this is, of course, a source of error. In general the theory predicts the trend of the data but differs somewhat in absolute magnitude. This is not unexpected since the theories are strictly applicable only for $Z_1/Z_2 \ll 1$ whereas in the present case $0.6 \leq Z_1/Z_2 \leq 0.9$. The PWBABCP+EC, which includes Coulomb and binding corrections,³ the Z^3 polarization correction⁴, and target electron capture⁴ by the projectile, should provide the best description of Coulomb excitation in its region of validity and this is, indeed, the case for $\text{Cl} \rightarrow \text{Cu}$. As Z_2 decreases the agreement becomes worse probably reflecting the non-Coulombic nature of the excitation for symmetric collisions. Since the PWBA and BEA overpredict the data in their region of validity, the good agreement for $\text{Cl} \rightarrow \text{K}$ and Ti must be regarded as fortuitous.

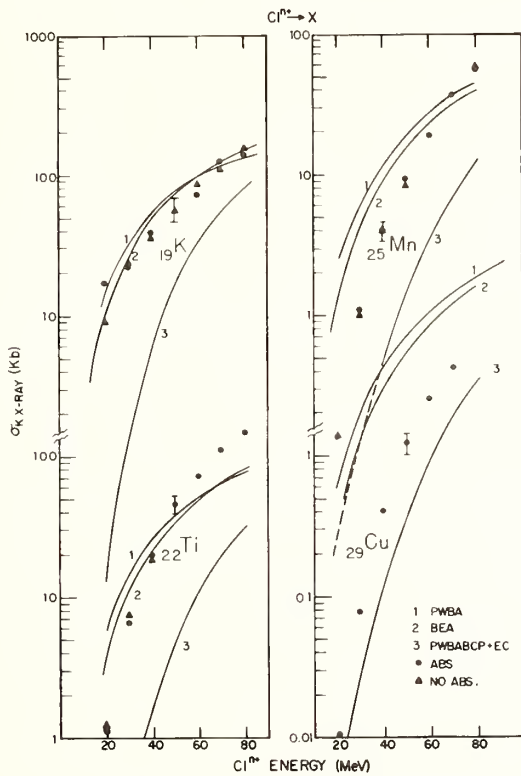


Fig. 3 Cross Sections

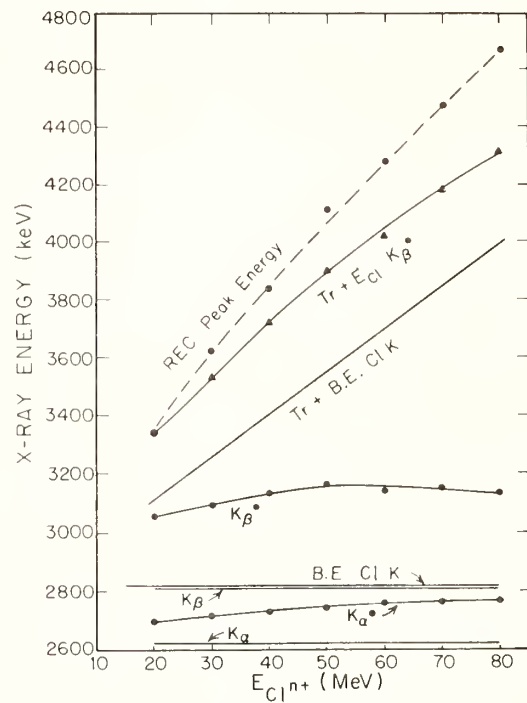


Fig. 4 R.E.C. and Projectile x-ray Energies

The observed Cl projectile K_{α}^* , K_{β}^* , and REC energies are shown in Fig. 4 as a function of E_{Cl} . For comparison, the single vacancy K_{α} , K_{β} and K binding energies are also shown. The line labeled $T_r + \text{BE ClK}$ is a lower limit to the REC energy and assumes capture of a "free" target atom electron into the K -shell of a Cl ion with a single K vacancy⁵. The measured REC energy is seen to be somewhat higher than this lower limit. A better approximation to the REC energy is obtained by using the measured Cl K_{β} energy shift to estimate the increase in K -shell binding energy and adding this to the relative K . E. of the captured electron as shown.

Fig. 5 shows the effect of Cl^{n+} bombarding energy on the widths of the K_α , K_β and REC peaks. It is interesting to note that the minimum REC peak width is 520 eV. This is much wider than would be expected from the model of Sohval et. al.⁶, which describes the REC width for O^{8+} on a variety of gaseous targets, including C_3H_8 , quite well. Much of the increased width in the present work is thought to be due to multiple ionization of the projectile passing through the foil.

Finally, the REC differential cross section vs. E_{Cl} at 90° is shown in Fig. 6. The measured cross sections assume that each target atom contains a single electron which can be captured. The agreement with the free electron calculation of Bethe and Salpeter⁷ is seen to be quite good although this agreement must be regarded with caution due to possible corrections for target thickness effects⁸ and the number of electrons available for capture.

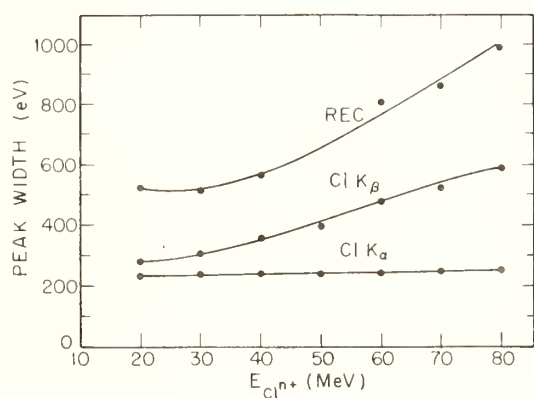


Fig. 5 Widths

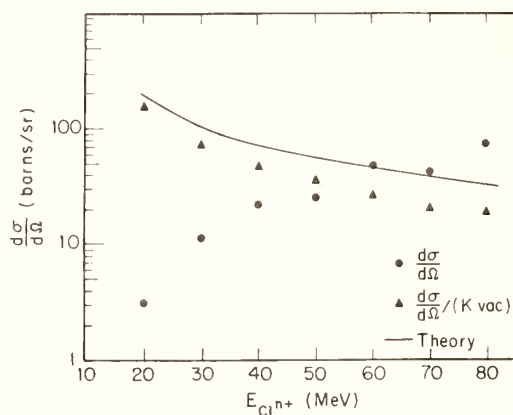


Fig. 6 σ R.E.C.

*Supported by U. S. Energy Research Development Administration
 +Supported by North Carolina Board of Science and Technology

References

1. D. H. Madison and E. Merzbacher, Atomic Inner Shell Processes, B. Craseman, Ed. Vol. 1, pg. 1, Academic Press, New York, 1975.
2. W. E. Meyerhof, Phys. Rev. Letters 31, (1973) 1341.
3. G. Basbas, W. Brandt, R. Laubert, Phys. Rev. A7, 783 (1973).
4. G. Lapicki, private communication, 1976.
5. H. W. Schnopper et al., Phys. Rev. Letters 29, 898 (1972).
6. A. R. Sohval et al., Phys. Letters 9, L25 (1976).
7. H. A. Bethe and E. E. Salpeter, Quantum Mechanics of One-and Two-Electron Atoms, (Academic Press, New York, 1957).
8. K. O. Groeneveld et al., Z. fur Physik A 277, 13 (1976).

R. L. Watson, B. I. Sonobe, A. K. Leeper, T. Chiao, and F. E. Jenson
Cyclotron Institute and Department of Chemistry
Texas A&M University, College Station, Texas 77843

One of the most striking differences between inner-shell vacancy production by electron bombardment or photoabsorption and that resulting from heavy-ion bombardment at intermediate velocities is the high degree of multiple ionization produced by the latter. K-shell ionizing collisions by heavy-ions are of particular interest in this regard because of the attendant high probability for simultaneous multiple ionization of the L-shell. As a result, the K α x-ray spectrum arising from the decay of K-vacancies produced in heavy-ion-atom collisions displays intense satellite structure. Despite the considerable amount of work which has been directed toward the investigation of heavy charged particle-induced K-shell ionization, the exact nature of the mechanism for multiple L-vacancy production is still unclear. Our recent work on three aspects of this problem is summarized below.

a. Projectile energy dependence

The shapes of the excitation functions for K α satellite production by light ions (H⁺ and He⁺⁺) have previously been examined and compared with the predictions of several theoretical formulations based upon a multiple Coulomb excitation mechanism [1,2]. Our recent results for K α satellite production by C, O and Ne ions are shown in Fig. 1. The

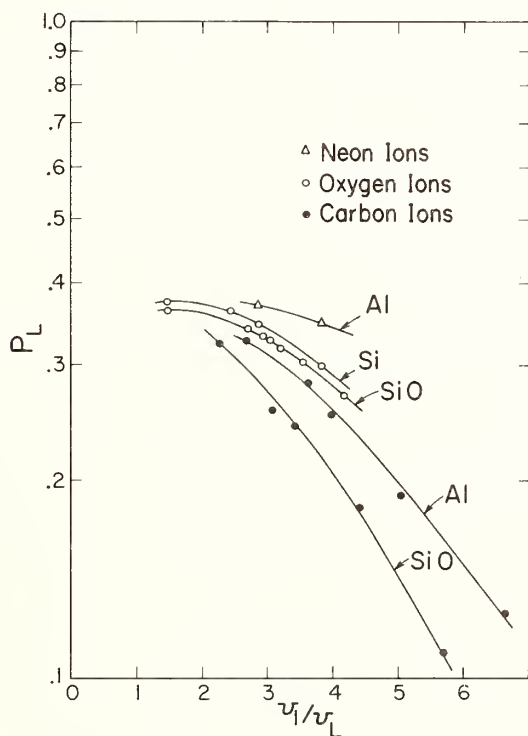


Fig. 1 The dependence of the average (apparent) L-vacancy fraction on the projectile-to-L-electron velocity ratio.

parameter p_L in this figure is the average (apparent) L-vacancy fraction defined as $\bar{N}_L/8$ where \bar{N}_L is the average (apparent) number of L-vacancies as determined from the observed satellite relative intensities. The character of the $K\alpha$ satellite energy dependence for heavier ions is appreciably different from that displayed by hydrogen and helium ions.

b. Intensity enhancement effects

The $K\alpha$ satellite intensity patterns produced by projectiles having atomic numbers much less than the target are generally well characterized by binomial distributions [3,4]. However, the $K\alpha$ satellite intensity patterns produced by projectiles having atomic numbers slightly greater than the target show striking departures from binomial distributions [4,5]. In Fig. 2 are shown the ratios of the experimental $K\alpha_{1,2}$ intensities to the $K\alpha_{1,2}$ intensities predicted from binomial fits to the satellite intensities for a number of projectile-target combinations. This behavior appears to indicate that more than one mechanism contributes to the production of K- and L-shell vacancies in near symmetric collisions.

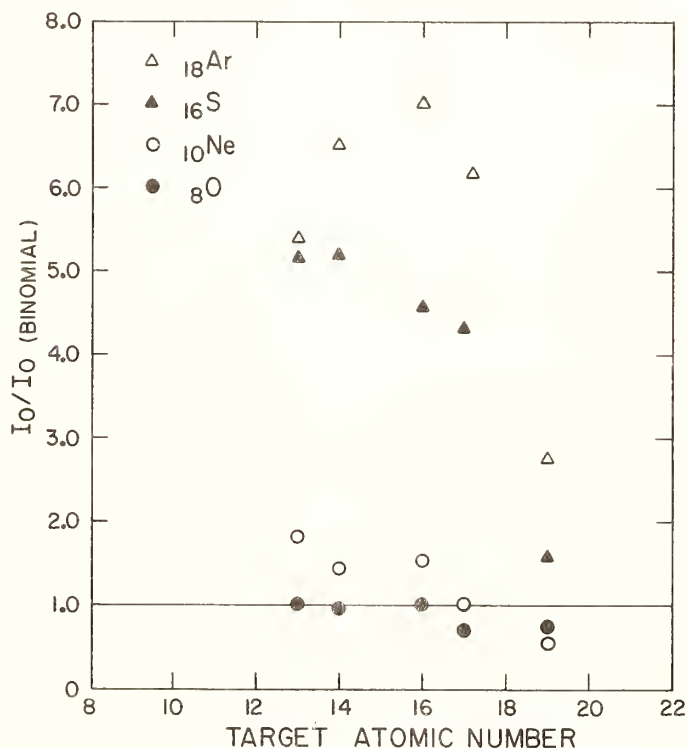


Fig. 2 The ratio of the experimental $K\alpha_{1,2}$ intensity to the binomial intensity for a number of projectile-target combinations.

c. L-vacancy transfer

If the rates of L-vacancy transfer processes are large enough to compete with $K\alpha$ transitions, a significant amount of alteration of the original L-shell vacancy distribution may be expected to occur between the time of the collision and the time of $K\alpha$ x-ray emission. We have previously observed significant differences in the $K\alpha$ satellite

intensity patterns for various sulfur and silicon compounds [6,7]. These measurements have since been extended to a number of chlorine compounds and the results are shown in Fig. 3.

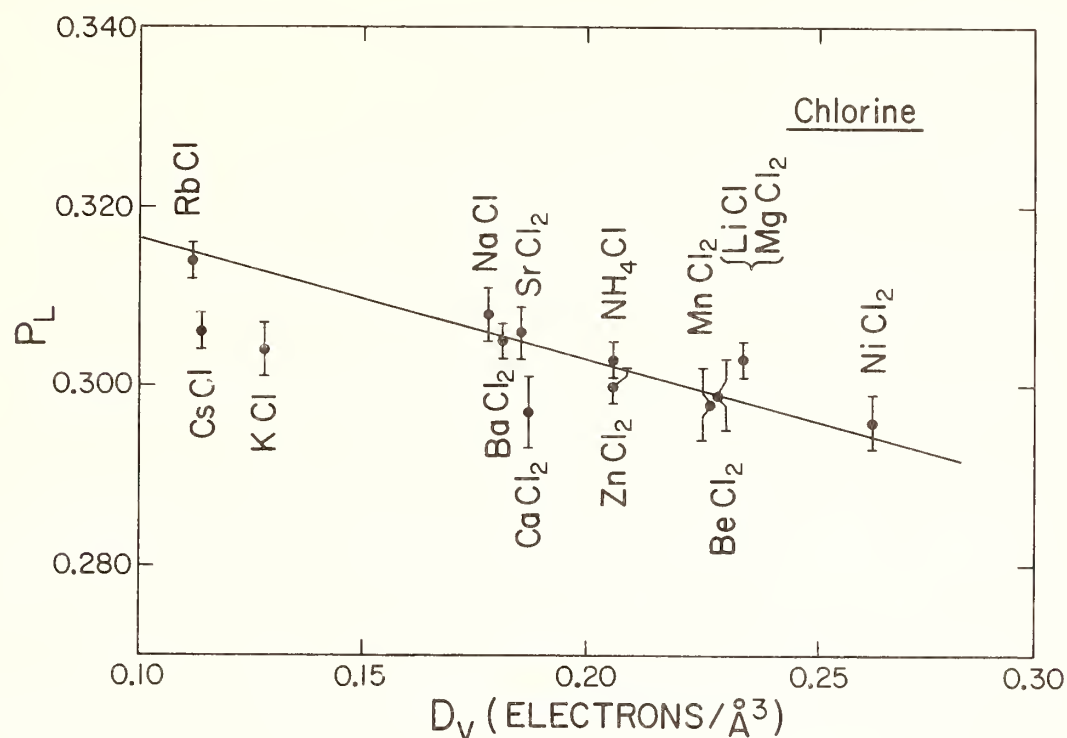


Fig. 3 The dependence of the average (apparent) L-vacancy fraction on average valence electron density for chlorine compounds.

We believe this behavior reflects the effect of chemical environment on the rates of L-vacancy transfer transitions which, for third-row elements, must involve the valence electrons.

References

*This work was supported in part by the U. S. Energy Research and Development Administration and the Robert A. Welch Foundation.

- [1] R. K. Li, R. L. Watson, and J. S. Hansen, Phys. Rev. A 8, 1258 (1973).
- [2] P. Richard, R. L. Kauffman, J. H. McGuire, C. F. Moore, and D. K. Olsen, Phys. Rev. A 8, 1369 (1973).
- [3] R. L. Kauffman, J. K. McGuire, P. Richard, and C. F. Moore, Phys. Rev. A 8, 1233 (1973).
- [4] R. L. Watson, F. E. Jenson, and T. Chiao, Phys. Rev. A 10, 1230 (1974).
- [5] A. R. Knudson, P. G. Burkhalter, and D. J. Nagel, Proc. of the Fifth Int. Conf. on Atomic Collisions, Gatlinburg, Tn. (1973).
- [6] R. L. Watson, T. Chiao, and F. E. Jenson, Phys. Rev. Lett. 35, 254 (1975).
- [7] R. L. Watson, et al., Proc. of the Fourth Int. Conf. on Beam-Foil Spectroscopy and Heavy-Ion Atomic Physics Symp., Gatlinburg (1975).

CALCULATIONS OF X-RAY BAND SPECTRA

D. A. Papaconstantopoulos

George Mason University, Fairfax, Virginia 22030

and

Naval Research Laboratory, Washington, D.C. 20375

During the last few years several calculations of X-ray spectra have been reported. These calculations which involve a variety of techniques and approximations, have been reviewed by Nagel and Baun and by Azaroff and Pease¹. Since then we note the work of Neckel et al², and of Gupta and Freeman³.

Here we present calculations of x-ray band emission and absorption spectra which we have performed for the elements Ca, V and Ni and for the compounds TiFe, TiNi, NbC and V₃Si.

We have followed the formalism set up by Goodings and Harris⁴, who derive formulae for the x-ray intensity in terms of the angular momentum components of the density of electronic states and the matrix elements formed by the core and band radial wave functions.

In order to do the x-ray calculations, band structure calculations were performed by the augmented plane wave method^{5,6}; and to obtain reliable wave functions the calculations were carried out self-consistently^{6,7}. The resulting eigenenergies and eigenfunctions were interpolated by either the "Quad"⁸ or the Slater-Koster⁹ interpolation schemes and the densities of states decomposed per site and per angular momentum component were found.

The calculated x-ray spectra were broadened using an energy-dependent Lorentzian function. This function included spectrometer window broadening, core-level life time width and electron life time broadening with one adjustable parameter.

Our results indicate that the main features of the x-ray spectra are reflected by the decomposed densities of states, with the energy dependent radial matrix elements playing a secondary role. The inclusion of the matrix elements was more crucial for L and M spectra than for K-spectra.

On comparing the calculated and measured spectra we find generally, good agreement for K and L spectra, and somewhat worse agreement for M spectra.

Although we have calculated both the emission and absorption K, L and M spectra, we will present only those results for which measurements were found in the literature. In particular, the calculated emission spec-

tra of V were compared with the measurements of Nemnonov and Finkelshteyn¹⁰ for the K spectrum, the measurements of Brytov¹¹ for the L spectra and the experiments of McAlister et al¹² for the M spectra.

For Ca^{13} and Ni^{14} we concentrated on the K-absorption edge and found good agreement with the measurements of Sugiura¹⁵ and Pease and Gregory¹⁶ respectively.

For the intermetallic compound TiFe^{17} we find excellent agreement with the experiments of Nemnonov and Kolobova¹⁸ for both emission and absorption K spectra of both components.

In the case of TiNi in comparing with the work of Cuthill et al¹⁹ and Källne²⁰ we find some discrepancies for the L and M spectra.

Our calculations on NbC and V_3Si are compared with the measured spectra of Ramqvist et al²¹ and Nemnonov et al²² and obtain generally good agreement.

In conclusion we note that accurate self-consistent band structure calculations produce energies and wavefunctions which can be used to account for most measured X-ray spectra, without invoking any subtle many body effects, beyond the effective one-electron Hamiltonian.

Collaborations with D. J. Nagel and J. W. McCaffrey on the X-ray calculations and with B. M. Klein and L. L. Boyer on the band calculations are gratefully acknowledged. I am also indebted to L. S. Birks for many useful discussions.

REFERENCES

- [1] D. J. Nagel and W. L. Baun; L. V. Azaroff and D. M. Pease, X-ray Spectroscopy (edited by L. V. Azaroff) McGraw-Hill New York (1974)
- [2] A. Neckel, K. Schwarz, R. Eibler, P. Rastl and P. Weinberger, Mikrochimica Acta [Wien], Suppl 6, 257 (1975)
- [3] R. P. Gupta and A. J. Freeman, Phys. Rev. Lett. 36, 1194 (1976)
- [4] D. A. Goodings and R. Harris, J. Phys. C, 2, 1808 (1969)
- [5] J. C. Slater, Phys. Rev. 51, 846 (1937)
- [6] L. F. Mattheiss, J. H. Wood and A. C. Switendick, Methods in Computational Physics Vol. 8, p. 123, Academic Press, New York (1968)
- [7] D. A. Papaconstantopoulos, J. R. Anderson and J. W. McCaffrey, Phys. Rev. B5, 1214 (1972)
- [8] F. M. Mueller, J. W. Garland, M. H. Cohen and K. H. Bennemann, Ann. Phys. (New York) 67, 19 (1971)
- [9] J. C. Slater and G. F. Koster, Phys. Rev. 58, 1498 (1954)
- [10] S. A. Nemnonov and L. D. Finkelshteyn Ann. Physik 18, 42 (1966)

- [11] I. A. Brytov, Phys. Metalmetal 24, 174 (1967)
- [12] A. J. McAlister, J. R. Cuthill, R. C. Dobbyn, M. L. Williams and R. E. Watson, Phys. Rev. B12, 2973 (1975)
- [13] J. W. McCaffrey and D. A. Papaconstantopoulos, Solid State Commun. 14, 1055 (1974)
- [14] D. J. Nagel, D. A. Papaconstantopoulos, J. W. McCaffrey and J. W. Criss, Proc. Int. Symp. on X-Ray Spectra and Electronic Structure of Matter (Edited by A. Faessler and G. Wiegh) p. 51 (1973)
- [15] C. Sugiura, Japan J. Appl. Phys. 11, 598 (1972)
- [16] D. M. Pease and T. K. Gregory, Solid State Commun. 18, 1133 (1976)
- [17] D. A. Papaconstantopoulos, Phys. Rev. Lett. 31, 1050 (1973)
- [18] S. A. Nemnonov and K. M. Kolobova, Phys. Metalmetal 23, 66 (1967)
- [19] J. R. Cuthill, A. J. McAlister and M. L. Williams, J. Appl. Phys. 39, 2204 (1968)
- [20] E. Källne, J. Phys. F4, 167 (1974)
- [21] L. Ramqvist, B. Ekstig, E. Källne, E. Noreland and R. Manne, J. Phys. Chem. Solids 32, 149 (1971)
- [22] S. A. Nemnonov, E. Z. Kurmaev, and V. P. Belash, Phys. Stat. Sol. 39, 39 (1970)

VALENCE BAND STRUCTURE OF DIAMOND, GRAPHITE, AND AMORPHOUS CARBON OBTAINED BY X-RAY AND PHOTOELECTRON SPECTROSCOPY

G. Wiech

Sektion Physik der Universität München, 8 Munich 40, FRG

The X-ray K-emission bands of diamond, graphite and evaporated carbon were measured, and are compared with recent X-ray photoelectron (XP) spectra (1) and theoretical calculations. The intensity distribution of these spectra is governed by the dipole selection rules and the photoionization cross-sections σ_s and σ_p , respectively. Since the core level of carbon has a well defined s orbital symmetry, the C K-emission bands reflect the p states in the valence band. In X-ray photoelectron spectroscopy of light elements the cross-section for valence s-like electrons is considerably larger than for p-like electrons. The XP spectra therefore arise predominantly from s-like electrons. Thus both experimental techniques for the light elements and compounds of them yield complementary results.

In diamond the electrons at the bottom of the valence band are mainly s-like, those of the top part are mainly p-like, and there is considerable s-p-mixing throughout the valence band. As Fig.1 shows, these properties are clearly reflected by the XP spectrum (1) and the C K-emission band.

Since the band structure and the density of states for diamond and silicon are in qualitative agreement, one expects close similarity between the distribution of s- and p-like electrons in the valence bands of the two elements. Fig.2 shows that the structural features of the Si K β - and C K-band agree well. There is also good agreement between the XP spectrum of diamond and the L_{2,3}-band of silicon which arises from s-like valence states. This indicates that $\sigma_s \gg \sigma_p$.

In graphite there are two classes of bands, the σ and the π bands. The low lying σ bands have s character with some admixture of p-like symmetry, while the π bands are predominantly p-like. The special bonding in graphite yields a band structure different to that of diamond, and these differences are clearly reflected by the XP and the X-ray spectra. The K-emission band of graphite is shown in Fig.3 together with the XP spectrum (1). As in the case of diamond, the intensity distribution of the spectra is complementary. In the region of a', a, and peak b the XP spectrum has its main intensity. It drops off sharply on the low-binding-energy side until 281 eV, the top of the σ bands. Where there are only π electrons (>281 eV) the

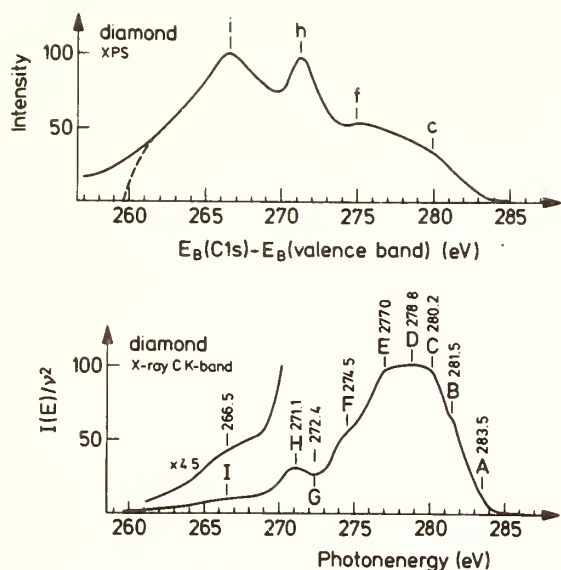


Fig.1 XP spectrum (1) and x-ray K-emission band of diamond

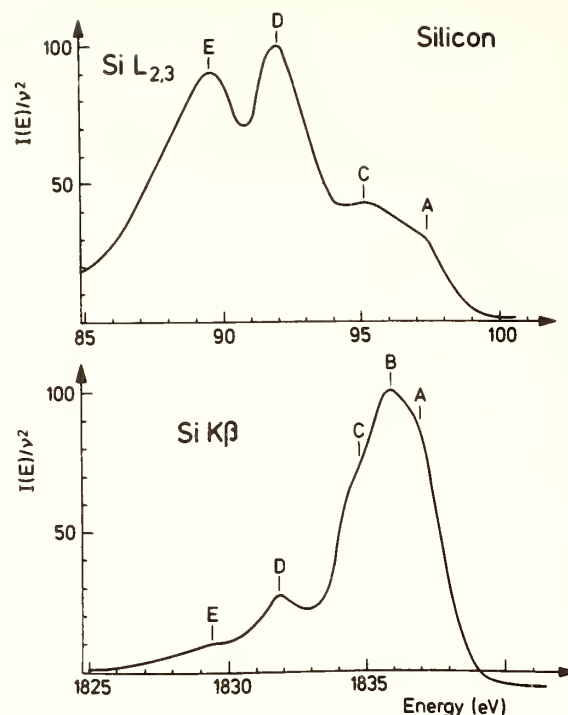


Fig.2 Si L_{2,3}- and Si Kβ-emission band of silicon (2)

intensity is extremely low, due to the large value of the cross-section ratio σ_s/σ_p .

While $\sigma \rightarrow 1s$ transitions yield an isotropically distributed radiation, the radiation resulting from $\pi \rightarrow 1s$ transitions is strongly anisotropic, no π -radiation being emitted parallel to the crystallographic c axis. By measuring the emitted radiation of a graphite single crystal as a function of the take-off angle, the width of the σ and π bands, and the region of overlap (Fig.3) could be determined (3). In the region of the π bands the x-ray emission band obtained at a take-off angle of 15° is intense and shows detailed structural features. For the 80° spectrum the intensity of structures E, F, and G is almost zero.

In Fig.4 the XP spectrum of glassy carbon (1) and the K-band of evaporated carbon are shown. The gross features of the spectra resemble those of graphite. All structural details, however, are smeared out as it is typical for amorphous materials: the over-all structure of the density of states depends on the short-range order in the material, while long-range order leads to additional fine structure.

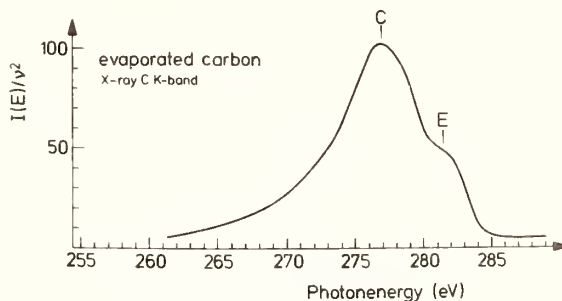
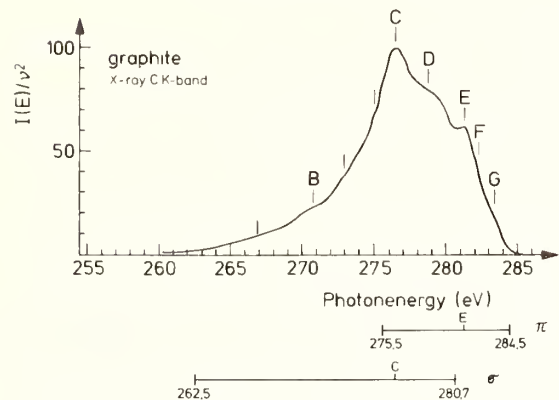
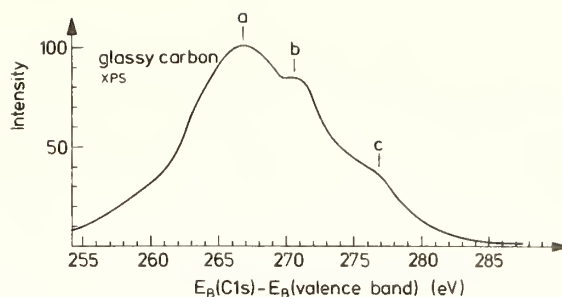
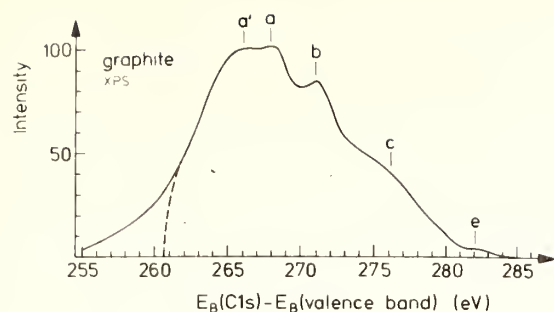


Fig.3 XP spectrum (1) and K-emission band of graphite

Fig.4 XP spectrum of glassy carbon (1) and K-emission band of evaporated carbon

References

- (1) F.R.McFeely, S.P.Kowalczyk, L.Ley, R.G.Cavell, R.A.Pallock, and D.A.Shirley, Phys.Rev. B 9, 5268 (1974)
- (2) G.Wiech and E.Zöpf, Journal de Physique 32, C4-200 (1971)
- (3) Chr.Beyreuther and G.Wiech, in: VUV Radiation Physics, edit. E.E.Koch, R.Haensel and C.Kunz, Pergamon Vieweg, 1974, p.517.

Physikalisches Institut, Universität, 7500 Karlsruhe (FRG)

Graphite exhibits a layered structure, where the monolayers consist of hexagonal arrays of carbon atoms. The bonds between the layers are weak and mainly due to van der Waals interactions. The strong covalent bonds in the monolayers consist of σ - and π -bonds. The σ -bonds evolve from the hybridisation of three electronic wavefunctions, namely the $2s$, $2p_x$ and $2p_y$ functions, which yields three half filled coplanar σ -bonds per atom with bond angles of 120° . The one half filled π -bond per atom is generated from the occupied $2p_z$ wave function.

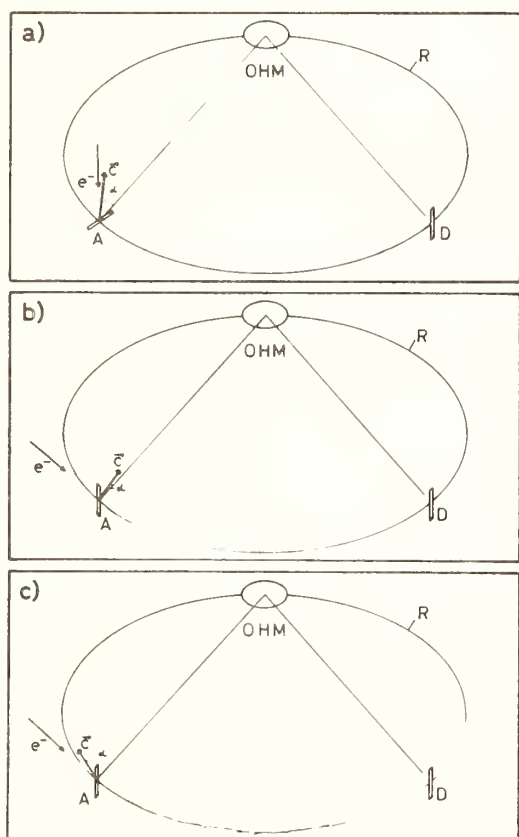


Fig. 1: Geometric arrangements of the \vec{c} -axis (perpendicular to the layer planes) of the probe relative to the Rowland circle R . The direction of the exciting electron beam is indicated.

- a) $\alpha = 87^\circ$; b) $\alpha = 3^\circ$;
c) $\alpha = 87^\circ$.

In the case of the σ -bonds the centers of gravity of the charge distributions are localised between all pairs of next neighbours. Therefore, if $1s$ -vacancies are produced in the atoms, transitions of electrons from the σ -bonds into the vacant states give rise to an X-ray emission which can be expected to be polarised in the plane of the layer, while its intensity distribution should be isotropic. As concerns the π -bonds, the charge due to one p_z -electron per atom is distributed above and below the layer atoms. Since the π -bond of a carbon atom is uniformly distributed over the three next neighbours, the center of gravity of the corresponding charge distribution should be situated exactly above and below the atoms. From this follows that the radiation due to transitions of π -electrons into $1s$ -vacancies should be polarised perpendicular to the layer plane, i.e., parallel to the \vec{c} -axis. As a consequence all directions of maximum emission intensity lie in the layer plane.

The σ - and π -subbands, which result from the respective radiating transitions overlap strongly in the C K-spectrum.

Investigations of monocrystalline carbon employing gratings as monochromators have been performed by Brümmer et al /1/ and Beyreuther and Wiech /2/. In both cases the anisotropy of the π -radiation could be demonstrated by the investigation of C K-spectra measured with different relative orientations of the sample. The obtained spectra showed a marked dependence of the relative intensity of the π -maximum on this orientation. These results have been used to estimate the shape of the π - and σ -subbands.

The presented contribution deals with the experimental verification of the proposed polarisation and anisotropy properties of the C K-spectrum. By making use of these properties the shapes and bandwidths of the π - and σ -subbands of monocrystalline graphite have been measured. The investigation has been performed employing an Octohydrogenmaleate - OHM - crystal as monochromator. This crystal exhibits a lattice constant of $2d = 63.39 \text{ \AA}$. Due to the investigated energy range of the C K-spectrum of $260 \text{ eV} < E < 284 \text{ eV}$ the Bragg angles vary between 48° and 42° . In this range the OHM-crystal monochromator acts simultaneously as a nearly perfect analyser ($> 96 \%$) for the polarisation of the monochromatized radiation, due to the Fresnel equations.

First orienting measurements of the C K-spectrum of different carbon samples employing an OHM-monochromator have been performed by McFarlane /3/.

Fig. 1 shows the investigated positions of the c-axis of the probe relative to the Rowland circle. The arrangement of Fig. 1a should yield the π -subband only, since the σ -component, which is polarised in the Rowland circle plane should be suppressed in the reflected beam. The spectrum measured with this arrangement is shown in Fig. 2. According to the expectations the dominating σ -maximum has disappeared.

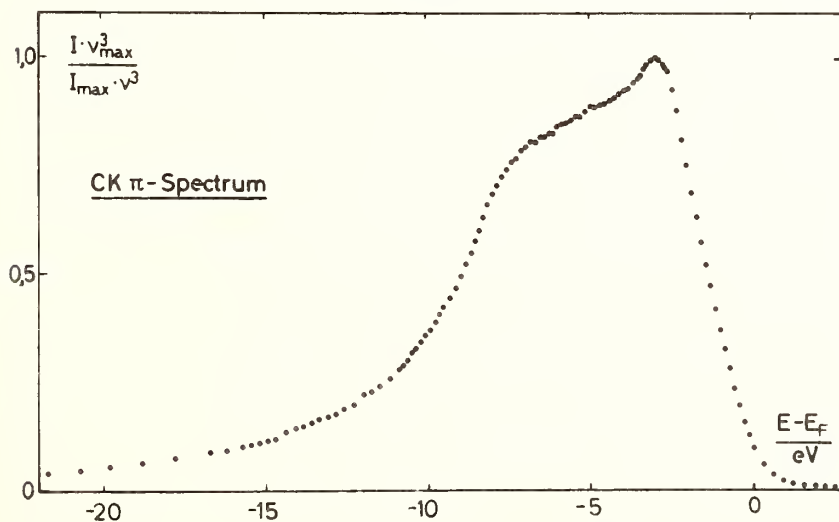


Fig. 2:
C K π -spectrum obtained with the arrangement of the probe according to Fig. 1a. The Fermi level corresponds to the zero of energy.

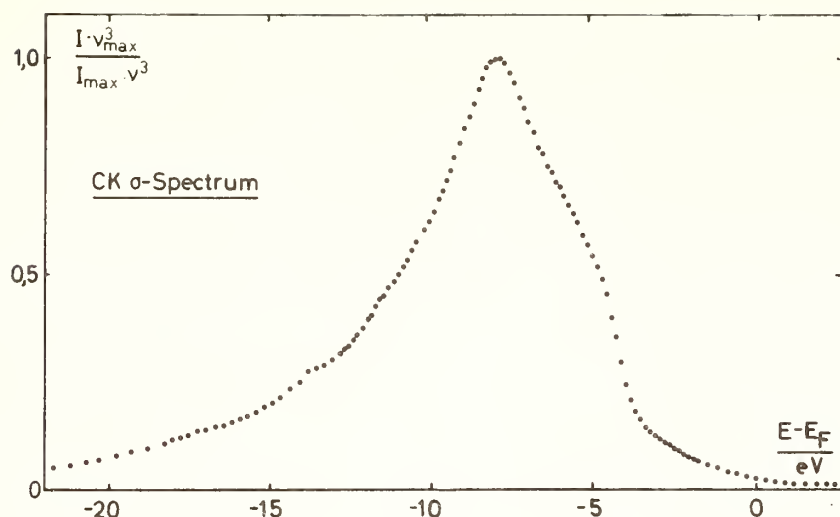


Fig. 3:
C K σ -spectrum
obtained with the
arrangement of the
probe according
to Figs. 1b and
1c. The Fermi level
corresponds to the
zero of energy.

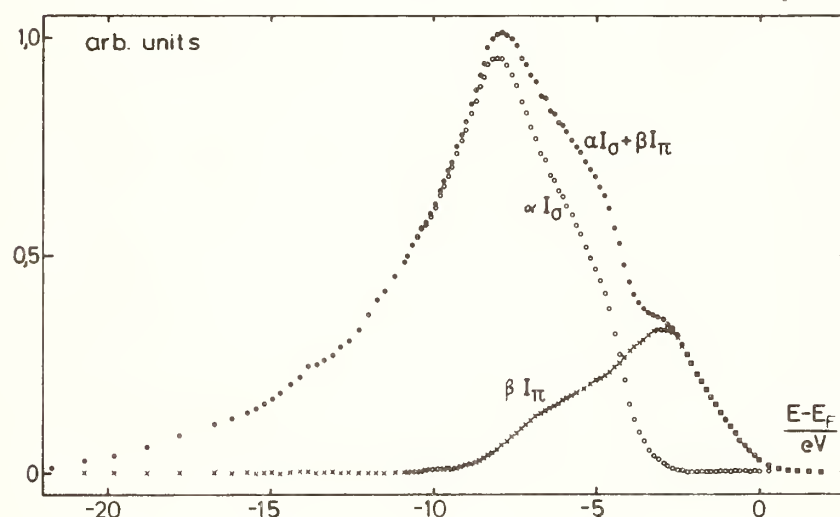


Fig. 4:
Corrected π - and
 σ -spectra and an
arbitrary linear
combination.
The Fermi level
of all curves
corresponds to the
zero of energy.

Figs 1b and c show two further mountings of the probe which are both useful for maximum suppression of the π -subband. In the first case no π -radiation reaches the monochromator due to its anisotropy. In the second case (Fig. 1c) the π -radiation is polarised in the Rowland circle plane and should therefore be suppressed by the monochromator. The C K σ -spectra obtained with the two mountings of Figs. 1b and c are identical within the experimental accuracy. This is a strong confirmation for the proposed anisotropy as well as polarisation properties of the C K-radiation. It further demonstrates the excellent polarising properties of the OHM monochromator.

Fig. 3 shows such a C K σ -spectrum.

The spectra of Figs. 2 and 3 contain a small amount of the suppressed component. This is mainly due to the used probes of natural graphite which were no perfect single crystals. Additionally even at the used pressure $< 2 \times 10^{-9}$ Torr carbon containing contaminations were deposited on the probe which caused a progressive smearing of the investigated

structure. Therefore a simple correction procedure has been applied to the measured spectra. The corrected 'pure' π - and σ -components are shown in Fig. 4 together with an arbitrary linear combination. This linear combination is nearly identical with a C K-spectrum taken from a polycrystalline graphite probe, as is shown in Fig. 5, thus confirming that the shapes of the subbands as shown in Fig. 4 are essentially correct.

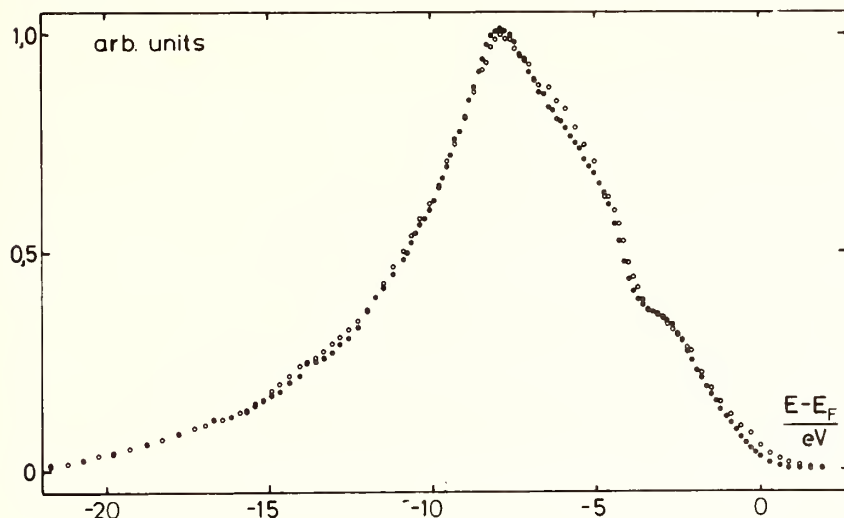


Fig. 5:
Comparison of the
linear combina-
tion of Fig. 4
(dots) with a
C K-spectrum from
polycrystalline
graphite (circles).

References

- /1/ Brümmer, O. et al in: X-Ray Spectra and Electronic Structure of Matter, ed. A. Faessler and G. Wiech, München 1973, Vol. I, p. 78.
- /2/ Beyreuther, Ch., Wiech, G.: Physica Fennica 9, Suppl. S. 1, 176 (1974).
- /3/ McFarlane, A.A.: Carbon 11, 73 (1973).

CALCULATION OF THE K-ABSORPTION SPECTRUM OF ALUMINUM[†]

F. Szmulowicz*

Case Western Reserve University
Cleveland, Ohio 44106

B. Segall

Case Western Reserve University
Cleveland, Ohio 44106

We have performed a first principles calculation of the K-absorption spectrum of aluminum using band structure and matrix elements of momentum determined by the symmetrized APW method (1). Comparison between theoretical and experimental results for the x-ray spectra provides a sensitive test of the one-electron band theory. Therefore, there has been a great need and interest concerning these calculations.

The potential for the calculation was obtained by superposition of free atom charge densities with Slater's free-electron exchange. Eigenvalues and wavefunctions were obtained at 89 k -points in the irreducible wedge in 4.2 Ry range above the bottom of the conduction band at Γ . The $1s$ level and its wavefunction were calculated with the muffin-tin potential and used to obtain transition strengths between the core level and states above the bottom of the conduction band by the $\nabla V(r)$ method.

An OPW non-linear least-squares fit (2) using 27 plane waves was performed for the purpose of interpolating energies and gradients throughout the wedge (rms deviation of .03 Ry for the first 10 bands). The integrals over the Brillouin zone for the density of states and linear absorption coefficient were done with the Gilat and Raubenheimer method (G-R) (3) while the Fermi energy was obtained by a variant of the G-R scheme for volumes.

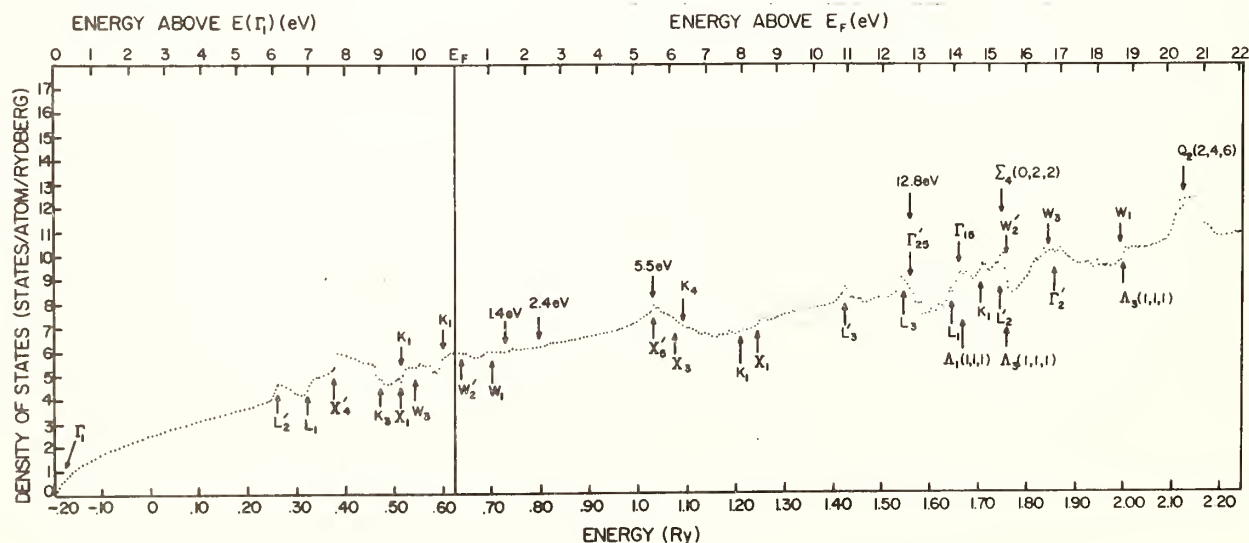


Fig. 1
202

Results for the density of states

$$D(\omega) = \frac{2\Omega}{(2\pi)^3} \sum_n \int d^3k \delta(E_n(\underline{k}) - \omega)$$

where Ω is the unit cell volume, are presented in Fig. 1 with identifications of points leading to the structure in the curve and of their locations in units of $(2\pi/8a)$. This plot is in good agreement with the previous density of states calculation of Connolly (4). Results for the absorption coefficient

$$\mu(\omega) = \frac{1}{nc\omega} \frac{4\pi^2 e^2 \hbar^2}{3m^2} \sum_n \int d^3k \frac{2}{(2\pi)^3} P_{1s,n}^2 \delta(E_n(\underline{k}) - E_{1s} - \omega)$$

are shown in Fig. 2. The curve above E_F represents the K-absorption spectrum of aluminum while the curve below E_F is proportional to the K-emission spectrum. The contributions to the plot are separated by bands with band symmetry and ℓ -character classifications, e.g. irreducible representation (band index, ℓ -character). The K-emission spectrum is in good agreement with the previous calculation of Smrčka (5).

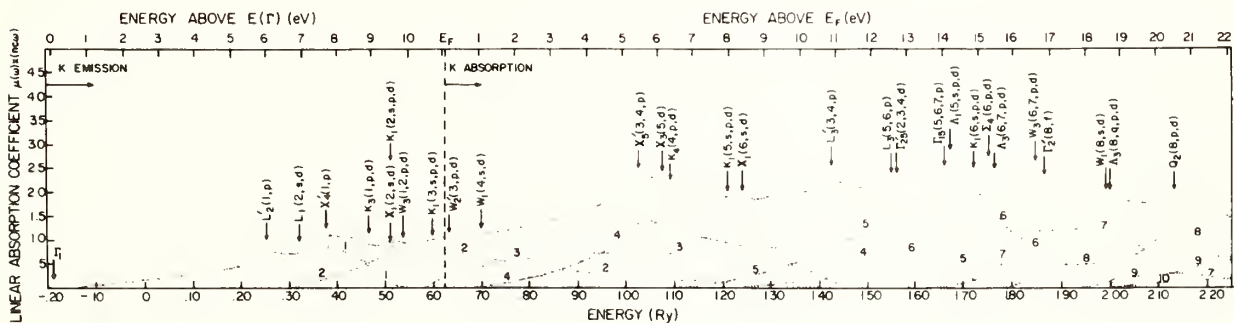


Fig. 2

The Lorentzian broadened (half-width at half-maximum of .02 Ry) absorption curve is shown in Fig. 3 together with the experimental result (6) normalized to 5.5 eV peak. We find that peak A, which can arise due to level W_1 is suppressed in going from $D(\omega)$ to $\mu(\omega)$ while there is no evidence for peak B. Peak C is at 5.5 eV in excellent agreement with the experiment and the structure around 12.8 eV peak D is flanked by other peaks not seen in the experiment. It should be

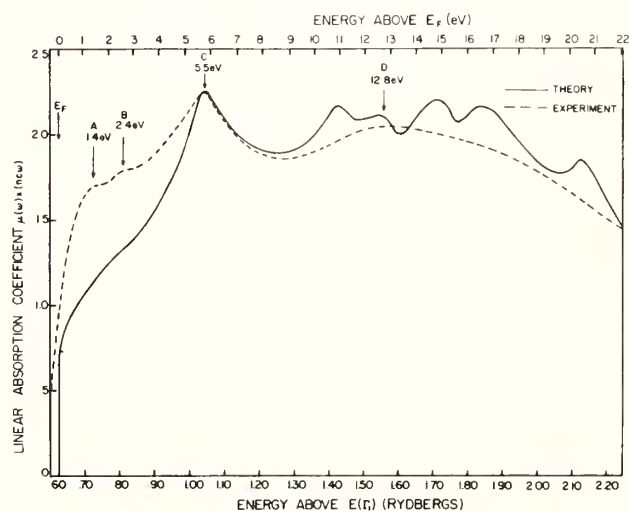


Fig. 3

noted that Shaw (7) reports a peak on the low side of the 12.8 eV peak. The appearance-potential spectrum also shows a peak of 21 eV which is reflected in the theoretical curve in Fig. 3.

[†] Work supported by AEC and grants from NSF.

^{*} Present address Institute of Materials Science, University of Connecticut, Storrs, Conn. 06268.

1. L. F. Mattheiss, J. H. Wood, A. C. Swidendeck (1968), in "Methods in Computational Physics" Vol. 8, (B. Alder, S. Fernbach, M. Rotenberg, editors), p. 63. Academic Press, New York.
2. J. W. D. Connolly (1971), in "Electronic Density of States" (L. H. Bennett, editor), p. 27. NBS Special Publication 323.
3. G. Gilat, L. J. Raubenheimer, Phys. Rev. 144, 144 (1966).
4. J. W. D. Connolly, Intern. J. Quant. Chem. 3, 807 (1970).
5. L. Smrčka, Czech. J. Phys. B21, 683 (1971).
6. C. Senemaud, M. T. Costa Lima, J. Phys. Chem. Solids 37, 88 (1975).
7. C. H. Shaw, in "Theory of Alloy Phases", (1956) pg. 13, American Society for Metals.
8. P. O. Nilsson, J. Kanski, Phys. Letters 41A, 217 (1972).

VALENCE BAND SPECTRA OF ALUMINIUM-NOBLE METAL ALLOYS

L.M. Watson, D.J. Fabian, J.C. Fuggle*, E. Källne[†], and P.R. Norris

Metallurgy Department, University of Strathclyde,
Colville Building, 48 North Portland Street,
Glasgow G1 1XN, Scotland.

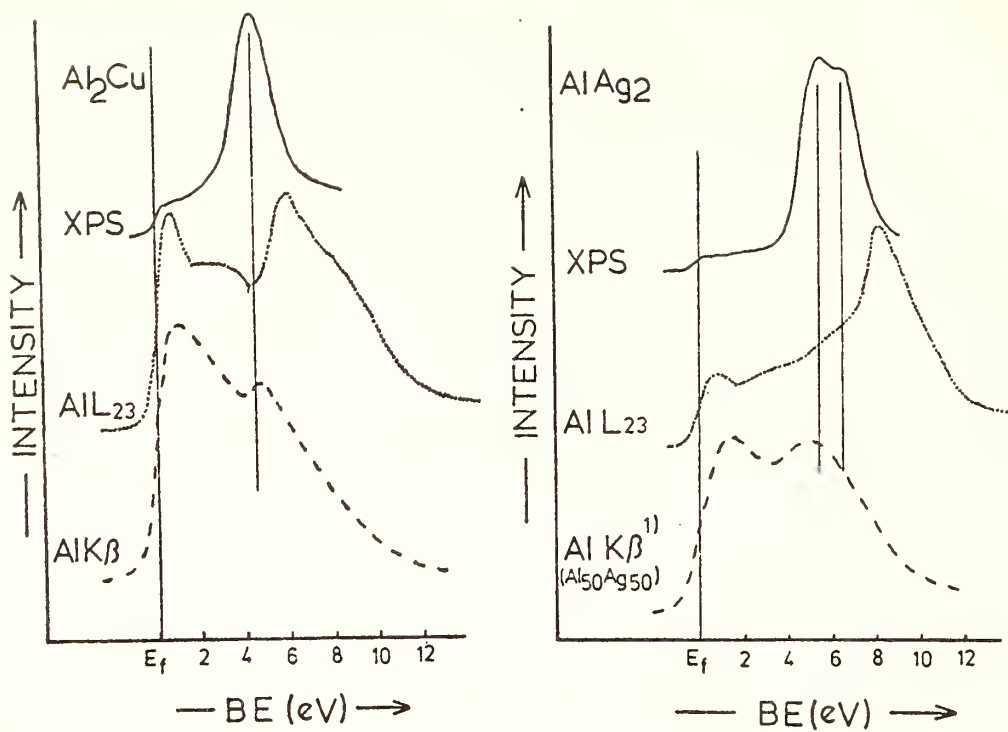
*Physik Departmente 20, Technische Universität München,
D-8046 Garching b, München, W. Germany.

[†]Los Alamos Scientific Laboratory, University of California,
Los Alamos, New Mexico, USA.

The valence band x-ray photoemission (XPS), the Al $L_{2,3}$ and the Al $K\beta$ spectra for a number of aluminium-noble metal alloys have been superimposed on the same energy scale for comparison. Those for Al_2Cu , $AlAg_2$ and Al_2Au are shown in figure 1. Although the emission process from solids is extremely complex, we assume to a first approximation that the XPS spectra reflect the overall density of states in the alloys, the Al $L_{2,3}$ the partial density of valence band s and d states in the spatial region of the aluminium 2p core wavefunctions, and the $K\beta$ spectra the partial density of valence band p-states in the spatial region of the aluminium 1s wavefunction. That this approximation is justified has been demonstrated by the excellent agreement between calculation and experiment for the Al $L_{2,3}$ emission from Al_2Au [2,3].

The Fermi level is clearly defined in all spectra and is taken as the zero of binding energy. The high intensity regions of the XPS spectra are attributed to the 3d, 4d and 5d states of Cu, Ag and Au respectively. Splitting of these levels is resolved in the silver and gold alloys but not in the copper alloys (resolution ~ 1 eV). The $L_{2,3}$ spectra show sharp peaks at high binding energies and coincide with the high binding energy onset of the d-bands. These are interpreted as being due to the mixing of the Al 3s states with the high binding energy d-band causing a flattening of the $E(k)$ curves and a consequent increase in the density of states. This occurs over a small energy region and the peaks are accentuated by a depletion of the s-state density at the aluminium sites in the region of the noble metal d-bands. This behaviour has been predicted by Kudrnovský et al [4] using CPA theory for disordered alloys and has been given experimental support by Norris et al [5].

Al_2Au is probably the most thoroughly investigated alloy and the Al s-state density predicted by Switendick is in general agreement with the overall shape of the $L_{2,3}$ spectrum. However, the calculation fails to predict the pronounced peak at 6.3 eV binding energy. Since the d-bands of gold are more spatially diffuse this peak plus a contribution to the main peak is attributed to the overlap of the gold d-bands with the Al $L_{2,3}$ core levels thus contributing to the emission. A similar effect has been observed in the $L_{2,3}$ emission from Mg-Au alloys [6]. Another remarkable feature of this alloy is the extremely sharp rise in the $L_{2,3}$ absorption spectrum 1.4 eV above the absorption edge measured by Gudat et al [7].



1) BAUN & FISCHER

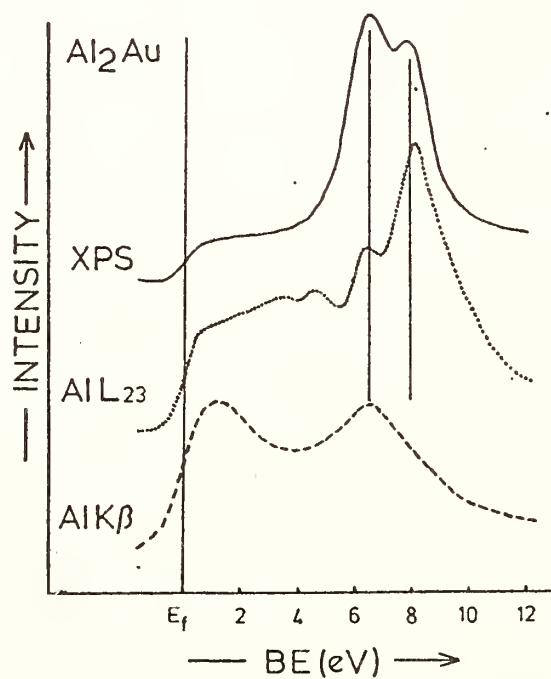


Figure 1

Valence band spectra of some aluminium-noble metal alloys.

In all cases the Al K β spectra show a second peak at high binding energies for the alloys. The d band widths decrease with increasing aluminium concentration. The high binding energy onset remains constant in energy within experimental error whereas the low binding energy onset recedes from the Fermi level. The peak in the K β spectra follows this recession and suggests that it is caused by the mixing of the Al 3p states with the low binding energy d-bands.

Many intermetallic compounds are strongly bonded and some indication of the types of bond could be expected from XPS core level shift measurements. However, in most of these alloys core levels from both species shift to a greater or lesser extent to higher binding energies. A striking example is again Al₂Au where the Au N₆ and N₇ levels shift by 2eV whereas the Al L₁ peak shifts in the same direction by 0.1eV. All these shifts being measured from the Fermi level.

References

- [1] D.W. Fischer and W.L. Baun, 1967, J. Appl. Phys., 38, 229, 2092.
- [2] A.C. Switendick, 1971, N.B.S. Spec. Publ. No. 323, p297.
- [3] M.L. Williams, R.C. Dobbyn, J.R. Cuthill and A.J. McAlister, 1971, N.B.S. Spec. Publ. No. 323, p303.
- [4] J. Kudrnovský, L. Smrčka and B. Velický, 1973, "X-ray Spectra and Electronic Structure of Matter" ed. A. Faessler and G. Wiech, Vol. II, p94.
- [5] P.R. Norris, D.J. Fabian, L.M. Watson, J.C. Fuggle and W. Lang, 1974, J. de Physique, 35, C4-65.
- [6] J.C. Fuggle, L.M. Watson, P.R. Norris and D.J. Fabian, 1975, J. Phys. F, 590.
- [7] W. Gudat, J. Karlau and C. Kunz, 1973, "X-ray Spectra and Electronic Structure of Matter" ed. A. Faessler and G. Wiech, Vol. I, p205.

SXS AND XPS IN THE INVESTIGATION OF ORDER IN ALLOYS AND LIQUID METALS.⁺

C. F. Hague, J.-M. Mariot, G. Dufour and R. C. Karnatak

Laboratoire de Chimie Physique (L. A. n° 176)
Université Pierre et Marie Curie
11, rue P. et M. Curie 75231 Paris Cedex 05 France

1. Introduction : the invariance of the lattice under translation is a fundamental aspect of band theory. So the study of the modifications to the band model when long-range order breaks down is most interesting. Two types of disorder can be met with :

- i) a composition disorder, which exists in disordered crystallized alloys,
- ii) a topological disorder, which is found in liquids and amorphous solids.

We report here two examples of work undertaken to study the alterations in the density of states upon disordering : the well known Ni_3Fe alloy, whose long-range ordering can be eliminated by quenching from a high temperature (1), and Fe in the liquid phase.

Ni_3Fe alloy was studied by soft X-ray spectroscopy (SXS) and X-ray photoelectron spectroscopy (XPS). These techniques are usefully complementary especially where alloys are concerned : on the one hand SXS gives an indication of the partial densities of states, depending on which type of atom is ionized in an inner shell ; on the other hand, XPS gives an overall picture of the combined densities of states.

Fe was studied in the liquid phase by SXS only.

2. Experimental : the Ni and Fe L_3 spectra were studied in the pure metals and in the Ni_3Fe alloys by electron bombardment (2 kV) with a 25 cm radius bent crystal spectrometer equipped with gypsum and KAP crystals respectively. The photoelectron spectra were induced by Mg $K\alpha$ radiation and run in UHV conditions. The details of the alloy experiments can be found elsewhere (2).

The L_3 spectrum of liquid Fe was obtained in a newly designed 50 cm radius bent crystal spectrometer (3). It is equipped with an electron gun to excite the L_3 spectrum and to melt the target. The vacuum in the source chamber is $< 5.10^{-8}$ Torr ; this can rise to 5.10^{-7} Torr at liquid phase temperatures. Results shown are from at least 8 runs on different samples.

⁺Sponsored in part by DGRST under contract n° 73-7-1586 and "Groupement Régional de Mesures Physiques pour la Chimie Paris Centre (Centre de Spectrochimie)".

3. Results and discussion :

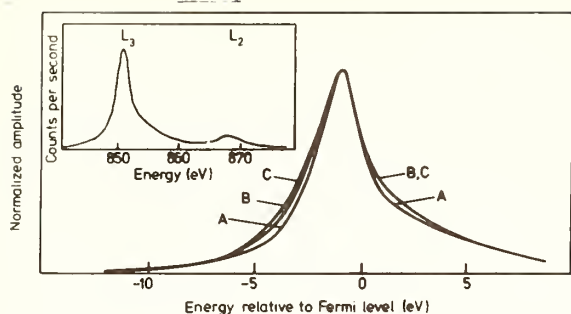
i) Ordered (O) and disordered (D) Ni_3Fe alloys : the SXS L_3 emission of Ni in the metal and the O and D Ni_3Fe alloys are given Fig. 1a. The corresponding spectra for Fe are given Fig. 1b. The spectra of the alloys are broader than those of the pure elements, the broadening being more important for the Ni spectra. Such band broadening could be explained by d electron tunnelling (4). Ni is 23 % and 20 % broader in the O and D alloy respectively ; the broadening is 6 % for Fe in either phase. This must be confronted with the number of nearest neighbours. There are 12 nearest neighbours in pure Ni but 4 Fe atoms only surrounding each Ni in the O alloy. Disorder would be expected to attenuate this situation. Fe goes from 8 nearest neighbours in the pure element to 12 nearest Ni atoms in the O alloy, and account taken for the presence of fewer Fe atoms, it would be expected to be less perturbed by disorder.

The XPS valence band spectra of the alloys (Fig. 2,3) are broader than that of pure Ni, but closely resemble it, indicating the lower concentration of Fe.

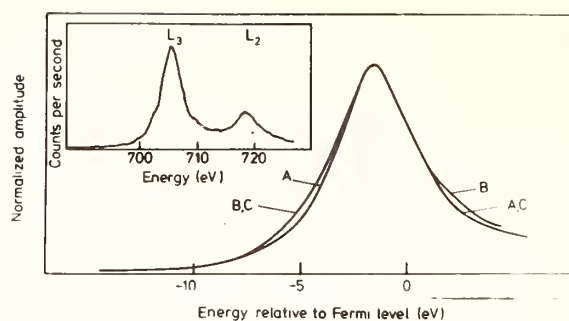
ii) L_3 absorption and emission of liquid Fe : the L_3 emission of liquid Fe is indistinguishable from the solid.

The absorption curves were obtained by the self-absorption method (5) and the $\ln (I_{2.5 \text{ kV}} / I_{5 \text{ kV}})$ is plotted Fig. 4. It is important to note that the penetration of the electron beam is inversely proportional to the density of the target, so the amount of matter traversed by the emitted radiation remains the same in the liquid and solid despite a decrease in density of the liquid phase of 14 %. The absorption curves presented here can thus be considered to reflect relative changes in the absorption coefficient on fusion. Hence we tentatively conclude that a change in the density of unoccupied states of the conduction band is observed. However, as in recent K emission results on Fe and Cu (6) no change is observed to within the experimental limits at the Fermi level in the emission or absorption curves. This is also true in the L_3 emissions of Co, Ni and Cu as we report elsewhere (3).

4. Conclusion : as expected from the small changes in the coordination numbers of liquid metals no modification is observed close to the Fermi level in the liquid relative to the solid. However 3d band broadening is observed in the O and D alloys where a change in coordination number is encountered. A confrontation with conflicting theoretical calculations for the densities of unoccupied states in liquid metals is at present a little hazardous.



a) Ni



b) Fe

Fig. 1 : L_3 emission (A: pure metal; B: D- Ni_3Fe ; C: O- Ni_3Fe)

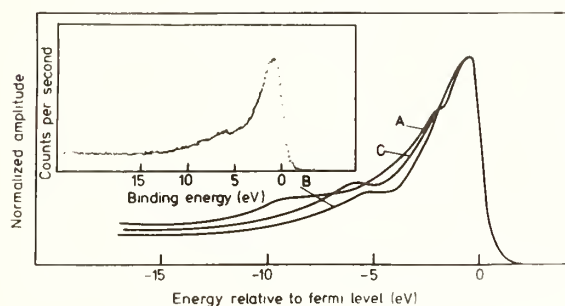


Fig. 2 : XPS valence band (A: Fe; B: Ni; C: O- Ni_3Fe ; insert: unsmoothed O- Ni_3Fe)

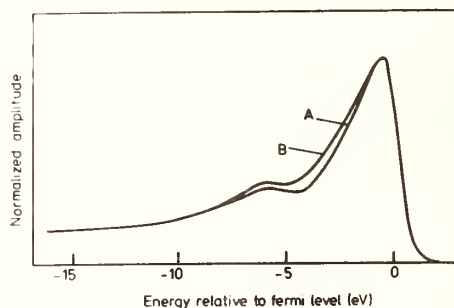
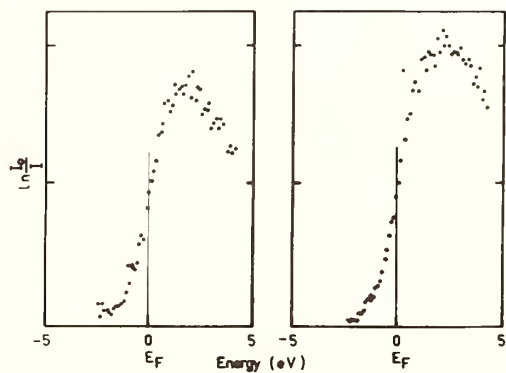


Fig. 3 : XPS valence band (A: O- Ni_3Fe ; B: D- Ni_3Fe)



Liquid

Solid

Fig. 4 : L_3 absorption spectrum of iron

References :

1. Y Calvayrac, M Fayard Phys Stat Solidi(a) 17 407 (1973)
2. C F Hague et al J Phys F: Metal Physics 6 899 (1976)
3. C F Hague, in Proceedings of the 3rd International Conference on Liquid Metals, Bristol, 1976 (The Institute of Physics Conference Series, to be published)
4. V L Moruzzi et al Phys Rev B 10 4856 (1974)
5. R J Liefeld, in Soft X-ray Band Spectra, editor D J Fabian (Academic Press, London, 1968) p 133
6. K B Garg, E Källne Phys Stat Solidi(b) 70 K121 (1975)

A NEW COMPARISON BETWEEN EXPERIMENT AND THEORY FOR THE X-RAY K-ABSORPTION EDGE OF NICKEL

D. M. PEASE and T. K. GREGORY*†

Institute of Materials Science

University of Connecticut

Storrs, Connecticut 06268

*Present Address: Frequency and Time Systems Inc., 182 Conant Street, Danvers, Massachusetts

Nagel, et. al., have calculated the K edge absorption spectrum of nickel using an APW approach, in which possible effects of the core hole on the final states are ignored [1]. Their calculated curve exhibits maxima at about 3 and 15 eV above the Fermi level, in general agreement with experiment. In addition to these peaks, however, the above authors calculate a shoulder at about 9 eV which they cannot correlate with a corresponding feature on any experimental spectrum. We have resolved in our experimental nickel K edge a similar shoulder occurring approximately 6 eV above the Fermi level, putting our results in better agreement with theory than previous spectra.

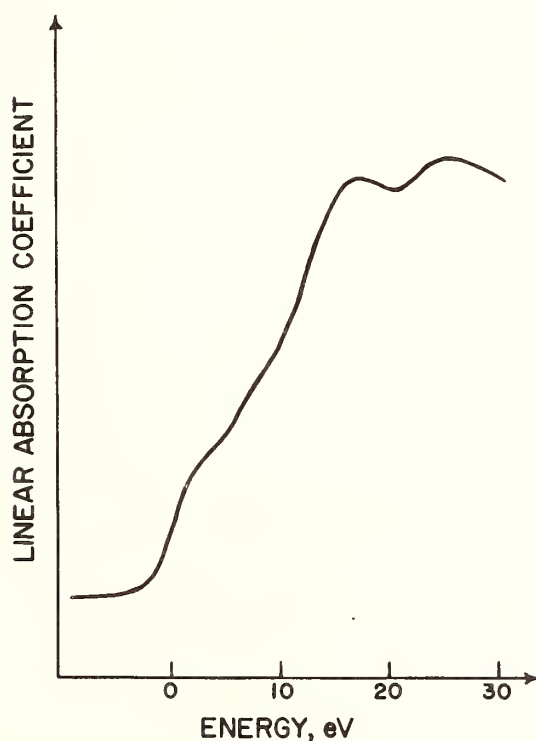


Fig. 1. Experimental nickel K edge for a 4 μ m foil using the (1,1) crystal setting.

The spectra were taken with an automatic two crystal spectrometer [2]. The x-ray tube had a tungsten target operated at 13 KV and 100 ma. Silicon analyzer crystals in the (1,1) setting were used, whose first order rocking curve was 9.5 arc seconds at the nickel K edge. 80,000 count statistics and scanning step sizes of $\frac{1}{2}$ eV were utilized. A four micron nickel foil was used, for which thickness effects will be small for the apparatus used. [3] The spectrum was reproduced with crystals in the (1,3) setting as well. Our experimental spectrum is shown in Fig. 1, and our deconvoluted spectrum at the top of Fig. 2. We point out that Borovskii and Batyrev, although not resolving the shoulder at B in their experimental nickel K spectrum, do deconvolute their results to obtain a double humped

structure somewhat similar to ours in the vicinity of the Fermi level [4]. The feature corresponding to shoulder B is located significantly closer to the Fermi energy in Borovskii and Batyrev's results than in our spectrum.

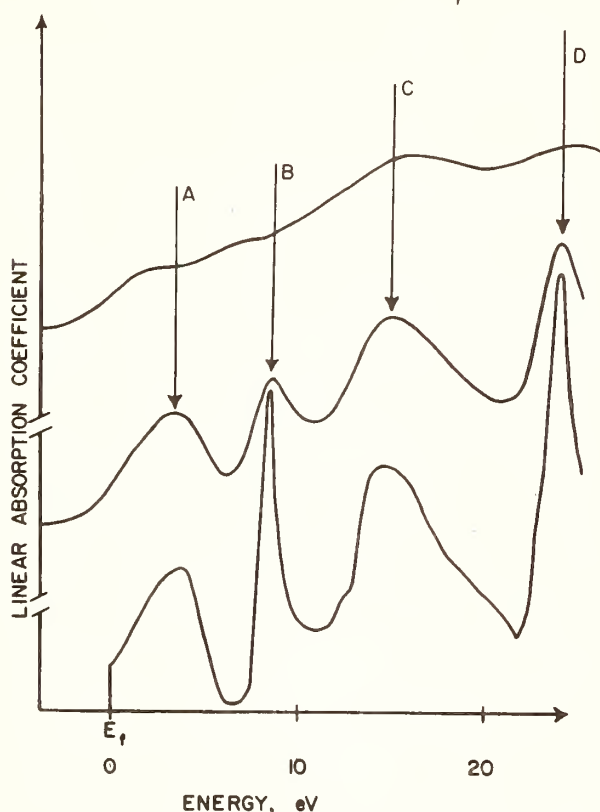


Fig. 2. Comparison between experimental and theoretical absorption edges. From top to bottom are the nickel K edge deconvoluted with the experimental rocking curve, the theoretical nickel K edge convoluted with a Lorentzian having the K level half width, and the unbroadened theoretical K edge.

are of interest lies in the possibility of resolving the old question of whether the K hole significantly modifies the Bloch states in a metal [6], [7]. From the above it appears that calculations neglecting the influence of the core hole on the final state do result in a rough qualitative agreement with experiment regarding the number and position of peaks. However, our results indicate that broadening effects on the final ejected electron states are quite important. In addition, since the two lowest energy experimental peaks are significantly shifted in energy relative to the calculated peak positions

Fig. 2 shows a detailed comparison between theory and experiment. The bottom curve is the unbroadened spectrum of Nagel, et. al. [5]. The central curve shows the calculated spectrum after our convolution with a Lorentzian corresponding to the K hole broadening. It may be seen that the theoretical spectrum with K hole broadening shows rough qualitative agreement with the deconvoluted experimental spectrum. However, the theoretical spectrum is much sharper than the experimental results, and the first two experimental peaks are shifted to lower energies relative to the theoretical curve by about 2-3 eV. Nagel, et al., point out that there is an important broadening correction which should be taken into account in addition to K-hole broadening, namely the "hot electron" broadening due to the finite time that the excited electron exists in a state above the Fermi level [1].

In conclusion, we note that one of the main reasons experimental and theoretical comparisons such as the above

the possibility also exists that core hole effects may modify the positions of spectral features.

+This investigation was supported by a grant from the National Science Foundation.

- (1) D. J. Nagel, D. A. Papaconstantopoulos, J. W. McCaffrey, and J. W. Criss. Proc. of the International Symposium on X-Ray Spectra and Electronic Structure of Matter, Ed A. Faessler and G. Wiech, 51 (1973).
- (2) T. K. Gregory and P. E. Best, Advances in X-Ray Analysis 15, 90 (1971).
- (3) Douglas M. Pease, to be published in Applied Spectroscopy.
- (4) I. B. Borovskii and V. P. Batyrev, Bull. Acad. Sci. USSR 24, 499 (1960).
- (5) The unbroadened spectrum was obtained by courtesy of D. A. Papaconstantopoulos.
- (6) L. G. Parratt, Rev. Mod. Phys. 31, 616 (1959).
- (7) E. N. Rumanov, Sov. Phys. - JETP 20, 1480 (1965).

APPLICATION OF Pt L EMISSION AND ABSORPTION SPECTRA FOR
THE INVESTIGATION OF CLUSTER STRUCTURES

J. Finster, P. Müller, F. Thiel and A. Meisel
Sektion Chemie der Karl-Marx-Universität
DDR-701 Leipzig, Linnéstr. 2

The knowledge of the electronic structure of clusters (small aggregations of atoms) is of great interest for several fields, especially in heterogeneous catalysis, where finely dispersed metals play an important role. However, for a long time the question existed, if these clusters have metallic properties or not. Depending on the chosen criterion, the number of atoms with which such an aggregation starts to be a metal (or a true solid) can vary from appr. 10 (where you can get already a rough picture of the solid band structure) to several hundred atoms (if you consider macroscopic properties). Up to now there are only a few investigations which uses X-ray and photoelectronspectroscopy for the exploration of the electronic structure of clusters [1 - 3].

We took as an example platinum and measured at first L β emission lines and L_{III} absorption spectra of the metal and some Pt compounds [4,5]. Additionally, XPS measurements have been made.

With the L β_1 , β_2 and β_4 lines we found long-wavelength shifts for Pt(II) and short ones for Pt(IV) in the order of 0.1 eV relative to metallic Pt. The L_{III} absorption edge showed shifts of +0.3 eV for Pt(II) and +0.5 eV for Pt(IV), whereas PtCl₂ (and also the clusters) gave a long-wavelength shift. The changes in the fine structure (especially intensity and width of the first absorption maximum) correlate with the changing density of unoccupied 5d states. The X-ray spectra together with the XPS measurements of PtCl₂, which exists in form of Pt₆Cl₁₂-clusters, account for the

existence of metal-metal-interaction [6].

The Pt clusters on a coal carrier exhibit mean diameters of 13, 18, 24 and 45 Å, determined by EXAFS [7]. The X-ray spectra of the clusters were measured with a high-resolution focussing spectrometer with linear stepwise movement of the proportional counter and with sample changing in each measuring point. The ESCA measurements were performed with the VG ESCA 4. In both spectrometers the spectra were taken from the original, air-influenced samples and from the samples after in-situ reduction with hydrogen at 150 °C. Thus we could distinguish between chemical effects and cluster-size-effects. The cluster in the 45 Å-sample showed metallic behaviour: the spectra were similar to those of the metal, and there is almost no difference before and after H₂ exposure. However, the smaller clusters of this noble metal with a high percentage of active surface atoms had been oxidized after contact with air.

For the cleaned samples we found 3 kinds of cluster-size-effects: 1) The Pt 4f lines show a somewhat lower B.E. in the clusters than in the bulk metal. This can be explained by the combination of the (positive) potential shift and the (negative) polarisation shift of core levels connected with the transition from the free atom to the metal, where the clusters are an intermediate state [8]. 2) The L_{III}-edge shifts to lower energies in the smaller clusters in agreement with the opposite directions of the shifts of core levels (decreasing B.E.) and of valence levels (increasing B.E.), going in the direction bulk metal → cluster → free atom. 3) The first absorption maximum of the L_{III} edge is more pronounced in the case of the smaller clusters. This fact (and also the second point) is supported by a quantumchemical calculation (SCCC calculation of a 13 atom Pt cluster), which shows a higher density of free d states near the Fermi energy.

References

- 1 Lewis P.H.: J.Phys.Chem. 67(1963), 2151
- 2 Erenburg S.B., Golovin A.V., Noskova S.P., Kuznetsov B.N. and Ovsianikova I.A.: React. Kinet. Cat. Lett. 1(1974), 507
Ovsianikova I.A., Erenburg S.B., Khlestov V.B., Gegusin I.I., Topol I.A., Sachenko V.P. and Kovtun A.P.: Izv. Akad. Nauk SSSR, Ser. fiz. 40(1976), 230
- 3 Borsyak P.G., Katrich G.A. and Samoilov V.S.: Proc. Intern. Symp. "X-ray Photoelectron Spectroscopy", Kiev, June 1975 (to be published)
- 4 Finster J., Müller P. and Meisel A.: Proc. XVIII^e Coll. Spectr. Internat., Grenoble 1975, Vol. II, p. 596
- 5 Müller P., Finster J. and Meisel A.: Izv. Akad. Nauk SSSR, Ser. fiz. 40(1976), 373
- 6 Finster J., Müller P. and Meisel A.: Z. Chem. (to be published)
- 7 Keilacker H., Meisel A.: Wiss. Z. KMU Leipzig, Math.-Naturw. R. 22(1973), 585 ; Kristallographia (Moscow) 20(1975), 245
- 8 Finster J.: Wiss. Z. KMU Leipzig, Math.-Naturw. R. 25(1976), No. 4 (to be published)

CONFIGURATION INTERACTION INTERFERENCE EFFECTS IN THE CORE ELECTRON EXCITATION EDGES OF TRANSITION METALS

R. E. Dietz and E. G. McRae

Bell Laboratories, Murray Hill, New Jersey 07974

The shapes of the low-lying core excitation edges in the transition metals are largely determined by an interference between the scattering matrix elements corresponding to the excitation of a core electron to empty d states near the Fermi level, and excitations of d conduction electrons to continuum f states [1]. This result applies to both electron energy loss (ELS) and soft X-ray absorption (SXA) spectroscopies, which give virtually identical lineshapes. The effect of the interference is to distort and shift the peaks in the spectral density from the resonant energy of the discrete d-state density. The interference effect must be taken into account in relating ELS or SXA resonant energies to the corresponding binding energies measured by X-ray photoemission spectroscopy (XPS). We report in Table I ELS peak energies measured in Ni, Pd and Pt together with resonant energies E_0 derived from the observed spectra with due consideration of the interference effect. The ELS resonance energies and XPS binding energies [2] shown in Table I are the same. We infer as explained below that the multiplet structure observed in XPS is that of the fully screened configuration [3].

Core excitation thresholds in metals as studied by SXA or ELS correspond to the transition

$$c^{n,m}_v \rightarrow c^{n-1,m+1}_v$$

and have a threshold energy $E_{cv} = \langle c^{n-1,m+1}_v \rangle - \langle c^{n,m}_v \rangle$. Here c and v represent the principal and orbital quantum numbers of, respectively, core and valence electrons, and $\langle \rangle$ indicates the energy of the lowest energy state of the enclosed configuration.

In XPS experiments, the threshold energy for core excitation is determined by the energy for the creation of a fully screened core hole in the long time limit. In the atomic limit we can represent this process by a two-atom excitation, equivalent to the one atom plus metal description:

$$2c^{n,m}_v \rightarrow c^{n-1,m+1}_v + c^{n,m-1}_v + e^-.$$

For emission of a valence electron: $c^{n,m}_v \rightarrow c^{n,m-1}_v + e^-$. The "relaxed" binding energy is then the energy difference between core and valence excitations:

$$\mathcal{E}_B^r = \langle c^{n-1,m+1}_v \rangle - \langle c^{n,m}_v \rangle.$$

Thus we find $E_{cv} = \mathcal{E}_B^r$. This equivalence will hold even if $c^{n-1,m+1}_v$ can be represented by a multiplet or band of states, since the threshold will simply correspond to the occupation of the lowest energy state. Whether the multiplet structure perceived in the spectral density corresponds to the structure expected for the fully screened configuration will depend on the relative time scales for the core transition and the screening processes. In cases where the structure in the

spectral density is dominated by incompletely screened configurations, as it may be in narrow-band metals or insulators, then the fully screened threshold energy may be difficult to ascertain, and the spectral density will be dominated by bound states.

Ni, Pd and Pt are particularly simple to study because these have only one d hole in their ground state, with the final ELS or relaxed XPS configuration consisting locally of a closed d shell. The final state multiplet structure should be simply that of the core hole spin-orbit splitting. Thus a doublet structure should be observed for core levels with $l > 0$. The components are broadened mainly by Coster-Kronig decay of the core hole, this effect being much larger than s-d hybridization which broadens the final electron state in ELS and SXA. In fact, band structure calculations in Ni, Pd and Pt indicate that the width of the empty d-band states is only ~ 0.2 eV. This means that one can treat the empty d density as a discrete level which would produce a sharp peak in the ELS or SXA spectral density in the absence of relaxation effects.

The configuration interaction process which is chiefly responsible for the np core hole decay can be represented by the exchange matrix element $\langle np, \epsilon f; nd', nd \rangle$. Here $n = 3, 4, 5$ respectively for Ni, Pd, and Pt. This matrix element mixes configurations (possessing a particular total angular momentum J) which result from the discrete $p \rightarrow d$ scattering, with configurations which result from $d \rightarrow \epsilon f$ scattering, as shown in Fig. 1. In this process, each of the $J = 3/2$ or $J = 1/2$ components of the 2P multiplet of the $np^5 nd^{10}(n+1)s$ configuration mixes with three continua which are derived from the $np^6 nd^8(n+1)s\epsilon f$ configuration by combining three of the L-S multiplets of d^8 , namely, 1G , 3F and 1D , with the f continuum to form 2P continua. In spherical symmetry each core hole component will mix with continua having the same J value, and the spectral lineshapes for each spin-orbit component can be computed simply from the Fano theory for the interference of a single discrete transition with a continuum.

In addition to the interference process discussed above, there are a number of less important interference processes which may contribute to the spectral density of the $J = 1/2$ spin-orbit component. These processes are summarized in Fig. 2. One of them (Fig. 2(b)) is resonant with the discrete $p \rightarrow d$ excitation and can lead to interference effects. The nonresonant processes (Fig 2c,d,e) merely contribute to the core-hole relaxation rate $\Gamma = \pi \sum_i V_i^2$, where the sum is taken over all contributing coulomb and exchange matrix elements (weighted by the density of states). These processes make a significant contribution to the XPS linewidth 2Γ in some metals. For example, in Ni metal, $\Gamma(3p_{3/2}) = 0.79$ eV while $\Gamma(3p_{1/2}) = 1.08$ eV [2]. In fourth and fifth row metals, processes (c) and (d) will not exist since the 4p and 5p spin orbit splitting is larger than the d bandwidth.

We have considered the possibility that departures from spherical

symmetry and many-body interactions might also be important in determining the experimental lineshapes. Trial ELS lineshapes computed for cubic potentials in Ni metal are qualitatively similar to shapes computed in the spherical approximation. On the other hand, the lineshapes are very sensitive to many-body interactions which appear to be very weak in the ELS spectra of Ni metal ($|\alpha| < 0.02$), although they are very important in XPS [3].

REFERENCES

1. R. E. Dietz, E. G. McRae, Y. Yafet, and C. W. Caldwell, Phys. Rev. Letters **33**, 1372 (1974).
2. G. K. Wertheim, unpublished data.
3. S. Hüfner and G. K. Wertheim, Phys. Lett. **51A**, 301 (1975).

TABLE I. XPS AND ELS CORE EXCITATION ENERGIES

		ϵ_B (XPS) ⁽²⁾	E_{peak} (ELS)	E_0 (ELS)
Ni	3p _{3/2}	65.9 eV	67.0	66.0 ± 0.1
	3p _{1/2}	67.6	68.4	67.7
	3s	110.6	110.6	110.6
Pd	4p _{3/2}	51.3	60	
	4p _{1/2}	54		
Pt	5p _{3/2}	51.9	58.0	52
	4f _{7/2}	71.2	72.0	71.3
	4f _{5/2}	74.6	75.3	74.6

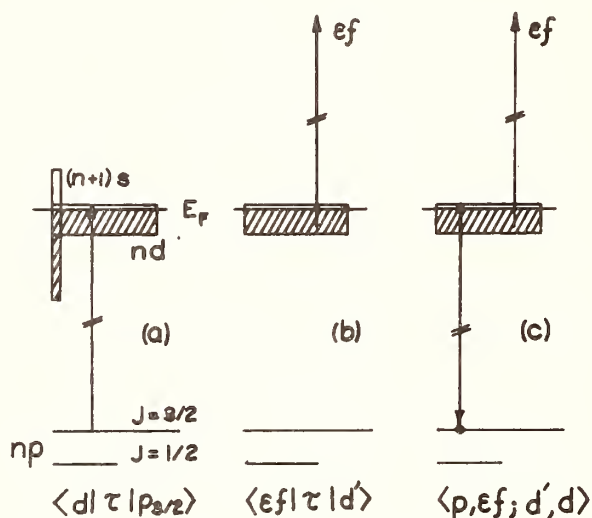


Fig. 1. Main interference process determining np ELS and SXA line-shapes in n=3, 4 and 5th row transition metals.

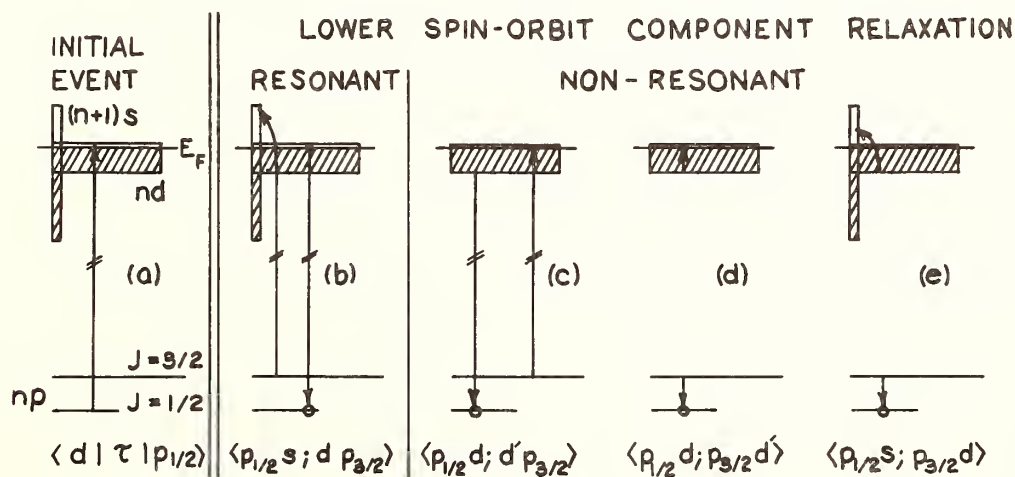


Fig. 2. Some additional processes affecting np_{1/2} excitation.

Kenjiro TSUTSUMI, Kouichi ICHIKAWA, and Osamu AITA

College of Engineering, University of Osaka Prefecture
Mozu, Sakai, Osaka 591, JAPAN

Transition-metal compounds are of fundamental interest in solid-state physics. It is not possible to adequately describe the optical, electronic and magnetic properties of many first-row transition-metal compounds within the theoretical framework provided by conventional band theory. The results of the energy band calculations which have been carried out for 3d transition-metal monoxides clearly predict that the transition-metal monoxides should be conductors[1,2]. However, experimentally the oxides MnO through NiO are insulators, though the oxide TiO is a good conductor. Determination of the electronic structures of these materials is essential to an understanding of these properties, and x-ray spectroscopy and x-ray photoelectron spectroscopy are powerful means for studying these structures. However, only a few investigations have been made on soft-x-ray absorption[3] and emission-band spectra of these substances. In the present study, the $M_{2,3}$ emission-band spectra of transition metals and their compounds, such as 3Ni , NiO, $NiCl_2$, $NiBr_2$, Co, CoO, $CoCl_2$, $CoBr_2$, etc. were obtained by using a Henke-type x-ray tube and a Vodar-type spectrometer consisting of a concave grating with the radius of 200cm and 1200 grooves per mm. In addition, the x-ray photoelectron spectra of the valence bands and the transition-metal 3p states of these substances were obtained by using an electron-energy analyser of hemi-spherical type with the radius of 12.5cm. All the experiments were carried out under the clean high vacuum. Also, the $M_{2,3}$ photoelectric-yield spectra of the transition-metal compounds had been obtained with a usual x-ray tube and the same Vodar-type spectrometer as mentioned above[4]. It is well known that the feature of the photoelectric-yield spectra is quite similar to that of the absorption spectra [5]. Besides, the $M_{2,3}$ absorption spectra of the transition-metal halides had been obtained by using a soft-x-ray spectrometer consisting of a plane-glass grating with 1080 grooves per mm and a concave mirror[6]. In this case synchrotron orbital-radiation from a 1.3GeV electron synchrotron had been used as a continuous light source.

The $M_{2,3}$ emission spectrum of these substances shows a structure accompanied with a tail (in some substances, very remarkable structure) in the high-energy region of the emission band. The photoelectron spectrum of the valence band shows detailed structures. The $M_{2,3}$ absorption spectrum of the transition-metal halides shows the fine structures on the low-energy side of the absorption threshold, and photoelectric-yield spectrum of the transition-metal monoxides also shows the similar structures. All these emission, absorption, photoelectric-yield and photoelectron spectra are compared one another. For the accurate comparison, the energy scale of the photoelectron spectrum is measured from the peak of the transition-metal 3p spectrum of these substances. Some of such comparisons are shown in Fig.1. Such comparisons show the following remarkable features: (1) The shapes of the $M_{2,3}$ emission-band spectrum and the x-ray photoelectron spectrum(XPS) of the same substance are quite

different each other. The structures which are observed in the high-energy region of the x-ray emission band are not observed in XPS. However, the peak of the band in XPS nearly coincides with the main peak in the x-ray emission-band spectra. (2) Even in the case of the compounds the energy gap is not observed between the absorption or photoelectric-yield spectra and both the x-ray emission-band spectra and XPS. (3) In the absorption and photoelectric-yield spectra the structures are observed on the low-energy side of the absorption threshold of all the transition-metal compounds except for the nickel compounds.

The structure observed in the high-energy region of the $M_{2,3}$ emission band appears not to be due to the M_2 component in the usual meaning, because its intensity ratio to the main peak of the emission band is sometimes much larger than the ratio generally expected (about 1:2) and changes with the substances. It is well known that the characteristic x-ray lines of the transition-metal compounds show the asymmetric shape and/or sometimes show the remarkable structures[7]. It is interpreted by the electrostatic interaction of a core hole created by x-ray transition with the d valence electrons[7,8], which gives rise to the multiplet structures of the lines. Recently Asada et al.[8] calculated the shape of the $K\beta_{1,3}$ line and the 3p-XPS of nickel compounds on the basis of the ligand field theory for molecular cluster in which the d electrons are mainly localized, and showed that the line broadening is due to the multiplet structure arising from the configuration p^5d^8 in a cubic field. Their result shows that such multiplet structures extend over ten electron volts on the high-binding-energy side of the state with the maximum multiplicity. According to this conception, it might be considered that the high-energy structure of the emission band may be due to the multiplet structure caused by the interaction between the 3d electrons and the inner-core p hole at the initial state of x-ray emission, that is, due to the multiplet structure arising from the configuration $3p^53d^n$ at the initial state of the $M_{2,3}$ emission, where n is the number of the 3d electrons of the substances

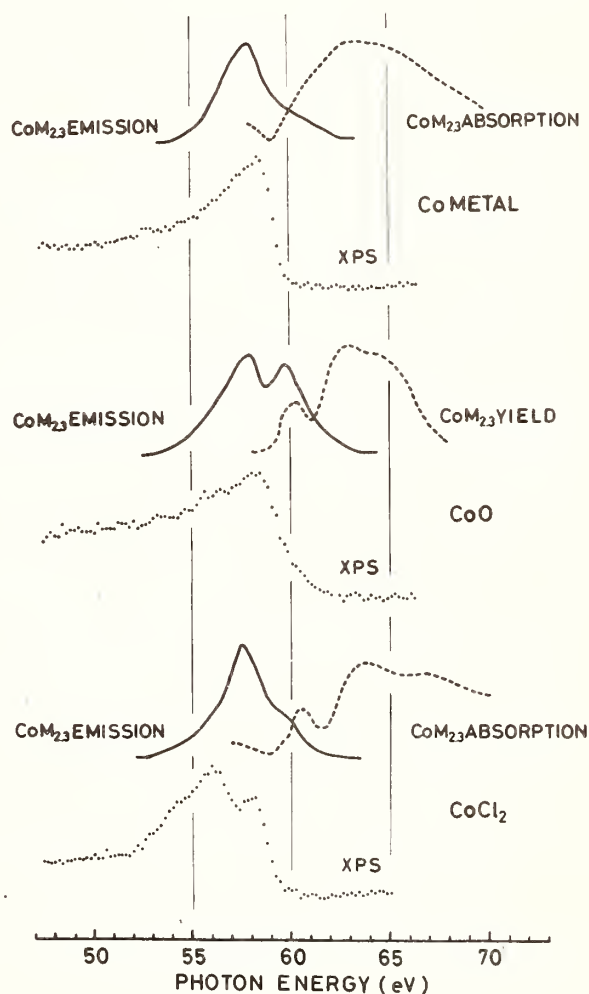


Fig.1. The $M_{2,3}$ x-ray emission band spectra, the $M_{2,3}$ absorption spectra, the $M_{2,3}$ photoelectric-yield spectra, and the photoelectron spectra(XPS) of the valence bands of metallic cobalt, CoO and $CoCl_2$.

in question.

Similarly, it might be considered that the structure which appears on the low-energy side of the absorption threshold in the $M_{2,3}$ absorption and $M_{2,3}$ photoelectric-yield spectra may be attributed to the multiplet structure arising from the configuration $3p^5 3d^{n+1}$ in the process of x-ray absorption. Kotani and Toyozawa[9] discussed the soft-x-ray absorption process of metal with an incomplete shell and suggested that the final state of the d level of the excited atom is lowered down due to a core hole left behind and sometimes is formed below the Fermi-level, though in the initial state of the absorption the unoccupied d level is above the Fermi-level. Similar phenomenon might occur in this case, and some of the $3p^5 3d^{n+1}$ multiplet states may be formed below the conduction band. This may give rise to the low-energy structure of the absorption threshold. The main absorption on the high-energy side of the absorption threshold may be caused by the transition to the empty 4s band and some of the $3p^5 3d^{n+1}$ multiplet states mixed with this band.

The x-ray photoelectron spectrum of the valence band is considered to show the most reliable feature of the electronic state of the valence band and its main peak appears to show the d character of the valence band of the substance in comparison with the $M_{2,3}$ emission band, absorption and photoelectric-yield spectra. The detailed structure in XPS are interpreted in terms of multiplet structure at excited state[10]. The tail observed on the low-energy side of the peak may be due to the p character of the anion[10].

As a conclusion, the soft-x-ray emission and absorption spectra of the transition-metal compounds are accompanied with the multiplet structures which are caused by the interaction between the core hole and the localized d electrons in these substances, and the results appear to support the model containing both localized and one-electron band states [8,11].

References

- 1) L.F. Mattheiss, Phys. Rev. B 5, 290,306 (1972).
- 2) J. Yamashita, J. Phys. Soc. Jap. 18, 1010 (1963).
- 3) F.C. Brown, C. Gähwiller, and A.B. Kunz, Solid State Commun. 9, 487 (1971).
- 4) K. Tsutsumi and S. Nakai, Physica Fennica 9, Suppl. 74 (1974).
- 5) W. Gudat and C. Kunz, Phys. Rev. Lett. 29, 169 (1972).
- 6) S. Nakai, H. Nakamori, A. Tomita, K. Tsutsumi, H. Nakamura, and C. Sugiura, Phys. Rev. B 9, 1870 (1974).
- 7) K. Tsutsumi and H. Nakamori, J. Phys. Soc. Jap. 25, 1418 (1968).
- 8) S. Asada, C. Satoko, and S. Sugano, J. Phys. Soc. Jap. 37, 855 (1975).
- 9) A. Kotani and Y. Toyozawa, J. Phys. Soc. Jap. 35, 1073,1082 (1973).
- 10) D.E. Eastman and J.L. Freeouf, Phys. Rev. Lett. 34, 395 (1975).
- 11) D. Adler and J. Feinleib, Phys. Rev. B 2, 3112 (1970).

INTERPRETATION OF THE RHENIUM L_{III} ABSORPTION DISCONTINUITY IN RHENIUM METAL AND IN SOME OF ITS COMPOUNDS

A.V. PENDHARKAR and C. MANDE

Department of Physics, Nagpur University, Nagpur (India)

---o---

The shape and fine structure of the Re X-ray L_{III} absorption discontinuity have been studied in rhenium metal, seven octahedral [K_2ReCl_6 , K_2ReBr_6 , $(PyH)_2ReCl_6$, $(dipyH)_2ReCl_6$, $Re(dipy)Cl_4$, $K_3ReO_2(CN)_4$ and ReO_3] and three tetrahedral ($KReO_4$, $NaReO_4$, NH_4ReO_4) compounds, using a Cauchois type bent crystal X-ray spectrograph of diameter 40 cm, equipped with a well tested mica crystal. Microphotometer traces with magnification $\times 100$ of the recorded spectra were taken on the Spectroline Scanner manufactured by the Applied Research Laboratories, California, U.S.A.

The shape and the absorption maxima in the extended fine structure obtained for rhenium metal can be interpreted on the basis of the reported band structure of the metal and Lytle's theory. It has been shown that an absorption maximum lying at 30 eV from the main L_{III} discontinuity can be explained using the concept of electronic plasma in solids.

The main absorption discontinuity for all the compounds is found to split into two components [1] whereas in the metal the discontinuity is not split. The splitting and near edge structures in the discontinuities of the ~~ten~~ ^{ten} compounds lying within 30-35 eV have been interpreted with the help of suitable qualitative molecular orbital diagrams. It is possible to assign specific electron transitions for the different spectral features in the discontinuities on the basis of the M.O. diagrams, taking account of the dipole selection rules.

In the absorption process, the initial level from which the electron is ejected is $2P_{3/2}$. We can interpret the absorption maxima of the ReL_{III} discontinuity as transitions of the $2P_{3/2}$ electrons into suitable vacant M.O. levels. In all the cases except that of $Re(dipy)Cl_4$, the $p(\sigma$ and $\pi)$ orbitals of the ligands are considered for interactions in constructing the M.O. pictures. In the case of $Re(dipy)Cl_4$, the $[2,2']$ dipy ligand behaves as a strong σ donor because of which one has to consider the interactions of mainly the $p(\sigma)$ orbitals of the chlorine ligands and the $p(\sigma)$ orbitals of the lone pairs of the nitrogen atoms in the $[2,2']$ dipy ligand for the construction of the M.O. diagram. It can be assumed that the qualitative M.O. picture for $K_3ReO_2(CN)_4$ is similar to that of metal hexacyanides. The final levels responsible for the absorption maxima in the

compounds are given in Table I. The resemblance of the main Table I: Final empty MO levels responsible for absorption maxima in the compounds.

Absorp- tion max.	Octahedral compounds			Tetrahedral compounds
	$K_2ReCl_6, K_2ReBr_6,$ $(pyH)_2ReCl_6,$ $(dipyH)_2ReCl_6,$ ReO_3	$Re(dipy)Cl_4$	$K_3ReO_2(CN)_4$	
b	$2t_{2g}$	$1t_{2g}$	$t_{2g}(\pi)$	$2e$
c	$3e_g$	$2e_g$	$e_g(\sigma^a)$	$4t_2$
d	$3a_{1g}$	$2a_{1g}$	$t_{2g}(\pi^a)$	$5t_2$
e			$a_{1g}(\sigma^a)$	$3a_1$

edge to the nondegeneracy of 5d levels renders the possibility of obtaining the magnitudes of the crystal field splitting, Δ , in these compounds.

Table II: Bond lengths (r_1) in A.U. obtained from the fine structure of the L_{III} edge.

Compound	ΔE	r_1 (in A)	r_1 (in A) (X-ray diffraction data)
K_2ReCl_6	27.6(e- γ)	2.34	2.37
K_2ReBr_6	23.2(e- γ)	2.55	2.50
$(pyH)_2ReCl_6$	29.0(e- γ)	2.28	-
$(dipyH)_2ReCl_6$	28.9(e- γ)	2.29	-
$Re(dipy)Cl_4$	33.9(e- γ)	2.11(av.)	-
$K_3ReO_2(CN)_4$	44.8(f- δ)	1.84(av.)	-
ReO_3	44.5(e- γ)	1.84	1.867
$KReO_4$	52.2(f- δ)	1.70	1.77
$NaReO_4$	50.4(f- δ)	1.73	1.68
NH_4ReO_4	43.7(f- δ)	1.86	1.84

Assuming that the fluctuations of the absorption coefficient are nearly sinusoidal in nature in the region of the escape peak, it is possible to extend the applicability of Levy's theory, originally developed for

the K discontinuity to the L_{III} and other X-ray discontinuities as well. The peak just beyond the M.O. region is considered as the escape peak. Utilizing the observed energy differences (ΔE) between this escape peak and the subsequent absorption minimum, we have been able to obtain the bond lengths in these compounds with reasonable accuracy. The standard error, obtained statistically, in the values of ΔE is found to be within ± 2 eV and therefore the errors in the determination of the bond lengths lie within ± 0.07 Å. Table II shows that the agreement between our values and those obtained from X-ray diffraction work is quite satisfactory. It is, thus, possible to employ the X-ray absorption edge fine structure method to determine the bond lengths of the compounds with sufficient confidence.

Reference

- 1) Pendharkar, A.V. and Mande, C. Chemical Physics (W.G.), 7 (1975) 244-254.

COHERENT-PSEUDOPOTENTIAL-PAIR CALCULATION FOR X-RAY PHOTOEMISSION STUDIES OF AG-PD ALLOYS

Vipin Srivastava and S.K.Joshi

Physics Department, Roorkee University, Roorkee 247667, India.

In the recent past there has been considerable activity, both theoretical and experimental [1-4], for the determination of the density of electronic states in disordered alloys. X-ray photoelectron spectroscopy (XPS) has emerged as one of the most powerful techniques for getting a direct view of the occupied electron states of such systems. On the theoretical side simplified models are being employed to deal with real alloys.

In the Ag-Pd system the lattice constant changes markedly with composition giving rise to an appreciable change in the site energies and bandwidths. The densities of states of Ag and Pd are also very dissimilar in nature. Though the coherent potential approximation (CPA) gives moderately good agreement with experimental data, it can not be held as a promising scheme for an adequate understanding of complex systems like Ag-Pd alloys. We propose here a scheme that can incorporate the special features of the Ag-Pd system mentioned above. The agreement of our results with XPS data is heartening.

THEORY AND RESULTS: The present scheme is an extension of our earlier work [4] based on the pseudopotential concept. We have considered two-site scattering in an effective medium framework to take into account off-diagonal disorder more rigorously. The Hamiltonian of the system is,

$$H = \sum_n |n\rangle \epsilon_n \langle n| + \sum_n \sum_{m \neq n} |n\rangle h_{nm} \langle m|, \quad \dots (1)$$

where site energies, ϵ_n and hopping integrals, h_{nm} , are random variables and satisfy the following equality for Ag-Pd system,

$$\begin{aligned} & \sum_n |n\rangle \epsilon_{Ag} \langle n| + \sum_n \sum_{m \neq n} |n\rangle h_{Ag-Ag} \langle m| \\ &= \sum_n |n\rangle \epsilon_{Pd} \langle n| + \sum_n \sum_{m \neq n} |n\rangle h_{Pd-Pd} \langle m| + \sum_n |n\rangle V(E) \langle n|. \quad \dots (2) \end{aligned}$$

$V(E)$ is the energy dependent pseudopotential, and is obtained such that it exactly interpolates between $\rho_{Ag}(E)$ and $\rho_{Pd}(E)$. $\rho_{Ag(Pd)}(E)$ is the density of states of Ag(Pd). With the help of (2) the expression for $V(E)$ is found to be,

$$\int_{E_{Ag}}^E \rho^{Ag}(Z) dZ = \int_{E_{Pd}}^{E-V(E)} \rho^{Pd}(X) dX . \quad \dots (3)$$

E_{Ag} and E_{Pd} respectively denote the bottoms of $\rho^{Ag}(E)$ and $\rho^{Pd}(E)$. The averaged properties of the disordered system are found by obtaining a configurationally averaged propagator, $\langle G \rangle (= \langle (E-H)^{-1} \rangle)$. $\langle G \rangle$ is related to an effective medium propagator, as,

$$\langle G \rangle = \tilde{G} + \tilde{G} \langle T \rangle \tilde{G}, \quad \dots (4)$$

where T is the scattering matrix, and the effective medium is denoted by the Hamiltonian

$$\tilde{H} = \sum_n |n\rangle \sum_1 \langle n| + \sum_n \sum_{m \neq n} |n\rangle \sum_2 \langle m|. \quad \dots (5)$$

The best estimate \tilde{G} , for $\langle G \rangle$ is made self-consistently by putting,

$$\langle T \rangle = \langle (H - \tilde{H}) / [I - (H - \tilde{H}) \tilde{G}] \rangle = 0. \quad \dots (6)$$

It is a formidable task to solve eqn.(6) exactly. We approximate T by a two-site scattering matrix, and obtain two self-consistent coupled equations in \sum_1 and \sum_2 :

$$\langle T_{nn}(\sum_1, \sum_2) \rangle = 0, \quad \dots (7a)$$

$$\langle T_{nm}(\sum_1, \sum_2) \rangle = 0, \quad \dots (7b)$$

where n and m are two nearest neighbour sites.

The self-energies \sum_1 and \sum_2 have been obtained by solving (7) iteratively for 40 at.% Ag, 60 at.% Pd alloy. The various input parameters have been taken from ref.3. The density of states for the alloy is found from the formula

$$\rho(E) = -\pi^{-1} \text{Im} \langle n | \langle G \rangle | n \rangle [1 - 0.4 \frac{\partial V(E)}{\partial E}], \quad \dots (8)$$

where $\langle n | \langle G \rangle | n \rangle = \frac{1}{1 - \sum_2} \int \frac{\rho^{Pd}(E') dE'}{(E - \sum_1) / (1 - \sum_2) - E' + \epsilon_{Pd}} .$

Figure 1 shows the results for $\rho(E)$ for the alloy under consideration. Comparison has been made with the CPA results and the optical density of states (XPS). The structures in the present result are distinctly close to the ones shown in the experimental result, and may be assigned to the structures in the parent densities of states. The positions of the prominent peaks are indicated in the figure. The present calculation shows excellent agreement with experiment.

REFERENCES:

1. C.Norris and H.P.Myers, J.Phys.F1,62(1971).
2. S.Hüfner, G.K.Wertheim and J.H.Wernick, Phys.Rev.B8,4511 (1973).
3. G.M. Stock,R.W.Williams and J.S.Faulkner, J.Phys.F3,1688 (1973).
4. V.Srivastava and S.K.Joshi, Proceedings of the IV International Conference on Vacuum Ultraviolet Radiation Physics(Hamburg,1974); Phys.Rev.B12, 2871(1975).

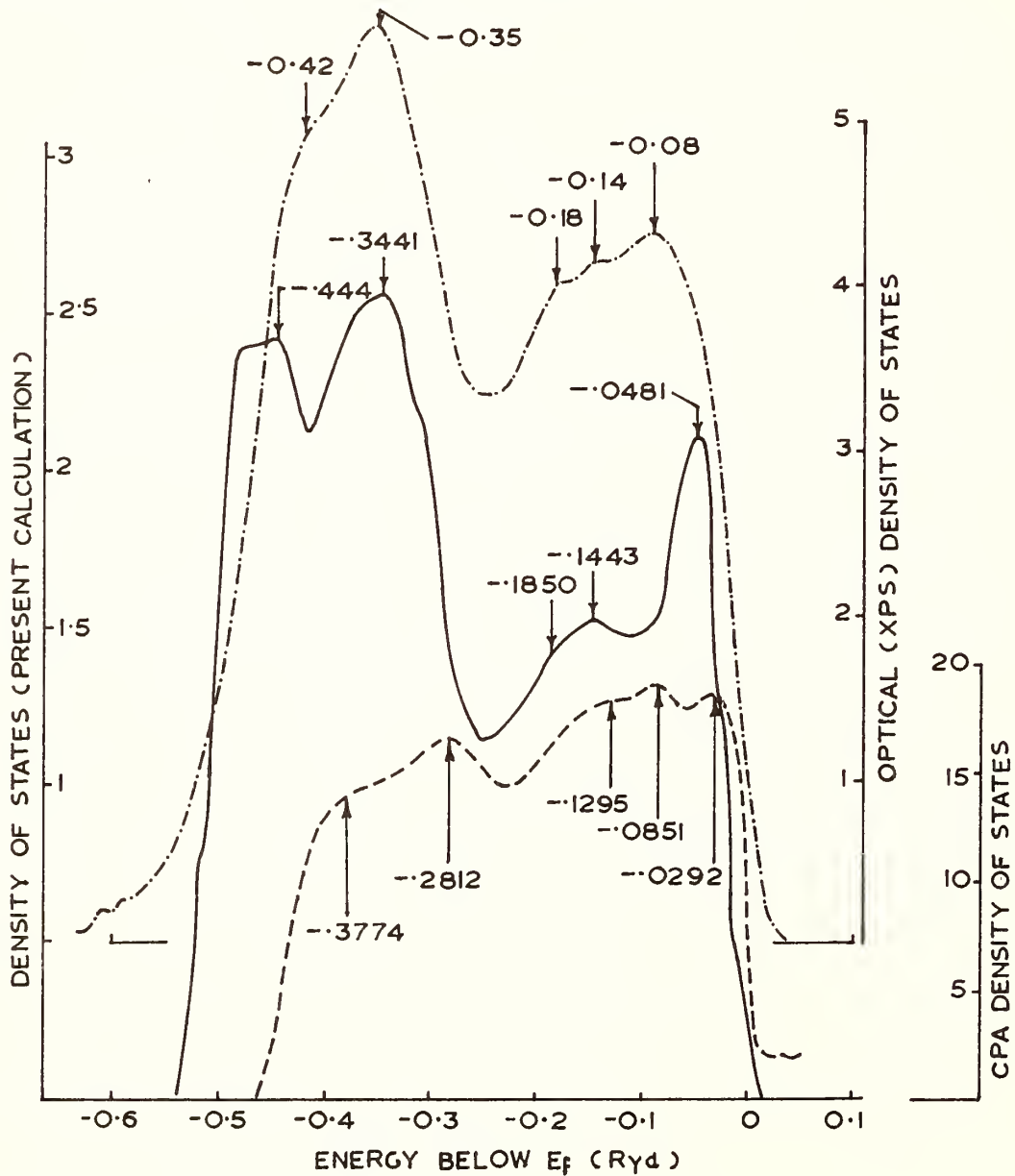


FIG.1. Plots of electronic density of states for 40at.% Ag, 60 at.%Pd alloy: Comparison of present calculation (—) with CPA results(---)and XPS results(-•-•-).

ON THE ELECTRONIC STRUCTURE OF PALLADIUM IN THE PD-H SYSTEM

E. Gilberg, Sektion Physik der Universität München
Geschwister-Scholl-Platz, D 8 München

Introduction

In 1971 EASTMAN et al. (1) reported on an experimental and theoretical investigation of the energy band structures of Pd metal and PdH_x . Using an APW calculation they found that the commonly accepted protonic model fails in explaining the changes occurring in the electronic structure when hydrogen enters the metal lattice. The calculation revealed a strong interaction between H 1s and Pd d states which leads to the formation of a new energy band located below the original Pd d bands. The electrons from the hydrogen fill up the free d states and the lowest vacant s-p band which is partly pulled down below the Fermi level. In an UPS investigation the authors indeed found an additional electron emission band below the main band for PdH_x , which they ascribed to the theoretically predicted low lying Pd-H bonding energy band.

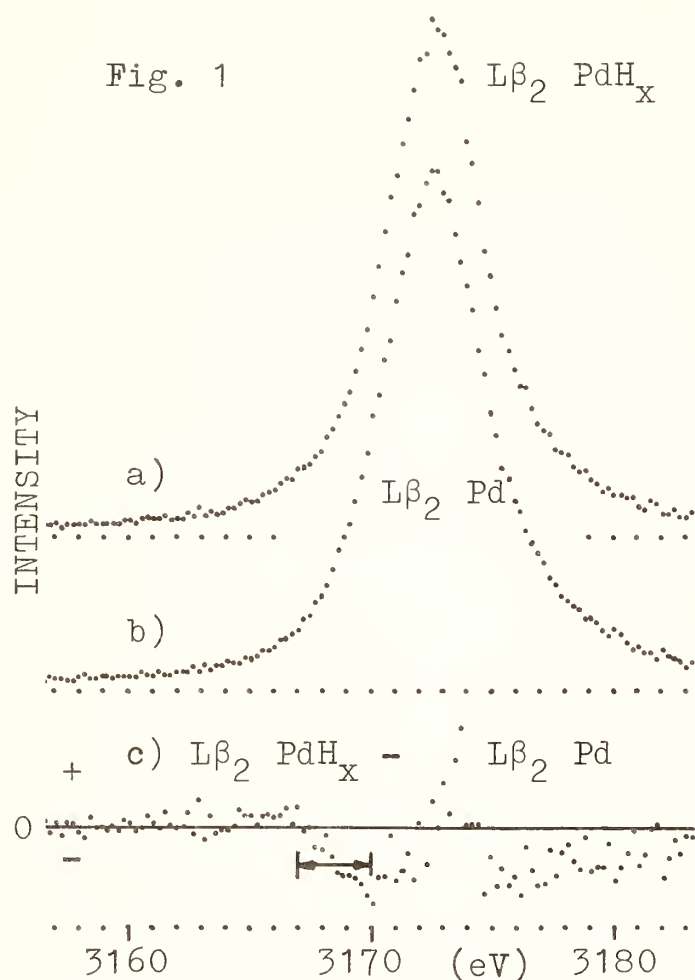
At room temperature the Pd-H system forms two phases, a low concentration α phase with a maximum atomic ratio H/Pd of about 0.03 and a high concentration β phase with a minimum atomic ratio of about 0.6; between these limits one finds the α, β two-phase region. The phase diagram is not yet well established for low temperatures, but probably the same phases still exist with only slightly changed limits at the temperature of liquid nitrogen. The fcc lattice of the Pd metal is slightly expanded when it is charged with hydrogen. The hydrogen atoms occupy octahedral interstitial sites.

In a previous investigation (2) we recorded the $L\beta_2$ valence band transition of pure Nb metal and NbH_x ($x \approx 0.6$). The spectrum from NbH_x showed an additional emission band below the main metal emission band which we ascribed to transitions from metal-hydrogen bonding states. The results were thus similar to the findings of EASTMAN et al. for PdH_x . It looked desirable to extend our investigation to the Pd-H system, as the experimental method used, although providing less energy resolution, yields results which are not affected by surface contaminations of the specimens, in contrast to the photoelectron spectra. As the main symmetry character of the Pd valence states is assumed to be d-like, we again choose transitions to and from the L_3 level, which probe the s- and d-like character of the local density of states at the Pd atoms.

Experimental

The spectra were recorded with a high resolution curved crystal spectrometer (2). The specimens consisted of $23 \mu\text{m}$ and $1.4 \mu\text{m}$ Pd foils of 99.9% purity, the first being used for the emission-, the second for the absorption spectra. The

Fig. 1



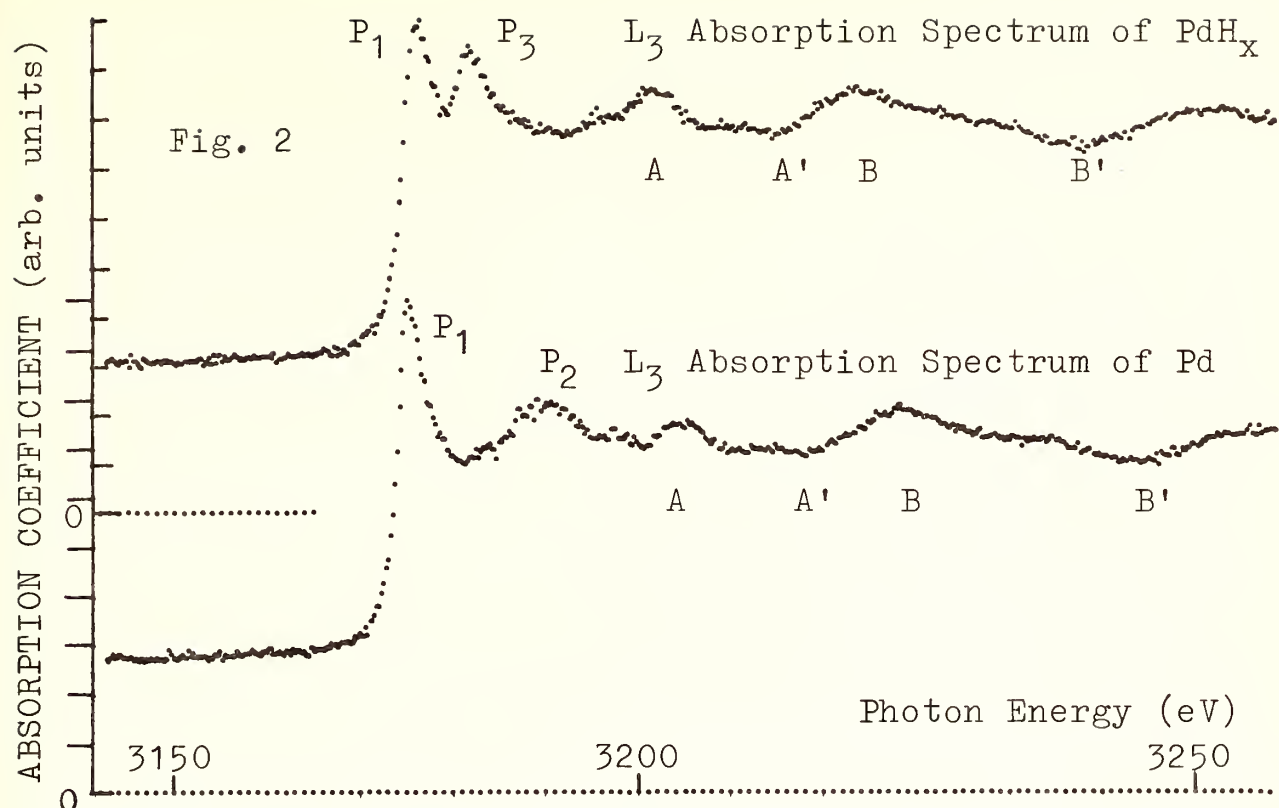
foils were charged with hydrogen by electrolysis in dilute sulphuric acid. The atomic ratios were determined by weighing to be 0.58 ± 0.04 in the emission- and 0.51 ± 0.08 in the absorption case. The target holders were cooled with liquid nitrogen in order to keep the hydrogen in the metal foil. The emission spectra were excited in fluorescence. As they were strongly affected by selfabsorption they were corrected using a method which will be described elsewhere. The L_3 absorption spectra were recorded using the continuum of a gold anode. They were corrected for the background accompanying the bremsstrahlung as reported in (3).

Results and Discussion

The corrected and normalized $L\beta_2$ emission spectra shown on Figs. 1a, b are almost identical in shape and position. Therefore the difference $L\beta_2 \text{ PdH}_x - L\beta_2 \text{ Pd}$ is given on Fig. 1c on an enlarged scale (2.7x). The region where according to EASTMAN et al. transitions from the additional energy band in PdH_x should occur is marked by arrows. As can be seen there is no corresponding feature in the x-ray spectrum of PdH_x . From Fig. 1c one has to conclude that in the energy region in question $L\beta_2 \text{ PdH}_x$ is even less intense than $L\beta_2 \text{ Pd}$. In the adjacent region between 3164 eV and 3167 eV the intensity of the PdH_x spectrum is slightly higher which might be regarded as some indication for an additional energy band.

There is some ambiguity in the relative positions of the emission spectra, as it is not possible to determine the Fermi edges in the spectra without further information. If one assumes the Fermi edges to be given by the points of inflexion of the absorption edges shown on Fig. 2, the spectrum of PdH_x would have to be shifted by 0.5 eV towards lower energies in order to achieve coincidence of the Fermi edges in the emission spectra. Then the difference $L\beta_2 \text{ PdH}_x - L\beta_2 \text{ Pd}$ becomes positive in the region between 3164 eV and 3172 eV with a maximum at 3171 eV. This again would not comply with the experimental findings of EASTMAN et al.

The low lying x-ray emission band, which is well pro-



nounced in the Nb $L\beta_2$ spectrum of NbH_x , is absent or has a very low intensity in the case of PdH_x . The corresponding energy band obviously has a very low density of states at the Pd atoms or a symmetry different from s and d.

In contrast to the emission spectra the absorption spectra show significant differences. The first peak P_1 decreases. Instead of the peak P_2 , which disappears completely, a new line P_3 arises between P_1 and P_2 . The interpretation of these results has to be postponed until appropriate calculations will be available. The extended fine structure regions marked with A, B, A', B' are rather similar. The distances in energy ΔE between corresponding features are smaller in the spectrum of PdH_x due to the lattice expansion. Using the $\Delta E \sim 1/a^2$ dependence we found the lattice parameter a to be increased by $(3.7 \pm 0.4)\%$. As the increase of a at the low concentration limit of the β phase amounts to 3.5% it is assured that the specimens of PdH_x were of rather pure β phase.

It is intended to complete this investigation by studying the corresponding transitions to and from L_1 which should give information on the p-like character.

Acknowledgements

The author is indebted to Prof. J. Peisl and to Prof. A. Faessler for several helpful discussions. Thanks are also due to cand. phys. B. Foltz for technical assistance.

Literature: (1) D.E. Eastman, J.K. Cashion, and A.C. Switendick, Phys. Rev. Letts. 27, 35 (1971); (2) E. Gilberg, phys. stat. sol. (b) 69, 477 (1975); (3) M.J. Hanus and E. Gilberg, J. Phys. B 9, 137 (1976)

CHARACTERISTIC AND CONTINUOUS X-RAY EMISSION MEASUREMENTS ON TiNi

Helmut Föll

Physikalisches Institut der Universität 7500 Karlsruhe, FRG

A special problem which arises in connection with the alloying of Ti with Ni is the possibility of a charge transfer. Investigations on this question have been performed by Källne [1] and Kolobova and Trofimova [2]. For clarification of this problem we have investigated the electronic DOS of the occupied and unoccupied part of the conduction band of the ordered alloy TiNi.

The electronic DOS of the unoccupied part of the conduction band can be investigated by means of continuum isochromats. Recently Nagel et al. [3] have given an anticipated shape of such a continuum isochromat for TiNi. These calculations are based on so-called local DOS of TiNi as have been given by Papaconstantopoulos et al. [4].

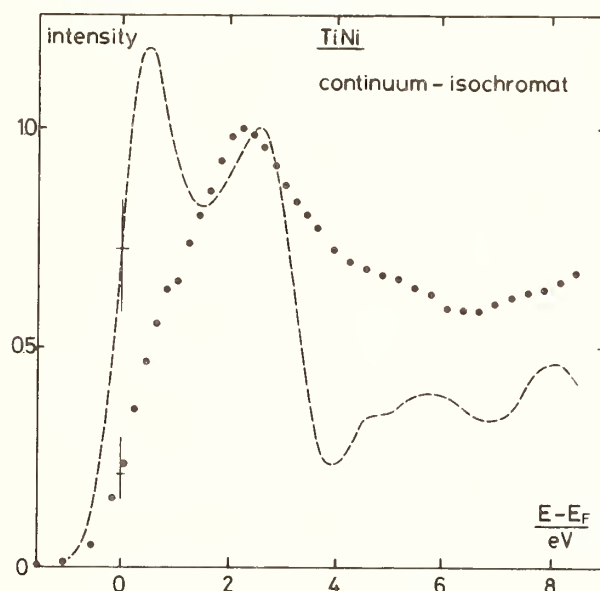


Fig. 1

Comparison of the theoretical and experimental isochromat. The theoretical isochromat (Nagel et al. [3]) is dashed lined.

The Fermi edge E_F is zero of energy. The curves are normalized to the same height of the second peak.

A comparison of the theoretical expectation with the measured continuum isochromat is shown in Fig. 1. The largest discrepancy between the two isochromats is the first high maximum of the theoretical isochromat immediately neighbouring the Fermi edge which is completely missing in the experimental isochromat. This high maximum of the theoretical curve corresponds to a high electronic DOS above the Fermi edge and arises according to Nagel et al. [3] from the unoccupied d-electron states localised at the Ni-sites in TiNi. The lack of such a high maximum in the experimental curve can be understood by a local transfer of electronic charge from Ti-sites to the Ni-sites on alloying.

Further arguments for a charge transfer from Ti- to the Ni-sites arise from a comparison of our measured isochromats of Ti, Ni and TiNi (Fig. 2) There is a conspicuous similarity of the TiNi-isochromat with the Ti-isochromat especially with regard to the intensity in the maximum. Concerning the high intensity of the Ni-isochromat this result can

only be explained by a completely filled local d-band of the Ni-spheres in TiNi.

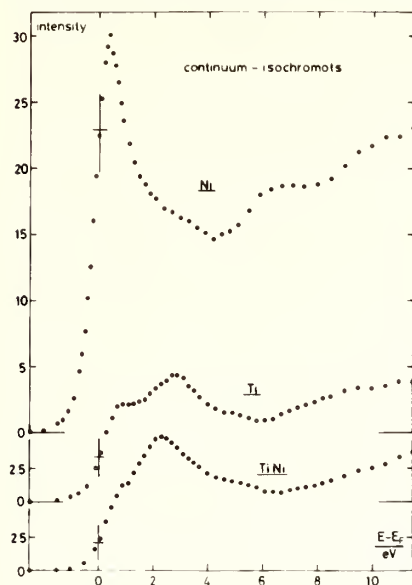


Fig. 2

Continuum isochromats from Ni, Ti and TiNi.

Measured with a quartz crystal in 1 st order of reflection.

Threshold voltage ≈ 1.5 kV.

The Fermi edge is zero of energy.

Supplementary to isochromat spectroscopy we have investigated the occupied part of the conduction band by measuring L_{III} -emission band spectra in the pure elements and in the ordered alloy. Here our conclusions are based mainly on the positions of the Fermi edges at the respective emission bands. With the exception of the TiL_{III} -spectrum from TiNi all these positions are determined from additional measurements of self absorption spectra.

Fig. 3 shows the NiL_{III} -bands in pure Ni and TiNi. Most important in our connection is the shift of the position of the Fermi edges at the spectrum. On going from pure Ni to TiNi the shift of the position of the Fermi edge towards the bottom of the spectrum in TiNi can be interpreted in terms of a filling up of the local DOS within the Ni-sphere of the ordered alloy TiNi. It supports the charge transfer concept from Ti to Ni.

Fig. 4 shows the TiL_{III} -bands in pure Ti and TiNi. The presentation is the same as that of Fig. 3. Because in TiNi the Fermi edge could not be localised by a pertaining self absorption spectrum, at present we cannot draw any conclusions from the positions of the Fermi edges in favor of charge transfer but on the other hand there is no evidence against charge transfer.

There are arguments for the assumption that the high energetic peak of the TiL_{III} -spectrum from TiNi doesn't reflect local DOS but possibly arises from cross transitions from the local Ni-d-band to the TiL_{III} -level. On this basis further arguments for a charge transfer from Ti to Ni can be given.

Normally one would expect that the area of the TiL_{III} -band from TiNi is half the area of the TiL_{III} -band from pure Ti.

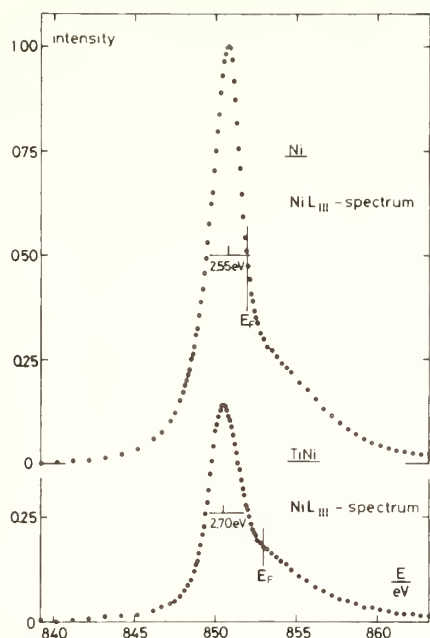


Fig. 3

NiL_{III}-emission band spectra from Ni and TiNi. Measured with an OHM-crystal in 4 th order of reflection. Excitation energy: 2.5 keV. The ordinal scale is the same for both spectra.

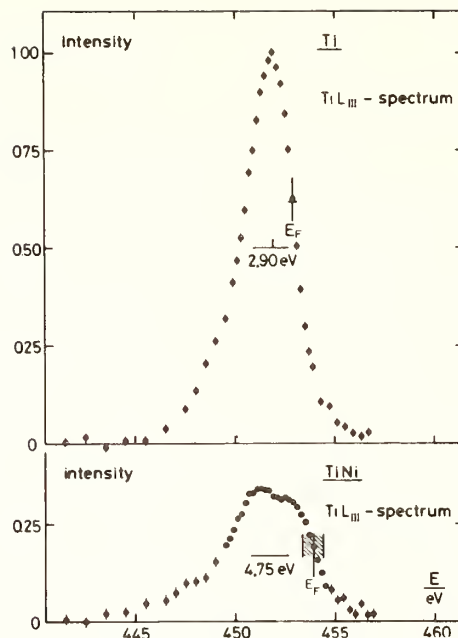


Fig. 4

TiL_{III}-emission band spectra from Ti and TiNi. Measured with an OHM-crystal in 2 nd order of reflection. Excitation energy: 2.5 keV. The ordinat scale is the same for both spectra.

Regarding the high energetic peak in the TiL_{III}-spectrum from TiNi as the result of cross transitions, the area due to the Ti-d-band in TiNi is significantly less than the expected 50 %. This can be interpreted in terms of a local charge transfer from the Ti- so the Ni-sites. In the case of the NiL_{III}-bands (Fig. 3) the area of the Ni-band from TiNi is significantly greater than the half area of the band from pure Ni. From this the same conclusion regarding charge transfer can be drawn.

References

- [1] Källne, E: J. Phys. F. Metal Phys. 4 167 (1974)
- [2] Kolobova, K.M., Trofimova, V.A.: Proc. Int. Symp. Kiev 1968 (Institute of Metal Physics Academy of Science of the Ukrainian SSR) pp. 172-83 (1969)
- [3] Nagel, D.J., Papaconstantopoulos, D.A., Mc Caffrey, J.W., Criss, J.W.: In X-ray Spectra and Electronic Structure of Matter pp. 51-80 ed. by A. Faessler and G. Wiech, München (1973)
- [4] Papaconstantopoulos, D.A., Mc Caffey, J.W., Nagel, D.J.: J. Phys. F 3, L 26 (1973)

RESOLUTION-ENHANCED Cu AND Co $K_{\alpha_{1,2}}$
X-RAY EMISSION SPECTRA OBTAINED BY
THE DECONVOLUTION METHOD

Jiro KASHIWAKURA, Yohichi GOHSHI and Isao SUZUKI

Toshiba Research and Development Center
Komukai-Toshiba, Saiwai, Kawasaki, 210 Japan

Introduction

It is well known that $K_{\alpha_{1,2}}$ X-ray emission lines of the iron-series first transition elements in chemical compounds show very broad line width and depart from a single Lorentzian distribution form. An elucidation of these experimental facts has been an objective of a number of theoretical studies. [1-3]

In an X-ray emission process, two hole states arise, either of which may be studied by X-ray photoemission technique. According to the theory of Weisskopf and Wigner, the lifetime widths of the initial and final hole states should contribute additively to the width of the X-ray emission spectra. Therefore appearance of fine structures due to multiplet splitting in the X-ray emission spectra is hindered by the large lifetime broadening factor. However, as is shown in the previous papers [4,5], application of successive pseudo-deconvolution method taking the lifetime broadening factor as a deconvoluting function to resolution enhancement treatment of the transition element $K_{\alpha_{1,2}}$ X-ray spectra makes it possible for fine structures to appear. The amount of fine structures is largely influenced by the number of unpaired 3d electrons, which also depends on the nature of the chemical bond in the compounds. The purpose of the present paper is to show fine structures of the $K_{\alpha_{1,2}}$ X-ray emission spectra of copper compounds CuCl and $\text{CuF}_2 \cdot 2\text{H}_2\text{O}$, and of cobalt acetyl acetonates $\text{Co}(\text{AA})_2$ and $\text{Co}(\text{AA})_3$.

Experimental

The original $K_{\alpha_{1,2}}$ spectra of copper and cobalt compounds were measured with a prototype TOSHIBA AFV 701 two-crystal X-ray spectrometer [6]. The tungsten target tube was used to produce primary exciting X-rays and was operated at 35KV-25mA. Si (220) crystals were used as analyzer crystals. The scanned 2θ regions for the cobalt and copper compounds are from 55.38 to 55.78 degrees and from 47.04 to 47.54 degrees, respectively.

Method

The pseudo-deconvolution technique, whose mathematical formulation is given in the following form in the frequency domain, was used.

$$G_n(\omega) = G_{n-1}(\omega) + [G_0(\omega) - G_{n-1}(\omega) \times L(\omega)] \quad (1)$$

Here, $G_0(\omega)$, $L(\omega)$ and $G_n(\omega)$ are the Fourier transform of the original spectrum, the Lorentzian distribution function expressing the lifetime broadening shape and the deconvoluted spectrum after n iterations, respectively. Though the exact values for the lifetime width of Co and Cu atoms are not known, 1.7eV and 2.0eV lifetime width values were used for Co and Cu atoms, respectively, which were estimated from the values given in a previous article [7].

In order to prevent the enhancement of the noise component contained in the spectra during the deconvolution process, the feedback term of Eq. (1) was smoothed $n-1$ times, using smoothing functions determined by the least-squares sliding polynomial method [8]. The frequency characteristics of these smoothing functions depend both on the number of polynomial fitting points and on the degree of polynomials. An appropriate smoothing function was decided upon through deconvolution treatment of the simulation spectra having a Lorentzian contour, which was formed by taking into account the experimental conditions and the measured spectra of the compound having no unpaired d electrons. The smoothing function determined in this way was a quartic 17-point function for the cobalt compounds and a quartic 15-point function for the copper compounds.

Results

In order to correctly judge the fine structures appearing in the resolution enhanced spectra, it was necessary to calculate the amount of false peaks or ringings caused by the deconvolution process. It was determined from the calculation on simulation spectra, whose results are shown in Table 1.

Resolution-enhanced Cu and Co $K_{\alpha_{1,2}}$ X-ray spectra are shown in Fig. 1 and Fig. 2. According to the Nefedov theory [2], when there are no unpaired d electrons, both K_{α_1} and K_{α_2} spectra are expected to be composed of a single peak. This seems approximately correct in the $\text{Co}(\text{AA})_3$ and CuCl compounds, though the spectra of the latter compound show some structure in a lower energy side of the main K_{α_2} peak. As the $\text{Co}(\text{AA})_2$ compound is known to have three unpaired d electrons, the resolution-enhanced K_{α_1} and K_{α_2} spectra are expected to be composed of four and two peaks, respectively. Though it is not clearly separated, the obtained K_{α_2} spectrum seems to consist of three peaks. The high resolution Cu $K_{\alpha_{1,2}}$ spectra of $\text{CuF}_2 \cdot 2\text{H}_2\text{O}$ rather resemble those of CuCl . As the $\text{CuF}_2 \cdot 2\text{H}_2\text{O}$ compound is known to have one unpaired d electron, its high resolution spectra should give two peaks for the K_{α_1} and K_{α_2} spectral lines. However, it is doubtful whether free spin localization on the Cu atom is firmly made.

References

- 1 K. Tsutsumi, J. Phys. Soc. Japan, 14, 1696 (1959)
- 2 V.I. Nefedov, Izv. Akad. Nauk. SSSR, Ser. fiz., 28, 816 (1964)
- 3 J. Finster, G. Leonhardt and A. Meisel, J. de Phys., 32, C4, 218 (1971)

- 4 Y. Gohshi and J. Kashiwakura, *Physica Fennica*, 9, 327, 330 (1974)
- 5 J. Kashiwakura and Y. Gohshi, *Spectrochim. Acta*, 30B, 471 (1975)
- 6 Y. Gohshi, Y. Hukao and K. Hori, *Spectrochim. Acta*, 27B, 135 (1972)
- 7 L. G. Parrat, *Rev. Mod. Phys.*, 31, 630 (1959)
- 8 A. Savitzky and M. J. E. Golay, *Anal. Chem.*, 36, 1627 (1964)

Table 1 Amount of false peaks or ringings

Element	FWHM of simulation spectra	Deconvolution width*	Percent of maximum false** peak height with regard to peak maximum (%)
Co	18.0 channels	14.24 channels	10.4 (8.8)
Cu	15.7 channels	12.0 channels	11.2 (8.9)

* Using a one-fourth value of this, deconvolution treatment was carried out four times.

** The entries in the parenthesis are values for noise free spectra.

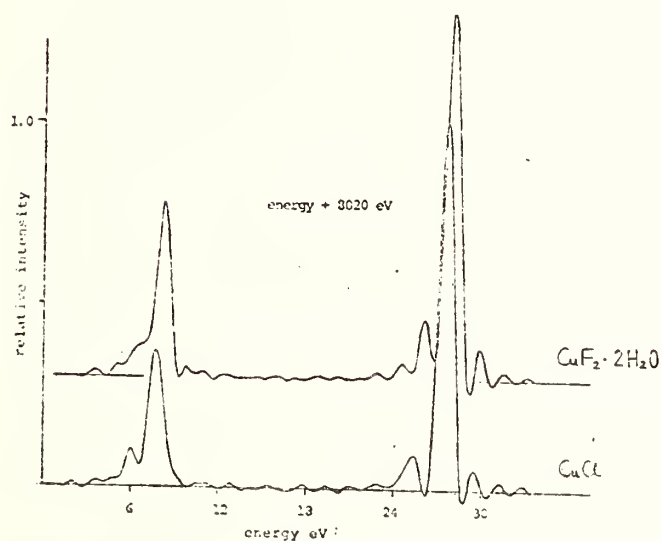


Fig.1 High resolution Cu $K_{\alpha_{1,2}}$ spectra

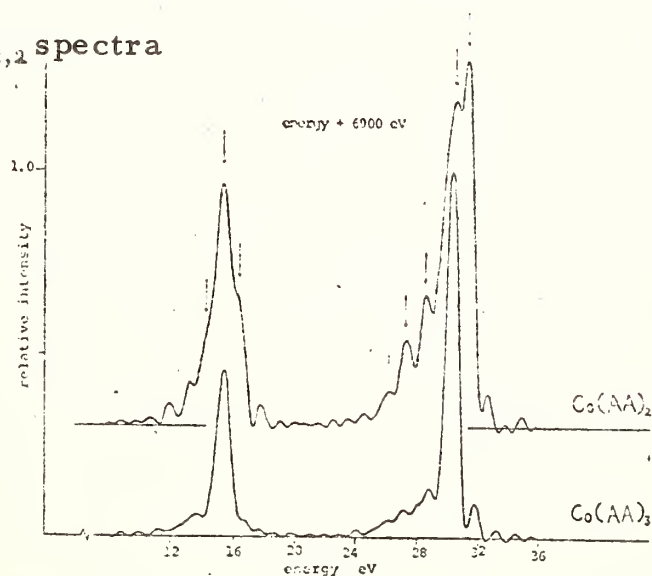


Fig. 2 High resolution Co $K_{\alpha_{1,2}}$ spectra

"A NEW COMPUTER CONTROLLED SOFT X - RAY SPEKTROMETER"

H.-E. Goldstein, R. Pfliegl, H. Kirchmayr
Institute for Experimental Physics
Technical University Vienna
Karlsplatz 13,
A-1040 Vienna / A U S T R I A

The activity in the field of Soft X - Ray Physics within the Institute for Experimental Physics is based on experiments performed in the 1950's by H. Herglotz and coworkers. ("Study of Structural Detail by X-Rays of Wavelength greater than 4 Å," Advances in X-Ray Analysis, Vol. 14, Plenum Press 1971)

In the last three years a completely new Soft X-Ray Spectrometer has been designed and built, trying to combine the technical advantages of different commercially available components in the field of vacuum, spectrometry, registration and computer science to a unique new apparatus. Thus we have put great weight on a sophisticated fully automatised vacuum system (Leybold), capable of 10^{-8} Pa in the sample chamber (see fig. 1) in which the facilities to clean the sample surface (sputter gun, scraper) and in which the electron gun are positioned. This electron gun (focus $3 \times 7 \text{ mm}^2$, max. current 30 mA) is home made and allows a normal incidence of electrons as well as a normal take off of the X-Rays, thus minimising the self-absorption.

The spectrometer is based on a Hilger & Watts vacuum spectrometer (E 580) adapted for photoelectric scanning, utilizing a blazed grating (Bausch & Lomb, 600 mm^{-1} , $3^\circ 31'$ blaze angle) with a radius of 2 m according to the Rowland radius of 1 m. In the spectrometer tank there is a pressure of 10^{-6} Pa. The entrance slit has the function of separation to the sample chamber.

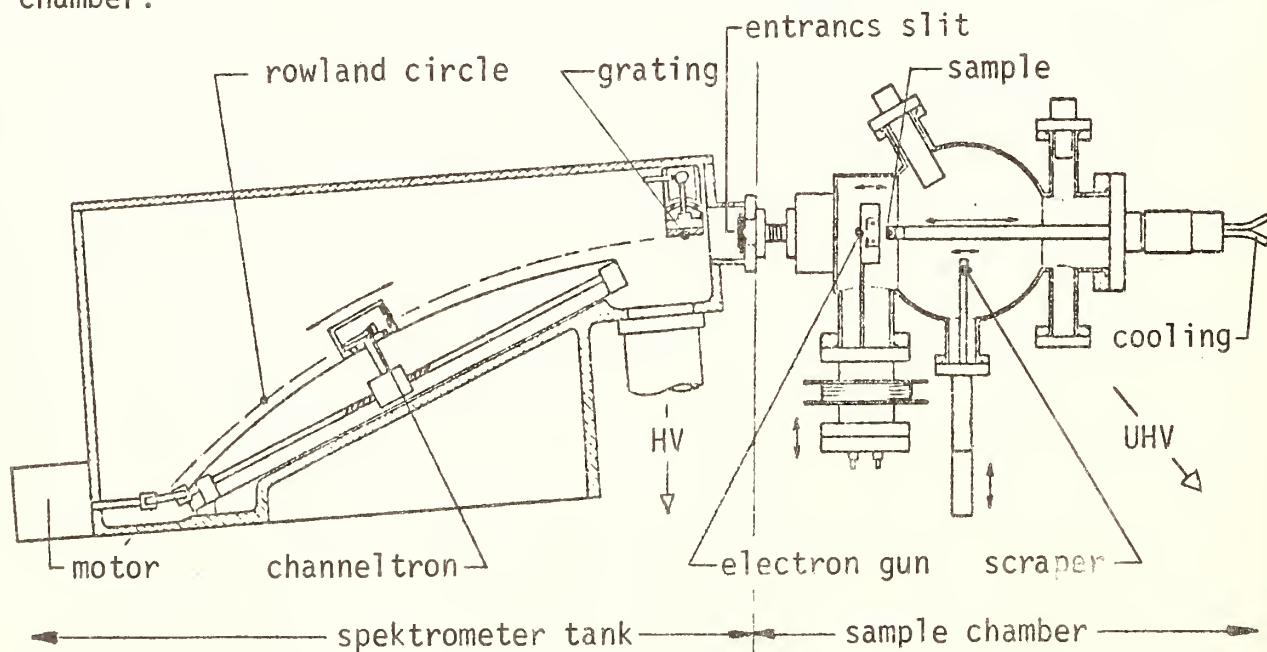


fig. 1: scheme of the spectrometer

Throughout the wavelength region of 50 to 1000 Å we expect to gain a resolution of at least 0,3 eV. The dedection system consists of a channeltron, which is moved along the Rowland circle (Valvo B 312-BL) by means of a step and scan motor (Bautz, Slo Syn). Both are controlled by a CAMAC system in connexion with a process computer (PDP 11/05 Digital Equipment) which controls the complete experiment and is also responsible for the fully automatic running and supervising of the experiment during an extended period up to several days. (See fig. 2)

Furthermore the PDP 11/05 allows the controll of a large number of parameters, e.g. of the pressure and composition of the residual gas, of the sample temperature, the electron current (from filament to sample) of fluctuations of the excitation, voltages, etc., during the whole experimental time. Therefore a distinct improvement of the reproducibility of the spectra is achieved. The concentration and primary treatment of the results is also done by the process computer PDP 11/05, but for the unfolding of the spectra and for the theoretical analysis there exists a connexion with a large computer, (PDP 11/45) the central computer for the Physics Institutes and also a large CYBER 70 computer. Simultaneously an X-Y plot may be obtained during the run of the experiment.

First results are presented.

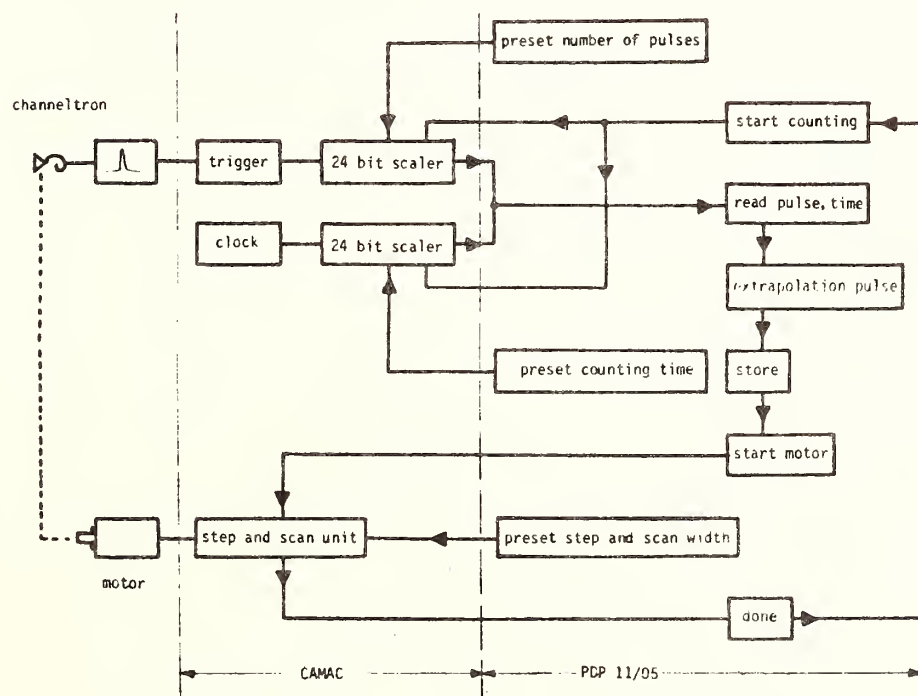


fig. 2: schematic registration diagram

Ultra High Resolution Capabilities of A 5M Grating Spectrometer
In The 10 to 250 Å Region

George Andermann, Lars Bergknut, Marri Karras^{*} and George Grieshaber
Department of Chemistry
University of Hawaii
Honolulu, Hawaii 96822

Our recently acquired Grating Measurements Ltd. (GML) 5 meter grating spectrograph has a number of interesting features. The standard features include highly precise and accurate "reference" Rowland circle railings as well as carefully aligned primary slit, grating and photographic assemblies. The optical elements may be demounted and reinserted without disturbing the alignment. The range of our spectrograph is from 10 to 250 Å.

Using a high voltage spark for a source GML personnel obtained in first order a spectral resolution of about .017 eV at 130 eV, i.e., a resolving power of about 7500, thus demonstrating ultra high resolution capability.

The standard GML spectrograph has been adapted by our group for molecular electronic structural characterization via x-ray emission studies. In our arrangement the identical spot on a sample may be viewed by the grating optics at any angle of incidence which itself may be varied continuously from 0 to 6°. A simple modular photoelectric attachment has been designed by our group which allows an easy insertion of the photographic detection assembly.

The unit is currently under evaluation with respect to resolution and intensity capabilities using conventional photon irradiation of samples.

^{*} Prof. Karras spent his sabbatical at the University of Hawaii. His regular address is Department of Electrical Engineering, University of Oulu, Finland.

K ABSORPTION SPECTRA OF FLUORINE IN ALKALIHALIDE CRYSTALS

S. Kiyono, Y. Hayasi and T. Muranaka

Department of Applied Physics, Faculty of Engineering,
Tohoku University, Sendai, Japan

Recently, several papers were published on measurements of soft X-ray spectra with a concave grating grazing incidence vacuum spectrometer. However, as yet there have been only a few works on the spectra studied $10 \sim 30 \text{ \AA}$ region. This is probably because of the complexity in experimental methods and technics.

We have designed and constructed a spectrometer operated by new mechanism <<Precision linear motion of curved mica crystal spectrometer>>. The center of Rowland circle is not fixed but moves around a fixed X-ray source, and a flow proportional X-ray counter moves also on this moving Rowland circle. Both crystal and detector move with high precision without backlashes ($< 1 \text{ }\mu\text{m}$) along the Rowland circle ($R = 300 \text{ mm}$), and accurate spectra can be recorded in the range of $11.43 \text{ \AA} \sim 19.68 \text{ \AA}$.

The spectrometer is operated by a simple pantagraph mechanism which provides precise straight motion along bearing V-slots and rotation around pivots. Since a guiding circle and gears are not needed, it is comparatively easy to construct a high precision spectrometer. A glancing angle of the analyzing crystal from anticathode is always kept constant and the displacement of the center of the crystal corresponds to the difference in X-ray wavelength.

An X-ray tube with tungsten target was used as a source of continuum X-rays. The tube was operated at 1.3 kV , 10 mA . The anticathode voltage was determined by the condition that the 2nd order reflection of the lowest energy X-ray in the spectrum did not appear. The output pulses of the detector were counted for 20 seconds at each point. The intensity transmitted through the substrate was approximately 5000 counts per 20 seconds. In this apparatus the absorption coefficient was determined by observing the difference in transmission of the two samples [1]. The measurement of transmission intensity of two samples were carried alternatively. The apparatus ran automatically for about 4.5 hours to obtain a set of data (201 data points).

The samples used in this investigation were prepared by vacuum evaporation upon aluminum thin foil ($\sim 5000 \text{ \AA}$) at pressures of about $2 \times 10^{-5} \text{ Torr}$. Two samples of different thicknesses, were prepared at each evaporation. In the case of LiF the thicknesses of the two samples were 600 \AA and 8000 \AA , respectively. But the LiF spectra were not so different from the one obtained by the difference method of transmission with the thicker sample and the substrate only. Therefore we determined the absorption coefficient of other

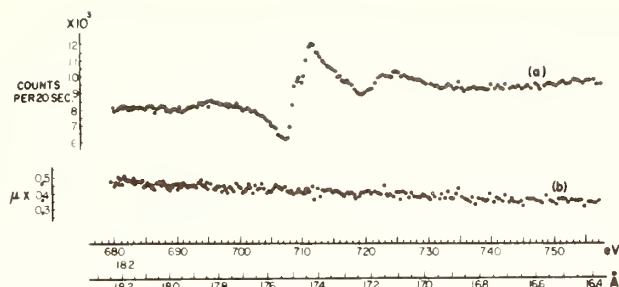


Fig. 1.

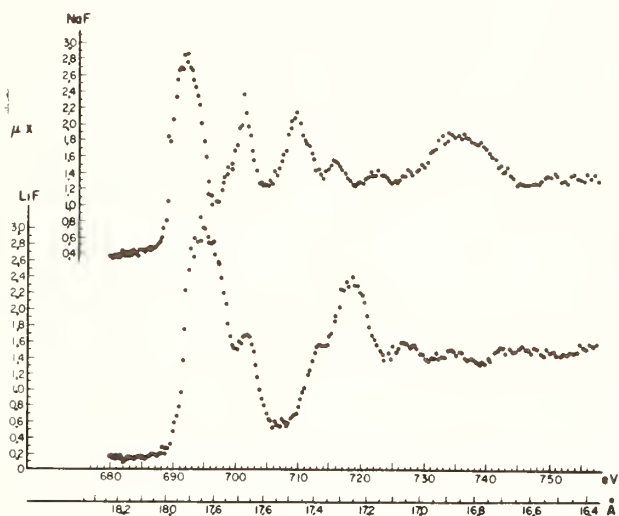


Fig. 2.

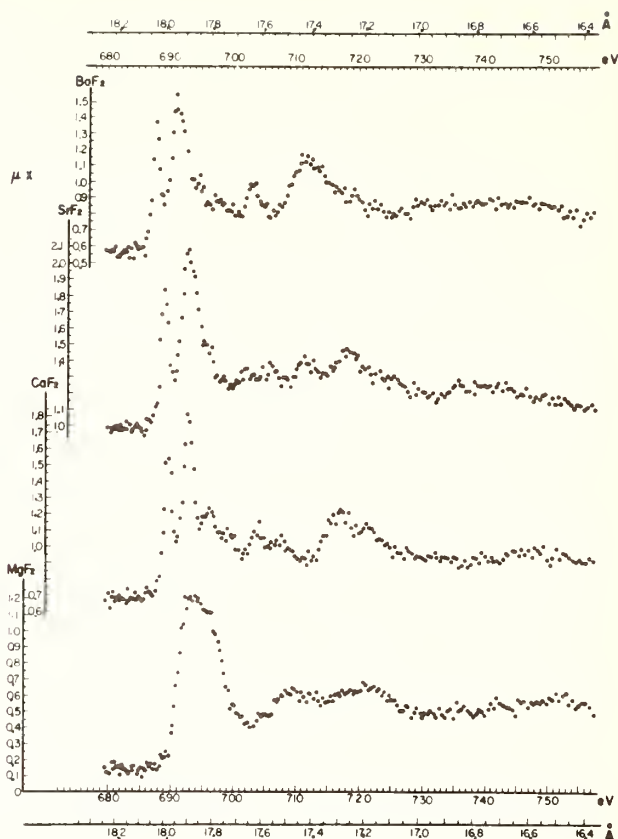


Fig. 3.

samples by the difference in the transmission of one sample and a substrate. Effects of small pinholes in the substrate were negligible compared to the transmission through a sample. At present we have managed to overcome the experimental difficulty of measuring absorption coefficient of such a hygroscopic sample as KF by the subsequent evaporation of carbon thin film on the sample.

Characteristic of the reflection intensity of mica analyser crystal is showed in Fig. 1(a). An anomalous appeared near at 710 eV. In Fig. 1(b), the absorption coefficient of aluminum substrate is showed. It is clear that the effect of anomalous reflection and fluctuation of the incident X-ray almost disappeared. We obtained the fine structure of the fluorine K absorption spectra in alkali halide (LiF, NaF) and alkali-earth fluoride (MgF_2 , CaF_2 , SrF_2 , BaF_2). In Figs. 2 and 3 these spectra are showed, respectively. In the measured spectra the absorption peak positions and relative intensities were almost consistent with those obtained by Zimkina et. al [2].

-
- [1] A. Milgram and M. Paker Givens, Phys. Rev. 125, 1506 (1962).
 - [2] T. M. Zimkina and A. S. Vinogradov, Journal de Physique, 32, 278 (1971).

A HIGH-RESOLUTION X-RAY SPECTROMETER:
DESCRIPTION AND PRELIMINARY EXPERIMENTAL RESULTS

William C. Sauder
Department of Physics
Virginia Military Institute
Lexington, Virginia 23669

and

Robert E. LaVilla
Optical Physics Division
National Bureau of Standards
Washington, D.C. 20234

The availability of crystals of high perfection has made possible a variety of novel X-ray diffraction devices. For example, a single crystal machined into a form that would allow an X-ray beam to diffract successively from two different crystal planes has been proposed as a monochromator [1]. This monolithic monochromator is equivalent to a conventional X-ray double crystal spectrometer with a fixed inter-crystal dihedral angle. Calculations [1,2] have identified several near coincidences between wavelengths of prominent characteristic X-ray lines and the wavelength transmitted by some silicon and germanium monochromators. These calculations were carried out under the assumption that the beam lies in a plane perpendicular to the line of intersection of the diffracting planes (the so-called plane of dispersion). Very limited tuning of the characteristic wavelength is possible if the temperature of the monolith is changed.

The passband wavelength of such a device can be varied over a much larger range by varying the angle ψ between the incident beam and the plane of dispersion. One method of accomplishing this would be to rotate the monolith about an axis that simultaneously lies in the plane of dispersion and is perpendicular to the incident beam. The diffraction process can be visualized by representing it in reciprocal space as a vector tetrahedron defined by the wave vectors of the incident beam (\vec{k}_0), the beam travelling between the two diffracting planes (\vec{k}_1), and the exit beam (\vec{k}). The base of this tetrahedron, bounded by the reciprocal lattice vectors \vec{H}_1 and \vec{H}_2 of the diffracting planes and the vector $\vec{H} = \vec{H}_1 + \vec{H}_2$ is the plane of dispersion. From such a geometrical representation, it is straightforward to determine the tuned wavelength of the device:

$$\lambda = (\sin \alpha / \vec{H}) \cos \psi$$

where α is the angle between \vec{H}_1 and \vec{H}_2 and ψ is the angle between \vec{k}_0 (and therefore also \vec{k}_1 and \vec{k}) and the base plane. If one employs this device in an arrangement that allows ψ to be varied, then he has a monolithic (tunable) double crystal spectrometer (MDCS) that functions over a narrow wavelength range, but one that can have a large dispersion if ψ is sufficiently small.

The high dispersion of the MDCS makes this spectrometer suitable for the study of X-ray line shapes. In order to test this concept, we fabricated an MDCS from dislocation free silicon; the first and second Bragg diffractions were of the type $\bar{4}4\bar{4}$ and 111, respectively. By operating this MDCS so that ψ lay in the neighborhood of 9° , we were able to use it to examine the Cu $K\alpha_{1,2}$ spectrum from a commercial X-ray diffractometer tube. Previous observations [3,4] have shown this spectrum to consist of a pair of smooth but asymmetric lines, but our data show definite evidence of underlying structure. We attribute this structure to electric dipole transitions between the double vacancy states [$1s^13d^9\ 1,^3D \rightarrow 2p^53d^9\ 1,^3PDF$ and $1s^13p^5\ 1,^3P \rightarrow 2p^53p^5\ 1,^3SPD$]. In order to support this interpretation, we have carried out non-relativistic atomic model calculations for the positions and relative strengths of the multiplet transitions. We find that the principal features of the observed spectrum are predicted by the theoretical model.

We shall discuss (1) the experimental arrangement of the MDCS, (2) the reasons for the apparently greater resolution of the MDCS as compared to other double crystal spectrometers, and (3) the comparison of the experimental spectrum with the theoretical spectrum predicted by our model to determine the intensities and widths of the multiplet transitions.

References

1. R.D. Deslattes, Appl. Phys. Lett. 12, 133 (1968).
2. M. Hart, Rep. Prog. Phys. 34, 435 (1971).
3. For earlier work on the copper $K\alpha_{1,2}$ spectrum, see K. Tsutsumi and H. Nakamori, Proceedings of the International Symposium "X-ray Spectra and Electronic Structure of Matter", (Munich, 1972), V.1, p. 100 and references therein.
4. P.H. Citrin, P.M. Eisenberger, W.C. Marra, T. Åberg, J. Ultrainen and E. Kallne, Phys. Rev. B10, 1762 (1974).

HOLOGRAPHIC TRANSMISSION GRATINGS: A NEW ANALYSER IN THE X-RAY REGION

E.Källne, Los Alamos Scientific Laboratory, P.O.Box 1663, Los Alamos,
N.M.87545, USA

H.W.Schnopper, L.P.VanSpeybroeck, J.P.Delvaille, and A.Epstein,
Center for Astrophysics, HCO/SAO, Cambridge, Mass.02138, USA

R.Z.Bachrach, XEROX Research Centre, Palo Alto, Calif.94304, USA

J.H.Dijkstra and L.J.Lantwaard, Laboratory for Space Research, Utrecht,
The Netherlands

The low efficiency of high resolution analysers together with the problem of overlapping orders for grating instruments in the soft x-ray region has already limited the variety of experiments which are feasible. Holographic transmission gratings are made using the photolithographic technique previously employed for producing zone plates [1,2]. Although intended primarily for use in a grating spectrometer in the High Energy Astronomical Observatory HEAO-B for extra-solar x-ray astronomical studies the gratings will be available in the near future for laboratory applications. The gratings consist of a thin gold wire system supported by a fine and a coarse random structure. Since the thin wires are not opaque to x-rays in the region of anomalous dispersion it is of importance to measure the efficiency over a large wavelength region. The gratings can be constructed to achieve first order transmission as large as 25% in the region of anomalous dispersion. The potentially achievable resolution exceeds one part in 10^3 . Future tests are planned to determine the resolution experimentally and extend the efficiency measurements to higher energies.

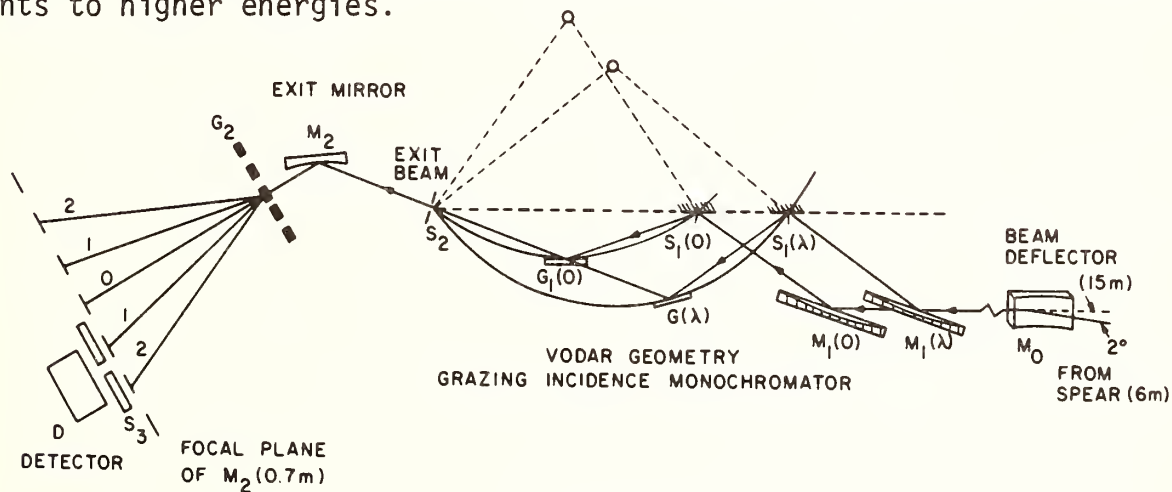


Fig.1

Fig.1 shows the apparatus for the grating tests. The tests were performed on the 4⁰ beam line of the Stanford Synchrotron Radiation Project[3]. The grazing incidence monochromator has been described earlier [4]. The exit mirror M_2 is adjusted for best focus on the 0.5mm entrance slit S_3 of a Mullard channel plate array located at a distance of about 70 cm from the grating. The detector can be scanned over the region of interest in the focal plane by a stepping motor. The detailed description of the experimental procedure as well as the theoretical

analysis of the data is described elsewhere [5]. Data were accumulated over the energy range 45-275 eV.

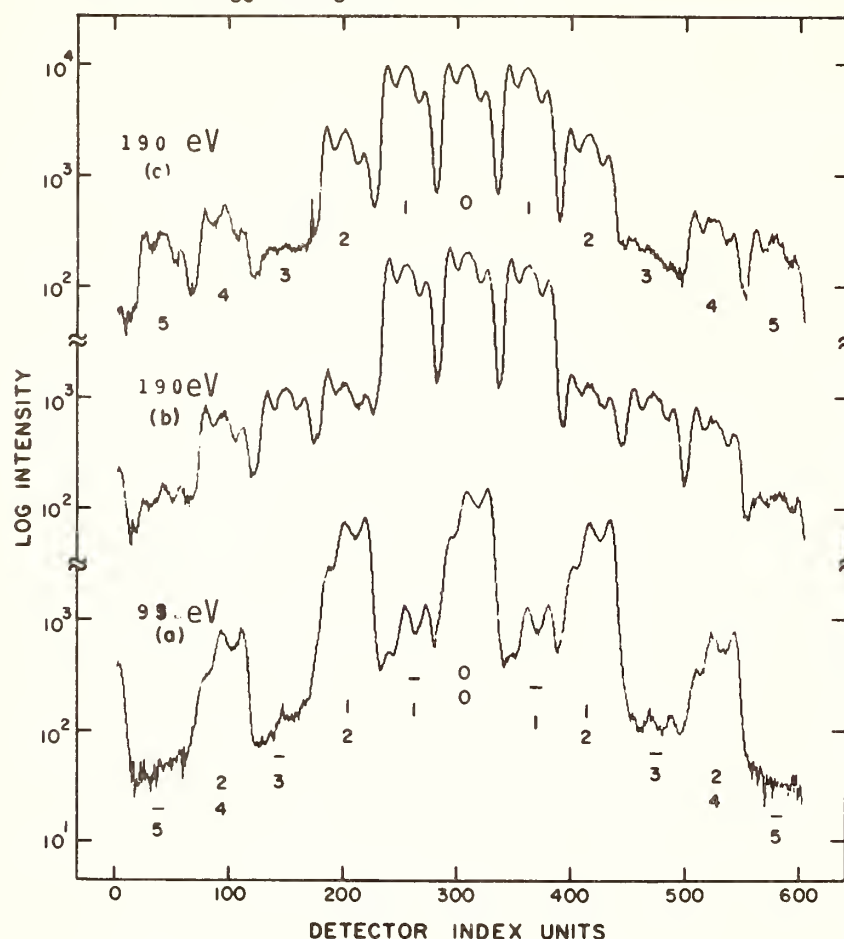


Fig.2

Several typical data scans are shown in Fig. 2 for two different gratings with 1000 l/mm. a) shows grating #1, $E=95\text{eV}$ in first order and $E=190\text{eV}$ in second order. In the labelling of orders the top numbers refers to 95eV and the lower one to 190 eV x-rays. b) grating #1, 190eV, little second order from the monochromator is present, c) grating #2, $E=190\text{eV}$. The difference in intensity relative to first order for orders two through five in c) when compared to the same orders in b) is indicative of a different fractional open grating spacing a/d for each grating. The broad structure of the zero order is attributed to the low quality focus of the exit mirror. A disturbing feature is the presence of second order from the monochromator which contributes to zero order from the test grating. Calibration data were taken by scanning the monochromator with the test grating in place at zero order and again with the grating removed from the beam.

The grating is modeled as an array of wires with rectangular cross sections. The number of counts received in a given order m as a function of photon energy (or wave number q) is calculated from the N-slit interference pattern which is modulated by the single slit diffraction pattern appropriate to the fractional slit opening a/d . The interference between the wave coming through the slit opening and the attenuated, phase-shifted wave coming through the wire is included in the calculation. By using previously measured values of the refractive index in this energy region [6], we have constructed curves of efficiency vs. photon energy based on the above model. Fig.3 shows the results of these calculations together with the experimental data. It is interesting to notice that the ratios in a) are energy dependent, which may be an indication of non-rectangular wire cross sections. Further development of the model of the grating in terms of a more complex wire cross section is in progress.

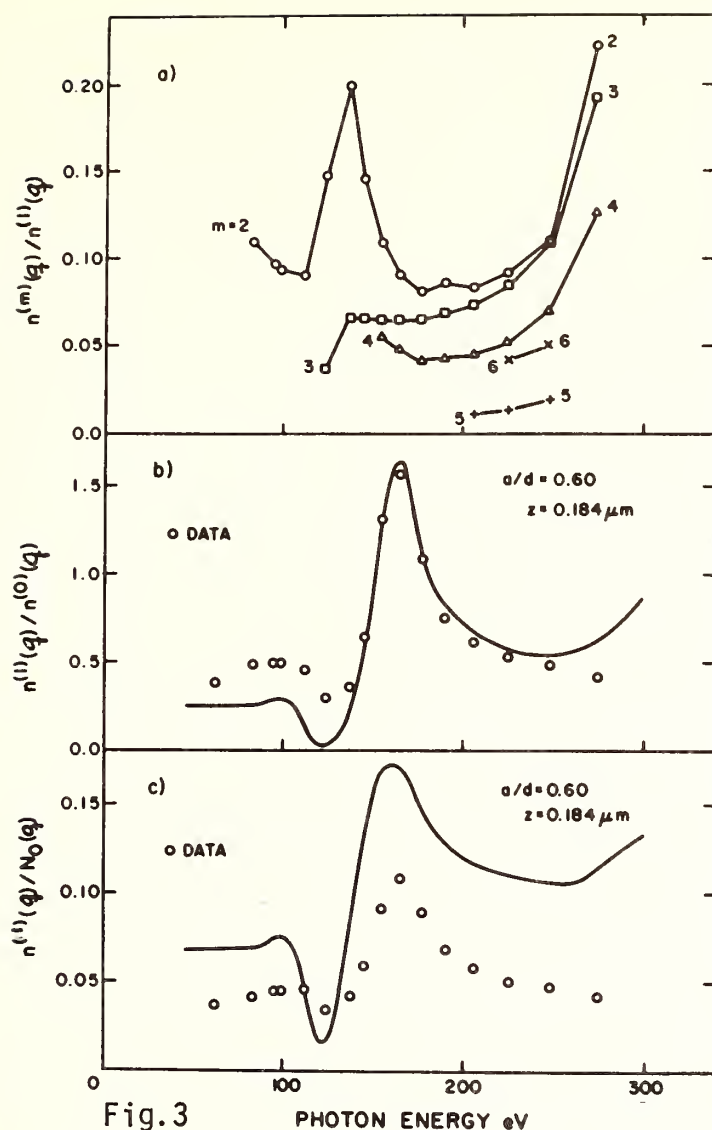


Fig.3

a) shows the relative efficiency of orders two through six compared to first order. b) gives the first order to zero order ratio values which can be used to obtain the grating thickness. c) gives the absolute efficiencies for the first order. The values in the experimental data may be low compared to the predicted values because of difficulties in obtaining absolute normalization to the incident beam. For future applications it is interesting to point out that the effects of the interference term between waves going through the slit opening and the waves coming through the wire can be used to advantage. A proper choice of grating material and thickness will minimize zero- and maximize first order transmission. In addition, even orders are cancelled when the slit opening and wire sizes are equal.

This research has been partially supported by NSF grant No. DMR 73-07692, in cooperation with SLAC and ERDA and by NASA contract NAS 8-30751.

1. Dijkstra, J.H., and Lantwaard, L.J., Optics Comm. 15,300 (1975)
2. Dijkstra, J.H., Space Science Instr. in press (1976)
3. Winick, H., in Vacuum Ultraviolet Radiation Physics, eds. E.E. Koch, R. Haensel and C. Kunz, Pergamon Vieweg, 1974, p. 776
4. Brown, F.C., Bachrach, R.Z., Hagström, S.B.M., Lien, N., and Pruett, C.H., in Vacuum Ultraviolet Radiation Physics, eds. E.E. Koch, R. Haensel and C. Kunz, Pergamon Vieweg, 1974, p. 785
5. Schnopper, H.W., VanSpeybroeck, L.P., Delvaille, J.P., Epstein, A., Källne, E., Bachrach, R.Z., Dijkstra, J.H., and Lantwaard, L.J., Proc. from International Workshop on Synchrotron Radiation Facilities, Quebec, Canada, June 1976
6. Hagemann, H.-J., Gudat, W., and Kunz, C., J. Opt. Soc. Am. 65,742 (1975)

I.A. Brytov, L.E. Mstibovskaya, N.I. Komyak and L.G. Rabinovitch
X-ray Institute
1, Stakhanovtsev, Leningrad, 195112
USSR

A vapor-jet source with a supersonic speed of the jet formed by an axisymmetric Laval nozzle has been developed. The source is placed into a vacuum chamber coupled with a PLASMA-type X-ray spectrometer [1]. To excite X-rays, a high-perveance three electrode electron gun is used.

The supersonic jet flowing out into vacuum has sharp boundaries within which a region of constant density and vapor speed is maintained.

Intensity assessment dictated by nozzle parameters, heating temperature of the metal to be analyzed and anode current is made for Dy $M\alpha$ band excited in atomic vapor. The intensity is calculated to be $10^{12} \frac{\text{quanta}}{\text{sec}}$, with allowance made for the spectrometer geometry and efficiency the recorded intensity should be $10^4 \frac{\text{quanta}}{\text{sec}}$ [2].

$M\alpha$ bands are obtained for Yb, Dy and Eu in vaporous and solid states.

$M\alpha$ -band width of atomic Yb is four times less than $M\alpha$ -band width of Yb in solid state. When passing from metal to atom, $M\alpha$ line shifts by 1.5 eV towards long wavelengths. The spectrum of atomic Yb reveals an extended short-wavelength structure. Similar differences are observed for Dy and Eu in vaporous and solid states.

A problem of multiatomic-particle/cluster/generation in a supersonic jet is discussed.

References

1. I.A. Brytov, M.C. Goldenberg, E.A. Oblenskii, N.I. Komyak et al Sbornyk, "Apparatura i metody rentgenovskogo analiza", vypusk XII, 3 SKB RA, Leningrad, Mashinostroenie (1973).
2. I.A. Brytov, L.E. Mstibovskaya, L.G. Rabinovitch, Izvestiya AN SSSR. Seriya phys. 40 (1976).

DETERMINATION OF THE DEPTH OF IMPURITY ATOMS IN BULK MATERIAL BY PROTON INDUCED X-RAYS

O. Benka, M. Geretschläger, A. Kropf and H. Paul
Institut Für Physik
J. Kepler Universität Linz
A-4045 Linz-Auhof, Austria

An attempt is made to determine the target composition by proton induced X-rays in the simple case of one layer of foreign atoms in a known bulk material. For this purpose, the X-ray yield $Y(E_1)$ is measured at various energies E_1 and at energies $E_1 - \epsilon$, where ϵ is taken as constant. If the foreign layer is infinitely thin, then its depth x_0 can be determined by comparison to a calibration function $f(E) = Y(E)/Y(E-\epsilon)$ measured beforehand on a pure sample of the foreign material, if the stopping power S_1 of the bulk material is known as a function of energy. If the layer is not infinitely thin, the depth can still be determined by iteration.

For proton energies E_1 of about 0.5 - 1 MeV we found a value $\epsilon = 0.2$ MeV to be most appropriate, if K-lines of elements with $Z \sim 30$ are to be measured. An error of about 5 keV in the energy loss $E_1 - E = S_1 x_0$ can be expected. To try the method, Ag-Cu-Ag and Ge-Cu-Ge sandwich targets were measured, with depths up to 1 mg/cm². For comparison, reference targets of all layers were prepared separately and measured by the backscattering technique. The deviations of the individual depth values measured by X-rays from the backscattering results were about 2-3% and hence consistent with the expected error. In addition, it was possible to determine the surface density of foreign atoms from the absolute X-ray yield.

The measured results can also be compared to yield ratios calculated by means of a computer program.

Because of the good elemental discrimination of the X-ray technique, this method can be applied in cases of nearby elements, and can thus give important information additional to that obtainable from backscattering analyses.

HIGH RESOLUTION L X-RAY EMISSION SPECTRUM OF ARGON

J. Nordgren, H. Ågren, C. Nordling and K. Siegbahn,
Institute of Physics, Uppsala University, Box 530,
S-751 21 Uppsala, Sweden.

Abstract. A high resolution L x-ray emission spectrum of gaseous argon has been recorded, using a holographic grating spectrometer at grazing incidence. The spectrum has considerably better resolution and contains a great deal more satellite lines than our previously reported spectra (1,2).

We have mounted a 3m-holographic grating with 2400 grooves/mm in our spectrometer at a grazing angle of 87° . Electrons of 10 keV were used for excitation and Kodak SC5 plates for detection of the x-rays. The holographic grating yields considerably higher dispersion than our former ruled grating. In fact, using a $10\text{ }\mu\text{m}$ entrance slit we obtain a width of the spectrometer function which is not greater than 50 meV in this energy region. This width is about one third of the natural width of the main x-ray lines. The energy calibration was made in second order against spark induced spectral lines from highly ionized silicon, aluminum and oxygen.

As can be seen in the figure the L_I line is rather broad, which is in accordance with the high Coster-Kronig decay rate of the L_I hole. The other two diagram lines, L_{II} and L_{III} , are separated by 2.148eV and their width is $\approx 0.19\text{eV}$.

Around 210 eV there is a group of satellite lines of considerable intensity. Some of these were observed in our previous spectrum and interpreted as $L_{2,3}\text{-M}$ x-ray transitions to the $3p^4nd(2S)$ states (see table I).

The main part of the lines in the spectrum are found on the high energy side of the L_{II}, L_{III} lines. Some of them can be attributed to transitions promoting an L-hole to the M shell while having a "spectator" hole in the M shell (see table I). A great deal of the lines are due to transitions in multiply ionized atoms created by Auger cascades from the $1s$ hole state, which the 10 keV impact electrons are likely to produce. This is supported by the observation that some of the lines are much narrower than the main lines and the fact that the fluorescence yield tends to increase with higher degree of ionization. The line energies are listed in table II.

As demonstrated in this work, grating spectrometers possess very high capabilities as resolution and energy measurements are concerned. Together with the straightforward dipole selection rules this makes soft x-ray grating spectroscopy a powerful tool for molecular (2) as well as atomic studies.

Reference

- 1/ L. Werme et al. C.R. Acad. Sc. Paris t279 (29 juillet-74).
- 2/ L. Werme et al. Z. Physik A272, 131-141 (1974).

ARGON L X-RAY EMISSION SPECTRUM

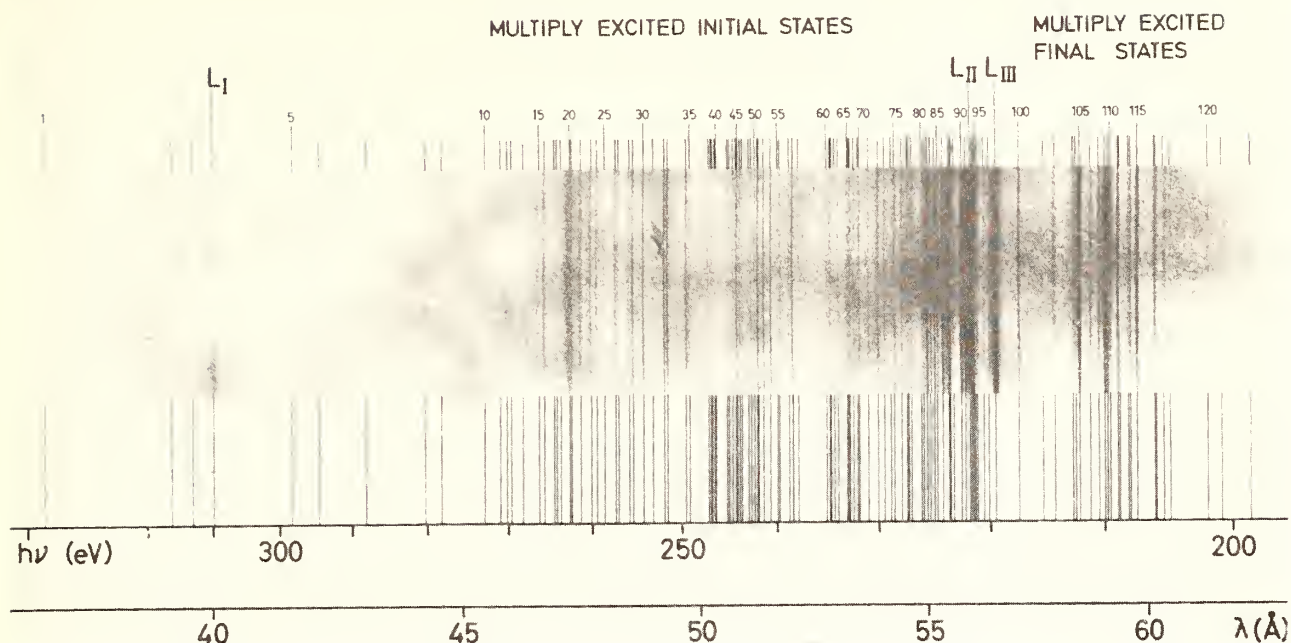


Table I

Energies and assignments of some of the Ar L x-ray lines

Line no	Energy (eV)	Assignment
4	309.64	$L_I - M_I$
84	224.899	$L_{II,III} M_{II,III} (^3P_1) - M_I M_{II,III} (^3P)$
85	224.590	$L_{II,III} M_{II,III} (^3P_0) - M_I M_{II,III} (^3P)$
86	224.142	$L_{II,III} M_{II,III} (^1S) - M_I M_{II,III} (^1P)$
87	223.563	$L_{II,III} M_{II,III} (^3D_1) - M_I M_{II,III} (^3P)$
88	223.468	$L_{II,III} M_{II,III} (^3P_2) - M_I M_{II,III} (^3P)$
90	222.408	$L_{II,III} M_{II,III} (^3D_2) - M_I M_{II,III} (^3P)$
91	222.079	$L_{II,III} M_{II,III} (^1D_2) - M_I M_{II,III} (^1P)$
92	221.537	$L_{II} - M_I$
93	221.405	$L_{II,III} - M_{II,III} (^3D_3) - M_I M_{II,III} (^3P)$
99	219.389	$L_{III} - M_I$
100	217.364	$L_{II,III} - M_{II,III} (^1P) - M_I M_{II,III} (^1P)$
105	212.144	$L_{II} - 3s^2 3p^4 3d (^2S)$
108	210.032	$L_{III} - 3s^2 3p^4 3d (^2S)$
110	209.548	$L_{II} - 3s^2 3p^4 4d (^2S)$
115	207.402	$L_{III} - 3s^2 3p^4 4d (^2S)$

Table II. Argon L x-ray energies. The accuracy is better than 10 meV for the main part of the lines.

Line no	Energy (eV)	Line no	Energy (eV)	Line no	Energy (eV)
1	336.20	42	245.039	83	225.233
2	315.67	43	244.648	84	224.899
3	313.06	44	244.408	85	224.590
4	309.64	45	244.250	86	224.142
5	298.43	46	243.948	87	223.563
6	294.77	47	243.682	88	223.468
7	288.10	48	243.021	89	223.193
8	280.29	49	242.760	90	222.408
9	278.43	50	242.407	91	222.079
10	272.55	51	242.118	92	221.537
11	270.922	52	241.975	93	221.405
12	270.135	53	241.486	94	221.276
13	269.586	54	240.766	95	221.111
14	268.206	55	240.058	96	220.968
15	266.371	56	239.811	97	220.452
16	265.667	57	238.940	98	219.976
17	264.415	58	238.584	99	219.389
18	264.143	59	237.883	100	217.364
19	263.563	60	235.152	101	214.818
20	262.752	61	234.849	102	214.358
21	262.509	62	234.689	103	212.647
22	261.449	63	234.394	104	212.464
23	260.272	64	234.034	105	212.144
24	259.604	65	233.158	106	211.232
25	258.729	66	232.939	107	210.556
26	257.473	67	232.702	108	210.032
27	257.214	68	232.517	109	209.804
28	255.944	69	232.162	110	209.548
29	255.514	70	231.972	111	208.967
30	254.345	71	231.071	112	208.852
31	253.308	72	230.175	113	208.111
32	252.048	73	229.561	114	207.937
33	251.674	74	228.904	115	207.402
34	249.629	75	228.599	116	205.952
35	249.300	76	227.946	117	205.788
36	247.273	77	227.474	118	205.198
37	246.999	78	227.309	119	204.695
38	246.814	79	227.005	120	201.815
39	246.579	80	226.052	121	200.707
40	245.572	81	225.871	122	198.435
41	245.283	82	225.579	123	194.565

THE USE OF LONG WAVELENGTHS FOR LOW-ANGLE SCATTERING

Yasuo SIOTA and Mamoru YOKOTA

Research Institute for Science Education, Miyagi
Univ. of Education, Aramaki, Aoba, Sendai, Japan

This report concerns with both our present work of low-angle X-ray scattering with long wavelengths and future use of synchrotron radiation as a very intense source of light for low-angle scattering with long wavelengths.

Several important advantages are gained. First, the effects of multiple scattering and refractions become small for long wavelengths. Second, owing to the large angle of scattering, an accurate determination of the central portion of the scattering pattern is possible and an important information about large particles is obtained. Third, low-angle scattering due to double Bragg reflections [1] could be removed by using long wavelengths. Finally, the use of long wavelengths suppresses the continuous background radiation against the characteristic radiation proportional to the atomic number of the target in an X-ray tube. Few workers [2],[3] have tried investigations in a long wave length region. Perhaps this is due to the necessity of hard working in a vacuum, low intensity of scattered X-ray and high absorption by the sample.

We have studied the low-angle X-ray scattering by polystyrene latex spherical particles and succeeded in obtaining several well-resolved peaks of higher orders. Close agreement between observed and calculated curves was obtained.

The source was an Al or C tube of Pierce type. For recording, a Kodak SWR-plate or a proportional counter was used. The counter was followed by a pulse height discriminator in connection with automatic scanning and recording devices. A special attention was paid for sample preparation.

Figs.1 and 2 represent observed and slit-corrected scattering curves (4) of polystyrene latex of diameter 0.234μ with Al-K radiation and of 1.011μ with C-K radiation, respectively. The numbers labelled by $K=2,3,4$ correspond to the orders of the peak positions of the intensity maxima calculated in the Rayleigh-Gans theory for a uniform sphere. An

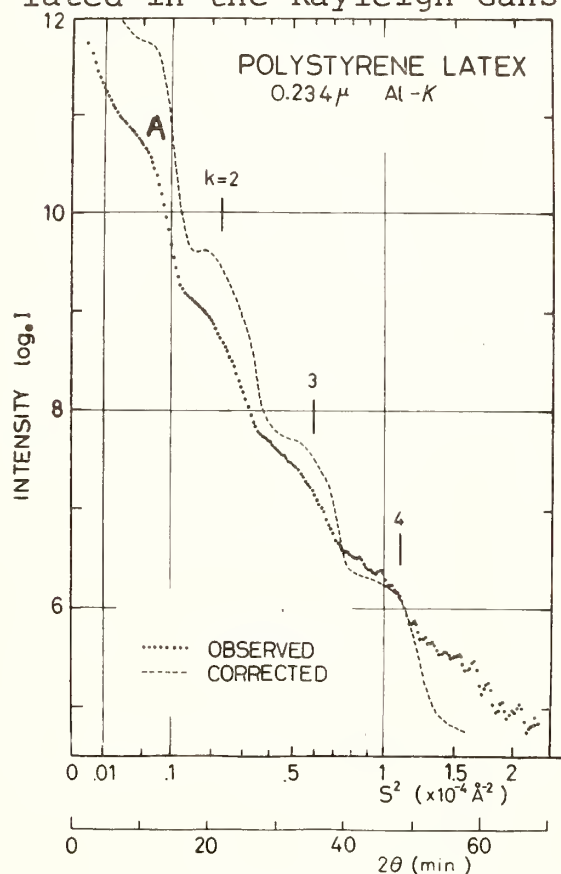


Fig.1. Curves of polystyrene latex of diameter 0.234μ with Al-K radiation.

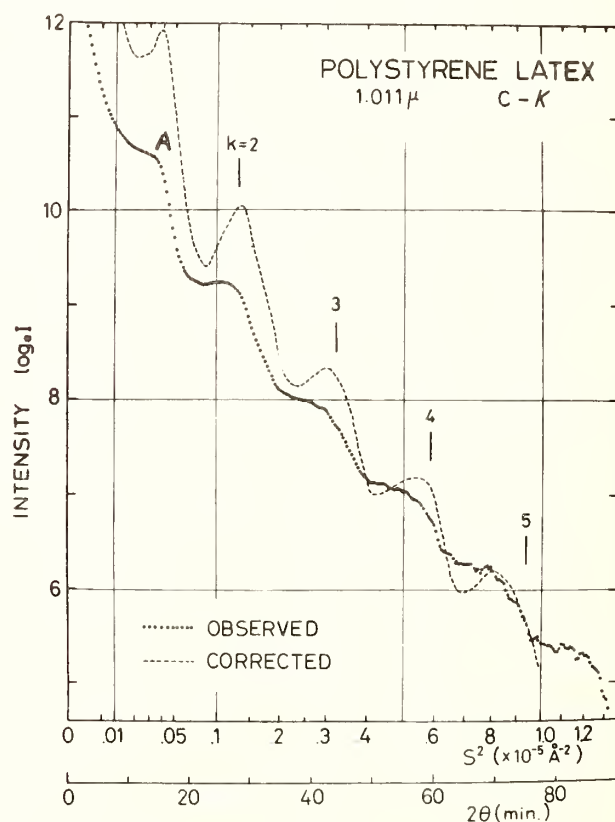


Fig.2. Curves of polystyrene latex of diameter 1.011μ with C-K radiation.

additional peak A is caused by interparticle interference (5), which was clearly observed by using long wave-lengths.

There is a limit in sampling times, in spite of a high power X-ray tube and a high sensitive detector. We are now planning to use synchrotron radiation from a 1.3 BeV electron synchrotron at the Institute for Nuclear Study, University of Tokyo, for the low-angle scattering with long wavelengths in a range of $50 \sim 100 \text{ \AA}$. The application of synchrotron radiation to low-angle scattering has been made at DESY (6).

A grazing-incidence spectrograph with high resolution is used. Experiment at any desirable wavelengths is possible by moving a slit on the Rowland circle continuously. First, we will investigate the same sample as studied by our X-ray tube. Details of experimental arrangements and technical considerations will be reported in the conference.

The authors appreciate ES-Machine group and INS-SOR group at the Institute for Nuclear Study, University of Tokyo, for their assistance. They are also greatly indebted to the Institute for Solid State Physics, University of Tokyo.

References

- (1) A.Franks and K.Thomas, Proc.Phys.Soc. B. 71, 861 (1958).
- (2) K.L.Yudowitch, J.App.Phys. 20, 174 (1949).
- (3) B.Henke and J.W.M.DuMond, Phys.Rev. 89, 1300 (1953).
- (4) J.Soller and J.Baldrian, J.App.Cryst. 7, 398 (1974).
- (5) U.Bonse and M.Hart, Z.Phys. 189, 151 (1966).
- (6) J.B.Leigh and G.Rosenbaum, J.App.Cryst. 7, 117 (1974).

X-RAY DETECTION FOR MEASUREMENT OF INNER SHELL IONIZATION BY RELATIVISTIC ELECTRON IMPACT*

H. Genz, D.H.H. Hoffmann, W. Löw and A. Richter
Institut für Kernphysik, TH Darmstadt, 61 Darmstadt, Germany

The measurement of the absolute yield of characteristic x rays emitted from a target bombarded by particles has become one of the major techniques in the determination of inner shell ionization [1,2]. Electron induced ionization has predominantly been restricted to K-shell ionization at nonrelativistic and ultra relativistic energies [3]. The lack of data in the intermediate range has now been overcome by measuring the K and L x-ray production cross section between 15 and 70 MeV [4-6]. The present work is motivated by this lack of data, by the lack of fully relativistic theories and by the speculation of a possible scaling behaviour of the cross section.

In the present work we report on the first L x-ray production cross section for energies between 15 and 70 MeV with electrons from the Darmstadt linear accelerator (DALINAC). The recent considerable improvements of its beam quality and transport system [7] enable x-ray detection at low background. The electron beam impinged on thin self supporting targets of Au and Bi ($\approx 200 \mu\text{g}/\text{cm}^2$) inside a scattering chamber and was then collected by a magnetically suppressive Faraday cup located about 5.3 m downstream. The produced x rays were detected with a Si(Li) detector. By means of a $20 \mu\text{m}$ Al foil placed between target and detector M-shell x rays were hindered from reaching the detector. For the measurement of the angular distribution of the emitted photons the detector can be placed under 14 angles from 45° to 165° . In order to avoid pile-up of two events due to the detection of two x rays within a single machine pulse of $6 \mu\text{s}$ duration every second photon detected within this time interval was electronically rejected. The beam current was kept at about 0.6 nA (i.e. 3×10^7 electrons per linac pulse) corresponding to about 0.1 detected event per machine pulse. A typical L-shell x-ray spectrum obtained by bombarding a Bi target with 60 MeV electrons is shown in fig. 1. The spectrum clearly exhibits a low and flat background. The solid line represents a fit of several asymmetric Gaussians to the data points after subtraction of the background.

The total cross section for L-shell ionization is determined from

$$\sigma_{\text{TOT}} = \sum_i N_i / [N_0 t \bar{\omega}_L \varepsilon(\Delta\Omega/4\pi)], \quad (1)$$

where N_i is the number of i-subshell photons corrected for absorption in the target, absorber and window of the scattering chamber, N_0 the number of incident electrons, t the target thickness in atoms/cm^2 , $\bar{\omega}_L$

✕

Supported in part by Deutsche Forschungsgemeinschaft

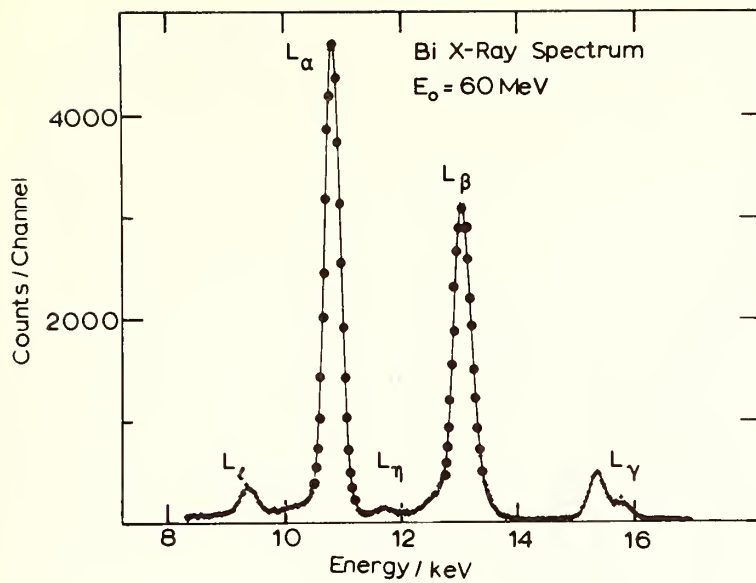


Fig. 1 L-shell x-ray spectrum observed with a Si(Li) detector by bombarding a Bi target with electrons of $E_0 = 60 \text{ MeV}$

the average L-shell fluorescence yield [8], ϵ the detector efficiency and $\Delta\Omega$ the solid angle subtended by the detector. The first results on the L-shell ionization cross section for Bi are shown in fig. 2 together with the values by Park et al. [9] at much lower and by Middleman et al. [10] at much higher electron energies. The solid line represents a theoretical prediction by Gryzinski [11]. It is interesting to note that the cross sections do not scale when plotted in the form suggested by this theory, i.e. $\sigma_{\text{TOT}} \propto I^2$ versus E_0/I , I being the aver-

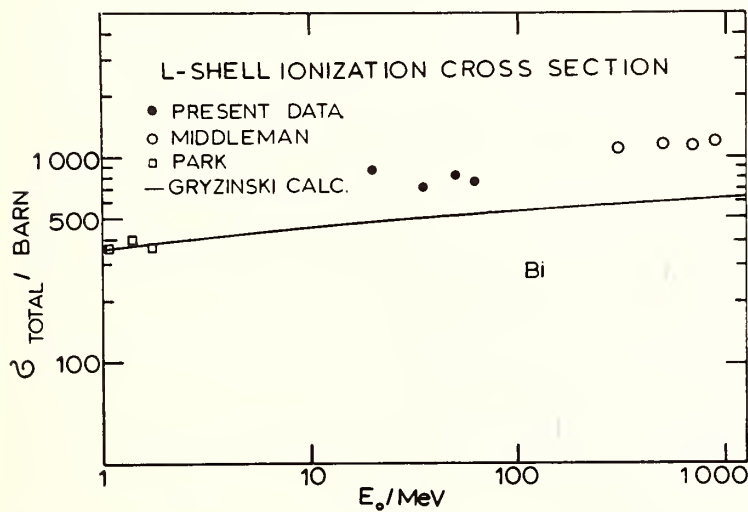


Fig. 2 L-shell ionization cross section for Bi with theoretical prediction [11]

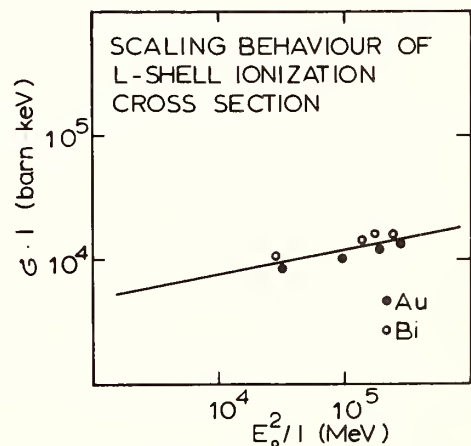


Fig. 3 L-shell ionization cross section in the σI vs E_0^2/I representation

age L-shell ionization energy, but they do scale in the form $\sigma_{\text{TOT}} \cdot I$ versus E_0^2/I . They then exhibit the same "scaling behaviour" (fig. 3) as observed for the K-shell [4].

The L_β/L_α ratio of x rays from Bi and Au has been measured at $E_0 = 60$ MeV. The result for the case of Bi is plotted in fig. 4 together with the values obtained from ref. [9] and [10]. There is clearly an increase of the ratio by about 14% over the considered energy region. This might be explained qualitatively by the fact that L_β x-rays result predominantly from 3p-2s and L_α from 3d-2p transitions. Because of their spatial extension 3d electrons are stripped off preferably to 3p with increasing bombarding energies and then L_β/L_α should also increase [12].

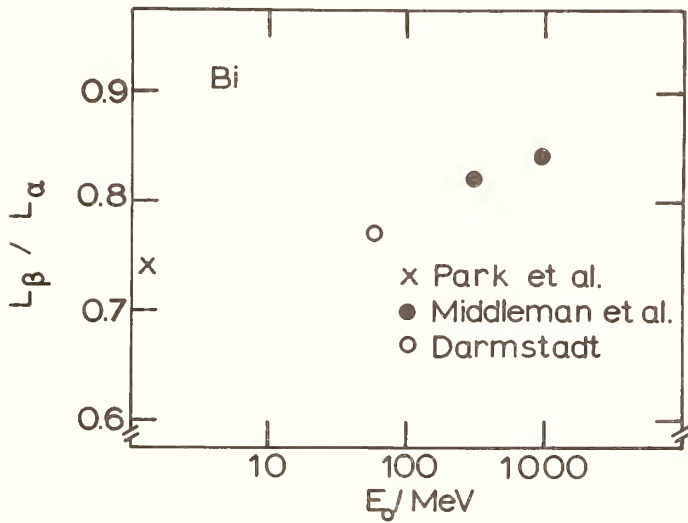


Fig. 4 L_β/L_α ratio versus bombarding energy

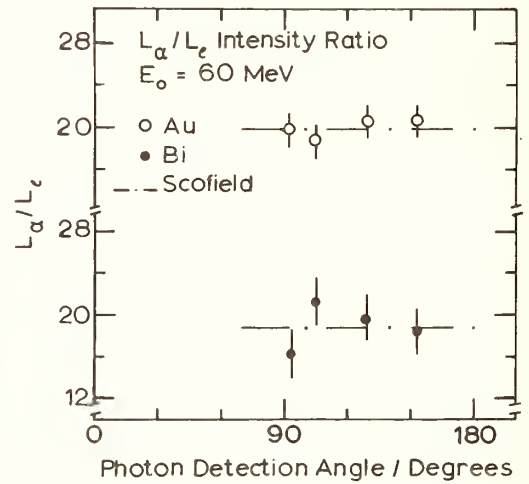


Fig. 5 Angular distribution of the L_α/L_l ratio

Figure 5 displays a preliminary angular distribution of the L_α/L_l ratio as obtained at four different angles together with a relativistic Hartree-Fock model prediction [13]. This prediction assumes isotropy of the ratio. The experimental angular distribution is indeed isotropic within 8%, the uncertainty still being large at present. Table 1 lists the measured L_α/L_l ratios for Au using different experimental methods of creating L-shell vacancies as well as the calculations by Scofield. Apart from the values of the measurement of ref. [16] there is an overall agreement between all ratios.

Finally, the spectra have been investigated for possible energy shifts of x-ray lines. Therefore the peak positions in the spectra have been compared with a careful calibration using standard low energy x-ray sources. In the case of Ag for example we detected an average energy shift for K_α lines of about 150 eV. This might reflect

effects of multiple ionization seen also in the production of x rays by heavier particles.

TABLE I

L_{α}/L_{ℓ} ratios of Au

X-ray fluorescence [14]	Proton bombardment [15]	Electron bombardment 25 keV 60 MeV [16]		Theory [13]
18.72 ± 1.2	19.7 ± 1.0	25.25 ± 3.0	19.9 ± 1.1	19.8

We should like to thank Drs. Folkmann and Liesen from GSI for the kind loan of the Si(Li) detector.

- [1] C.J. Powell, Rev. Mod. Phys. 48 (1976) 33
- [2] D.H. Madison and E. Merzbacher, in Atomic Inner-Shell Processes, B. Crasemann, ed., Acad. Press, Inc., New York (1975), p. 11
- [3] Proc. Second Int. Conf. on Inner Shell Ionization Phen., Freiburg 1976, ed. R. Brenn and W. Mehlhorn, Fakultät für Physik, Universität Freiburg
- [4] H. Genz, D.H.H. Hoffmann, A. Richter and E. Spamer, ref. [3] Abstracts p. 229
- [5] S. Morita, ref. [3]
- [6] D.H. Madison, ref. [3]
- [7] H. Miska, H.D. Gräf, A. Richter, R. Schneider, D. Schüll, E. Spamer, H. Theissen and O. Titze, Phys. Lett. 58B (1975) 155
- [8] W. Bambynek, B. Crasemann, R.W. Fink, H.U. Freund, H. Mark, C.D. Swift, R.E. Price and P.V. Rao, Rev. Mod. Phys. 44 (1972) 716
- [9] Y.K. Park, M.T. Smith and W. Scholz, Phys. Rev. A12 (1975) 1358
- [10] L.M. Middleman, R.L. Ford and R. Hofstadter, Phys. Rev. A2 (1970) 1429
- [11] M. Gryzinski, Phys. Rev. A138 (1965) 336
- [12] B. Crasemann, private communication
- [13] J.H. Scofield, Phys. Rev. A10 (1974) 1507
- [14] J.H. McCrary, L.V. Singmann, L.H. Ziegler, L.O. Loomey, C.M. Edmonds and C.E. Harris, Phys. Rev. A5 (1972) 1587
- [15] J.R. Chen, J.D. Reber, D.J. Ellis and T.E. Miller, Phys. Rev. A13 (1976) 941
- [16] S.I. Salem, D.C. Clark and R.T. Tsutsui, Phys. Rev. A5 (1972) 2390

Two regular Kossel lines have been observed in germanium crystal with wavelengths of 1.134 and 1.246 Å due to germanium $K\beta_1$ and $K\alpha_{1,2}$ radiation. Two additional Kossel-type lines on the low energy side of germanium $K\alpha_{1,2}$ with wavelengths 1.391 and 1.544 Å have also been observed. The energy of these newly observed lines correspond to the kinetic energies of the Auger electrons of germanium involving K and L levels. The newly observed radiation is characterized by the following properties: (i) a non-linear rise in intensity with pumping, (ii) anomalous mass absorption coefficient in aluminum and silicon so far studied, (iii) preliminary results reveal an unusually narrow fundamental width of the newly observed lines.

Kossel cones of semi-vertical angle α are generated in good single crystals due to internal Bragg interference of characteristic x-ray lines of the atoms of the crystal by sets of lattice planes (hkl) given by the equation $2\cos\alpha = \lambda |r(hkl)|$. The axis of the Kossel cone is the direction of the reciprocal lattice vector $r(hkl)$. Borrmann effect is characterized by an anomalous transmission, that is a low mass absorption coefficient μ/ρ , when a collimated beam of x-rays is set at the Bragg angle for a set of lattice planes of the crystal. In studying Kossel lines from germanium single crystal, the mass absorption coefficients μ/ρ for germanium $K\beta_1$ and $K\alpha_{1,2}$ radiation of wavelengths 1.129 and 1.256 Å respectively were expected to be absorbed by the germanium crystal of thickness 1.2 mm. I have observed strong Kossel lines K_1 and K_2 , Fig. 1 (a), (b), and (c), due to germanium 1.129 and 1.256 Å in crystals of thicknesses 1.2-1.3 mm. The crystal is cut parallel to (111) planes and is excited by x-rays from silver, molybdenum, copper, and cobalt target radiation in different sets of experiments. Kossel lines K_1 and K_2 were observed with target radiation at 20, 25, 30, 35, and 40 keV and tube currents between 30-10 mA. Because of the high penetrability of Kossel lines K_1 and K_2 through thick germanium crystal, these lines have been designated as Kossel-Borrmann lines. In addition to the lines K_1 and K_2 , I have observed two more Kossel-Borrmann type lines A_1 and A_2 , Fig. 1 (a), (b), and (c), of longer wavelengths than germanium $K\alpha$ lines. The lines A_1 and A_2 have been observed in different sets of experiments when germanium crystal was irradiated by the target radiation from silver, molybdenum, copper, and cobalt operated at 20, 25, 30, 35, and 40 keV and tube currents 30-10 mA. Some of these preliminary results using copper target radiation as the exciting source have been reported.[1]

It has been established by a series of experiments with more than 20 different pieces of germanium crystals that the new type of Kossel-Borrmann lines A_1 and A_2 are generated in the germanium crystal and not at the target of the x-ray tube that excites the crystal. We have measured the increase in intensity of the unusually strong portion of A_1 and A_2 lines at the terminal with increase of the x-ray tube current from molybdenum target that excites the germanium crystal radiation. We have observed a non-linear rise in intensity of A_1 and A_2 with increase

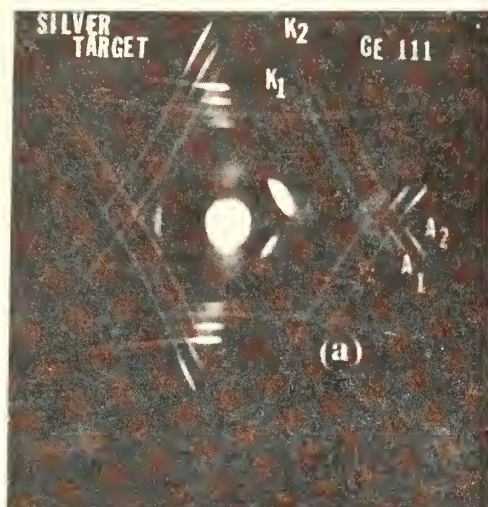


Fig. 1(a) Silver Target
30 kV, 20 mA
15 hrs. exposure

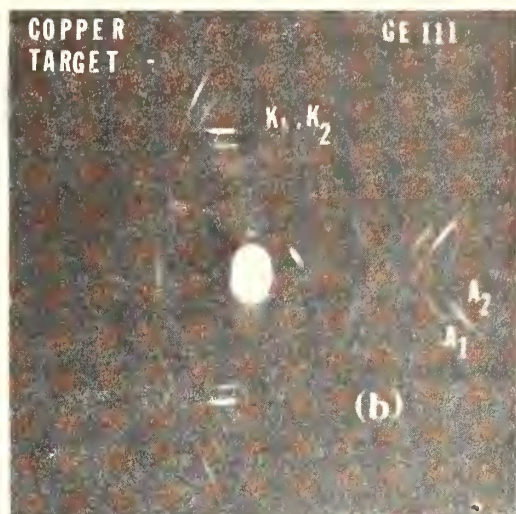


Fig. 1(b) Copper Target
35 kV, 10 mA
20 hrs. exposure

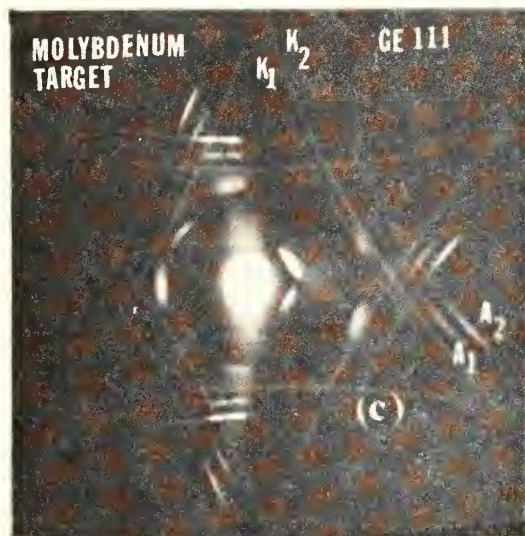


Fig. 1(c) Moly Target
35 kV, 15 mA
10 hrs. exposure

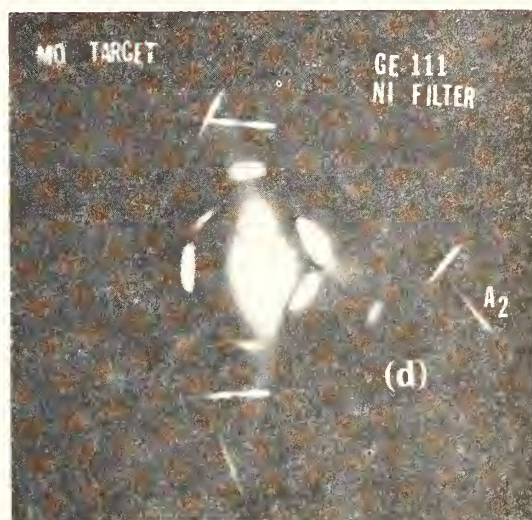


Fig. 1(d) Moly Target with
Nickel Filter
35 kV, 15 mA
15 hrs. exposure

Fig. 1(a), (b), and (c): Kossel-Borrmann lines K_1 , K_2 and Kossel-Borrmann type lines A_1 , A_2 from Ge {220} planes. The collimated beam of x-rays from the target strikes normally the Ge crystal of thickness 1.2 mm cut parallel to (111) planes.

Fig. 1 (d): Kossel-Borrmann lines K_1 , K_2 , and Kossel-Borrmann type lines A_1 are absorbed with a 0.015 mm thick nickel filter.

of the tube current. We have checked at the same time that the intensity of $K\alpha$ radiation from molybdenum monochromatised with a silicon crystal increases linearly with increase of the tube current. Preliminary results with a multi-channel analyzer reveal an unusual narrowing of A_1 and A_2 , similar to the narrowing of lines reported earlier by Das Gupta.[2]

In a series of experiments, I have studied, in collaboration with Peter Seibt and James White, the mass absorption coefficients of A_1 and A_2 with aluminum and silicon filters. The values of μ/ρ are suprisingly low by a factor of 40-50. This work is currently being continued with an energy sensitive detector and generating A_1 and A_2 at various potentials of the x-ray tube that excites germanium crystal radiation. I have reasons to believe that Auger electrons from germanium involving K and $L_{2,3}$ levels and K and L_1 levles could generate Kossel type electron cones in germanium crystal with the same set of $\{220\}$ lattice planes. In earlier papers [3,4] I have tried to explain the origin of low energy satellites in soft x-ray band spectra from solids to be due to a radiative Auger-Raman process in crystals. An understanding of A_1 and A_2 lines as a stimulated Kossel-Borrmann radiative Auger-Raman process will be reported in a separate article.

*This work has been supported by the Robert A. Welch Foundation and the Air Force Office of Scientific Research.

[1] K. Das Gupta, J. Appl. Phy., 47, 2765, (1976).

[2] K. Das Gupta, Phys. Letters, 46A, 179, (1973).

K. Das Gupta, Colloquium Spectroscopicum Internationale XVII, II, 482, (1973).

[3] K. Das Gupta, Nature, 166, 563, (1950).

[4] K. Das Gupta, Nature, 167, 313, (1951).

THEORY AND MEASUREMENT OF X-RAY DIFFRACTION
FROM SEVERAL ACID PHTHALATES

D. M. Barrus, R. L. Blake, and A. J. Burek*

University of California, Los Alamos Scientific Laboratory

P. O. Box 1663, MS 436

Los Alamos, New Mexico 87545

Acid phthalate crystals have been widely used in the laboratory and cosmic x-ray spectroscopy because of their large interplanar spacings, reasonable diffraction properties, and availability in large sizes with good quality. Liefeld (1) evaluated KAP by double spectrometer measurements, after which this crystal was widely used. Burek, Barrus, and Blake (2) - prompted by concern that variations among samples could limit the validity of higher precision measurements - studied several samples of KAP from several sources and under a variety of experimental conditions. They found only minor variations among samples. For practical purposes all KAP without obvious visible flaws could be considered the same. Nevertheless we were keenly aware of the need for some analytical guidelines for the evaluation of additional crystals, especially for long wavelength x-ray spectroscopy where we were unable to find any application of diffraction theory in the literature. Elimination of this deficiency was undertaken (2,3) with results that have been gratifying not only for KAP but also for several other crystals of importance in soft x-ray studies.

The basic theory of x-ray diffraction in crystals has been available for a long time (4). Successful application to long wavelengths (5-25 Å) is critically dependent upon knowledge of the ultrasoft x-ray absorption coefficients for atoms in the crystal structure, especially near the edge frequencies because anomalous dispersion dominates the diffraction properties. We have now extended both the calculations and measurements to several additional crystals. In this report results will be given for the most readily available acid phthalates and some interesting properties will be noted. Calculations far more extensive than shown here are available on request.

The table summarizes the calculated and average-measured values of the single crystal coefficient of reflection, R_c , at characteristic line wavelengths. All calculated values are from Darwin-Prins theory. For each order of reflection the upper number is the calculated R_c and the bottom number is the measured value, with error estimate replacing the power of 10 designation. Quoted errors are estimates of upper bounds to systematic effects - statistical errors being negligible. Individual specimens can vary outside these limits due to poor production or handling procedures. KAP shows excellent agreement over a wide wavelength range and three orders of reflection. When reflection coefficients are small the calculated values are very sensitive to small errors in atomic locations and measurements are sensitive to systematic errors; hence, agreement within a factor two should be considered good when $R_c < 10^{-5}$. RAP shows good agreement in three orders of Al(K) but the measured values fall below calculated values at longer wavelengths. This probably means the Rb absorption coefficients at long wavelengths are larger than our input values. We believe this same factor is responsible for the excess of calculated values for TlAP, the effect in this case reaching all the

way down to 8 Å. Uncertainties inherent in our present knowledge of anomalous dispersion effects combined with uncertain absorption coefficients in Rb and Tl are sufficient to account for any discrepancy presently found between calculated and measured values. Note the good agreement between calculated and measured values from KAP, NaAP, and NH₄AP in three orders of reflection.

When displayed graphically against complete calculated curves the measurements show remarkably good agreement. However, it has long been known that rocking curve profiles and peak reflection coefficients provide far more sensitive tests of the quality of crystals for spectroscopy. Unfortunately our laboratory facilities do not include a double crystal instrument required for such measurements. In order to achieve at least a qualitative evaluation of acid phthalate rocking curve widths we employed the Ne 1s→3p absorption line technique suggested by Liefeld (5). The figure shows this sharp-line profile measured with nominal one arc minute FWHM collimation of the Ni Lβ line passed through a Ne absorption cell and diffracted from KAP, RAP, and TlAP. Detailed comparison shows KAP resolving power very slightly superior to RAP as predicted by calculations. TlAP has such poor resolving power that the line is hardly distinguishable, also in agreement with theory. NaAP and NH₄AP are not suited to this technique.

Some conclusions to be drawn from this work are as follows. RAP, because it has twice the reflectivity of KAP and nearly equal resolving power, should replace KAP as a standard for general spectroscopy. For quantitative analysis where reflectivity is most important TlAP is far superior at all useful wavelengths. Both RAP and TlAP have good ratios of first to all higher order reflections. NH₄AP has the interesting property that the second order R_c exceeds the first order by a factor two or more from 15 to 60 degrees of theta angle, and above 68 degrees. It is particularly useful for high dispersion measurements around 12 Å. We have been able to resolve the solar NeX resonance doublet with this crystal in a rocket experiment.

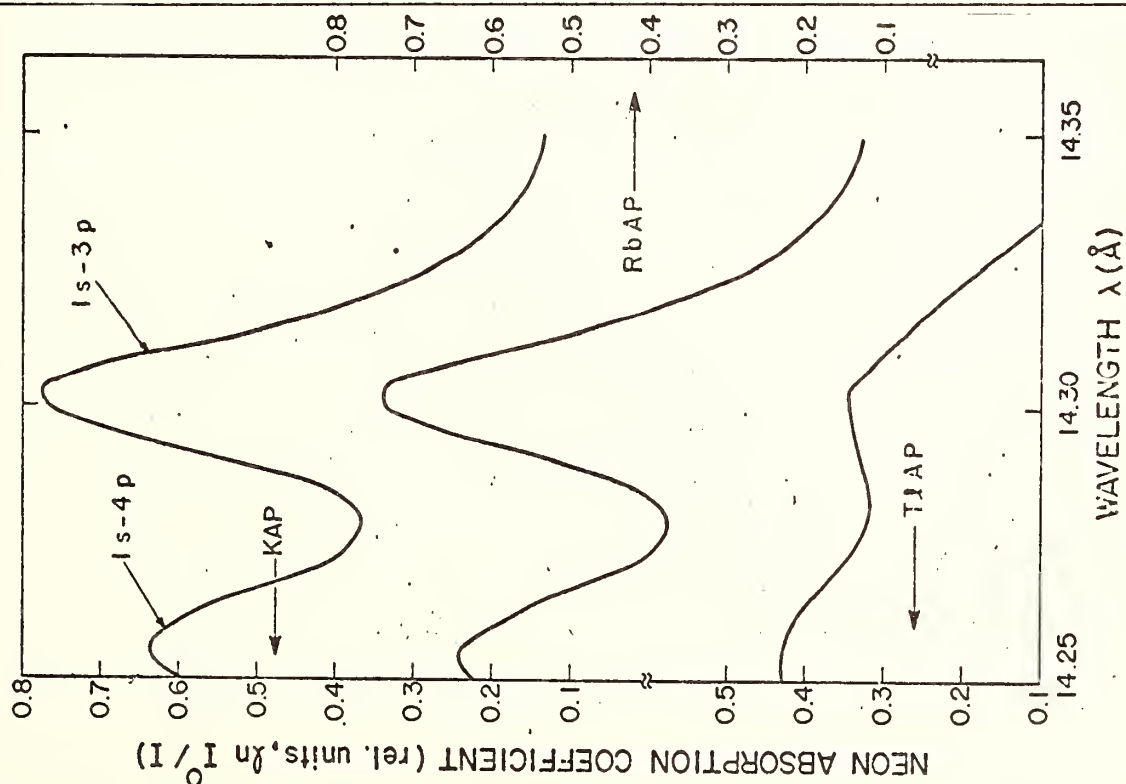
References

1. Liefeld, R. J. Hanzely, S., Kirby, T. B. and Mott, D. 1970, *Advances in X-Ray Analysis*, 13, 373 (results were general knowledge as early as 1963).
2. Burek, A. J., Barrus, D. M. and Blake, R. L. 1974, *Ap. J.*, 191, 533.
3. Burek, A. J. 1976, *Space Science Instrumentation*, to be published.
4. Batterman, B. W. and Cole, H. 1964, *Rev. Mod. Phys.*, 36, 681.
5. Liefeld, R. J. 1965, *Appl. Phys. Ltrs*, 7, 267.

*Work performed under the auspices of the U.S. Energy Research and Development Administration.

CALCULATED AND MEASURED R_c OF ACID PHTHALATE CRYSTALS

WAVE- LENGTH (Å)	KAP (001)	RbAP (001)	TlAP (001)	NaAP (002)	NH ₄ AP (002)	ORDER n
1.54	3.14×10^{-5} 3.59±5%	6.19×10^{-5} -----	1.20×10^{-4} -----	2.76×10^{-5} -----	8.59×10^{-6} -----	1
	1.92×10^{-6} 1.88±5%	9.97×10^{-6} -----	3.67×10^{-5} -----	3.57×10^{-6} -----	1.36×10^{-6} -----	2
	3.15×10^{-7} -----	7.85×10^{-6} -----	2.08×10^{-5} -----	2.16×10^{-6} -----	1.92×10^{-6} -----	3
8.34	7.93×10^{-5} 8.45±2%	1.04×10^{-4} 1.10±2%	2.56×10^{-4} 2.79±2%	6.15×10^{-5} 6.21±2%	1.12×10^{-5} 1.12±2%	1
	3.46×10^{-6} 3.27±4%	3.97×10^{-7} 2.94±4%	3.45×10^{-5} 3.59±4%	3.17×10^{-6} 3.39±4%	2.63×10^{-5} 2.58±4%	2
	2.40×10^{-8} 4.41±6%	7.87×10^{-6} 4.83±6%	1.15×10^{-4} .906±6%	3.42×10^{-6} 5.75±6%	6.26×10^{-6} 7.35±6%	3
14.6	5.77×10^{-5} 5.49±5%	1.16×10^{-4} -----	2.39×10^{-4} -----	3.30×10^{-5} -----	6.09×10^{-6} -----	1
18.3	5.04×10^{-5} 5.21±2%	1.11×10^{-4} .896±2%	2.57×10^{-4} 2.00±2%	2.53×10^{-5} 2.67±2%	4.86×10^{-6} 5.20±3%	1
21.7	5.35×10^{-5} 5.61±10%	1.34×10^{-4} -----	3.65×10^{-4} -----	1.90×10^{-5} -----	9.12×10^{-6} -----	1
23.6	1.43×10^{-5} 1.78±4%	1.21×10^{-4} .733±4%	5.23×10^{-4} 2.81±4%	2.77×10^{-5} 2.94±4%	6.02×10^{-5} 6.66±4%	1
24.3	2.87×10^{-5} 2.85±15%	2.13×10^{-4} -----	7.63×10^{-4} -----	1.10×10^{-5} -----	3.36×10^{-5} -----	1



Relative absorption coefficient of Ne using crystals of KAP, RAP, and TlAP.

A SPECTROGRAPH FOR STUDIES OF HIGH SPEED DISCHARGE

B. Sundbom and S.K. Händel

Institute of Physics, University of Uppsala,
Box 530, S-751 21 UPPSALA, Sweden

Abstract. A spectrograph using the convex de Broglie configuration designed for studies of high speed discharges in vacuum, plasma, wire etc. has been developed. The instrument covers the spectral range 1-17 Å and can also be supplied with a time resolving equipment. Spectra from flash X-ray (FXR) discharges are recorded and will be discussed.

Introduction. The discharge mechanism of FXR discharges has been studied at this institute during the last decade. In these studies the X-ray bursts have shown to be very important for the understanding of the transient discharge mechanism. However, no studies of the spectral distribution have been carried out. Therefore, we have developed a spectrograph in which we have used the simple but rarely practised spectroscopic geometry suggested by de Broglie in 1914 (1). With this geometry a large spectral range could be recorded simultaneously during one discharge.

Spectrograph Design. In the convex de Broglie configuration one utilizes the crystal bent to a very small radius of curvature, Fig.1, compared to that in a conventional concave spectrograph.

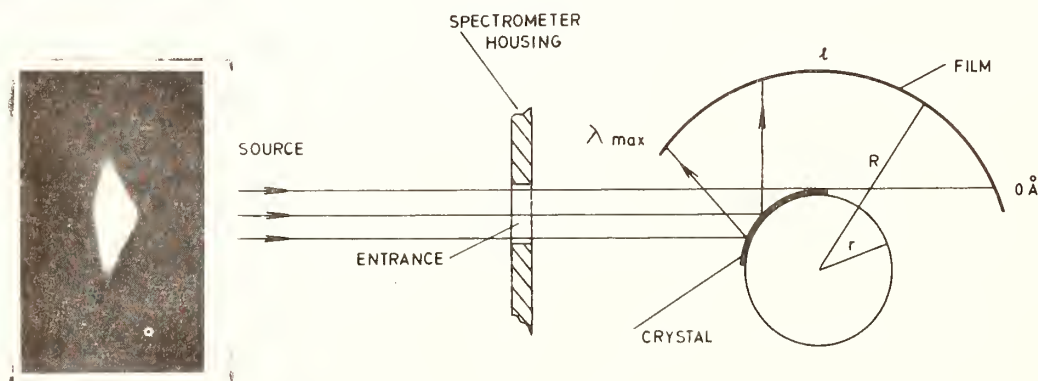


Fig.1. Arrangement of spectrograph to FXR discharge. To left pinhole picture recorded from side.

We intended to study wavelengths up to 15-20 Å. The Bragg law puts the condition on $2d$ to be at least the size of the maximum wavelength to be diffracted. This made mica (001) with $2d=19.9$ Å suitable since this material is very easy to bend to small radius if the crystal is thin enough. As shown in Fig.1, the film contour forms a circular arc concentric with that of the crystal. When radiation from the small X-ray source which is situated relatively distant from the crystal and hence forms a nearly parallel beam, strikes upon the cry-

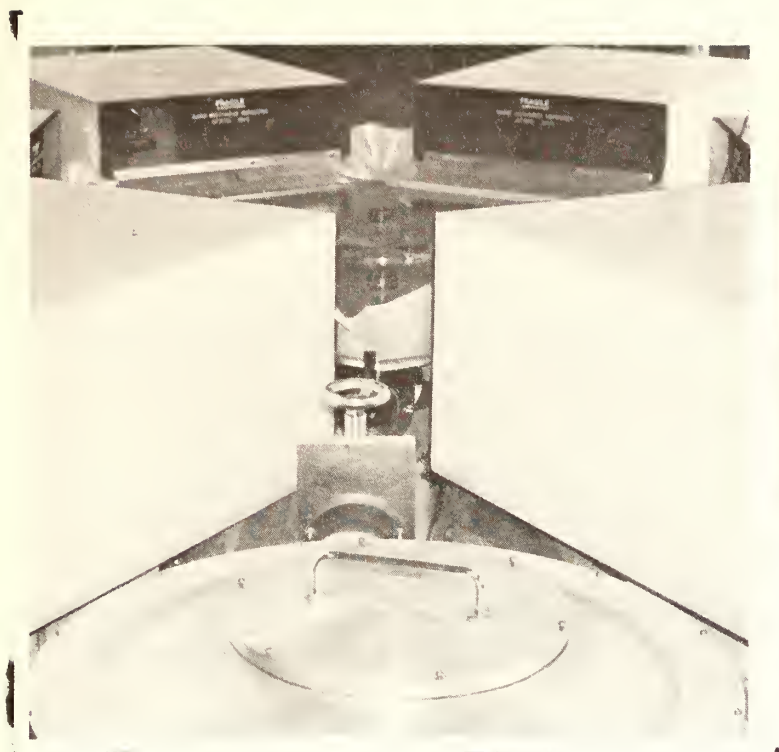


Fig.2. The spectrograph arranged to a 23 kJ vacuum discharge

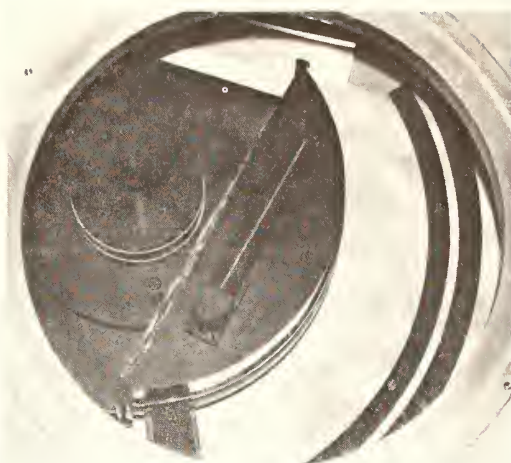


Fig.3. Dispersion arrangement in the spectrograph

stal all wavelengths from $2d$ to 0 will find their Bragg angles somewhere on the surface and thus be diffracted onto the film. Tangential incidence on the crystal corresponds to 0 \AA . No aperture system is needed except for preventing direct radiation. The spectrograph can be seen in Fig.2.

In Fig.3 the dispersion arrangement is shown. The mica was bent towards a brass cylinder, 75 mm in diameter. The cassette was constructed for a 35 mm film. The film forming arc had a radius of 113,3 mm. The front side of the cassette was covered by a $5 \mu\text{m}$ thick Al-foil in order to protect the film from visible light. It was also necessary to put a shield, $25 \mu\text{m}$ thick mylar, in front of the crystal to protect this from being contaminated by the various discharge products. The Al-foil in the passage of the diffracted radiation of course strongly reduces the recorded intensities of the wavelengths smaller than 8 \AA . The spectrograph is also prepared to contain a detector system so that the building up time of the spectral lines can be registered simultaneously as the film is exposed.

Calibration. The position ℓ on the film contour (measured from the point of tangential incidence) versus the wavelength λ and the order is according to the geometry, see Fig.1, given by the expression

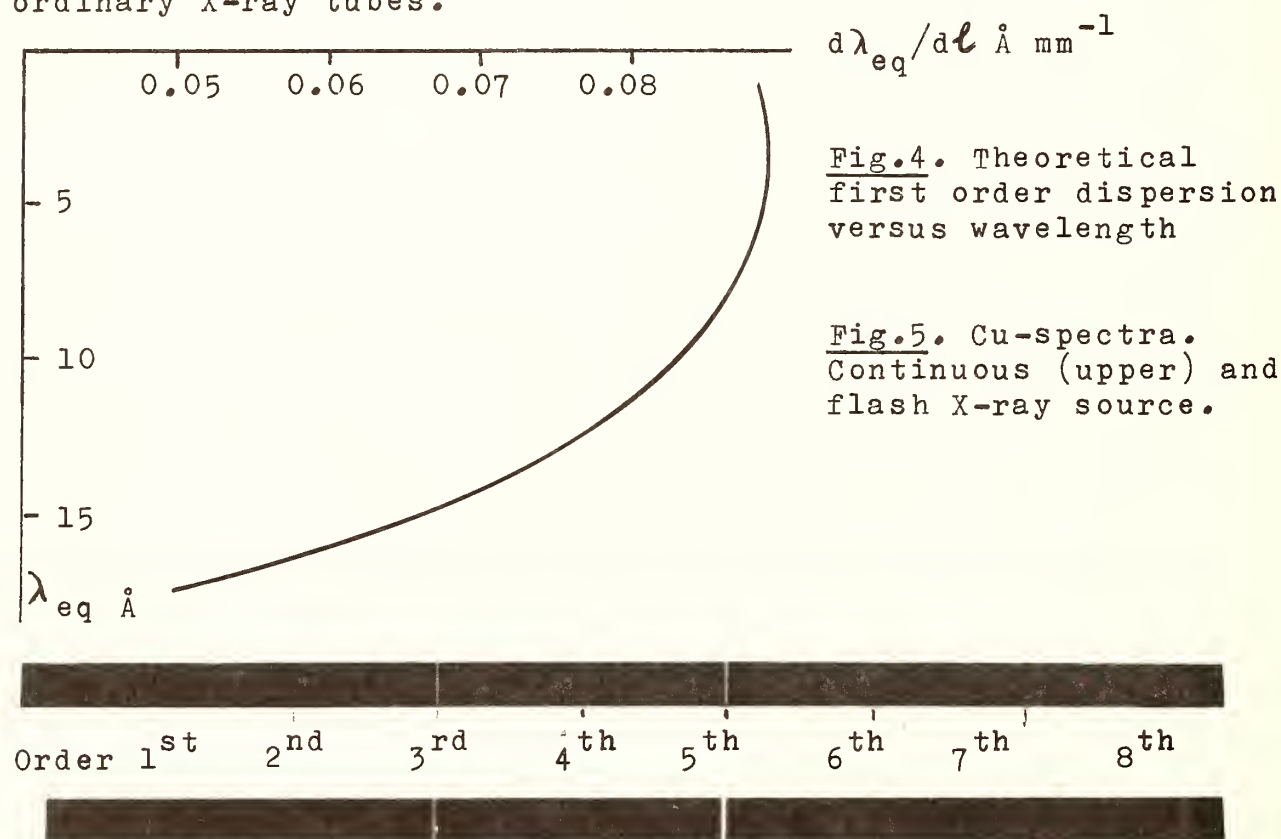
$$\ell = R(2 \arcsin n\lambda/2d + \arcsin \frac{r}{R} \sqrt{1-(n\lambda/2d)^2} - \arcsin \frac{r}{R}),$$

where d is the lattice constant and n order of diffraction. In practice, this expression will give a very good approximation for a small source (about 1 mm) situated about 1 m from the crystal. When using mica one can expect that the diffraction order n can have relatively high numbers. Therefore, for more accurate measurements it is necessary to take into consideration the refraction index of the crystal for X-rays. This is done in a convenient way by calculating a corrected lattice constant d_n for each order n of diffraction. Working with calibration of the spectra it is convenient to reduce all wavelengths to the corresponding equivalent of first order,

$$\lambda_{eq} = n \lambda d_1 / d_n$$

In Fig.4 the dispersion for the first order diffraction is shown.

Spectra. In Fig.5 two spectra recorded by the spectrograph are shown. One of these represents ordinary or continuous X-rays and the other flash X-rays from a Cu electrode. As seen, the lines from the FXR discharge are broader than those from ordinary X-ray tubes.



- (1) M. de Broglie and F.A. Lindemann, Compt. Rend. 158, 944 1914.

X-RAY SPECTROSCOPIC INVESTIGATION OF ENERGY BANDS FINE STRUCTURE AND THE INTERPRETATION OF CONDUCTIVITY CHARACTER OF PHOSPHOROUS COMPOUNDS OF VARIOUS CHEMICAL BOND TYPES

A.N. Gusatinski, M.A. Blokhin, G.I. Alperovich, M.A. Bunin, I.A. Topol
Department of Solid State Physics, Rostov State University
344006 Rostov-on-the-Don, USSR

In [1] it was shown that the energy distribution of local partial electron states density of p- and s-symmetry (with d-admixture) for the third period elements is well reproduced by X-ray K- and $L_{2,3}$ -spectra.

Fluorescent K-bands, K-absorption and $L_{2,3}$ -emission spectra of phosphorous in semiconductor compounds of types $A^{III}B^V$ and $A^{II}B^{IV}C^V_2$ and in the 3d-transition metal monophosphides had been studied. The Ti $M_{2,3}$ -emission band was investigated in the TiP-compound. The phosphorous K- and $L_{2,3}$ -spectra were matched to a common energy scale with the aid of the $PK\alpha$ -line for the same compounds. The P K-spectra were corrected for the inner energy level width using a method, which ensures small boundary distortions.

As an example for the $A^{III}B^V$ compounds the results of X-ray spectral study of InP (Fig. 1a and b) are compared with the calculated $N(E)$ distribution (Fig. 1d and e) and with the X-ray photoelectron spectra (Fig. 1c). Such a comparison was also made for GaP. The positions and related amplitudes of individual elements of the curves in the Fig. 1b,c,e are similar to each other. F- and G-maxima of the absorption spectra (Fig. 1a) and of the $N(E)$ curve (Fig. 1e) are in accordance also. All this shows that for polyhedra of phosphorous atoms the curve of local states density distribution reproduces well such a distribution for the whole crystal. This can be explained as the bonds in such materials are mainly of a covalent type and that both types of atoms are mutually identical surrounded with atoms of the other type. As can be seen from Fig. 1a the 1-st subband (A) contains mainly s-states, the 2-d, 3-d and 4-th subbands (B,C,D) - mainly p-states but with some s-states admixture.

The comparison of various emission spectra series for various components of indium phosphide justifies an assumption of d-states admixture in polyhedra containing the indium atoms. The MO calculation confirms this assumption.

For $ZnGeP_2$ (an isoelectronic analog of GaP) a comparison of phosphorous K-spectra with the calculated $N(E)$ curve shows a correspondence of separate elements of these curves (Fig. 2).

Phosphorous K emission and absorption spectra in $A^{III}B^V$ compounds corrected for the inner level width allows us to determine the energy gap ΔE , which (in the accuracy limits for measuring this quantity) is equal to the forbidden band width E_g for these compounds as determined by other physical methods [1]. As appears from the above there is a sufficiently large p-state density both near the top of the valence band and near the bottom of the conductivity band. Thus, the combined effect of several physical causes leading to a difference between ΔE and E_g in this special case is not greater than the error in the ΔE determination.

The main structure features of the investigated X-ray emission and absorption spectra of phosphorous in monophosphides of Sc, Ti, Cr and Mn are similar in all these compounds. As an example the emission K-bands

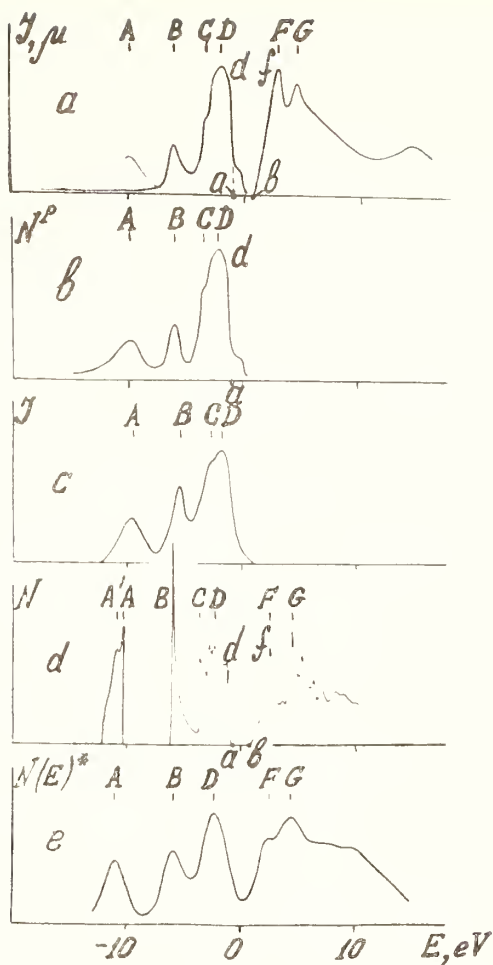


Fig. 1. InP:

- X-ray K (thick line) and $L_{2,3}$ (thin line) phosphorous spectra.
- Local states density in polyhedra of phosphorous atoms, derived from the X-ray spectra.
- X-ray photoelectron spectrum of the valence band [3].
- Calculated $N(E)$ curve.
- Calculated $N(E)^*$ curve, convoluted with a Lorentz curve of 1.2 eV width.

and the absorption K-spectra of phosphorous in TiP and MnP are shown in Fig. 3. The corrected spectra slightly overlap (~ 0.4 eV) each other, but this overlapping is within the limit of experimental errors. Therefore, we can conclude that these compounds must have a metallic conductivity. According to [4] TiP does have a metallic conductivity.

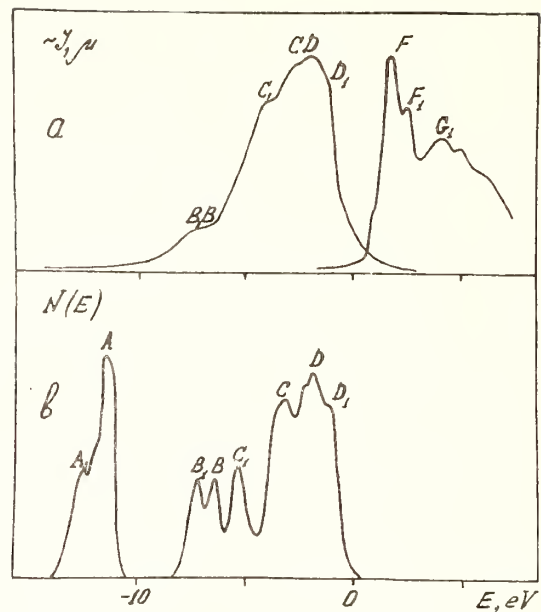


Fig. 2. $ZnGeP_2$: X-ray PK-spectra (a), valence band states density after convolution with a gaussian [2] (b).

The emission K- and $L_{2,3}$ -bands of phosphorous and the $M_{2,3}$ -bands of titanium in TiP are shown in Fig. 4. In these spectra one can see a display of three main energy subbands A, C (with a shoulder B) and D. The intensity ratios of these subbands are different for the spectra of various series and components.

The A and C subbands in the considered spectra have a genetic connection to the s- and p-states of the phosphorous atoms, respectively, and the D subbands - with the d-state of titanium (Fig. 4).

The s-like subband A is not reproduced in the phosphorous K-spectra. Apparently an admixture of p-states of phosphorous is practically absent in this region. The appearance of a high energy shoulder in the K-emission spectra of phosphorous, which is prominent in

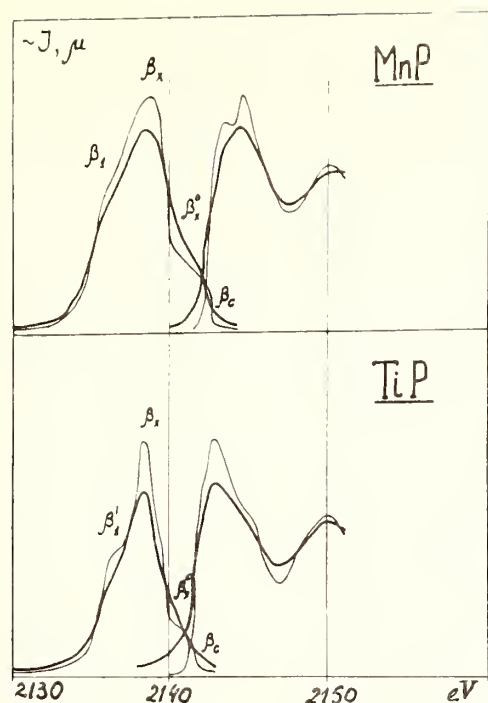


Fig. 3. Fluorescent PK-bands in MnP (a) and TiP (b); experimental (thick lines) and corrected for the inner level width (thin lines).

phosphorous compounds with transition elements, is connected with an admixture of a fraction of phosphorous p-states to the crystal valence band, which contains mainly d-states of the transition metal. In the $L_{2,3}$ -spectra of phosphorous the faint peak D corresponds to this shoulder. As can be seen on the K- and $L_{2,3}$ -spectra of the phosphides of Sc, Cr, Ti and Mn the intensity of the D structure features increases with the atomic number of the transition element. In the titanium emission $M_{2,3}$ -spectrum the main peak corresponds to the subband D.

Thus, the results of X-ray investigations can give important information on the energy band structure and on the electric conductivity type for compounds of the considered classes.

The authors express their deep gratitude to N.A. Gurunova, A.S. Borshchevski, V.D. Prochukhan, V.I. Torbov and V.I. Chukalin for the compounds they had synthesized and placed at our disposal for this investigation, and to L.M. Monastirski

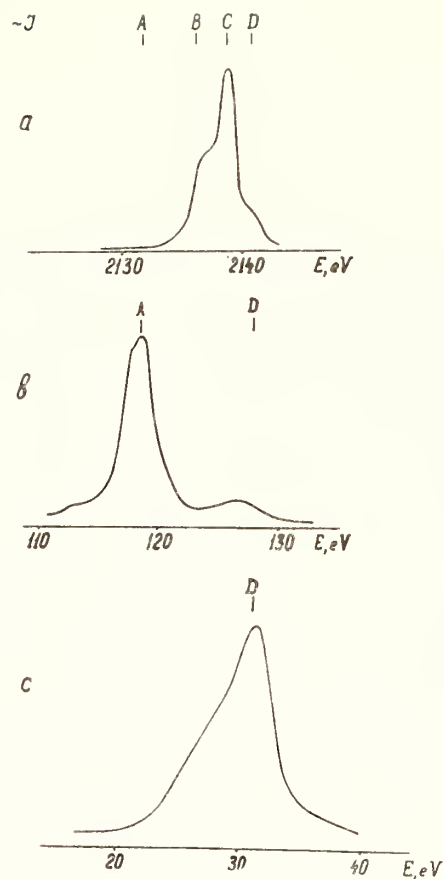


Fig. 4. Emission bands of TiP: a) PK-band. b) $PL_{2,3}$ -band. c) $TiM_{2,3}$ -band.

and I.G. Shweizer for their aid in the experimental part of this work.

References

1. A.N. Gusatinski, in "X-ray Spectra and Electron Structure of Materials", Kiev, 1969, p. 328 (in Russ.).
2. C.V. de Alvarez, M.L. Cohen et al, Phys. Rev. B 10, 596 (1974).
3. L. Ley, R.A. Pollak et al, Phys. Rev. B 9, 600 (1974).
4. I.R. Fakidov, V.P. Krasovski, Physika Metallov i Metallovedeniye 7, 156 (1959) (in Russ.).

TARGET K X-RAY PRODUCTION FOR HEAVY IONS MOVING IN THIN SOLID FILMS*

Tom J. Gray,[†] Patrick Richard, R. K. Gardner,
K. A. Jamison, and J. M. Hall

Department of Physics, Kansas State University
Manhattan, Kansas 66506

There have been several works reported [1-4] on the production of target x rays as a function of target thickness for various heavy ion projectiles incident on thin solid films. Betz et al. [5] reported a new technique for measuring inner-shell atomic lifetimes by measuring the projectile x-ray yield vs target thickness. The approach of the latter group was to account for the microscopic interactions affecting the projectile K shell as the incident ion moved through the solid at high velocities. The results of their work are dependent on the rate equation which relates the K-shell single-vacancy population, Y_1 , to the K-shell vacancy production cross section, σ_v , the quenching cross section, σ_Q , and the natural decay cross section, σ_T :

$$dY_1/dX = \sigma_v(1 - Y_1) - (\sigma_Q + \sigma_T)Y_1 \quad (1)$$

Hopkins [2], Groeneveld et al. [3] and Feldman et al. [4] have used a similar approach to that of Betz et al. as a starting point for their respective studies of film thickness on target x-ray production.

We have studied the target x-ray production vs target thickness for various incident charge states of the projectile at high energies. The initial system studied was Cl ions on thin solid Cu targets. It has been shown by Winters et al. [6] that the target x-ray production rate for gas targets under single collision conditions increases by factors of 2 or greater for H-like incident projectiles on argon. Admixtures of the bare nucleus or H-like component in a beam is expected to enhance the x-ray production rate. Shown in Fig. 1 are the results of measurements for Cl on Cu at 60 MeV for three different target thicknesses. Beginning with Eq. (1) and assuming that there are two components in the ion beam within the targets; those with a K vacancy, Y_1 , and those without a K vacancy, Y_0 , the target K-shell x-ray production cross section averaged over the target thickness is

$$\overline{\sigma_{KX}} = 1/T \int_0^T [\sigma_{K0} Y_0 + \sigma_{K1} Y_1] dX \quad (2)$$

where σ_{K0} = target x-ray cross section for the Y_0 component, and σ_{K1} = target x-ray cross section for the Y_1 component. The resulting expression for $\overline{\sigma_{KX}}$ is

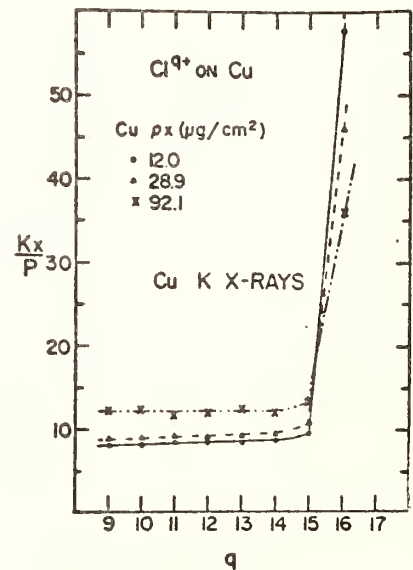


Fig. 1

$$\overline{\sigma_{KX}} = \sigma_{K0} [1 + (\alpha-1) \sigma_v/\sigma - ((\alpha-1)/\sigma_T)(\sigma_v/\sigma - A)(1 - \exp(-\sigma T))] \quad (3)$$

where A is the initial fraction of ions with one K-shell vacancy incident on the target, $\sigma = \sigma_V + \sigma_Q + \sigma_T$ and $\alpha = \sigma_{K1}/\sigma_{K0}$.

Experimentally, α is determined for vanishing target thickness. The measurements and model calculations for 60 MeV Cl ions on Cu are shown in Fig. 2. The relevant parameters obtained from the model calculations are given in Table 1.

At energies of 1-2 MeV/amu the two component model begins to break down as the atomic number of the projectile is decreased. The projectile must then be described by three components Y_0 , Y_1 and Y_2 , where Y_2 is the fraction with 2 K-shell vacancies. Using the solution of Allison [7] for the 3-component system an effective cross section $\overline{\sigma_{KX}}$ for target x-ray production is formulated analogous to the 2-component system. Solutions of the form

$$\overline{\sigma_{KX}} \sim \sigma_{K0} \{ 1 + (\alpha - 1) [f_1 \gamma_1 + f_2 \gamma_2 + \xi_1] + (\beta - 1) [f_3 \gamma_1 + f_4 \gamma_2 + \xi_2] \},$$

where

$$\gamma_i = \exp(r_i T) - 1; f_i = f_i(r_i, C_i, T) \text{ and } \xi_i = \xi_i(\sigma_{V1}, \dots).$$

The quantities r_i and C_i are, respectively, the eigenvalues of the diagonalized coefficient matrix of the rate equations and the constants determined from the boundary conditions.

Fig. 3 gives measurements of $\overline{\sigma_{KX}}$ for Si on Cu at a bombarding energy of 48 MeV. Similar measurements have been made for Al and F on Cu at energies of 48.5- and 38.0-MeV, respectively. Model calculations for the 3-component system are shown in Fig. 3. Work is in progress on the interpretation of the projectile cross sections obtained from the model calculations of $\overline{\sigma_{KX}}$ in terms of single collision cross sections.

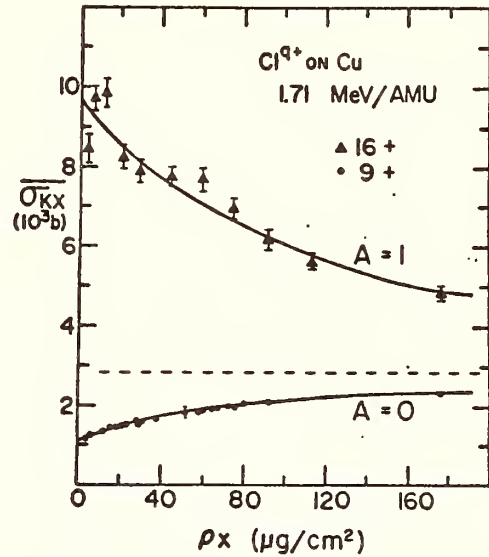


Fig. 2

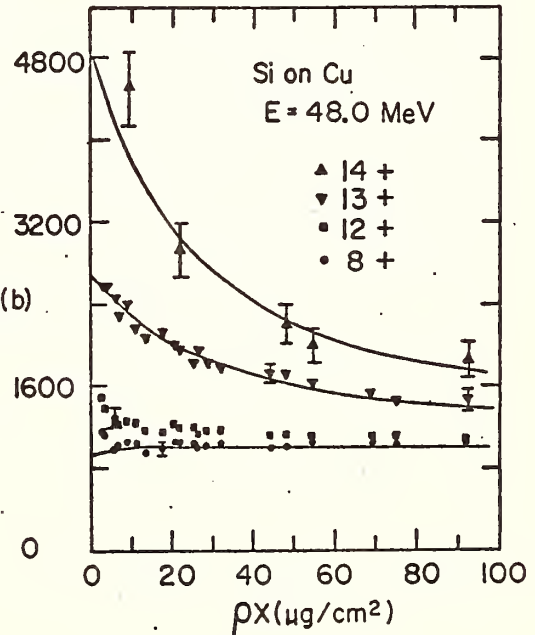


Fig. 3

TABLE 1
Values of the parameters for 60 MeV Cl on Cu

	Present Work	Other Sources
σ_V	$3.5 \times 10^{-19} \text{ cm}^2$	$\sim 6 \times 10^{-19} \text{ cm}^2$ [6]
σ'	$15.4 \times 10^{-19} \text{ cm}^2$	$15.7 \times 10^{-19} \text{ cm}^2$
α	8.1	8.4
σ_{K0}	$1.18 \times 10^{-21} \text{ cm}^2$	--
w	--	2.80×10^{-2}
σ_R	--	$7.07 \times 10^{-19} \text{ cm}^2$
ω_{cu}	--	0.443

REFERENCES

* Work supported in part by the U. S. Energy Research and Development Administration under Contract No. E(11-1)-2753, and the Faculty Research Fund, North Texas State University.

⁺ Presently on leave from North Texas State University.

- [1] W. Brandt, R. Laubert, M. Mourino, and A. Schwarzschild, Phys. Rev. Lett. 30, 358 (1973).
- [2] Forrest Hopkins, Phys. Rev. Lett. 35, 270 (1975).
- [3] K. O. Groeneveld, B. Kolb, J. Schader, and K. D. Sevier, Z. Physik A 277, 13 (1976).
- [4] L. C. Feldman, P. J. Silvermann, and R. J. Fortner, Nuc. Instr. Meth. 132, 29 (1976).
- [5] H. D. Betz, F. Bell, H. Panke, G. Kalkoffen, M. Solz, and D. Evers, Phys. Rev. Lett. 33, 807 (1974).
- [6] L. Winters, M. D. Brown, L. D. Ellsworth, T. Chaio, E. W. Pettus, and J. R. Macdonald, Phys. Rev. A 11, 174 (1975).
- [7] S. K. Allison, Rev. Mod. Phys. 30, 1137 (1958).

AR $K\alpha$, $K\beta$, AND K-REC X-RAY ENERGIES AND
INTENSITIES VS $AR^{+12} \rightarrow C$ -FOIL THICKNESS

F.Folkmann*, K.-O.Groeneveld**, P.Mokler*, J.Schader**, K.D.Sevier**§

*G.S.I., Postfach 541, 61 - Darmstadt, W. Germany.

**I.K.F., August-Euler-Str. 6, 6 - Frankfurt/Main 90, W. Germany.

Investigation of X-ray emission from the system $Ar^{+12} \rightarrow Ni$ (on C-substrate) or $\rightarrow C$ -foil with a Si(Li) spectrometer enables one to study the projectile and target or only the projectile X-ray emission cross section, respectively, with varying target thickness. The first article in this series treated the Ni $K\alpha$ and $K\beta$ intensities and energies /1/. The results were similar to an earlier study of $Ne^{+2} \rightarrow Al$ of varying target thickness /2/.

The present report deals with the Ar $K\alpha$, β , and -REC energies and intensities using 56 MeV $Ar^{+12} \rightarrow C$ -foil (8 to 440 $\mu g/cm^2$ thick) at the UNILAC at Darmstadt. The foil normals bisected the beam-Si(Li) spectrometer right angle. A 19 μm Al-foil was used as absorber, a 19 μm hostaphan foil acted as vacuum chamber window which was situated 3 mm (of air) from the 12.7 μm Be-foil spectrometer window. The detector acceptance solid angle was 0.75% of 4π , and the beam current was integrated by use of a Faraday cup (20 mm ϕ) 20 cm behind the target.

Figure 1 shows a typical measured spectrum, the components being clearly distinguishable. The intensity maximum near 1.4 keV may be due to K-fluorescence radiation from the Al absorber foil.

Figure 2 shows the average X-ray production cross sections for the Ar $K\alpha$, $K\beta$, and K-REC spectral components: These values are calculated by dividing the absorption and solid angle corrected Gaussian-fitted and integrated peak intensities by the number of projectiles per run and the used foil thickness (measured by alpha-scattering) expressed in units of atoms/cm². (Absorption of the Ar $K\alpha$ radiation is less than 4% in the thickest C-foil.) Such a cross section calculation is quite suitable for the Ar K-REC radiation, which originates within the foil. However, the Ar $K\alpha$

§ Recipient of an Alexander von Humboldt scholarship.

and $K\beta$ radiation originates both from within and from without the foil. As the foil thickness increases, the relative radiation contribution from outside the foil decreases. This variation need not be linear, depending on solid state effects.

Qualitatively, the data can be easily understood. First, the general weak fall in average cross section values for all three rays is due to projectile energy loss in the foil. This loss is estimated to be ~ 12 MeV after traversing a $500 \mu\text{g}/\text{cm}^2$ thick C-foil. One may extract from such measurements the energy dependence of projectile K X-ray yield for a given target material. (The extrapolation of this component toward smaller thicknesses is drawn in.) Secondly, one observes an initial increase in the average Ar K-REC production cross section with thickness, and this tends to saturate. This tendency can be fitted in the first approximation by the formula $(KR) \propto 1 + (\exp(-\sigma_T x_0) - 1)/\sigma_T x_0$, where x_0 is the foil thickness and σ_T is the sum total of all excitation and de-excitation cross sections for projectile K-vacancies /1/. Thirdly, the Ar $K\alpha$ and $K\beta$ production cross sections are made up of an in-foil contribution, similar to the K-REC case, and a post-foil contribution from the decay of the excited projectiles after the foil, with mean fluorescence yields $\bar{\omega}'$ and $\bar{\omega}$ respectively. The latter contribution to the mean cross section will have the general form $(KAB) \propto (1 - \exp(-\sigma_T x_0))/\sigma_T x_0$. The total $K\alpha$ and $K\beta$ production cross sections will be expected to have the general form

$$\bar{\sigma} \propto \bar{\omega}(KR) + \bar{\omega}(KAB) = \bar{\omega}' + (\bar{\omega} - \bar{\omega}')(1 - \exp(-\sigma_T x_0))/\sigma_T x_0,$$

which describes in general the upper two curves in Figure 2 when $\bar{\omega} > \bar{\omega}'$. Of course, $\bar{\omega}$ and $\bar{\omega}'$ may vary with target thickness, because the average projectile excitation state may be a function of the duration of the ion's being in the foil.

Also, the foil thickness dependent variations of the X-ray peak centroid energy values, shown in Figure 3, indicate larger changes with foil thickness for the thinner foils than for the thicker. This may result from mean projectile state variation with penetration depth in the foil, as above. These and other points will be discussed.

References:

- /1/ K. D. Sevier, F. Folkmann, K.-O. Groeneveld, P. Mokler, and J. Schader, 5th International Conference on Atomic Physics, Berkeley, California, July 26-30, 1976.
- /2/ K.-O. Groeneveld, B. Kolb, J. Schader, and K. D. Sevier, Z. Physik A277(1976)13.

Figure 1. Ar K X-ray spectrum from (1.4 MeV/amu) Ar^{+12} bombarding a $113 \mu\text{g}/\text{cm}^2$ thick carbon foil.

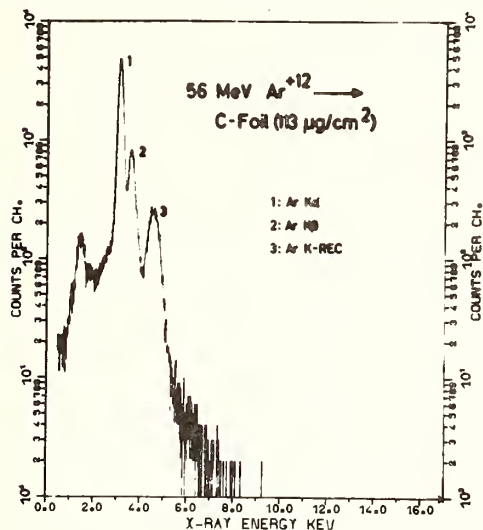
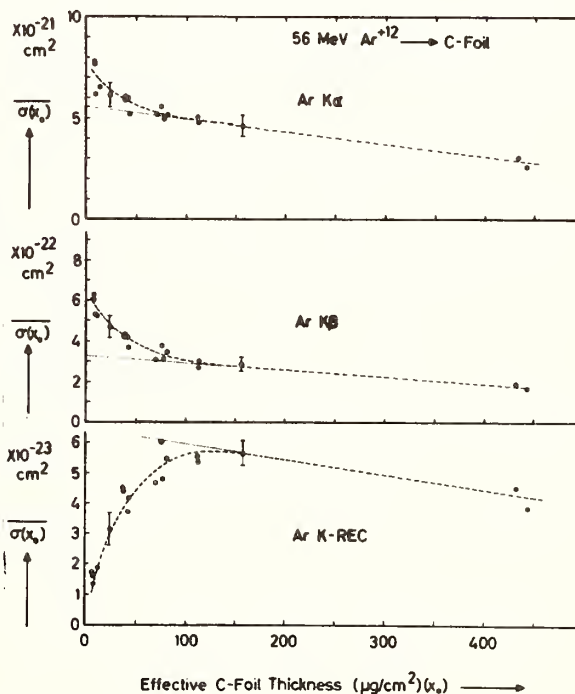
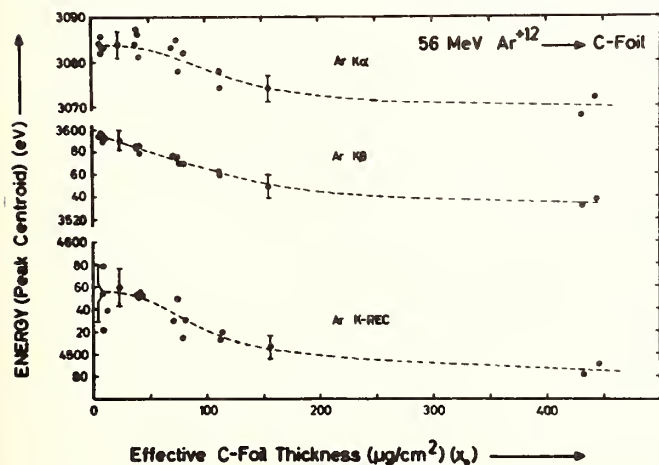


Figure 2. Average Ar K X-ray production cross sections as functions of C-foil thickness. Note the transient components for $x \geq 120 \mu\text{g}/\text{cm}^2$ and the projectile straggling dependent general decrease with increasing foil thickness. Dashed curves to guide the eye.

Figure 3. Ar K X-ray energies as functions of C-foil thickness. Note transient and general features, analogous to those seen in Figure 2. Dashed curves to guide the eye.



The effect that the degree of projectile ionization becomes much higher when heavy ions pass through solids rather than gases is explained in the Betz-Grodzins model (1) by assuming inner shell excitation of the projectile in the solid. Outside the solid the excited states preferentially decay via nonradiative transitions enlarging the ion charge-state.

Recently, in the case of Ar ions incident on Carbon targets (2, 3), investigations have been made to determine the influence of inner shell vacancies on charge-state distributions. The measurements of the absolute Auger yield (3) have shown that the observed Ar L-excitation cannot account for the differences in the charge-state of ions emerging from solids and gases. In this work we extended the earlier experiments by measuring electron yields at angles as small as 5° making use of the Doppler-effect. Due to shifting of the electrons to higher energies it was easier to discriminate the autoionization emission from the lower background.

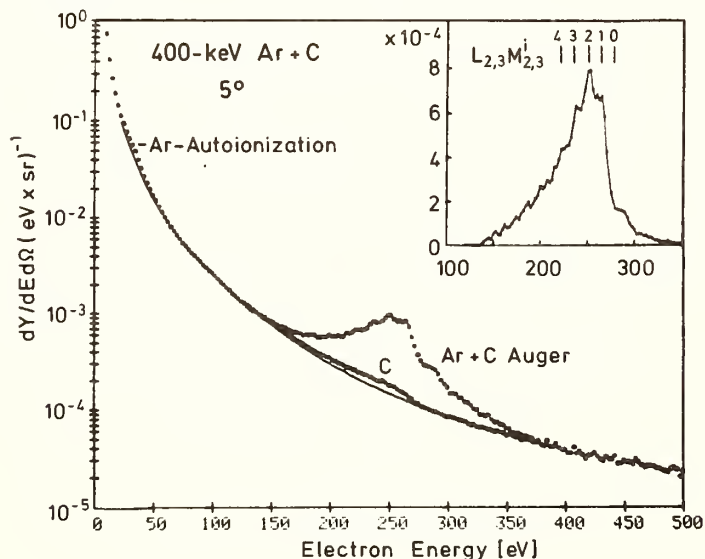


Fig.1 The electron yield of 400-keV Ar ions incident on $2\mu\text{g}/\text{cm}^2$ C-foils observed at 5° . The C K-emission at 140° is added to the background. The inset shows the Auger yield after background subtraction. Also given are theoretical transition energies for different multiple ionized initial states.

Fig. 1 shows the electron emission of 400-keV Ar ions having passed a $2\mu\text{g}/\text{cm}^2$ C-foil using a spectrometer with 1.3% resolution, the observation angle being 5° . Autoionization electrons (at 50 eV) and Auger electrons (150 to 300 eV) of the target and the emerging projectile are detected apart from the continuous background. In the reverse direction (140°) only C K-Auger electrons have been observed with the same intensity as in forward direction (3). Apparently, due to multiple M-shell ionization of the Ar ions within the first four C-layers, MO-swapping occurs so that C K-electrons can be promoted.

The inset of Fig. 1 depicts the Auger electron emission at 5° after subtracting the background. The labels denote the theoretical energies of electrons produced by $L_{2,3} M_{2,3}^i - M_{2,3}^{i+1}$ ($i=0,1..4$) transitions (4) indicating that the step-like shape of the peak is probably due to satellite Auger transitions; whereby, the $L_{2,3} M_{2,3}^2$ state is the most likely excited one (in agreement with ref. (5)). The peak intensity near 300 eV is caused by transitions involving electrons which are excited to upper bound states. A detailed discussion comparing Ar-CH₄ experiments will be given at the conference.

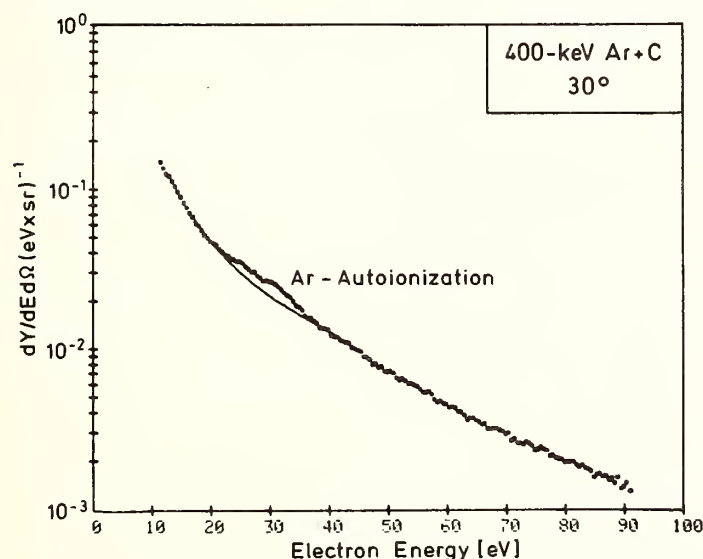


Fig.2 The electron yield for 400 keV ions observed at 30° showing the autoionization electrons between 20 and 35 eV.

The new experiments enabled a better detection of the Ar autoionization electrons as seen in Fig. 2. The plot indicates that this emission is superimposed on a steeply increasing background which makes detection difficult. Nevertheless, we could estimate that the yield of autoioniza-

tion electrons was nearly equal to the yield of Auger electrons. Thus, we may conclude that the autoionization process strongly contributes to the charge-state increase of ions emerging from the surface.

The fraction f_L of L-shell ionized Ar ions passing C-foils with energies from 100 to 800 keV (3) has been reproduced within 20%. Also the same fraction f_L was found for $2\mu\text{g}/\text{cm}^2$ and $10\mu\text{g}/\text{cm}^2$ C-foils. Hence, it appears that the f_L equilibrium is already reached at 100 \AA (thickness of $2\mu\text{g}/\text{cm}^2$ C-foils). This result allows for estimating the upper and lower limit of the lifetime τ and the production cross section σ_v of Ar L-vacancies in C-foils; this estimation is similar to the procedure used in ref. (6). It follows for 400-keV Ar projectiles that $\sigma_v \geq 3.6 \cdot 10^{-18} \text{ cm}^2$ and $\tau \leq 4.3 \cdot 10^{-15} \text{ sec}$. This lifetime τ is smaller by a factor of two than that obtained from the analysis of thick target x-ray yield (2). Supposing an underestimation of collisional quenching in ref. (2) the differences in the fraction f_L between x-ray yield (2) and Auger yield measurements (3) could be discerned.

We are indebted to G. Wüstefeld for his assistance during the experiments.

Footnotes and references.

+ Permanent address: Centro Atomico Bariloche, 8400 S.C. de Bariloche, R. N., Argentina

- 1) H. D. Betz, L. Grodzins Phys. Rev. Lett. 25(1970)211
- 2) R. Fortner, J. D. Garcia Phys. Rev. A12(1975)856
- 3) R. A. Baragiola, P. Ziem, N. Stolterfoht (Sec. Int. Conf. on Inner Shell Ionization Phenomena, Freiburg 1976, Abst. of pap. p 109)
- 4) F. P. Larkins J. Phys. B4(1971)1
- 5) A. B. Wittkower, H. D. Betz Atomic Data 5(1973)113
- 6) K. H. Schartner, Th. P. Hoogkamer, P. Woerlee, F. W. Saris Nucl. Inst. Meth. 132(1976)35

CONTINUOUS THERMAL X-RAY SPECTRUM FROM HOT PLASMAS.
BREMSSTRAHLUNG AND RADIATIVE ELECTRON CAPTURE PROCESSES*

C. M. Lee and R. H. Pratt
Department of Physics and Astronomy
University of Pittsburgh
Pittsburgh, Pennsylvania 15260

The x-ray emission from a plasma consists a continuum of free-free bremsstrahlung, free-bound electron capture radiation, and bound-bound line radiation [1]. We have attempted to carry out systematic theoretical surveys of both the bremsstrahlung process [2,3] and the direct radiative electron capture process [4,5]. Both processes are described as single electron transitions in a relativistic self-consistent screened central potential, using full relativistic partial wave expansion calculations which include all important photon-multipole contributions. Theoretical bremsstrahlung energy spectra $k(d\sigma/dk)$ from neutral atoms ($Z = 2-92$) with incident electron energy 1-500 keV are now available [2]. Similar analysis for the bremsstrahlung energy spectra from atomic ions is in progress [3]. Regarding the direct radiative electron capture process, we recently proposed a simple theoretical method for calculating the needed cross sections [4]. Applying quantum defect theory, the radiative capture and the tip bremsstrahlung processes can be treated together because, at atomic distances, bound and continuum wave-function shapes, of energies close to the ionization threshold, are similar and vary slowly with energy. As a result only two smoothly varying quantities, the quantum defect and the cross section density, need to be calculated for each partial wave channel of the final-state electron. This then suggests a convenient way to carry out systematic analysis of radiative capture cross sections. We have reported some preliminary results [4,5] of such analysis.

The bremsstrahlung and the direct radiative capture processes give rise to the continuous x-ray spectrum from a plasma. The continuous spectrum [1] usually consists of the continuous thermal x-ray spectrum and a runaway tail at higher photon energies due to non-thermal high energy electrons. From the cross sections for these two basic processes, the radiation power loss density of the thermal x-rays (defined as power loss per unit volume per unit photon energy, e.g. Watt/cm³keV) can be calculated as

$$(dW^{th}/dk) = \sum_i \eta_e \eta_i (dW_i^{th}/dk) ,$$

where η_e and η_i are the densities for electrons and for atomic ions of the i th kind respectively. The "specific radiation power loss density" (dW_i^{th}/dk) , defined as power per unit density of the i th kind of atomic ion per unit photon energy, e.g. Watt cm³/keV, is related to the basic cross sections through the following Maxwellian folding,

$$\frac{dW_i^{th}}{dk} = \sum_n \int k \sigma_n^i(T) \delta(k-T-|\epsilon_n|) f_{Max}(T, T_e) dT$$

$$+ \int_k^\infty k \frac{d\sigma^i(T, k)}{dk} f_{Max}(T, T_e) dT$$

where k is the photon energy, T the electron kinetic energy and $f_{Max}(T, T_e)$ the Maxwellian energy distribution of the electron at the electron temperature T_e . Also $\sigma_n^i(T)$ is the direct radiative electron capture cross section into the unoccupied bound state with binding energy ϵ_n ; the summation here covers all unoccupied states. Finally, $d\sigma^i(T, k)/dk$ is the Bremsstrahlung cross section from the i th kind of atomic ion. In Fig. 1, we plot the specific radiation power loss density dW_i^{th}/dk for Ne-like Mo ions vs. the photon energy k at various electron temperatures $T_e = 0.4, 0.8, 1.5, 3, 6$, and 9 keV. We also present the corresponding partial specific radiation power from the bremsstrahlung process, indicated by the dashed lines in Fig. 1. At low electron temperatures, the direct radiative capture process is dominant for continuous thermal x-ray radiation. However, at higher electron temperature, the bremsstrahlung process will have an appreciable contribution and will be even more important than the direct radiative electron capture process. In such a semilog plot, the continuous thermal x-ray intensity has almost a linear dependence on photon energy k with a slope equal to about $-0.434/T_e$. Thus, a complete set of such data, (i.e. extended to various atomic ions) would be helpful for quick estimates and/or checks of the average electron temperature, electron density and atomic ion densities in a hot plasma.

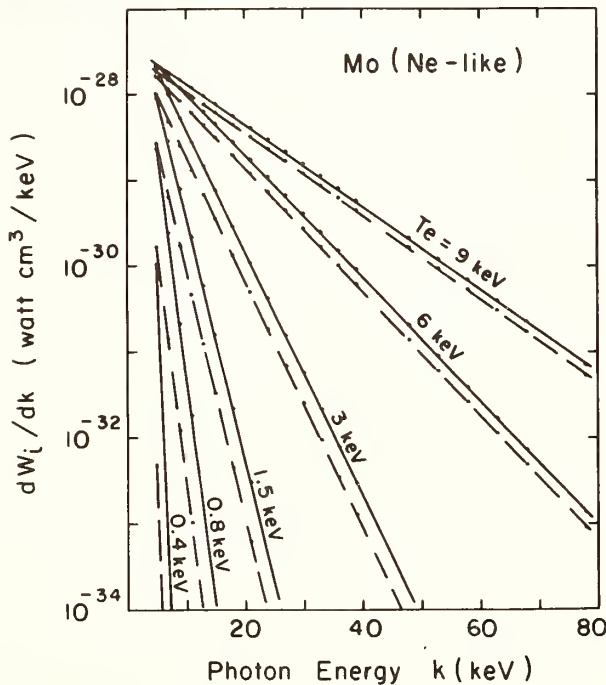


Fig. 1. Specific radiation power density (Watt cm³/keV vs. photon energy k (keV)

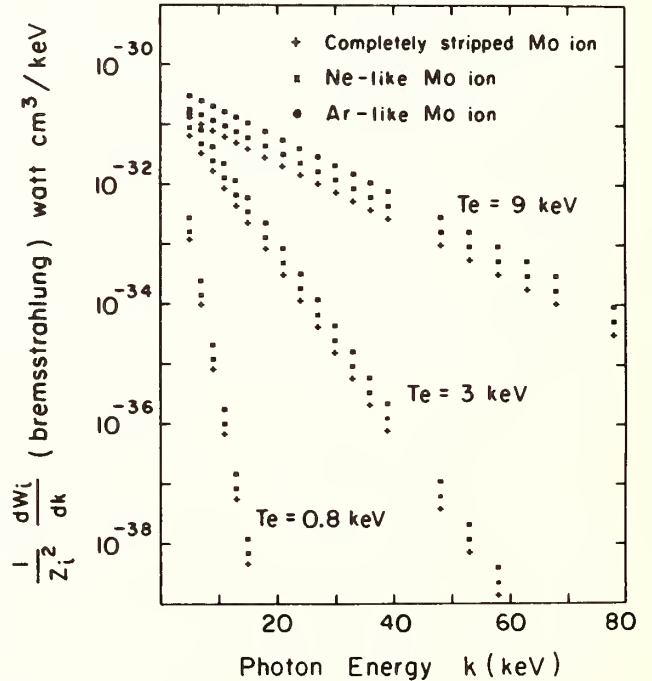


Fig. 2 "Reduced" specific radiation power density vs. photon energy.

In order to examine the validity of the conventional effective charge approximation for the bremsstrahlung process, we present, in Fig. 2, the "reduced" partial specific radiation power loss density, $(1/Z_f^2)(dW_i^{th}/dk)$ vs. the photon energy k for bremsstrahlung from Ar-like, Ne-like, and completely stripped Mo ions. Our data here indicate inadequacy of the effective charge approximation, understandable since such a hard-photon bremsstrahlung process involves small distances where an adequate treatment for the screening effect is necessary in the case of partially ionized atoms.

Finally, for the total radiation power loss, one should integrate over the whole photon energy range and should also include the contribution of the "discrete line" spectrum and the "runaway tail" in addition to that of the thermal continuous x-ray spectrum. At higher electron temperature, the bremsstrahlung process will become more important.

References

* Supported in part by the National Science Foundation.

1. S. Von Goeder, W. Stodiek, H. Fishman, S. Grebenschchikov and E. Hinnoy, Nuclear Fusion 15, 301 (1975).
2. C. M. Lee, L. D. Kissel, R. H. Pratt and H. K. Tseng, Phys. Rev. A, 13, 1714 (1976).
3. C. M. Lee and R. H. Pratt, Bull. Am. Phys. Soc. 21, 574 (1976).
4. C. M. Lee and R. H. Pratt, Phys. Rev. A 12, 1825 (1975).
5. C. M. Lee and R. H. Pratt, (to appear in Phys. Rev. A, 1976.)

RELATIVE INTENSITIES OF ION-INDUCED $K\alpha$ X-RAY
SATELLITE SPECTRA OF Si AND Mg AS A FUNCTION
OF THE CHEMICAL ENVIRONMENT

Robert L. Kauffman, L. C. Feldman and P. J. Silverman
Bell Laboratories
Murray Hill, New Jersey 07974

High resolution spectra of ion-induced $K\alpha$ x-rays contain a number of satellite lines which are due to multiple L-shell vacancies present at the time of K x-ray emission. The intensity of the satellite lines is greater than that observed for x-ray bombardment and in some cases the satellites may dominate the spectrum. In a recent letter the relative intensities of the satellite lines for the third row elements of Si and S are observed to depend upon the chemical environment of the element when 2 MeV/amu O and Ne projectiles are used [1]. Such dependences have been explained by changes in the L-shell decay rate. The systematics of such changes suggest that interatomic transitions are a major contribution to the effect. In this abstract preliminary results are reported of the relative intensities of x-rays from Mg and Si compounds using proton and He projectiles. Dependence of the satellite intensities on the chemical compound in these collision systems is also observed. Possible effects of the chemical environment on the production of the multiple L-shell distribution is discussed.

In this experiment thick targets of Mg and Si compounds are bombarded with beams of protons and He^+ at 1.9 MeV. The x-rays are resolved using a flexed mica crystal in first order. Typical spectra from Mg compounds produced by 1.9 MeV He are shown in Fig. 1. The spectra are taken in scans of decreasing wavelength in constant 2θ steps of 0.02° . The first peak at about channel 25 is the $K\alpha_{1,2}$ peak. The higher energy peaks correspond to transitions with n L-shell vacancies accompanying the K shell vacancies and are designated $KL_1, KL_2, \dots K\alpha_{1,2}$ in this nomenclature is KL_0 . From these scans peak areas can be extracted and relative intensities are obtained.

In Table I the relative intensities, $I(n)$, of the satellite lines normalized to $K\alpha_{1,2}$ are given. Errors due to counting statistics and peak area extraction are less than 3%. The relative intensities of the satellite lines in the compounds are decreased with respect to the element. This is opposite to the trend observed from x-ray fluorescence whose values are also listed in Table I.

The changes in satellite intensities of the ion-induced measurements can be explained by the interatomic Auger hypothesis, but the theory would not predict the x-ray fluorescence results. Another possible mechanism which can

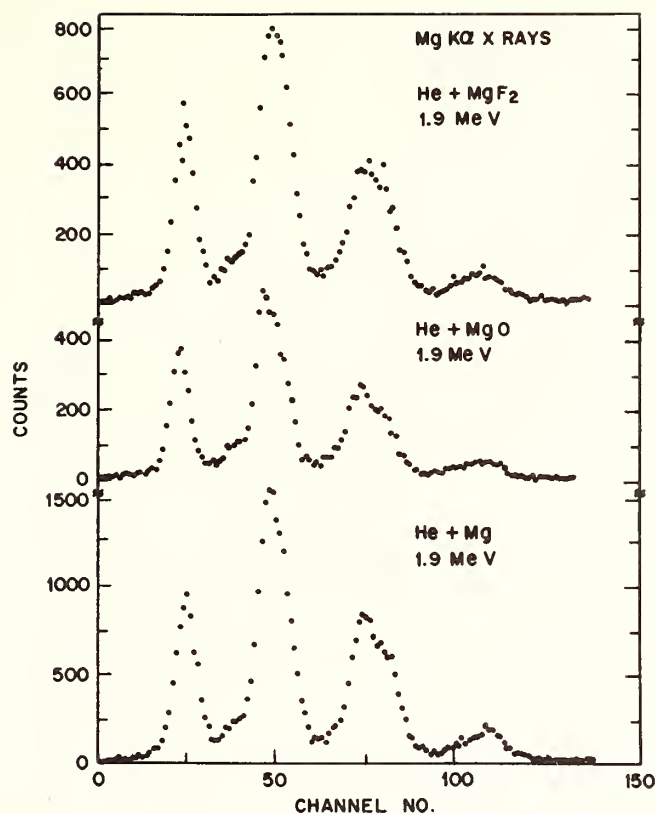


Fig. 1. 1.9 MeV He induced $K\alpha$ structures of Mg compounds.
The peak at channel 25 is the $K\alpha_{1,2}$ line.

qualitatively predict the changes in the ion-induced satellites is the variation of the L-shell ionization probability, P_L . P_L should be related to the L-shell ionization cross section which varies with binding energy, U_L , as U_L^{-2} or U_L^{-1} in this energy range [3]. In Table I the U_{2p} binding energy of the various material determined from ESCA measurements are given. Using such arguments the correct sign of the change and the correct order of magnitude can be predicted. The S results are also consistent with such arguments. The Al results, which are not in agreement with the interatomic Auger hypothesis [2], cannot be understood in this formalism. A more thorough investigation is needed before a quantitative comparison can be made.

Table I
The Relative Intensities of the $K\alpha$ Satellite
Lines for Mg and Si Compounds

	p 1.9 MeV		He 1.9 MeV		Fluore- scence[2]	$U_{2p}[4,5]$
	I(1)	I(1)	I(2)	I(3)	I(1)	(eV)
Mg	0.21	2.45	1.82	0.47	0.140	48.9
MgO	0.21	2.32	1.54	0.39	0.158	50.8
MgF ₂	-	2.26	1.47	0.37		53.5
Si	0.18	1.65	0.78	0.12	0.078	99.
Si ₃ N ₄	0.17	1.46	0.67	0.09		101.8
SiO ₂	0.17	1.52	0.68	0.10	0.090	103.0

References

- [1] R. L. Watson, T. Chiao, and F. E. Jensen, Phys. Rev. Lett., 35, 254 (1975).
- [2] J. Utriainen, M. Linkoaho, E. Rantavuori, T. Åberg and G. Graeffe, Z. Naturforsch. 23a, 1178-82 (1968).
- [3] J. H. McGuire and P. Richard, Phys. Rev. A 8, 1374-84 (1973).
- [4] G. Wertheim, private communication.
- [5] R. Nordberg, H. Brecht, R. G. Albridge, A. Fahlman and J. R. Van Wazer, Inorganic Chem. 9, 2469-74 (1970).

IMPACT PARAMETER DEPENDENCE OF NONCHARACTERISTIC RADIATION EMITTED IN Cl - Cl COLLISIONS

I. Tserruya⁺

Max Planck Institut für Kernphysik, 69 Heidelberg, Germany

H. Schmidt-Böcking, R. Schulé, and K. Bethge

Institut für Kernphysik der J. W. Goethe Universität

6 Frankfurt/Main, Germany

R. Schuch and H.J. Specht

Physikalisches Institut der Universität Heidelberg

69 Heidelberg, Germany

The structureless shape of the non characteristic radiation (NCR) emitted in heavy-ion-atom collisions makes it difficult to associate (in a clear cut way) this radiation with transitions between molecular orbitals transiently formed during the collision.

In this work we present results of a new experimental approach to the problem, namely measurements of the continuum radiation upon the impact parameter of the collision /1/. Such measurements are expected to show a strong dependence of the cross section on the impact parameter.

A 35-MeV Cl beam was used to bombard thin targets of NaCl on a carbon backing. X rays emitted at 90° were detected with a Si(Li) detector in coincidence with particles scattered at laboratory angles of 1.5° , 3° , 6° , 7° , 13° , and 25° corresponding to impact parameters of $b = 450$ to 25 fm. Scattered-particle detection was accomplished by the use of a parallel plate avalanche detector with an azimuthal 2π geometry.

The coincidence spectrum is only slightly different from the single spectrum, normalised at the ClK x rays. The measured photon emission probabilities for different x-ray energy intervals are given in Fig. 1, as well as the Cl x-ray emission probability. The photon emission probabilities are quite insensitive to the impact parameter of the collision, similar to the characteristic x-ray emission probability. A small increase for small impact parameter and high x-ray energies is in qualitative agreement with what is expected from induced transitions.

Quasistatic /2/ and dynamic /3/ theories, however, predict strong dependence of the NCR yield and shape on the impact parameter of the collision.

One may think of several reasons of the similitude of "singles" and "coincidence" spectra. If the NCR is produced mostly in a two-step process, i.e. production and decay of the vacancy in two subsequent collisions, the information on the impact parameter may be lost. In a one-step process the vacancy might be produced only at the moment of closest approach of the two nuclei, and the radiation is emitted in the separating system, by this removing all interference effects.

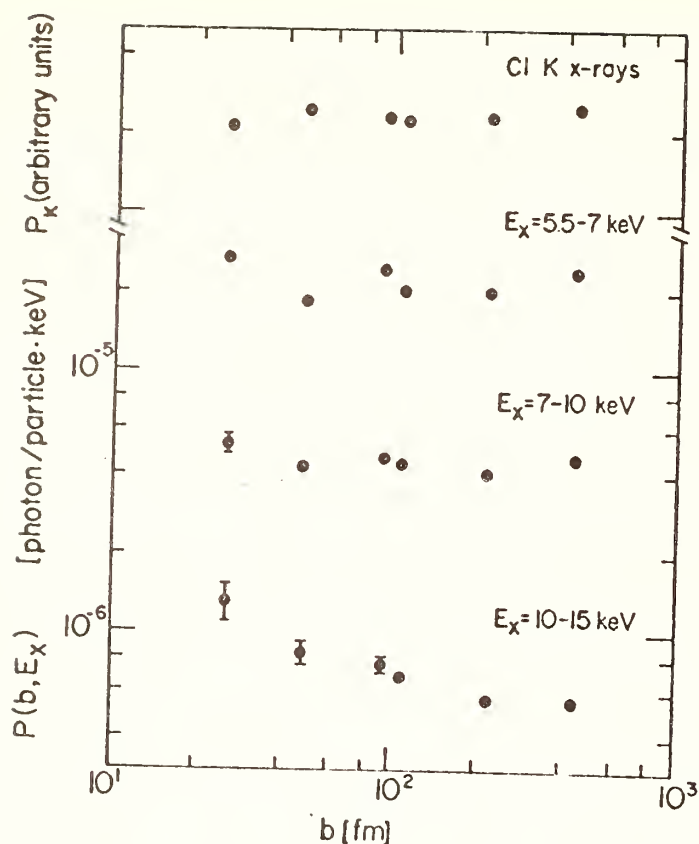


Fig. 1

For the clarification of this point, we undertook the measurement of the NCR excitation function for similar systems using gaseous and solid targets.

The spectral shape of the NCR-continuum is very similar for both types of targets at 35 MeV in accordance to previous results. At low energies, however, considerable differences are seen, the NCR yield almost vanishing for gaseous targets.

+ supported by a Minerva fellowship;
present address:
Weizmann Institute
of Science, Rehovot,
Israel.

- /1/ I. Tserruya, H. Schmidt-Böcking, R. Schulé, K. Bethge, R. Schuch, and H.J. Specht, Phys. Rev. Lett. 36 (1976) 1451.
- /2/ W.E. Meyerhof et al., Phys. Rev. Lett. 32 (1974) 1279.
- /3/ J.H. Macek and J.S. Briggs, J. Phys. B7 (1974) 1312;
K. Smith, B. Müller, and W. Greiner, J. Phys. B8 (1975) 75.

ANGULAR DISTRIBUTION AND PROJECTILE-ENERGY DEPENDENCE OF THE RADIATIVE ELECTRON CAPTURE X RAYS

R. Schulé and H. Schmidt-Böcking

Institut für Kernphysik der J. W. Goethe Universität

6 Frankfurt/Main, Germany

I. Tserruya[†]

Max Planck Institut für Kernphysik

69 Heidelberg, Germany

X-ray spectra induced by energetic heavy-ion collisions show a peak-like continuum at x-ray energies above the characteristic K-lines of the projectile, which is due to the radiative capture of target electrons into the projectile shell /1/.

We investigated the angular distribution of these x rays for 20-, 30- and 115-MeV ^{32}S ions on Be, C, and Ni targets. Fig. 1 shows for 115 MeV incident energy the resultant

distributions. The experimental results are in good agreement with a pure $\sin^2\theta$ distribution in the rest frame of the projectile, thus indicating the dipole nature of the radiation emitted in the capture process.

For ^{32}S ions in the range of bombarding energies from 5 to 115 MeV incident on Ni targets, we stu-

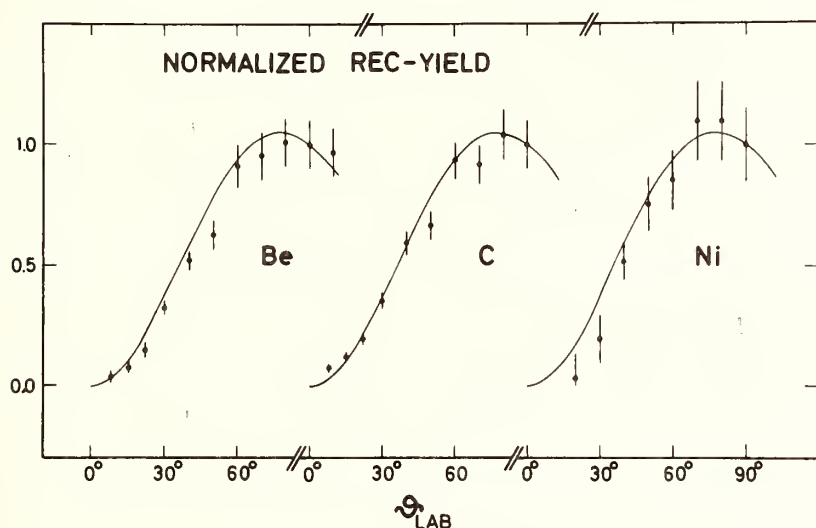


Fig. 1

died the energy dependence of the radiative electron capture (REC). The centroid energy of the REC peak was found to depend linearly on the bombarding energy, if one allows for an increase of the projectile K-shell binding energy in function of the charge state and hence in function of the bombarding energy.

The width of the REC peak, however, is proportional to the ion velocity. The ratio of the width and the projectile velocity is supposed to yield some information on the momentum distribution of the electrons captured. The value of the average kinetic energy of the target electrons derived from the data, 113 eV, is in reasonable agreement with the expected one for Ni M-shell electrons, 80 eV. This over-

estimation of the average kinetic energy, however, seems to be a common result in all REC investigations /2/. The REC cross section σ_{REC} was obtained from the yield ratio of REC to characteristic x rays,

$$Y_{\text{REC}}/Y_{\text{K x ray}} = n \cdot v \cdot \lambda_{\text{rad}}^{-1} \cdot \sigma_{\text{REC}}.$$

Here n denotes the number of target atoms per unit volume, λ_{rad} the decay constant for radiative decay of the projectile K vacancy and v the projectile velocity. The REC cross sections obtained in this way are given in Fig. 2.

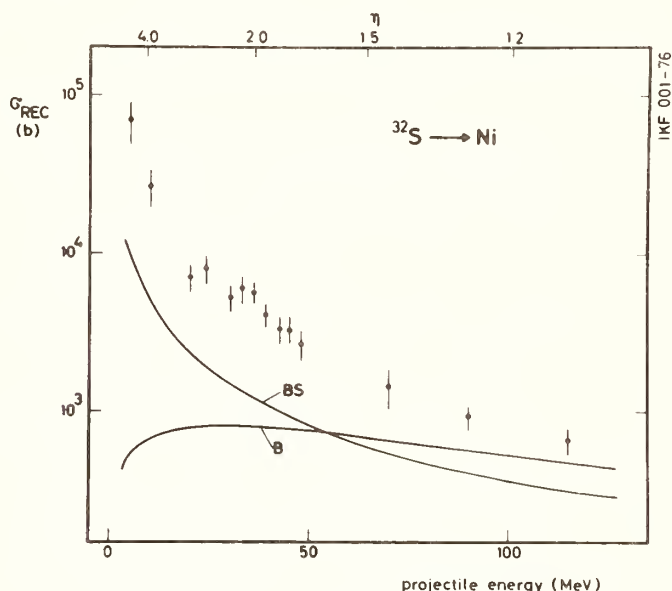


Fig. 2

We compare our results with the formulation of the REC cross section in the Bethe-Salpeter theory /3/ and the Born approximation /4/. The Bethe-Salpeter theory is supposed to be relevant for this case, since it is more appropriate for slow collisions. In both theories we made the assumption that 18 electrons, the number of M- and N-shell electrons of nickel,

contribute to the capture process. The theories are also given in Fig. 2 by the curves labelled B and BS for the Born approximation and the Bethe Salpeter theory, respectively. A qualitative agreement with the Bethe-Salpeter theory is observed, the discrepancies ranging from a factor of 7 at the lowest energy to a factor of 2 at the highest energy measured. The Born cross section, although closer to the experiment for energies exceeding 60 MeV, fails completely to describe the shape of the excitation function.

The discrepancy between the experiment and the Bethe Salpeter theory may be partially due to the way the experimental cross sections were deduced. For λ_{rad} we adapted the neutral atom value /5/, since the real value for these highly ionized projectile states is unknown. One can estimate, however, that the real value of λ_{rad} should be smaller, thus decreasing the experimental cross sections. Also the determination of the yield of S K x rays may be in error due to the absorbers used in the measurements. In Fig. 2 only the statistical errors are given, the absorber correction is estimated to be correct within a factor of 2. Considering these uncer-

tainties, the description of the excitation function by the Bethe Salpeter theory is quite satisfactory.

+ Supported by a Minerva fellowship; present address: Weizmann Institute of Science, Rehovot, Israel.

- /1/ H.W. Schnopper et al., Phys. Rev. Lett. 29 (1972) 898;
P. Kienle et al., Phys. Rev. Lett. 31 (1973) 1099.
- /2/ H.D. Betz et al., "The Physics of Electronic and Atomic Collisions, Review Papers and Progress Reports", University of Washington Press, Seattle (1975).
- /3/ H.A. Bethe and E.E. Salpeter, "Quantum Mechanics of the One- and Two-Electron Atoms", Handbuch der Physik, Springer, Berlin (1957) p. 408.
- /4/ M. Kleber and D.H. Jakubassa, Nucl. Phys. A252 (1975) 152.
- /5/ E.J. McGuire, Phys. Rev. A2 (1970) 273;
D.L. Walters and C.P. Bhalla, Phys. Rev. A3 (1971) 1919.

CONTINUOUS X-RAY SPECTRA BELOW 2 MEV IN RELATION WITH
NUCLEAR RESONANCE

Y. Cauchois
Laboratoire De Chimie Physique
11, Rue P. Et M. Curie
75231 Paris Cedex 05, France

ABSTRACT NOT AVAILABLE

SOLAR X-RAY ASTRONOMY
Allen S. Krieger
American Science & Engineering, Inc.
Cambridge, Mass.

Introduction

Solar X-ray astronomy is a branch of astrophysics. As such it is concerned with determining the properties of the solar corona from its radiations. Soft X-rays provide an advantageous waveband for examination of the lower corona. Soft X-rays are thermally emitted by plasmas with temperatures in the range of 10^6 K or more, therefore they are (along with XUV radiation) the characteristic emission of the coronal plasma. There is no background radiation at soft X-ray wavelengths from the lower, cooler regions of the solar atmosphere. Thus the corona can be observed in projection against the disk without ambiguity. This property provides coronal physics with (quite literally) a new perspective on the corona which is not available at visible wavelengths.

It is now possible to produce X-ray emitting plasmas under laboratory conditions. Many of the experimental and analytical techniques which have been developed for coronal studies may also be applicable to these laboratory plasmas. Accordingly, before proceeding on a short tour through the coronal zoo, it would be appropriate to review the techniques with which these results were obtained.

Detection Techniques

At this time solar soft X-rays are observed by three techniques:

- 1) Broad-band soft X-ray flux measurements are usually obtained with gas filled counters. Such counters are usually designed to have very good time resolution, and high efficiency.
- 2) High spectral resolution is achieved by Bragg reflection crystal spectroscopy. Recently, most crystal spectrometers have been preceded by multi-grid collimators in order to reduce the field of view. The collimators serve two purposes. They reduce the angular spread of the incident radiation to a width less than that of the crystal rocking curve in order to maximize the spectral resolution, and they restrict the field of view to a single solar feature.
- 3) High spatial resolution is obtained through the use of grazing incidence optical systems. At the present time, photographic film is almost always used as the image detector and full disk photographs of the X-ray corona can now be obtained routinely.

In the future, X-ray spectrometers will be coupled to X-ray telescopes. This will permit the acquisition of data combining both high spatial and spectral resolution. This advance has required the development of systems with higher efficiency than have been available in the past.

Interpretation of Solar X-ray Measurements

The X-ray spectrum $I(\lambda)$ emitted from a volume V on the sun may be written as:

$$I(\lambda) = \int_V F[\lambda, T(\underline{r})] N_e^2(\underline{r}) dV \quad (1)$$

where N_e and T are the electron density and temperature respectively at a point \underline{r} in V . $F(\lambda, T)$ is a spectral power function which depends only on atomic physics and solar abundances. A number of estimates of $F(\lambda, T)$ have been published.

If the corona or any coronal feature were isothermal, two measurements of $I(\lambda)$ or of $\int_{\lambda_1}^{\lambda_2} I(\lambda) d\lambda$

would suffice to reveal both the temperature and the emission integral $\int_V N_e^2 dV$.

In actuality, the corona is not isothermal. It is made up of loop like structures of various dimensions, each of which possesses its own temperature distribution. Accordingly, it is customary to rewrite equation (1),

$$I(\lambda) = \int_{T_1}^{T_2} Y(T) F(\lambda, T) dT \quad (2)$$

where $Y(T)$, called the differential emission measure represents the total emission integral within the volume V at temperatures between T and $T + dT$. It can be shown that

$$Y(T) = \sum_{i=1}^N \int_{S_i(T)} N_e^2(\underline{r}) |\nabla T|^{-1} dS \quad (3)$$

where the sum is over elementary volume elements V_i each possessing its own temperature and density distribution, and the integral is a surface integral over the closed isothermal surface $S_i(T)$ at temperature T . Unless high spatial resolution is achieved the measured $Y(T)$, a sum of the elementary $Y_i(T)$, may not resemble the individual $Y_i(T)$ very closely.

Equation (2) is not easy to invert because coronal lines are typically formed over a range of temperatures which is large compared to the variations in $Y(T)$. Individual line intensities are not independent. Thus, equation (2) is mathematically ill-conditioned. A number of approximate methods have been developed for its solution.

Solar Coronal Structures

Study of soft X-ray images of the corona has allowed us to identify five types of coronal features which emit X-rays continuously, three classes of transient X-ray brightenings, and two types of coronal features which do not emit X-rays. The five types of coronal structures which emit X-rays continuously are active regions, the interconnections between active regions and their surroundings, large scale coronal arcades, X-ray bright points, and regions of disorganized coronal structure. The three classes of transient X-ray brightenings are solar flares, bright point "flares", and filament or prominence eruptions. The two types of features which do not emit X-rays are coronal holes, and filament cavities. The nomenclature of solar physics is often obscure to the non-specialist, but all of these are coronal structures whose morphological and physical characteristics can be defined in detail. Some of the relationships described above have been well known for many years (e.g. active regions and solar flares emit X-rays), and they have been extensively studied. Others are brand new. Both bright point "flares" and the transient X-ray brightenings associated with filament or prominence eruptions were discovered from observations obtained by Skylab.

K-SHELL EXCITATION AND X-RAY SPECTRA IN HOT LABORATORY AND ASTROPHYSICAL PLASMAS

Leonid P. Presnyakov

P.N. Lebedev Physical Institute, USSR Academy of Sciences,
Moscow, USSR

At present time the most effective methods of X-ray spectroscopy diagnostics are based on measurements of relative intensities for resonance and satellite lines of highly charged ions in plasmas [1-3]. The following processes are important for spectra formation: i) dielectronic recombination, ii) direct K-shell excitation. The last one is less investigated.

The problem of excitation of highly charged ions by electron impact is considered. The system of coupled integral equations is solved for the case $Z \gg 1$, where $Z-1$ is the ion charge. The representation obtained for the radial Green function of the Coulomb field permits construction of a solution in the form of correct expansion in small parameter Z^{-1} . The asymptotically exact expression for the scattering matrix contains two terms which describe respectively potential and resonance scattering. Coupling of open channels leads to small corrections in the parameter Z^{-1} to the potential scattering, whereas the resonance contribution has the same order of magnitude as potential scattering, and in number of cases it is dominant [4-5]. As to the potential scattering, the electronic exchange effect should be taken into consideration [7]. For any specific ion the following selection rule is valid: either resonance contribution or exchange effect is important [6]. In a case of K-shell excitation of many-electron ions one should take into consideration presence of equivalent electrons in an initial and final channel [8]. The scattering theory under consideration permits to obtain a regular asymptotic expansion for autoionization rate coefficients. Results of numerical calculations are given both for resonance lines and satellites. X-ray spectra of solar flares and laser produced plasmas are discussed.

References.

1. A.H. Gabriel. Mon. Not. Roy. Astr. Soc. 160, 99 (1972)
2. C.P. Bhalla, A.H. Gabriel, L.P. Presnyakov. Mon. Not. Roy. Astr. Soc. 172, 359 (1975)
3. L.A. Vainstein, U.I. Safronova. Short Communications Physics. Lebedev Inst. 3, 40 (1972).
4. L.P. Presnyakov, A.M. Urnov. Sov. Phys. - JETP 41, 31 (1975)

5. L.P.Presnyakov, A.M.Urnov. J.Phys. B.8, 1218 (1975)
6. L.P.Presnyakov. Uspekhi Fys. Nauk. 119, 49 (1976)
7. L.A.Vainstein. Sov. Phys. - JETP, 40, 32 (1975)
8. L.P.Presnyakov. Apleton Laboratory Report No.I.M.369 (1975).

X-RAYS FROM TOKOMAKS

W. Stodiek
Princeton University
Plasma Physics Lab
Princeton, New Jersey 08540

ABSTRACT NOT AVAILABLE

300 - 500 Å LASERS AND POSSIBLE LASERS OF SHORTER λ

I.I. Sobelman
P.N. Lebedev Physical Institute
Moscow, USSR

ABSTRACT NOT AVAILABLE

ELECTRON TEMPERATURE AND DENSITY MEASUREMENTS FROM LASER PRODUCED PLASMAS*

T.C. Bristow
Laser Energetics Laboratory
University of Rochester
Rochester, New York 14627

One of the most important measurements in laser produced plasma research is the determination of the electron density and temperature. These measurements are crucial for understanding such basic problems as thermal conduction, ablation, and compression in laser fusion experiments, as well as studies of the possibility of soft x-ray laser action in this environment. Typical conditions in laser plasmas are electron temperatures of 1 keV and electron densities of 10^{21} cm^{-3} . A measurement of these conditions can be determined from relative soft x-ray line intensities. However, the results are often complicated by the non-steady state nature of the plasma. Previous interpretation of these intensities have used only a few of the observed lines, as well as an assumption of steady state ionization models (e.g., corona model). For laser plasmas the line intensities can be effected by a non-steady state population density of the ground level. The result is that steady state models will then incorrectly predict the intensities of the emitted line radiation.

It will be shown in this work that one can determine the electron density and temperature for non-thermal, non-steady state plasmas. The method consists of examining relative line intensities from an ion using the Collisional-Radiative model. Implicit in this model is the use of a non-steady population density of the ground level. Results will also extend the collisional-radiative model to include helium-like ions. The extent to which departures from steady state conditions occur will be examined for various times and Z dependencies.

An illustration of the above method will include experimental spectra of an aluminum plasma, produced by irradiating a slab target by a 10^{11} watt, 10^{-10} sec laser pulse, focussed to 10^{15} watts/cm². The spectra includes both the Lyman series of hydrogen and helium-like ions. Results will include electron density and temperature measurements using the collisional-radiative model, and a comparison of these results with those obtained from steady state models.

* Research supported in part by the National Science Foundation and by ARPA, Contract No. N00014-67-A-0398-0017.

K X-RAY EMISSION SPECTRA FROM A HIGH POWER DENSITY PLASMA

T. N. Lee

U.S. Naval Research Laboratory
Washington, D.C. 20375

Vacuum spark discharges have been used as a source of EUV and x-radiation since at least the 1890's [1]; however, in spite of its long history, this extremely simple device still finds a place in the modern laboratory. In general, when such a device is operated with an increased energy input, it is known [2], [3], [4] to emit the K x-ray radiation of highly stripped, high-Z atoms. This line radiation originates from one or more small ($\sim 10^{-9} - 10^{-7}$ cm³), high-temperature ($\sim 10^7 - 10^8$ °K) plasmas. The x-ray energy density (in both line and bremsstrahlung radiation) in such a plasma volume reaches a value of $10^6 - 10^8$ J/cm³ in a time interval of about 5×10^{-9} sec, giving a power density of $10^{14} - 10^{16}$ watts/cm³ [5]. In addition to the highly concentrated hot plasmas, the discharge also produces somewhat cooler, low-energy-density plasmas. Accordingly, the integrated spectral contributions from all the components of different plasma temperatures and states makes it difficult to unambiguously interpret the spectra obtained, unless one can also produce spatially resolved spectra with a resolution of a few tens of micrometers. Another difficulty in understanding the x-ray spectrum obtained with multiple discharge exposures is a consequence of the shot-to-shot nonreproducibility of the discharge, i.e., such spectrum is an integration of a large variety of spectral features emitted by individual discharges.

In this study, space-and-time-resolved K x-ray line spectra emitted by a vacuum spark plasma are analyzed in order to better understand the physics of the x-ray spectrum. These spectra are obtained with a single discharge exposure. The vacuum spark source used here is a laser-pulse-triggered discharge and is essentially the same device used in the previous investigation [6]. The capacitive discharge takes place between a bullet-shaped anode tip and a relatively flat cathode which is separated from the anode by a gap of approximately 5 mm. The anode material used here is iron. After triggering, the discharge current reaches its maximum value of 250 kA in about 2 μ sec. A flat LiF analyzing crystal is used, and the spectrum is recorded on Polaroid film in an XR-7 film back. Spatially resolved (in an axial direction) spectra of the discharge x-ray emission is obtained by simply mounting a 150 to 250 μ m-wide slit (oriented perpendicular to the discharge axis) onto the x-ray window (125 μ m-thick Be-foil). Pinhole (50 μ m in size) x-ray photographs are also taken simultaneously with each spectral exposure to aid in the interpretation of the spectral data. Fig. 1 shows three microdensitometer tracings taken by scanning across three different axial locations of the discharge gap in a space-resolved spectrum. The three locations correspond respectively to a plasma cloud near the anode tip (1st trace) and two axially well-separated (600 μ m in distance) point plasmas which constitute the main x-ray emitting plasmas in this particular run. The 1st tracing suggests that the plasma cloud emits

predominantly $K\alpha$ -type transition lines mainly from Fe II through about Fe X, according to the normal line intensity ratio between a $K\alpha$ and $K\beta$ line. One of the point plasmas (2nd trace) is hot enough to produce the $2p \rightarrow 1s$ transition lines of Fe XXIV, Fe XXV, and H-like Fe XXVI ions; whereas the other point plasma (3rd trace, the farthest from the anode tip) does not emit these lines. Negligibly weak $K\beta$ -type ($3p \rightarrow 1s$) lines in the 3rd trace, however, indicates that this relatively cool point plasma emits predominantly $K\alpha$ -type lines arising from Fe XI through Fe XVIII ions. It is likely that the main contribution to this feature may be Fe XVIII ions which are produced by innershell ionizations of Ne-like closed-shell Fe XVII ions. Examination of a number of pinhole x-ray photographs and spectra obtained indicate that a single, isolated hot point plasma is rarely produced but generally accompanies a cooler point plasma (or a small cloud) occurring in the immediate vicinity ($\leq 25 - \sim 100 \mu\text{m}$). For instance, the point plasma which produced the spectrum indicated in the 2nd tracing of Fig. 1 is surrounded by a small plasma cloud, according to the monitoring x-ray pinhole photograph. However, on several occasions, we were able to obtain spectra emitted by

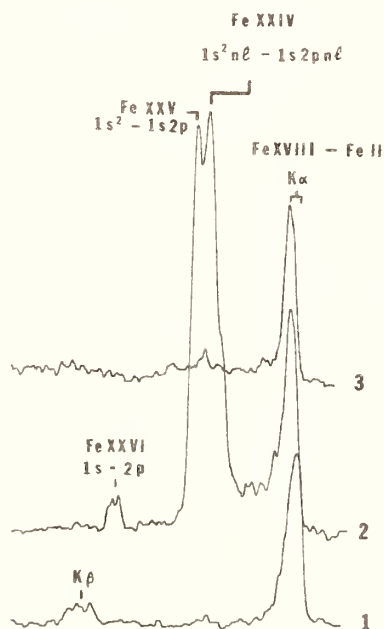


Fig. 1 - Microdensitometer scans of a space-resolved K x-ray spectrum of iron. Scan 1 is taken at the plasma cloud near the anode, and scans 2 and 3 are at two separated ($600 \mu\text{m}$) point plasmas, respectively.

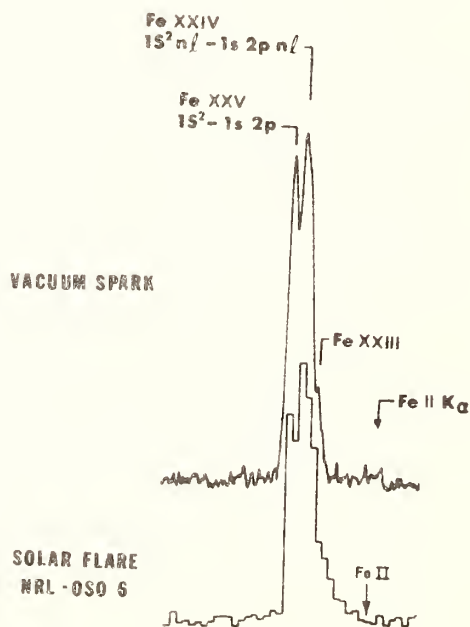


Fig. 2 - Microdensitometer scan of a space-resolved K x-ray spectrum emitted by a well-isolated point plasma. Also shown is a corresponding Fe x-ray spectrum [7] of the solar flare for comparison. . . Note the negligibly weak Fe II $K\alpha$ line in both cases.

what is believed to be an isolated point plasma. Such a spectrum is shown in Fig. 2, where a microdensitometer scan of the point plasma is shown along with a corresponding Fe spectrum [7] of the solar flare (NRL-OSO 6) for comparison. Note the strong Fe XXV $1s2p \rightarrow 1s^2$ and Fe XXIV $1s2p\ n\ell \rightarrow 1s^2\ n\ell$ lines with negligibly weak emission of the Fe II - Fe XVIII $K\alpha$ and $K\beta$ lines. This result contradicts the previous assumption [8] that a laboratory transient plasma inevitably produces K transition lines of lower stages of ionization due to the extremely transient ionizing condition (in this experiment, $\sim 10^{-9}$ sec). On the other hand, the result is in good agreement with a recent study by Feldman, et al. [9], who deduced the spectral contributions from a two-temperature plasma based on space-resolved x-ray absorption measurements. Time-resolved x-ray line radiation of Fe XXV $1s2p \rightarrow 1s^2$ and its satellite lines are obtained by properly positioning an x-ray detector and a slit at the film plane of the crystal spectrometer. The data is analyzed by comparing the signals with the simultaneously obtained pin-hole x-ray photographs or the space-resolved spectra (time integrated) obtained with the second LiF analyzing crystal. The result will be described.

I would like to thank Mr. R. H. Dixon for reading the paper and Dr. R. C. Elton for helpful discussions.

-
- [1] R. W. Wood, Phys. Rev. V, no. 1, p. 1 (1897).
 - [2] L. Cohen, U. Feldman, M. Swartz, and J. H. Underwood, J. Opt. Soc. Am. 58, 843 (1968).
 - [3] T. N. Lee and R. C. Elton, Phys. Rev. A 3, 865 (1971).
 - [4] J. L. Schwob and B. S. Fraenkel, Space Sci. Rev. 13, 589 (1972).
 - [5] T. N. Lee, Ann. New York Acad. Sci. 251, 112 (1975).
 - [6] T. N. Lee, Astrophys. J. 190, 467 (1974).
 - [7] G. A. Doschek, J. F. Meekins, R. W. Kreplin, T. A. Chubb, and H. Friedman, Astrophys. J. 170, 573 (1971).
 - [8] A. H. Gabriel, M.N.R.A.S. 160, 99 (1972).
 - [9] U. Feldman, S. Goldsmith, J. L. Schwob, and G. A. Doschek, Astrophys. J. 201, 225 (1975).

C. M. Dozier, P. G. Burkhalter and D. J. Nagel

Naval Research Laboratory, Washington, D.C. 20375

Exploded-wire plasmas are used to excite x-ray transitions in highly-ionized atoms (1). X-ray emitting plasmas are produced by passing energetic currents through thin metallic wires stretched between the output electrodes of electron-beam generators. Spectra for high atomic number elements have shown that high ionization states are produced. For example, 51-times-ionized gold has been observed (2). It has also been observed that the high ionization states are not produced uniformly along the length of plasma, but are related to pinch and flare regions that occur along the plasma length (3). The spatial information from the earlier work was somewhat limited. The purpose of this paper is to report newer results of spatially-resolved spectra from several exploded-wire plasmas.

Plasmas formed from exploding wires have rather complex structures. Figure 1 shows an x-ray pinhole image which exhibits tightly-pinched regions plus more extended flares between the pinches. The x-ray spectra from exploded wires contain three types of features: (a) thermal emission from high temperature (~ 1 keV) pinches, (b) thermal emission from cooler plasma (~ 0.1 keV), and (c) inner shell transitions excited by non-thermal electrons (3). Space-resolved spectra obtained in this work yield two types of results. Firstly, they permit association of spatial regions (pinches and flares) with spectral features (thermal and non-thermal emission). Secondly, it is possible to examine pinch-to-pinch variations in the emitted spectra.

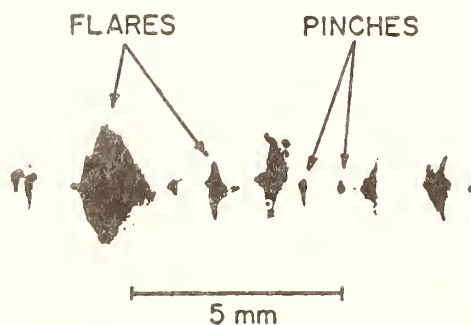


Fig. 1. X-ray pinhole image of exploded wire plasma showing pinch and flare regions.

The experimental arrangement is shown schematically in Figure 2. Wires of Al, Cu, and W were exploded in the Naval Research Laboratory's Gamble II facility. Pinhole images, such as the one in Figure 1, were obtained with a 100 μ m pinhole camera containing films of varying sensitivity. Spectra were recorded with a convex-curved-crystal spectro-

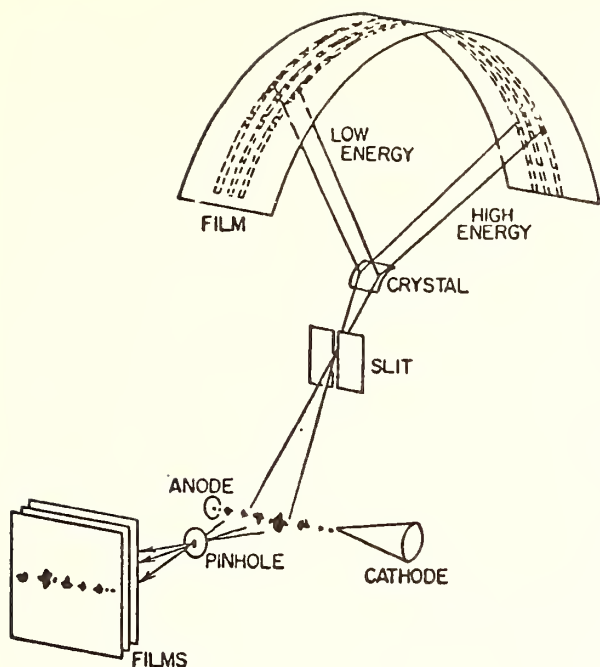


Fig. 2 Schematic of the experiment. The pinhole camera imaged the plasma. The spectrograph with slit made it possible to collect spectra from distinct regions along the plasma.

graph. The bending axis of the crystal was parallel to that of the wire. Spatial information along the plasma (wire) axis was obtained by placing a 0.025 cm slit, perpendicular to the crystal and wire axes, between the plasma and spectrograph. In addition, some spatial information was available from x-ray line widths along the dispersion direction of the spectra.

The types of results available are illustrated below:

(1) Al spectra show K lines from transitions in He-like and H-like ions. Figure 3 contains densitometer traces for two pinched regions in an Al plasma. Although the intensity varies significantly from pinch to pinch, only small variations in the temperatures are observed.

(2) Cu spectra contain L spectra from Ne-like and F-like ions. A coronal model (4) predicts plasma temperatures of 150-200 eV to produce these transitions. The spatially-resolved spectra shown these transitions are emitted from regions containing small clusters of pinches. Also, Cu L spectra were emitted from the larger cool-plasma flare regions. Spectral lines from the pinches are narrow, while those from the flares are broad.

(3) W spectra contain both M spectra from Ni-like ions and L spectra from inner-shell transitions. The M spectra are only emitted from pinched regions and indicate plasma temperatures in these regions of ~ 900 eV (3). The L-line spectra are found to come from flare regions in the W plasmas. Line-above-background intensities suggest that they are excited by electrons with energies in excess of 30 keV (5).

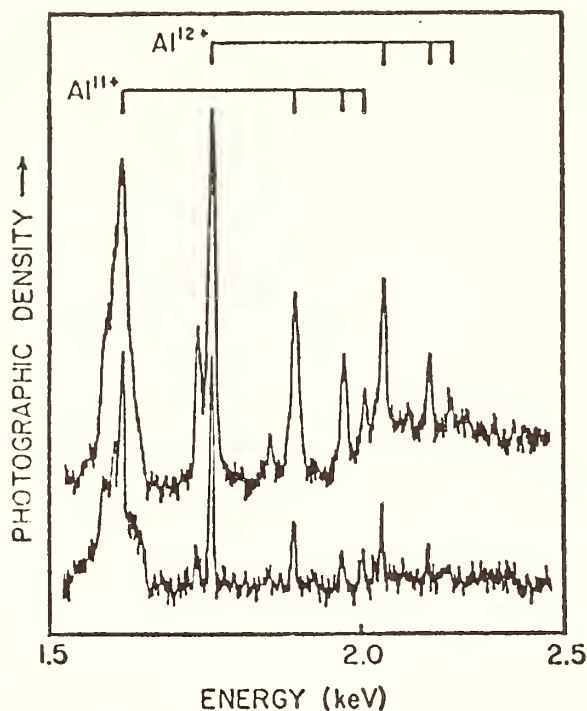


Fig. 3. Densitometer traces of Al spectra from two pinched regions.

In summary, spatially-resolved spectra have provided valuable insight into the origin of the different types of x-ray emission in exploded-wire plasmas. The spatial origin of various x-ray spectral features were determined and variations in x-ray intensity along the wire were obtained.

* This work was partially supported by DNA and ERDA.

- (1) D. Mosher, S. J. Stephanakis, I. M. Vitkovitsky, C. M. Dozier, L. S. Levine and D. J. Nagel, Appl. Phys. Lett. 23, 429 (1973).
- (2) C. M. Dozier, P. G. Burkhalter and D. J. Nagel (to be published).
- (3) P. G. Burkhalter, C. M. Dozier and D. J. Nagel (to be published).
- (4) D. Mosher, Phys. Rev. A 10, 2330 (1974).
- (5) D. B. Brown (private communication).

PICOSECOND PROXIMITY-FOCUSED X-RAY STREAK CAMERA

A. J. Lieber, H. D. Sutphin, and C. B. Webb

University of California
Los Alamos Scientific Laboratory
Los Alamos, New Mexico 87545

It has been recognized for several years in the LASL laser-fusion program that x-ray diagnostics with temporal resolution better than 1 ps and good spatial resolution are essential for understanding the basic laser-fusion process. Compression instabilities are predicted to be 1 to 2 ps. Therefore, a program was initiated to develop a new streak camera with picosecond x-ray resolution, since all existing cameras were based upon a streak tube capable of delivering only 10 to 20 ps resolution in the design limit.

Among the old tube's weaknesses are its pinhole electron geometry requires operation at low peak conductance or gain to reduce the effect of space-charge distortion at the pinhole and the loss of temporal and spatial resolution. Expensive follow-on intensifiers must be used in an attempt to restore system gain for recording. The overall length of the basic tube of 22 cm from photocathode to phosphor allows longitudinal photoelectron velocity dispersion to reflect as intolerable time dispersion for true picosecond operation. Finally, such features as overall package size, vacuum compatibility, dynamic range, and trigger jitter limit the utility of the overall camera package as a practical diagnostic in the laser-fusion laboratory where experimental space around the target is at a premium, and the cost of each shot requires a record each time.

Our camera, the Pico-X, was developed primarily as an x-ray diagnostic although application of the design to the visible spectrum represents an advance in the state-of-the-art of these cameras as well.[1] A schematic of the tube is shown in Fig. 1.

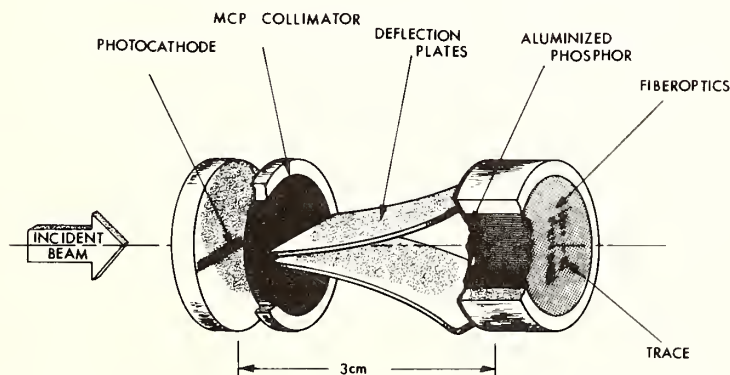


Fig. 1. Schematic of proximity-focused streak tube.

The tube utilizes a microchannel plate in a new manner--as a passive collimator for transverse photoelectron velocity control.[2,3] The overall distance of 3 cm from photocathode to phosphor minimizes longitudinal electron dispersion without the need for a lens for longitudinal velocity selection. Such a lens would result in a longer tube which in turn would require high selectivity and reduced sensitivity. In this type of intensifier resolution and conduction are practically independent eliminating the need for an expensive high-gain follow-on intensifier. Proximity-focused devices require maximum electric fields to map photoelectrons from cathode to phosphor making them ideal for producing maximum photocathode extraction fields at the same time. Peak extraction fields generated between polished plates far exceed those that can be generated using the grid structure of the old tube, thereby yielding the highest possible photocathode sensitivity.

The overall limit on tube length has required care be taken in the design of the sweep electrodes. Our plates were designed using a computer simulation code.[4] A comparison of the prototype Pico-X with a standard visible RCA C 73435 (which is the basis for most x-ray tubes) is shown in Fig. 2. Using this tube, an instrument package that is vacuum compatible and small enough to fit inside the chamber without blocking the field of other diagnostics has been developed. This camera is capable of taking 24 frames without breaking vacuum--a fact that has greatly speeded data recording. To ensure a streak each cycle of the laser, a new low-jitter power supply had to be developed. Basic to this system is a laser triggered solid dielectric spark gap which has shown less than 20 ps jitter in over 400 cycles.



Fig. 2. Comparison of prototype Pico-X with standard RCA C 73435 streak tube.

Streaks formed when a 200- μm -diameter-nickel ball is irradiated by two Nd:YAG laser beams are shown in Fig. 3. The left beam has been optically delayed from the right by 20 ps for calibration of the camera sweep. Quality of the profiles allows quantitative densitometer profiles. Data will be presented showing the irradiation of hollow 50- μm -diameter-glass microballoons using the dual beam laser. These data include a trace showing an instability of less than 3 ps in the collapse of a microballoon. This serves to verify, experimentally, the theoretical prediction of 2.7 ps resolution for the prototype (the design should be capable of 0.6 ps resolution).

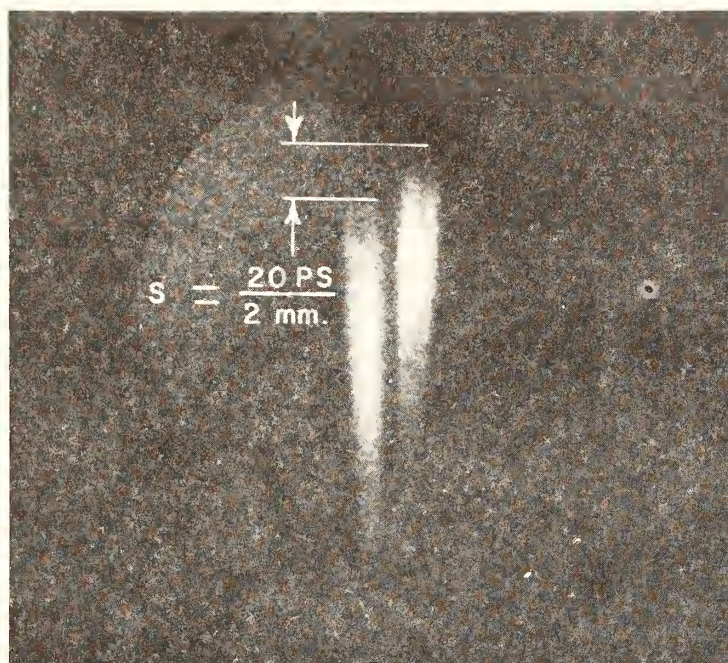


Fig. 3. Sweep calibration using x-rays generated when nickel ball is irradiated by a dual beam Nd:YAG laser of 70 ps duration.

REFERENCES

1. "Pico-X" patent waiver applied for by General Engineering Applied Research, Inc., 260 Sheridan Avenue, #414, Palo Alto, CA 94306.
2. A. Lieber, R. Benjamin, H. Sutphin, and C. Webb, Nuc. Inst. and Methods, 127 (1975) pp 87-92.
3. C. Webb, A. Lieber, H. Sutphin, and R. Benjamin, Rev. Sci. Instrum. 47, 1 (Jan 1976) pp 149-150.
4. S. Gitomer, R. Benjamin, W. Hall, A. Lieber, and H. Sutphin, IEEE Conference on Plasma Science, Ann Arbor, MI, May 14-16, 1975.

THEORETICAL INVESTIGATIONS CONCERNING THE EVOLUTION OF THE ATOMIC
EFFECTS CONTRIBUTION IN THE SPECTRA (40 TO 400 eV)

F. Combet Farnoux and F. Keller

E R "Spectroscopie Atomique et Ionique" Université Paris-Sud
Bâtiment 350 - 91405 Orsay (France)

The atomic origin of inner shell ionization processes in the photoabsorption and electron energy loss spectra obtained with solid state samples is well known now. However, the exact formulation and the importance of the atomic effects (compared with the environment effects) vary with the energy range and the elements considered. We will give a brief review of these spectra recently studied both by optical absorption using a synchrotron light source and by electron energy loss spectroscopy, in the energy range from 40 to 400 eV. Among them, we will mention: the rare gases (np and (n-1)d ionization), Ag, Sn, Te, Cs, Ba and the rare-earth metals (4d ionization), Na, Mg, Al (2p ionization), some transition metals Sc, Ti, Mn, Ni, Ir ... (np ionization), and some heavy elements (Au, Hg, Bi, U ...).

We will emphasize the various atomic calculations of photoionization cross sections σ which have been performed to interpret these spectra; they are relevant to various techniques, among them:

- independent particle models taking into account some final state correlations, as we use for heavy elements,
- many body perturbation theory as used by Kelly (1),
- random phase approximation with exchange, as used by Amusia (2) and Wendin (3).

The comparison of these calculations with spectra obtained from gaseous and solid samples allows us to distinguish several situations, according as we consider the atomic configuration of the ionized element or the energy range.

A) If the photon energy $\hbar\omega < E_0$ (generally less than 100 eV), the calculated structures of σ and $df/d\omega$ (oscillator strength distribution) are seen modified in the absorption curves ($\mu \propto df/d\omega \cdot (1/n)$), since the refraction index n may vary strongly. So, entirely different theoretical methods are used to treat photoeffect in solids (4): they are based on the spectral response of the free-electron gas due to the change in the effective potential seen by the conduction electrons. However, Figure 1 shows that an atomic calculation of $df/d\omega$ relative to the 5d subshell of Au would give a right envelope of the experimental curve if the threshold value took into account both the atomic and extraatomic relaxation effects (5).

B) If $\hbar\omega > E_0$, except some edge singularities explained by the

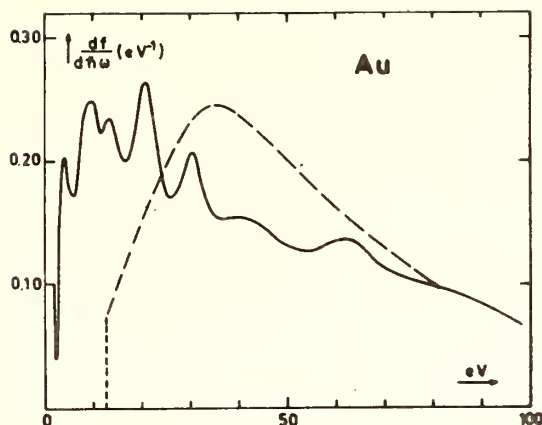


Figure 1

Oscillator strength density: solid line represents the results of Wehenkel and Gauthé(10) calculated from their electron energy loss spectrum; dashed line shows our theoretical results obtained with Hartree-Fock continuum wave functions.

solid state physicists and some resonant structures well resolved in the metallic vapor spectra, the general trend of absorption and its amplitude is approximately the same in both gases and solids. However, the atomic contribution may be modulated by the environment as shown by Na, Al and Si, beyond the L_2L_3 thresholds (6): this modulation was interpreted by backscattering of the outgoing electron from neighboring atoms. Also, the relaxation effects are still more important than above: first, atomic relaxation effects, as mentioned for Ba by Wendin (7) when comparing his RPAE calculations with the Ba vapor spectrum (8), and extraatomic relaxation effects which we will discuss from our calculations for Au and Hg (see Figure 2).

According to the atomic configuration of the ionized element, we must distinguish 2 situations: a) Ionization of nl subshells in atoms such as no $n, l+1$ electron is bound in the ground state: in this case, the transitions to the continuum ($nl \rightarrow \epsilon, l+1$) are major, compared to the discrete transitions ($nl \rightarrow n, l+1$), but their maximum is delayed as long as the potential barrier (for $l \gg 2$) is not reached. It is clearly seen in Figure 2 for the calculated $5d$ and $4f$ cross sections of Hg. The transitions ($nl \rightarrow n', l-1$) may give resonant structures near the threshold, as observed near the N_6N_7 thresholds of heavy elements.

b) Ionization of nl subshells in atoms such as the $n, l+1$ subshell is partially filled in the ground state: the $4d$ subshell in rare-earth elements, the $5d$ in actinides and the $3p$ in the first series transition metals are concerned. In

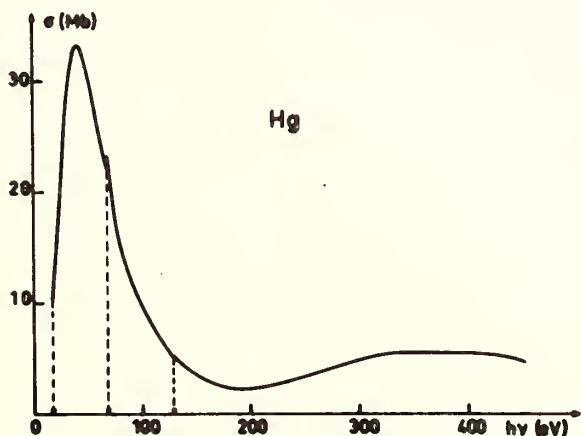
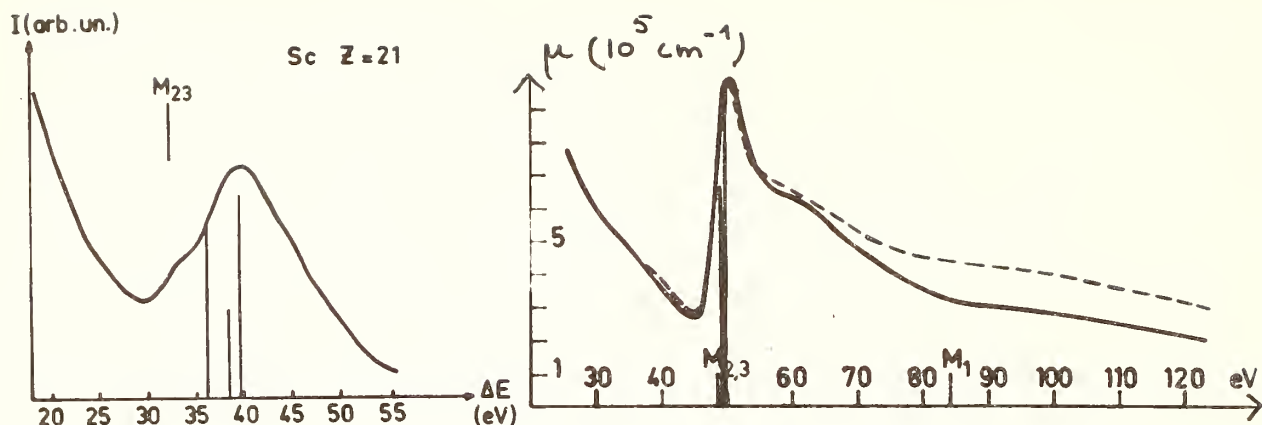


Figure 2:

Total Hg cross section = sum of partial cross sections σ_{5d} , σ_{5p} , σ_{4f} calculated with Hartree-Fock continuum wave functions.



Figures 3 (left) and 4 (right) we show some experimental results relative to the $3p$ excitation in Sc (Fig.3) and Mn (Fig.4). The solid line represents the electron energy loss spectrum obtained by Colliex and Trebbia (9) for Sc, and the absorption coefficient calculated by Wehenkel and Gauthé (10) from their electron energy loss spectrum of Mn. In Fig.4, the dashed line represents the absorption spectrum obtained at DESY (11). In both figures, the vertical lines show the relative intensities and the position of the final states for the transitions $3p^6 3dN \rightarrow 3p^5 3dN+1$; we have calculated them in an intermediate coupling scheme (12). While such a scheme allows to understand well the $4d$ excitations in the rare-earths (13), it is not so evident for the transition elements in which the $3d$ electrons are not so localized as the $4f$ in the rare-earths. However, the model suggested by Dietz et al. (14) for Ni has been extended recently by Davis and Feldkamp (15) to treat other $3d$ transition metals.

- (1) H.P.Kelly and A.Ron Phys.Rev.5A ,168 (1972)
- (2) M.Ya.Amusia in "Vacuum Ultraviolet Radiation Physics"
ed.Pergamon Vieweg (1974) p.205
- (3) G.Wendin ibid. p.225
- (4) J.Friedel Comm.Sol.State Phys. 2, 21 (1969)
- (5) D.A.Shirley Chem.Phys.Lett. 16, 220 (1972)
- (6) J.J.Ritsko,S.E.Schnitterly and P.C.Gibbons Phys.Rev.Lett.
32 ,671 (1974)
- (7) G.Wendin Phys.Lett.51A ,291 (1975)
- (8) P.Rabe,K.Radler and H.Wolff Proc.Int.Conf.on VUV Radiation
Physics, Hamburg, 1974 , ed. E.E.Koch ,p.247
- (9) C.Colliex and P.Trebbia Physica Fennica,9 Suppl.S1,83(1974)
- (10) C.Wehenkel and B.Gauthé Phys.Stat.Sol.(b) 64 ,515 (1974)
- (11) B.Sonntag,R.Haensel and C.Kunz Sol.State Comm.7,597 (1969)
- (12) F.Combet Farnoux Physica Fennica,9 Suppl.S1,80(1974)
- (13) J.L.Dehermer,A.F.Starace,U.Fano,J.Sugar,J.W.Cooper Phys.Rev.Lett.26 ,1521 (1971)
- (14) R.E.Dietz,E.G.McRae,Y.Yafet and C.W.Caldwell Phys.Rev.Lett.33 ,1372 (1974)
- (15) L.C.Davis and L.A.Feldkamp Solid State Communications
(In press)

ANALYTIC CALCULATION OF SCREENED PHOTOEFFECT CROSS SECTIONS*

James McEnnan, Sung Dahm Oh and R. H. Pratt

Department of Physics and Astronomy, University of Pittsburgh
Pittsburgh, Pennsylvania 15260

Renewed interest in atomic inner shell photoionization processes has been stimulated by the needs of the thermonuclear fusion program. In particular cross sections for highly ionized systems are of concern. Numerical studies of photoeffect from ions have been reported by Manson [1], and we have reported similar studies for ionic bremsstrahlung [2]. Since it may not be practical to produce numerical tabulations for all ionic species of interest, it is clear that further theoretical insight would be useful so that simple analytic interpolation schemes can be introduced. It is, thus, important to understand the circumstances in which the atomic potential in the interior of the atom (characterized by a few parameters) suffices to determine the complete photoeffect process, since this leads to a convenient analytic description of photoeffect cross sections in terms of atomic number, ionic charge and photon energy.

We have recently developed an analytic perturbation theory for non-relativistic radial wave functions in a screened Coulomb potential [3,4] which is particularly convenient for the description of atomic inner shell processes. The method is based on the expansion of the potential inside an atom as a series in λr having the form,

$$V(r) = (-a/r)[1 + V_1\lambda r + V_2(\lambda r)^2 + V_3(\lambda r)^3 + \dots]. \quad (1)$$

where $\lambda = \alpha Z^{1/3}$ is a small parameter characterizing the screening. The coefficients, V_k , may be chosen such that the form (1) converges rapidly and gives a good approximation to realistic atomic potentials, such as those of Herman and Skillman, in the interior of the atom. Wave functions are obtained as series in λ with simple analytic coefficients, due to the special symmetries of the Coulomb problem. Both bound and continuum shapes are correctly treated in the region $\lambda r < 1$. For inner bound states this includes all of the region where the wave function is large. Similarly, high energy continuum wave functions will have completed several oscillations in this region so that, by $r = \lambda^{-1}$, the asymptotic region has been reached. Hence, expressions for bound state normalizations as series in λ are accurate, in general for the K-shell, and for other low lying levels of high Z elements. Continuum normalizations are valid at energies on the order of the K-shell binding energy above threshold. Bound state energies and continuum phase shifts are also obtained in these circumstances.

We note that this approach is complimentary to other analytic methods used in photoeffect; for example, quantum defect theory and its generalizations. In quantum defect theory one uses the fact that at large distances the potential seen by an electron is essentially Coulombic. The effect of inner-electron screening, then, is only to

change the normalization and phase of the exterior Coulomb wave function. Moreover, at low energies the phase shift can be determined semi-empirically by analytically continuing the quantum defect parameter to positive energies. In this way one obtains analytic expressions for screened photoeffect cross sections which are valid for transitions of outer electrons at photon energies near threshold. On the other hand, because of our expansion of the potential (1), we can construct analytic screened wave functions which are accurate in the interior region.

We have used the wave functions obtained with this perturbation theory to calculate K and L shell atomic photoeffect in nonrelativistic dipole approximation. The resulting cross sections are expressed analytically in terms of the point Coulomb Stobbe formula together with wave function normalization and shape corrections due to screening, given as simple elementary functions. At high energies we reproduce the result of normalization screening theory; the screened cross section is just the point Coulomb result multiplied by the square of the ratio of screened to point Coulomb bound state normalizations. At low energies, shape corrections may be significant. In this region the screened corrections can be given in terms of an expansion in powers of $1/v^2 = 2(\omega - T_c)/a^2$, where $T_c = a^2/2n^2$ is the point Coulomb binding energy, $a = \alpha Z$ and ω is the photon energy. In particular, for the K-shell (assuming $v \gg 1$) we have for the screened cross section the simple result,

$$\sigma = \sigma^c (N/N^c)^2 \{ 1 - \Lambda_2 \left[\frac{58}{15} - \frac{34}{7} \frac{1}{v^2} + \frac{110}{21} \frac{1}{v^4} \right] - \Lambda_3 \left[\frac{310}{21} - \frac{10274}{315} \frac{1}{v^2} + \frac{34246}{693} \frac{1}{v^4} \right] \}, \quad (2)$$

where $\Lambda_k = v_k (\lambda/a)^k \equiv v_k (1.13\alpha Z^{-2/3})^k$ and σ^c is the Stobbe formula.

Comparisons of our analytic results with exact numerical screened calculations for the nonrelativistic dipole cross section and also with the full numerical relativistic multipole calculations are given for the K shell of several elements in the following table.

Table I. Comparison of our analytic results for the K shell, σ_{An} , with exact numerical values of the K shell nonrelativistic dipole cross section, σ_{Num} , and with the full relativistic results of Scofield, σ_{Rel} . T_B is the Herman-Skillman ground state binding energy, $T_c = a^2/2$ the corresponding point Coulomb energy. All energies are in keV. Cross sections are in barns.

Z	ω	σ_{An}	σ_{Num}	σ_{Rel}
20($T_B = 3.99$) ($T_c = 5.44$)	6	2.223(4)	2.217	2.218
	10	5.526(3)	5.544	5.560
	20	7.511(2)	7.544	7.583
	40	9.252(1)	9.293	9.396
	60	2.619(1)	2.631	2.681
	80	1.055(0)	1.059	1.091

36($T_B=14.0$) ($T_c = 17.6$)	15	1.416(4)	1.394	1.383
	20	6.633(3)	6.571	6.609
	40	9.709(2)	9.667	9.793
	60	2.987(2)	2.979	3.044
	80	1.269(2)	1.266	1.306
	100	6.459(1)	6.448	6.728
	200	7.543(0)	7.538	8.501
79($T_B=73.4$) ($T_c = 84.9$)	80	2.317(3)	2.294	---
	90	1.695(3)	1.680	---
	100	1.277(3)	1.267	1.273
	120	7.771(2)	7.719	---
	150	4.178(2)	4.155	4.416
	200	1.843(2)	1.835	2.057

Good results are obtained even for relatively low Z at energies close to threshold. At higher energies there is agreement with the relativistic multipole results beyond the expected range of validity of the nonrelativistic dipole approximation. Since one can show that relativistic or multipole effects separately become important above 10 keV, these results imply an effective cancellation between relativistic and higher multipole contributions in the total cross section from S states. It is due to this cancellation, which had previously been noted by Ron in the point Coulomb case, that we obtain such good results even for high Z .

Similar results are obtained for the L shell. Applications to ionic cases will also be discussed.

* Work supported in part by the National Science Foundation under Grants MPS74-03531-A01 and GF-36217.

1. S. T. Manson, Bull. Am. Phys. Soc. 19, 1106 (1975); 20, 1461 (1975); 21, 179 (1976); 21, 690 (1976).
2. C. M. Lee and R. H. Pratt, Bull. Am. Phys. Soc. 21, 574 (1976).
3. James McEnnan, Lynn Kissel and R. H. Pratt, Phys. Rev. A 13, 532 (1976); (E) (1976).
4. James McEnnan, Lynn Kissel and R. H. Pratt, Phys. Rev. A (to be published).

LOW ENERGY PHOTOIONIZATION CROSS SECTIONS
FROM PROTON INDUCED X-RAY SPECTROSCOPY

Allen Lurio, Wilhad Reuter and Johann Keller
IBM Watson Research Center
Box 218, Yorktown Heights, N.Y., 10598

INTRODUCTION

The atomic photoelectric effect is by far the dominant process by which electromagnetic radiation is absorbed in the soft x-ray region. The photoionization cross section, σ , for this process is directly related to the mass absorption coefficient $\mu = (N_A/M)\sigma$, where N_A is Avogadro's number and M is the atomic weight.

At the present time there exists very little experimental data on mass absorption coefficients $\mu(\text{cm}^2/\text{gm})$ in the wavelength range 10-100 Å. Of the existing data, reliable measurements are principally available only for those elements which can be studied in the gaseous state. [1] The reason for this circumstance is that previous techniques applicable to solids required very thin, large area, self-supporting films of the absorber. Difficulty in making uniform films and in accurately measuring their areal density and purity (e.g., surface oxides) have limited reliable measurements to a few special cases. For this reason, researchers needing reliable mass absorption coefficients in the soft x-ray region are presently using Henke's tabulation [1] which is based on interpolations from the calculated results of Veigele [2] which agree well with the measured mass absorption coefficients of gases.

We shall present in this paper a new and reliable technique for measuring the mass absorption coefficients of solids in the soft x-ray region. In this technique the absorbing film is supported directly on a substrate which, under proton bombardment, will generate the characteristic x-rays whose absorption will be measured.

EXPERIMENTAL

Metal absorber films in the thickness range 300 to 2500 Å were evaporated onto polished vitreous carbon substrates. For each film we measured the area density ρ_A , the number of atoms per square cm, by two different techniques. For the non-destructive measurements we used Rutherford backscattering (RBS) of 2 MeV He^+ ions. [3] In this method ρ_A is determined by counting the number of He ions backscattered from the surface film into a known solid angle for a measured number of incident ions. We estimate the overall accuracy of this technique to be $\pm 5\%$.

After this non-destructive measurement, the films were dissolved and analyzed wet chemically. Atomic absorption spectroscopy with an estimated accuracy of $\pm 3\%$ was used for the determination of Ag, Au, Ni and Co. Colorimetric methods were used for all other elements with an accuracy of $\pm 5\%$ except for Hf where we claim an accuracy of only $\pm 10\%$.

In addition to measuring the film areal density, RBS also yields a quantitative estimate of the oxygen content and impurities present in the films. In most cases we observe two small oxygen peaks in the RBS

spectrum corresponding to oxygen in the front and back sides of the film. The largest oxygen content occurred for the 2400 Å Ti film where in contrast to all other metal films the oxygen was distributed throughout the entire film. We calculated that $1.98 \mu\text{gm}/\text{cm}^2$ of oxygen was present but since $\mu_{\text{oxygen}}^{(44.7 \text{ Å})} = 6044$ this would cause less than 1.5% transmission loss.

A beam of protons from our Van de Graaf accelerator was normally incident onto our sample targets thereby exciting C K α radiation from the substrate. The radiation is dispersed by a crystal α spectrometer with an LSD crystal and is detected by a gas flow proportional counter. Other details of our vacuum chamber and spectrometer have been described previously. [4]

For each sample we counted the number of C K α x-rays for the same number of protons incident onto the reference and film coated carbon substrates at a number of different positions on the film.

The thick target x-ray yield for protons on carbon goes through a rather flat maximum near 950 keV, [6] and in this region a ± 100 keV energy change of the proton beam causes a change in the emitted x-ray intensity of approximately 1%. The greatest energy loss for protons passing through our films was 14.5 keV for the case of 2400 Å thick Ti film. In view of this we took all our data at 1 MeV.

RESULTS

As previously explained, we may ignore the change in x-ray production due to the energy loss in the film. Let I_o be the detected x-ray intensity generated in the carbon substrate and I_F be the intensity from the film coated substrate. We may write therefore:

$$I_F = I_o e^{-\mu \rho_A / \cos \theta} \quad \text{or} \quad \mu = (\cos \theta / \rho_A) \ln(I_o / I_F)$$

We selected absorber thicknesses yielding I_o / I_F in the range from 10 to 2.5 permitting the use of relatively thick films without an appreciable increase in error. This minimized problems associated with the substrate topography and with the analytical determination of the absorber mass.

In Table 1 we list for all samples used in our experiments, the areal density ρ_A , the experimental value of μ and Veigele's theoretical value for comparison. In most cases the agreement is quite good. Two cases showed significant disagreement with Veigele. These are Mo and Nb. Since rather thin films of these elements, of the order of 300 Å were used in the first measurement we suspected possible non-uniformity on a 100 Å scale as the cause for the observed discrepancy between experiment and theory. We therefore repeated the measurements using films two to three times thicker.

The second set of results shown in Table 1 for Zr, Nb, and Mo were obtained from these films. Consistently higher mass absorption coefficients were found for the thicker films, which may indicate some non-uniformity problems leading to erroneously low values if the mass deposition is less than $30 \mu\text{gm}/\text{cm}^2$.

The very large difference in μ between theory and experiment for C K $_{\alpha}$ in Mo and also to a lesser extent in Nb is far outside our experimental uncertainty and must be attributed to the presence of the M V absorption edge in Mo (227 eV) and Nb (205 eV) close to the energy of the radiation source (277 eV). The omission of solid state effects in the free atom absorption theory becomes critical in such cases and explains the large observed deviation found for Mo.

REFERENCES

1. B. L. Henke and E. S. Ebisu, University of Hawaii, AFOSR Report 72-2174.
2. W. J. Veigele, Atomic Data Tables 5, 51 (1973).
3. See "Ion Beam Surface Layer Analysis," ed. by J. W. Mayer and J. F. Ziegler, Elsevier Co., Lausanne, Switzerland (1974).
4. W. Reuter, A. Lurio and J. F. Ziegler, J. Appl. Phys. 46, 3194 (1975).
5. J. M. Khan, D. L. Potter and R. D. Worley, Phys. Rev. 139 A1735 (1965); L. H. Toburen, Phys. Rev. A5, 2482 (1972).

Table 1

Experimental Results for the Mass Absorption Coefficient μ at C K $_{\alpha}$ (44 Å)

Element	ρ_A ($\mu\text{gm}/\text{cm}^2$) RBS	ρ_A ($\mu\text{gm}/\text{cm}^2$) Wet Chemistry	μ (cm^2/gm) Present Exp.	μ (cm^2/gm) Veigele
Al	35.4	34.8	28800	30200
Ti	104.3	106	8056	8094
V	56.3	60.2	10600	8840
Co	58.9	57.4	16300	14730
Ni	72.3	75.7	19100	17270
Zr	31.0	31	26100	31300
	66.0		28200	
Nb	23.7	26	22400	33900
	63.8		25000	
Mo	27	27.4	17900	32420
	72.1		19200	
Ag	98.9	106	6610	5507
Hf	46.1	49 \pm 5	18600	18030
Ta	45.6	43	18100	18390
W	42.2	47	16200	18750
Au	65.8	62.3	13800	15200
	114		14000	

STUDY OF 4d SHELL EXCITATIONS
BY ELECTRON SCATTERING

C. P. Franck, P. C. Gibbons*, S. E. Schnatterly

Joseph Henry Laboratories
Princeton University
Princeton, New Jersey 08540

We will present inelastic electron scattering measurements at and above the transitions of 4d electrons in tellurium and barium fluoride into the conduction band. We are particularly interested in broad resonances similar to those seen in Xe [1] which have been described as atomic plasma oscillations [2]. Our apparatus [3] enables us to make detailed shape measurements in the electric dipole limit as well as surveys of the loss spectrum as a function of momentum transfer (q).

Types of Measurements

We have performed three types of electron scattering experiments on Te and Ba in BaF_2 . The first, low momentum transfer energy loss studies, have the advantage of good statistics because of the high counting rates experienced at low q . Also, the spectral shapes can be compared to photoabsorption results, since for small q , inelastic electron scattering and optical absorption yield the same information. We have obtained low momentum transfer data in the 0 to 200 eV energy range with a resolution of between 75 and 300 MeV.

The study of other than electric dipole transitions becomes possible at non-zero momentum transfer, the second type of measurement. The limiting factors here are decreased counting rates and elastic-inelastic multiple scattering. This latter problem is a type of incoherent multiple scattering which causes the $q = 0$ spectrum to appear in measurements made at high momentum transfers. The process consists of an elastic scattering of the incident electron from a phonon or structural defect and an independent inelastic scattering event. In Te, we have noticed the appearance of elastic-inelastic double scattering at $q = 1.3 \text{ \AA}^{-1}$.

Electron diffraction patterns, the third type of measurement, have been taken with our apparatus out to $q = 5 \text{ \AA}^{-1}$. They help characterize the order and composition of the targets. The high count rates experienced at zero energy loss facilitate these measurements.

Target Design

We have used two types of evaporated film preparations for the study of Te and BaF_2 . The first kind of target uses a Formvar film

*Present address: Department of Physics, Washington University,
St. Louis, MO. 63130

substate over which we deposit between 500 and 1000 Å of material. The second type of target differs only in that the substate is a 200 Å carbon film on a copper wire grid. This substate has the advantage of greater stability than the Formvar during the high-temperature evaporation of BaF₂.

Results

Our $q = 0$ spectra for Te and BaF₂ qualitatively agree with those produced by photoabsorption experiments [4,5]. Additional structure is present in our observations of the broad resonances of BaF₂ when a comparison is made with earlier metallic and vapor phase Ba studies [5].

One of our primary interests is the evaluation of the first few moments of the broad peaks in Ba and Te. The zeroth moment is a measure of the strength of the excitation, the first moment provides the center of gravity, or average energy of the excitation, and the second moment gives the width. We evaluate the moments as a function of momentum transfer. The variation of the first moment with q corresponds to plasmon dispersion in bulk solids. Moment evaluation requires careful subtraction of the underlying background due to lower energy excitations. Results will be presented for both the 80 eV feature in Te and the structures in Ba between 100 and 165 eV.

References

1. R. Haensel, G. Keitel, P. Schreiber, C. Kunz; Phys. Rev. 188, 1375 (1974).
2. S. Lundqvist in Elementary Excitations in Solids, Molecules and Atoms, Part A, ed. J. Devreese et al., 281-312 (Plenum, New York, 1974).
3. P. C. Gibbons, J. J. Ritsko, S. E. Schnatterly; Rev. Sci. Inst. 46, 1546 (1975).
4. P. Rabe, K. Radler, H. W. Wolff in Vacuum Ultraviolet Radiation Physics, ed. E.E. Koch et al., 247-249 (Pergamon, Vieweg, 1974).
5. B. Sonntag, T. Tuomi, G. Zimmerer; Phys. Stat. Sol. 58, 101 (1973).

EXPERIMENTAL STUDY OF PHOTOABSORPTION IN Gd AND Dy IN THE VICINITY OF THE 4d IONIZATION THRESHOLD

M. Cukier, P. Dhez, P. Jaeglé

E. R. "Spectroscopie Atomique et Ionique" N° 184 du C. N. R. S.
Université Paris Sud, Bât. 350 -91405 ORSAY - France .

Photoabsorption of rare earths in solid phase in the energy range of the $4d \rightarrow 4f$ transitions is a very particular case where the observed discrete transitions are similar to the ones observed in free atoms .

It is now clear that this is due to several facts. In rare earths the 4f shell is incomplete and well localized. This shell is also closer to the nucleus than other more outer shell filled before in lighter elements, in particular 5s and 5p subshells. The f-electrons are embedded and do not participate to the chemical bonding as manifested by the well known chemical identity between all rare earths. For these reasons $4f^N$ configuration in rare earths, where N varies from 0 for La to 13 for Yb, present the same behaviour and keep then atomic character independently of the phase. In this case the 4f states do not contribute to the conduction band and are well localized below the Fermi level in the ground state (1)

In 1967, in a systematic study of rare earths absorption in the 50-500 eV region with thin films, Zimkina et al (2) were the first to observe a large absorption feature due to the excitation of the 4d-electrons. Haensel et al (3) then, with a better resolution, studied Ce, Pr, Nd, Sm and gave the first absolute values for the absorption coefficient. Explanation for presence of peaks in the absorption curve was given in 1972 by Sugar (4). Calculations for transitions of the type $4d^{10}4f^N \rightarrow 4d^94f^{N+1}$ were performed with radial integral considered as adjustable parameters and fitted to the observed resonances. The lines observed were supposed to arise from triply ionized atoms, which explained all structures spread over 10eV and the large peak by transitions on $4d^94f^{N+1}$, corroborating the assumption made.

We present here experimental results obtained with synchrotron light and a spectromonochromator described elsewhere (5, 6). In this case the system was used in the one grating mode with a 576 gr/mm-1° blaze angle grating. Grazing incidence angle of 7°5 was used to increase the intensity in the wavelength range of interest in the first positive order and without orders over lapping. Continuous electron multiplier was fixed directly behing the exit slit. Solid thin samples have been prepared under good vacuum and then transfered in the experimental chamber.

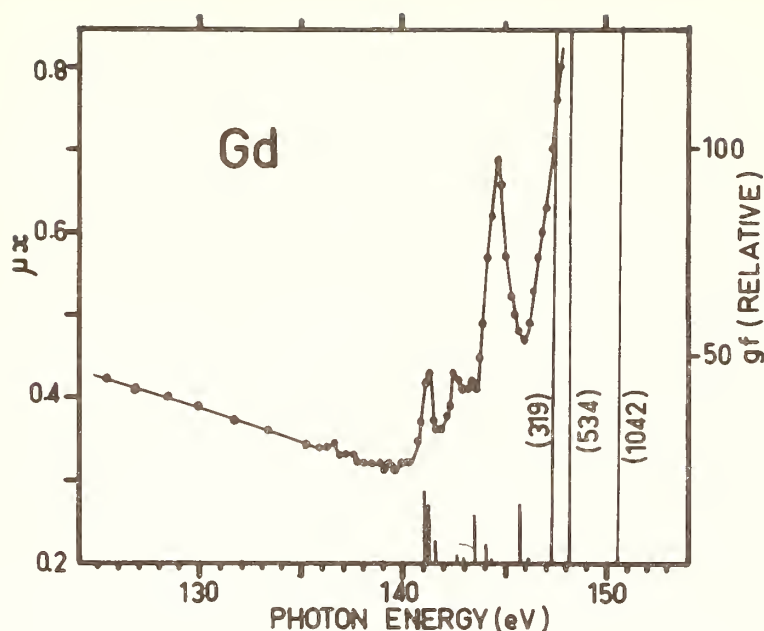


Fig. 1: Comparison of μx absorption coefficient for gadolinium, with the calculated oscillator strength gf of the $4d^{10}4f^78S_{7/2} \rightarrow 4d^94f^8$ from ref. (4). The three gf values out of scale are given between parenthesis.

Figure 1, shows the relative absorption coefficient μx obtained with unbacked gadolinium thin film at energies lower than the energy of the large peak. Each point corresponds to one measurement for direct and absorbed light. Relative oscillator strength gf from ref(4) was drawn. The relative intensities experimentally observed are not in as good agreement with the calculated values in the case of Gd as for Ce, Pr and Er (4). This is particularly evident when the intensities of the peak around 140 and 145eV are compared. After the measurements the free film was oxidized but new measurement did not give any shift or change in intensities. Other measurements with Gd backed on aluminium or carbon gave the same result.

Figure 2 shows the case of Dysprosium over a larger energy range. For this element a thin film was evaporated on carbon and the measurement of the thickness allowed to deduce absolute values for the absorption coefficients. Curve in figure 2 compared with relative values obtained by Zimkina (2) shows more details in fine structures because of our better resolution. Unfortunately, oscillator strengths do not exist for Dy, as for Gd and only Bearden values (7) for the $N_{IV,V}$ threshold can be indicated.

We have not tested the oxydation effect on Dy sample as in the Gd samples and nothing can be inferred from the insensitivity observed with Gd. Oxydation effects have been observed resulting in a change of intensities of small peaks and a shift for the large maximum for Ce and CeO by Haensel(3). Suzuki et al(5) reported also small differences in these features for La and Ce when combined with halides. Recently Dufour et al (9) have observed the X-Ray photoemission spectra from the 4d levels for Gd and Dy in metal and oxyde showing that only broadening appears in Gd but broadening and shift occur in Dy. In fact,

spectras obtained by XPS or UPS, X-ray emission and photoabsorption are not directly comparable because of differences in selection rules and final state involved ; however such a comparison can bring valuable informations to understand more deeply the very particular situation occuring in rare earths 4f shell. As a general rule more direct comparisons can be done between photoabsorption and electron energy loss spectra (10) or with yield spectra as demonstrated for $N_{IV, V}$ excitation in metallic cesium obtained with synchrotron light (11).

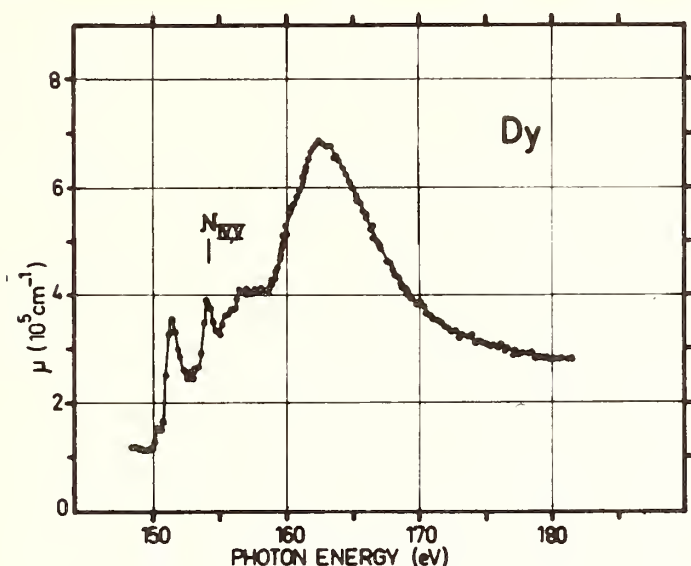


Fig. 2: Absolute photon absorption coefficient μ measured for dysprosium in the region of $N_{IV, V}$ threshold.

The authors wish thank P. Marin for his help in the use of the ACO storage ring , M. Berland for his contribution to the measurements and M. Gasnier for the preparation of Gd sample.

+ Work carried out in Orsay at LURE, Laboratory jointly created by the C. N. R. S. and the University Paris Sud.

- (1) Y. Baer, G. Busch-J. of Electron Spectroscopy 5, 611(1974).
- (2) T. M. Zimkina, V. A. Fomichev, S. A. Gribovskii, I. I. Zhukova Soviet Phys. -Solid State 9, 1128 and 1163(1967).
- (3) R. Haensel, P. Rabe, B. Sonntag-Solid State Com. 8, 1845(1970).
- (4) J. Sugar-Phys. Rev. B5, 1785(1972).
- (5) P. Jaeglé, P. Dhez, F. Wulleumier-IVth Conference on Vacuum U. V. Rad. Phys. (Hambourg 1974)Ed. E. Koch et al. p. 788
- (6) P. Jaeglé, P. Dhez, F. Wulleumier-Rev. Sci. Inst. (to be published)
- (7) J. A. Bearden, A. F. Burr-Rev. Mod. Phys. 39, 125(1967).
- (8) S. Suzuki, T. Ishii, T. Sagawa-J. Phys. Soc. Japan, 38, 156(1975).
- (9) G. Dufour-Thèse d'Etat (to be published)
- (10) M. Cukier, P. Dhez, P. Jaeglé, F. Combet Farnoux -Phys. Let. 51, 173, (1975).
- (11) H. Petersen-Phys. Stat. Sol. B72, 591(1975).

Lynn Kissel and R.H. Pratt
Department of Physics and Astronomy
University of Pittsburgh
Pittsburgh, Pennsylvania 15260

Using the numerical partial wave method developed by G.E. Brown [1] and extended by W.R. Johnson [2], we are continuing the study of elastic scattering of photons from isolated atoms. The method is exact for the scattering from each atomic electron, described by a single-electron wave function in a screened static central potential. We identify the individual contributions to the total scattering amplitude made by each atomic orbital and contributions due to specific electric and magnetic multipole transitions. Sensitivity of the result to the choice of potential can be explored; we have primarily used self-consistent fields of the Hartree-Fock-Slater type. These results permit a systematic comparison with experimental observations. We will first give a brief survey of the current status of theory and experiment. Since most previous theoretical work has been based on the simpler form factor approximation, with emphasis placed on the choice of wave functions within that approximation rather than on the validity of the form factor itself, we will then present results of a detailed comparison of the form factor with exact numerical results for the K-shell. Preliminary results of a similar survey for higher shells will be presented. Our discussion will reflect two different interests in Rayleigh scattering; its role in elastic scattering and its contribution to total photon attenuation.

Previous work of this type has focused either on the zero frequency limit or on the energy range 100-1000 keV. The work and some of the motives for interest in the process are summarized in the accompanying table. In the zero frequency limit, Rayleigh scattering is related to the electromagnetic susceptibility of the atom. Johnson and Feiok [2] used this method to calculate electric and magnetic dipole susceptibilities of the noble gases. They found good agreement with experimental values only for magnetic susceptibilities. For the electric susceptibilities, the numerical calculation, while agreeing with previous nonrelativistic calculations, seriously overestimated the experimental values.

<u>ENERGY</u>	<u>PREVIOUS WORK</u>	<u>INTEREST IN RAYLEIGH</u>
Threshold	Johnson [2]	electromagnetic susceptibilities dominates total attenuation
Threshold to K-edge	none	apparent singularities in amplitudes
K-edge to 1000 keV	Johnson [3] Brown [1]	contribution to total attenuation dominates elastic scattering
> 1000 keV	Brown [4] Cornille [5]	needed to detect Delbruck scattering

The original work of Brown, et. al. [1] focused on the K-shell of mercury over the energy range 164-1130 keV using the point Coulomb potential. Johnson and Cheng [3] have calculated exact Rayleigh scattering amplitudes for atomic numbers in the range 30-82, for photon energies on the range 100-1000 keV using self-consistent fields. They compared this data with experiments at angles 30-150 degrees. On the average, agreement of 5% to 20% was found. While such data is probably sufficient for prediction of elastic differential cross sections for angles in the region 30-150 degrees, it is quite inadequate for calculation of total elastic cross sections since Rayleigh scattering is becoming increasingly forward peaked with increasing energy. For still higher photon energies, other elastic scattering processes begin to become important. Interest in measurement of the real part of the Delbrück scattering amplitude requires the accurate theoretical prediction of the Rayleigh amplitude. Only two exact numerical calculations have been reported above 1 MeV. Considering the K-shell of mercury, Brown [4] performed a calculation at 1.13 MeV while Cornille and Chapdelaine [5] calculated scattering at 2.615 MeV. Above several MeV, Rayleigh scattering becomes extremely forward peaked and is vanishingly small at ordinary angles.

All present tabulations of elastic scattering cross sections by bound electrons and tables of attenuation coefficients for photons in matter have been based on the form factor approximation. Relativistic derivations of the form factor have generally required some nonrelativistic assumptions, suggesting that its validity should be restricted to low energies. However recently Gavrilu and

Florescu [8] studied for the point Coulomb case elastic scattering of photons by K-shell electrons at high energies and found that neglecting terms of order $(Z\alpha)^2$, the form factor approximation in fact becomes exact in the high energy limit and so should be expected to improve with increasing energy.

We have made a systematic and detailed study of Rayleigh scattering amplitudes for K-shell electrons over a wide range of atomic numbers and for photon energies 1-1000 keV. Comparison of the exact amplitudes with those predicted by the form factor have been made. It has been found that for momentum transfers of 0-5 (inverse Angstroms), the form factor differs from exact calculations by a constant multiple, depending upon the incident photon energy. This range of momentum transfers represents the angles through which more than 75% of the scattered photons pass and provides the dominant contribution to the total Rayleigh scattering cross section. In most cases, these are angles considerably less than 30 degrees. Over this energy range the form factor prediction for high Z elements deteriorates with increasing energy, while for low Z elements the prediction improves with increasing energy. At larger angles, the form factor gives poor predictions for elastic scattering, often wrong by a factor of two from the exact results. A similar study of validity of the form factor is currently being completed for higher shells. Sample comparisons for the L-shell will be presented.

References:

- [1] G.E. Brown, R.E. Peierls, J.B. Woodward, Proc. Roy. Soc. A227, 51-58 (1955)
- [2] W.R. Johnson, F.D. Feiock, Phys. Rev. 168, 22-31 (1968)
- [3] W.R. Johnson, K. Cheng, Phys. Rev. A13, 692-698 (1976)
- [4] G.E. Brown, D.F. Mayers, Proc. Roy. Soc. A242, 89-95 (1957)
- [5] H. Cornille, M. Chapdelaine, Nuovo Cimento 14, 1386 (1959)
- [6] V. Florescu, M. Gavrilă, "Elastic Scattering of Photons by K-shell Electrons at High Energies", Phys. Rev. (to be published)

ANGULAR CORRELATION BETWEEN K AND L X RAYS IN PLATINUM

A. L. CATZ

Department of Physics, University of Massachusetts at Boston
Boston, Mass. 02116

During the past several years angular correlations between K and L x rays were measured in a number of elements [1] to test the accuracy of the theoretically predicted [2] admixtures to the x-ray transitions of magnetic quadrupole (M2) radiation, admixtures, which were shown to affect the angular correlation functions [3]. The expected effects of the M2 admixtures are small however and their quantitative determination imposes stringent requirements on the experimental system regarding stability and absence of spurious anisotropies. Unfortunately the extent to which the system meets such requirements is difficult to ascertain for lack of easily accessible cascades of known anisotropies and in the energy range of interest, which could serve for comparison purposes.

In the present experiment aimed at determining the angular correlation between K α 1 and L x rays in Platinum an improved experimental system was employed which allowed the simultaneous recording of all K-L x-ray coincidences and use of the known isotropic K-L x-ray cascades as internal standards relative to which the anisotropies of the other cascades could be accurately determined.

THE X-RAY SOURCE. Platinum x rays were obtained from a radioactive source of Au 195. The x rays are emitted from the Au 195 source, in part, as a result of the Au 195 decay by electron capture to Pt 195 and, in part, following the deexcitation by K electron internal conversion of several excited states of Pt 195 populated in the Au 195 decay. A source of approximately 40 μ Ci intensity was prepared by evaporating a small droplet of Au 195 chloride in HCl solution on a thin (0.84 mg/cm²) Mylar sheet.

X-RAY DETECTORS AND DATA ACQUISITION SYSTEM. The K x rays were detected with a cooled Intrinsic Germanium detector 10 mm in diameter and 5 mm thick the energy resolution of which was sufficient to completely resolve the Pt K α 1 from the K α 2 x rays. The L x rays were detected with a cooled Si(Li) detector 4 mm in diameter and 3 mm thick. The L α , L β and L γ peaks were well resolved.

Spectra of coincident K and L x rays were accumulated using a system which combined a time-to-amplitude converter (TAC) and a computer-based multichannel analyzer capable of storing on magnetic tape for each coincidence K-L x-ray event the following three parameters: the energies of the coincident K and L x rays and the time interval between their detection as measured by the TAC. This last parameter allowed the separation of the true coincidences from the random ones. Measurements were performed using a standard angular correlation table at relative angles between the two detectors ranging from 90 to 270 degrees in steps of 30 degrees; angles were interchanged at random at measured time intervals.

DATA ANALYSIS AND RESULTS. The data accumulated in each individual measurement were analyzed as follows: 1) For all K-L x-ray cascades the number of true, random and net-true coincidences recorded were determined; in the process, background contributions to both K and L x-ray peaks due to higher energy radiations were subtracted. 2) For all K α 1 and K α 2-L x-ray cascades contributions due to K α -L x-ray coincidence events involving "unrelated" K α and L x rays i.e. K α and L x rays emitted in different cascades which occur in the same atom in quick succession (See Ref [4] p 638) were subtracted. In the present experiment the number of such coincidences is determined with high accuracy from the measured numbers of K β -L x-ray coincidences, all of which are of this nature, [5], [6], and the simultaneously measured ratios of intensities of K α to K β x rays. 3) Following the above two steps, for all K α 1-L x-ray cascades the numbers of net, coincidence events involving "related" K and L x rays recorded during the measurements were normalized relative to one of the following quantities: the number of random coincidence events recorded for the given cascade in the measurement (with proper correction for radioactive source decay), or the numbers of K β -L α , K β -L β , or K α 2-L β true coincidences recorded. Each of these quantities is expected to be independent of the angle of measurement, thus providing the internal standard of normalization desired, relative to which the anisotropies of the K α 1-L x-ray cascades could be determined. The results obtained using the different normalization procedures were in close agreement with each other. In the final stage of analysis the normalized values of the numbers of coincidences recorded for each cascade in all measurements performed at a given angle were properly averaged and the resulting weighted averages $N(\theta)$ were fitted by a weighted least square procedure to functions of the form $N(\theta) = N(0) + N(2) P(2) (\cos \theta)$. From these, the angular correlation coefficients $A_{22} = N(2)/N(0)$ were then determined (See Ref. [4]).

The following results were obtained for the coefficients A_{22} from data analyzed thus far: 0.236 ± 0.027 for the K α 1-L1 cascade; 0.024 ± 0.006 for the K α 1-L α cascade and 0.021 ± 0.017 for the K α 1-L β cascade. These results are slightly lower than the values of 0.2983, 0.0348 and 0.0535 theoretically predicted [2] for these three cascades, respectively. The experiment is still in progress and results of higher precision are expected to be available for presentation at the conference. Possible causes for deviation from theoretical predictions will also be discussed.

REFERENCES

- [1] M. R. Zalutsky, E. S. Macias and A. L. Catz Phys. Rev. A 11, 75 (1975). This work contains references to most previous works on the subject.
- [2] J. H. Scofield, U CRL Report No. 51232, 1972 (unpublished).
- [3] A. L. Catz Phys. Rev. Letters 24, 127 (1970)
- [4] A. L. Catz Phys. Rev. A 2, 634 (1970)
- [5] A. L. Catz and E. S. Macias Phys. Rev. A 9, 87 (1974)
- [6] E. S. Macias and M. R. Zalutsky Phys. Rev. A 9, 2306 (1974)

SOFT X-RAY PHOTOIONIZATION OF XENON BY PHOTOELECTRON SPECTROMETRY WITH SYNCHROTRON RADIATION ^{✱ +}

F. Wuilleumier, M.Y. Adam

E.R. "Spectroscopie Atomique et Ionique" n° 184 du CNRS
Université Paris Sud, Bât.350, 91405-Orsay, France
and

V. Schmidt, N. Sandner, W. Mehlhorn

Fakultät für Physik der Universität Freiburg, Freiburg i.B.
D-7800 - Germany

Photoelectron spectrometry is an unique method to delineate the electronic structure and dynamics of atoms. In particular, electron correlations can be investigated with accuracy, indirectly through their influence on single electron properties, and directly through the existence and intensity of multiple ionization or excitation processes (1).

Up to recently the number of photon sources supplying a photon beam of well defined energy and high intensity was very limited. Most of the electron spectrometry experiments have been carried out either with UV resonance lines of low energy or with the $MgK\alpha$ and $AlK\alpha$ lines. In the last few years, the use of soft X ray emission lines brought new informations about the energy dependence of various atomic properties in He (2) and Ne (3). These first energy analysis revealed clearly the interest to use a continuous photon source such as synchrotron radiation to investigate, as a function of the photon energy, the atomic subshell properties by photoelectron spectrometry ; in addition, many interesting processes can only be studied with a continuously adjustable photon energy.

Up to now only one group had obtained some results in the study of gaseous species by electron spectrometry with synchrotron radiation. Using the Daresbury synchrotron, single subshell cross sections and angular distributions of photoelectrons have thus been measured in neon (4), argon (5) and xenon (6). However, in these experiments, the band pass of the monochromator had to be set at 3 to 7 eV in the 100 eV region. Only the gross features of single photoionization processes have been observed and neither the fine structure of the photoelectron and Auger lines nor the multiple excitation processes could be studied.

We present here the first results of an experimental program devoted to the study of atomic subshell properties (3) and Auger processes (7) by electron spectrometry with the synchrotron radiation emitted by the ACO storage ring in Orsay (8). The electron produced are energy analyzed with a cylindrical mirror analyzer with the cylinder axis parallel to the incident radiation. The acceptance of a 2π azimuthal angle

around the incoming photon beam is the only experimental set up giving independence from the state of polarization of the incident radiation (9). In these first experiments, the analyzer accepted electrons about the magic angle of $54^{\circ}44'$ which makes the results independent of the angular distribution effects. The apparatus has been designed to work in the first order focusing mode with intermediate focus point (10). A detailed description of this spectrometer and of the operating procedure will be given elsewhere (11). We just mention here that the residual magnetic field is less than 2 milligauss and that the resolution (FWHM) can be varied from about 0.2% to 1.5%, except at very low kinetic energy, where the limit is around 30 meV. In the first experiments with ACO, this resolution was set at 0.9 %.

Continuum radiation from ACO operated at 540 meV-100 mA, was monochromatized with the 1m grazing incidence monochromator specially designed for the laboratory LURE (12). In the experiments presented here, the apparatus has been used in the one grating mode with a fixed exit slit between 60 and 150 eV with a band pass of 0.4 to 1.5 eV. A gold foil-electrometer amplifier combination monitored the incident radiation. Photon flux of typically 10^9 photons/Å/sec at 100 Å in the source volume of the electron spectrometer were measured.

In the first experiments, electrons ejected from xenon at various photon energies were analyzed. Spectroscopically pure xenon was introduced into the spectrometer via a multicapillary array at pressures varying in the source volume from 10^{-5} to 10^{-4} Torr.

Figure 1 shows the electron spectrum following photoionization of

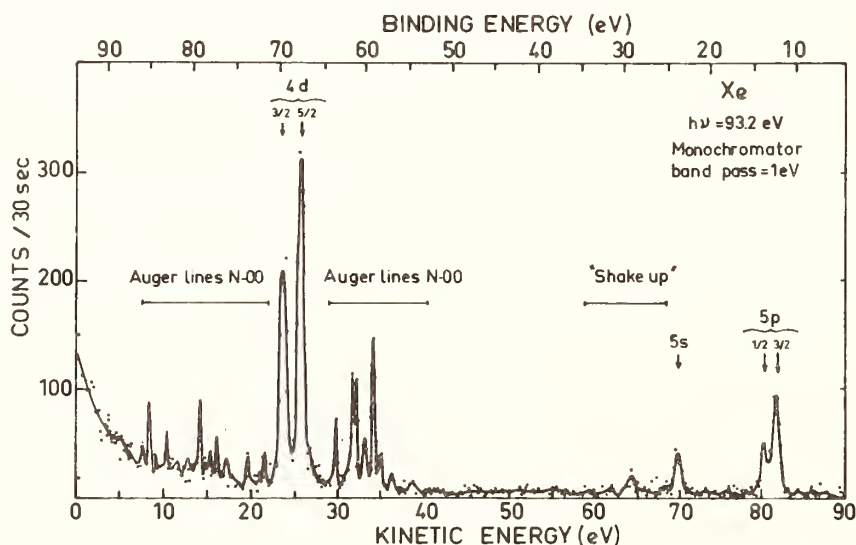


Fig. 1 - Electron spectrum of Xe after photoionization. "Shake up" indicates both true shake up and configuration interaction processes.

Xe with 93.2 eV photon energy and a monochromator band pass of 1 eV. All main features of the photoelectron and Auger spectra can be distinctly seen. The spin-orbit splitting of the 4d and 5p subshells is well re-

solved, the Auger lines previously observed after electron impact (13) are clearly resolved and identified, and, in the 60-70 eV kinetic energy region, some processes corresponding to the simultaneous excitation of a 5p electron accompanying the ionization of another 5p electron are clearly observable. The width of the Auger lines shows that the experimental resolution of the electron spectrometer is about 0.9 % and thus equal to the calculated one. The width of the 4d peaks, about 1 eV, is mainly due to the monochromator band pass. One can also note the high peak to background ratio at the 4d peaks (~ 30).

The detailed study of all the features observed in this spectrum is now undertaken as a function of the photon energy. Preliminary results have already been obtained showing that the energy and width of the Auger lines increases with decreasing photon energy near threshold. This demonstrates that post collision effects occur also in the Auger decay of atoms following photoionization, as can be expected from the investigation of Auger spectra after electron impact (14) or in the ion charge distribution after quasi-photon ionization (15).

The authors gratefully acknowledge the contribution of Dr P.Dhez to the success of these experiments by setting the monochromator. They would like also to thank Dr P.Jaeglé for his constant support and Dr P.Marin for his help in operating the storage ring.

*Work carried out in Orsay at LURE, laboratory jointly created by the C.N.R.S. and the Université Paris-Sud.

[†] Research supported by the Centre National de la Recherche Scientifique, France, and the Deutsche Forschungsgemeinschaft, Germany.

- (1) M.O.Krause, "Photoionization and Other Probes of Many-Electron Interactions", ed. F.Wuilleumier, Plenum Press (1976), p.133.
- (2) M.O.Krause and F.Wuilleumier, J. Phys. B., 5, L143 (1972)
- (3) F.Wuilleumier and M.O.Krause, Phys. Rev. A 10, 242 (1974)
- (4) K.Codling et al., J. Phys. B, 9, L83 (1976)
- (5) R.G.Houlgate et al., J. Phys. B, 7, L 470 (1974)
- (6) J.B.West et al., J. Phys. B, 9, 407 (1976)
- (7) S.Flügge, W.Mehlhorn and V.Schmidt, Phys.Rev.Lett.29,7 (1972)
- (8) F.Wuilleumier, LURE Report 74/03, Orsay (1974)
- (9) V. Schmidt, Phys. Lett. 45A, 63 (1973)
- (10) J.S.Riesley, Rev. Sci. Instrum., 43, 95 (1972)
- (11) M.Y.Adam, F.Wuilleumier and N.Sandner, V.Schmidt, W.Mehlhorn (to be published)
- (12) P.Jaeglé, P.Dhez and F.Wuilleumier, Rev.Sci.Instrum (to be pub.)
- (13) L.Werme, T.Bergmark and K.Siegbahn, Phys.Scrip., 6, 141 (1972)
- (14) S.Ohtani et al., Phys.Rev.Lett., 36, 863 (1976)
- (15) M.Van der Wiel, G.R.Wight and R.R.Tol, J.Phys.B,9, L5 (1976)

ABOUT THE $L\alpha$ SATELLITE SPECTRUM
CAN $L\alpha$ DIAGRAM LINES BE OBSERVED ?

J.P. Briand, M. Frilley, P. Chevallier, A. Chetoui, A. Touati,
M. Tavernier and J.P. Rozet
Institut du Radium and Université Pierre et Marie Curie
11, rue P & M Curie, 75231 Paris Cedex 05, France.

The LX ray spectra exhibit a large amount of satellite lines which are generally not well identified namely in the case of heavy elements. For heavy elements most of the double vacancy production in photo or electron ionization is due to Auger (KLX) or Coster-Krönig transitions, direct multiple ionization by shake-off (+ up) processes having a probability which is some orders of magnitude lower. In this paper, we intend to present experiments in which direct identification of LX ray satellites is performed and to give the interpretation of an old experiment, done by M. Frilley (1), and the results of which were never explained. It can also be pointed out how important may be the contamination of XL diagram lines by satellites, the energy shift of which is lower than the natural width of monoionization rays.

Let us first present the main features of the Frilley's experiment. Frilley studied with a curved mica crystal spectrograph, the L spectrum of bismuth, and namely the $L\alpha_1$ spectra observed in two different modes of excitation :

- the usual electron bombardment in a conventional X ray tube with a bismuth anode. In this case, the approximate ratio of direct ionization for the L subshells is 22/23/55 for $L_I/L_{II}/L_{III}$.

- the internal conversion of the 46,5 keV nuclear energy level of Ra D. The ^{210}Pb (Ra D) β decay leads to the 46,5 keV nuclear energy level of ^{210}Bi which can only be converted into L subshells. In this case, the $L_I/L_{II}/L_{III}$ direct ionization ratio is very different from the previous one and equal to 92/5/3. Then, we can say that in this case, the direct ionization roughly occurs only in the L_I shell.

In the first case, he observed the conventional $L\alpha_1$ spectrum which is characterized by the appearance, near the diagram line, of a main satellite which is situated at 34 eV with respect to the $L\alpha_1$ line and the relative intensity of which is about 3-10%.

In the second case, the same satellite appeared but with an intensity of 50% of the diagram ray which was also observed.

This experiment was not understood because it was expected that in the second case, the diagram ray would not be observed and that only a $L\alpha$ satellite spectrum would appear.

In order to explain these results and to give an identification of the observed lines, we performed two different experiments.

(i) The energy shifts of L satellite lines emitted by a $L_{III} + X$ hole for instance, following a $L_I L_{III}$ X Coster-Krönig transition can be measured, in principle, in a coincidence experiment, between the emitted Coster-Krönig electron and the corresponding $L\alpha_1$ line. In fact, it seems not to be possible to detect at present time such an electron line with a detector having a transmission good enough to allow us to realize an electronic coincidence. (The energy of a Coster-Krönig electron is of few keV for heavy elements.) However, it is possible, using SiLi solid state detectors in a special experimental arrangement to realize an other coincidence experiment which can give the same information ; if one creates a hole in the K shell, one can do a coincidence with the KL_{III} X Auger line which leads to the same doubly ionized configuration. These Auger lines have a large energy (~ 70 keV) and can be detected in a SiLi detector. We realized such an experiment using a radioactive sample which decays by K electron capture. The resolution of a SiLi detector for electron detection is in fact, very poor, but using selected detectors the resolution of which can be of the order of 600 eV at 60 keV, it is possible, in biparametric coincidence to separate a special group of Auger lines as the $KL_{III} M_{IV,V}$ group for instance, from the others. One needs then to use a special housing for the detector in order to introduce the sample without any change of the cooling of the detector and of the vacuum. The X rays were recorded in an other but conventional, SiLi detector the resolution of which was about 200 eV. In order to avoid problems connected with random coincidences and background, a biparametric coincidence set-up was used. This experiment was realized using ^{207}Bi sample which leads to K shell ionization of lead atom. It was deduced from the shift of the $L\alpha$ line observed in coincidence with the $KL_{III} M$ Auger line, that the satellite following $L_{III} M_{IV,V}$ ionization states is shifted in energy by about 42 eV with respect to the diagram line, i.e. with an energy which is in rough accordance with the satellite observed by Frilley.

(ii) We then realized another experiment for lead atoms in order to know the energy shift of a $L\alpha_1$ satellite coming from a $L_{III} N$ initial state. Such state can be obtained in a coincidence experiment between a $K\alpha_2$ line and the subsequent $L\alpha_1$ line. The L_{II} ionization due to the $K\alpha_2$ transition is followed by an $f_{2,3}$ Coster-Krönig transition which can only lead for energetic reasons to $L_{III} N'$ (or $L_{III} O$) final ionization states. Using long time exposure, because the $f_{2,3}$ Coster-Krönig transition has a low intensity and because we need a great number of points in order to have a good accuracy in energy, we then found that this energy shift is about 6 eV. The natural width of this line being 10 eV we can say that there is in fact no observed energy shift. There is so two different groups of satellites, the first for M additional hole which is shifted by 42 eV and the second for N or O additional hole which nearly lie at the same energy that the one of the diagram line. The ratio of the $L_I L_{III} M$ and $L_I L_{III} (N \text{ or } O)$ Coster-Krönig transitions was calculated by Mac Guire (2) and there is a good fit between the predicted ratio of the two satellites and the Frilley's results. This experiment gives the only direct identification of L satellites and we can then

see how it is difficult to interpret the L satellite series spectra. Another interesting conclusion is also given by this type of experiment : the diagram lines are generally not pure and sometimes (that is exactly the case for lead or bismuth) the degree of satellite contamination is so high that the diagram line is not really observed. Such a similar conclusion was presented by Krause, Wuilleumier and Nestor (3) who calculated using a relativistic Hartree-Slater program, the energies of the LX ray satellites of zirconium and also found that only double ionization states with LM adjacent shells can lead to energy shifts higher than the natural widths.

We thank Dr. M.O. Krause for helpful discussions.

References

- (1) M. Frilley, B.G. Gokhale and M. Valadares. C.R. Acad. Sci. Paris 232 (1951) 157.
- (2) E.J. Mc Guire. Phys. Rev. A3 (1971) 1801.
- (3) M.O. Krause, F. Wuilleumier and C.W. Nestor Jr. Phys. Rev. A6 (1972) 871.

A DIRECT PROOF OF THE SHAKE MODEL :
 THE K_{α} SATELLITE SPECTRUM FOLLOWING ELECTRON CAPTURE
 J.P. Briand, P. Chevallier, A. Chetoui, J.P. Rozet, M. Tavernier
 and A. Touati. Institut du Radium and Université P & M Curie
 11, rue Pierre et Marie Curie, 75231 Paris Cedex 05, France.

In the shake-off (+ shake-up) model, the ionization in a given (n, ℓ) shell can be due to the imperfect relaxation of the atomic cloud during a sudden change of the atomic central charge. When K ionization occurs during the nuclear electron capture, the change of the central charge, for L, M... electrons is nearly zero and no (or very few) additional vacancy should then be created. The K electron capture should be the unique case when quasi pure K ionized state can be observed.

We intended in the experiment, we describe in the present paper, to give a direct proof of the shake model, studying K_{α} spectra emitted by radioactive samples decaying by electron capture and comparing them to those emitted after conventional K ionizations. The $K^{-1}L^{-1}$ double ionization states can be studied by observing usual K_{α} satellites ; the $K^{-1}(M, N...)^{-1}$ double ionization states cannot be directly observed, the energy of the corresponding satellites being too close to those of the diagram lines (their energy shifts are less than the natural width of the diagram line ; see for instance the other paper we present in this conference). These satellites then strongly contaminate the K_{α} monoionization lines. The K_{α} spectra emitted following electron capture must then be roughly exempt from satellites as well in the vicinity of the diagram lines as inside the diagram lines and should be the purest observable K_{α} spectra.

We studied two different atoms decaying by electron capture : ^{55}Fe and ^{71}Ge . The X ray spectra were analyzed with a curved crystal spectrometer (Ge 333, $R = 50\text{cm}$, detection performed with either a SiLi detector moving along the Rowland circle or a localization chamber of the Gabriel's type). One of our preliminary spectra is presented in Fig. 1. The usual most intense satellite spectrum ($K_{\alpha 3}$ and $K_{\alpha 4}$ lines : characteristic lines emitted by $(1s)^{-1}(2p)^{-1}$ ionized state) is not observed or is much less intense than in the Parratt's spectra (1). However, at the energies of the K_{α}'' and $K_{\alpha}'_{3,4}$ lines (characteristic lines emitted by $(1s)^{-1}(2s)^{-1}$ ionized states) which are very low in intensity in the usual X ray spectra, we observe in both cases (^{55}Fe and ^{71}Ge) a line, the intensity of which is not negligible.

The first experimental result agree with previous considerations (shake-off (+ up) in 2p shell) but the second one (shake-off (+ up) in 2s shell) seems to be in contradiction with the proposed model and does not agree with the recent calculations of Mukoyama and al (2) who found probability values one or two orders of magnitude lower than those of our preliminary results.

These results can however be explained in a very simple way. In general,

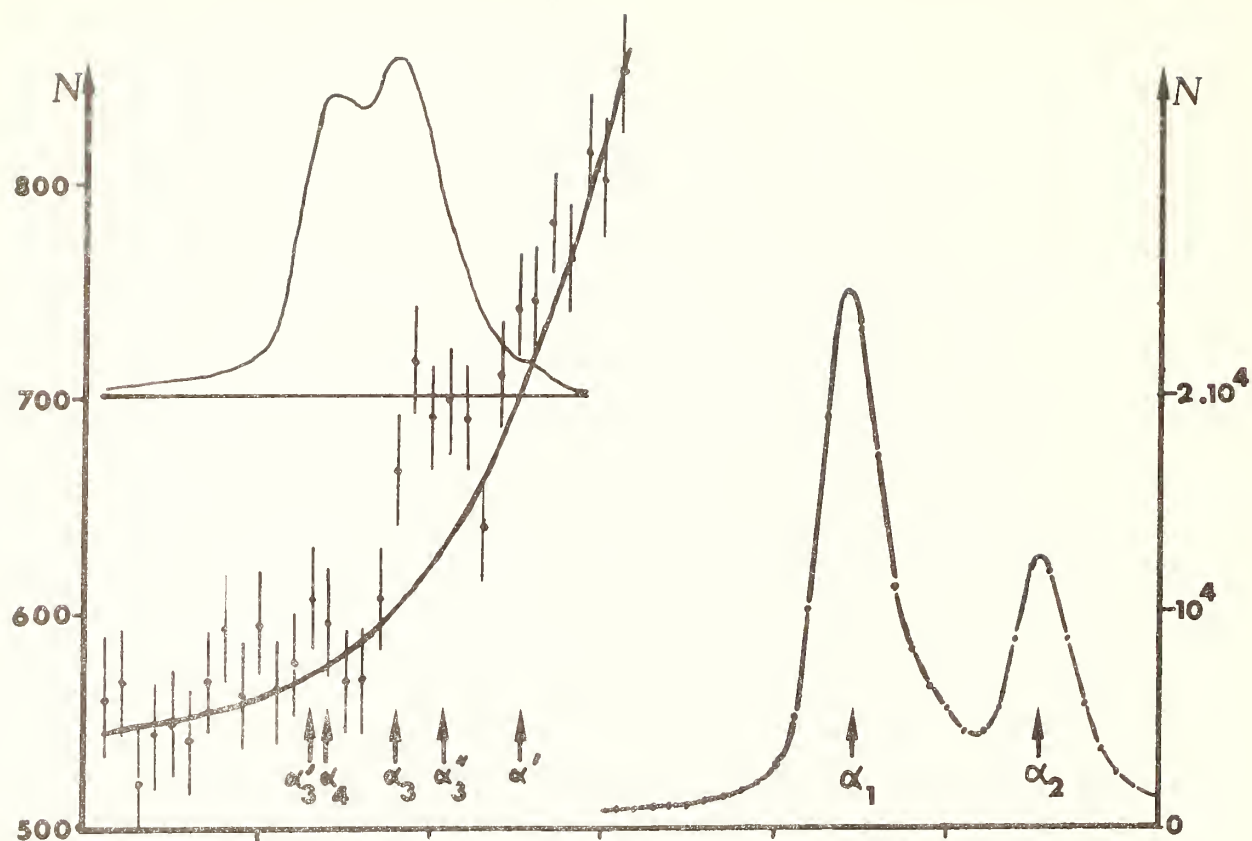


Fig. 1. K_{α} spectrum of Mn in electron capture decay of ^{55}Fe (upper part at left : $K_{\alpha 3}$ $K_{\alpha 4}$ satellites observed by Parratt (1) same scale).

K ionization				β^- decay			
	L _I	L _{II}	L _{III}		L _I	L _{II}	L _{III}
Ne	1.71	5.44	10.63	Ne	4.77	5.55	11.10
Ar	0.3	0.54	1.07	Ar	0.914	0.703	1.41
Kr	0.06	0.089	0.18	Kr	0.185	0.124	0.230
Xe	0.023	0.032	0.061	Xe	0.079	0.049	0.082

Table 1. L shake-off (+ up) probabilities in K ionization and β^- decay in % from ref. (3) and (4).

when sudden approximation applies, the probability of a shake-off (+ up) process increases when the value of the change of the central charge increases.

Let us first compare the 2s and 2p shake-off (+ up) probability in two different cases of change of the central charge : β^- decay and K ionization (this last case being the most usual process : photoionization, particle bombardment or internal conversion). In the case of β^- decay the change of the central charge is exactly equal to one elementary charge when it has to be lower in the case of K ionization due to screening effects. Carlson (3) (4) calculated this probability in both cases. In Table 1, it can be seen that the 2p ionization probability is roughly equal in both cases ($\Delta Z \simeq 1$) when it is roughly 3 times lower, for 2s shell, in K ionization than in β^- decay. This last result being due to the strong penetration of the 2s electron inside 1s radius.

These remarks can qualitatively explain our results because the change of the central charge in K ionization and electron capture are complementary (if ΔZ is in a classical picture, the change of charge seen by a given electron in K ionization, the change of charge in the case of electron capture is then equal to $1 - \Delta Z$). The change of the central charge is then roughly equal to zero for the 2p shell in electron capture when that of the 2s shell has to be relatively important. These conclusions are then in qualitative agreement with our preliminary results. However, to go further it should be necessary to know how important are the 2s \rightarrow 2p Coster-Krönig transitions when the atom is ionized in the 1s shell. The study of K_α satellites emitted in electron capture decay which is characteristic of the $(1s)^{-1} (2s)^{-1}$ ionized states can then give us valuable information on the validity of the assignments of these particular lines (which is still an open problem).

References

- (1) L.G. Parratt. Phys. Rev. 50 (1936) 1.
- (2) T. Mukoyama and S. Shimizu. Phys. Rev. C9 (1974) 2300.
- (3) T.A. Carlson, C.W. Nestor and J.C. Tucker. Phys. Rev. 169 (1968) 168.
- (4) T.A. Carlson and C.W. Nestor Jr. Phys. Rev. A8 (1973) 2887.

RIGOROUS SCREENING AND EFFECTIVE PRINCIPAL QUANTUM NUMBERS

Z.J. Horák,^{x)} M.N. Lewis,⁺ H. Říhová^{x)}

^{x)} Institute of Solid State Physics, Czechosl. Acad. Sci.,
Cukrovarnická 10, 162 53 Praha 6, Czechoslovakia

⁺ Center for Astrophysics, Harvard Coll. Observatory
60 Garden St. Cambridge. Mass. 02138

A common drawback of the atomic screening theories is that they are either semiempirical or introduce nonorthogonal orbitals [1] inconvenient for refined calculations. In this contribution we obtain an ab initio and rigorous scheme of screening constants and principal quantum numbers by means of the perturbation theory. The quality of our wave functions is tested by a calculation of the dipole transition probability $K \rightarrow L$ in neon; $K \equiv 1s(2s)^2(2p)^6$, $L \equiv (1s)^2(2s)^2(2p)^5$.

The proposed perturbation scheme is defined by writing the atomic Hamiltonian

$$H = - \sum_{i=1}^N [1/2 \Delta_i + Z(r_i)^{-1}] + \sum_{i < j}^N (r_{ij})^{-1}$$

as $H = Z_0^2 H_0 + Z_0 V$

where $H_0 = - \sum_{i=1}^N [1/2 \bar{\Delta}_i + (\bar{r}_i)^{-1} + B(\bar{r}_i)^{-2}]$
 $V = \sum_{i < j}^N (\bar{r}_{ij})^{-1} + \sum_{i=1}^N [-\sigma(\bar{r}_i)^{-1} + \beta(\bar{r}_i)^{-2}]$

$$r_i = \bar{r}_i (Z_0)^{-1}, \quad \bar{\Delta}_i = \Delta_i (Z_0)^{-2}, \quad Z_0 = Z - \sigma, \quad \beta = Z_0 B$$

and σ, β are arbitrary Z_0 - independent constants. The unperturbed problem $(H_0 - E_0)\Psi_0 = 0$ can be solved in closed form [2] : $2E_0 = - \sum_{i=1}^N (n_i^*)^{-2}$; $n^* = n - \Delta n$; $\Delta n = (\ell + 1/2) \times \{1 - [1 - 8B(2\ell + 1)^{-2}]^{1/2}\}$. We find σ, β by expanding $Z_0^2 E_0$ in powers of Z and comparing with the Hylleraas Z -expansion of exact nonrelativistic energy $-Z^2 \sum_{i=1}^N 1/2(n_i)^{-2} + \epsilon_1 Z + \epsilon_2 + \dots$ [3]. This analysis gives for the K and L states of neon $\beta_K = 0.566$ and $\beta_L = 0.501$ respectively.

To find the reduced matrix element I [4] for the transition $K \rightarrow L$ we computed first two terms of the exact Z -expansion $I = I_0 Z^{-1} + I_1 Z^{-2} + \dots$. The zero order of our generalized perturbation scheme gives $I = I_0(B)Z_0^{-1} = I_0 Z^{-1} + (I_0 \sigma + I'_0 \beta)Z^{-2}$, where $I_0(0) = I_0$; $I'_0(0) = I'_0$. We took $\beta = \beta_K$ or β_L and adjusted σ such that $I_0 \sigma + I'_0 \beta = I_1$. The results for the emission rate (in units eV/h) are 0.0041 ($\beta = \beta_K$) and 0.0045 ($\beta = \beta_L$) in agreement with the Hartree Fock 0.0044 [5].

References:

- [1] D. Layzer: Ann. Phys. (N.Y.) 8 271 (1959)
- [2] S. Flügge: Practical Quantum Mechanics I (Springer 1971) Problem 69
- [3] E.P. Ivanova, U.I. Safronova: J. Phys. B 8 1591 (1975); U.I. Safronova, A.N. Ivanova, N.V. Rabinkina, V.N. Kharitonova: Optika i Spektroskopiya 38 841 (1970)

- [4] C. Laughlin, M.N. Lewis, Z.J. Horák: J. Phys. B 6
1953 (1973) Eq. (4)
- [5] J.H. Scofield: Phys. Rev. A 9, 1041 (1974)

CONTRIBUTION OF RADIATIVE AND AUGER TRANSITION ON $K\beta'$ SATELLITE OF TRANSITION ELEMENTS

Takeshi Watanabe and Chuji Horie

Department of Applied Physics
Tohoku University, Sendai 980, Japan

There have been several experimental studies on the $K\beta$ emission spectra of transition elements in pure and compound materials. In comparison to the parent line the $K\beta'$ satellite is characterized by (1) a broad band spectrum locating in the lower energy side of the parent line, (2) a large amount of the integrated intensity which is far greater than other satellite lines, and (3) a spectral intensity highly dependent on the bonding nature of electrons.

Interpretations of this satellite have been also carried out along with experiments. In the analyses based on the electrostatic interaction of p-d electrons[1~3] the energy spread of the satellite is attributed to the energy split of multiplets created by p-dⁿ electron interactions and the intensity distribution is given by the envelope of these multiplets weighted by their multiplicity. Tsutsumi proposed that the total spin of unpaired 3d electrons plays an essential role and the satellite structure is produced as a result of difference in the spin state of a 3p hole relative to that of 3d electrons[4]. However, in these analyses the line width of the observed spectrum was assumed to consist of the life-time broadening of a K hole and the instrumental broadening, and when the theoretical result is compared with observed spectra a smearing function with an empirically determined width is convoluted to the discrete spectrum. Here the line width is assumed to be constant for all multiplets, and a broad nature of the $K\beta'$ line is not fully explained. Also, other proposals such as by Parratt[5] and Sawada[6] are too far qualitative and no positive interpretation seems to be deduced from them.

In the present work we restrict ourselves to the $K\beta'$ satellite of transition metal compounds such as MnO and MnO₂. Noticing that a large member of these compounds are anti-ferromagnetic we consider, like Tsutsumi, that unpaired 3d spins give rise to significant effects on the state of a 3p hole. In contrast to the previous works we take into account effects of Auger transitions on a 3p hole which occur among 3p, 3d and continuum levels. As shown by McGuire[7] for the photoelectron spectrum of pure elements the Auger width is expected to be different for each multiplet also in the present case. Moreover, because of absence of screening

due to 4s electrons in the compounds considered the Auger width of $p-d^n$ configurations should be larger in comparison to pure metallic elements. We show that this difference in the Auger width of each multiplet causes a broadening of the $K\beta'$ satellite.

It is assumed that the self-energy $\Sigma(3p)$ of a 3p hole is given by the contribution of direct Coulomb and exchange interactions between 3p hole and 3d electrons and of the Auger transition associated with 3d electrons. The first order diagrams of electrostatic interactions (Hartree-Fock) contribute only to $\text{Re } \Sigma(3p)$, while the Auger transition gives rise to non-zero contribution to $\text{Im } \Sigma(3p)$ when the spin orientation of a 3p hole is antiparallel to that of a 3d electron. An example of this case is the 5P state of a $p-d^5$ configuration. In the opposite case, e.g., the 7P state in the above example, the Auger contribution to $\text{Im } \Sigma(3p)$ vanishes because the spin conservation cannot be satisfied. Since we are interested in the broadening of the spectrum, the imaginary part of the self-energy is mainly discussed.

The Auger contribution to $\text{Im } \Sigma(3p)$ can be expressed as

$$\text{Im } \Sigma(3p) = \pi \sum_1 | \langle 3p \ k1 | (1/r_{12}) | 3d \ 3d \rangle |^2 \delta(\tilde{\omega}_{3p} + \epsilon - 2\omega_{3d}) ,$$

where $\tilde{\omega}_{3p}$ is the renormalized energy of a 3p hole and ϵ is the energy of an Auger excited electron. Other quantities have the conventional meaning. Although the wave number k ($\epsilon = k^2/2$) or the energy ϵ of the continuum should be determined self-consistently, they are approximated by using the experimentally measured binding energies of 3p and 3d states [8], where $\tilde{\omega}_{3p}$ is replaced by ω_{3p} . The value of k used is 1.75 (in a.u.) for Mn.

In evaluation of the matrix element we have used hydrogenic wavefunctions with Slater's screening constants for the 3p and 3d states of Mn, and a spherical Bessel function for the continuum state. For calculation of the angular parts McGuire's table [7] was used. Because of the choice of wavefunctions the matrix elements can be calculated analytically and it is found that the f-continuum state contributes to the matrix element one order of magnitude smaller than the p-continuum state in the present case. Therefore, we consider the contribution from the p-continuum state only. Putting the renormalization constant for a 3p hole to unity, we obtain the Auger line width as $2\text{Im } \Sigma(3p)$. In Table are shown non-vanishing Auger widths and the effective charges used for the calculation along with the electron configurations and spectral terms for some of manganese ions.

The present calculation indicates that the Auger width of a 3p hole $\Gamma(3p)$ of some manganese ions is much larger than the K width $\Gamma(K)$ of a manganese atom which is estimated to be about one eV [9]. Therefore, according to our assign-

ment of the $K\beta'$ satellite, the line width should be given by $\Gamma(3p)+\Gamma(K)$ and its peak intensity is reduced by a factor of $\Gamma(K)/(\Gamma(3p)+\Gamma(K))$ from what to be expected from the spin multiplicity. Putting $\Gamma(K)$ to be 1.1 eV, we calculated the expected peak intensity ratios of the $K\beta'$ to $K\beta_{1,3}$ line. These ratios are compared with the observed values of MnO and MnO₂ [10] in Table. When the electrostatic interaction splits the spin multiplet, the present analysis should be applied to each multiplet. As shown in Table, at least with these elements, agreements are quite satisfactory. One thing to be mentioned is that the instrumental width smears both lines equally and does not affect the present argument.

In conclusion it is shown that the Auger width gives rise to significant effect on the $K\beta'$ satellite of transition metal compounds. A similar analysis is being made for chromium ions. Use of better wavefunctions as well as inclusion of 4s electrons in the formalism is for future work.

Table: Auger widths, effective charges, and calculated and observed intensity ratios of the $K\beta'$ satellite to the parent line.

	Multiplet	Z_{3p}	Z_{3d}	$\Gamma(3p)$	$I_{\beta'}/I_{\beta_{1,3}}$	
					cal.	obs.
MnO	(pd ⁵) 5_p	13.75	6.6	1.8eV	0.26	0.19
MnO ₂	(pd ³) 3_F	13.75	7.3	1.1	0.30	0.14
	3_D	13.75	7.3	0.8	0.35	

REFERENCES

- [1] B. Ekstig, E. Källne, E. Noreland, R. Manne, Phys. Scr. 2 38 (1970).
- [2] R. P. Gupta and S. K. Sen, Phys. Rev. B10 71 (1974).
- [3] S. Asada, C. Satoko and S. Sugano, J. Phys. Soc. Japan 38 855 (1975).
- [4] K. Tsutsumi, J. Phys. Soc. Japan 14 1696 (1959) and 25 1418 (1968).
- [5] L. G. Parratt, Rev. Mod. Phys. 31 352 (1959).
- [6] M. Sawada, Sci. Mem. Kyoto Imper. Univ. A15 43 (1932).
- [7] E. McGuire, Phys. Rev. A10 32 (1974).
- [8] A. Bearden and A. F. Burr, Rev. Mod. Phys. 39 125 (1969).
- [9] V. O. Kostroun, M. H. Chen and B. Crasemann, phys. Rev. A3 533 (1971).
- [10] K. Tsutsumi, H. Nakamori and K. Ichikawa, Phys. Rev. B13 929 (1976)

THEORETICAL X-RAY SPECTRUM FOR DOUBLE VACANCY IN 2p SHELL OF ARGON*

C.P. Bhalla

Kansas State University, Department of Physics
Manhattan, Kansas 66506 U.S.A.

Measurements of L x-rays from ion-argon collisions show the production of double-hole (2p) states in addition to single 2p vacancy configurations with different degrees of multiple ionization in the M shell. The cascade of the double-hole states leads to a nonstatistical distribution of the terms. We present the theoretical results for argon.

The Auger rate is given by

$$\Gamma_A(\alpha_i S_i L_i \rightarrow \alpha_f S_f L_f) = 2\pi \sum_{i < j} |\langle \psi_f | \sum (1/r_{ij}) | \psi_i \rangle|^2.$$

The evaluation of the matrix elements requires special theoretical techniques [1] when there is more than one spectroscopic term for an initial electron configuration. The Auger rates can be expressed in terms of the coefficients of fractional parentage, the angular momentum recoupling coefficients and the generalized Slater integrals. The relevant theoretical expressions for the three terms of the 2p shell double-hole configuration were derived. The radial matrix elements were calculated with the HFS atomic model [2,3] for argon.

Table 1 contains the Auger rates for the three initial terms to the various terms representing the core and a continuum electron after the 2p-3s-3p transition. Similarly the individual Auger rates after the 2p-3p-3p transition are listed in Table 2. The 2p-3s-3s Auger rate for all the initial terms is 1.402×10^{-4} a.u. The +(-) subscript in the final terms denotes the upper (lower) state of the same symmetry.

Table 1.

Auger rates $\times 10^4$ in a.u. for the $2p \rightarrow 3s, 3p$ transition from the three initial terms of the $1s^2 2s^2 2p^4 3s^2 3p^6$ configuration of argon leading to the various terms of the $1s^2 2s^2 2p^5 3s 3p^5$ configuration.

Final Term	Initial State		
	1_D	1_S	3_P
$2D_+$	5.14	0.015	0.0001
$2D_-$	24.4	0.010	0.013
$2P_+$	0.011	0.0	16.3
$2P_-$	0.0005	0.0	0.26
$2S_-$	0.0	21.7	0.0
$2S_+$	0.0	7.86	0.0
$4D$	0.0	0.0	0.006
$4P$	0.0	0.0	13.0

The x-ray transition energies and multiplet fluorescence yields are given below:

$1S \rightarrow 1P$	247.34eV	$1.65 \cdot 10^{-4}$
$3P \rightarrow 3P$	241.5eV	$1.54 \cdot 10^{-4}$
$1D \rightarrow 1P$	235.5eV	$1.43 \cdot 10^{-4}$

Table 2

Auger rates $\times 10^4$ in a.u. for the $2p\ \bar{2}\ 3p_4\ 3p$ transition from the three initial terms of the $1s^2\ 2s^2\ 2p^4\ 3s^2\ 3p^6$ configuration of argon leading to the various final states of the $1s^2\ 2s^2\ 2p^5\ 3s^2\ 3p^4$ configuration.

Final Term	Initial States		
	1_D	1_S	3_P
2_P	18.9	2.14	16.7
2_P	0.88	89.9	2.20
2_P	5.51	5.93	3.09
2_D	33.5	0.0	26.2
2_D	1.05	0.0	5.56
2_F	32.5	3.87	2.58
2_S	0.0	0.0	1.82
4_S	0.0	0.0	14.5
4_D	0.0	0.0	18.2
4_P	0.0	0.0	10.9

References

*Work supported by the U.S. Army Research Office, Durham, North Carolina.

[1] U. Fano, Phys. Rev. 140, A67(1965).

[2] C. P. Bhalla, Phys. Rev. A 12, 122(1975).

[3] C. P. Bhalla, N. O. Folland and M. A. Hein, Phys. Rev. A 8, 649(1973).

SYSTEMATICS OF X RAY SATELLITES

Sidheshwar Rai

Physics Department, Lucknow University, Lucknow-226007, India.

1. INTRODUCTION

The problem of the origin of x ray satellites has been a subject of interesting debate among x ray researchers all over the world. The construction of their energy level diagrams is still an open question. The challenge in this field has been to select the fundamentally new and interesting phenomena and to relate these to various probable satellite generation processes. The interpretations offered so far to explain the physics of the so-called x ray non-diagram(satellite)lines have, in a few outstanding instances, been remarkably fruitful but many have ended in frustration. A possible reason for this seems to be the lack of research on systematics of these lines. However, a considerable amount of work on this aspect has recently been done in India. The aim of the present paper is to review this work. The results are being discussed in the following sections.

2. SCREENING AND SPIN DOUBLET FORMATION

Spectroscopic analysis has led [1] to the establishment of two types of doublets in x ray satellite spectra, viz., (a) screening doublets and (b) spin doublets. Screening doublets are characterized [2-4] by the relation

$$\Delta(\nu/R)^{1/2} = (\Delta\sigma_1/n) = C \quad \dots \quad (1)$$

where C is not an absolute constant but increases very slowly with increasing Z. A critical study [4] of the data for x ray satellites on the basis of equation (1) has led to the discovery of the following pairs of screening doublets:

2.1 The K Region : $\alpha_3' \alpha''$ (Z = 16-28), $\alpha_3' \alpha'$ (Z = 14-33), $\alpha'' \alpha_4$, $\alpha'' \alpha_3'$, $\alpha'' \alpha_3$, $\alpha'' \alpha'$ (Z = 14-29), $\alpha_5 \alpha_7$ (Z = 11-14), $\alpha' \alpha_3$, $\alpha' \alpha_4$, $\alpha_3 \alpha_4$ (Z = 11-40), $\alpha_5 \alpha_6$ (Z = 11-17), $\alpha_3 \alpha_3'$ (Z = 14-40), $\alpha_3'' \alpha_3'$, $\alpha_3'' \alpha_4$, $\alpha_3'' \alpha'$ (Z = 19-28), $\alpha_6 \alpha_7$ (Z = 11-19), $\beta''' \beta'$ (Z = 15-30), $\beta_3 \beta'''$ (Z = 20-27), $\beta_3 \beta_6$, $\beta_3 \beta_7$, $\beta_8 \beta_{II}'$, $\beta_6 \beta_7$, $\beta_0 \beta_3'$ (Z = 33-44).

2.2 The L Region : $\alpha_4 \alpha_6$, $\alpha_4 \alpha_7$, $\alpha''' \alpha^{IV}$ (Z = 37-53), $\alpha_5 \alpha_7$, $\alpha_6 \alpha_7$ (Z = 37-56), $\alpha_5 \alpha_8$, $\alpha_6 \alpha_8$ (Z = 41-56), $\alpha_5' \alpha_7$, $\alpha_5' \alpha_5$, $\alpha_5' \alpha_8$ (Z = 46-51), $\alpha^y \alpha^x$, $\alpha^y \alpha^{ix}$ (Z = 73-82), $\alpha^{ix} \alpha_a$ (Z = 73-92), $\alpha_2' \alpha''$, $\alpha_2' \alpha_6$, $\alpha_2' \alpha_5$, $\alpha_2' \alpha_7$, $\alpha_2' \alpha^{VI}$ (Z = 42-48), $\alpha_3 \alpha_4$, $\alpha_5 \alpha_6$ (Z = 37-49), $\alpha_7 \alpha_8$ (Z = 41-49), $\alpha'' \alpha'''$ (Z = 27-53), $\alpha^{ix} \alpha^x$ (Z = 73-92), $\beta_2^I \beta_2^V$, $\beta_2^I \beta_2^{VII}$, $\beta_2^{II} \beta_2^V$, $\beta_2^{II} \beta_2^{VII}$, $\beta_2^V \beta_2^{VII}$, $\beta_2^V \beta_2^{III}$, $\beta_2^{VII} \beta_2^{III}$,

$\beta_2^{VII} \beta_2^{IV} (Z = 75-90), \beta_2^{I} \beta_2^{III}, \beta_2^{II} \beta_2^{III} (Z = 73-90), \beta_2^{VII} \beta_2^{VI}, \beta_2^{III} \beta_2^{VI}, \beta_2^{VI} \beta_2^{IV},$
 $\beta_2^{II} \beta_2^{VI} (Z = 78-90), \beta_2^{III} \beta_2^{IV} (Z = 74-90), \beta_1^{III} \beta_1^{IV} (Z = 42-49), \beta_2^b \beta_2^b, \beta_2^b \beta_2^{I'}$
 $(Z = 40-50), \beta_2^b \beta_2^c, \beta_2^b \beta_2^c (Z = 42-50), \beta_2^{I'} \beta_2^c (Z = 39-51), \beta_1^b \beta_1^{I'} (Z = 26-50),$
 $\beta_2^b \beta_2^{I'} (Z = 40-53), \beta_5^b \beta_5^{I'} (Z = 78-88), \beta_2^a \beta_2^b, \beta_2^a \beta_2^{I'} (Z = 44-53), \beta_2^a \beta_2^b, \beta_2^a \beta_2^c$
 $(Z = 44-50), \gamma_2^b \gamma_2^{I'} (Z = 72-82), \gamma_1^b \gamma_2^b, \gamma_1^b \gamma_2^{I'} (Z = 73-83), \gamma_1^b \gamma_9 (Z = 58-69).$
2.3 The M Region : $\alpha^I \alpha^{IV}, \alpha^{II} \alpha^{IV} (Z = 71-92), \alpha^b \alpha^{I'} (Z = 72-83), \beta_I \beta_{III},$
 $\beta_{II} \beta_{III} (Z = 72-92), \beta_I \beta_{II} (Z = 73-83).$

On the other hand spin doublets of x ray satellites are characterized [5,6] by the relation,

$$(\Delta \nu / R)^{1/4} = \eta Z + \gamma \quad \dots \quad \dots \quad \dots \quad (2)$$

where $\eta = \frac{\sqrt{\alpha}}{n} \left(\frac{n}{1} - \frac{n}{1+1} \right)^{1/4}$ and $\gamma = -\sigma_2 \cdot \eta$

The x ray satellite data have been critically analysed [6] on the basis of equation (2). As a result following spin doublets are found out :

2.4 The K Region : $\beta_3^b \beta_6, \beta_3^b \beta_7, \beta_3^b \beta_{II}, \beta_7^b \beta_{II}, \beta_0^b \beta_{II}, \beta_3^b \beta_8 (Z = 33-44).$

2.5 The L Region : $\alpha_s \alpha^x, \alpha_s \alpha^{Ix}, \alpha_s \alpha_a (Z = 73-90), \beta_2^I \beta_5^I, \beta_2^{II} \beta_5^I, \beta_2^{III} \beta_5^I$
 $(Z = 77-88), \beta_2^I \beta_5^{II}, \beta_2^{II} \beta_5^{II} (Z = 76-88), \alpha_4 \beta_1^b, \alpha_4 \beta_1^{I'}, \alpha_3 \beta_1^b, \alpha_3 \beta_1^{I'} (Z =$
 $33-50), \alpha_4 \beta_1^{I'}, \alpha_6 \beta_1^{I'}, \alpha_7 \beta_1^{I'}, \alpha_8 \beta_1^{I'}, \alpha_3 \beta_1^{I'}, \beta_2^c \gamma_1^b (Z = 42-50), \alpha_6 \beta_1^b, \alpha_6 \beta_1^{I'},$
 $\alpha_7 \beta_1^b, \alpha_7 \beta_1^{I'} (Z = 38-50), \alpha_8 \beta_1^b, \alpha_8 \beta_1^{I'} (Z = 41-50), \beta_{14} \gamma_9 (Z = 58-70), \beta_2^I \gamma_2^b$
 $(Z = 72-82), \beta_2^{II} \gamma_2^b (Z = 72-83), \beta_2^{III} \gamma_2^b, \beta_2^{III} \gamma_1^b (Z = 73-83), \beta_2^{II} \gamma_1^b$
 $(Z = 42-83), \beta_2^I \gamma_1^b (Z = 41-82).$

2.6 The M Region : $\alpha^I \beta_{II}, \alpha^{II} \beta_{II} (Z = 71-92), \alpha^I \beta_I, \alpha^I \beta_{III}, \alpha^{II} \beta_I,$
 $\alpha^{II} \beta_{III}, \alpha^{IV} \beta_I (Z = 72-92), \alpha^{IV} \beta_{II}, \alpha^{IV} \beta_{III} (Z = 70-92).$

A coupling of the knowledge of the screening and spin doublets in x ray satellite spectra is expected to be helpful in solving the problem of the formation of energy level diagrams for the so-called x ray non-diagram lines (satellites).

3. NEW LINEAR LAW

It has been found that the empirical linear law [7], in its general form, $(\nu/R)_{Z+1} - (\nu/R)_Z = \alpha (Z - n) \dots \dots (3)$

is equally valid for all the high-frequency (HF) satellites in the K, L and M regions as well as for the K and L low-frequency (LF) satellites [8-10]. On the basis of these studies Deodhar [11] has concluded that

the LF satellites arise in the same way as the HF ones by single electron jump in the multiply ionized atoms supporting the basic idea of Wentzel-Drayvesteyn theory [12]. It is interesting to note that this empirical linear law also plays two subsidiary roles, viz., (a) it enables one to check the accuracy of the measurement of a particular satellite for a given element and also to ascertain its correct assignment and (b) it can be readily applied for predicting a satellite for an element which has been left uninvestigated.

4. DIAGRAM LINE ASSOCIATES (PARENT LINES)

The diagram line associates of almost all the HF satellites have been determined [13] on the basis of the following criteria :
 (a) semi-Moseley diagram based on double jump hypothesis of Richtmyer stating that $[(\nu/R)_s - (\nu/R)_p]^{1/2}$ holds a linear relation with Z and (b) 'new criterion' proposed by Deodhar [2] stating that $[(\nu/R)_s]^{1/2} - (\nu/R)_p^{1/2}$ holds a linear relation with Z. As a result it has been found that the satellites α' , α_3 , α_4 , α_3' , α_5 and α_6 in the K series are associated with $K\alpha_1$ whereas α'' , α_3' that with $K\alpha_2$. In the L series the satellites α_2' , α_3 , α_5 , α_6 , α_7 , α_5' , α_8 , α_9 , α' , α^{ix} , α^x and α_a are associated with $L\alpha_2$ whereas α_4 that with $L\alpha_1$. Our results for $L\beta$ and $L\gamma$ satellites agree with those of Cauchois and Hulubei [14]. In the M series the satellites α^I , α^{III} and α^{IV} are associated with $M\alpha_2$ whereas α^{II} that with $M\alpha_1$. The diagram line associate of all the $M\beta$ satellites is $M_{IV}N_{VI}(\beta)$ line whereas that of the satellite $M\gamma'$ is $M_{III}N_{IV}$.

5. SEMI-EMPIRICAL ENERGY LEVEL DIAGRAM :

Recently, it has been found [15] that a pair of common x ray terms (Ls, Ls') is involved in the emission of L satellite spin doublets (β_1', α_4) and (β_1''', α_7). The energy of the satellite $L\beta_1'$ is given [1] by $(E_{L\beta_1'})_Z = [(E_{L_{II}})_Z + (E_{M_{II}})_{Z+1}] - [(E_{M_{II}})_Z + (E_{M_{IV}})_{Z+1}] \dots (4)$ If Ls is the initial term for the emission of $L\beta_1'$ then,

$$(E_{Ls})_Z = (E_{L_{II}})_Z + (E_{M_{II}})_{Z+1} \dots \dots \dots (5)$$

and hence,

$$(E_{Ls'})_Z = (E_{Ls})_Z - \{(\Delta\nu/R)_{LsLs'}\}_Z \dots \dots \dots (6)$$

If F_1 and F_2 are, respectively, the final terms for the emission of spin doublets (β_1', α_4) and (β_1''', α_7) then,

$$(E_{F_1})_Z = (E_{M_{II}})_Z + (E_{M_{IV}})_{Z+1} \dots \dots \dots (7)$$

$$\text{and } (E_{F_2})_Z = (E_{Ls})_Z - (E_{L\beta_1'''})_Z^{\text{Expt.}} \dots \dots \dots (8)$$

Knowing the energy values for L_s , L_s' , F_1 and F_2 from equations (5)-(8) we can construct energy level diagram as shown in Fig. 1 (not drawn to the scale).

In conclusion, this report is thought to be useful in unifying the majority of x ray satellites specially those which have been thought to be emitted by Wentzel-Dryvesteyn process (WDP).

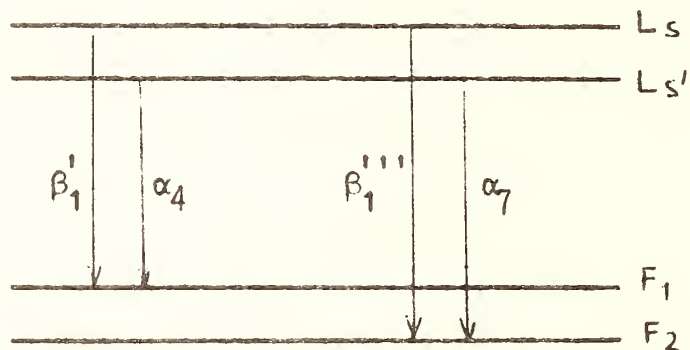


Fig. 1. Energy level diagram for the L satellites β_1' , α_4 , β_1''' and α_7 .

ACKNOWLEDGMENTS : The author is grateful to Professor B.G.Gokhale, Head of the Physics Department, Lucknow University, for useful discussions, interest in the work and encouragement. The financial assistance of the Department of Atomic Energy, Government of India, is also thankfully acknowledged.

REFERENCES :

- [1] Rai, S. , D. Phil. Thesis ,University of Allahabad ,India (1972).
- [2] Deodhar, G.B., Proc. Roy. Soc. A131(1931)476.
- [3] Deodhar, G.B., and Padalia, B.D., Z. Phy. 172(1963)490.
- [4] Deodhar, G.B., and Rai, S. , J. Phys. B 5(1972)418.
- [5] Deodhar, G.B., and Rai, S. , Nature 222(1969)661.
- [6] Deodhar, G.B., and Rai, S. , J. Phys. B 2(1969)1402.
- [7] Deodhar, G.B., and Abidi, S.T.H., Naturwiss. 47(1960)319.
- [8] Deodhar, G.B., and Padalia, B.D., Ind. Jour. Pure Appl. Phys. 21B(1962)4
- [9] Singh, R.B. , Ind. Jour. Pure Appl. Phys. 3(1965)486.
- [10] Singh, R.B. , D. Phil. Thesis, University of Allahabad, India (1968).
- [11] Deodhar, G.B., Proc. Nat. Acad. Sci. A32 (1962) 320.
- [12] Dryvesteyn, M.J., Z. Phy. 43 (1927)707.
- [13] Deodhar, G.B., and Rai, S., J. Phys. B 3 (1970) 1260.
- [14] Cauchois, Y., and Hulubei, H., Longueurs d' Onde des Emission X et des Discontinuites d' Absorption X (Paris :Hermann) (1947).
- [15] Rai, S. , Nature 243 (1973)34 .

ON THE SATELLITES OF THE $K\alpha$ -DOUBLET OF FLUORINE IN LITHIUM-FLUORIDE

Y. Hayasi

University of Munich, Department of Physics, Munich, West Germany
and Tohoku University, Department of Applied Physics, Sendai, Japan

The K-emission spectrum of fluorine in solid LiF ($\lambda=18.3 \text{ \AA}$) was studied using a focussing crystal spectrometer with a gas counter. If the spectrum is excited by radiation from either Cu, W or Co targets, satellites $K\alpha_3$ and $K\alpha_4$ appear with considerable intensity. However, these satellites appear only faintly when radiation from an Fe target ($h\nu$ of Fe $L\alpha=705 \text{ eV}$) was used for excitation (Fig.1).

The threshold energies for the K, $KL_{2,3}(^3P)$ and $KL_{2,3}(^1P)$ states of F^- ion in LiF crystal lattice were calculated under several assumptions to be 693.07, 715.53 and 719.00 eV, respectively. These energy values were compared with present experimental observations and with our recent results for the K-absorption spectrum of fluorine in LiF (Fig.2).

This comparison indicates that:

(i) The satellites $K\alpha_3$ and $K\alpha_4$ in the F K-spectrum of LiF correspond to transitions $KL_{2,3}-L_{2,3}^2$ of F^- ion in LiF, which support the assignment made by Kennard and Ramberg. The weak maxima which appear at the sites of the satellites in the case where radiations from an Fe target (Fig.3) was used for excitation may be caused by weak Fe $L\beta$ radiation ($h\nu=718.5 \text{ eV}$) or by bremsstrahlung.

(ii) The second absorption edge observed in the fluorine K-absorption spectrum of LiF at 710-718 eV may be attributed to double electron excitation ($KL_{2,3}$) of the F^- ion in LiF.

(iii) The markedly asymmetric profile of the $K\alpha_{1,2}$ line of fluorine in LiF is not due to the overlapping of a satellite, but rather to the structure of the L band of fluorine in LiF.

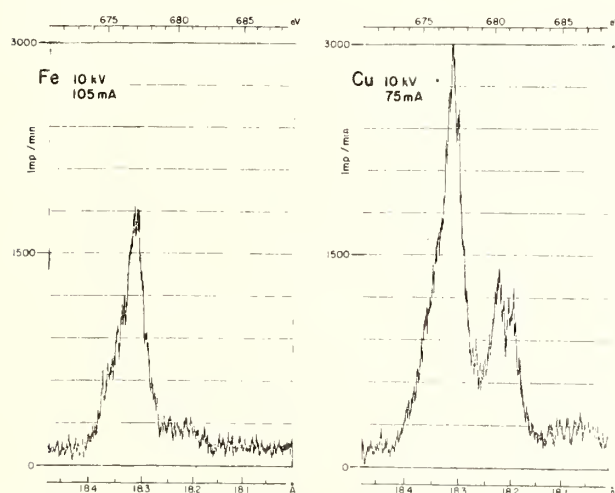


Fig.1. K-emission spectra of fluorine in LiF excited by radiation from Fe or Cu targets.

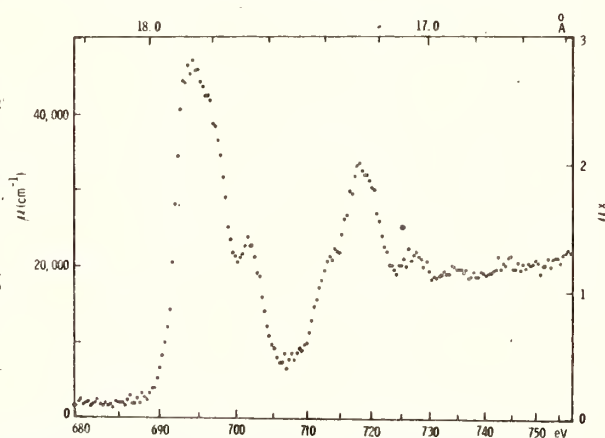


Fig.2. K-absorption spectrum of fluorine in LiF.

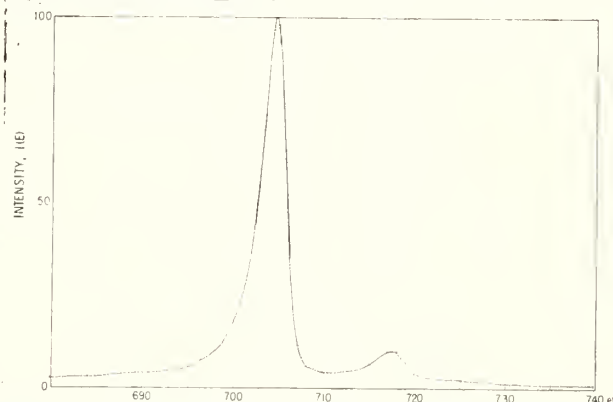


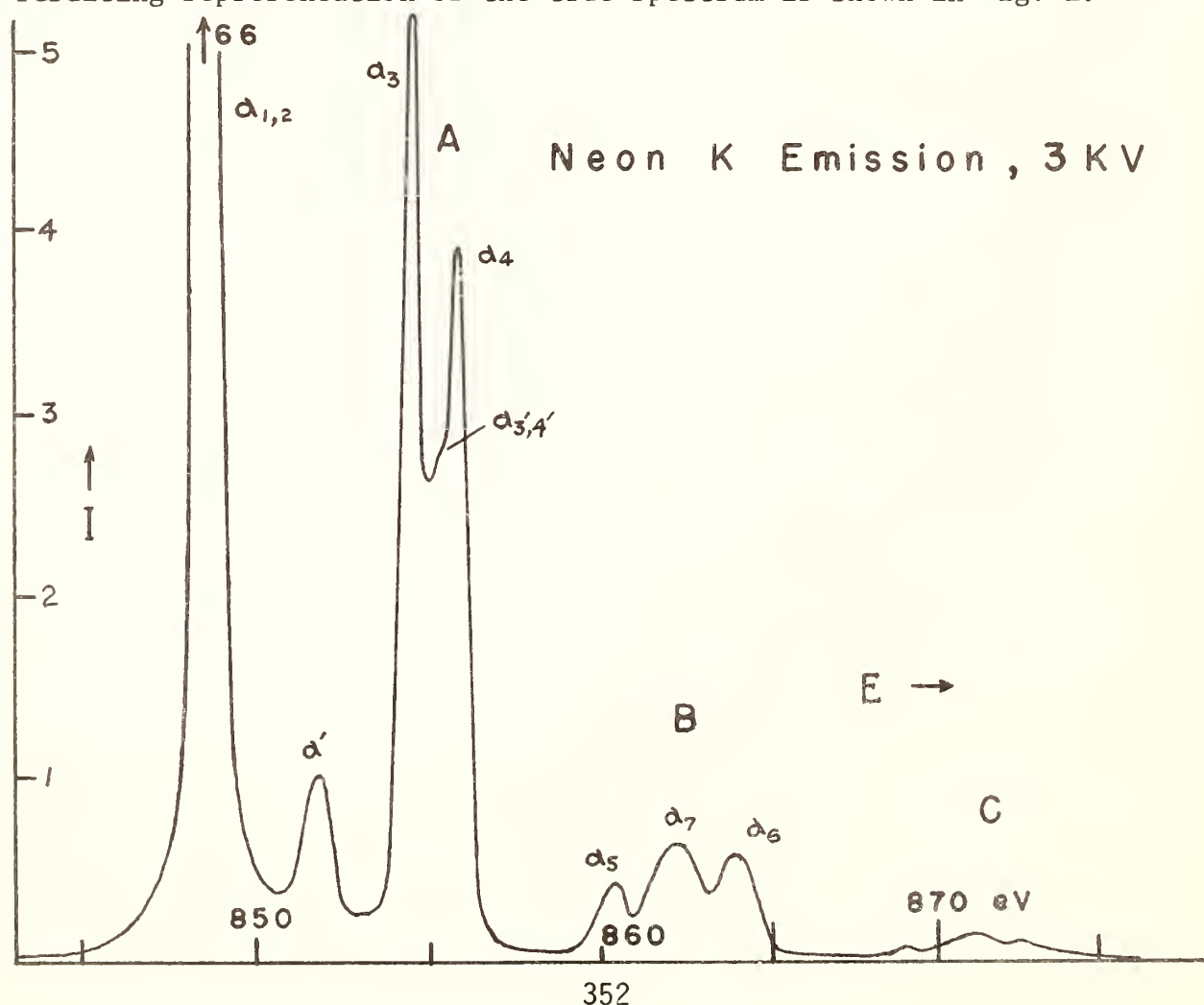
Fig.3. Intensity distribution $I(E)$ of Fe L radiation from an Fe target (anode potential 10 kV).

ELECTRON EXCITED K SERIES SPECTRA OF NEON GAS

T.P. Tooman and R.J. Liefeld, New Mexico State University
Las Cruces, New Mexico, 88003

A novel gas target x-ray tube has been used in conjunction with a vacuum two crystal spectrometer to obtain high resolution K series spectra of Neon [1]. The x-ray tube uses a microchannel plate nozzle to provide a neutral beam of gas. This gas beam is crossed by a monoenergetic electron beam and x-rays produced in the intersection region pass through a thin Formvar window into the spectrometer. There they are energy analyzed and detected by a two crystal (potassium acid phthalate) scanning monochromator and a flowing gas proportional counter. The gas beam density is regulated and the electron beam current is precisely integrated to permit counting for times corresponding to equal amounts of charge delivered to the gas beam. After passing through the x-ray tube the gas beam is scattered into the jets of a high speed diffusion pump, compressed, purified and returned to the microchannel plate to permit long term operation with small quantities of gas.

A composite of eight spectra of the neon K series obtained with the new gas target tube has been subjected to appropriate smoothing and computer deconvolution of the spectral window of the monochromator. The resulting representation of the true spectrum is shown in Fig. 1.



Careful analysis of the $K\alpha_{1,2}$ line reveals an essentially lorentzian shape, a width for the α_1, α_2 composite of 0.24 eV, and no detectable separation larger than 0.05 eV. The satellite groups A, B and C are identified as $K\alpha$ line transitions with, respectively, one, two and three spectator vacancies in the outer shell. Each group appears to have three components. Integrated intensity ratios are

$$\frac{\alpha'_1 \alpha_3 \alpha_{3'4'} \alpha_4}{\alpha_{1,2}} = 0.4 \quad \text{and} \quad \frac{\alpha_5 \alpha_7 \alpha_6}{\alpha_{1,2}} = 0.1$$

Both wide range and threshold region $K\alpha_{1,2}$ line excitation curves have been obtained but the threshold region excitation curves show no structures such as are observed in photon absorption.

[1] T.P. Tooman, Ph.D. Dissertation, New Mexico State University, 1975.

PLASMON SATELLITES IN AUGER SPECTRA OF METALS

D. CHASTENET,
Laboratoire de Chimie Physique, Université de
Paris VI, 11, rue P. et M. Curie, F-75231 Paris
Cedex 05, France

P. LONGE,
Institut de Physique, Université de Liège,
Sart Tilman, B-4000 Liège, Belgium

The low energy satellites in Auger spectra of metals, due to bulk plasmon excitation, is investigated in the frame of the many body theory. The total intensity of these satellites is compared to the main band intensity. Attention is paid to two types of processes : the intrinsic plasmon production directly related to the core state transition and the extrinsic plasmon production by the Auger electron on its way to the detector. These two processes may present an important cancellation effect by quantum interference. We investigate the importance of this effect in the K; VV and L_{23} ; VV Auger spectra of various light metals. The plasmon satellites in Auger spectra are also compared to the same satellites appearing in the X-ray spectra, which present similar cancellation effects.

MULTIPLE PLASMON EXCITATION IN CHARACTERISTIC ENERGY LOSS SPECTRUM OF POLYCRYSTALLINE AL .

By

K.S.Srivastava, S.P.Singh, & R.L.Shrivastava
Physics Department. K.N.Govt. P.G. College
Gyanpur. Varanasi. (U.P.) India.

Abstract:- Ashley and Ritchies' theory for the mean free path for the second order process of double plasmon excitation in a free electron gas has been extended to third order process. The relative intensities of double and triple plasmon loss peaks of aluminum have been calculated. The calculated results agree fairly well with the experimental value estimated from Henerich curve on the characteristic energy loss spectra of polycrystalline aluminum.

Multiple plasmon peaks upto several orders have been observed in the characteristic energy loss spectra by Henerich (1), in the Auger spectra by Jenkins et.al. (2), in SXAPS spectra by Broadshaw & Menzel (3), and in the photo-emission spectra by Smith & Spicer (4). These multiple plasmon peaks have, so far, been attributed as due to single plasmon-multiple scattering process. The contribution of multiple plasmon-single scattering process has not been taken into account.

Few years ago, Ashley & Ritchie (5) have calculated the probability of the second order process of double plasmon-single scattering and found that for metals (e.g. Al) having $r_s \approx 2$, the probability is about 8 %. Later on Spence and Spargo (6), assuming that the above probability for the second order process is enough to be detected, performed an experiment on the characteristic energy loss spectrum of Al and found that at the double plasmon energy loss distance, both the processes i.e. double plasmon-single scattering and single plasmon-double scattering are contributing. Thus the loss at $n\hbar\omega_p$ excitation energies may be due to two processes namely (a) single plasmon-multiple scattering and (b) multiple plasmon-single scattering. The contribution of the first process will overlap with the contribution of the second process and due to this overlapping, we get an enhanced intensity of the peak at the same energy position. Therefore, we present here the calculation of the probability of exciting multiple plasmon peaks in Al upto third order and their relative intensities with respect to the main peak. The calculated results agree fairly well with the experimental values estimated from Henerich curve (1) on characteristic energy loss spectrum of Al.

Henerich (1) has recently reported plasmon peaks at 10 eV, 15 eV, 30 eV. and 45 eV. in the characteristic energy

loss spectrum of aluminum. The peaks at 10 eV and 15 eV are due to surface and volume plasmon losses respectively. These losses have already been studied extensively by several workers (7-9). The other peaks at $2\hbar\omega_p$ (30 eV) and $3\hbar\omega_p$ (45 eV) are due to double and triple plasmon losses respectively and is the subject of present study.

Following Ashley and Ritchie (5) and Spence & Spargo (6) the zeroth, first and second plasmon loss probabilities can be written as

$$W_0(t) = e^{-t/\lambda} \quad (1)$$

$$W_1(t) = (t/\lambda_1) e^{-t/\lambda} \quad (2)$$

$$W_2(t) = \frac{1}{2} (t/\lambda_1)^2 e^{-t/\lambda} + (t/\lambda_2) e^{-t/\lambda} \quad (3)$$

where 't' is the plasmon thickness of the material foil used, λ is the effective mean free path and are connected to λ_1 and λ_2 as

$$\lambda^{-1} = \lambda_1^{-1} + \lambda_2^{-1} \quad (4)$$

and

$$\lambda_2^{-1} = 0.0103 r_s^2 \lambda_1^{-1} \quad (5)$$

In eqn. (3), the first term is the contribution of single plasmon- double scattering process and the second term represent the contribution due to double plasmon- single scattering process. Extending the work of Ashley and Ritchie (5) the probability for the energy loss of $3\hbar\omega_p$ has been derived as

$$W_3(t) = \left[\frac{1}{6} (t/\lambda_1)^3 e^{-t/\lambda} + (t/\lambda_3) e^{-t/\lambda} + \frac{W_1 \times W_2}{W_1 + W_2} \right] \quad (6)$$

and
$$\lambda^{-1} = \lambda_1^{-1} + \lambda_2^{-1} + \lambda_3^{-1} \quad (7)$$

Equation (6) has been obtained by taking the contribution of the following three processes (at the same energy position).

- (a) Single plasmon- triple scattering
- (b) Triple plasmon- single scattering
- (c) Double plasmon- single scattering and single plasmon- single scattering event occurring simultaneously.

From the above expressions ~~for~~ for the probabilities of plasmon losses, one can also derive the expressions for the intensities ratios of the plasmon peaks (I_n) with respect to the main peak (I_0): At $t = \lambda$, eqns.(1) and (2) can give

$$\frac{I_1}{I_0} \approx \frac{\lambda}{\lambda_1} \quad (8)$$

The value of I_1/I_0 can be estimated from Henrich curve (1). ~~Table 1 gives the values of λ and the intensities ratios~~ The values of λ and the intensities ratios are given in tables 1 and 2 respectively. From table 2, it appears that the calculated values of intensities ratios are in fair agreement with the estimated values from Henrich curve(1). Thus we can safely assign the peaks at $2\hbar\omega_p$ (i.e. 30 eV) and $3\hbar\omega_p$ (i.e. 45 eV) as due to double and triple plasmon excitations respectively.

References:-

1. V.E.Henrich, Phys.Rev. B7, 3512 (1975)
2. L.H.Jenkins, D.M.Zehner & M.F.Chung, Surf.Sci. 38, 327 (1973)
3. A.M.Bradshaw & D.Menzel., Phys.Stat.Soli.(b) 56, 135(1973)
4. N.V.Smith & W.E.Spicer, Phys.Rev.Lett. 23, 769 (1969)
5. J.C.Ashley & R.H.Ritchie., Phys.Stat.Soli. 38, 425 (1970)
6. J.C.H.Spence & A.E.C.Spargo., Phys.Rev.Lett. 26, 895(1971)
7. C.V.Von Koch., Phys.Rev.Lett. 25, 792 (1970)
8. W.Steinmann., Phys.Stat.Soli. 28, 437 (1968)
9. K.S.Srivastava, S.P.Singh & R.L.Shrivastava., Phys.Lett. 47 A, 305 (1975) and Phys.Rev. 13B, 3213 (1976)

Table 1.

S.No.,	Mean free path,	Value in Angstrom
1.	λ	0.01422×10^5
2.	λ_1	0.01490×10^5
3.	λ_2	0.33853×10^5
4.	λ_3	3.6×10^5

Table 2:- Probabilities for energy losses.

Energy Loss	Authors' Calculated Value	Estimated value from Henrich curve(1)
$2\hbar\omega_p$	0.18	0.19
$3\hbar\omega_p$	0.069	0.075

Review and Status of X-Ray Laser Research

Ronald W. Waynant
U. S. Naval Research Laboratory
Washington, D. C. 20375

The possibility of developing lasers in the x-ray region of the spectrum has attracted serious attention over the past few years. This attention has occurred for several reasons: (1) the success of generating vacuum ultraviolet laser wavelengths as short as 1100 Å; (2) the success of nonlinear tripling and mixing processes to up-convert existing laser frequencies to attain wavelengths as short as 887 Å; (3) the construction of extremely powerful laser systems to study laser fusion; and (4) the occurrence of results which have been attributed to stimulated emission from several x-ray experiments. Along with these developments numerous ideas for advancements have been made. This discussion collects the last results and proposals and places them within the framework of basic x-ray laser theory. Limitations of experimental technology and the lack of needed theoretical data are discussed.

Construction of lasers below 1000 Å is impeded by the lack of conventional optics. Window and reflector materials are used to make resonators in the visible, but below 1000 Å no material transmits until the 10-50 Å region is reached and the reflectance of metal coatings is usually below 50%. It is possible to use Bragg reflectors, but these are very difficult to align in practice. Distributed feedback also would be a possibility for obtaining resonance in an x-ray oscillator, but the intense pump power required may destroy the delicate lattice spacing required. Because of these practical limitations x-ray lasers are likely to resemble the single-pass, high-gain, mirrorless amplified spontaneous emission (ASE) lasers developed in the uv and vuv. Further study of the general properties of ASE lasers likely will indicate the operating characteristics of x-ray lasers.

Single-pass lasers of length L have gain given by $\exp(\alpha L)$ where α , the small signal gain coefficient, is given by

$$\alpha = \frac{\lambda^2 AN}{8\pi\Delta\nu}.$$

Here λ is the wavelength, $\Delta\nu$ is the linewidth in frequency units, A is the transition probability, and N is the inversion density. Substituting the wavelength dependency for Doppler broadening, the gain factor scales approximately as λ^3 . The pumping power per unit volume (W-cm^{-3}) scales as λ^{-4} . Typical values for $\alpha = 5$, $L = 1$ cm and particle velocity of 10^7 cm/sec are shown in Table I. This table shows the extremely high

TABLE I

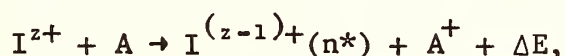
$\lambda[\text{\AA}]$	1	10	100	1000	2000
$P[\text{W-cm}^{-3}]$	10^{19}	10^{16}	10^{11}	10^7	10^6

power densities required in the 1-10 Å wavelength region. At present only high-power focused lasers can approach this power density.

The rate coefficients for energy transfer depend on the specific pumping process involved. Most of the excitation processes have rates which scale inversely with wavelength, the exception being resonance charge transfer. The use of metastable states to store excitation prior to rapid transfer to radiative states may alleviate the requirement for rapid excitation.

Perhaps the most important pumping process is electron collisional excitation. All of the vacuum ultraviolet lasers generated have been excited by electron collision, primarily collisions with molecules. It does not seem likely that molecules can be used in this manner to produce wavelengths much below 600 Å, however. Progress toward x-ray lasers will involve collisions with ions. One such proposal utilizes the electron-collision excitation process to invert the 3p-3s levels in ions. Since this transition has lifetimes connected with it that make lasing rather easy to produce in the visible and near uv, it may be possible to reach short wavelengths by following the isoelectronic ion sequence to higher stages of ionization. For example, the 3p-3s transition of U^{+85} gives a wavelength of 11 Å.

Various electron attachment processes can lead to population inversion. Three-body collisional recombination preferentially fills upper ion levels leading to population inversion with respect to the lower levels. This process is dependent on rather high densities to achieve a high pumping rate and may be best achieved in laser-produced plasmas. Some observations of population inversion in expanding laser plasmas have already been made. Dielectronic capture, where a free electron is captured and a second electron excited, is a possible means of creating a population inversion. Charge transfer interactions proceed as



where an ion, I^{z+} , interacts with a neutral atom, A, reducing the ionic charge, z, by removing an electron from A and promoting the remaining ion to an excited level, n^* . Charge transfer occurs spontaneously only when the defect energy, ΔE is exothermic. Stimulated charge transfer with the defect energy supplied by a laser also has been considered. Charge exchange experiments are presently underway.

Photoabsorption has been considered for the production of a population inversion because of the possibility of tuning the pumping source to produce a specific innershell vacancy. Both $K\alpha$ and full-shell vacancies in alkalis have been studied. The alkalis have the advantage of only one outershell electron and therefore no Auger effects. The analysis of both the alkalis and the $K\alpha$ laser proposals are positive provided photoionization losses of the laser frequency can be minimized and provided a strong pumping source can be found. Such a source could come from a suitably tailored laser-produced plasma.

Other means of possible x-ray laser production include the use of nuclear transitions and the use of stimulated Compton scattering. Serious consideration of nuclear transitions is definitely increasing and could produce an early breakthrough if methods are found to reduce the lifetime of long-lived isomers or if the shorter-lived excited nuclei can be rapidly assembled into a laser configuration. Stimulated Compton scattering has also received increased attention, but the attainment of wavelengths much below 200 Å does not seem possible due to the present limitations of electron and photon beams.

It must be pointed out that the verification of gain becomes very difficult in the far ultraviolet and soft x-ray regions. This is especially true for the very small, single-pass lasers anticipated. Techniques for the verification of gain will likely require the ability to vary the length or other geometry of the gain region as well as the ability to control the pumping intensity. Methods of examination for gain can follow those used for single-pass longer-wavelength vuv lasers, but it is essential that gain be measured to insure that laser action is present.

Many of the above difficulties can be avoided by starting with a powerful infrared laser and using the nonlinear susceptibility of vapors to generate harmonic frequencies or to sum several frequencies. These techniques avoid the pumping intensities required at shorter wavelengths and transfer much of the high-quality spatial and temporal characteristics from the infrared to the far ultraviolet. The extremely low efficiencies associated with nonlinear processes have been improved greatly by using materials with resonances near the incoming laser frequencies or their harmonics. Wavelengths as short as 887 Å have been generated, and mixing of tunable visible or near uv wavelengths has produced tunable vacuum uv in the 1000-2000 Å region. Conversion efficiencies range from 10^{-3} to 10^{-7} for these processes. Some prospects exist for the generation of shorter wavelengths via nonlinear processes employing higher-order harmonics in ionized vapors. It may also be possible to start with high-power vacuum-uv lasers rather than infrared lasers. Nonlinear processes will be available for mixing and tuning of x-ray laser wavelengths when these lasers are developed.

While it is difficult to predict the impact that an x-ray laser is certain to have on future research, it is likely to be most valuable in materials research. Its coherence will be valuable in producing x-ray holograms having high resolution. Its temporal and spatial properties also will be quite valuable in many areas. It is likely that the most important applications have not been anticipated at this time.

References

R. W. Waynant and R. C. Elton, "Review of Short Wavelength Laser Research," Proc. IEEE, vol. 64, pp. 1059-1092 (July 1976) and the 268 references therein.

G. Jamelot, A. Carillon, P. Jaeglé, A. Sureau

Laboratoire de Spectroscopie Atomique et Ionique du C.N.R.S.
 Université Paris-Sud, Centre d'Orsay, Bat. 350
 91405, ORSAY, FRANCE

We present new results on the observation of a negative absorption, in the soft X-ray range, in an aluminium laser-produced plasma. In our previous works, the absorption measurements were time integrated, due to the use of a slow proportional counter(1) or photographic technique(2) for detecting the X-ray radiation of the plasma. Here, the grazing incidence monochromator is equipped with a

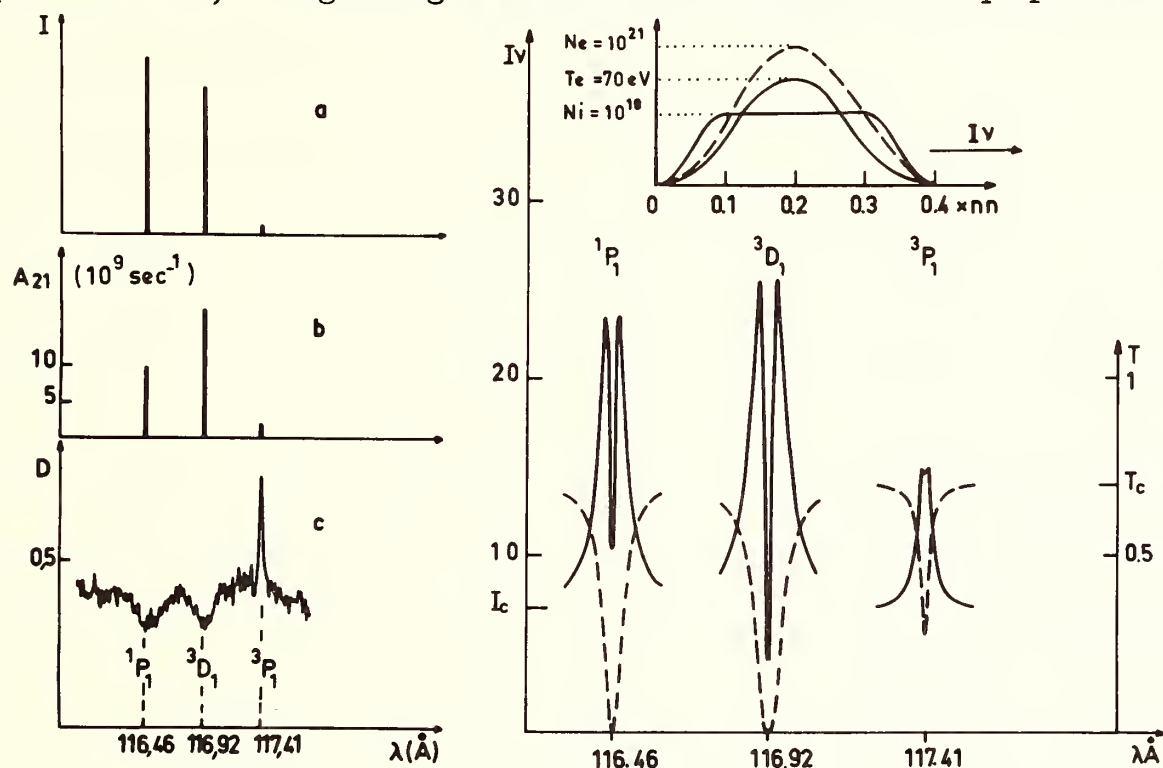


Fig. 1: I-c shows the intensity anomaly occurring in the dense part of a laser-produced plasma; on I-a are the relative intensities of the same lines in common situations; I-b gives calculated transition probabilities.

Fig. 2: For comparison with fig. 1-c, spectrum calculated in assuming i) an absorbing external plasma shell, ii) the equalization of the upper level populations by collisions (L.T.E. equilibrium); inset: ion and electron density distribution (cm^{-3}) and temperature (eV) for which the calculation is made. The figure shows the transmission of the light through the plasma (dashed curves). I_c and T_c are the values corresponding to the continuous spectrum.

Work supported by the D.G.R.S.T. under contract n° 75.7.08I2.

fast detection system, leading to a time-resolution of 1 nanoseconde.

Fig. 1 shows the spectral features in the region under investigation. The surprisingly high intensity of the $4d^3P_1 \rightarrow 2p^1S_0$ line of the Al^{3+} ion, at 117.4 \AA , is observed in several neon-like ions as Mg^{2+} , at 171.9 \AA , and Si^{4+} , at 85.8 \AA . It occurs in the narrow plasma zone where the absorption of the very powerful impulse of the Nd-laser by the plasma initiates turbulences and particle velocity distributions turning away from the equilibrium. Since it was stated that the feature shown on fig. 1-c should be due to the reabsorption in unhomogeneous plasma, without the necessity of invoking any upper level population anomaly, (3,4) we performed a detailed calculation of intensity and profile of the three $4d^1P_1, ^3D_1, ^3P_1 \rightarrow 2p^1S_0$ lines, assuming the equalization of the upper level populations by collisions and a strong reabsorption in an external shell. Fig. 2 gives an example of result of these calculations for a plasma surrounded by a dense cold shell which absorbs the radiation emitted by the center of the plasma. It is obvious that these assumptions are quite inadequate in interpreting the spectrum of fig. 1-c.

The absorption has been measured at the wavelength of the 3P_1 line (117.4 \AA) and in the continuous spectrum, at the wavelength of 118.2 \AA , in using the two plasma technique described elsewhere. The absorption caused by the pure discrete transition is deduced from these two measurements. The time-resolved emission curves of each plasma and of both plasmas together have been averaged over 30 shoots

Fig. 3: An example of time-resolved measurement of the plasma absorption. I - total absorption at 117.4 \AA ; II - continuous absorption measured at 118.2 \AA ; III - absorption caused by the pure discrete transition.

On the left, emission of the "source" plasma, of the "sample" plasma, of both plasmas together, after averaging over 30 shoots. The lower curves, on the right, are the smoothed line emission curve ("sample" plasma) and continuum emission curve (118.2 \AA , in the "sample" plasma).

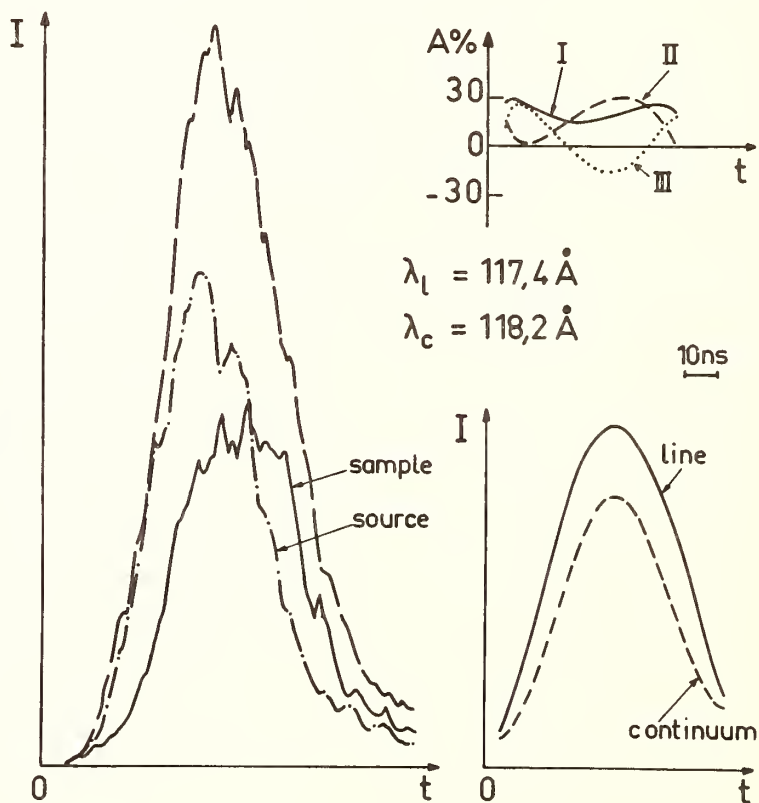
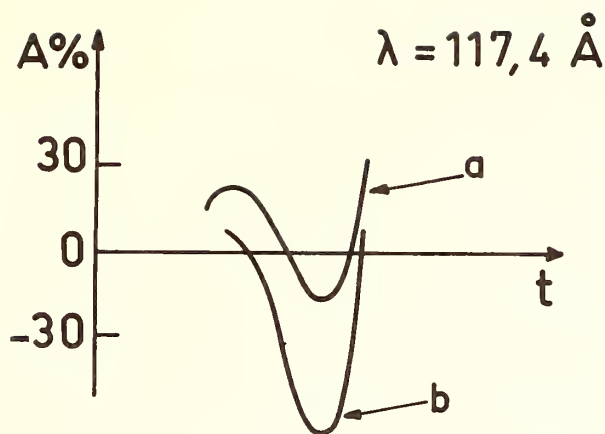


Fig. 3



In spite of the averaging, the curves keep some irregularities and we smoothed them, by a last square polynomial regression, before the calculation of the resulting absorption. This is shown on fig. 3 for the line "sample" emission curve.

In the case represented on fig. 3, the line effects a negative absorption, which is counterbalanced by the positive absorption of the continuum. Such a result is very sensitive to the exact position of the target with respect to the axis of observation (few tens of microns); this can slightly change, by mechanical inaccuracy and surface erosion, over a set of 90 shoots.

With the most accurate sighting attainable in the present device, we achieved the measurement plotted on fig. 4, where the negative absorption appears during a few nanoseconds, without taking off the positive absorption of the continuum (curve a). Moreover, the absorption reaches a large negative value, when deduction of the continuum is made up. These results are to be added to the ones we reported recently(5) with a discussion on population inversions.

REFERENCES

- 1 - A. Carillon, P. Jaeglé, G. Jamelot, A. Sureau, P. Dhez, M. Cukier, Phys. Letters, 36A, 1971, 167.
- 2 - P. Jaeglé, G. Jamelot, A. Carillon, A. Sureau, P. Dhez, Phys. Rev. Letters, 33, 1974, 64.
- 3 - J.P.J. Valero, Appl. Phys. Letters, 25, 1974, 64.
- 4 - W.T. Silfvast, J.M. Green, O.R. Wood, Phys. Rev. Letters, 35, 1975, 435.
- 5 - P. Jaeglé, Report at the 2nd International Conference on Inner Shell Ionization Phenomena, Friburg, W. Germany, March 29 - April 2, 1976, in the press.

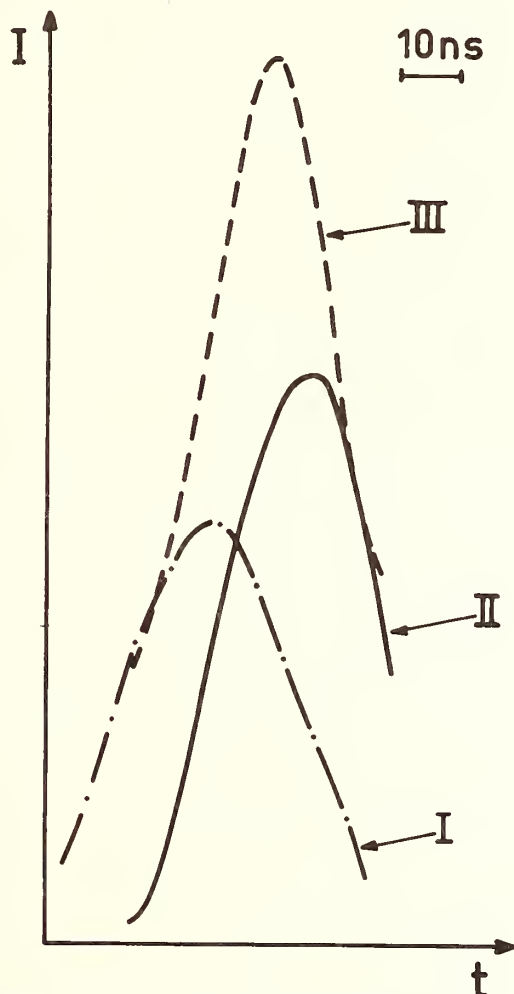


Fig. 4: Plasma absorption, a) total absorption at the wavelength of the line, b) absorption after taking off the continuous absorption. Smoothed emission curves of, I) the "source" plasma, II) the "sample" plasma, III) both plasmas together.

POPULATION INVERSIONS AND THE MEASUREMENT
OF GAIN IN HIGH DENSITY PLASMAS

W.T. Silfvast, O.R. Wood and J.M. Green^{*}
Bell Telephone Laboratories
Holmdel, New Jersey 07733

Population inversions in high-density plasmas are considered and some general problems relating to the interpretation of gain measurements in such plasmas are described. General conditions will be discussed under which population inversions might occur between excited states and also with respect to ground states in these plasmas. Examples of possible inversions in He^+ at 304Å and also in some specific metal vapors will be included. In addition, it will be shown theoretically that population inversions with respect to the ground state are probably not possible in an adiabatically expanding plasma. Experimental evidence will be presented indicating that the measurement of gain in a laser-produced plasma using the so called "two-plasma technique" can be unreliable. Qualitative explanations for the origin of these measurement difficulties will be given.

^{*}Present address: Culham Laboratory, Abingdon, Oxfordshire, United Kingdom.

L. J. Palumbo
 Naval Research Laboratory
 Washington, D.C. 20375

A steady-state computer model for estimating atomic level population densities and short-wavelength laser gain has been developed and applied to electron-collisionally pumped, single-ion, quasi-cw lasing schemes in the carbon-like and helium-like isoelectronic sequences. The carbon-like scheme is an isoelectronic extrapolation to higher atomic number ions and shorter wavelengths of transitions observed [1] to lase in the near UV. The analysis described here is a detailed extension of previous analytical estimates [2] for $3p \rightarrow 3s$ lasing following electron collisional pumping from a $2p$ ground-state reservoir; important refinements include the addition of ionization equilibrium and radiation trapping, extension to high densities [3], the inclusion of more energy levels and more mixing transitions, and the solution for the relevant population densities by simultaneous rate equations.

Because of the close similarity between the carbon-like scheme and another electron-collisional pumping scheme involving $3s \rightarrow 2p$ lasing (collisionally pumped $1s \rightarrow 3s$) in the 10-50 Å range in moderate-Z helium-like ions, the computer code developed for the carbon-like ions was also used with minor modifications to model this two-electron scheme.

In both of these schemes, the lower laser term is rapidly depleted by spontaneous dipole emission into the ground term, while the upper laser term can decay spontaneously only via the lasing transition and is pumped from the ground "reservoir." Such "single-ion" schemes in which the relevant levels are all the same ionization stage result in a maintenance of population inversion independent of atomic lifetimes and ionic regeneration; thus, gain occurs for as long as appropriate plasma conditions can be maintained, and the population inversion is said to be quasi-cw.

A set of steady-state rate equations, each of the form

$$\frac{dN_j}{dt} = 0 = \sum_{k \neq j} N_k W_{kj} - N_j \sum_{k \neq j} W_{jk},$$

was solved for the population densities, N_j , of the levels considered in the present model. The W 's in this equation represent the rates for appropriate atomic processes involving transitions between levels j and k and include electron collisional excitation and deexcitation, electron collisional ionization and (three-body) recombination, spontaneous photoemission, photoabsorption (through an escape-factor treatment of radiation trapping [4], and radiative recombination. Photoionization and transitions induced by ion collisions were negligible in all important cases considered here. In order to allow efficient computation, simple analytical estimates [5], [6] and semi-empirical fits [7] were used to

derive rates needed in the above equations, and the necessary energy-level spacings and oscillator strengths were extrapolated from published tables [8] by scaling appropriately with atomic number. For both the carbon-like and the helium-like schemes, a set of rate equations was solved for the population densities of five levels which included the term ($3d\ ^3D$ in C-like ions and $3p\ ^1P$ in He-like ions) most strongly collisionally coupled to the upper laser term and also strongly coupled by dipole emission to the ground reservoir term, the ground term of the lasing species, and the ground term of the next higher ionization stage.

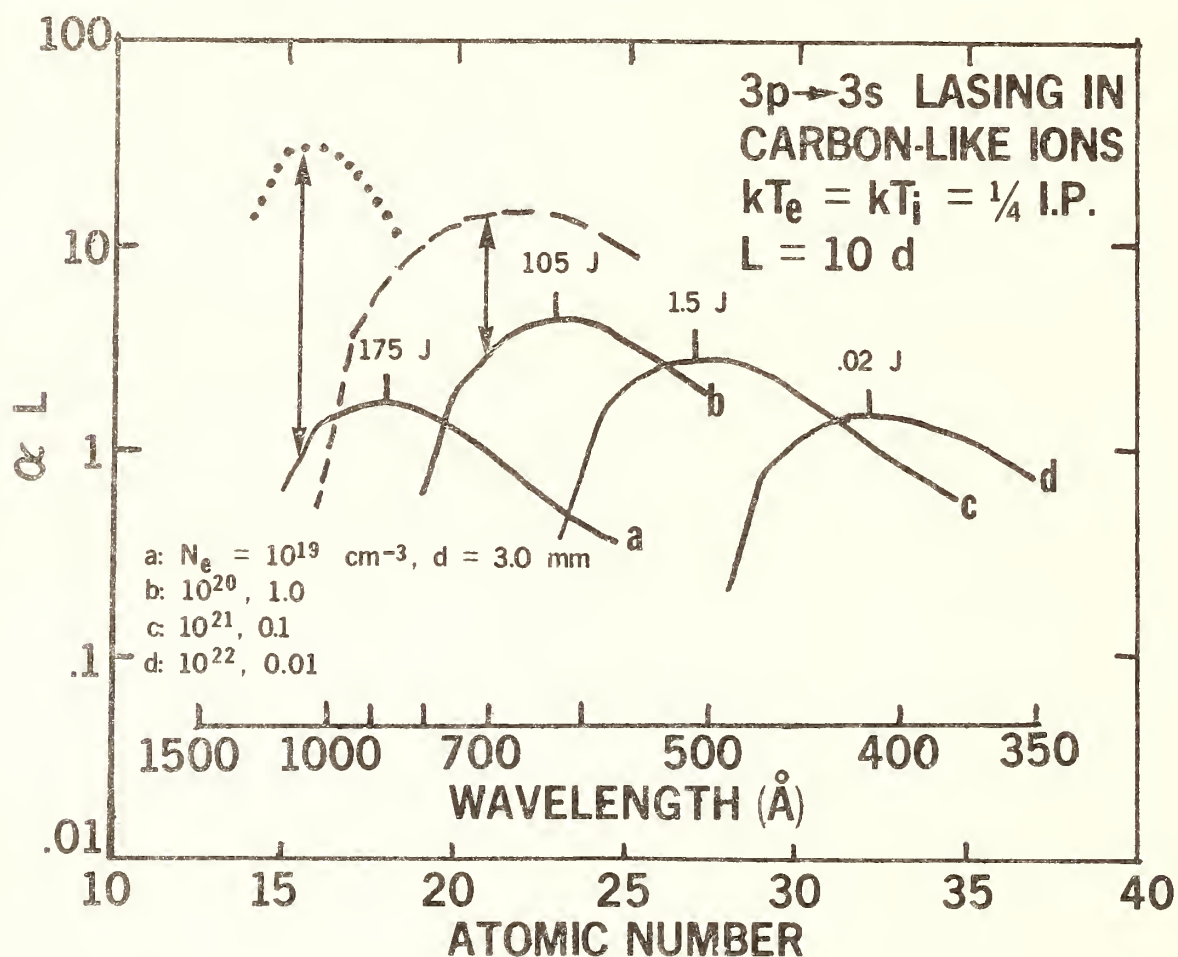


FIGURE 1. Computed product of gain coefficient, α , times plasma length, L , versus atomic number for ions of the carbon isoelectronic sequence at a temperature of one-fourth the ionization potential (for most cases). Solid curves are plotted for various practical electron density (N_e)/plasma diameter (d) combinations. The required plasma particle kinetic energy plus ionization energy is indicated for each curve. The dashed curve indicates the strong effect on curve (b) of varying the 3s - 3p collisional mixing rate by decreasing the effective Gaunt factor from 0.75 to 0.2. Also, the effect of increasing the electron temperature by a factor of four while limiting the ionization rate to maintain an abundance of the carbon-like species equal to one-third the total ion density (as might be the case in a transient heating phase) is indicated for curve (a) by the dotted curve.

Computations were performed for a variety of electron densities and plasma diameters (the size alters the populations through optical depth effects) selected to model conditions presently attainable by plasma discharges or by high-power laser/target interaction. For most of the carbon-like runs, a temperature of one-fourth the ionization potential was selected to assure adequate abundance of the lasing species while still maintaining a high $2p \rightarrow 3p$ pumping rate. Some typical gains calculated for carbon-like ions in a cylindrical plasma of length ten times its diameter are shown in Fig. 1, where curves (a) and (b) represent plasmas created in high-density discharge devices and curves (c) and (d) are typical of smaller high-density laser plasmas. Similar curves generated for helium-like ions under a variety of conditions exhibit population inversion on $3s \rightarrow 2p$ transitions yielding lasing in the 10-50 Å range, but the computed gains in plasmas of reasonable length are two to three orders of magnitude less than those shown in Fig. 1.

*Supported in part by the Defense Advanced Research Projects Agency, DARPA Order 2694.

- [1] Y. Hashino, et al., Jap. J. Appl. Phys. 11, 907 (1972); 12, 470 (1973).
- [2] R. C. Elton, Appl. Opt. 14, 97 (1975).
- [3] R. C. Elton, in Progress in Lasers and Laser Fusion, eds., B. Kursunoglu, A. Perlmutter, and S. M. Widmayer (New York: Plenum Press, 1975).
- [4] T. Holstein, Phys. Rev. 72, 1212 (1947); 83, 1159 (1951).
- [5] R. C. Elton, in Methods of Experimental Physics, Volume 9A, Plasma Physics, eds., H. R. Griem and R. H. Lovberg (New York: Academic Press, 1970) Chapter 4.
- [6] H. R. Griem, Plasma Spectroscopy, (New York: McGraw-Hill, 1964).
- [7] H. J. Kunze, Phys. Rev. A 3, 937 (1971).
- [8] W. L. Wiese, et al., Atomic Transition Probabilities - Volume I: Hydrogen through Neon, NSRDS-NBS-35 (Washington, D.C.: U.S. Government Printing Office, 1971).

AUTHOR INDEX

- Åberg, T., 35, 171
- Adam, M.Y., 329
- Agren, H., 250
- Ahmed, M., 46
- Aita, O., 220
- Alperovich, G.I., 269
- Andermann, G., 240
- Avdeev, V.I., 53
- Bachrach, R.Z., 245
- Baer, Y., 29
- Bagus, P.S., 114
- Baragiola, R., 278
- Barchewitz, R., 81
- Barrus, D.M., 263
- Basilier, E., 119, 126
- Benka, O., 249
- Bergknut, L., 240
- Best, P.E., 98
- Bethge, K., 287
- Bhalla, C.P., 46, 344
- Blake, R.L., 263
- Blokhin, M.A., 145, 269
- Blumberg, W.E., 86
- Bonnelle, C., 81
- Briand, J.P., 332, 335
- Bristow, T.C., 300
- Brown, G.S., 86, 88
- Brytov, I.A., 248
- Bunin, M.A., 269
- Burek, A.J., 263
- Burkhalter, P.G., 304
- Burr, A.F., 95
- Carillon, A., 361
- Catz, A.L., 327
- Cauchois, Y., 292
- Caudano, R., 119, 126
- Chastenet, D., 354
- Chetal, A.R., 163
- Chetoui, A., 332, 335
- Chevallier, P., 332, 335
- Chiao, T., 189
- Chu, C.C., 98
- Citrin, P.H., 29, 86
- Combet Farnoux, F., 310
- Costa Lima, M.T., 133
- Crasemann, B., 1
- Cukier, M., 321
- Curelaru, I., 102
- Das Gupta, K., 260
- Dehmer, J.L., 75
- Delvaille, J.P., 245
- den Boer, M.L., 105
- Dhez, P., 321
- Dietz, R.E., 217
- Dijkstra, J.H., 245
- Dill, D., 75
- Dow, J.D., 10, 111
- Doyle, B.L., 177, 186
- Dozier, C.M., 304
- Drahokoupil, J., 154
- Dufour, G., 208
- Eisenberger, P., 86
- Epstein, A., 245
- Fabian, D.J., 108, 205
- Faessler, A., 60
- Feldman, L.C., 284
- Finster, J., 214
- Flynn, C.P., 26
- Folkman, F., 275
- Föll, H., 232
- Fortner, R., 183
- Franschetti, D.R., 43
- Franck, C.P., 319
- Freeman, A.J., 16
- Frilley, M., 332
- Fuggle, J.C., 205
- Fukuda, Y., 105
- Gardner, R.K., 272
- Gelius, U., 119, 126
- Gel'mukhanov, F.K., 53
- Genz, H., 256
- Geretschlager, M., 249
- Gibbons, P.C., 23, 319
- Gilberg, E., 229
- Girvin, S.M., 13
- Gohshi, Y., 168, 235
- Goldstein, H.-E., 238
- Gonzalez, L., 40
- Goscinski, O., 35
- Graeffe, G., 157
- Gray, T.J., 272
- Green, J.M., 364
- Greenberg, J.S., 180
- Gregory, T.K., 211

- Griesehaber, G., 240
 Groeneveld, K.-O., 275
 Gupta, R.P., 16
 Gupta, S.N., 166
 Gusatinski, A.N., 269

 Haensel, R., 89
 Hagström, S.B.M., 122
 Hague, C.F., 208
 Hall, J.M., 272
 Handel, S.K., 266
 Hayasi, T., 64
 Hayasi, Y., 64, 241, 351
 Haycock, D., 139
 Hoffmann, D.H.H., 256
 Hopfield, J.J., 13
 Horak, Z.J., 338
 Horie, C., 341
 Howat, G., 35
 Humbert, H., 101

 Ichikawa, K., 220
 Iguchi, Y., 130
 Ishii, T., 116

 Jaeglé, P., 321, 361
 Jacobs, W.W., 177, 186
 Jamelot, G., 361
 Jamison, K.A., 272
 Jenson, F.E., 189
 Johansson, L.I., 122
 Jones, J.B., 136
 Joshi, S.K., 226
 Juslen, H., 157

 Källne, E., 205, 245
 Kanski, J., 102
 Karlsson, S.E., 122
 Karnatak, R.C., 208
 Karras, M., 240
 Kashiwakura, J., 168, 235
 Kasrai, M., 136
 Kauffman, R.L., 284
 Keller, F., 310
 Keller, J., 316
 Kieser, J., 198
 Kincaid, B.M., 86
 Kirchmayr, H., 238
 Kissel, L., 324
 Kiyono, S., 241
 Klokocníková, H., 154
 Komyak, N.I., 248

 Kondawar, V., 148
 Kondratenko, A.V., 53
 Kosakow, A., 57
 Kosuch, N., 60
 Krause, M.O., 32
 Krieger, A.S., 293
 Krishna, V., 151
 Kropf, A., 249
 Kunz, C., 19
 Kurmaev, E.Z., 125

 Lähdeniemi, M., 142
 Lang, W.C., 108
 LaVilla, R.E., 243
 Lee, C.M., 281
 Lee, T.N., 301
 Leeper, A.K., 189
 Leonhardt, G., 57
 Lewis, M.N., 338
 Lichten, W., 180
 Lichtenberg, W., 174
 Lieber, A., 307
 Liefeld, R.J., 95, 352
 Lindau, I., 78
 Longe, P., 354
 Low, W., 256
 Lurio, A., 316
 Lytle, F.W., 84

 Mahan, G.D., 7
 Malmqvist, P.-Å., 119, 126
 Mande, C., 148, 223
 Mariot, J.-M., 208
 Martens, G., 89
 Matsukawa, T., 168
 Matthews, D., 183
 Mazalov, L.N., 53
 Mehlhorn, W., 329
 Meisel, A., 63, 214
 Merz, H., 101
 McEnnan, J., 313
 McRae, E.G., 217
 Miller, D.L., 43, 111
 Mokler, P., 275
 Mstibovskaya, L.E., 248
 Muller, P., 214
 Muranaka, T., 241

 Nagel, D.J., 304
 Nakai, S., 168
 Nicholls, C.J., 139
 Nigam, H.L., 151

Nilsson, P.O., 102
 Nolte, G., 174
 Nordgren, J., 250
 Nordling, C., 250
 Norris, P.R., 108, 205

 Obashi, M., 168
 Oh, S.D., 313
 Okusawa, M., 116
 Orlova, E.G., 145

 Padalia, B.D., 108
 Palumbo, L.J., 365
 Papaconstantopoulos, D.A., 192
 Park, R.L., 105
 Paul, H., 249
 Pease, D.M., 211
 Pendharkar, A.V., 223
 Petersen, H., 19
 Petke, M., 57
 Pfliegl, R., 238
 Pianetta, P., 78
 Pireaux, J.J., 119, 126
 Platzman, P.M., 67
 Prasad, J., 151
 Pratt, R.H., 281, 313, 324
 Presnyakov, L.P., 296

 Rabe, P., 86
 Rabinovitch, L.G., 248
 Radler, K., 54
 Rai, S., 347
 Rao, P.V., 38
 Reed, J., 86
 Reed, W.A., 70
 Reuter, W., 316
 Richard, P., 272
 Richter, A., 256
 Rihova, H., 338
 Rozet, J.P., 332, 335

 Sagawa, T., 116
 Salem, S.I., 160
 Sandner, N., 329
 Sarode, P.R., 163
 Sauder, W.C., 243
 Sayers, D.E., 84
 Schader, J., 275
 Schlüter, M., 29
 Schmidt, V., 329
 Schmidt-Böcking, H., 174, 287, 289
 Schnatterly, S.E., 23, 319

 Schnopper, H.W., 245
 Schuch, R., 174, 287
 Schulé, R., 174, 287, 289
 Schwarz, W.H.E., 49
 Schweizer, I.G., 145
 Schwentner, N., 89
 Segall, B., 202
 Senemaud, C., 133
 Sevier, K.D., 275
 Shafroth, S.M., 177, 186
 Shrivastava, R.L., 355
 Shulman, R.G., 86
 Siegbahn, K., 119, 126, 250
 Silfvast, W.T., 364
 Silverman, P.J., 284
 Simunek, A., 154
 Singh, S.P., 355
 Siota, Y., 253
 Skibowski, M., 89
 Slusky, S.G., 23
 Sobelman, I.I., 299
 Sommer, H., 57
 Sonntag, B., 19, 54
 Sonobe, B.I., 189
 Soong, S.C., 46
 Specht, H.J., 287
 Spicer, W.E., 78
 Srivastava, K.S., 355
 Srivastava, V., 226
 Stern, E.A., 84
 Stiebing, K.E., 174
 Stodiek, W., 298
 Stolterfoht, N., 278
 Sugiyura, C., 168
 Sundbom, B., 266
 Suoninen, E., 142
 Sureau, A., 361
 Sutphin, H.D., 307
 Suzuki, I., 235
 Suzuki, T., 72
 Svensson, S., 119, 126
 Szargan, R., 63
 Szmulowicz, F., 202

 Tanis, J.A., 177, 186
 Tavernier, M., 332, 335
 Tegeler, E., 60
 Testardi, L., 88
 Thiel, F., 214
 Topol, I.A., 269
 Tooman, T.P., 352
 Touati, A., 332, 335

Tserruya, I., 174, 287, 289
Tsutsumi, K., 220

Ulmer, K., 92
Urch, D.S., 136, 139

Vaño, E., 40
Van Speybroeck, L.P., 245
Viinikka, E.-K., 114, 157
Vincent, P., 180
Vipayavargiya, V.P., 166

Waltner, A.W., 177
Watanabe, T., 341
Watson, L.M., 108, 205
Watson, R.L., 189
Waynant, R.W., 358
Webb, C.B., 307
Weber, W.M., 90
Werner, A., 89
Wertheim, G.K., 29
Wiech, G., 60, 195
Wolff, H.W., 54
Wood, O.R., 364
Wuilleumier, F., 329

Yokota, M., 253

Ziem, P., 278

PENN STATE UNIVERSITY LIBRARIES



A000070902419